

# Biomass gasification: the understanding of sulfur, tar, and char reaction in fluidized bed gasifiers

Xiangmei MENG

Process and Energy  
Faculty 3mE  
Delft University of Technology



# Biomass gasification: the understanding of sulfur, tar, and char reaction in fluidized bed gasifiers

## Proefschrift

ter verkrijging van de graad van doctor  
aan de Technische Universiteit Delft,  
op gezag van de Rector Magnificus prof. ir. K.C.A.M. Luyben,  
voorzitter van het College voor Promoties,  
in het openbaar te verdedigen op dinsdag 11 december 2012 om 15:00 uur

door

Xiangmei MENG

Master of Science in Mechanical Engineering, Tianjin University  
Geboren te Shan, China

Dit proefschrift is goedgekeurd door de promotor:  
Prof. dr. ir. A. H.M. Verkooijen

En de copromotor:  
Dr. ir. W. de Jong

Samenstelling promotiecommissie:

Rector Magnificus	voorzitter
Prof.dr.ir. A.H.M. Verkooijen,	Technische Universiteit Delft, promotor
Dr.ir.W. de Jong,	Technische Universiteit Delft, copromotor
Prof.dr.ir. E.A. Blekkan,	Norges Teknisk-Naturvitenskapelige Universitet
Prof.dr.ir. G. Brem,	Universiteit Twente
Prof. dr.ir. L.P.H. de Goey,	Technische Universiteit Eindhoven
Prof. dr.ir. D.J.E.M. Roekaerts,	Technische Universiteit Delft
Prof. dr.ir. B.J. Boersma	Technische Universiteit Delft

This research is related to the project, the 7<sup>th</sup> Framework Integrated Project “GreenSyngas” (Project NO. 213628), which was financially supported by the European Commission.

ISBN/EAN: 978-94-6186-090-3

Copyright ©2012 by X. MENG<sup>1</sup>

All rights reserved. No part of the material protected by this copyright notice may be reproduced or utilized in any form or by any means, electronic or mechanical, including photocopying, recording or by any information storage and retrieval system, without the prior permission of the author.

Printed by Ipskamp Drukkers, the Netherlands

---

<sup>1</sup> Author e-mail contact: meizi1006@msn.com



*To  
my dear  
parents, brother and sister,  
Rinko and lovely son Johannes MengLong,  
and friends*

献给

我亲爱的

父母, 弟弟(祥锁)和妹妹(祥杰),

老公林可和可爱的儿子约翰孟龙,

和朋友们

## Summary

---

As one of the currently available thermo-chemical conversion technologies, biomass gasification has received considerable interest since it increases options for combining with various power generation systems. The product gas or syngas produced from biomass gasification is environmental friendly alternatives to conventional petrochemical fuels for the production of electricity, hydrogen, synthetic transportation biofuels and other chemicals. The product gas normally contains the major components such as CO, H<sub>2</sub>, CO<sub>2</sub>, CH<sub>4</sub> and H<sub>2</sub>O, in addition to some organic (e.g., light hydrocarbon species, tar) and inorganic (e.g., H<sub>2</sub>S, HCl, NH<sub>3</sub>) impurities depending on operational conditions and gasification processes. Among these impurities, tar can hamper filtration operation and cause equipment fouling due to condensation at lower temperatures, while H<sub>2</sub>S can cause corrosion as well as poisoning of catalysts. Therefore, to avoid these undesired problems, these compounds need to be removed or reduced to certain level prior to the end use of the product gas.

Furthermore, the most important heterogeneous reactions occurring in biomass gasification are the water-gas and the Boudouard reactions. Concerning these reactions for several biomass fuels reliable char reaction kinetics are missing, though they are very important for the effective modeling and operation of gasification processes, and the conversion of char has a large influence on the overall gasification efficiency and the yield of the product gas. To improve the product gas quality and the overall gasification efficiency of the process, it is necessary to effectively measure and reduce the formation of sulfur and tar during biomass gasification, as well as to understand char reaction kinetics. This dissertation focuses on these three issues by performing biomass gasification experiments on both an atmospheric 100kW<sub>th</sub> steam-O<sub>2</sub> blown circulating fluidized bed (CFB) gasifier at the Delft University of Technology (TUD) and a steam blown 30-40kW<sub>th</sub> pressurized bubbling fluidized bed (PBFB) gasifier at the Technical University Munich (TUM), and studying char reaction characteristics by using a thermogravimetric analyzer (TGA) coupled with a Fourier transform infrared spectrometer (FTIR). The dissertation is divided into 10 chapters and organized as follows:

**Chapter 1** briefly addresses the background (i.e., world energy outlook and biomass conversion options) and motivation for this research, the methodology as well as the outline applied in this dissertation. **Chapter 2** presents a broad literature overview which mainly consists of four parts: sulfur formation and capture methods, tar formation and measurement techniques, char reactions and kinetics models, and models of (C)FB biomass gasification. Desulfurization can be carried out both in situ by using calcium based sorbents such as limestone and dolomite, and downstream by using regenerable single, mixed, and supported metal oxides. A special attention is paid to experimental conditions of sulfidation and the regeneration of used sorbent materials. Tar formation, primary tar reduction by optimizing of operational conditions and tar measuring techniques in particular on-line during biomass gasification is further introduced. Subsequently, a brief literature study regarding char combustion and gasification with an emphasis on char conversion kinetic models is presented. Finally, currently developed models of CFB biomass gasification are discussed.

**Chapter 3** presents experimental setups and measuring techniques used in this research. Three different pelletized fuels: a commercial wood pellet product “Agrol”, willow, and a by-product obtained from ethanol production dried distiller’s grains with solubles (DDGS) have been tested on the CFB gasifier and the PBFB gasifier. The product gas produced from gasification has been analyzed using different analytical instruments. Three different tar measuring techniques have been used to quantify tar concentrations: a quasi-continuous TA120-3 on-line tar analyzer (OTA) using a flame ionization detector (FID) originally developed by IVD, an on-line laser instrument based on induced fluorescence spectroscopy (LIFS) developed by TUM and an off-line solid phase adsorption (SPA) technique developed by KTH. A TGA-FTIR system has been used to study the pyrolysis of three fuels and the reaction behavior of their residual chars: CFB-Char obtained after three fuels gasification in the CFB gasifier and TG-derived PYR-Char obtained after three fuels pyrolysis in the TGA. The physical and chemical properties of CFB-Chars were studied by using powder X-Ray diffraction

(XRD), X-Ray fluorescence (XRF), N<sub>2</sub> adsorption/desorption at -196 °C and scanning electron microscopy (SEM) coupled with energy dispersive scattering (EDS).

Although experimental study of sulfur distribution and capture during biomass gasification is very important, the process could be time-consuming as well as challenging due to limitations and availabilities of sulfur measuring techniques. Thus, thermodynamic equilibrium simulations concerning sulfur species have been performed in two parts using Factsage<sup>TM</sup> software package version 5.4.1 and the results are presented in **chapter 4**. Part 1: the distribution of sulfur species during the gasification of six different biomass fuels at various temperatures ranging from 700-1200 °C, where effects of different operational parameters, including fuel properties and types, temperature, pressure, equivalence ratio (ER) and mineral content on the distribution behavior of sulfur species are systematically investigated and compared with the available experimental data. Part 2: sulfur capture behavior of various sorbent materials like limestone, lime, CuO, ZnO, FeO and MnO by using a simulated gas composition obtained from three different gasifiers, where sulfidation and regeneration capacities of different sorbents are examined. In general, the predicted results show that H<sub>2</sub>S is the predominant sulfur species and its maximum concentration is closely related to the fuel-S content. For all the fuels, around 95% fuel-S is converted into H<sub>2</sub>S during the reaction. Minerals in the fuels, especially the metal Fe, play an important role in the retention of sulfur in the solid phase. Sulfidation and regeneration simulation results indicate that copper, manganese and zinc oxides are the most favorable metals, which are capable of reaching even ppb level at a temperature of about 650 °C, while at temperatures higher than 900 °C calcium based oxides exhibit a better potential than other metal oxides, only their desulfurization capabilities are strongly limited by the temperature range and gas composition especially the H<sub>2</sub>O and CO<sub>2</sub> contents.

**Chapter 5** and **chapter 6** mainly discuss the experimental results obtained from biomass gasification on both gasifiers. **Chapter 5** analyses effects of operational conditions (e.g., steam to biomass ratio (SBR), ER, gasification temperature, pressure) and bed materials on the distribution of the main product gas, sulfur and tar formation from Agrol, willow and DDGS gasification. The results indicated that under atmospheric pressure higher temperatures and SBR were more favorable for H<sub>2</sub> production but less advantageous for the formation of CO and CH<sub>4</sub>, whereas a higher SBR also led to a lower carbon conversion efficiency (CCE%), cold gas efficiency (CGE%) and heating values of the product gas. Higher pressures can significantly promote the formation of CH<sub>4</sub>. Due to a relatively high K and Cl content in DDGS fuel, continually adding 3 to 10% kaolin (based on feeding rate) into the reactor was needed to avoid agglomeration. Furthermore, different amounts of tar were produced from three fuels, but in all cases it mainly contains phenol, cresol, naphthalene, indene and pyrene. Higher temperatures and higher SBR were favorable for tar decomposition.

**Chapter 6** compares the results obtained from three tar measuring techniques in three different ways: on-line analysis behavior of the LIFS and OTA methods, individual tar components quantification of the SPA and LIFS methods and the total tar content analysis using the SPA, LIFS and OTA methods. Possibilities for improving the OTA analyzer have been recommended based on experimental results. The analyzed results showed that the measured concentrations of 10 individual tar species obtained from the CFB and PBFB atmospheric pressure tests using the SPA and LIFS methods agreed reasonably well with a difference of less than 10% between the measured tar concentrations. Both the LIFS and OTA methods can be used as an indicator to monitor the change of the gasifier performance in real time; however, it appeared that the LIFS method was more accurate, and a regular calibration - preferably daily- of the OTA method is required in order to achieve reliable tar measurement results.

**Chapter 7** and **chapter 8** discuss the experimental results concerning the pyrolysis of three fuels, and gasification and combustion of their derived chars. **Chapter 7**, firstly presents the characterization results of CFB-Chars obtained from different analytical techniques; then it analyses the pyrolysis behavior of the three fuels under different heating rates (HR); finally it compares the gasification behavior of CFB-Char and char obtained after pyrolysis (PYR-Char) under different operational conditions (e.g., gasification temperature, CO<sub>2</sub> concentration). The kinetic parameters have been determined using the volumetric reaction model (VRM) and the shrinking core model (SCM). The

analyzed results from TGA-FTIR tests showed that Agrol and willow had a similar pyrolysis behavior, and the volatiles released from Agrol, willow and DDGS pyrolysis were mainly CO, CO<sub>2</sub> and H<sub>2</sub>O, followed by a small amount of CH<sub>4</sub>. Char gasification rate increased with increasing temperature, CO<sub>2</sub> concentration and HR. At low gasification temperature with low CO<sub>2</sub> concentration, CFB-Chars were much more reactive than PYR-Chars. Agrol char samples despite showing large specific surface areas had a low reactivity, due to their low ash content and related high crystalline order. On the other hand, the large ash content in DDGS char, in particularly K component, might catalyze its char gasification, balancing the reduced surface area.

**Chapter 8** analyses the experimental results regarding the combustion of willow and DDGS CFB-chars, and pure charcoal under both isothermal and non-isothermal conditions, as well as the modeling results obtained from a 3D TG furnace model which has been built by using COMSOL Multiphysics<sup>TM</sup> software in order to better understand both temperature and gas velocity profiles within the TG furnace under the condition with and without considering char combustion. The results showed that the char combustion rate increased with increasing either O<sub>2</sub> concentrations or combustion temperatures. Within the temperature range of 750 to 900 °C, it was impossible to determine kinetic parameters for combustion experiments of DDGS and willow chars, but well possible for charcoal under conditions with 15 vol.% O<sub>2</sub> (Ea was around 120 kJ/mol calculated by using the SCM model). Furthermore, a fairly good agreement was observed between the predicted results from COMSOL Multiphysics<sup>TM</sup> model and experimental ones.

**Chapter 9** presents the modeling of the 100kW<sub>th</sub> steam-O<sub>2</sub> blown CFB gasifier with an emphasis on the product gas distribution and equilibrium analysis of water-gas shift (WGS) reaction and methane steam reforming (MSR) reaction. Three different types of models: an equilibrium model (EM) and a kinetic model (KM) setup in Aspen Plus<sup>TM</sup> software, and a fluidization model (FM) written in C Language and compiled using software Bloodshed Dev-C++ have been developed. The modeling results achieved from different software are compared and validated with the experimental data. Compared to the product gas composition obtained from experiments, H<sub>2</sub> concentration predicted from the EM model was much higher, while CO, CO<sub>2</sub>, H<sub>2</sub>O concentrations were slightly lower and almost no CH<sub>4</sub> was predicted from the pure EM model; however, as expected, the concentrations of all gas species predicted from the KM model agreed fairly well with those obtained from experiments. Both the EM and KM models indicated that the WGS reaction and the MSR reaction largely influenced the concentration of H<sub>2</sub>, CO, CO<sub>2</sub>, H<sub>2</sub>O and CH<sub>4</sub>. Finally, **chapter 10** concludes the main experimental and modeling results and provides some recommendations for further research as well.

Xiangmei MENG, October, 2012



## Samenvatting

---

Biomassa vergassing heeft, als een van de hedendaags beschikbare thermo-chemische conversie technologieën, de grootste aandacht, omdat het een hoge gemiddelde systeem efficiëntie vertoont en de mogelijkheid biedt tot integratie met conventionele warmte of elektriciteitscentrales. Productgas of synthesesgas geproduceerd op basis van biomassa vergassing is een milieuvriendelijk alternatief voor conventionele petrochemische brandstoffen voor de productie van elektriciteit, waterstof, synthetische transportbrandstof vervangers en andere chemische producten. Het productgas bevat gebruikelijk de volgende componenten CO, H<sub>2</sub>, CO<sub>2</sub>, CH<sub>4</sub> en H<sub>2</sub>O; hiernaast zitten er ook organische verbindingen (bijvoorbeeld teer) in en verder ook anorganische componenten (bijvoorbeeld H<sub>2</sub>S, HCl, NH<sub>3</sub>), afhankelijk van operationele condities en het vergassingsproces. Teer kan de filtratie belemmeren en andere apparatuur vervuilen vanwege condensatie bij lagere temperaturen, terwijl H<sub>2</sub>S een corroderende werking kan vertonen en de katalysator kan vergiftigen. Om deze negatieve bijwerkingen te omzeilen dienen deze chemische componenten te worden verwijderd of tot een werkbaar niveau te worden gereduceerd. Verder zijn de meest belangrijke heterogene reacties die optreden tijdens biomassavergassing de water-gas reactie en de Boudouard reactie. Wat betreft deze reacties ontbreken voor diverse biobrandstoffen betrouwbare gegevens, hoewel deze erg belangrijk zijn voor de effectieve modellering en operatie van vergassingsprocessen; ook heeft de koolstofresidu conversie een grote invloed op de totale vergassingsefficiëntie en de opbrengst van productgas. Om de productgas kwaliteit en de totale vergassingsefficiëntie van het proces te verbeteren is het nodig om de vorming van zwavel- en teerverbindingen gedurende biomassavergassing effectief te meten en te reduceren, alsmede een beter begrip te verkrijgen van koolstofresidu (char) reaktiekinetiek.

Dit proefschrift richt zich op deze drie uitdagingen door middel van biomassavergassingsexperimenten met een atmosferische 100 kW<sub>th</sub> stoom en zuurstof bedreven circulerend wervelbed (CFB) vergasser bij de Technische Universiteit Delft (TUD) en een 30-40kW<sub>th</sub> stoom bedreven stationair wervelbed (PBFB) drukvergasser bij de Technische Universiteit München (TUM), en verder het bestuderen van koolstofreacties gebruikmakend van thermogravimetrische analyse (TGA) gekoppeld aan een Fourier transform infrared spectrometer (FTIR). De proefschrift is in 10 hoofdstukken verdeeld en op de volgende manier georganiseerd.

**Hoofdstuk 1** behandelt in vogelvlucht de achtergrond (wereld energie verwachting en biomassa conversie mogelijkheden) en motivatie voor dit onderzoek, verder de methodiek, alsmede de opbouw van dit proefschrift. **Hoofdstuk 2** presenteert een uitgebreid literatuur overzicht welke 4 onderdelen behandelt: de vorming van zwavelcomponent en zwavelafvang methodes, teervorming en meettechnieken, koolstofreacties en bijbehorende kinetische modellen, alsmede modellen van (C)FB biomassa vergassing. Ontzwaveling kan of in-situ worden uitgevoerd met calcium gebaseerde absorberende materialen zoals kalksteen en dolomiet of verderop in het proces door gebruik van regenereerbare zuivere, gemengde, alsmede metaaloxides op drager. Er wordt dieper ingegaan op de experimentele condities van zwavelbinding en de regeneratie van gebruikte absorbentia. Teervorming, primaire teerreductie door optimalisatie van procescondities en teer meettechnieken tijdens biomassavergassing, wordt verder uitgewerkt. Hierna wordt een korte literatuurstudie gepresenteerd over koolstofverbranding en -vergassing met een verdieping wat betreft kinetische koolstofconversie modellen. Als laatste zal de huidige stand van CFB biomassavergassing worden besproken.

**Hoofdstuk 3** beschrijft de experimentele opstellingen en meettechnieken welke in dit onderzoek zijn gebruikt. Drie verschillende biomassasoorten, te weten een commercieel verkrijgbare Agrol houtpellets, een alledaagse houtsoort wilg en een bijproduct verkregen van ethanol productie ('dried distiller's grains with solubles', DDGS), zijn getest met de CFB vergasser en de PBFB vergasser. Het geproduceerde product gas van de vergassing is geanalyseerd door middel van verschillende instrumenten. Drie verschillende teer meetinstrumenten zijn gebruikt om de teerconcentratie te kwantificeren: een semi-continue TA120-3 on-line teer analyzer (OTA) gebaseerd op vlam ionisatie detector (FID) ontwikkeld door IVD, een on-line laser instrument gebaseerd op laser geïnduceerde

fluorescentie spectroscopie (LIFS) ontwikkeld door TUM en een off-line vaste fase adsorptie (SPA) techniek ontwikkeld door KTH. Een TGA-FTIR systeem is gebruikt om de pyrolyse en de reactie van de koolstofresiduen van drie verschillende biomassa-soorten te bestuderen: CFB-char verkregen na vergassing van drie biomassa brandstoffen in de CFB vergasser en de PYR-Char verkregen na pyrolyse van deze drie biomassa soorten in de TGA. De fysische en chemische eigenschappen van CFB-chars zijn bestudeerd door middel van poeder X-ray diffractie (XRD), X-Ray fluorescentie (XRF), N<sub>2</sub> adsorptie/desorptie op -196 °C en scanning elektron microscopie (SEM) gecombineerd met 'energy dispersive scattering' (EDS).

Hoewel experimentele studie van zwavelpartitie en -vangst tijdens biomassa vergassing erg belangrijk is, kan het erg tijdsinwendend en uitdagend zijn door limiteringen en beschikbaarheid van zwavel meettechnieken. Daarom zijn thermodynamische evenwichtssimulaties met betrekking tot zwavel verbindingen gemodelleerd uitgevoerd in twee delen met Factsage<sup>TM</sup> versie 5.4.1. Deze resultaten worden gepresenteerd in **Hoofdstuk 4**. Deel 1: de distributie van zwavelverbindingen tijdens de vergassing van zes verschillende biomassa-brandstoffen bij verschillende temperaturen tussen 700 tot 1200 °C, waar de effecten van verschillende operationele parameters, inclusief biomassa eigenschappen en soorten, temperatuur, druk, 'equivalence ratio' (ER) en mineraal concentratie op het verdelingsgedrag van zwavel componenten systematisch zijn onderzocht en vergeleken met de beschikbare experimentele data. Deel 2: zwavelvangstgedrag van verschillende absorberende materialen zoals kalksteen, kalk, CuO, ZnO, FeO en MnO, gebruikmakend van een modelgas samenstelling op basis van drie verschillende vergassers, waar de verzwaveling en regeneratie capaciteiten van de verschillende absorbentia wordt onderzocht. Gemiddeld genomen tonen de voorspelde waarden dat H<sub>2</sub>S de belangrijkste zwavelcomponent is en dat de maximum concentratie gecorreleerd is aan de brandstof-S hoeveelheid. Voor alle brandstoffen wordt ongeveer 95% van de brandstof-S omgezet in H<sub>2</sub>S tijdens de reactie. Mineralen in de brandstof, vooral het metaal Fe, spelen een belangrijke rol in de retentie van zwavel in de vaste fase. Verzwaveling en regeneratie simulatie resultaten laten zien dat koper-, mangaan- en zinkoxides de beste metalen zijn. Deze hebben de mogelijkheid om een ppb niveau te behalen bij een temperatuur van ongeveer 650 °C, terwijl op een temperatuur van 900 °C op calcium gebaseerde oxides een betere potentie hebben dan andere metaal-oxides, alleen is hun ontzwavelingscapaciteit sterk gelimiteerd door de temperatuur range en gas-samenstelling, en hierbij zijn water en koolstofdioxide concentratie zeer belangrijk.

**Hoofdstuk 5** en **Hoofdstuk 6** zetten voor een groot deel de experimentele resultaten verkregen van biomassavergassing van beide vergassers uiteen. **Hoofdstuk 5** analyseert de effecten van operationele condities (bijvoorbeeld de stoom:biomassa verhouding (SBR), ER, vergassingstemperatuur en -druk) en bed materialen op de verdeling van de belangrijkste productgas componenten, zwavel- en teervorming van Agrol, Wilg en DDGS vergassing. De resultaten laten zien dat bij atmosferische druk hogere temperaturen en SBR-waarden gunstig waren voor H<sub>2</sub> productie, maar ongunstig voor de vorming van CO en CH<sub>4</sub>, terwijl een hogere SBR-waarde ook leidde tot een lagere koolstofconversie efficiëntie (CCE%), koud gas efficiëntie (CGE%) en stookwaarden van het productgas. Hogere drukken kunnen de formatie van CH<sub>4</sub> significant vergroten. Door een relatief hoge K en Cl concentratie in DDGS brandstof, was het nodig om continue 3 tot 10 % kaoliniet (gebaseerd op de voeding) in de reactor te transporteren om agglomeratie te verhinderen. Verder zijn er verschillende hoeveelheden teer geproduceerd bij de 3 brandstoffen, maar in alle drie gevallen bevatte het productgas hoofdzakelijk phenol, cresol, naftaleen, indeen en pyreen. Hogere temperaturen en hogere SBR-waarden waren gunstig voor de teerontleding.

**Hoofdstuk 6** vergelijkt de resultaten verkregen van drie teer meettechnieken op verschillende manieren: on-line analyse gedrag van LIFS en OTA methoden, individuele teer componenten kwantificatie van SPA en LIFS methodes en de totale teer inhoud analyse gebruik makend van de SPA, LIFS en OTA methoden. Mogelijkheden om de OTA te verbeteren zijn gebaseerd op experimentele resultaten. De geanalyseerde resultaten laten zien dat de gemeten concentratie van 10 individuele teersoorten bemonsterd bij de CFB en de PBFB atmosferische testen, gebruikmakend van de SPA en LIFS methoden, goed corresponderen met een verschil van minder dan 10% tussen de gemeten teerconcentraties. The LIFS en de OTA methode kunnen beide worden gebruikt als een



indicatie om de verandering van de vergasser in de tijd te monitoren. Echter, het lijkt dat de LIFS methode het stabielst en meest accuraat was. Een reguliere kalibratie, bij voorkeur dagelijks, is nodig om een goede en stabiele teermeting te verkrijgen.

**Hoofdstuk 7** en **Hoofdstuk 8** geven de experimentele resultaten weer op basis van de pyrolyse van de drie biomassa brandstoffen, vergassing en verbranding van de verkregen koolstofresiduen. **Hoofdstuk 7** presenteert eerst de karakteriseringsresultaten van de CFB-Chars verkregen door middel van verschillende analytische technieken; daarna analyseert het de pyrolyse gedrag van de drie verschillende biomassa onder verschillende verhittingssnelheden en uiteindelijk wordt het vergassingsgedrag van CFB-Char en PYR-Char onder verschillende operationele condities (zoals vergassingstemperatuur, CO<sub>2</sub> concentratie) vergeleken. De kinetiek parameters zijn bepaald op basis van het volume reactie model (VRM) en het krimpende kern model (SCM). De geanalyseerde resultaten van de TGA-FTIR test laten zien dat Agrol en wilg een vergelijkbaar pyrolysegedrag vertonen en dat de vluchtige stoffen vrijgekomen uit Agrol, Wilg en DDGS pyrolyse vooral CO, CO<sub>2</sub> en H<sub>2</sub>O waren gevolgd door een kleine hoeveelheid CH<sub>4</sub>. De vergassingssnelheid van het koolstofresidu wordt vergroot door hogere temperaturen, CO<sub>2</sub> concentratie en verhittingssnelheid. Bij een lage vergassingstemperatuur met een lage CO<sub>2</sub> concentratie, was CFB-koolstofresidu veel meer reactief dan PYR-koolstof. Agrol koolstofresidu monsters, hoewel ze een groot specifiek oppervlakte laten zien, vertoonde een lage reactiviteit. Dit komt door het lage asgehalte en een relatief hoge kristalliniteit. Aan de andere kant kan het hoge asgehalte in DDGS koolstofresidu, in het bijzonder het K-gehalte, de vergassing van het koolresidu katalyseren, hetgeen de lage reactie oppervlakte kan compenseren.

**Hoofdstuk 8** analyseert de experimentele resultaten van de verbranding van CFB-koolstofresidu van wilg en DDGS en pure houtskool onder zowel isotherme als non-isotherme condities. Verder zijn modelresultaten verkregen van een 3D TG oven model welke gemodelleerd is gebruikmakend van COMSOL Multiphysics<sup>TM</sup> Software om een beter inzicht te krijgen van de temperatuur- en gassnelheidsprofielen in de TG oven onder condities met en zonder koolstof verbrandingsreactie. De resultaten laten zien dat de koolstof verbrandingssnelheid hoger wordt met een toenemende O<sub>2</sub> concentratie of een hogere verbrandingstemperatuur. In de temperatuurgebied van 750 tot 900 °C was het onmogelijk om de kinetische parameters voor de verbrandingsexperimenten van DDGS en wilg koolresiduen te bepalen, maar dit was goed mogelijk voor koolstof onder de conditie van 15 vol.% O<sub>2</sub> (Ea was rond 120 KJ/mol, berekend door toepassing van het SCM model). Verder is een tamelijk goede overeenkomst aangetoond tussen de voorspelde resultaten van het COMSOL Multiphysics<sup>TM</sup> model en de experimenten.

**Hoofdstuk 9** behandelt de modellering van de 100kW<sub>th</sub> stoom en zuurstof bedreven CFB vergasser met de nadruk op de productgas distributie en evenwichtsanalyse van de water-gas shift (WGS) reactie en methaan stoom 'reforming' (MSR) reactie. Drie verschillende typen modellen zijn opgesteld: een Evenwichtsmodel (EM) en een kinetisch model (KM) in Aspen Plus<sup>TM</sup> Software, en een fluidisatie model (FM) geschreven in C en gecompileerd met Bloodshed Dev-C++. De modelresultaten verkregen op basis van de verschillende modellen is vergeleken en gevalideerd met de experimentele data. Vergeleken met de productgassamenstelling verkregen tijdens de experimenten is de voorspelde H<sub>2</sub> concentratie door het EM model een stuk groter, terwijl CO, CO<sub>2</sub> en H<sub>2</sub>O concentraties een stuk lager waren. Verder werd er bijna geen CH<sub>4</sub> voorspeld door het pure EM model; aan de andere kant, de concentraties van alle gassoorten voorspeld door het KM model correleerde vrij goed met de verkregen resultaten van de experimenten. De EM en de KM modellen indiceerden dat de WGS reactie en de MSR reactie voor een groot deel de concentratie van H<sub>2</sub>, CO, CO<sub>2</sub> H<sub>2</sub>O en CH<sub>4</sub> beïnvloedden. Als laatste vat **Hoofdstuk 10** de belangrijkste experimentele en modelresultaten samen en geeft een verwijzing naar mogelijkheden tot verder onderzoek.



# Nomenclature

## Abbreviations

AC	:	activated carbon	FID	:	flame ionization detector
ACF	:	activated carbon fiber	FM	:	fluidization model
a.r.	:	as received	FPD	:	flame photometric detector
BBM	:	black-box models	FT	:	Fischer-Tropsch
BET	:	Brunauer-Emmet-Teller	FTIR	:	Fourier transform infrared spectrometer
BFD	:	bubbling fluidized bed	GC	:	gas chromatograph
BTX	:	benzene, toluene, xylenes	GOR	:	(steam+oxygen)/biomass mass ratio
BTG	:	Biomass Technology Group BV	HGD	:	hot gas desulfurization
BW	:	bio-dried wood	HHV	:	higher heating value
CA	:	calcium acetate	HK	:	Horvarth-Kavazoe
CCE%	:	carbon conversion efficiency	HR	:	heating rate
CEN	:	European Committee for Standardization	HTR	:	high temperature range
CFB	:	circulating fluidized bed	ICP-OES	:	inductively coupled plasma optical emission spectroscopy
CFBG	:	circulating fluidized bed gasifier	IEO	:	international energy outlook
CFD	:	computational fluid dynamics	IGCC	:	integrated gasification combined cycle
CFDM	:	computational fluid dynamic models	IUPAC	:	International Union of Pure and Applied Chemistry
CGE%	:	cold gas efficiency	IVD	:	University of Stuttgart
CHP	:	combined heat and power	KTH	:	Royal Institute of Technology, Sweden
CMA	:	calcium magnesium acetate	LHM	:	Langmuir–Hinshelwood model
CST	:	conventional cold solvent	LHV	:	lower heating value
daf	:	dry ash free	LIFS	:	laser induced fluorescence spectroscopy
d.b.	:	dry basis	LTR	:	low temperature range
DDGS	:	dried distiller's grains with solubles	MBMS	:	molecular beam mass spectrometer
DFB	:	downdraft fixed bed	MR	:	measuring range
DSC	:	differential scanning calorimetry	MSR	:	methane steam reforming
DTG	:	the time derivative of weight loss	MSW	:	municipal solid waste
EDS	:	energy dispersive scattering	MT	:	miscanthus
EM	:	equilibrium model	NDIR	:	non dispersive infrared analyzer
ER	:	equivalence ratio	Ni-GDC	:	Nickel gadolinium-doped ceria
KM	:	kinetic model	NR	:	Not reported
FB	:	fluidized bed	NREL	:	National Renewable Energy Laboratory
FBC	:	fluidized bed combustion	OECD	:	Organization for Economic Cooperation and Development
FICFB	:	fast internally circulating fluidized bed	OTA	:	on-line tar analyzer
FCC	:	fluid catalytic cracking	PAHs	:	poly-aromatic hydrocarbons

*To be continued on the next page*

*To be continued*

## **Abbreviations**

PBFB	:	pressurized bubbling fluidized bed	SPA	:	solid phase absorption
PCFB	:	pressurized circulating fluidized bed	SPE	:	solid phase extraction
PF	:	particle filter	SS	:	sewage sludge
PFPD	:	pulsed flame photometric detector	ST	:	straw 97
PID	:	photo ionization detector	TGA	:	thermogravimetric analyzer
PLC	:	programmable logical controller	TUB	:	Technical University of Berlin
PM	:	paramagnetic analyzer	TUD	:	Delft University of Technology
RDF	:	refuse derived fuel	TUM	:	Technical University Munich
RF	:	response factor	UFB	:	updraft fixed bed
RPM	:	random pore model	VRM	:	volumetric reaction model
RT	:	railroad ties	WB	:	wood B-quality
SBR	:	steam to biomass mass ratio	WGS	:	water-gas shift
SCM	:	shrinking core model	XRD	:	X-Ray diffraction
SCR	:	selective catalytic reduction	XRF	:	X-Ray fluorescence
SEM	:	scanning electron microscopy	ZF	:	zinc ferrite
SOFC	:	solid oxide fuel cell	ZT	:	zinc titanate

<b>Mathematical symbols</b>			<b>Unit</b>
$C_{Ab}$	:	Bulk fluid gas concentration	kmol/m <sup>3</sup>
$C_{AS}$	:	Surface fluid gas concentration	kmol/m <sup>3</sup>
$C_i^n$	:	Gaseous reactant concentration ( i= CO <sub>2</sub> , O <sub>2</sub> )	kmol/m <sup>3</sup>
$C_{ib}$	:	Gas concentration in the bubble phase( i= CO <sub>2</sub> , O <sub>2</sub> , H <sub>2</sub> , CH <sub>4</sub> , O <sub>2</sub> , N <sub>2</sub> , H <sub>2</sub> O, C <sub>2</sub> H <sub>4</sub> )	mol/m <sup>3</sup>
$C_{ie}$	:	Gas concentration in the emulsion phase	mol/m <sup>3</sup>
$C_{ic}$	:	Gas concentration in the core phase	mol/m <sup>3</sup>
$C_{ia}$	:	Gas concentration in the annulus phase	mol/m <sup>3</sup>
$C_p$	:	The specific heat capacity of the fluid gas	kJ/kg K
$c_{vc}$	:	Solid volume fraction in the core	-
$c_{va}$	:	Solid volume fraction in the annulus	-
$c_{vb}$	:	Solid volume fraction in the bed zone	-
$\overline{c_v}$	:	Average solid volume fraction in the core and annulus phase	-
$C_D$	:	Drag coefficient	-
$D_e$	:	Effective diffusivity	m <sup>2</sup> /s
$d_b$	:	Bubble diameter	m
$d_t$	:	CFB riser diameter	m
$d_d$	:	CFB downcomer diameter	m
$d_p$	:	Solid particle diameter, $d_p = 2 R_p$	m
$E_a$	:	Activation energy	kJ/mol

*To be continued on the next page*

*To be continued*

<b>Mathematical symbols</b>			<b>Unit</b>
$F$	:	The vector of volume forces	N/m <sup>3</sup>
$f_a$	:	Annulus area fraction	-
$G$	:	Total arriving radiative flux- the irradiation	W/m <sup>2</sup>
$H_t$	:	CFB riser length	m
$H_{bz}$	:	CFB bed zone height	m
$h$	:	Heat transfer coefficient	kJ/m <sup>2</sup> ·s·K
$h_{ig}$	:	Enthalpy of vaporization of water	kJ/kg
$\Delta H$	:	Heat of reaction	kJ/kmol
$I$	:	The identity matrix	-
$J_0$	:	The total outgoing radiative flux - the radiosity	W/m <sup>2</sup>
$K_{be}$	:	Mass transfer coefficients the bubble and emulsion phase	1/s
$K_{ca}$	:	Mass transfer coefficients the core and annulus phase	1/s
$k_g$	:	Mass transfer coefficient	m/s
$k_n$	:	n <sup>th</sup> order specific reaction rate constant	(m <sup>3</sup> /kmol) <sup>n-1</sup> (m/s)
$k_m$	:	Kinetic coefficient	((m <sup>3</sup> /kmol) <sup>n-1</sup> /s)
$K$	:	Elutriation rate constant	-
$MW_i$	:	Molar weight of different elements (C, H, O, N, S)	-
$m_{i,daf}$	:	Mass fraction of different elements (C, H, O, N, S) in fuel on a daf basis	-
$m_0$	:	The initial char weight	kg
$m_t$	:	The char weight at time t	kg
$m_f$	:	The residue char weight	kg
$n$	:	Reaction order	-
$Q$	:	Heat source	W/m <sup>3</sup>
$p$	:	Static pressure	Pa
$R_p$	:	Solid particle radius	m
$R$	:	Char reactivity	-
$R_g$	:	Universal gas constant	J/(mol K)
$r'_A$	:	Reaction rate per unit mass of solid particle	kmol/kg-solid·s
$S_a$	:	Surface area of the solid particle	m <sup>2</sup> /kg
$T$	:	Temperature	K or °C
$U_a$	:	Gas velocity in the annulus	m/s
$U_b$	:	Gas velocity in the bubble phase	m/s
$U_c$	:	Gas velocity in the core	m/s
$U_e$	:	Gas velocity in the emulsion phase	m/s
$U_{mf}$	:	Minimum fluidization velocity	m/s
$U_0$	:	Superficial velocity	m/s
$U_t$	:	Particle terminal velocity	m/s

*To be continued on the next page*

*To be continued*

<b>Mathematical symbols</b>			<b>Unit</b>
$X$	:	Char reaction rate or reaction degree	-
$f(X)$	:	Account for the effects of available internal surface	-
$u$	:	The velocity vector	m/s
$\alpha$	:	The splitting factor for char combustion	
$\beta$	:	Heating rate	°C /min
$\mathcal{E}$	:	Surface emissivity	-
$\varepsilon_b$	:	Bubble fraction voidage	-
$\varepsilon_e$	:	Emulsion phase voidage	-
$\varepsilon_{bed}$	:	Bed porosity	-
$\varepsilon_{mf}$	:	Minimum fluidization stage voidage	-
$\eta$	:	Internal effectiveness factor	-
$\kappa$	:	Thermal conductivity of the materials	W/(m.K)
$\mu_g$	:	The dynamic viscosity of the fluid	Pa·s
$\rho_s$	:	The density of different solid fuels	kg/m <sup>3</sup>
$\rho_g$	:	Gas density	kg/m <sup>3</sup>
$\rho_p$	:	The density of the char solid particle	kg/m
$\sum_{g-g} \nu_{ij} R_{ia,g-g}$	:	Gas and gas reaction rate in the annulus phase	mol/(m <sup>3</sup> s)
$\sum_{g-s} \nu_{ij} R_{ia,g-s}$	:	Gas and solid reaction rate in the annulus phase	mol/(m <sup>3</sup> s)
$\sum_{g-g} \nu_{ij} R_{ib,g-g}$	:	Gas and gas reaction rate in the bubble phase	mol/(m <sup>3</sup> s)
$\sum_{g-g} \nu_{ij} R_{ic,g-g}$	:	Gas and gas reaction rate in the core phase	mol/(m <sup>3</sup> s)
$\sum_{g-s} \nu_{ij} R_{ic,g-s}$	:	Gas and solid reaction rate in the core phase	mol/(m <sup>3</sup> s)
$\sum_{g-g} \nu_{ij} R_{ie,g-g}$	:	Gas and gas reaction rate in the emulsion phase	mol/(m <sup>3</sup> s)
$\sum_{g-s} \nu_{ij} R_{ie,g-s}$	:	Gas and solid reaction rate in the emulsion phase	mol/(m <sup>3</sup> s)
$\sigma$	:	The Stefan-Boltzmann constant	W/(m <sup>2</sup> ·K <sup>4</sup> )
$\phi_n$	:	Thiele modulus	-
$\phi_s$	:	Solid particle shape factor	-
$\Phi_{m, oxygen}$	:	Oxygen supplied mass flow rate	kg/h
$\Phi_{m, fuel (daf)}$	:	Biomass fuel supplied mass flow rate on a daf basis	kg/h
$\Phi_{m, gas}$	:	Gas mass flow rate	kg/h

# Contents

<b>Summary .....</b>	<b>i</b>
<b>Samenvatting .....</b>	<b>v</b>
<b>Nomenclature.....</b>	<b>ix</b>
<b>1 Introduction .....</b>	<b>1</b>
<b>1.1 World energy outlook .....</b>	<b>1</b>
<b>1.2 Biomass as renewable energy .....</b>	<b>3</b>
1.2.1 Pyrolysis .....	4
1.2.2 Combustion.....	4
1.2.3 Gasification.....	5
1.2.4 Summary of thermochemical conversion .....	8
<b>1.3 Main research questions .....</b>	<b>9</b>
1.3.1 Problems with sulfur.....	9
1.3.2 Problems with tar.....	9
1.3.3 Problems with char reaction .....	10
1.3.4 Main research question .....	10
<b>1.4 Methodology .....</b>	<b>10</b>
1.4.1 Experimental work .....	11
1.4.2 Modeling work .....	11
<b>1.5 Outline of this dissertation .....</b>	<b>11</b>
<b>2 Literature overview — sulfur, tar, char reaction and (C)FB models.....</b>	<b>13</b>
<b>2.1 Sulfur formation and capture .....</b>	<b>14</b>
2.1.1 Sulfur formation .....	14
2.1.2 In bed sulfur capture .....	15
2.1.3 Downstream sulfur capture.....	17
<b>2.2 Tar reduction and measuring techniques .....</b>	<b>19</b>
2.2.1 Tar definition and formation.....	19
2.2.2 Tar reduction .....	21
2.2.3 Tar measuring techniques.....	25
<b>2.3 Char combustion and gasification .....</b>	<b>29</b>
2.3.1 Char reaction and reactivity.....	29
2.3.2 Char kinetic models.....	31
2.3.3 Char combustion.....	32
2.3.4 Char gasification.....	34
<b>2.4 Modeling of (C)FB biomass gasification .....</b>	<b>36</b>
2.4.1 Kinetic models.....	36
2.4.2 Equilibrium models (EM).....	39
<b>2.5 Summary .....</b>	<b>40</b>

<b>3 Experimental setups and measuring techniques .....</b>	<b>41</b>
<b>3.1 Gasification experiments .....</b>	<b>42</b>
3.1.1 The 100kW <sub>th</sub> steam-O <sub>2</sub> blown CFB gasifier .....	42
3.1.2 The 30-40kW <sub>th</sub> PBFB gasifier .....	44
3.1.3 Biomass fuels, bed materials and additives .....	45
3.1.4 Main product gas sampling and analysis .....	47
3.1.5 Sulfur species analysis .....	48
3.1.6 Tar measuring techniques .....	50
3.1.7 Investigating variables definition .....	54
<b>3.2 TGA-FTIR experiments .....</b>	<b>55</b>
3.2.1 TGA-FTIR .....	55
3.2.2 Char characterization .....	56
3.2.3 Char gasification procedure .....	57
3.2.4 Char combustion procedure .....	57
3.2.5 Sulfidation procedure .....	58
<b>4 Thermodynamic modeling of sulfur distribution and capture during biomass gasification .....</b>	<b>61</b>
<b>4.1 Sulfur distribution modeling procedure .....</b>	<b>62</b>
4.1.1 Biomass fuels .....	62
4.1.2 Factsage <sup>TM</sup> modeling .....	63
<b>4.2 Sulfur distribution modeling results .....</b>	<b>63</b>
4.2.1 Comparison of experimental and predicted H <sub>2</sub> S emission .....	63
4.2.2 Effect of temperature .....	65
4.2.3 Effect of pressure .....	66
4.2.4 Effect of ER .....	67
4.2.5 Effect of minerals .....	67
<b>4.3 Conclusion of sulfur distribution modeling .....</b>	<b>69</b>
<b>4.4 Sulfur capture modeling procedure .....</b>	<b>69</b>
<b>4.5 Sulfur capture modeling results .....</b>	<b>70</b>
4.5.1 Sulfidation simulation analysis .....	70
4.5.2 Regeneration simulation analysis .....	73
<b>4.6 Conclusion of sulfur capture modeling .....</b>	<b>78</b>
<b>5 Biomass gasification in the steam-O<sub>2</sub> blown CFB and the steam blown PBFB gasifiers: Effects of operational conditions on product gas distribution and tar formation .....</b>	<b>79</b>
<b>5.1 Biomass gasification using the CFB gasifier .....</b>	<b>80</b>
5.1.1 Effects of operational conditions on product gas composition .....	83
5.1.2 Effects of different operational conditions on tar formation/reduction .....	87
<b>5.2 Conclusion of gasification using the CFB gasifier .....</b>	<b>93</b>
<b>5.3 Biomass gasification using the PBFB gasifier .....</b>	<b>94</b>



5.3.1	Effects of different operational conditions on product gas compositions.....	94
5.3.2	Effects of different operational conditions on tar formation .....	97
<b>5.4</b>	<b>Conclusion of gasification using the PBFB gasifier.....</b>	<b>98</b>
<b>6</b>	<b>Tar formation in the steam-O<sub>2</sub> blown CFB and the steam blown PBFB gasifiers: comparison between different on-line measurement techniques and the off-line SPA sampling and analysis method .....</b>	<b>99</b>
<b>6.1</b>	<b>On-line analysis comparison .....</b>	<b>102</b>
<b>6.2</b>	<b>Individual tar component comparison .....</b>	<b>103</b>
6.2.1	Individual tar compounds from CFB gasification tests .....	104
6.2.2	Individual tar compounds from PBFB gasification tests .....	106
<b>6.3</b>	<b>Total tar concentration comparison .....</b>	<b>110</b>
6.3.1	Total tar concentration from CFB gasification tests .....	110
6.3.2	Total tar concentration from PBFB gasification tests.....	110
<b>6.4</b>	<b>Conclusion.....</b>	<b>112</b>
<b>7</b>	<b>Characterization of different CFB gasification residual chars and comparison of their gasification behavior with TG-derived pyrolysis chars .....</b>	<b>113</b>
<b>7.1</b>	<b>Char samples .....</b>	<b>114</b>
<b>7.2</b>	<b>Char gasification conversion models .....</b>	<b>114</b>
<b>7.3</b>	<b>Characterization of CFB-Char .....</b>	<b>115</b>
<b>7.4</b>	<b>Fuel pyrolysis results.....</b>	<b>120</b>
7.4.1	Fuel pyrolysis behavior .....	120
7.4.2	Product yields from pyrolysis.....	124
7.4.3	Light volatiles from pyrolysis.....	125
<b>7.5</b>	<b>Char gasification results .....</b>	<b>129</b>
7.5.1	Char gasification behavior.....	129
7.5.2	Char gasification kinetics .....	135
7.5.3	Recalculation of TG.....	136
<b>7.6</b>	<b>Conclusion.....</b>	<b>139</b>
<b>8</b>	<b>Combustion behavior study of willow and DDGS CFB gasification residual chars using TG analysis and COMSOL Multiphysics<sup>TM</sup> modeling .....</b>	<b>141</b>
<b>8.1</b>	<b>Char combustion conversion models.....</b>	<b>142</b>
<b>8.2</b>	<b>COMSOL Multiphysics<sup>TM</sup> modeling procedure .....</b>	<b>143</b>
<b>8.3</b>	<b>Char combustion results.....</b>	<b>146</b>
8.3.1	Isothermal combustion .....	146
8.3.2	Non-isothermal combustion .....	148
8.3.3	Kinetic constants for char combustion .....	150
8.3.4	The recalculated TG curves.....	154
<b>8.4</b>	<b>Comsol Multiphysics<sup>TM</sup> modeling results.....</b>	<b>155</b>
8.4.1	Velocity and temperature distribution without reaction .....	155

8.4.2	Velocity and temperature distribution with reaction .....	158
<b>8.5</b>	<b>Conclusion.....</b>	<b>160</b>
<b>9</b>	<b>Modeling biomass gasification in the 100kW<sub>th</sub> CFB gasifier using different models .</b>	<b>161</b>
<b>9.1</b>	<b>Model development .....</b>	<b>162</b>
9.1.1	Equilibrium model (EM) in Aspen Plus .....	162
9.1.2	Kinetic model (KM) in Aspen Plus <sup>TM</sup> .....	163
9.1.3	Fluidization model (FM) in C Language .....	171
<b>9.2</b>	<b>Experimental setup and model validation .....</b>	<b>176</b>
<b>9.3</b>	<b>Results and discussion.....</b>	<b>176</b>
9.3.1	Predicted results from the EM models.....	176
9.3.2	Predicted results from the KM models .....	180
9.3.3	Predicted Results from the FM model .....	185
9.3.4	Sensitivity analysis of the FM model .....	190
9.3.5	Comparison of EM, KM and FM models .....	191
<b>9.4</b>	<b>Conclusion.....</b>	<b>192</b>
<b>Chapter 10</b>	<b>Conclusions and recommendations .....</b>	<b>195</b>
<b>10.1</b>	<b>Conclusions .....</b>	<b>195</b>
10.1.1	Experimental results from CFB and PBFB tests .....	195
10.1.2	Experimental results from TGA-FTIR tests .....	196
10.1.3	Modeling results.....	196
<b>10.2</b>	<b>Recommendations .....</b>	<b>197</b>
<b>Bibliography</b>	<b>.....</b>	<b>199</b>
<b>Appendix</b>	<b>.....</b>	<b>213</b>
<b>List of publications</b>	<b>.....</b>	<b>245</b>
<b>Acknowledgments</b>	<b>.....</b>	<b>247</b>
<b>Curriculum Vitae</b>	<b>.....</b>	<b>249</b>

# 1 Introduction

---

*This chapter presents the research background, motivation, methodology and outline of this dissertation.*

## 1.1 World energy outlook

Over the past several decades, the world has dramatically changed, largely thanks to the contribution of fossil fuels (e.g., coal, oil and natural gas). Fossil fuels have provided us with cheap and convenient energy which we use for heating and electric power generation, and been widely used as transportation fuels and for chemical production as well. With a continuous population increase and economies expansion, global energy consumption is increasing fast, whereas cheap fossil fuels as non-renewable sources are rapidly depleting. Moreover, their massive utilization has also caused many problems such as environmental damage (e.g., ozone depletion, global warming) associated with various emissions. Changes in the energy supply structure are required to meet the growing demand for energy. Therefore, researchers are exploring renewable energy sources to decrease our dependence on fossil fuels and increase energy security. Renewable energy is energy which comes from natural resources such as sunlight, wind, rain, biomass and geothermal heat which are naturally replenished (Chang et al., 2003).

Regarding world energy sources consumption and future predictions, several scenarios have been developed by different institutions based on different perspectives and techniques (Fischer & Schrattenholzer, 2001; Petroleum, 2011; Schiffer, 2008; Shell International Petroleum Company & Environment, 2001; Tanaka, 2010). According to the International Energy Outlook (IEO) 2010 published by the International Energy Agency (IEA), world marketed energy consumption will increase by 49% from 2007 to 2035 in the reference case. The most rapid growth in energy demand from 2007 to 2035 occurs in nations outside the Organization for Economic Cooperation and Development (non-OECD nations) and their total energy demand will increase by 84% compared with an increase of 14% in OECD countries (Tanaka, 2010).

**Figure 1- 1** presents world marketed energy consumption from different fuel sources over the 2007-2035 projection periods. It can be seen that fossil fuels are going to continue sharing more than 80% of world marketed energy consumption. Among them, liquid fuels remain the world's largest source of energy due to their importance in the transportation and industrial end-use sectors, whereas their share decreases from 35% in 2007 to 30% in 2035, as the supply is projected to be driven by high and fluctuating world oil prices. Nuclear energy is predicted to grow relatively moderately. Renewables' share of world marketed energy consumption will increase from 10% in 2007 to 14 % in 2035.

World net electricity generation by different fuel sources over the 2007-2035 projection periods is presented in **Figure 1- 2**. It can be seen that world net electricity generation will increase by 87% in the reference case, from 18.8 trillion kWh in 2007 to 25.0 trillion kWh in 2020 and 35.2 trillion kWh in 2035. From 2007 to 2035, world renewable energy use for electricity generation grows by an average of 3.0 % per year, and the renewable share of world electricity generation increases from 18% in 2007 to 23 % in 2035. Coal-fired power generation increases by an annual average of 2.3% in the reference case, making coal the second fastest-growing source for electricity generation in the projection. The outlook for coal could be altered substantially; however, by any future legislation that would reduce or limit the growth of greenhouse gas emissions. Power generation from natural gas and nuclear power—which produces relatively low levels of greenhouse gas emissions (natural gas) or none (nuclear)—will increase by 2.1 and 2.0 % per year, respectively, in the reference case. Furthermore, of the 4.5 trillion kWh of increased renewable electricity generation over the projection period, 2.4 trillion kWh (54 %) is attributed to hydroelectric power and 1.2 trillion kWh (26 %) to wind. Renewable sources other than hydroelectricity and wind—including solar, geothermal, biomass, waste, and tidal/wave/oceanic energy—do increase at a rapid rate over the projection period which can be clearly seen in **Figure 1- 3**.

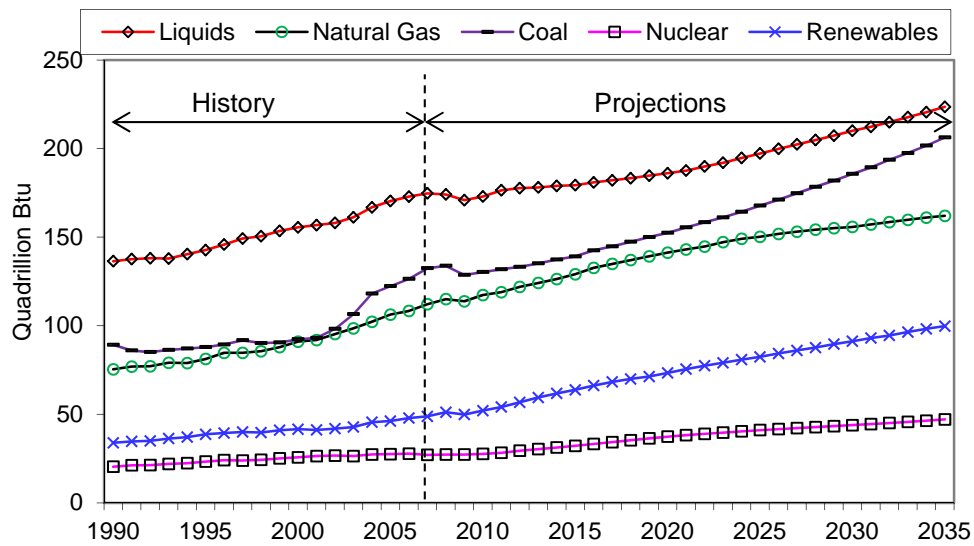


Figure 1- 1 World marketed energy use from different fuel sources over 2007-2035 (Tanaka, 2010)

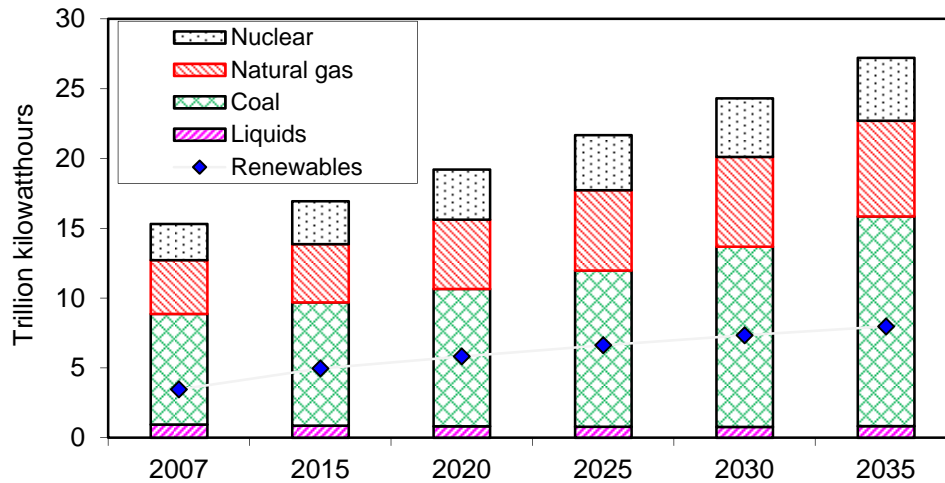


Figure 1- 2 World net electricity generation by different fuel sources over 2007-2035 (Tanaka, 2010)

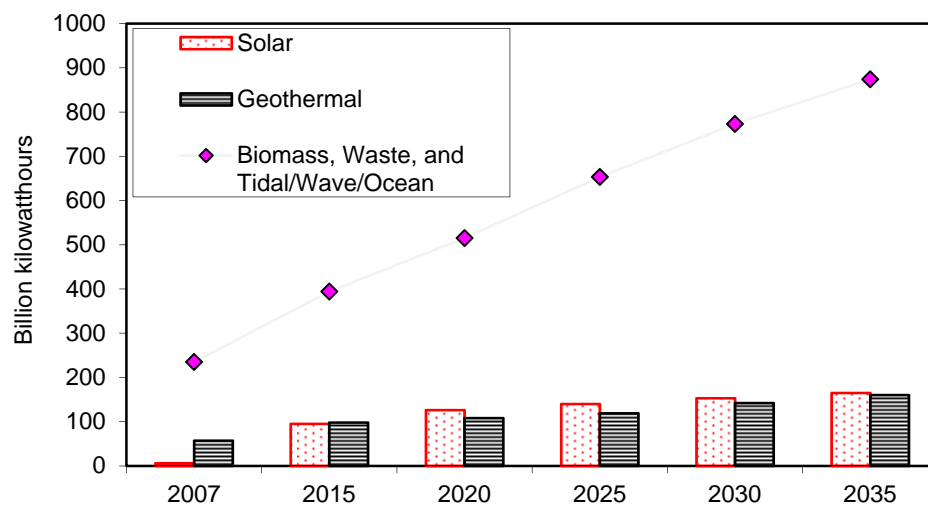


Figure 1- 3 World renewable electricity generation: excluding wind and hydropower (Tanaka, 2010)

According to abovementioned projected data in the IEO 2010, it is obvious that no combination of alternative technologies can completely replace the current usage of fossil fuels and the highest increase in world-wide energy consumption is predicted to be from all three fossil fuels. However, in order to mitigate global warming, it is inevitable to reduce the quantity of fossil fuels consumed as much as possible and increase the global production from alternative renewable energy sources as well. As it is well-known, most common renewable energy resources include wind, solar, hydropower, geothermal and biomass. Unfortunately, none of renewable energy resources are equally distributed over the world. The deployment of renewable energy should be based on the availability of local resources. Biomass is the most promising renewable energy resource to satisfy future energy needs, since it can produce many chemical products and be used in many applications just as fossil fuels. How to efficiently convert biomass into various energy forms will be explained in the section below.

## 1.2 Biomass as renewable energy

Biomass, a renewable energy source, is biological material from living, or recently living species, such as woodchips, sawdust, bark, straw, municipal solid waste (MSW) and wastes from the food industry (McKendry, 2002a). Biomass can be converted into more valuable energy forms via physical, biochemical/biological (i.e., anaerobic digestion and fermentation) (Demirbas, 2005a; Goldemberg et al., 2008) and thermochemical conversion (i.e., combustion, pyrolysis and gasification) (Kumar et al., 2009; McKendry, 2002b; Stiegel & Maxwell, 2001; Wang et al., 2008a). The possible options for converting biomass into various energy forms such as power and heat or chemicals and liquids are presented in **Figure 1- 4** (Scahill, 2004).

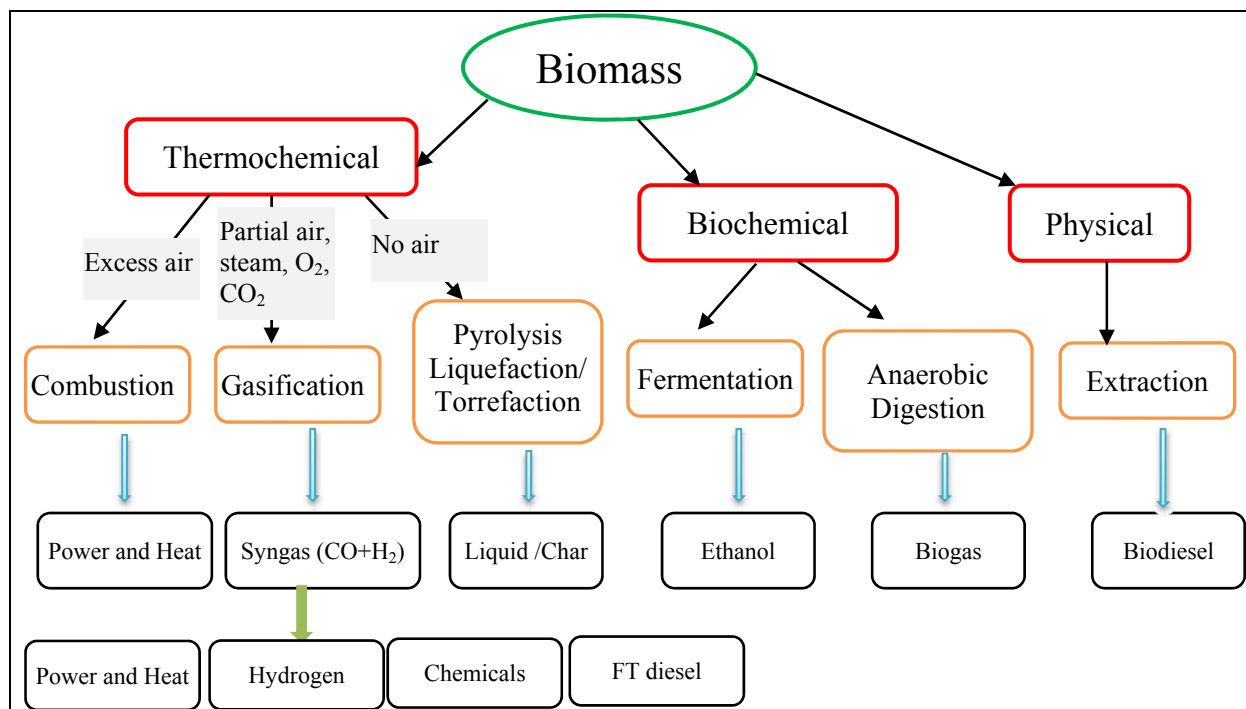


Figure 1- 4 Biomass to energy conversion technologies modified from (Scahill, 2004)

As we can see in **Figure 1- 4**, biochemical and physical conversion technologies are mainly used to convert specified biomass fuels into liquid fuels such as ethanol, biodiesel or biogas, whereas a broad range of biomass fuels can be used to produce electricity, heat, liquid fuels and chemicals via thermochemical processes. Biochemical and physical conversion technologies are out of the scope of this research, thus a brief description with a focus on thermochemical conversion of biomass will be further presented.

### **1.2.1 Pyrolysis**

Pyrolysis converts biomass into liquid (bio-oil or bio-crude), solid and gaseous fractions by heating biomass fuels at a temperature of 450-600 °C in the absence of air (Babu, 2008). Pyrolysis is also the first reactive step occurring during biomass gasification and combustion. Depending on operational conditions (e.g., heating rate and residence time), pyrolysis can be classified into conventional slow pyrolysis and fast pyrolysis. Conventional slow pyrolysis has been mainly used for the production of charcoal, while fast pyrolysis is currently of particular interest for bio-oil production (heating value of about 17 MJ/kg). The conversion of biomass to crude bio-oil show efficiencies up to 70% for flash pyrolysis processes (Demirba, 2001). However, crude bio-oil normally has a high viscosity, high oxygen content, high corrosivity and poor thermal stability. Crude bio-oil can be upgraded (e.g., hydrogenation or catalytic cracking) to biofuels or to intermediates which can be used in boilers, engines and turbines for heat and/or electricity generation (Balat et al., 2009; Demirba, 2001). The high concentration of oxygenates in the crude bio-oil can be largely reduced by using different acidic zeolite catalysts which have been studied by several groups (Aho et al., 2008; Horne & Williams, 1996; Lappas et al., 2002). However, pyrolysis and bio-oil upgrading technology is not currently widely commercially available, although considerable experience has been gained and several pilot plants or demonstration projects are in operation (Bioenergy, 2011).

### **1.2.2 Combustion**

Combustion is a widely practiced commercially process for converting biomass fuels to heat, power or heat and power with excess of air. Worldwide it provides more than 90% of the energy generated from biomass (Koppejan & van Loo, 2002). The energy produced from biomass combustion can be used to provide heat for cooking, space heating and heat and/or steam for industrial processes, or for electricity generation. Biomass of different forms can be used to produce power and heat in small-scale distributed generation facilities and in industrial scale applications as well as in larger scale electricity generation and district heating plants (Koppejan & van Loo, 2002). Various combustion conversion technologies (e.g., fixed bed combustion, fluidized bed combustion (FBC), pulverized fuel combustion) are available to produce energy from different qualities of biomass fuels. Among them, FBC has emerged as a viable alternative over conventional firing system as it has significant advantages, such as: flexibility with fuels, higher combustion efficiency and reduced emissions of noxious pollutants (i.e.,  $\text{SO}_x$  and  $\text{NO}_x$ ). The FBC generally takes place within a temperature range of 800 to 1000°C, since this temperature range is much below the ash fusion temperature, melting of ash and thus associated problems are avoided (Maciejewska et al., 2006). In general, less homogeneous and low-quality biomass fuels need more sophisticated combustion systems.

A classic application of biomass combustion is heat production for domestic applications, which still remains a major market in countries like Austria, France, Germany, Finland, Sweden, Denmark and Norway. However, this way combustion generally has a low efficiency (some even as low as 10%) accompanied with considerable indoor emissions (e.g., CO,  $\text{NO}_x$ , dust and soot). In order to improve its efficiency, automated heating systems by using standardized fuel (e.g., pellet) with catalytic gas cleaning have been developed. With these improvements, the advanced domestic heaters can obtain a high efficiency of 70–90% with significantly reduced emissions (Faaij, 2006). Combined heat and power production (CHP) also called cogeneration is currently recognized as one of the most cost effective ways of using biomass for energy conversion purposes. Compared to a conventional power station which has an operating efficiency of 40%, a CHP plant can achieve an overall efficiency of around 75% with 25% of electric efficiency and 50% of thermal efficiency (Biomass, 2010).

Co-combustion of biomass with coal in traditional coal-fired power plants is becoming increasingly popular due to its low risk and investment cost as well as the capacity for reducing traditional pollutants (i.e.,  $\text{SO}_x$ ,  $\text{NO}_x$ ) and net greenhouse gas (i.e.,  $\text{CO}_2$ ,  $\text{CH}_4$ ) emissions (Demirbas, 2005b). Biomass co-fired in existing combustors is usually limited to 5–10% of the thermal input due to concerns about plugging existing coal feed systems (Wang et al., 2008a). Although significant progress has been achieved in co-combustion over the last decade, biomass properties pose several challenges to coal plants that may affect their operation and lifetime. According to Nussbaumer

(Nussbaumer, 2003), co-combustion may require some additional investment costs for biomass pretreatment, de-NO<sub>x</sub> installation and boiler retrofitting, as well as higher operation cost due to increased slagging, fouling, corrosion and potential poisoning of selective catalytic reduction (SCR) catalyst. On another hand, “the desire to burn uncommon fuels, improve efficiencies, reduce costs, and decrease emission levels continuously results in improved technologies being developed ” (Koppejan & van Loo, 2002). Jappe Frandsen (Jappe Frandsen, 2005) wrote an excellent paper concerning their findings in the field of utilizing biomass and waste for power production, with a focus on the problems of ash and deposit formation and corrosion during coal and biomass con-firing in utility boilers. He reported that due to the production of fly ash and deposits with very high contents of K and Cl (40-80 wt.%), ash deposition and corrosion may constitute a significant problem in straw-fired grate-boilers, particularly if the metal temperature is raised above 520 °C, but they will likely not be the major problems during coal straw co-firing in pulverized fuel boilers since coal ash can capture the K from straw and only low concentrations of KCl (<5wt.%) are observed in the fly ash and deposits from these plants. Currently, biomass co-combustion in modern coal power plants with efficiencies up to 45% is the most cost effective biomass use for power generation.

### 1.2.3 Gasification

Biomass gasification has attracted considerable interest worldwide probably due to the high overall system flexibility and efficiency it offers with respect to biomass combustion and pyrolysis (Ruoppolo et al., 2010). Gasification converts biomass to a combustible product gas or syngas at a typical temperature range of 800 to 1000 °C by using various gasifying agents such as air, O<sub>2</sub>, steam, CO<sub>2</sub> or their mixtures. Unlike combustion where oxidation is practically complete in one process, during gasification biomass undergoes several steps: drying to evaporate moisture, pyrolysis to produce gases, vaporized tars or oils and a solid char residue, and gasification or partial oxidation of the residual char, pyrolysis tars and pyrolysis gases (Bridgwater, 2003). Major reactions involved in the gasification process are summarized in **Table 1- 1**. Several parameters such as gasifier types, reaction temperature, biomass fuels properties, bed materials and gasifying agents have a substantial influence on the product gas composition, carbon conversion efficiency and tar formation.

*Table 1- 1 Major reactions involved in the gasification process(Gómez-Barea & Leckner, 2010)*

NO.	Name	Reaction	$\Delta H_{298}^0$ (kJ/mol)
<i>RI- 1</i>	Devolatilization	<i>biomass</i> → Volatiles + C + Ash	>0
<i>RI- 2</i>	Partially combustion	$C + 0.5O_2 \rightarrow CO$	-111
<i>RI- 3</i>	Complete combustion	$C + O_2 \rightarrow CO_2$	-394
<i>RI- 4</i>	Boudouard reaction	$C + CO_2 \rightarrow 2CO$	+173
<i>RI- 5</i>	H <sub>2</sub> gasification	$C + 2H_2 \rightarrow CH_4$	-75
<i>RI- 6</i>	H <sub>2</sub> O gasification	$C + H_2O \rightarrow CO + H_2$	+131
<i>RI- 7</i>	CO oxidization	$CO + 0.5O_2 \rightarrow CO_2$	-283
<i>RI- 8</i>	H <sub>2</sub> oxidization	$H_2 + 0.5O_2 \rightarrow H_2O$	-242
<i>RI- 9</i>	CH <sub>4</sub> reforming	$CH_4 + H_2O \leftrightarrow CO + 3H_2$	+206
<i>RI- 10</i>	Water-gas shift reaction	$CO + H_2O \leftrightarrow CO_2 + H_2$	-41
<i>RI- 11</i>	CH <sub>4</sub> oxidization	$CH_4 + 0.5O_2 \rightarrow CO + 2H_2$	-37.5
<i>RI- 12</i>	Tar thermal cracking	$pC_nH_x \rightarrow qC_mH_y + rH_2$	+ (200-300)
<i>RI- 13</i>	Tar steam reforming	$C_nH_x + nH_2O \rightarrow \left(n + \frac{x}{2}\right)H_2 + nCO$	
<i>RI- 14</i>	Tar dry reforming	$C_nH_x + nCO_2 \rightarrow \frac{x}{2}H_2 + 2nCO$	
<i>RI- 15</i>	Tar carbon formation	$C_nH_x \rightarrow \frac{x}{2}H_2 + nC$	

Two of the most frequently used reactor types for biomass gasification are fixed bed and fluidized bed (FB) reactor with variations within each type (Warnecke, 2000). A third type is the entrained-flow gasifier. The residence time of an entrained flow gasifier is of the order of seconds or tens of seconds, thus the gasifiers must operate at high temperatures to achieve high carbon conversion. According to Higman and Van der Burgt (Higman & Van der Burgt, 2003), entrained-flow gasifier requires a very small biomass particle size of the order of magnitude 100 $\mu$ m or less to promote mass transfer and also high O<sub>2</sub> for maintaining the relatively high operational temperature, which make the process largely unsuitable for most biomass fuels.

The fixed bed gasifier can be classified as updraft, downdraft or cross-flow. A schematic of updraft and downdraft fixed bed gasifier is presented in **Figure 1- 5** (Lettner et al., 2007). The updraft fixed bed (UFB) gasifier can handle biomass fuels with high ash (up to 15 %) and high moisture content (up to 50 %) (Chopra & Jain, 2007). In an UFB gasifier, biomass enters from the top of the gasifier, while the gasifying agent enters from the bottom of the gasifier via a grate. Due to the low temperature (200-300 °C) of the product gas leaving the gasifier, the overall energy efficiency of the process is high but the product gas normally contains high tar content (30-150 g/Nm<sup>3</sup>). The downdraft fixed bed (DFB) gasifier can handle only uniformly sized biomass fuels which contain moisture content and ash content less than 20 % and 5 %, respectively. In a DFB gasifier, biomass enters through the hopper and flows down, gets dried and pyrolyzed before being partially combusted by the gasifying agent entering at the nozzles. Because the product gas leaves the gasifier at temperatures about 900–1000 °C, the overall energy efficiency of the process is low, due to the high heat content carried over by the hot product gas. The product gas from DFB gasifier generally has lower contents of tar-oils (0.015-3.0g/Nm<sup>3</sup>), higher temperature (ca. 700 °C) with more particulate matter than that from an UFB gasifier (Chopra & Jain, 2007; Prabir, 2010).

To sum up, the fixed bed gasifiers are simple and most suitable for small-scale with capacities of less than a 100 kW<sub>th</sub> up to a few MW<sub>th</sub> heat, and power applications combined with the gas cleaning and cooling system normally consisting of filtration through cyclones, wet scrubbers and dry filters (Demirbas, 2002).

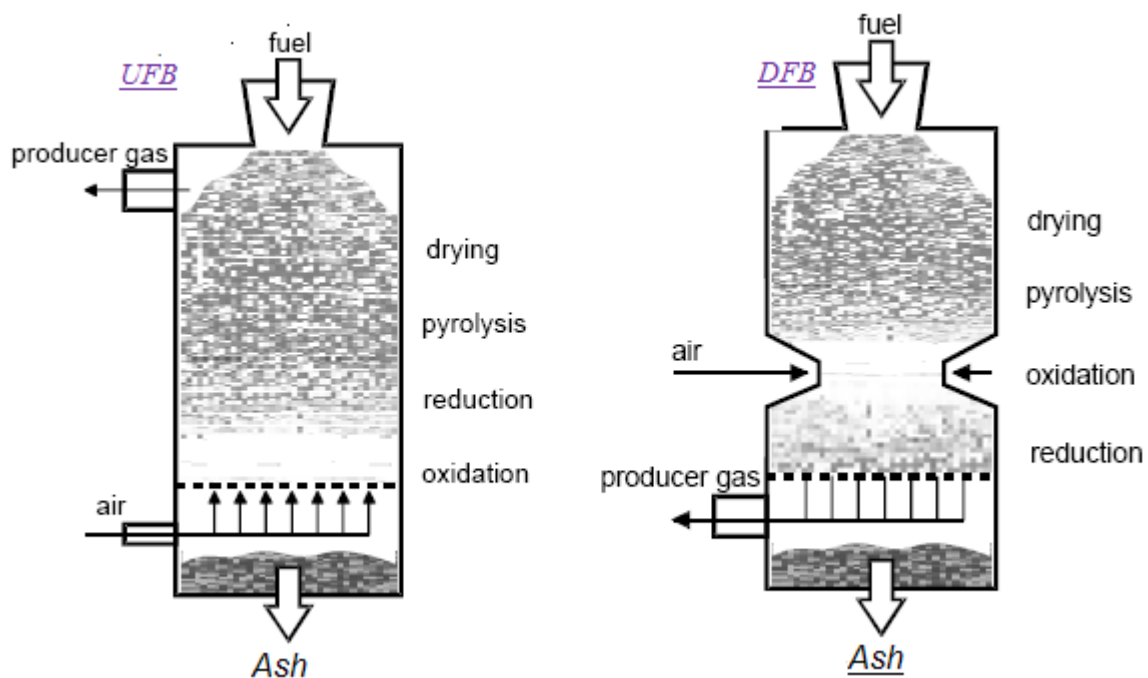


Figure 1- 5 Schematic of updraft and downdraft fixed bed gasifier (Lettner et al., 2007)

Current development activities on large scale biomass gasification have been mainly devoted to FB technologies, since FB gasifiers have better heat and mass transfer between the gas and solid phases, and can also meet the challenges of wide variations in fuel quality with a broad fuel particle-size



distribution. FB gasifiers can be divided into two main types: bubbling fluidized bed (BFB) and circulating fluidized bed (CFB). A schematic of bubbling and circulating fluidized bed gasifier is presented in **Figure 1- 6**. The main difference between them are fluidizing velocity and gas path. The velocity of the upward flowing gasifying agent in a BFB gasifier is normally around 1–3 m/s, while in a CFB gasifier is around 3–10 m/s. Consequently, in the BFB gasifier the expansion of the inert bed regards only the lower part of the reactor, and bed materials and char do not leave the reactor; while in the CFB gasifier the expanded bed occupies the entire reactor and a fraction of sand and char is carried out of the reactor together with the gas stream and further captured and recycled back to the reactor using a cyclone that intercepts the gas stream. FB gasifiers can be operated either at atmospheric pressure or elevated pressure. According to Bridgwater (Bridgwater, 2003), atmospheric CFB gasifiers have been proven very reliable with various biomasses with capacities scale up from a few MW<sub>th</sub> up to 100 MW<sub>th</sub>, even above 100 MW<sub>th</sub>, while commercial applications of atmospheric BFB gasifiers are in the small to medium scale up to about 25 MW<sub>th</sub>. Pressurized FB gasifiers either circulating or bubbling show relatively limited market attractiveness probably due to the more complex operation of the installation and the additional costs related to the construction of pressurized vessels.

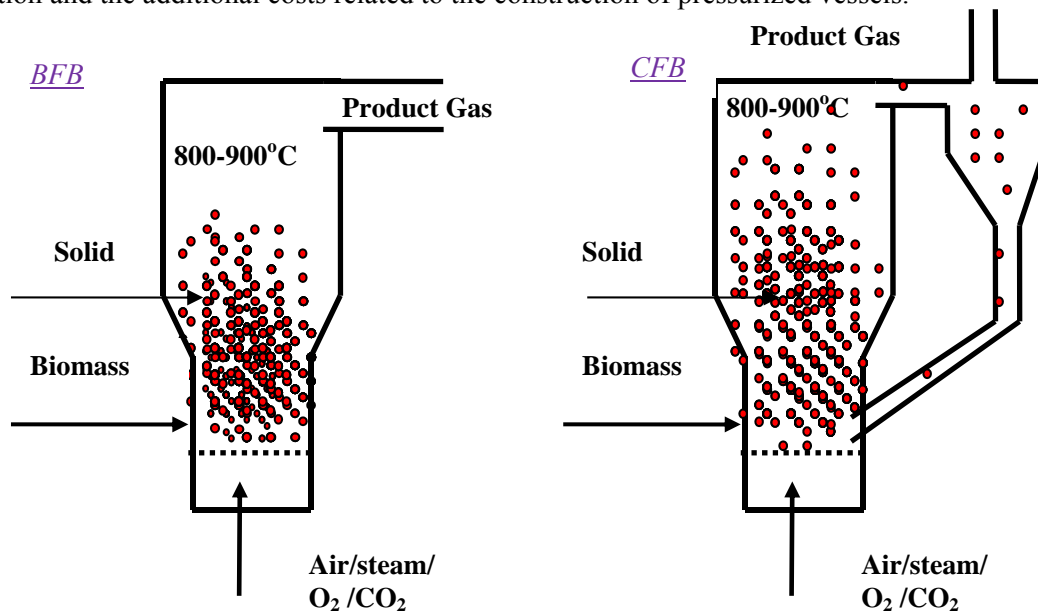


Figure 1- 6 Schematic of bubbling and circulating fluidized bed gasifier

The product gas produced from biomass gasification normally contains the major components CO, H<sub>2</sub>, CO<sub>2</sub>, CH<sub>4</sub> and H<sub>2</sub>O, in addition to organic (e.g., tar) and inorganic (e.g., H<sub>2</sub>S, COS, HCl, NH<sub>3</sub>, alkali metals) impurities and particulates. Depending on the gasifying agent and operational conditions used, the quality of product gas can vary significantly. Air is the mostly used gasifying agent currently at demonstration or commercial scale because of its extensive low-cost availability. However, the product gas from FB air-blown biomass gasification normally containing 50 vol.% N<sub>2</sub> has a lower heating value (LHV) of 4-7MJ/Nm<sup>3</sup> and it can be used only for electricity production or heat generation (Narvaez et al., 1996). The dried product gas produced from biomass gasification with O<sub>2</sub> or steam generally has a medium heating value (MHV) of 10–15 MJ/Nm<sup>3</sup> and 13–20 MJ/Nm<sup>3</sup>, respectively (McKendry, 2002c). A schematic of application of product gas produced from biomass gasification is presented in **Figure 1- 7**. In general, MHV product gas is better suited to synthesis of transport fuels and commodity chemicals due to the absence of N<sub>2</sub> which reduces process efficiency and increase costs. However, high N<sub>2</sub> content from air biomass gasification could favor ammonia synthesis. There is no evident benefits difference between LHV and MHV product gas regarding electricity generation. The combination of biomass gasification with fuel cells such as solid oxide fuel cells (SOFCs) is attracting lots of interest as an efficient and environmentally benign method of producing electricity and heat. However, tars in the product gas produced from biomass gasification can deposit carbon on the SOFC anode, having detrimental effects to the life cycle and operational

characteristics of the fuel cell. According to Hofmann et al. (Hofmann et al., 2009), the SOFC had a Nickel gadolinium-doped ceria (Ni-GDC) anode can stand a short-term operation ( $\sim 7$  h) with a high tar load ( $>10$  g/Nm<sup>3</sup>) without having immediate problems. No performance loss was observed and no carbon or other product gas trace constituents contamination of the anodes was found when the SOFC membranes were examined with scanning electron microscopy (SEM) coupled with energy dispersive scattering (EDS) after the tests. Lorente et al. (Lorente et al., 2012) pointed out that model tar compounds (toluene, benzene, naphthalene) may fail to simulate the degradation effects of real tars on SOFC anodes, thus they performed an experimental study on the impact of a real gasification tar on two commercially available anode materials, Ni/YSZ (yttria stabilised zirconia) and NiO/GDC. They found that less degradation of the anode powders by carbon formation occurred when the anodes were exposed to humidified H<sub>2</sub> gas containing the real tar compared with toluene as model tar. Furthermore, product gas can also be biologically converted into bio-based products including organic acids, alcohols and polyesters (Datar et al., 2004).

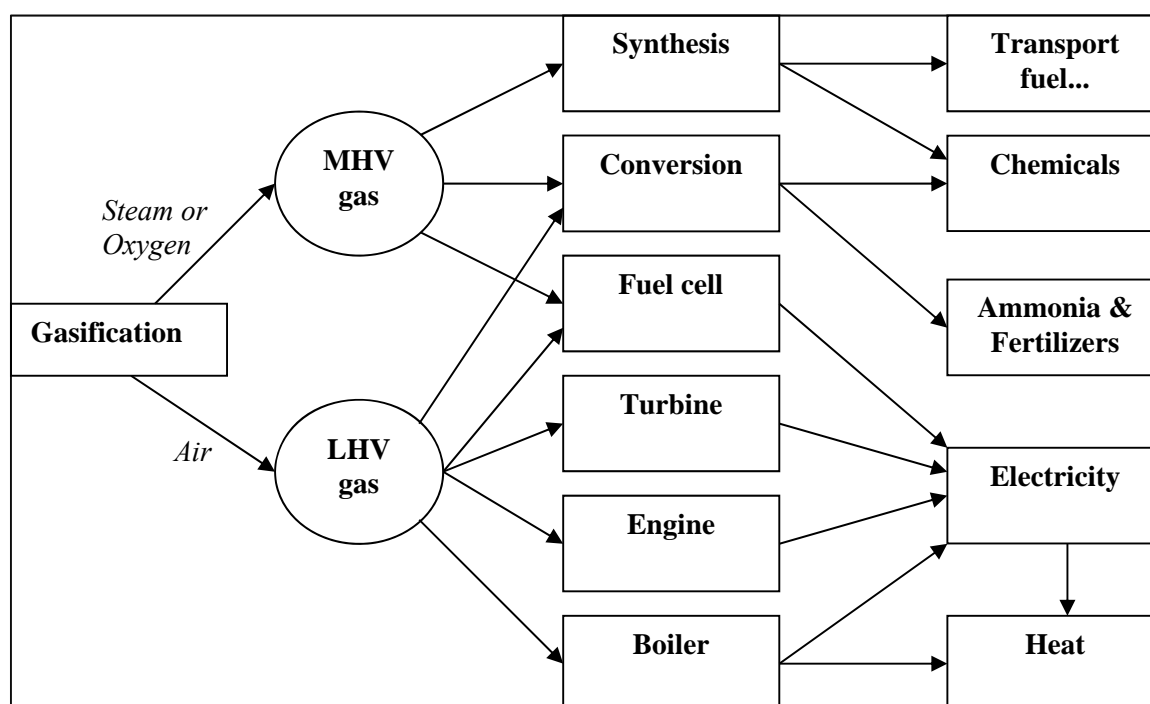


Figure 1- 7 Application of syngas produced from biomass gasification (Bridgwater, 2003)

### 1.2.4 Summary of thermochemical conversion

From the aforementioned information, it can be generally concluded that biomass combustion is the most developed and commercially available process to provide heat and power. Co-combustion biomass with coal in modern coal power plants is currently the most cost-effective biomass use for power generation. Fast and /or catalytic pyrolysis is suitable for producing bio-oil, which can be upgraded or used as transportation fuels in diesel engines and gas turbines as well as the potential to supply a number of valuable chemicals. Biomass gasification has received lots of interest since it offers high overall system efficiency and increases options for combining with various power generation systems. The broad applications of biomass gasification technology strongly depend on syngas quality control technologies. Current development activities on large scale biomass gasification have been mainly devoted to BFB and CFB technologies. CFB gasification is now undergoing rapid commercialization for biomass. Fundamental and pilot studies are, nevertheless, required for scale-up, as well as to fill the gaps in understanding the underlying principles. This dissertation presents these studies and intends to fill the gaps.

### 1.3 Main research questions

From **Figure 1- 7** it can clearly be seen that product gas derived from biomass gasification further has many applications, such as a fuel for internal combustion engines, gas turbines and fuel cells for heat and power generation or as a feedstock for the synthesis of liquid fuels (e.g., Fischer-Tropsch (FT) diesel, methanol) and chemicals. However, contaminants contained in product gas largely limit its applications, since tars can cause equipment fouling due to condensation at lower temperatures, while  $H_2S$  can cause corrosion as well as poisoning of catalysts. Therefore, to avoid detrimental effects on downstream equipment, these compounds need to be removed or reduced to certain level prior to the use of product gas. The main contaminants contained in the product gas and their allowable concentrations for some applications are summarized in **Table 1- 2**. Furthermore, the conversion of char also a large influence on the product gas yield, which can be clearly seen from **Table 1- 1** char involved reactions.

*Table 1- 2 Product gas quality requirements for some applications (Siedlecki, 2011)*

Contaminant	FT synthesis	Methanol synthesis
Particles	0.1 mg/Nm <sup>3</sup>	low
Tar and BTX	Below dew point	low
Halogens (HCl, HF)	<10 ppbv	<10ppbv
Alkaline metals	<10 ppbv	-
N-compounds	<1 ppm, 20 ppb	10 ppmv NH <sub>3</sub> , 0.01 ppmv HCN
S-compounds	<1 ppm, 20 ppb	<1 ppm, 0.1ppmv
Pressure (bar)	20-30	140
Temperature (°C)	200-400	100-200

#### 1.3.1 Problems with sulfur

Sulfur in the biomass feedstock, of which the content is often low, is mainly converted to hydrogen sulfide ( $H_2S$ ), with some amounts of carbonyl sulfide (COS), carbon disulphide ( $CS_2$ ), mercaptans ( $CH_3SH$ ,  $CH_3CH_2SH$ ) and thiophene ( $C_4H_4S$ ) etc. Removing these sulfur species from product gas is important to minimize poisoning of catalysts and corrosion of downstream equipment. Sulfur species can generally be captured in two stages: in-situ (or in-bed) and downstream of the gasifier. Even though many methods are currently available, a robust and completely reliable technology has not yet been developed especially for high temperature cleaning over 600 °C. In order to optimize the gas cleaning system to ensure the cleaned gas satisfying with requirements of different applications, a thorough comparison of different sulfur capture methods by using different sorbents at different stages is required, meanwhile an efficient measuring technique for quantifying sulfur species is necessary to know the sulfur capture capacities of different sorbents. Furthermore, a full understanding of sulfur species distribution during gasification is needed for effectively using feedstock and reducing their sulfur emissions. Nevertheless, probably due to low sulfur content present in most biomass fuels, the fate of sulfur species during the gasification of various biomasses in FB gasifiers as well as an overview of high temperature desulfurization methods is lacking in the literature.

#### 1.3.2 Problems with tar

Tar is one of the most problematic compounds produced from biomass gasification, and its formation is highly dependent on the operational conditions such as reaction temperature, equivalence ratio and gasifying agent used. To avoid various problems associated with tar condensation and formation of tar aerosols, tar reduction is necessary before the final use of the product gas. Tar removal technologies can broadly be divided into two approaches: treatments inside the gasifier (primary methods) and hot gas cleaning after the gasifier (secondary methods). Primary methods are gaining lots of attention as they may eliminate or reduce the need for downstream cleanup. Despite the fact that extensive studies have been published on biomass gasification with air, steam and air steam as gasifying agent, how different operational conditions affect tar formation produced from steam- $O_2$  blown biomass gasification using a CFB gasifier is currently far less available.

Furthermore, quantitative measurement of tar concentration in product gas is important to assess the effectiveness of cleanup and conditioning processes. So far several methods for the sampling and analysis of tars have been developed, such as off-line methods including conventional cold solvent trapping (CST) and solid phase adsorption (SPA), and on-line methods such as the on-line tar analyzer (OTA) and laser induced fluorescence spectroscopy (LIFS). A major disadvantage of off-line methods is their complexity and time delay needed for sample treatment, which does not deliver the direct and fast monitoring of gas quality. To monitor real time tar concentration as well as the performance of the gasifiers, on-line tar sampling and measurement methods are gaining increasing attention. However, the accuracy and reliability of on-line tar measuring techniques have not been fully evaluated.

### ***1.3.3 Problems with char reaction***

Studies of the pyrolysis of biomass fuels and their residual char reaction behavior are important to optimize and model gasification processes. Pyrolysis as the first reactive step largely influences the quality and quantity of the product gas produced further, while char gasification reactions are much slower and thus become the rate-limiting step during biomass gasification (Di Blasi, 2009). Although, under similar operational conditions, char combustion is normally much faster than its gasification, it is still slower than the pyrolysis process. Recently, Di Blasi (Di Blasi, 2009) has published an extensive literature review towards combustion and gasification rates of lignocellulosic chars. From this review paper, it can clearly be seen that there is a significant variation among kinetic parameters reported by different researchers depending on biomass fuel types, reaction conditions and model types used. Therefore, a good understanding of char reaction kinetics is important for the effective modeling and operation of gasification processes.

### ***1.3.4 Main research question***

In view of aforementioned problems, to improve the product gas quality and the gasification efficiency of the process, it is necessary to effectively measure and/or reduce the formation of sulfur and tar during biomass gasification, as well as master char reaction kinetics for effectively modeling. To be in details, the main research question dealt in this work is, during biomass gasification in FB gasifiers, how operational conditions influence sulfur and the formation of tar compounds, associated with how to measure them (i.e., tar) effectively on-line by using different techniques and compare with associated standard techniques, and then how pyrolysis and reaction conditions influence char reactivity as well as how the applied char kinetics influence the predicted product gas distribution by using different models. To solve this main question, this work has concentrated on biomass gasification concerning two typical types of gasifiers, and studied char reactions using a thermogravimetric analyzer (TGA) coupled with a Fourier transform infrared spectrometer (FTIR). The coming section will explain the methodology which has been applied to this work.

## **1.4 Methodology**

This research work includes experimental and modeling two parts. Agrol, willow, and dried distiller's grains with solubles (DDGS) pellets have been chosen for this work, and also designated fuels for the Greensyngas project due to the following reasons (Greensyngas, 2008-2011). Agrol is a commercial solid biofuel as a kind of wood pellets which is made from pure sawdust and shavings from sawmills using 100% virgin timber from sustainably managed plantation forestry. This commercial solid biofuel has been produced by Lantmännen (Sweden) and widely used for heating. Willow is a common woody biomass and widely available in the world, especially in European countries. On the other hand, DDGS is a by-product of the so-called dry-grind process to produce ethanol from wheat. During past years, the rapid growth in the production of ethanol led to a parallel rise in DDGS production. To avoid the adverse effect on ethanol production which could be caused by saturated DDGS market, the potential applications of DDGS need to be explored and therefore its potentiality for gasification to produce a gaseous fuel is investigated in this work.

### **1.4.1 Experimental work**

Agrol, willow and DDGS gasification experiments are carried out on an atmospheric pressure 100kW<sub>th</sub> steam-oxygen blown circulating fluidized bed (CFB) gasifier at the Delft University of Technology (TUD) and a steam blown 30-40 kW<sub>th</sub> pressurized bubbling fluidized bed (PBFB) gasifier, called BabyHPR (Heatpipe Reformer) at the Technical University Munich (TUM), respectively. Effects of different operational conditions (e.g., temperature, steam/biomass ratio, ER, pressure) and bed materials on the formation of main product gas, sulfur and tar have been investigated. Three different tar measuring techniques have been used to quantify tar concentrations: a quasi-continuous TA120-3 on-line tar analyzer (OTA) using a flame ionization detector (FID) which is commercially available (Ratfisch company, Germany) and originally developed by the University of Stuttgart (IVD, Germany), an on-line laser instrument based on induced fluorescence spectroscopy (LIFS) developed by TUM and an off-line Solid Phase Adsorption (SPA) technique developed by the Royal Institute of Technology, Sweden (KTH). A TGA-FTIR system has been used to study the pyrolysis of three fuels and the reaction behavior of their residual chars: CFB-Char obtained after three fuels gasification in the CFB gasifier and TG-derived PYR-Char obtained after three fuels pyrolysis in the TGA.

### **1.4.2 Modeling work**

Thermodynamic modeling of sulfur species partitioning and H<sub>2</sub>S sorption using different sorbents during biomass gasification is performed using Factsage<sup>TM</sup> software package. In order to better understand the temperature and velocity distribution in TGA during char combustion, a computational fluid dynamics (CFD) model using COMSOL Multiphysics<sup>TM</sup> software is developed. This model will be a useful tool for the interpretation of experimental results. By applying experimental operational conditions used during Agrol, willow and DDGS gasification, and char reaction kinetic parameters derived from TG analysis and adapted from the literature, the modeling of the 100kW<sub>th</sub> steam-O<sub>2</sub> blown CFB gasifier with an emphasis on product gas distribution has been performed. The modeling results achieved from different models are compared and validated with the experimental data. These different types of models developed in this work aim at improved prediction of the product gas distribution during biomass gasification under different operational conditions.

## **1.5 Outline of this dissertation**

**Figure 1- 8** illustrates the outline of this dissertation. The dissertation is divided into 10 chapters and organized as follows:

**Chapter 2** presents a broad literature overview which mainly consists of four parts: sulfur formation and capture methods, tar formation and measurement techniques, char reactions and kinetics models, and models of (C)FB biomass gasification.

**Chapter 3** presents experimental setups and measuring techniques used in this research, which includes: the main characteristics of the CFB gasifier and the PBFB gasifier, different instruments for measuring the product gas, sulfur and tar compounds, and for char characterization analysis, and experimental procedure for the pyrolysis of three fuels, char gasification and combustion.

**Chapter 4** presents thermodynamic equilibrium simulation results about the partitioning of the various sulfur compounds during the gasification of different biomass fuels under different operational conditions and sulfur capture behavior of various sorbent materials using simulated gas composition obtained from typical gasifiers using Factsage<sup>TM</sup> software package version 5.4.1.

**Chapter 5** and **chapter 6** mainly discuss the experimental results obtained from biomass gasification on both gasifiers. **Chapter 5** analyses the effects of operational conditions (e.g., steam to biomass ratio (SBR), oxygen to biomass stoichiometric ratio (ER), gasification temperature, and pressure) and bed materials on the distribution of the main product gas, sulfur and tar formation from Agrol, willow and DDGS gasification. **Chapter 6** compares the results obtained from three tar measuring techniques in three different ways: on-line analysis behavior of the LIFS and OTA methods, individual tar

components quantification of the SPA and LIFS methods and the total tar content analysis using the SPA, LIFS and OTA methods.

**Chapter 7** and **chapter 8** discuss the experimental results concerning the pyrolysis of three fuels, and gasification and combustion of their derived chars. **Chapter 7**, presents the characterization results of CFB-Chars, analyses the pyrolysis behavior of the three fuels, and compares the gasification behavior of CFB-Char and PYR-Char. **Chapter 8** analyses the experimental results regarding the combustion of willow and DDGS CFB-Chars, and pure charcoal under both isothermal and non-isothermal conditions, as well as the modeling results obtained from a 3D TG furnace model which is set up using COMSOL Multiphysics™ software version 4.1.

**Chapter 9** performs the modeling of the 100kW<sub>th</sub> steam-O<sub>2</sub> blown CFB gasifier with an emphasis on the product gas distribution and equilibrium analysis of water-gas shift (WGS) reaction and methane steam reforming (MSR) reaction. The modeling results achieved from different model approaches is compared and validated with the experimental data. Finally, **chapter 10** concludes the main experimental and modeling results and also provides some recommendations for further research.

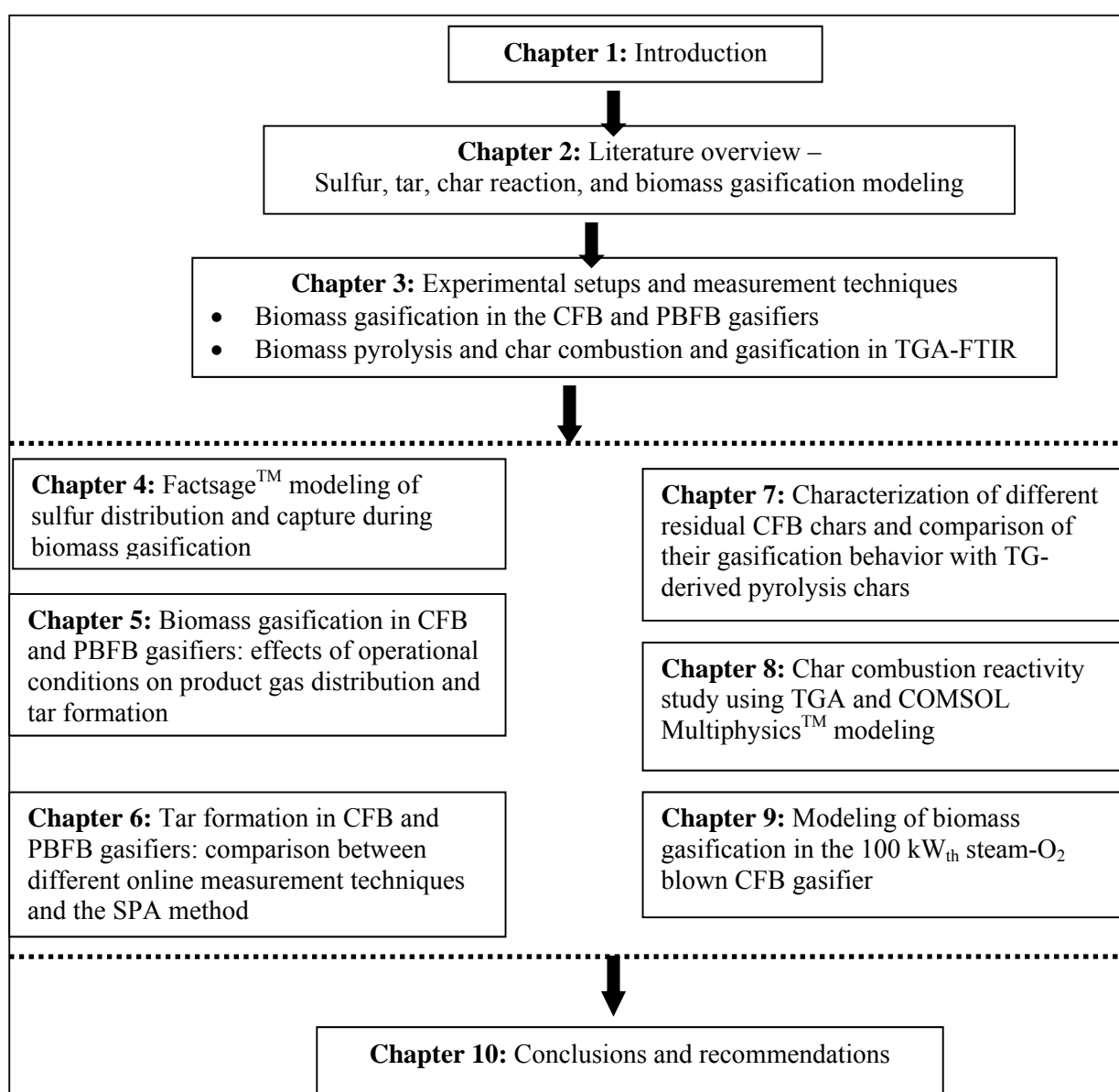


Figure 1- 8 Schematic of the outline of this thesis

## 2 Literature overview — sulfur, tar, char reaction and (C)FB models

---

*As aforementioned in chapter 1, the product gas produced from biomass gasification can be further used to synthesize chemicals and liquid fuels. Gasification technology has been successfully demonstrated at large scale and several demonstration projects are under implementation. Although significant progress has been achieved, contaminants contained in product gas such as organic components (e.g., tar), inorganic components (e.g.,  $H_2S$ ) and particles largely limit the applications of product gas produced from biomass gasification. The efficient removal and reduction of these components still presents the main technical barrier to be overcome.*

*This chapter presents a literature overview which mainly consists of four parts: sulfur formation and capture methods, tar formation and measurement techniques, char reactions and kinetics models and models of (C)FB biomass gasification. Firstly, special attention is paid to literature concerning in bed and downstream sulfur capture methods. Then, tar formation, primary tar reduction by optimizing of operational conditions and tar measuring techniques during biomass gasification are introduced. Subsequently, a brief literature study regarding char combustion and gasification with an emphasis on char conversion kinetics models is presented. Furthermore, the developed models of (C)FB biomass gasification are discussed. Finally, refined research requirements for this research work based on the literature overview are determined.*

**Meng, X., De Jong, W., Pal, R., Verkooijen, A.H.M.** 2010. In bed and downstream hot gas desulfurization during solid fuel gasification: A review. *Fuel Processing Technology*, 91(8), 964-981.

**Meng, X., De Jong, W.** 2009. A report on tar analysis and possibility for improvement - the State of the art Literature, Greensyngas Project, Deliverable report 4.4, 22<sup>nd</sup> October, TU Delft, the Netherlands

## 2.1 Sulfur formation and capture

### 2.1.1 Sulfur formation

The main sulfur species produced from biomass gasification is  $H_2S$  next to small amounts of COS,  $CS_2$ , mercaptans and thiophene (Jazbec et al., 2004). Sulfur species are normally formed via the reactions (**R2- 1**  $\rightarrow$  **R2- 11**, see below) during combustion and gasification (Zevenhoven & Kilpinen, 2001). These reactions also affect the major product gas distribution to certain extent. Removing these sulfur species from the product gas is required to minimize poisoning of catalysts, corrosion of downstream equipment and to meet various emission requirements (Leibold et al., 2008; Ma et al., 2008; Okabe et al., 2009). The tolerable level of sulfur for certain important applications is shown in **Table 2- 1**. From **Table 2- 1**, it can be seen that different allowable sulfur concentrations for various syngas applications are reported by different researchers.

No	Name	Reaction
R2- 1	Fuel devolatilization	$Fuel - S + heat \rightarrow H_2S + COS + \dots + Char - S$
R2- 2		$Char - S + CO_2 \rightarrow COS + \dots$
R2- 3	Char oxidation	$Char - S + H_2O \rightarrow H_2S + \dots$
R2- 4		$Char - S + O_2 \rightarrow SO_2 + \dots$
R2- 5		$H_2S + 1.5O_2 \rightarrow SO_2 + H_2O$
R2- 6		$CO_2 + H_2S \rightleftharpoons COS + H_2O$
R2- 7	Gas phase reactions	$H_2S + CO \rightleftharpoons H_2 + COS$
R2- 8		$COS + H_2S \rightleftharpoons CS_2 + H_2O$
R2- 9		$CS_2 \rightleftharpoons C + \frac{2}{x}S_x$
R2- 10	S species oxidation	$SO_2 + 0.5O_2 \rightleftharpoons SO_3$
R2- 11		$H_2O + SO_3 \rightleftharpoons H_2SO_4$

Table 2- 1 Allowable sulfur concentrations for various syngas applications (Meng et al., 2010b)

No.	Application	Allowable sulfur levels (ppmv)
1	Ammonia production	<0.1
2	Methanol synthesis	<0.5 <0.1 < 1 0.1-15
3	Solid oxide fuel cell	<1 <9 < 60 ppb
	Fuel cell	
	Phosphoric acid fuel cell	<50 <20 <sup>a</sup> +30 <sup>b</sup>
	Molten carbonate fuel cell	< 0.5
4	Fischer-Tropsch process	<1 ppmv <60 ppb
5	Gas turbines	<100 < 750 < 20 <sup>c</sup>

Remark: a: for  $H_2S$  in the fuel;  
b: for COS in the fuel;  
c: for selective catalytic reduction



### 2.1.2 In bed sulfur capture

Hot gas desulfurization (HGD) for cleaning of product gas is gaining more attention since it can improve the overall system thermal efficiency by eliminating fuel gas cooling and associated heat exchangers. Generally, sulfur can be captured either in-situ (or in-bed) or downstream of the gasifier (see **Figure 2- 1**).

In bed desulfurization has been achieved with calcium based sorbents which are naturally available such as limestone or dolomite. Some commercially available sorbents such as calcium acetate and calcium magnesium acetate are reported to be more efficient than limestone and dolomite (Adanez et al., 1999; Garcia-Labiano et al., 1999). The decomposition and sulfidation reactions of calcium based sorbents are shown below (**R2- 12**→**R2- 17**). The product CaS is a relatively unstable product and can react with O<sub>2</sub> in oxygen rich reactor parts via an unwanted side reaction (**R2- 18**) to form CaSO<sub>4</sub>, which forms a tight layer on the surface of the sorbent thereby reducing the extent of reaction. In bed sulfur capture by using calcium based sorbents has been studied by different researchers.

No	Name	Reaction
R2- 12	Direct sulfidation	$\text{CaCO}_3 + \text{H}_2\text{S} \rightarrow \text{CaS} + \text{CO}_2 + \text{H}_2\text{O}$
R2- 13		$\text{CaCO}_3 \cdot \text{MgO} + \text{H}_2\text{S} \rightarrow \text{CaS} \cdot \text{MgO} + \text{CO}_2 + \text{H}_2\text{O}$
R2- 14	Calcination	$\text{CaCO}_3 \rightarrow \text{CaO} + \text{CO}_2$
R2- 15		$\text{CaCO}_3 \cdot \text{MgO} \rightarrow \text{CaO} \cdot \text{MgO} + \text{CO}_2$
R2- 16	Sulfidation of calcined sorbents	$\text{CaO} + \text{H}_2\text{S} \rightarrow \text{CaS} + \text{H}_2\text{O}$
R2- 17		$\text{CaO} \cdot \text{MgO} + \text{H}_2\text{S} \rightarrow \text{CaS} \cdot \text{MgO} + \text{H}_2\text{O}$
R2- 18	Side reaction	$\text{CaS} + 2\text{O}_2 \rightarrow \text{CaSO}_4$

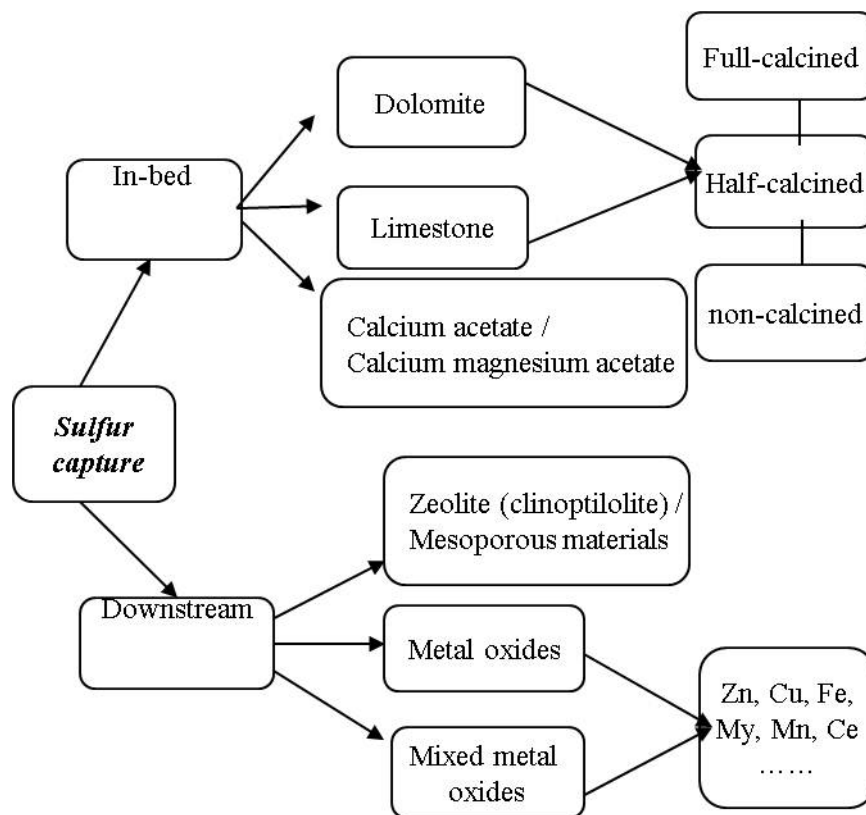


Figure 2- 1 In bed and downstream sulfur capture sorbents

### 2.1.2.1 Limestone and dolomite

Squires et al. (Ruth et al., 1972; Squires et al., 1971) performed pioneering studies concerning sulfur capture using dolomite and limestone. Squires et al. (Squires et al., 1971) proposed that half-calcined dolomite can be used as sulfur capture agent for fuel gas cleaning at high pressure and temperature. Based on the thermodynamic equilibrium for reaction **R2- 12**, the authors concluded that the optimum sulfur sorption temperature would be above about 750 °C. Borgwardt and Roache (Borgwardt & Roache, 1984) studied the reaction of limestone between H<sub>2</sub>S and elemental sulfur in the temperature range of 570 to 850 °C. The authors found that the reaction between H<sub>2</sub>S and limestone was inhibited by H<sub>2</sub> and HCl which reacted with limestone to form CaCl<sub>2</sub>. Limestone also reacted with elemental sulfur, but the activation energy and reaction rate were much lower than those of the H<sub>2</sub>S reaction.

In order to obtain the sulfidation reaction rate related to the gasification process with in situ sulfur removal, Abbasian et al. (Abbasian et al., 1990) studied the activity of limestone and dolomite for in bed desulfurization in a FB gasifier. The authors found that sulfur capture appeared to be independent of temperature within the gasification temperature range of 925 to 1040 °C, and sulfur capture can be effectively performed by using both limestone and dolomite without a significant influence on the conversion efficiency, although dolomite captures sulfur almost twice as rapidly as limestone due to their difference in porosity. Yrjas et al. (Yrjas et al., 1996) studied the sulfur capture abilities of different calcium based sorbents at elevated pressure (2MPa). The authors found that partially calcined dolomites had a significantly higher H<sub>2</sub>S absorption capacity than the uncalcined limestone. The difference was caused by the higher porosity of half-calcined dolomite due to calcination of MgCO<sub>3</sub>, which makes the effect of CaS sintering less pronounced. The authors concluded that if the conditions in the gasifier cause Ca-based sulfur sorbent to remain in its uncalcined form, dolomite should be used as a desulfurization agent, but limestone and dolomite in calcined form both were efficient sulfur sorbents. Fenouilt and Lynn (Fenouil & Lynn, 1995) also reported that calcination temperature of dolomite and limestone has a significant influence on their sulfur capture capacities. At temperatures below calcination temperatures, dolomite and dolomitic limestone were not such effective sorbents for H<sub>2</sub>S sorption.

### 2.1.2.2 Other calcium based sorbents

Besides dolomite and limestone, some commercially available sorbents such as calcium acetate (CA) and calcium magnesium acetate (CMA) prove to be more efficient in HGD. Garcia-Labiano et al. (Garcia-Labiano et al., 1999) studied desulfurization capacities of 12 calcium based materials which were either naturally or commercially available or modified by adding certain additives. They found that CA and CMA had the highest sulfur capture capacity of 90% and 59%, respectively, followed by dolomite, commercial calcium hydroxide and Alborg limestone with a sulfur capture capacity around 50%. Similar H<sub>2</sub>S removal capacities of CA and CMA were also reported by the same authors along with Adanez et al. (Adanez et al., 1999) in their previous work. Yang and Shen (Yang & Shen, 1979) studied the utilization of calcium silicates and the silica supported lime as regenerative sorbents for desulfurization of hot combustion gases. Except for  $\gamma$ -Ca<sub>2</sub>SiO<sub>4</sub> and Ca<sub>3</sub>SiO<sub>5</sub>, all the calcium silicates and the silica supported calcium oxide are equally or more reactive than pure CaO and the regeneration rates of these sorbents are substantially higher than that of CaO. There was no tendency of reduction of the reactivity after eight cycles of sorption and regeneration.

### 2.1.2.3 Summary of in bed sulfur capture

In general, calcium-based sorbents can remove sulfur in FB gasifiers which improves the overall efficiency of the process and also simplifies the system by using less downstream equipment. However, limestone suffers from the problem of attrition and incomplete conversion below the calcining temperatures. An increase of Mg to Ca ratio in dolomite causes increased attrition though there is an increased reaction rate and reduced sintering. Some literature also suggests the use of calcium acetate and calcium magnesium acetate as alternatives to limestone and dolomite which resulted in very good sulfur capture capabilities. For calcium based sorbents, the achieved sulfur level at the exit largely depends on the partial pressure of steam and CO<sub>2</sub> and the reaction temperature. Also, the large quantities of spent sorbents produced with limestone and dolomite contain CaS which is not

environmentally stable and can react with water to release  $H_2S$  again thus requires a further stabilization step to oxidize  $CaS$  to environmentally acceptable  $CaSO_4$  material for landfill disposal. So far, only a very limited number of studies considered regenerating spent calcium-based sorbents, largely for economic issues. Therefore, to achieve a  $H_2S$  concentration lower than 100 ppmv and reduction of the environmental problem, regenerable metal oxide sorbents have recently received much attention and broadly used in downstream desulfurization. In the coming sections, sulfidation and regeneration reaction conditions of some regenerable metal oxide sorbents as well as their exhibited problems during desulfurization will be reviewed.

### 2.1.3 Downstream sulfur capture

Downstream HGD is mainly focused on using regenerable single /mixed/ supported metal oxide sorbents or micro-porous structure materials. Zeolites are widely used as adsorbents or as supports for metal based sorbents in order to form a well-structured sorbent. Based on thermodynamic calculations performed by Westmoreland and Harrison (Westmoreland & Harrison, 1976), the metal oxides of Fe, Zn, Mn, Mo, V, Ca, Sr, Ba, Co, W and Cu are feasible for HGD. The general desulfurization and regeneration reactions for  $H_2S$  reacting with a metal oxide is given by reaction equations **R2- 19** to **R2- 22**. From **R2- 21** and **R2- 22** it can be seen that the regeneration reaction equilibrium strongly depends upon the  $O_2$  and  $SO_2$  partial pressure. An unwanted side reaction is the formation of sulfate via **R2- 23** which should be avoided as the formed sulfate is inert with respect to the desulfurization and thus leads to a loss of material activities. General requirements for the metal oxide sorbent are summarized by Bakker et al. (Bakker et al., 2003) as follows:

- High equilibrium constant and fast kinetics for the sulfidation reaction;
- High selectivity towards sulfur capture to minimize side reactions;
- High mechanical stability to minimize mass losses by attrition.
- Good regeneration capabilities at optimal cost.

Among all available sorbent materials, zinc, copper, manganese and iron oxide based sorbents are the most extensively studied, and they are discussed in the sections below.

No	Name	Reaction
<i>R2- 19</i>	Sulfidation	$Me_xO_y(s) + xH_2S(g) + (y - x) H_2(g) \rightarrow x MeS(s) + yH_2O(g)$
<i>R2- 20</i>		$MeS(s) + H_2O(g) \rightarrow MeO(s) + H_2S(g)$
<i>R2- 21</i>	Regeneration	$(x)MeS(s) + (y/2)SO_2(g) \rightarrow Me_xO_y(s) + (x + y/2)S(g)$
<i>R2- 22</i>		$(x)MeS(s) + (x + y/2) O_2(g) \rightarrow Me_xO_y(s) + xSO_2(g)$
<i>R2- 23</i>		$MeS(s) + 2O_2(g) \rightarrow MeSO_4(s)$

#### 2.1.3.1 ZnO based sorbents

ZnO is known to be among the best metal oxide sorbents as it shows the most favorable sulfidation thermodynamics. An escalation in interest regarding zinc oxide as a sorbent began in 1977 with a study by Westmoreland and Harrison (Westmoreland & Harrison, 1976). ZnO has been widely used for more than 30 years as an  $H_2S$  removal sorbent for natural gas. Although ZnO has a high  $H_2S$  sorption capacity, the reduction of ZnO in the highly reducing atmosphere followed by vaporization of elemental Zn can be a severe problem when the temperature is higher than 600 °C. Consequently, extensive research work has been carried out in this field which mainly focused on two types of ZnO based materials: zinc ferrite ( $ZnFe_2O_4$ , ZF) and zinc titanate (ZT).

Early testing of ZF as desulfurization sorbent was mainly conducted in a fixed bed reactor system using cylindrical extrudates. General Electric Environmental Services Inc. later developed a moving-bed, high-temperature desulfurization system for integrated gasification combined cycle (IGCC) power systems where ZF was used as desulfurization sorbent (Ayala et al., 1992). Gupta et al. (Gupta et al., 1992) developed several ZF sorbents for FB application using different techniques such as spray drying, impregnation, crushing and screening. However, the applications of ZF sorbents were limited

to a maximum temperature of about 550 °C, above which excessive sorbent weakening was observed possibly due to chemical transformations evidenced as excessive reduction of  $\text{Fe}_2\text{O}_3$  and  $\text{ZnO}$ , followed by some evaporation of metallic Zn. In order to improve ZF sorbents performance, Ikenaga et al. (Ikenaga et al., 2004) prepared ZF in the presence of carbon materials such as activated carbon (AC), activated carbon fiber (ACF), and Yallourn coal (YL). Liang et al. (Liang et al., 2007) found that the prepared ZF sorbent by adding kaolinite showed high reactivity in three-cycles of sulfidation regeneration tests. Zhang et al. (Zhang et al., 2007) reported that ZF sorbent prepared using a sol-gel (SG) auto-combustion method had a larger specific surface area and higher reactivity compared with those achieved by a solid mixing method.

Although ZF sorbent shows substantial improvements over pure  $\text{ZnO}$ , Zn reduction and regeneration still impose practical problems. Zinc titanate (ZT) compounds have emerged as sorbents with most of the advantages and few of the limitations of ZF (Elseviers & Verelst, 1999; Lew et al., 1992). In order to improve the reactivity, stability and regenerative characteristics of ZT sorbent, Poston (Poston, 1996) produced a Lanthanum-doped ZT sorbent using  $\text{ZnO}$  and  $\text{TiO}_2$  with a molar ratio of 2 to 1.5 wt.%  $\text{La}_2\text{O}_3$  and 3.5 wt.% bentonite as a binder. The author found that the addition of the  $\text{La}_2\text{O}_3$  reduces/eliminates sorbent spalling without negatively impacting performance. Sasaoka et al. (Sasaoka et al., 1999) found that the addition of 5 or 10 mol.%  $\text{ZrO}_2$  to 50 mol.%  $\text{ZnO}$ –50 mol.%  $\text{TiO}_2$  greatly improved the reactivity for  $\text{H}_2\text{S}$  removal and the regenerability of the sorbent. Jun et al. (Jun et al., 2001) found that the modified zinc titanates (ZTC-25) sorbents prepared by the physical mixing of the ZT sorbent with 25 wt.% of  $\text{Co}_3\text{O}_4$  showed an excellent sulfur capture capacity within the temperature range of 480 to 650 °C. Bu et al. (Bu et al., 2008) also prepared two new ZT sorbent using a dry-mixing method by adding some amounts of Cu and Mn metal oxide for HGD.

### **2.1.3.2 CuO based sorbents**

In parallel with the development of  $\text{ZnO}$  based sorbents,  $\text{CuO}$  based sorbents have been predominantly studied as well, due to their favorable thermodynamics and high sorption rate under reducing and oxidizing atmospheres.  $\text{CuO}$  based sorbents can reduce  $\text{H}_2\text{S}$  from several thousand ppmv to sub-ppmv levels. However,  $\text{CuO}$  in uncombined form is readily reduced to metallic copper by the  $\text{H}_2$  and  $\text{CO}$  contained in fuel gases, which lowers the desulfurization efficiency and leads to impractical operation (e.g., sintering). To improve the performance of  $\text{CuO}$  based sorbents, mixed and dispersed copper oxides sorbent have been extensively researched. An early systematical study of dispersed Cu-containing sorbents has been carried out by Kyotani et al. (Kyotani et al., 1989). In order to retain copper at the +2 or +1 oxidation state, Li and Flytzani-Stephanopoulos (Li & Flytzani-Stephanopoulos, 1997) studied the desulfurization and regeneration abilities of Cu-Cr-O and Cu-Ce-O oxide sorbents. The authors concluded that the desulfurization efficiency and reactivity as well as the regenerability of the sorbent can all be optimized for a real reactor system by suitable sorbent composition and structure selection. Gasper-Galvin et al. (Gasper-Galvin et al., 1998) performed a comprehensive study of zeolite-supported mixed-metal oxide sorbents consisting of various combinations of Cu, Mn and Mo. For the stabilization of  $\text{CuO}$  against complete reduction to elemental Cu, Abbasian and Slimane (Abbasian & Slimane, 1998) demonstrated a sorbent designated as “CuCr-29” which was prepared by using  $\text{Cr}_2\text{O}_3$  as the support for  $\text{Cu}_2\text{O}$  along with binder materials. Karvan and Atakul (Karvan & Atakul, 2008) prepared two types of  $\text{CuO}$ /mesoporous SBA-15 sorbents by the wet impregnation method.

### **2.1.3.3 MnO based sorbents**

$\text{MnO}$  based sorbents have also attracted considerable attention of a number of researchers, especially in the past decade. The earlier kinetic study of Westmoreland and Harrison (Westmoreland & Harrison, 1976) showed that the reactivity of  $\text{MnO}$  was higher than those of  $\text{CaO}$ ,  $\text{ZnO}$ , and  $\text{V}_2\text{O}_3$  in  $\text{H}_2\text{S}$  removal.  $\text{MnO}$  was found to be stable from temperatures in excess of 1000 °C down to 400 °C, thereby allowing greater flexibility in sulfidation and regeneration temperatures without loss of sorbent. In the 1990s,  $\text{MnO}$  based sorbents have also been extensively researched by Ben-Slimane and Hepworth (Ben-Slimane & Hepworth, 1994a; Ben-Slimane & Hepworth, 1994b; Ben-Slimane & Hepworth, 1995). In order to improve the pore structure of  $\text{MnO}$  based sorbents, Atakul et al. (Atakul

et al., 1995) developed a  $\gamma$ - $\text{Al}_2\text{O}_3$  supported MnO sorbent which was prepared by wet impregnation and contained 8 wt.% MnO. To prevent sulfate formation during regeneration, mixtures of manganese and copper oxides have been proposed as regenerable sorbents. The porous Mn-Cu and Mn-Cu-V mixed-oxide sorbents were prepared by Karayilan et al. (Karayilan et al., 2005) using a wet co-impregnation method in the presence of  $\text{H}_2$ . García et al. (Garcia et al., 2000) also prepared Mn and Cu oxides prepared by calcination at 950 °C of  $\text{MnO}_2$  and CuO powders in different mole ratios.

#### **2.1.3.4 FeO based sorbents**

Among transition metal compounds, the oxides of Zn, Cu and Mn have been investigated most extensively. Compared to the above materials, iron oxide desulfurization potential is somewhat lower. The earliest research, which started in the 1950s, by using iron oxide at high temperatures for removal of  $\text{H}_2\text{S}$  from a crude coke oven gas, was performed by the Appleby-Frodingham Steel Company (Reeve, 1958). In order to develop low cost and highly reactive and durable FeO based sorbents, Sasaoka et al. (Sasaoka et al., 1993) prepared eight kinds iron sorbents from iron ore powder and blast furnace dust using  $\text{SiO}_2$ ,  $\text{TiO}_2$ , and  $\text{Al}_2\text{O}_3$  as binders. Fan and Li (Fan & Li, 2005) prepared iron oxide sorbents from red mud using mixed clay as the binder. Shirai et al. (Shirai et al., 1999) developed composite sorbents by mixing iron oxide and ZF particles with ultra-fine silica particles. Wang et al. (Wang et al., 2008b) synthesized a mesoporous material SBA-15 supported  $\text{Fe}_2\text{O}_3$  sorbent using a post-synthesis method. Recently, Xie et al. (Xie et al., 2010) studied simultaneous removal of  $\text{H}_2\text{S}$  and COS within the temperature range of 400 to 650 °C at 1 bar by using iron-based sorbents, which were prepared by a physical mixing method using iron oxide and cerium oxide with fine coal ash as the support.

#### **2.1.3.5 Summary of downstream sulfur capture**

From aforementioned literature overview, it appears that ZnO sorbent exhibits the most favorable thermodynamic property of  $\text{H}_2\text{S}$  capture. However, due to Zn vaporization and migration problems at high temperature, using pure ZnO as sulfur sorbent is limited to a temperature of around 600 °C. CuO can reduce  $\text{H}_2\text{S}$  from several thousand ppmv to sub-ppmv levels. However, CuO in uncombined form is easily reduced to metallic Cu by the  $\text{H}_2$  and CO contained in fuel gases, which lowers the desulfurization efficiency. Manganese oxides combine the advantages of high sulfur capacity and high reactivity in the moderate temperature range, without any requirement for sorbent preconditioning or activation. However, manganese oxide sorbents are easily prone to sulfate formation and need to be regenerated at high temperature. Iron oxide desulfurization potential is somewhat lower, mainly because of severe sorbent cracking problem due to excessive reduction and iron carbide formation at a temperature higher than 550 °C. However, iron sulfide formed during the sulfidation or absorption step can be most conveniently regenerated by oxidizing it with air or  $\text{N}_2$ -diluted air at considerably lower temperatures than other metal oxides. In order to overcome these problems, additives, such as Ti, Al, Si, Zr, Co, Ni, and Fe, and promoters (Co, Ni, and Fe) are added to different metal oxide based sorbents to improve their sulfur capture capacity during multiple cycles and their regeneration properties. Also, mesoporous materials and zeolites, which mainly consist of  $\text{Al}_2\text{O}_3$ ,  $\text{TiO}_2$ ,  $\text{Fe}_2\text{O}_3$  and  $\text{SiO}_2$ , are used as the supporters to create and maintain the desirable sorbent structure. Regarding sulfur capture methods, a more detailed literature review is available in one of published papers within this research (Meng et al., 2010b). In this published paper, the major advantages and disadvantage of various sulfur sorbents were compared, and the sulfidation and regeneration conditions applied for desulfurization were analyzed as well.

## **2.2 Tar reduction and measuring techniques**

### **2.2.1 Tar definition and formation**

“Tar” represents a lump term comprising thousands of single substances. Due to its complexity, different definitions have been given by various research groups working on biomass gasification. In Milne’s review report, tar is defined as “the organics produced under thermal or partial-oxidation regimes of any organic material and generally assumed to be largely aromatic” (Evans & Milne, 1998;

Milne et al., 1998). A consensus on the definition of tar was agreed by the European Committee for Standardization (CEN) and “tar” is defined as “all organic compounds present in the gasification product gas with molecular weight higher than benzene” (Li & Suzuki, 2009; Tar, 2007).

During biomass gasification, tar is generally formed in a series of complex reactions and its formation is highly dependent on process conditions. The tar formation scheme proposed by Elliott and summarized by Milne (Milne et al., 1998) is presented in **Figure 2- 2**, which shows the transition of tar as a function of process temperature from primary products to phenolic compounds to aromatic hydrocarbons. Evans and Milne (Evans & Milne, 1998) suggested that tar can be classified into four product classes which are identified as a result of gas-phase thermal cracking reactions:

- primary products which are characterized by cellulose-derived, hemicellulose-derived and lignin-derived products;
- secondary products which are characterized by phenolics and olefins;
- alkyl tertiary products which are mainly methyl derivatives of aromatic compounds;
- and condensed tertiary products which are PAH series without substituent.

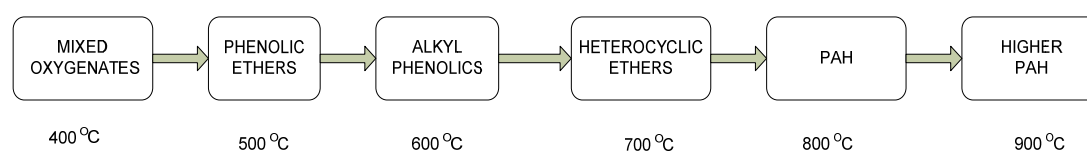


*Figure 2- 2 One pathway for tar formation (Milne et al., 1998)*

Another classification based on the number of aromatic rings and physical properties of tar is shown in **Table 2- 2** (El-Rub & Kamel, 2008; Li & Suzuki, 2009).

*Table 2- 2 Tar classification system(El-Rub & Kamel, 2008)*

Class	Type	Examples
1	GC undetectable tars.	Biomass fragments, heaviest tars (pitch).
2	Heterocyclic compounds. These are components that exhibit high water solubility	Phenol, cresol, quinoline, pyridine.
3	Aromatic components. Light hydrocarbons, which are important from the point view of tar reaction pathways, but not in particular towards condensation and solubility.	Toluene, xylems, ethyl benzene (excluding benzene.)
4	Light poly-aromatic hydrocarbons (2-3) rings PAHs). These components condense at relatively high concentrations and intermediate temperatures.	Naphthalene, indene, biphenyl, anthracene.
5	Heavy poly-aromatic hydrocarbons (>4-rings PAHs). These components condense at relatively high temperature at low concentrations.	Fluoranthene, pyrene, chrysene.
6	GC detectable not identified compounds.	Unknown

Generally the composition, properties and quantity of tar in product gas vary remarkably depending upon the biomass feedstock, gasifier type and gasification conditions. Among them, the type of gasifier is one of the most important parameters affecting the tar content. The average and range of tar content in different gasifiers are summarized in **Table 2- 3**. As seen in **Table 2- 3**, downdraft fixed bed (DFB) was the best effective method in suppressing the formation of tar during biomass gasification. Furthermore, some extreme low tar concentration was also reported by some research institutes. For example, Technical University of Denmark developed a two-stage gasifier in 1980–1990; the tar content in the product gases was even below 25 mg/Nm<sup>3</sup>. The reason for that is in this two-stage gasifier, the pyrolysis and gasification processes were separated into two different zones, which resulted in the volatiles from the pyrolysis zone were partially oxidized between these two

zones. Hence, most of the tar was able to be decomposed into gases. Asian Institute of Technology (AIT), Thailand also developed a two-stage wood gasification process, and the product gas produced by biomass gasification using this gasifier only contained about 19–34 mg/Nm<sup>3</sup> tar (Han & Kim, 2008).

For different end-use applications the maximum allowable tar content is different. For instance, Boerrigter et al. (Boerrigter et al., 2004) reported that for Fischer–Tropsch (FT) diesel synthesis the naphthalene concentration in product gas should be less than 2 ppmv to avoid condensation during the compression step before catalytic conversion. Bui et al. (Bui et al., 1994) mentioned that the preferable tar and dust loads in gases for engines must be lower than 10 mg/Nm<sup>3</sup>. The allowable global tar concentrations for some applications are summarized in **Table 1- 2**. Therefore, suitable options to reduce tar need to be chosen based on the required quality of the product gas for different applications.

Table 2- 3 Typical tar concentration in the product gas in different gasifiers (Han & Kim, 2008)

	Fixed bed		Fluidized bed	
	Updraft	Downdraft	Bubbling	Circulating
Mean tar content (g/Nm <sup>3</sup> )	50	0.5	12	8
Mean tar content (g/Nm <sup>3</sup> )*	50	1	10	
The range of tar(g/Nm <sup>3</sup> )	10-150	0.01-6	1-23	1-30

Remark: \* from Milne et al. (Milne et al., 1998)

## 2.2.2 Tar reduction

According to Devi et al. (Devi et al., 2003), tar removal technologies can broadly be divided into two approaches: primary methods and secondary methods. The primary options include (a) the proper selection of the operating conditions; (b) the use of a proper bed additive or a catalyst during gasification; and (c) a proper gasifier design. Secondary methods consist of chemical (thermal or catalytic cracking) or physical (mechanical separation or scrubbing) treatment (Campoy et al., 2010). Regarding these two methods, Corella et al. (Corella et al., 1999) made an comparison between them and found no significant difference in their effectiveness concerning tar reduction. Sutton et al. (Sutton et al., 2001) reported that a suitable combination of different primary and secondary treatments is likely to improve gasifier performance and produce a syngas with minimum tar concentration. For both methods, tar decomposition generally mainly occurs due to a series of complex, multiple and simultaneous reactions such as cracking, steam and dry reforming reactions as shown below:

No	Name	Reaction
R2- 24	Tar thermal cracking	$pC_nH_x \rightarrow qC_mH_y + rH_2$
R2- 25	Tar steam reforming	$C_nH_x + nH_2O \rightarrow (n + \frac{x}{2})H_2 + nCO$
R2- 26	Tar dry reforming	$C_nH_x + nCO_2 \rightarrow \frac{x}{2}H_2 + 2nCO$
R2- 27	Tar carbon formation	$C_nH_x \rightarrow \frac{x}{2}H_2 + nC$

Where  $C_nH_x$  represents tar and  $C_mH_y$  represents hydrocarbon with smaller carbon number than  $C_nH_x$ .

Although, secondary methods are reported to be very effective in tar reduction, in some cases they are not economically viable (Devi et al., 2003). Since they are out of the scope of this research, detailed information is available in the excellent reports by Milne et al. (Milne et al., 1998), Neeft et al. (Neeft et al., 1999) and the paper from Han and Kim (Han & Kim, 2008). Primary methods are gaining much attention as they may eliminate or strongly reduce the need for downstream cleanup. Extensive studies have been conducted by different researchers concerning effects of operational conditions (e.g., temperature, steam to biomass mass ratio (SBR), and pressure and residence time) and active materials (e.g., bed material, additive) on tar formation during biomass gasification. A proper selection of

operational conditions can largely reduce the amount of tar produced. In addition to the optimized operational conditions, using catalytically active materials during biomass gasification can also promote char reaction, reduce the tar yield and prevent the solid agglomeration tendencies.

### 2.2.2.1 Effect of temperature

The temperature is one of the most influential factors affecting the overall biomass gasification process. Temperature can influence the amount of tar formed as well as the composition of tar. Kinoshita et al. (Kinoshita et al., 1994) observed that the total number of detectable tar species produced from sawdust gasification decreased with increasing temperature. Lower temperatures favored the formation of more aromatic tar species with diversified substituent groups, while higher temperatures favored the formation of fewer aromatic tar species without substituent groups. Li et al. (Li et al., 2004) reported that the amount of tar obtained from biomass gasification decreased drastically from 15 to 0.54 g/Nm<sup>3</sup> as the average temperature increased from 700 to 820 °C.

van Paasen and Kiel (van Paasen & Kiel, 2004) revealed that tar concentration decreased with temperature varying from 750 to 950 °C, and simultaneously tar compositions shifted from alkyl-substituted poly-aromatic hydrocarbons (PAHs) to non-substituted PAHs, and the effect of gasification temperature on tar concentration is shown in **Figure 2- 3**, from which it can be seen that gasification temperature largely affects the formation and composition of tar. Kurkela et al (Kurkela et al., 1993) and Simell and Leppälahti (Simell & Leppälahti, 1992) studied the effects of operational conditions on the formation of tar produced from different feedstocks ranging from hard coals to wood wastes gasification in a pressurized fluidized bed (PFB) gasifier. They found that the total tar concentration in the PFB product gas seems to depend mainly on the feedstock and on the gasification temperature, which can be clearly seen in **Figure 2- 4** which shows the tar content produced from for wood, peat, and Rhenish brown coal gasification in the PFB gasifier at different freeboard temperatures.

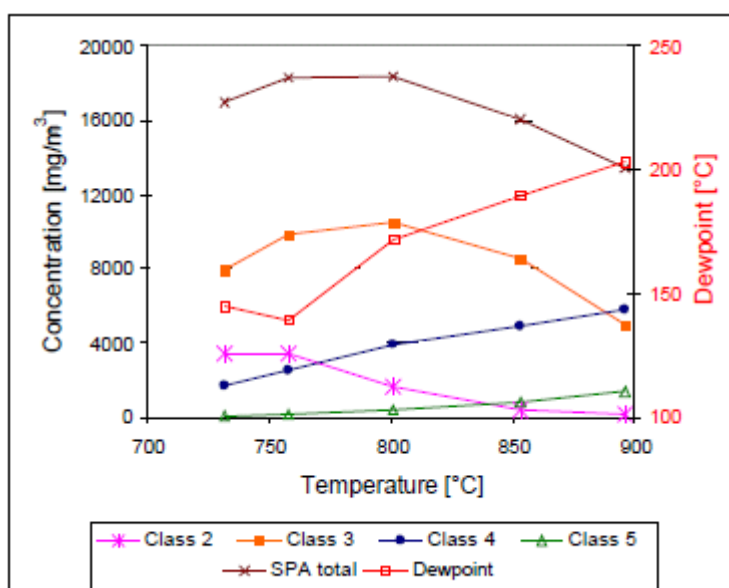


Figure 2- 3 Effect of gasification temperature on tar concentration and dew point (van Paasen & Kiel, 2004)



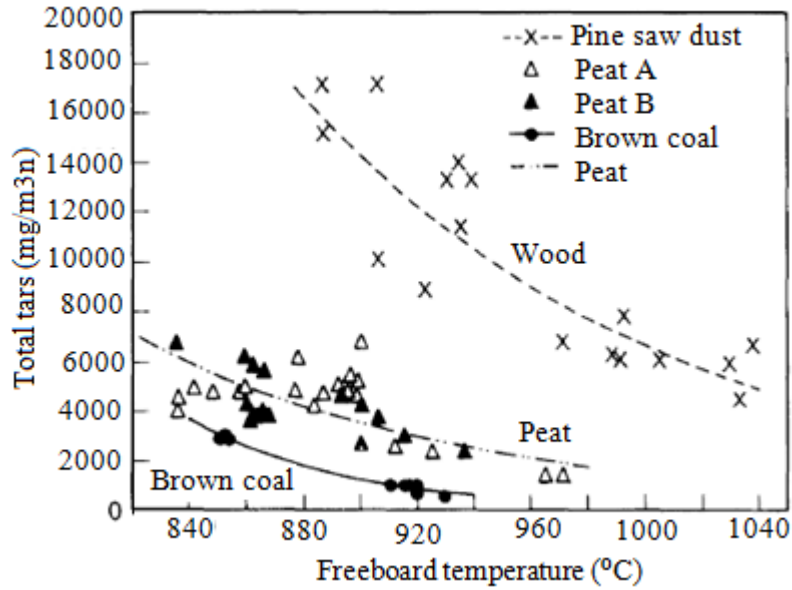


Figure 2- 4 Effect of freeboard temperature on the total amount of tar +benzene in the PFB-gasification with different feedstocks (Kurkela et al., 1993)

#### 2.2.2.2 Effects of ER and SBR

Similar to temperature, an increase in ER also has a beneficial effect on reducing tar formation. Narváez et al. (Narvaez et al., 1996) studied operational conditions on the product gas produced from pine sawdust gasification with air in an atmospheric bubbling fluidized bed (BFB) gasifier. The effect of ER on the tar yield in the product gas is shown in **Figure 2- 5** for two H/C ratios in the gasifier.

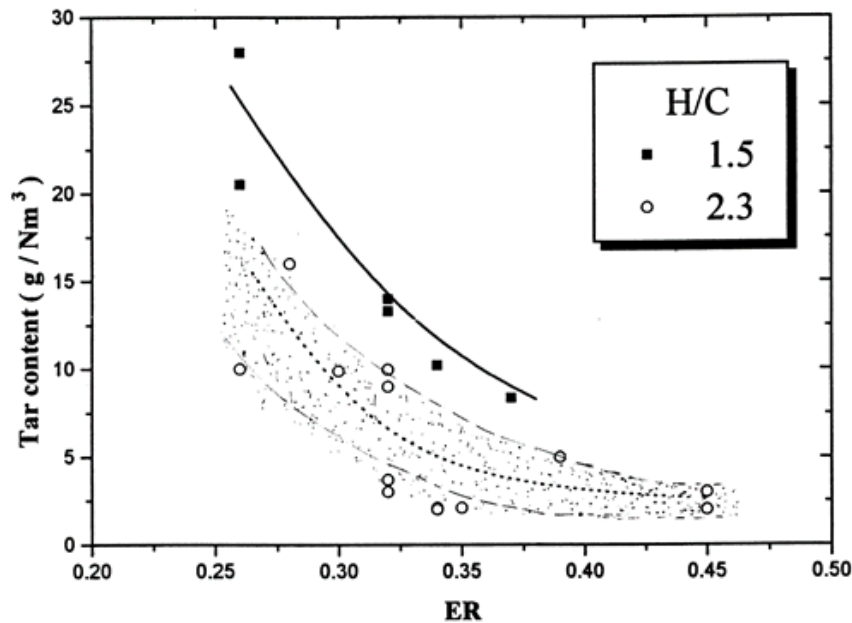


Figure 2- 5 Tar concentration at different ER values at gasification temperature 800°C (Narvaez et al., 1996)

From **Figure 2- 5**, it can be seen that the tar content produced from pine sawdust gasification at a temperature of 800 °C decreased with increasing ER and a tar content of about 2–7 g/Nm<sup>3</sup> was obtained at an ER value of 0.45. Meanwhile, the H/C ratio is also very important and the tar content

decreases with increasing H/C ratios. Lv et al. (Lv et al., 2004) reported that the lower heating value (LHV) of the product gas decreased with an ER increase due to strengthening oxidization reactions of product gases. SBR also influences tar formation due to more / less tar steam reforming reactions. Herguido et al. (Herguido et al., 1992) reported that the amount of tar sharply decreased from 8 wt.% to negligible content with an increasing SBR range from 0.5 to 2.5. Aznar et al. (Aznar et al., 1998) reported that with varying GOR ((steam+oxygen) / biomass mass ratio) from 0.7 to 1.2 more than 85% reduction in the total tar was achieved.

### 2.2.2.3 Effects of pressure and residence time

Besides temperature, ER and SBR, reactor pressure and residence time also influence tar formation. According to Kinoshita et al. (Kinoshita et al., 1994) residence time can significantly influence the composition of tar, but slightly affect tar yield. With increasing residence time, yields 1- and 2-ring compounds (except benzene and naphthalene) decreased whereas that of 3- and 4-ring compounds increased in the total tar fraction. Knight (Knight, 2000) studied operational conditions (e.g., temperature, and pressure) on the tar composition produced from the gasification of different biomass fuels in a PFB gasifier. The effect of system pressure on tar concentration produced from Wisconsin whole tree chips gasification is shown in **Figure 2- 6**.

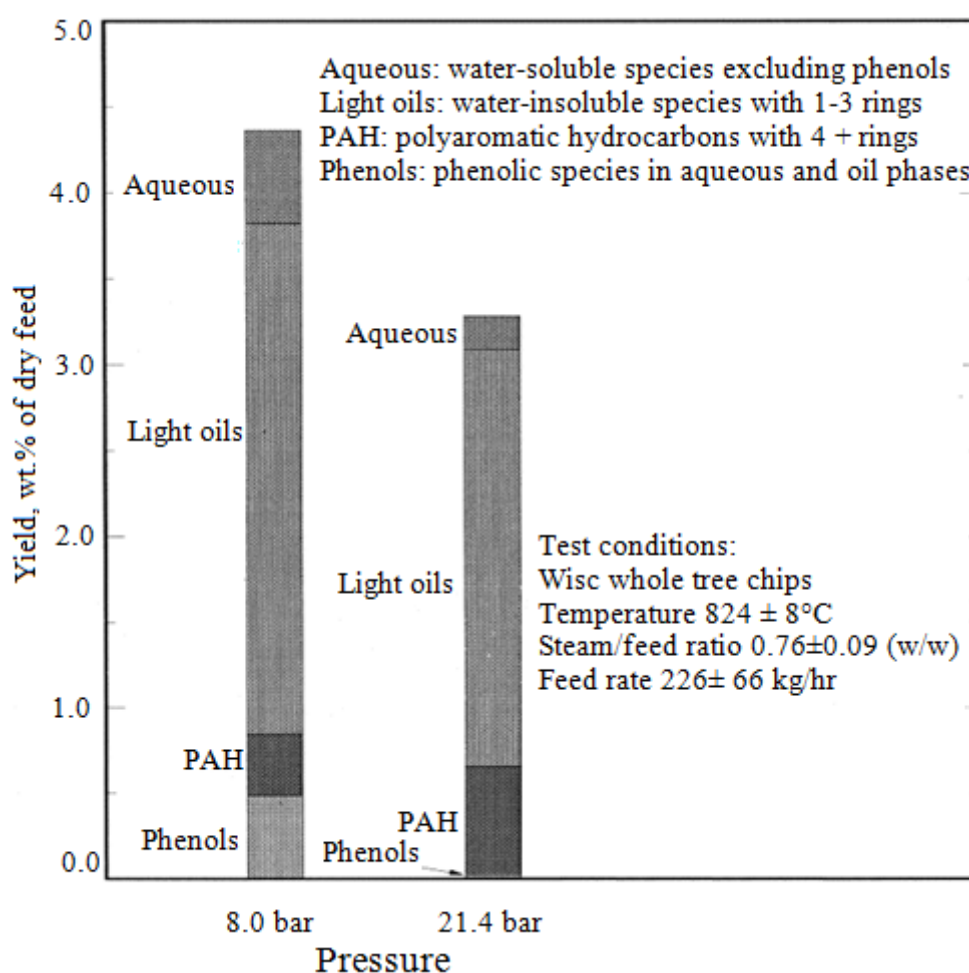


*Figure 2- 6 Tar concentration produced from whole tree chips gasification at different pressures (Knight, 2000)*

From **Figure 2- 6**, it can be clearly seen that the oxygenated components, especially phenols, were largely eliminated when the gasifier was operated at higher pressure; however, the fraction of PAH increased with increasing pressure though the total amount of tar decreased. Padban et al. (Padban et al., 2000) studied tars produced from an air-blown pressurized bubbling fluidized bed (PFBF) 90 kW<sub>th</sub>

pilot biomass gasifier and compared the results from tar measurement from Värnamo integrated gasification combined cycle (IGCC) demonstration plant, which is a 18 MW air-blown, pressurized circulating fluidized bed (PCFB) gasifier. They found that for the same fuel the conversion to tars from Värnamo plant was lower by one magnitude compared to the results obtained from their gasifier, which could be attributed to several reasons like reactor construction, operation temperature and pressure. They concluded that higher pressure resulted in slower devolatilization and consequently a lower amount of tars produced.

#### **2.2.2.4 Effect of active materials**

There are many active materials (may act as catalysts) available for biomass gasification which are classified into different categories by different researchers. Bridgwater (Bridgwater, 1994) divided catalysts into three groups: dolomites, fluid catalytic cracking (FCC) catalysts and nickel and other metals such as platinum, palladium, and rhodium. Sutton et al. (Sutton et al., 2001) divided them into dolomites, alkali metals and nickel catalysts. El-Rub et al. (El-Rub et al., 2004) divided them into two classes based on their production methods: minerals (calcined rocks, olivine, clay mineral and iron ores) and synthetic catalysts (char, FCC, alkali metal-based, active alumina and transition metal-based). So far, only few of these materials have been tested as active bed materials/additive inside the gasifier during biomass gasification. Olivine showed some promising results in the control of tar content obtained in fluidized bed biomass gasifiers. For instance, Rapagnà et al. (Rapagnà et al., 2000) investigated the catalytic activity of olivine and observed that it has a good performance in terms of tar reduction and the activity is comparable to calcined dolomite. More than 90% reduction in average tar content was observed, leading to a tar amount of 2.4 g/Nm<sup>3</sup> compared to 43 g/m<sup>3</sup> with only sand. Mastellone and Arena (Mastellone & Arena, 2008) reported that the use of a natural olivine as an in-situ tar reduction agent greatly catalyzes the reactions of heavy hydrocarbon cracking and carbon formation and considerably improved the quality of the syngas. Siedlecki et al. (Siedlecki, 2011; Siedlecki et al., 2009) studied the effect of magnesite as bed material on tar formation in the CFB gasifier and found that magnesite largely enhanced the water–gas shift (WGS) reaction, (steam) reforming of methane and C<sub>2</sub> hydrocarbons toward their equilibrium, and also reduced the tar total concentration of toluene, xylenes, PAHs and phenolics circa 6.7 g/Nm<sup>3</sup> compared to circa 9 g/Nm<sup>3</sup> measured during a base-case experiment with quartz sand as the bed material. Among these compounds, the concentration of PAHs and phenolics was reduced even to 1.9 g/Nm<sup>3</sup>.

### **2.2.3 Tar measuring techniques**

Since tar composition supplies quantitative and qualitative chemical information about pyrolysis and gasification conditions, tar analysis is complementary to gas analysis in monitoring and controlling process and catalyst performance (Milne et al., 1998). Quantitative measurement of tar in product gas is essentially important to assess the effectiveness of cleanup and conditioning processes and verify the suitability of the cleaned product gas for its final intended downstream utilization.

Up to now, a large variety of tar sampling and measurement methods, such as cold solvent trapping (CST) (e.g., tar standard), solid phase adsorption (SPA), molecular beam mass spectrometer (MBMS), on-line tar analyzer (OTA) and laser induced fluorescence spectroscopy (LIFS), have been developed by different manufacturers and researchers to determine tar concentration in biomass-derived product gas. Among these methods, CST and SPA are off-line methods. A major disadvantage of off-line methods is their complexity and time delay needed for sample treatment, which does not deliver the direct and fast monitoring of gas quality. To monitor real time tar concentration and thereby the performance of the gasifiers, on-line tar sampling and measurement methods are gaining increasing attention.

#### **2.2.3.1 Off-line methods**

CST is the conventional method for integral tar sampling and is commonly based on cold trapping using water condensers and cooling traps, occasionally combined with solvent absorption in impingers (Esplin et al., 1985). The CST method has been improved several times by different organizations (Neeft et al., 2001; Ståhlberg et al., 1998; van de Kamp et al., 2005; van Paasen et al., 2002). The

Biomass Gasification Task Working Group of the International Energy Agency (IEA) has completed an impinger-based, standardized international CEN Technical Specification (CEN/TS 15439 tar standard) “*Biomass gasification- Tar and Particles in Producer Gases-Sampling and Analysis*” to assist developers and end-users of biomass gasification technologies in measuring tar in the product gas (van de Kamp et al., 2005). A normalized CST method is designed to cover different gasifier types under a wide range of process conditions (0 to 900 °C, 0.6 to 60 bars) and concentration ranges from 1 to 300 g/Nm<sup>3</sup> (van de Kamp et al., 2005). A schematic of the impinger sampling train described in the tar standard is shown in **Figure 2- 7** (Tar, 2007). The CST method has some advantages such as being simple, using inexpensive equipment and near-universal applicability to gasifier operating conditions. However, this method also has several shortcomings: it is time-consuming and requires a high degree of expertise by the operator to ensure reproducible sampling and results.

**The solid phase adsorption (SPA) method** has originally been developed by the Royal Institute of Technology (KTH) to quantify tar species ranging in molecular weight from benzene to coronene, prevailing in product gas produced from biomass gasification within the temperature range from 700 to 1000 °C (Brage & Sjöström, 1991; Brage et al., 1997). A schematic of the SPA sampling system is shown in **Figure 2- 8**. The sampling method consists of a solid phase extraction (SPE) tube which is filled with aminopropylsilane phase bonded to silica gel connected to a syringe needle and a 100 ml gas tight syringe (plastic). An amount of 100 ml of gas is sampled directly from the process line through a silicone septum. To prevent contact with the atmosphere, the SPE column is placed in a likewise conditioned test tube and tightly capped with a stopper before and after sampling. The sampling line is normally kept at 250 to 350 °C to minimize tar condensation. The favorable features that distinguish SPA method from CST methods include reliability, speed of sampling, simplicity and reproducibility. Compared with one or two samples per hour using the CST method, the sampling step allows collection of one sample per minute and correspondingly more information on the process dynamics is obtained. As a result of this improvement, the quality of the gasification process in terms of tar molecular distribution is followed much easier.

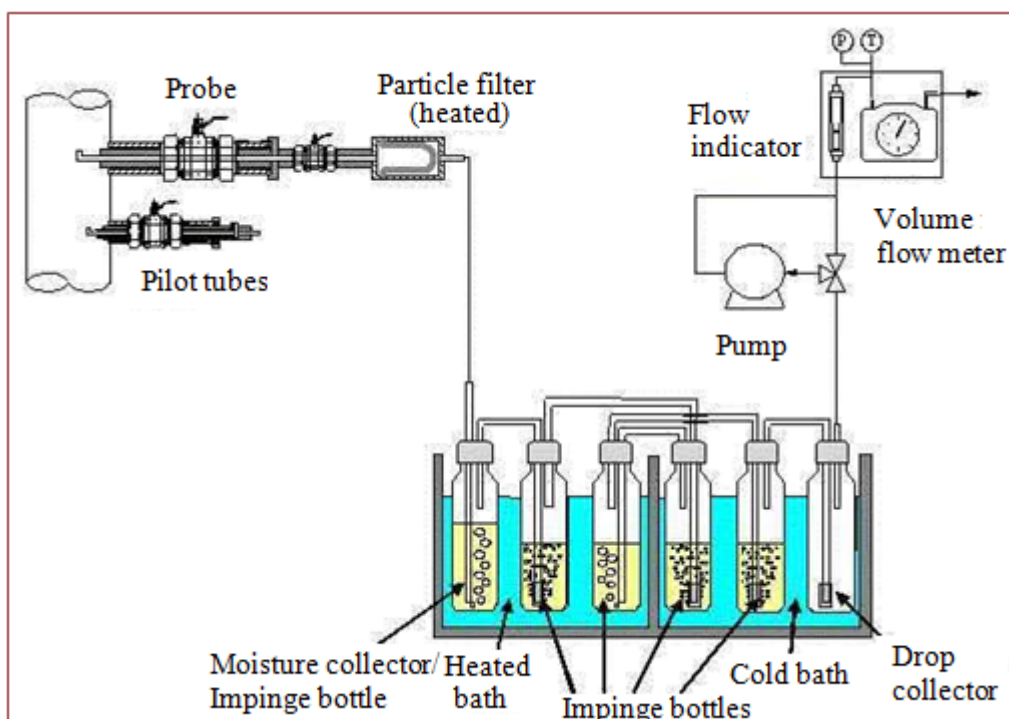


Figure 2- 7 Impinger sampling train in tar standard (van de Kamp et al., 2005)

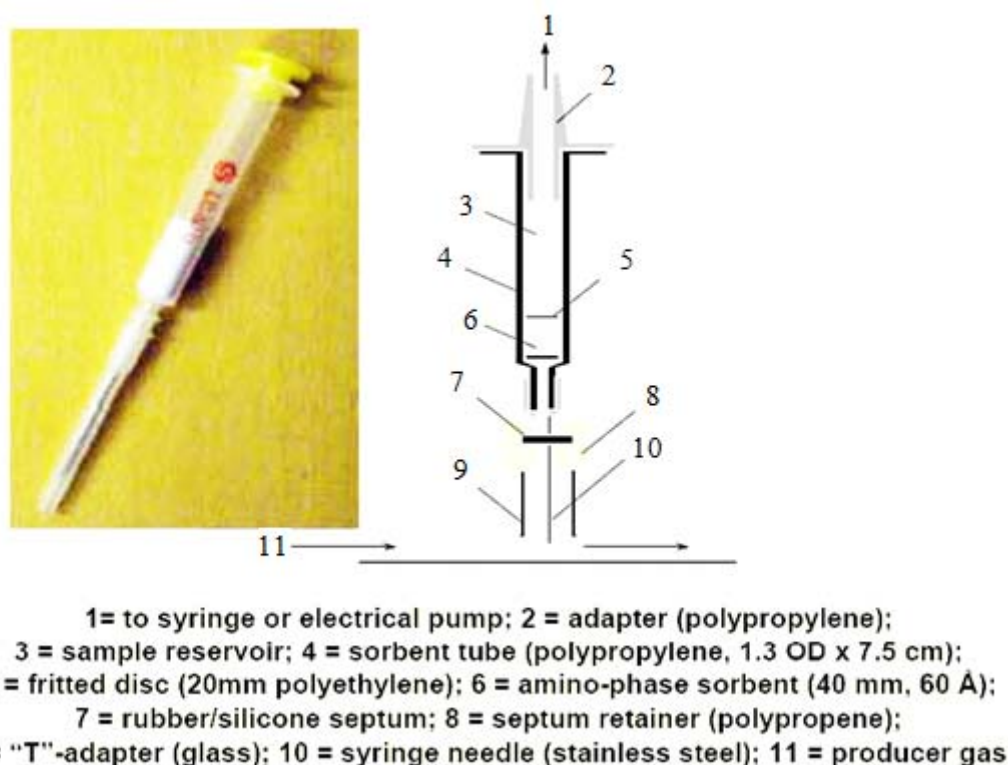


Figure 2- 8 A schematic of SPA sampling system (Liliedahl, 2007)

### 2.2.3.2 On-line methods

The aforementioned classical off-line methods consisting of sampling, enrichment, preparation and detection are not capable to generate on-line signals which can be used for process dynamic control. In order to avoid drawbacks of these techniques, on-line tar sampling and measurement methods have been developed of particular interest, since they can yield fast results by analyzing tar components in the vapor phase without condensation and re-evaporation. Several research institutions has developed different on-line/semi-online tar sampling and measurement methods, such as the molecular beam mass spectrometry (MBMS) (Carpenter et al., 2007; Gebhard et al., 1994), an on-line laser spectroscopic technique based on laser induced fluorescence spectroscopy (LIFS) (Karellas & Karl, 2007; Mitsakis et al., 2008; Sun et al., 2010), on-line tar analysis based on a photo ionization detector (PID) (Ahmadi et al., 2011) and on-line tar analyzer (OTA) based on flame ionization detector (FID) (Moersch et al., 1997; Moersch et al., 2000). Regarding the working principles of aforementioned tar analysis and measurement methods, a literature review of their applications in details is available in the one of Greensyngas Project deliveries (Meng & de Jong, 2009). Here, a simple comparison between these on-line and off-line tar sampling and measurement method is shown in **Table 2- 4**.

From **Table 2- 4**, it can be seen that both off-line and on-line methods have some advantages and disadvantages. In general, off-line methods are capable to analyze more tar components than on-line methods, but they also require longer response time for analysis. Compared to tar standard, the SPA method is much more flexible and require less special skills for sampling. PID and FID ( i.e., OTA) based analysis can both measure the global tar content on-line, while FID based analysis is capable to measure higher tar content than PID basis. Therefore, these two on-line methods can be as an indicator to show tar change trend during biomass gasification and as well monitor the performance of the gasifier in real time; however they are not able to measure individual tar components. In this way, LIFS and MBMS methods have more advantages. In this research, three tar methods such as the OTA developed by IVD-Stuttgart, LIFS developed by TUM and SPA developed by KTH have been selected to characterize the fate of tars in fluidized bed biomass gasification based on their aforementioned advantages and disadvantages. Concerning these two on-line tar measuring techniques, a detailed introduction about their working principles is presented in the coming chapter 3.

Table 2- 4 Comparison between on-line and off-line tar methods

Name	Developer	On/off-line	Detected tar species	Advantages	Drawbacks
Tar standard	IEA	Off-line	gravimetric tar and GC detectable tar	Simple, inexpensive equipment and near-universal applicability to gasifier operating conditions	Time consuming and handling of organic solvents requires special skills and extra attention
SPA	KTH	Off-line	GC detectable tar	Short sampling time, simple, accurate and reproducible	Off-line, cannot determine heavy tar and BTX is not reliable when samples are not analyzed on the same day
MBMS	NREL	On-line	GC detectable tar	Quantitative, continuous, and real-time monitoring of tar concentration in gasifier	Sensitivity is affected by differences in electron ionization cross-sections etc.
PID	KTH, BTG	On-line	the global volatile aromatic compounds	Can measure global tar concentration in the real-time	Needs calculation method to link tar concentration to PID signal
LIFS	TUM, TUB	On-line	GC detectable tar	Can measure individual tar species in the real-time.	Can be affected by adding fuel to the gasifier, reactor pressure
OTA	IVD	On-line	the global non condensable hydrocarbon	Can measure global tar concentration in the real-time	Can not measure individual tar species and needs regular calibration

Remarks:

IEA: International Energy Agency

NREL: National Renewable Energy Laboratory

TUB: Technical University of Berlin

BTG: Biomass Technology Group BV

## 2.3 Char combustion and gasification

As the most important heterogeneous reactions occurring during biomass gasification, char reactions have been investigated by different researchers using different models. The main char reactions occurring during biomass gasification are summarized in **Table 2- 5**. Among all reactions, char combustion reaction is normally faster than char gasification reactions. Char gasification with steam is reported to be faster (about 2–5 time) than with CO<sub>2</sub>. Char gasification with H<sub>2</sub> is generally neglected for most applications due to its very low reaction rate. Char combustion and gasification have been broadly studied due to their importance for biomass gasification processes.

Table 2- 5 Main char reactions occurring during gasification

NO	Name	Reaction	$\Delta H_r^{298}$ (kJ/mol)
R2- 28	Boudouard reaction	$C + CO_2 \rightarrow 2CO$	+173
R2- 29	Steam gasification	$C + H_2O \rightarrow CO + H_2$	+131
R2- 30	Hydrogen gasification	$C + 2H_2 \rightarrow CH_4$	-75
R2- 31	Partially combustion	$C + 0.5O_2 \rightarrow CO$	-111
R2- 32	Complete combustion	$C + O_2 \rightarrow CO_2$	-394

### 2.3.1 Char reaction and reactivity

In general, the char conversion process in a fluidized bed consists of several fundamental kinetic steps (Di Blasi, 2009)

- (1) External mass and heat transfer: from the bulk gas to the char external surface layer;
- (2) Internal mass and heat transfer through the ash layer and the char particles;
- (3) Pore diffusion and heat conduction inside the char particle
- (4) Surface chemical reaction on the external and internal surfaces of the char particles;

According to some researchers (Di Blasi, 2009; Hurt, 1998; Winter et al., 1997), three main regimes are divided during solid conversion based on the Thiele modulus (the ratio of the overall reaction rate to the internal diffusion rate) and the effectiveness factor (the ratio of the actual reaction rate to that which would occur if all the surface throughout the internal pores were exposed to the gaseous reactant at the same conditions as that existing at the external surface of the particle):

- (1) Regime I- kinetic control when reaction occurs at low temperature with small char particles. Under this situation, the Thiele modulus is small and the effectiveness factor is ideally unity, and conversion occurs throughout the particle with changes in density but with a constant size.
- (2) Regime II- intra-particle mass transfer control when the particle size is increased which lead to a limited gaseous reagent penetration into the char surface. Under this situation, the Thiele modulus is much greater than unity and the effectiveness factor much less than unity and conversion occurs the particle exterior surface and the particle size decreases without much change in density.
- (3) Regime III- external mass transfer control when reaction occurs at high temperature with larger char particles. Under this situation, the reaction rate is proportional to the external surface of the particle while the conversion time to the particle diameter.

Furthermore, heat transfer may also affect char conversion due to heat release and absorption during combustion and gasification reaction, respectively, may enhance the temperature gradient between surface and core of the char particle. Both mass and heat transfer effects are enhanced by high temperatures. To estimate effects of mass and heat transfer during char reactions, various criteria are available in the literature. For instance, Mears criterion (Mears, 1971) is widely used to estimate effects of external mass transfer (**Eq.2- 1**) and intraphase heat transfer (**Eq.2- 3**). Weisz-Pater criterion (Fogler, 1999) is normally used to determine the effect of internal mass transfer (**Eq.2- 2**). When these equations (**Eq.2- 1 to Eq.2- 4**) are satisfied, it means that the influences of external mass transfer, internal mass transfer and intraphase heat transfer effects can be neglected.



$$k_{ex} = \frac{-r'_A \rho_p (1 - \varepsilon_{bed}) R_p n}{k_g C_{Ab}} < 0.15 \quad Eq.2- 1$$

$$C_{wp} = \eta \phi_1^2 = 3(\phi_1 \coth \phi_1 - 1) \ll 1 \quad Eq.2- 2$$

$$k_{heat} = \left| \frac{-\Delta H (-r'_A) \rho_p (1 - \varepsilon_{bed}) R_p E_a}{h T^2 R_g} \right| < 0.15 \quad Eq.2- 3$$

$$\phi_n = R_p \sqrt{\frac{k_n \rho_p S_a C_{As}^{n-1}}{D_e}} \quad Eq.2- 4$$

Where:

- $C_{Ab}$  : Bulk fluid gas concentration (kmol/m<sup>3</sup>)
- $C_{AS}$  : Surface fluid gas concentration (kmol/m<sup>3</sup>)
- $D_e$  : Effective diffusivity (m<sup>2</sup>/s)
- $d_p$  : Solid particle diameter (m),  $d_p = 2 R_p$
- $h$  : Heat transfer coefficient, (kJ/m<sup>2</sup>·s·K)
- $k_g$  : Mass transfer coefficient (m/s)
- $k_n$  : n-order specific reaction rate constant  $((m^3/kmol)^{n-1} \cdot (m \cdot s^{-1}))$
- $n$  : Reaction order
- $r'_A$  : Reaction rate per unit mass of solid particle (kmol/kg-solid·s)
- $R_p$  : Solid particle radius (m)
- $S_a$  : Surface area of the solid particle (m<sup>2</sup>/g)
- $\rho_p$  : Density of the solid particle (kg/m<sup>3</sup>)
- $\varepsilon_{bed}$  : Bed porosity (-)
- $\Delta H$  : Heat of reaction (kJ/kmol)
- $\phi_n$  : Thiele modulus(-)
- $\eta$  : Internal effectiveness factor (-)

Di Blasi (Di Blasi, 2009) reported that the char conversion rate was critically determined by several fundamental factors, such as char surface area and surface accessibility, porosity, carbon active sites and catalytically active sites created by indigenous or added inorganic matter and the local gaseous reactant concentration. However, these parameters are very difficult to measure practically and vary significantly with the conversion level. To simplify the situation, char conversion rate is normally evaluated via its reactivity (**Eq.2- 5**), where  $dX/dt$  can be expressed by means of a chemical kinetic term  $k_m C_i^n$  accounting for effects of temperature and reactant concentration, and a structural term,  $f(X)$  is used to describe the effects of available internal surface (actual surface over initial surface, available active or reactive sites and pore evolution) (Di Blasi, 2009; Risnes et al., 2001).

$$R = -\frac{1}{m_i} \frac{dm_i}{dt} = \frac{1}{1-X} \frac{dX}{dt} [kg / (kg \cdot s)] \quad Eq.2- 5$$

$$X = \frac{m_0 - m_i}{m_0 - m_f} \quad Eq.2- 6$$

$$\frac{dX}{dt} = k_m f(X) \times C_i^n \quad Eq.2- 7$$

Where:



$C_i^n$	: Gaseous reactant concentration ( $i = \text{CO}_2, \text{O}_2$ ) (kmol/m <sup>3</sup> )
$f(X)$	: Account for the effects of available internal surface
$k_m$	: Kinetic coefficient $\left( (m^3/kmol)^{n-1} \cdot s^{-1} \right)$
$m_0$	: The initial char weight (kg)
$m_t$	: The char weight at time $t$ (kg)
$m_f$	: The residue char weight (kg)
$R$	: Char reactivity
$X$	: Char conversion or reaction degree (-)

### 2.3.2 Char kinetic models

The char reaction mechanism has been extensively investigated and multi-steps models have been proposed in the literature. For example, Tseng and Edgar (Tseng & Edgar, 1985) proposed a multi-step model for the char combustion reaction which consists of a series of adsorption and desorption processes. Laurendeau (Laurendeau, 1978) reported that char gasification with CO<sub>2</sub> is based on an oxygen exchange mechanism. A simplified semi-global mechanism for char combustion and CO<sub>2</sub> gasification in terms of kinetic laws of the Langmuir–Hinshelwood (LHM) is can be expressed as:

$$r_{C-O_2} = \frac{k_1 k_2 P_{O_2}}{k_1 P_{O_2} + k_2}; \quad r_{C-CO_2} = \frac{k_1 P_{CO_2}}{1 + k_2/k_3 P_{CO} + k_1/k_3 P_{CO_2}}$$

Where:  $P_{O_2}$ ,  $P_{CO_2}$  and  $P_{CO}$ , are the partial pressure of O<sub>2</sub>, CO<sub>2</sub> and CO, respectively. To simplify the computation, a one-step n-th order global reaction model like the volumetric reaction model (VRM), shrinking core model (SCM) and the random pore model (RPM) have been widely proposed for char combustion and gasification which is expressed as equation **Eq.2- 7**. Empirical expressions  $f(X)$  and their integral form  $g(X)$  used for common gas solid state reactions models are summarized in **Table 2- 6** (Khawam & Flanagan, 2006).

Table 2- 6 Solid-state rate expressions for different reaction models(Khawam & Flanagan, 2006)

Model	Differential form $f(X) = \frac{1}{k} \frac{dX}{dt}$	Integral form $g(X) = kt$
<i>Nucleation models</i>		
Power law (P2)	$2X^{1/2}$	$X^{1/2}$
Power law (P3)	$3X^{2/3}$	$X^{1/3}$
Avrami-Erofe'ev (A2)	$2(1-X)[- \ln(1-X)]^{1/2}$	$[- \ln(1-X)]^{1/2}$
Avrami-Erofe'ev (A3)	$3(1-X)[- \ln(1-X)]^{2/3}$	$[- \ln(1-X)]^{1/3}$
<i>Geometrical Contraction models</i>		
Contraction area (R2)	$2(1-X)^{1/2}$	$[1-(1-X)^{1/2}]$
Contraction volume (R3)	$3(1-X)^{2/3}$	$[1-(1-X)^{1/3}]$
<i>Diffusion models</i>		
1-D diffusion (D1)	$\frac{1}{2}X$	$X^2$
2-D diffusion (D2)	$[- \ln(1-X)]^{-2}$	$[(1-X)\ln(1-X)] + X$
<i>Reaction-order models</i>		
Zero-order (F0/R1)	1	$X$
First-order (F1)	$(1-X)$	$- \ln(1-X)$
Second-order (F2)	$(1-X)^2$	$(1-X)^{-1} - 1$
Third-order (F3)	$(1-X)^3$	$0.5((1-X)^{-2} - 1)$

Among these expressions, the VRM (F1) assumes that the char particle reacts homogeneously with CO<sub>2</sub> and that the particle size remains constant while the density decreases during the reaction (Murillo et al., 2004). The SCM (R3) assumes that the reaction initially occurs at the external surface of char and gradually CO<sub>2</sub> diffuses through the gas film, the ash layer and reacts on the un-reacted core surface which keeps on shrinking but always exists during the reaction progress (Bhat et al., 2001; Lee & Kim, 1996).

### 2.3.3 Char combustion

Char combustion reaction has been investigated by different researchers. For example, Di Blasi (Di Blasi, 2009) summarized the rate expressions for char combustion reaction with the estimated kinetic parameters for both one-step and multi-step models. She reported that most researchers incorporated the effect of the oxidant partial pressure on char reactivity into the pre-exponential factor. Both moderate and fast heating rates were applied during pyrolysis of various fuels like wood, agricultural residues, refuse-derived fuel (RDF) and biomass components (cellulose, lignin). The char combustion experiments have been conducted either under isothermal or non-isothermal conditions within the temperature range from 350 to 1000 °C in the environment of air or reduced O<sub>2</sub> concentrations below its content in the air. The Ea values for the main combustion reaction were roughly between 76 and 229 kJ/mol. Quantitative differences could be caused by operating condition, experimental devices, pyrolysis conditions and biomass properties etc. Only some char combustion studies are reviewed here in order to get an insight into the kinetic parameters for the combustion of different fuel chars.

Luo and Stanmare (Luo & Stanmore, 1992) studied combustion behavior of sugar cane char and the reported the Ea value of around 180 kJ/mol. Janse et al. (Janse et al., 1998) studied the combustion kinetics of rapidly pyrolyzed wood within the temperature range of 300–500 °C with O<sub>2</sub> concentration range of 2.25–36 vol.%. They found that the combustion kinetics can be described by a simple rate equation and the Ea value was 125 kJ/mol. Di Blasi et al. (Di Blasi et al., 1999a) studied the reactivities in air of wheat straw, olive husks and grape residues chars for applications in fixed-bed gasification. They reported that the weight loss curves could be well interpreted by a one-step global reaction, whose rate presented a power law dependence on the char conversion and Ea values in the range 70–110 kJ/mol. Zolin et al. (Zolin et al., 2001) studied combustion reactivities of chars from wheat straw and leached wheat straw pyrolyzed within the temperature range of 900–1400 °C in a TGA. They found that inorganic material present in parent fuel enhanced char reactivity significantly at heat treatment temperatures up to 1000 °C. Above 1000 °C the catalytic activity of the inorganic materials was severely reduced and a change in the char oxidation mechanism took place. Cozzani (Cozzani, 2000) studied combustion reactivities of chars obtained from refuse derived fuel (RDF) pyrolysis in a fixed-bed reactor at a low heating rate of 60 °C/min within the temperature range of 500 and 800 °C. He found that the RDF chars showed a reactivity in oxygen similar to that of chars obtained from municipal solid wastes (MSW) and wood, but higher than that of graphite of about 5 orders of magnitude. Raising the final temperature of the pyrolysis process from 500 to 800 °C resulted in a significantly lower combustion reactivity of char.

Branca and Di Blasi (Branca & Di Blasi, 2003) studied combustion reactivities of chars obtained from different fuels at conventional or fast pyrolysis. They found that an n<sup>th</sup> order global reaction provided a poor description of the differential curves from char combustion and obtained also lower Ea values. The combination with an additional first-order reaction for the devolatilization stage produced accurate predictions of both integral and differential curves. Varhegyi et al. (Várhegyi et al., 2006) studied the combustion reactivity of corncobs charcoal. They found that a partial removal of minerals from corncobs using acid-washing significantly enhanced the specific surface area of the charcoal, but the produced charcoal had evidenced a much lower reactivity. Kinetic parameters and char combustion conditions of above-stated literature are summarized in **Table 2- 7**, where it can be seen that there is a significant variation among kinetic parameters reported by different researchers as mentioned by Di Blasi (Di Blasi, 2009).

Table 2- 7 The kinetic parameters and char combustion conditions presented in the literature

Reference	Char type	Kinetic model	O <sub>2</sub> vol.% in N <sub>2</sub>	Kinetic parameters		Combustion conditions	
				Ea (kJ/mol)	n	T (°C)	setup
(Janse et al., 1998)	Pine wood	power-law	2.25-36	125	0.53	300-500	TGA
(Di Blasi et al., 1999a)	wheat straw, olive husks, grape residues and pine wood	VRM	21	70-100	1	400-600	Quartz reactor
		RPM		70-110	0.7-2.0		
(Zolin et al., 2001)	Wheat straw	VRM	10	106-208	-	200-1000	TGA
	Leached wheat straw			99-160	-		
(Branca & Di Blasi, 2003)	Beech, pine, redwood, chestnut, Douglas fir	Two steps model	21	114-183	0.9-1.34	Up to 700	Quartz reactor
(Várhegyi et al., 2006)	corncoobs	power-law	20-100	88-152	0.22-0.91	310-460	TGA
(Luo & Stanmore, 1992)	Sugar cane Bagasse	VRM	0-21	180	0.65	450-550	TGA
(Cozzani, 2000)	RDF	VRM	6-21	162	0.64	300-900	TGA

### 2.3.4 Char gasification

Char gasification is the rate limiting step during biomass gasification due to its slow rate compared to other reactions as reported by some researchers. Peters and Bruch (Peters & Bruch, 2001) studied the thermal decomposition of wood particle with a diameter of 4cm and found that the drying process reached completely at approximately 140 s with the evaporation temperature of 100 °C, Maschio et al. (Maschio et al., 1992) studied the influence of kinetic and diffusion phenomena on the pyrolysis of biomass particles using TG techniques and other apparatus. They found that the pyrolysis process of biomass particles could be either kinetics or both heat transfer and kinetics reaction controlled depending on particles sizes, and the pyrolysis process last about 250 s. Chen and Gunkel (Chen & Gunkel, 1987) reported that char gasification reaction occurred generally at high temperature and could take around 3000s. A broad literature review about the char conversion rates together with parameter values for char gasification with CO<sub>2</sub> and H<sub>2</sub>O is presented by Di Blasi (Di Blasi, 2009). Attention is only focused on char gasification with CO<sub>2</sub> in this research.

Gasification kinetics of various biomass chars such as wood, cotton wood (Groeneveld & Van Swaaij, 1980; Standish & Tanjung, 1988), Douglas fir (DeGroot & Shafizadeh, 1984; Okumura et al., 2009), Eucalyptus wood (Tancredi et al., 1996), rice husk (Bhat et al., 2001), olive residue (Ollero et al., 2003), beech wood char and oil palm shell (Klose & Wolki, 2005), olive husk and pine seed shells (Senneca, 2007), pine and birch (Khalil et al., 2008) with CO<sub>2</sub> have been investigated using different models. Bhat et al. (Bhat et al., 2001) reported that VRM and SCM agreed well. Ollero et al. (Ollero et al., 2003) reported that the LHM fitted well in the presence of CO. Lee and Kim (Lee & Kim, 1996) and Murillo et al. (Murillo et al., 2004) studied gasification kinetics of waste tire char with CO<sub>2</sub> using the SCM, VRM and the modified VRM models. Matsumoto et al. (Matsumoto et al., 2009) investigated gasification kinetics of four Japanese wood chars with CO<sub>2</sub> using the RPM model by considering surface porosity, constant particle size and specific surface area. Seo et al. (Seo et al., 2010) reported that RPM predicted the experimental data better than the SCM and VRM. Fermoso et al. (Fermoso et al., 2009) reported that the LHM fitted the reactivity data better for char gasification at atmospheric and at elevated pressures.

Pyrolysis temperature and heating rate largely affect char reactivity, which has been reported by some researchers. Fermoso et al. (Fermoso et al., 2009), Kumar and Gupta (Kumar & Gupta, 1994) and Lu et al. (Lu et al., 2002) reported that an increase in pyrolysis temperature substantially decreased the char reactivity, because char structures such as amorphous concentration and crystallite size became more ordered at higher temperatures and thus lower the concentration of reaction sites. Okumura et al. (Okumura et al., 2009), Chen et al. (Chen et al., 1997), Cetin et al. (Cetin et al., 2005; Cetin et al., 2004), Guerrero et al. (Guerrero et al., 2005), Kurosaki et al. (Kurosaki et al., 2003) and Mermoud et al. (Mermoud et al., 2006) reported that char obtained under high heating rates possessed a higher reactivity than chars obtained under low heating rates, which is because chars obtained under high heating rate during pyrolysis generally had sparse, large internal cavities and macroporous structure and/or a higher concentration of active sites. Fushimi et al. (Fushimi et al., 2003) reported that the increase in the maximum rate of weight loss and volatile yield observed at high heating rates during pyrolysis also shortened tar vapors residence time in the pores, thus reducing the activity of condensation reactions and preventing char agglomeration and condensation of fragments on the char surface. Kinetic parameters and gasification conditions of above-stated literature are summarized in **Table 2- 8**, where it can be seen that there is a large variation among kinetic parameters reported by different researchers depending on biomass types, gasification conditions and model types used.

Table 2- 8 The kinetic parameters and char gasification conditions presented in the literature

Reference	Char type	Kinetic model	P <sub>CO2</sub> (kPa)	Kinetic parameters		Gasification conditions	
				Ea (kJ/mol)	n	T (°C)	setup
(Groeneveld & Van Swaaij, 1980)	wood	a local volumetric rate model	0.88-23	217	0.6	800-1100	Quarts container
(Standish & Tanjung, 1988)	wood	SCM	20-101	210	0.71	900–1100	Tube furnace
(DeGroot & Shafizadeh, 1984)	Douglas Fir	VRM	0.05-0.5	220	0.6	700-900	Chamber furnace
	Cottonwood			196	0.6		
(Okumura et al., 2009)	Douglas Fir	RPM	-	-	-	700-1100	PTGA
(Tancredi et al., 1996)	eucalyptus wood	-	101	230–261	-	775-850	TGA
(Bhat et al., 2001)	Rice husk grain	VRM	101	200	1	750-900	TGA
	Rice husk power	VRM		197	1		
	Rice husk power	SCM		83	1		
(Matsumoto et al., 2009)	Japanese wood	RPM	25-300	94	0.22	900–1200	drop tube furnace
(Klose & Wolki, 2005)	beech wood	LHM	70, 100	200	-	720-730	TGA
	oil palm shell			300	-	730-780	
(Senneca, 2007)	olive husk	n-th order model	5-100	230	0.5	750-910	TGA
	pine seed shells			245	0.59		
	wood chips			298	0.64		
(Khalil et al., 2008)	Pine and birch	n-th order model	51, 101	262–263	0.4	600-1000	TGA
(Lee & Kim, 1996)	waste tire	the modified VRM	30-101	238	0.68	850–1000	Thermo-balance reactor
(Murillo et al., 2004)	waste tire	VRM	20-40	191.79	0.7	850–1000	Thermo-balance reactor
		the modified VRM		191.40	0.5		
		SCM		197.45	1		
		RPM		197.70	1		
(Ollero et al., 2003)	olive residue	n-th order model	20-50	133	0.43	800–950	TGA
(Seo et al., 2010)	Pinus densiflora for Multicaulis	VRM	2-10	172	-	850-1050	Fixed bed reactor
		SCM		142	-		
		RPM		134	-		
(Fermoso et al., 2009)	Pinus elliottii	VRM	20-101	184	0.33	750-900	Pressurized TGA (PTGA)
		SCM		185			
		RPM		184			

## 2.4 Modeling of (C)FB biomass gasification

Although experimental investigation towards the fluid dynamics, reaction kinetics and heat transfer during biomass gasification is essentially important, a good simulation model can provide lots of valuable information for process parameter optimization, product gas formation. Several reviews of the current knowledge on FB models have been published (Basu & Kaushal, 2009; Gómez-Barea & Leckner, 2010; Puig-Arnabat et al., 2010).

According to Gómez-Barea and Leckner (Gómez-Barea & Leckner, 2010), the existing FB models can be generally divided into three groups: Computational fluid-dynamic models (CFDM), Fluidization models (FM) and Black-box models (BBM). They reported that less CFDMs have been developed due to the requirement details of complex gas–solid dynamics and considerable computational times for CFD computations. FM models are a compromise between BBM and CFDM. They are the most successful models applied up to date with the major fluid-dynamics effects captured by assuming a multiphase pattern in the bed (e.g., two or three phase theory of fluidization) and simplified by semi-empirical correlations. BBM models deal with less or no kinetics involved in the particle conversion process and two approaches have been widely used among BBM: equilibrium models (EM) or modified equilibrium models complemented by empirical correlations obtained from experiments. An overview of the mathematical gasifier models based on kinetic models presented in the literature has been summarized by De Jong (De Jong, 2005). Here emphasis is put on the application of FM and EM models during CFB biomass gasification.

### 2.4.1 Kinetic models

Among currently developed FB models, in general the development of models for BFBs preceded that of CFBs. Also, the field of combustion was ahead of that of gasification and the conversion of coal proceeded biomass. Regarding the hydrodynamics of CFB modeling, a number of CFB coal combustor and gasifier models have been developed and reported in the literature, which can be classified in three broad groups of details of sophistication:

- Group I: 1D models based on two phase bubbling bed model with a simple mass and energy balance, where gases are in plug flow and solids are well mixed. The models only predict the axial variation of solids holdup and do not consider solid flow in the annular region of the riser where temperature, gas concentration and velocity can differ from that in the core (Basu et al., 1987; Heinbockel & Fett, 1995; Smolders & Baeyens, 2001; Sotudeh-Gharebaagh et al., 1998).
- Group II: 1.5-2D core-annulus models with broad consideration; they predict the axial and the radial variation of solids holdup (Adanez et al., 2001; Fang et al., 2001; Gungor & Eskin, 2007; Gungor & Eskin, 2008; Hua et al., 2004; Huilin et al., 2000; Kim et al., 2000; Siedlecki, 2011; Wang et al., 2003).
- Group III: 3D models based on gas and solid phase continuity equations, energy momentum balances and the appropriate constitutive equations with detailed consideration of chemical kinetics and individual physical processes (Hartge et al., 1999; Hyppanen et al., 1991; Knoebig et al., 1999; Yunhau et al., 2006).

According to Corella et al. (Corella & Sanz, 2005), modeling studies of coal based CFB reactors offer valuable information and help to model CFB biomass gasification, but they are not adequate enough due to the difference in physic-chemical property of biomass compared to coal.

#### 2.4.1.1 Fluidization models (FM)

So far, some FM models of CFB biomass gasifier are available in the literature. Kersten et al. (Kersten et al., 2003) provided a two-dimensional model for the pilot CFB biomass gasifier at ECN validated with the results obtained from measurements with the pilot plant and the cold-flow model. Liu and Gibbs (Liu & Gibbs, 2003) developed a CFB biomass gasifier model which was mainly addressed to  $\text{NH}_3$  and  $\text{HCN}$  emissions. Corella et al. (Corella & Sanz, 2005; Sanz & Corella, 2006) presented a 1-

dimensional model for an atmospheric CFB biomass gasifier under stationary state which was based on the kinetic equations for the reaction network solved together with mass and heat balances and with several hydrodynamic considerations. Petersen and Werther (Petersen & Werther, 2005a; Petersen & Werther, 2005b) developed 1.5D and 3D models of a CFB sewage sludge gasifier which used continuous radial profiles of velocities and solids hold-up with regard to the description of fluid mechanics and also contained a complex reaction network of sewage sludge gasification. Jennen et al. (Jennen et al., 1999) developed a mathematical model of CFB wood gasifier, which consists of the description of the flow structure, the kinetics of the gasification reactions, the particle-size distributions of the solids and the energy balances. A summary of the FM models for modeling of biomass gasification in CFB gasifier is presented in **Table 2- 9**.

#### **2.4.1.2 Aspen Plus<sup>TM</sup> models**

To avoid complex process description but still incorporating chemical kinetics of relevant reactions involved in the gasification process, some models using Aspen Plus<sup>TM</sup> software, a flowsheeting software package, have been developed. For example, Mansaray et al. (Mansaray et al., 2000) simulated a dual-distributor-type FB rice husk gasifier using Aspen Plus<sup>TM</sup>. Two different types of thermodynamic models have been developed: a one-compartment model, in which the hydrodynamic complexity of the FB gasifier was neglected and an overall equilibrium approach was used; and a two-compartment model, where the complex hydrodynamic conditions presented within the gasification chamber were taken into account. Mitta et al. (Mitta et al., 2006) modeled an FB tyre gasification plant using Aspen Plus<sup>TM</sup>, where the gasification model was divided into three different stages: drying, devolatilization and gasification-combustion, but an overall equilibrium approach was employed by neglecting the hydrodynamic complexity of the gasifier. Nikoo and Mahinpey (Nikoo & Mahinpey, 2008) developed a model capable of predicting the steady-state performance of an atmospheric FB gasifier by considering the hydrodynamic and reaction kinetics simultaneously. Doherty et al. (Doherty et al., 2009) studied the effect of air preheating in a biomass CFB gasifier using Aspen Plus<sup>TM</sup> based on the restricted thermodynamic equilibrium method. van der Meijden et al. (van der Meijden et al., 2010) used Aspen Plus<sup>TM</sup> as a modeling tool to quantify the differences in overall process efficiency for producing synthetic natural gas in three different gasifiers: entrained-flow, allothermal and CFB. Recently, Nilsson et al. (Nilsson et al., 2012) performed the modeling of the gasification of biomass and waste in a staged FB gasifier using Aspen Plus<sup>TM</sup>. In the model, the process includes three main stages: devolatilization of the fuel, homogeneous reactions of volatiles, and heterogeneous reforming of gas and the generated char. And each thermochemical stage is modeled using kinetics data obtained in dedicated tests in a laboratory-scale FB reactor or taken from the literature.

Table 2- 9 FM from literature for modeling of biomass gasification in a CFB gasifier (Gómez-Barea & Leckner, 2010)

Author, year	(Corella & Sanz, 2005; Sanz & Corella, 2006)	(Petersen & Werther, 2005a; Petersen & Werther, 2005b)	(Liu & Gibbs, 2003)	(Jennen et al., 1999)
Bed model	Constant solids void fraction = 0.77	Modified two-fluid model with some parameters from own data	Treated as input from literature data	Based on two-phase fluidization theory
Freeboard model	Constant porosity in splash and dilute zones	Core-annulus with some key parameters from own data	Treated as input from literature data	Based on core-annulus
Pyrolysis model	Instantaneous gas distribution from literature data	Instantaneous gas distribution from own measurements	N-compound from previous model, other from literature data	Not reported
Gas-phase reactions (kinetics)	kinetics from several sources with some ad-hoc corrections	kinetics from several sources	kinetics from several sources with some ad-hoc corrections	Not reported the sources
Tar model	Two lumps reacting with O <sub>2</sub> , H <sub>2</sub> O and by thermal cracking	Benzene is taken as tar model, reaction with O <sub>2</sub> is considered	One lump reacting with O <sub>2</sub> , H <sub>2</sub> O and by thermal cracking	Reaction with O <sub>2</sub> , H <sub>2</sub> O and by thermal cracking
Fuel	Pine wood chips	Dried sewage sludge	Wood	Wood
Biomass feed rate (kg/h)	11800–23700	NR	7200–14400	110
Gasifying agent	Air	Air	Air	Air
ER	0.20 — 0.45	0.3 and 0.6	0.20 — 0.40	0.25 (estimated)
Bed inventory	Silica sand	Silica sand	Silica sand	Not reported



## **2.4.2 Equilibrium models (EM)**

Unlike kinetic models which can predict the composition of the product gas at different positions along a reactor, an equilibrium model predicts the maximum achievable yield of a desired product from a reacting system. Kinetic models generally require many parameters which limit their applicability to different plants, while EM models are independent of gasifier design which make them more suitable for process studies on effects of the most important operational parameters. Equilibrium modeling uses two generally approaches: stoichiometric and non-stoichiometric, of which the former requires a defined reaction mechanism and employs equilibrium constants of all constituent reactions, while the latter does not require a specified reaction mechanism and minimizes the Gibbs free energy subject to mass balance and non-negativity constraints (Li et al., 2001). According to some researchers (Jarungthammachote & Dutta, 2007), these two approaches are essentially equivalent. A stoichiometric EM may use free energy data to determine the equilibrium constants of a proposed set of reactions. However, the second one is more flexible in handling multiple feed streams of unclear or unknown molecular formulation, as in biomass gasification (Mathieu & Dubuisson, 2002; Thompson & Argent, 2002). Here, one of the important inputs required in EM is the elemental composition of the fuel, which can be easily obtained from the ultimate analysis of the fuel. According to Prins et al. (Prins et al., 2007), EM models are based on some general assumption to achieve better predictive capabilities: the gasifier is assumed as zero-dimensional, perfectly insulated and mixed, having a uniform temperature, fast gasification reaction rates and long residence time enough to reach the equilibrium state etc. Due to these assumptions, EM models normally overestimate of the yields of  $H_2$  and CO and underestimate of the yields of  $CO_2$ ,  $CH_4$ , tars and char (Villanueva et al., 2008), which is why some modified EM models complemented by empirical correlations obtained from experiments have been developed.

### **2.4.2.1 Stoichiometric EM**

Up to now, various EM models have been developed in order to model different types of gasifiers, like fixed bed (Huang & Ramaswamy, 2009; Jarungthammachote & Dutta, 2007; Zainal et al., 2001), spouted-fluid bed (Jarungthammachote & Dutta, 2008), FB (Kinoshita, 1991; Schuster et al., 2001) and CFB (Li et al., 2004; Li et al., 2001). Jarungthammachote and Dutta (Jarungthammachote & Dutta, 2008; Jarungthammachote & Dutta, 2007) developed a stoichiometric EM model to predict the composition of the product gas obtained from municipal solid waste (MSW) gasification in a downdraft fixed bed gasifier. Five unknown species ( $CO$ ,  $CO_2$ ,  $H_2$ ,  $H_2O$  and  $CH_4$ ) were calculated by using five equations which were generated based on mass balance and equilibrium constant relationships. In order to improve the model, some coefficients obtained from the author and other researchers' experiments were applied to improve the equilibrium constant of the water–gas shift (WGS) reaction and the methane reaction. Zainal et al. (Zainal et al., 2001) developed a similar EM model to predict the composition of the product gas obtained from different biomass gasification process.

### **2.4.2.2 Non-Stoichiometric EM**

To predict more gaseous species as well as solid, carbon and inorganic species, released during biomass gasification, non-stoichiometric EM models are better to be applied. Li et al. (Li et al., 2001) developed a non-stoichiometric EM to predict the composition and heating values of the product gas and cold gas efficiency obtained from coal CFB gasification. This model considered five elements and 44 species in both the gas and solid phases. They found that except for the amount of  $CH_4$ , predicted product gas compositions were reasonably well comparing with measured ones. Schuster et al. (Schuster et al., 2001) performed an extensive parametric study regarding effects of operational conditions and fuel parameters on the heating value of the product gas and the overall performance of a gasification plant to produce electricity and energy for district heating. They found that the discrepancies in the prediction of the gas composition did not significantly influence the overall gasification efficiency.

## 2.5 Summary

In this chapter, a literature study regarding the main research questions related to biomass gasification has been performed, which includes: sulfur capture methods, tar formation, reduction and measuring techniques, char reaction as well as models used for (C)FB biomass gasification. Several important points can be concluded from this literature study:

In-bed and downstream sulfur capture has been widely studied by different researchers. However, the formation and distribution behavior of various sulfur species produced from the gasification of different biomass fuels is still lacking in the literature. Despite the fact that an experimental study of sulfur distribution and capture during biomass gasification is very important, the process could be time-consuming as well as challenging due to limit and availabilities of sulfur measuring techniques. Thus, the thermodynamic equilibrium simulations of the distribution performance of the variation of sulfur species during biomass gasification will be helpful to optimize gasifier operating conditions as well as to design downstream gas cleaning systems.

Using primary tar reduction methods is very attractive since operational conditions have a large influence tar yield and formation. In order to investigate the fate of tar during biomass gasification, tar measurement and analysis is primarily required. A thorough comparison between both on-line and off-line tar measuring techniques is currently not available in the literature for different FB biomass gasifiers.

There is a significant variation among kinetic parameters derived for combustion and gasification of different biomass chars reported by different researchers depending on biomass fuel types, reaction conditions studied and conversion model types used. To offer reliable kinetic data for modeling biomass gasification process, in this research gasification and combustion reaction kinetics of some specified chars is studied.

Despite the fact that many models have been developed by different researchers, the choice of a model largely depends on the objectives and the experimental information available. From this literature review, it appear that most published biomass gasification models from the simplest to the most advanced formulation generally fit reasonably well the selected experiments. However, modeling results which have been obtained from simulations based on different models could be different due to different assumptions. Therefore, the accuracies and reliabilities of different models should be validated by experimental data and the differences between them need to be studied and explained, an analysis which currently is not available in the literature.

### **3 Experimental setups and measuring techniques**

---

*An extensive literature overview has been presented in chapter 2, and the information summarized offers valuable sources for performing experiments and modeling in order to investigate “gaps” regarding sulfur, tar, char reaction and biomass gasification.*

*This chapter presents experimental setups and measuring techniques used in this research. A atmospheric pressure 100kW<sub>th</sub> steam-O<sub>2</sub> blown circulating fluidized bed (CFB) gasifier at the Delft University of Technology (TUD) and a steam blown 30-40kW<sub>th</sub> pressurized bubbling fluidized bed (PBFB) gasifier, called BabyHPR (Heatpipe Reformer) at the Technical University Munich (TUM) have been used to carry out biomass gasification experiments. A TA Instruments thermogravimetric analyzer (TGA) Q600 coupled with a Fourier transform infrared spectrophotometer (FTIR) (Nicolet 5700) (TGA-FTIR) is used to perform char reaction, pyrolysis and sulfidation experiments.*

*The product gas produced from biomass gasification has been analyzed using different analytical instruments such as Hartmann Braun Uras10P NDIR (on-line CO<sub>2</sub>, CO), Hartmann Braun Magnos6G PM (online O<sub>2</sub>), Varian CP4900  $\mu$ -GC (semi-online CO, CO<sub>2</sub>, H<sub>2</sub>, CH<sub>4</sub>, benzene, toluene and xylenes (BTX)), Varian GC 450 (semi-online CO, CO<sub>2</sub>, H<sub>2</sub>, CH<sub>4</sub>, BTX, H<sub>2</sub>S, COS and methyl mercaptan) and a FTIR from ThermoElectron Nicolet 5700 (semi-online CO<sub>2</sub>, CO, COS, CH<sub>4</sub>, C<sub>2</sub>H<sub>4</sub>, C<sub>2</sub>H<sub>2</sub>, H<sub>2</sub>O).*

*Three different tar measuring techniques have been used to quantify tar concentrations. The first one is a quasi-continuous TA120-3 on-line tar analyzer (OTA) using a flame ionization detector (FID) which is commercially available (Ratfish company, Germany) and originally developed by the University of Stuttgart (IVD, Germany), the second method is an on-line laser instrument based on laser induced fluorescence spectroscopy (LIFS) developed by TUM and the third one is the off-line solid phase adsorption (SPA) technique developed by Royal Institute of Technology, Sweden (KTH).*

### 3.1 Gasification experiments

To investigate effects of operational parameters on the formation of main product gas, sulfur and tar, a series of gasification experiments have been carried out on an atmospheric pressure 100kW<sub>th</sub> steam-O<sub>2</sub> blown circulating fluidized bed (CFB) gasifier at TUD and a steam blown 30-40kW<sub>th</sub> pressurized bubbling fluidized bed (PBFB) gasifier at TUM.

#### 3.1.1 The 100kW<sub>th</sub> steam-O<sub>2</sub> blown CFB gasifier

The experimental setup at TUD is an atmospheric pressure 100kW<sub>th</sub> steam-O<sub>2</sub> blown CFB gasifier. Some technical details of this facility are available in several papers which have been published in international conference proceedings, journals and Siedlecki's PhD thesis (Meng et al., 2011a; Meng et al., 2010a; Siedlecki, 2011; Siedlecki & de Jong, 2011; Siedlecki et al., 2009). The schematic diagram of the 100kW<sub>th</sub> steam-O<sub>2</sub> blown CFB gasifier and its some pictures is shown in **Figure 3- 1**.

In general, the main characteristics of the CFB test rig are described as 5 parts: reactor geometry and materials, reactor heating system, gas and solid supply system, gas cleaning system, and reactor control and measurement system:

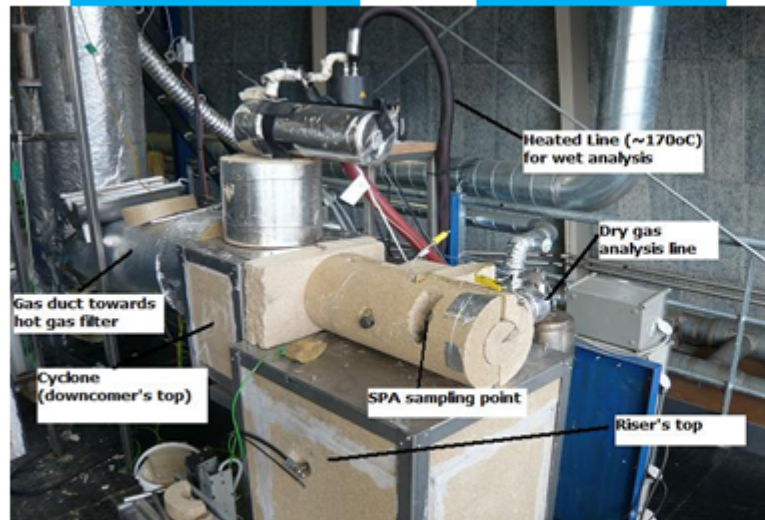
- The CFB test rig consists of a riser with length of 5.5 m and an inner diameter of 83 mm, a downcomer with an inner diameter of 54 mm, and a cyclone with an inner diameter of 102 mm. The material used for the parts exposed to nominal process temperature and to contact with the reactants and/or products is AISI 310, DIN 1.4845, while for other parts is AISI316, DIN1.4404.
- The riser (except the bend in the top part), downcomer and the cyclone are heated by using modular, semi-cylindrical ceramic fiber radiant heaters supplied by ZMC Zamac (Poland). Length of each module is 40 cm with a maximum heating power 2.4kW at 230V and a maximum operating temperature of 1200 °C. The top part of the riser and the gas ducts to the filters are heated by using heating cables supplied by Tyco Thermal Controls, type KMIN with maximum operating temperature of 1000 °C. Furthermore, the fluidization medium (i.e., steam) is preheated by using electrical circulation pre-heater (6kW) supplied by Watlow. Its maximum operating temperature is 400 °C, but normal operating temperature is 360 °C.
- The feeding system is able to supply biomass at a maximum rate of 20 kg/h plus the possibility of independent co-feeding of bed materials and additive. The gas distribution plate consists of nine tuyeres with a diameter of 6 mm with two holes each of a diameter of 2 mm. As primary fluidized flows, N<sub>2</sub>, steam and O<sub>2</sub> can be supplied independently.
- There are two high temperature filters (ceramic tissue candle filter (BWF, Germany) operating normally at 450 °C and Si-SiC ceramic candle filter (Pall Filter systems–Werk Schumacher, Germany) operating normally at 800 °C) which are connected in parallel downstream the cyclone and can be switched during operation.
- Steam flow is measured by Hauser Prowirl 72 vortex flow meter and other primary flows are measured by Endress and Hauser AT70 thermal flow meters. Product gas flow is measured by a differential pressure flow meter (McCrometer V\_cone). All primary gaseous input streams are controlled by Samson pneumatic controller. Purge nitrogen flows and L-valve nitrogen flows are controlled by mass flow controllers (M +W Mass-Stream). Temperature is measured by 8 thermocouples (K-type) of which 7 are located on the riser and 1 on the downcomer. Pressure drop over different parts of the reactor is measured by 9 dp-cells. In-house implemented supervision, control and data acquisition (SCADA) package are coupled to a programmable logical controller (PLC, ABB, and type SattCon 200).



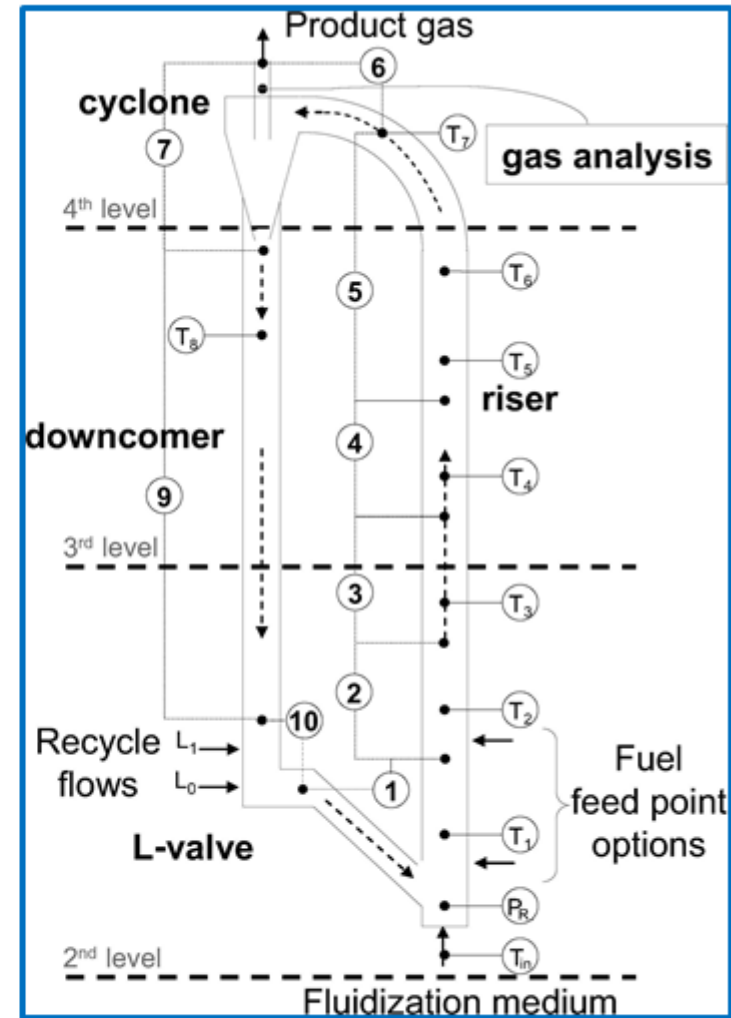
Feeding system



Filter system



Riser top



CFB gasifier flow chart

Figure 3- 1 The schematic diagram and some pictures of the 100kW<sub>th</sub> steam-O<sub>2</sub> blown CFB gasifier

### 3.1.2 The 30-40kW<sub>th</sub> PBFB gasifier

The experimental setup at TUM is an allothermal PBFB gasifier BabyHPR where the required heat for the endothermic gasification reactions is provided by means of heatpipes. A simple flow diagram of the facility is presented in *Figure 3- 2*.

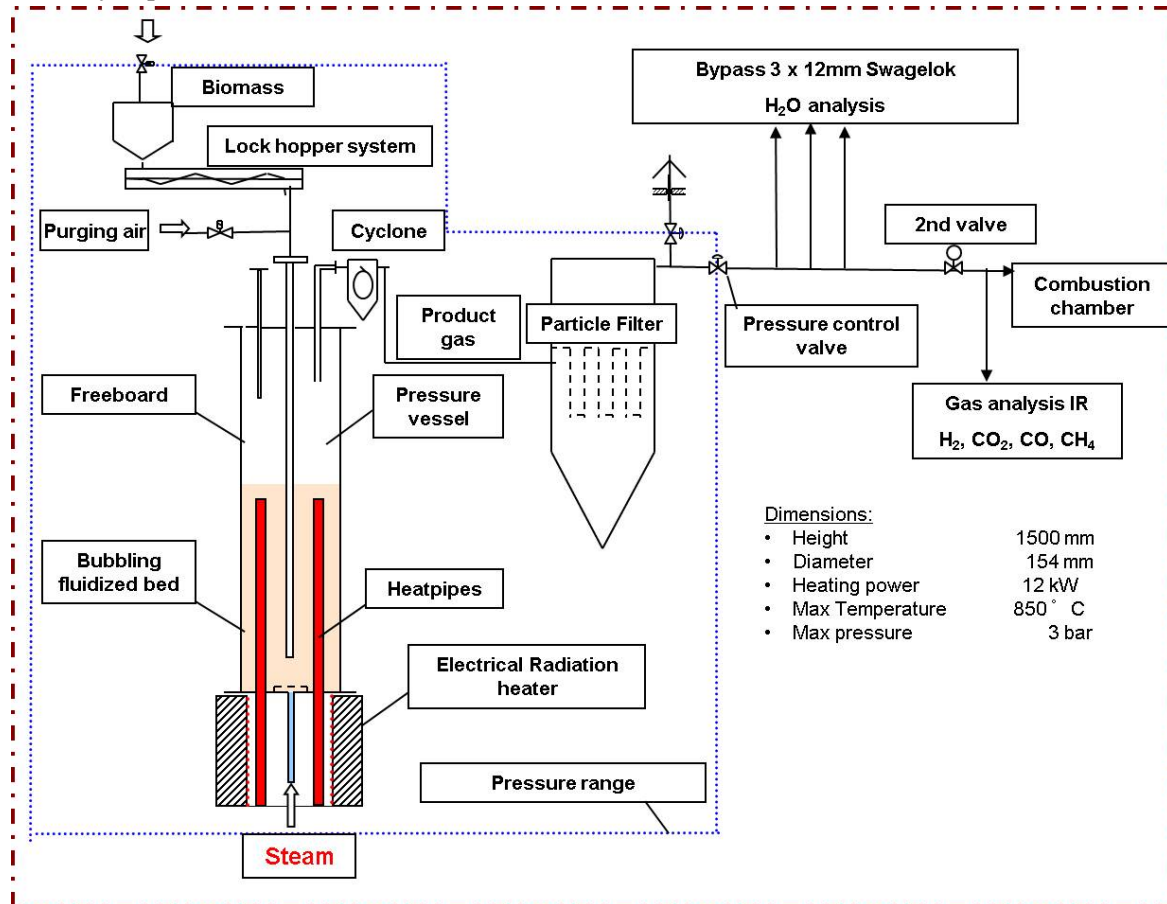


Figure 3- 2 The process flow diagram of the PBFB at TUM (Mayerhofer et al., 2011)

The PBFB gasifier is 1.5 m high with a diameter of 15.4 cm and it mainly consists of four parts: the reactor and pressure vessel, electrical radiation heater, high temperature heat pipes and a pressurized screw conveyor with lock hopper cycle for biomass supply. The biomass is fed through a lock hopper system into the PBFB gasifier. The bed has a height of approximately 700 mm and is fluidized with steam which is also used as gasifying agent. The product gas together with some un-reacted char leaves the reactor, passes through a cyclone where the entrained char is separated and then enters a particle filter for further purification.

During the experiments, a small amount of nitrogen is used to flush the biomass feeding system to avoid the product gas and steam to exit the reactor over the lock upstream hopper system. The necessary heat for the process is provided by electrical radiation heater and transferred into the fluidized bed via high temperature alkali metal containing heat pipes which work nearly isothermal over the entire length into the gasification zone. The heat pipes have a diameter of 20 mm and a length of 660 mm. The heat pipes have an evaporation zone which is located in the electrical radiation heater and a condensation zone which is placed into the gasifier. The working fluid medium (e.g., sodium) is evaporated by the input heat, flows to the gasification zone where it condensates by heat emission providing the heat for the endothermic gasification reaction, and the condensed liquid metal flows back by gravity and capillary effects into the evaporation zone and so on. The facility is controlled through an SPC (realized with Simatic). This facility and its characteristics are described by Mayerhofer et al. (Mayerhofer et al., 2011) in detail.

### 3.1.3 Biomass fuels, bed materials and additives

Agrol, willow, and DDGS used for gasification experiments were obtained from Greensygnas Project partner Lantmännen Company, Sweden. The compositions of these fuels and their ashes (obtained at 550 °C) were analyzed by Forschungszentrum Jülich GmbH, Germany, and they are presented in **Table 3- 1**. The following analytical methods have been used for chemical analysis: main inorganic components of the fuel were analyzed by inductively coupled plasma optical emission spectroscopy (ICP-OES). C, H, N, O and S were analyzed by CHNSO-IR spectrometry (LECO) analyzer, where C, H and S oxides formed were measured by the IR-absorption of the combustion gases CO<sub>2</sub>, H<sub>2</sub>O and SO<sub>2</sub>, N was quantified based on the thermal conductivity of N<sub>2</sub> and O<sub>2</sub> was measured separately. Chlorine was analyzed by Cl-Ion chromatography (IC) after Wickbold combustion. The water content was measured after drying the milled fuel in a vacuum oven at 105 °C for 60 h. All X-ray analysis was made by a Siemens D500, radiation source: Cu-K $\alpha$ . The proximate analysis of three fuels was carried out by using SDT Q600 from TA Instrument.

*Table 3- 1 Chemical composition of biomasses and ashes of biomasses obtained at 550 °C*

Types of fuel	Agrol	Willow	DDGS
Moisture (wt.% a.r.)	8	8	12
Volatile matters	74.7	69.8	67.2
Fixed carbon	16.0	20.1	15.5
Ash content	0.14	2.52	4.82
Ultimate analysis (wt.%, dry)			
C	51.0	50.3	48.2
H	6.26	6.17	6.54
O	38.2	37.4	31.2
N	0.15	0.69	5.52
S	0.002	0.002	0.76
Cl	0.01	0.01	0.21
Elemental ash analysis (wt.% of Ash at 550 °C )			
Al <sub>2</sub> O <sub>3</sub>	2.68	4.23	0.05
CaO	33.3	26.3	2.87
Fe <sub>2</sub> O <sub>3</sub>	1.32	1.54	0.26
K <sub>2</sub> O	16.5	13.13	38.1
MgO	7.79	2.89	8.87
Na <sub>2</sub> O	1.0	1.67	10.04
SiO <sub>2</sub>	6.46	33.8	1.86
SO <sub>3</sub>	2.46	2.27	10.04
Some element molar ratios			
K/S	18.1	103	1.92
K/Si	3.52	0.82	23.9
S/Cl	0.44	0.32	3.97
K/Cl	8.00	32.5	7.62
Ca/S	31.2	188	0.11
(K+Na)/Si	4.61	0.93	32
Ca/(K+Na)	1.32	1.60	0.04



It can be seen in **Table 3- 1** that DDGS sample ash is rich in K, Na and Mg, but the total quantified ash composition only sums up to 72%, which could be due to the unavailable analysis of  $P_2O_5$ . For all fuels, except for C, H, O, N, S, Cl main elements, some amounts of K, Na, Ca, Si and so on were also detected. Giuntoli et al. (Giuntoli et al., 2009b) reported that there is approximately 29%  $P_2O_5$  in the ash of another, similar DDGS sample. Agrol and willow are fairly “clean” and contain almost no sulfur and relatively low ash content.

It can also be seen in **Table 3- 1** that compared to Agrol and willow, DDGS fuel has a much higher (K+Na)/Si value, while extreme low Ca/(K+Na) value. According to Mettanant et al. (Mettanant et al., 2009), K and Na contents of the biomass are the major contributors to the agglomeration in biomass fired fluidized beds. Fuels with high (K+Na)/Si and Ca/(K+Na) values will have high agglomeration as well as sintering risks during combustion and gasification. Therefore, during DDGS gasification tests, kaolin was chosen as an alkali-getting additive to prevent agglomeration, since kaolin can be transformed to meta-kaolinite particles which potentially adsorb potassium species. The main constituent of the kaolin is the mineral kaolinite ( $Al_2Si_2O_5(OH)_4$ ), with a small amount of halloysite ( $Al_2Si_2O_5(OH)_4(H_2O)_2$ ) (Öhman et al., 2000; Siedlecki et al., 2009). Kaolin used in this work is a fine powder with a mean particle size of 12  $\mu m$ . Around 50% of the particles are in the range of 0.063 to 63  $\mu m$ . Its composition is 57.5%  $SiO_2$ , 37.5%  $Al_2O_3$ , 3.1%  $K_2O$ , 0.9%  $Fe_2O_3$ , and trace amounts of CaO,  $Na_2O$ , MgO and  $TiO_2$ . Kaolin was added together with biomass during DDGS gasification. The amount of kaolin added to the reactor varied from 3 to 10 wt.% of total feeding rate, depending the fluidization condition during experiments.

Four different bed materials have been used during measurement campaigns at TUD. Their main compositions are summarized in **Table 3- 2**. Bed 1 and Bed 2 are Austrian olivines which were received from Greensygnas Project partner Biomasse Kraftwerk Güssing GmbH & Co KG, Austria. The difference between these two Austrian olivines is that Bed 1 was pre-treated by about 1000 redox cycles in a fast internally circulating fluidized bed (FICFB) real gasification process, while bed 2 was untreated natural olivine (Bed 2). Bed 3 was a mixture of quartz sand and pre-treated olivine with a mass ratio around 50:50. The quartz sand consists of more than 99 %  $SiO_2$ , with trace amounts of  $Fe_2O_3$ , CaO,  $K_2O$ ,  $Na_2O$  and MgO. Bed 4 was untreated Scandinavian olivine. Another type of olivine was as the only bed material during measurement campaign at TUM. The reason olivine has been chosen as bed material is due to its high attrition resistance and its attractive chemical composition (being a natural mineral containing magnesium, iron and silica). From **Table 3- 2**, it can be seen that all types of olivines mainly contain MgO,  $SiO_2$  and  $Fe_2O_3$ . Besides these components, olivines also contain trace amounts of other components, for the untreated natural olivine (Bed 2) are  $Cr_2O_3$ ,  $Mn_3O_3$ , CaO and  $Al_2O_3$ , for untreated Scandinavian olivine (Bed 4) are NiO, MnO and  $Al_2O_3$ , while for olivine used at TUM are MnO, CaO and  $Al_2O_3$ .

*Table 3- 2 Compositions of different bed materials used during three fuel gasification*

Components (wt.%)	Bed 1 (treated Austrian olivine)	Bed 2 (natural Austrian olivine)	Bed 3 <sup>a</sup> ( 50%Bed 1 + 50% quartz sand)	Bed 4 (untreated Scandinavian olivine)	Olivine (TUM)
MgO	1000 redox of bed 2 in a FICFB gasifier	48-50	-	44.2	47.6
$SiO_2$		39-42	99	43.9	42
$Fe_2O_3$		8-10.5	-	9.44	9.8
Others		Trace	1	2.46	0.6

Remark: a: elements present for bed 3 here only show those from quartz sand

A brief summary about experiments and their relevant conditions applied during Agrol, willow and DDGS gasification at TUD and TUM is given in **Table A-1** and **Table A-2** (Appendix), respectively. For DDGS gasification using Bed 1 and 2 on the CFB gasifier has been tested only within a temperature range from 700 to 760 °C, as it is very difficult to reach a higher temperature during operation because of bed agglomeration risks as reported by some researchers. For example, Öhman et



al. (Öhman et al., 2005) studied bed agglomeration characteristics and mechanisms during biomass fuels gasification and combustion. They found that high-alkali-containing biomass fuels had a high risk of agglomeration. Grimm et al. (Grimm et al., 2011) studied the initial defluidization temperatures of different fuels in controlled bench-scale fluidized bed agglomeration tests. They found that DDGS fuel showed high bed agglomeration tendencies and the initial defluidization temperature was lower than 800 °C.

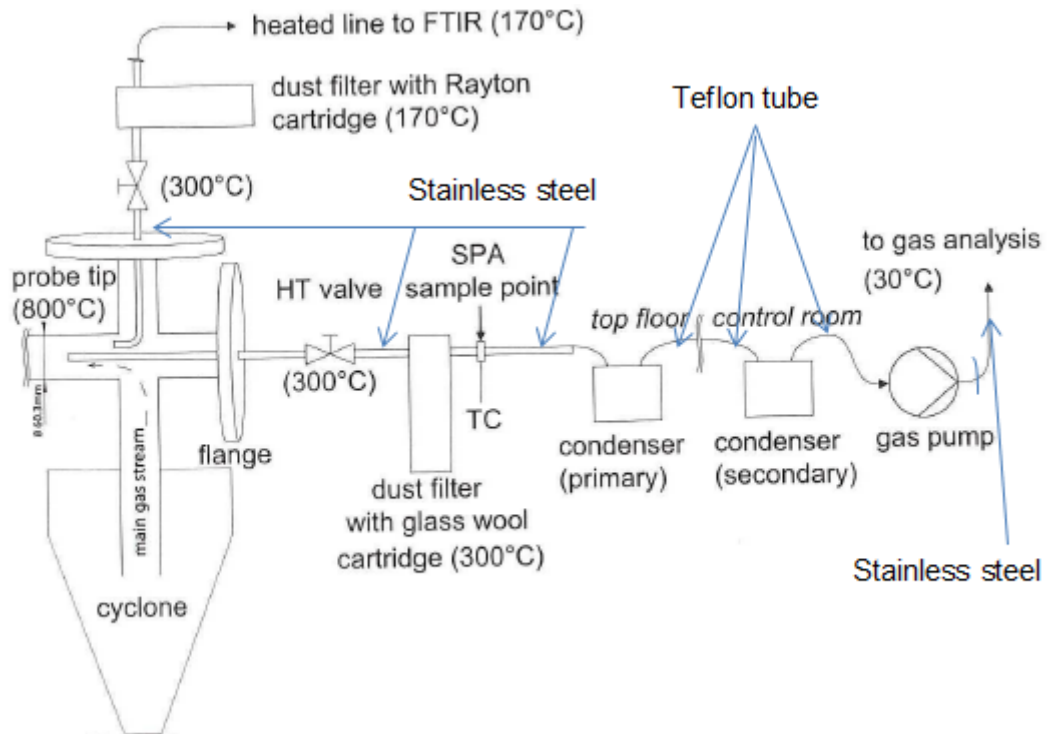
### 3.1.4 Main product gas sampling and analysis

The composition of the product gas produced from the CFB gasifier test-rig at TUD has been analyzed by using different analytical instruments which are summarized in **Table 3- 3**. As it can be seen in **Table 3- 3**, the FTIR is applied to both dry and wet gas analysis. The water concentration determined from FTIR is calculated from the dry and wet FTIR gas analysis data by comparing the respective concentration of CH<sub>4</sub> (Siedlecki, 2011). As a comparison, the water content is also measured by gravimetric method. The composition (CO, CO<sub>2</sub>, H<sub>2</sub> and CH<sub>4</sub>) of the product gas produced from the PBFB gasifier at TUM has been measured on-line by Infrared (IR) spectroscopy. The schematic drawing of the gas sampling line downstream of the CFB gasifier and pictures of Varian GC CP4900  $\mu$ -GC and GC 450 are shown in **Figure 3- 3**( also see **Figure 3- 1**).

*Table 3- 3 Overview of the analytical instruments and their analyzed components*

Technique / instrument	Specification	Components
Hartmann Braun Uras10P (NDIR)	online	CO <sub>2</sub> and CO
Hartmann Braun Magnos6G (PM)	online	O <sub>2</sub>
Varian CP4900 $\mu$ -GC Module: Cp-Sil 5 CB, 4m	semi-online	BTX (benzene, toluene, xylenes)
Varian CP4900 $\mu$ -GC Module: Cp-COX, 1m	semi-online	CO <sub>2</sub> , CO, H <sub>2</sub> , N <sub>2</sub> , CH <sub>4</sub>
Varian GC 450 Module CP-Sil 5CB, 15m×0.32 mm	semi-online	BTX
Varian GC 450 Module Hayesep T, Q Ultimetel, 0.5m Molsieve Ultimetel, 1.5m	semi-online	CO <sub>2</sub> , CO, H <sub>2</sub> , N <sub>2</sub> , CH <sub>4</sub> ,
Varian GC 450 Module CP-Sil 5CB, 50m×0.32 mm	semi-online	H <sub>2</sub> S, COS, CH <sub>3</sub> HS
FTIR ThermoElectron Nicolet 5700 heated gas cell (150 °C), 2m optical length, resolution 0.125cm <sup>-1</sup>	off-line, dry/wet	CO <sub>2</sub> , CO, COS, CH <sub>4</sub> , C <sub>2</sub> H <sub>4</sub> , C <sub>2</sub> H <sub>2</sub> , NH <sub>3</sub> , H <sub>2</sub> O
Gravimetric water measurement	off-line	H <sub>2</sub> O

To analyze the product gas produced from the gasification of three fuels using the CFB gasifier, a sample flow of the product gas is continuously extracted from the main stream downstream of the gas outlet of the cyclone. To avoid the coarsest particles from penetrating the line, the gas analysis probe which is made of stainless steel points into the direction of the flow. The gas sampling line is heated by using a trace heating cable from Horst (type HSS-450 °C). Additionally, the particle filter vessel is heated by using a heating jacket (Tyco IJ-GL glass silk heating jacket). The temperature of both the sampling line and particle filter vessel is maintained at ca. 300 °C using temperature controllers. The sampled product gas is then led by using Teflon tube through a primary condenser (located on the top floor and expose to air) to remove the condensables with the highest boiling point, predominantly heavy tar and some water, before leading the gas via a gas pump to the control room where the gas analysis equipment is located. After passing through a secondary condensation vessel, the dried gas passes through a short distance stainless steel tube and reaches different analytical instruments where the gas is characterized. For the analysis of the wet gas, both condensers are removed and a heated line (170 °C) is connected, leading the product gas to the FTIR analyzer.



Varian Micro-GC



Varian GC 450

Figure 3- 3 Drawing of the dry gas sampling line downstream of the CFB gasifier (top) modified from (Siedlecki et al., 2009) and pictures of the Varian GCs (bottom)

### 3.1.5 Sulfur species analysis

H<sub>2</sub>S, COS and methyl mercaptan are three common gaseous sulfur species present in product gas produced from biomass gasification. During experiments, these three main sulfur species are analyzed by Varian GC 450 (see in **Figure 3- 3**) which contains a pulsed flame photometric detector (PFPD). Compared to conventional flame photometric detector (FPD), the PFPD operates in a pulsed-flame rather than in a continuous-flame mode, thus achieves substantial improvements in both detectivity and selectivity by lowering the flow rates of the combustible mixtures (i.e., air and H<sub>2</sub>). The flame pulsation in the PFPD general involves 4 stages which is shown in **Figure 3- 4** (Varian, 2008):

- **Fill:** air (Air 1) and H<sub>2</sub> mix and then enter the combustion chamber at two points: part of the combustible gas stream combining with the column effluent moves upward through the interior of combustor chamber, while the second part of the gas stream sweeps along the outside of the combustor tube and into the igniter chamber.
- **Ignite:** the combustible gas mixture reaches the continuously heated igniter coil which is located in the igniter chamber and then ignites.

- **Propagate:** the flame front propagates downward into the combustion chamber and then extinguishes at the bottom of the combustion chamber. During this propagation phase, the sample molecules in the flame are broken down into simpler molecules or atoms.
- **Emit:** during and after flame propagation, the sample atoms of interest undergo further reaction to form electronically excited species, from which light is emitted. The flame background emission is complete within less than 3-4 milliseconds after propagation, whereas S molecular species emit over a much longer time.

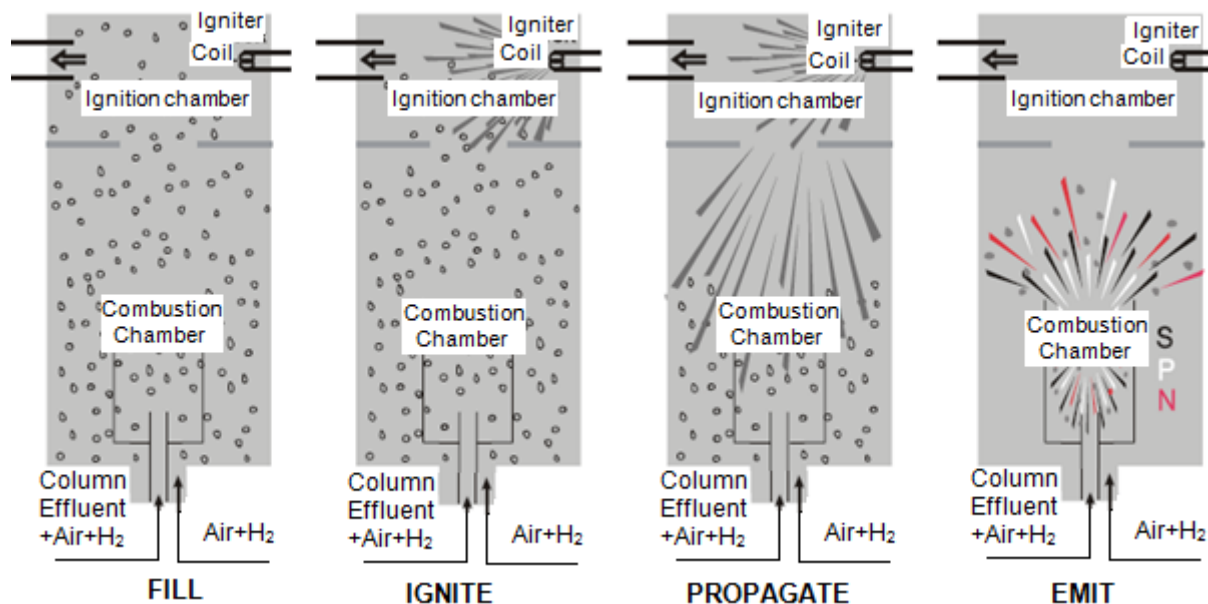


Figure 3- 4 Stages of the PFPD's pulsed-flame operation(Varian, 2008)

To analyze sulfur species accurately, it is important that the GC column and PFPD have appropriate setup, and the chosen setup of GC column and PFPD during experiments is shown in **Table 3- 4**.

Before performing sulfur compounds analysis, the calibration curves of three different sulfur species need to be made. The calibration has been performed using a cylinder gas mixture (2000 ppm  $\text{H}_2\text{S}$ , 200 ppm COS, 50 ppm methyl mercaptan,  $\text{N}_2$  as balance) and (500 ppm  $\text{H}_2\text{S}$ , 200 ppm COS,  $\text{N}_2$  as balance) which have been purchased from Linde Gas BV Company. The GC chromatography of three sulfur species and calibration curves for  $\text{H}_2\text{S}$  and COS are shown in **Figure A-1** and **Figure A-2** (see Appendix).

Table 3- 4 Setup of GC column and PFPD

Items	Setup/ specification
Column	CP-Sil 5CB, 50m×0.32 mm, df=5μm, CP7690
Temperature	Initial 50 °C for 2 min, ramping at 10 °C / min to 100 °C
Carrier gas	He, 2mL/min, constant flow
Injector	Gas sample valve, sample loop 50μL
Split ratio	1:50
Detector	PFPD, T =250°C
Combustion $\text{H}_2$	13mL/min
Combustion air	17mL/min (Air1), 10mL/min (Air 2)
Gate wide	10 milliseconds
Gate delay	4 milliseconds
Trigger level	200 millivolts

### 3.1.6 Tar measuring techniques

Three different tar measuring techniques have been used to quantify tar concentration: the first one is a quasi-continuous TA120-3 on-line tar analyzer (OTA) using a flame ionization detector (FID) which is commercially available (Ratfisch company, Germany) and originally developed by the University of Stuttgart (IVD, Germany), this second one is an on-line laser instrument based on induced fluorescence spectroscopy (LIFS) developed by TUM and the third one is the off-line solid phase adsorption (SPA) technique developed by the Royal Institute of Technology, Sweden (KTH).

#### 3.1.6.1 TA 120-3 on-line tar analyzer (OTA)

The TA 120-3 on-line tar analyzer (OTA) (Moersch et al., 1997; Moersch et al., 2000) was used to measure the global tar content on-line (see **Figure 3- 5**). The OTA analyzer is designed for semi-continuous on-line measurements of condensable aromatic hydrocarbons (tars), and is operated with help of a number of gases of which the connections are located on its back side (see **Figure 3- 5**). The specifications of gas flow connections and operational parameters for tar measurement are shown in **Table 3- 5**.

*Table 3- 5 Specifications of gas connections and operating parameter for tar measurement*

Name	Gas ( or criteria)	Specifications
Sample gas	the product gas	100-300 L/hr, 30-50 mbar
FID Fuel	H <sub>2</sub>	~2L/hr, ~ 2bar
FID air	Air	~20L/hr, ~ 3bar
Carrier gas	N <sub>2</sub> /He/Air	~5L/hr, ~ 2bar
Compressed air	Air	~50L/hr, ~ 5bar
Calibration gas	5-9 vol.% CH <sub>4</sub> in N <sub>2</sub>	~ 2bar
Oven temperature	To avoid water condensation	300 °C
Filter temperature	To remove tar	20 °C
Loading Time	Loading and Back flush	30s
Analysis Time	Analysis loop 1, 2 or 3	30s

A simple flow diagram of the OTA analyzer is presented in **Figure 3- 6**. The main components of the device include sample loops, high temperature switching valves, a FID and tar filters. The OTA is equipped with a sample valve (SV) which allows sample gas to enter via four different inlets: two inlets (sample line 1, 2) equipped with particle filters (PF1, PF2) are used to sample hot product gas from the gasifier, and the other two inlets (calibration line 1, 2) with high pressure magnetic valves (MV1, MV2) are used to calibrate the device before performing tar measurement. Each measuring cycle consists of two steps: loading sample gas (see blue line in **Figure 3- 6**) and then the analysis of gas from loop one, two and three (see pink and red line in **Figure 3- 6**). During loading, hot sample gas from the gasifier is sucked in by means of a heated venturi pump (Venturi sample) and then loaded simultaneously into three sample loops (S1, S2, S3), after having been purified by particle filters. Sample loops 1 and 2 are equipped with tar filters (F1, F2), which can be filled by different filter materials and used to remove all condensable substances from the sampled gas. After the loading, the valves switch to analysis mode and three sample loops are flushed in sequence with the carrier gas (N<sub>2</sub>) to the FID for combustion and hydrocarbon quantification. The sample loops 1 and 2 measure the content of non-condensable hydrocarbons (HC1, HC2), while the sample loop 3 (without filter) measures the total content of hydrocarbons (HC3). The difference between sample loop 3 and loop 1 or 2 (HC3-HC1 or HC3-HC2) yields the total amount of condensable tar in the sampled gas.

Before each measurement series, the OTA analyzer needs to be calibrated using a gas of known hydrocarbons (HC) concentration (e.g., 5 or 7 vol.% CH<sub>4</sub> in N<sub>2</sub>). The selection of a calibration gas is a critically important step in order to achieve the best measured results. During the calibration, the measuring range Low and High (MR Low & High), and measuring range high (MR High) need to be

selected based on carbon concentration. The aim of the calibration is to determine the response factor (RF) which reflects the relation between the determined peak areas (PK) from the FID and the total hydrocarbon content (HC) ( $RF=HC/PK$ ). The RF can be determined by using equation (*Eq.3- 1*) as follows (Moersch et al., 2000).

$$C - \text{concentration} \left[ \text{mgC/m}^3 \right] = \text{Concentration}(\text{vol.}\%) \times \text{Density} \left[ \text{kg/m}^3 \right] \times C - \text{Quota} \left[ \text{kgC/kg} \right] \times 10^6 \left[ \text{mg/m}^3 \right] \quad \text{Eq.3- 1}$$

For a calibration gas with 7vol.% CH<sub>4</sub> in N<sub>2</sub> the resulting carbon concentration is around 37.8 g/m<sup>3</sup> which can be calculated as follows:

- the specific density of CH<sub>4</sub> at standard temperature and pressure is 0.72 kg/Nm<sup>3</sup>
- the carbon content in CH<sub>4</sub> (C-Quota) is 0.75[kg C/kg] (=12/16=0.75)
- therefore the C-concentration is 37.8 g/Nm<sup>3</sup>

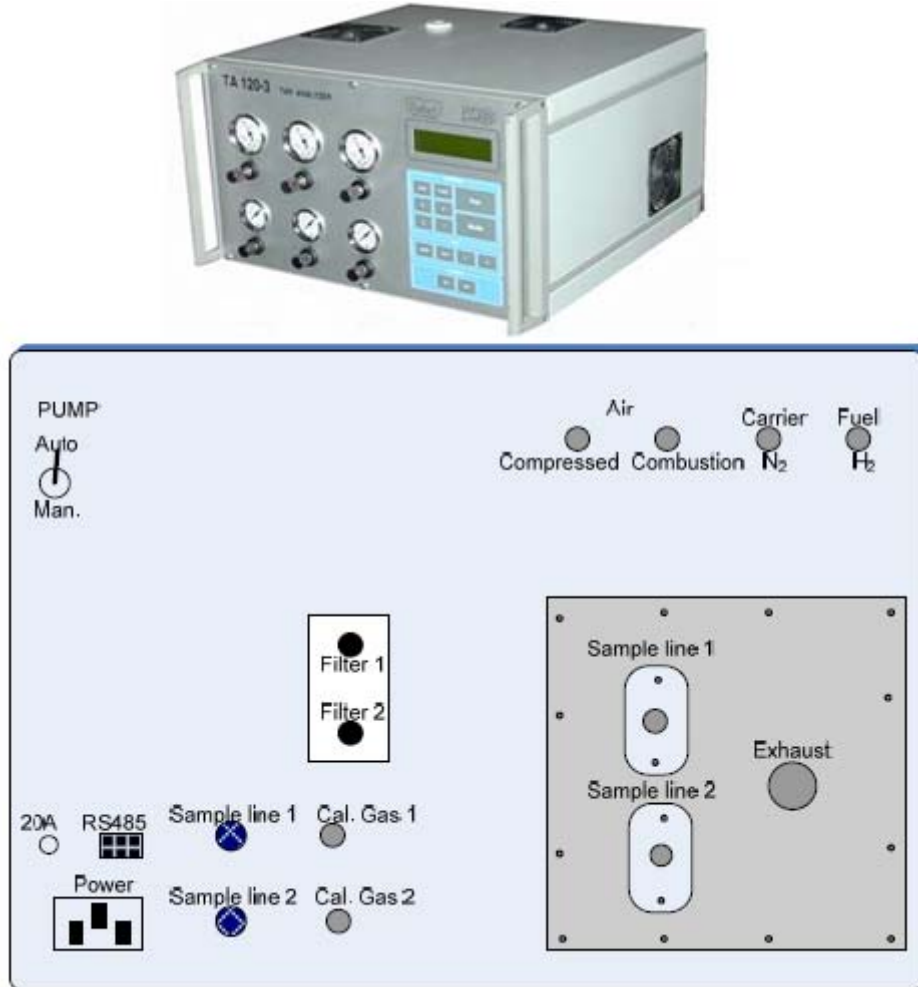


*Figure 3- 5 Picture of TA 120-3 on-line tar analyzer*

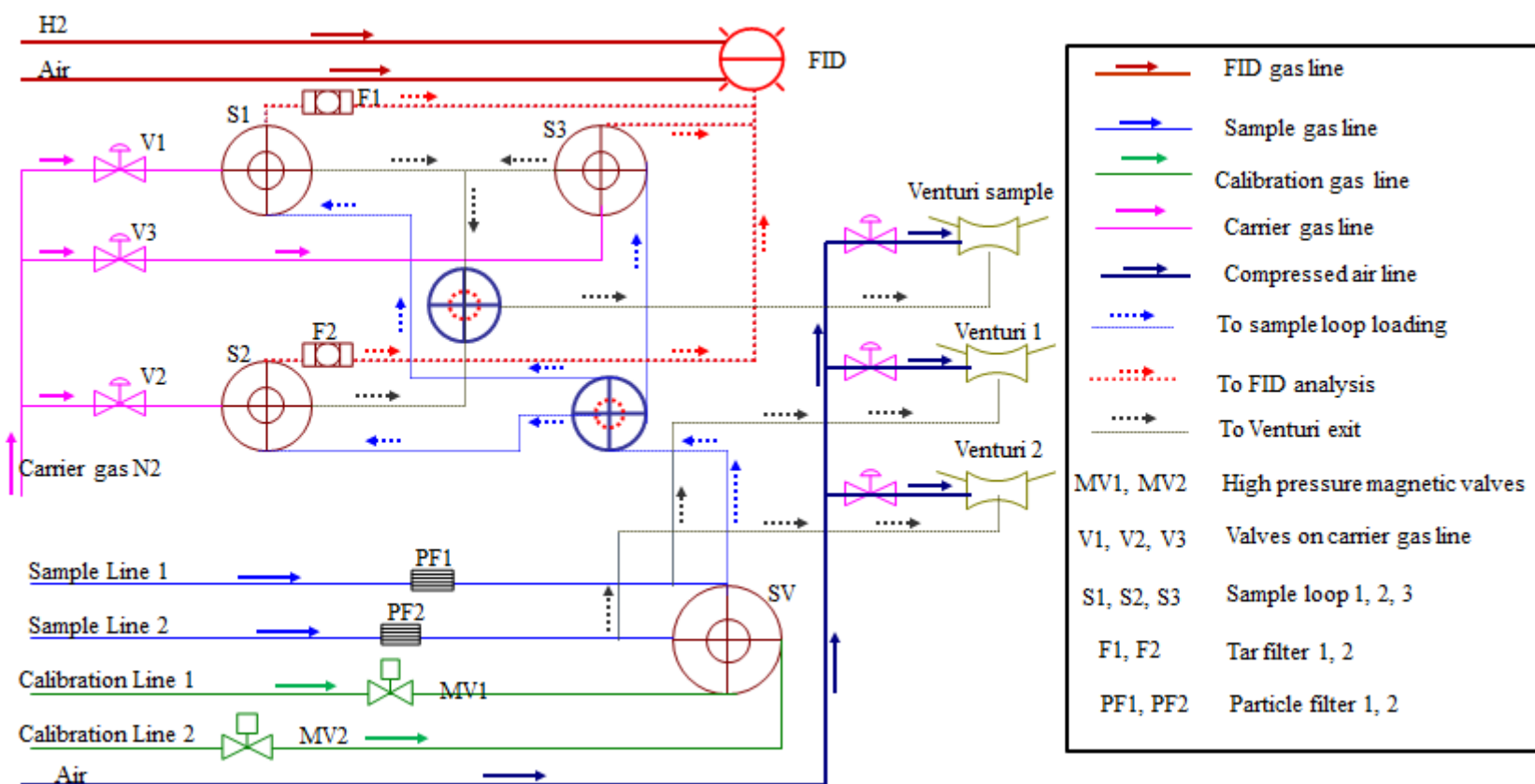


Figure 3- 6 Process flow diagram of TA 120-3 on-line tar analyzer



### 3.1.6.2 Laser induced fluorescence spectroscopy (LIFS)

An innovative laser spectroscopic technique developed by TUM (Karellas & Karl, 2007; Mitsakis et al., 2008) was used to measure 14 individual tar components which include phenol, o/m-cresol, toluene, styrene, o-xylene, indene, biphenyl, anthracene, fluorene, naphthalene, fluoranthene, pyrene and perylene on-line. A simple flow diagram of this laser instrument is presented in **Figure 3- 7**.

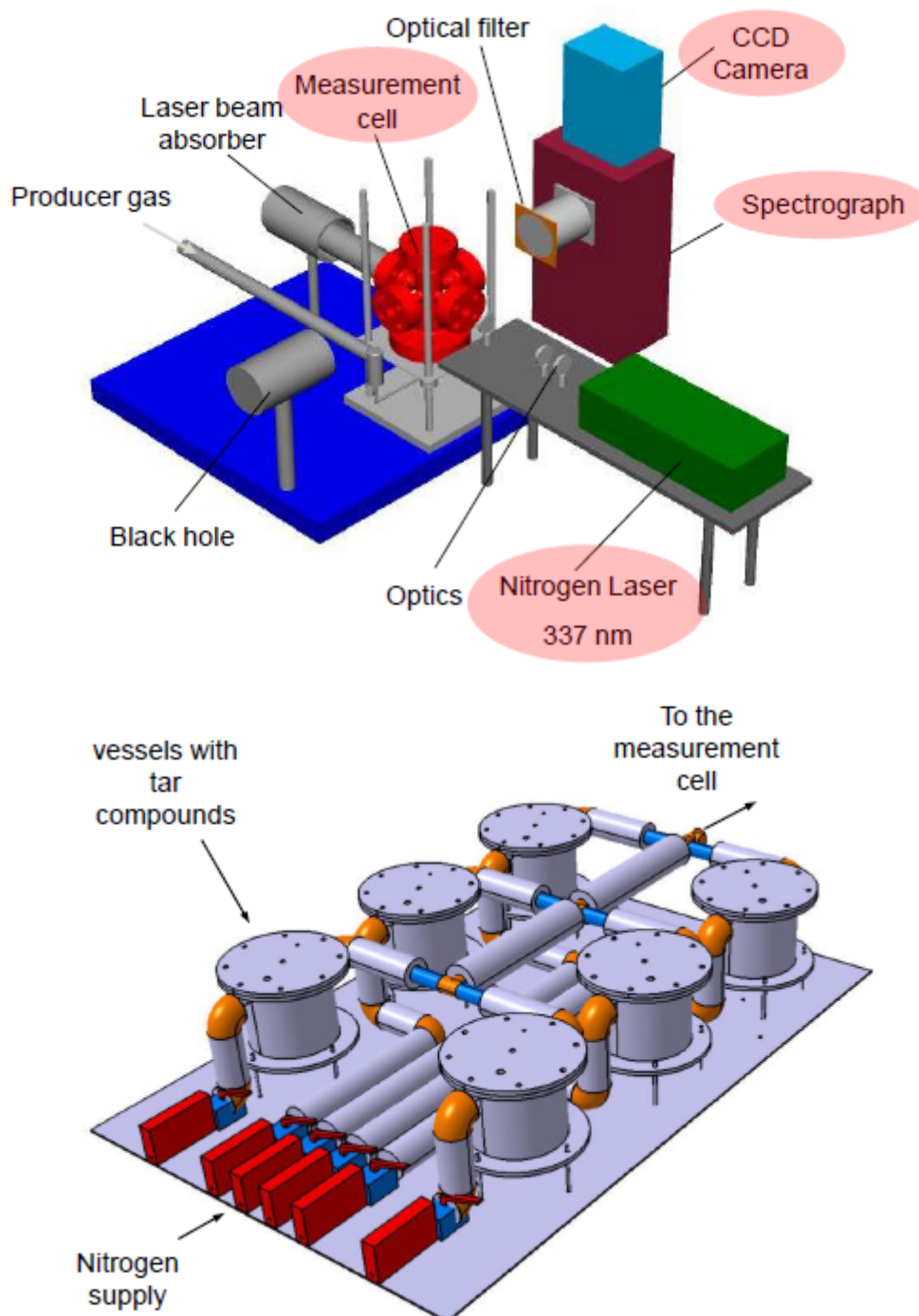


Figure 3- 7 The experimental setup of the LIFS (upper) and tar mixing station (bottom) developed by TUM (Mitsakis et al., 2008)

The LIFS system consists of a N<sub>2</sub> pulsed laser (Lasertechnik Berlin, GmbH) used as an excitation source which emits a light at  $\lambda=337.1$  nm with an average power of about 10 mW, an appropriate CCD

camera with an external image intensifier, a spectrophotometer and specific software. The product gas from gasification is sucked through heated pipes to a specially designed and electrically heated measurement cell so that condensation of tars is avoided. The temperature inside the measurement cell is 300°C, measured by a thermocouple which is placed in the center of the cell. The spectrophotometer together with the CCD camera is placed perpendicular to excitation in order to measure the emitted light from the gas in the cell. With the help of the software, pictures and profiles of the measured tars are continuously collected and saved on the computer. The evaluation of the experimental results takes place on-line by means of specially constructed macro commands.

Just as the OTA analyzer, the LIFS system also needs to be calibrated before tar measurement. The LIFS system has initially been calibrated with the help of a tar mixing station (see in **Figure 3- 7**), which enables the generation of well-defined gas phase tar compound mixtures. The tar mixing station consists of six different vessels, which contain the individual tar compounds of interest, which are either in the liquid or in the solid phase at room temperature. Each vessel can be electrically heated and N<sub>2</sub> is applied to the headspace of each vessel as carrier gas in order to provide an inert atmosphere and carry the vapors to the vessel vent and through heated pipes (condensation of tars is avoided) directly into the measurement cell. Evaporation of the tar compounds takes place within the vessel and continues at a steady rate as long as the flow of fresh purge gas is maintained and the solid or liquid content exists. The generated tar concentrations are validated by applying a tar protocol measurement downstream the exit of the tar mixing station. The calibration of the LIFS system implies the detection of the fluorescence signal that is emitted by the 14 model tar compounds of interest. In order to quantify and qualify tars, several spectra of individual tar compounds and test mixtures are recorded. The calibration process includes experiments with different concentrations of each model tar compound as well as with mixtures of them. The temperature of the vapors in the measurement cell as well as the parameters of the optical setup (e.g., gain, width and delay of the CCD camera, data acquisition timing) are kept unaltered during the whole calibration process as well as during gasification experiments.

Since the aromatic compounds studied have a linear fluorimetric response in relation to different concentrations, a linear mathematical model based on the partial least squares fit is adopted in order to evaluate the signal from the mixtures of different tar compounds and be able to obtain further information not only about the quality of the mixture, but also about the quantity of each compound in it. Therefore, since the calibration procedure is successfully been achieved, the LIFS system is able to identify single compound in complex mixtures and is used for the online and continuous monitoring of tar produced from a gasifier. Further information about the characteristics and specifications of the LIFS system, the tar mixing station and the calibration process as well as the accuracy and the detection limits of the LIFS system can be found elsewhere (Mitsakis, 2011; Mitsakis et al., 2009).

### **3.1.6.3 Solid phase absorption (SPA)**

As a reference method, the SPA measuring technique (Brage & Sjöström, 1991; Brage et al., 2000; Brage et al., 1997) is also used to sample tar during gasification experiments under specified different operational conditions. All SPA samples were put in the freezer and later were packed and sent to KTH for analysis. The following polycyclic aromatic hydrocarbons (PAHs) compounds were quantitatively analyzed: benzene, toluene, m/p-xylene, o-xylene, indan, indene, naphthalene, 2-methylnaphthalene, 1-methylnaphthalene, biphenyl, acenaphthylene, acenaphthene, fluorene, phenanthrene, anthracene, fluoranthene, and pyrene. The phenolic fraction consisted of phenol, o-cresol, m-cresol and p-cresol. Also, the non-identified peaks could be quantified using an internal standard. Among all identified components, BTX is usually lost by evaporation, thus their quantified amounts are not very accurate.

### **3.1.7 Investigating variables definition**

Several important ratios are applied in order to characterize the gasification conditions. The ER (oxygen to biomass stoichiometric ratio, or equivalence ratio) was calculated as the ratio of oxygen supplied to the oxygen required for the complete stoichiometric combustion of the biomass on a daf



(dry ash free) basis (see **Eq.3- 2**). SBR (steam to biomass mass ratio) was calculated as the ratio of steam supplied to biomass supplied on an a.r. (as received) basis. In the following equations,  $m_{i, \text{daf}}$  is the mass fraction of element  $i$  ( $i = \text{C, H, N, S, O}$ ) in the fuel on a daf basis and  $\Phi_{m, i}$  is mass flow rate of  $i$  [kg/h] ( $i = \text{oxygen, fuel, gas}$ ).  $m_{\text{O}_2, \text{air}}$  is the mass fraction of oxygen in the air.

$$\text{ER} = \frac{\left[ \Phi_{m, \text{oxygen}} / \Phi_{m, \text{fuel (daf)}} \right]_{\text{Actual}}}{\left[ \Phi_{m, \text{oxygen}} / \Phi_{m, \text{fuel (daf)}} \right]_{\text{Stoich}}} \quad \text{Eq.3- 2}$$

Where

$$\left[ \frac{\Phi_{m, \text{oxygen}}}{\Phi_{m, \text{fuel (daf)}}} \right]_{\text{Stoich}} = \frac{\left\{ \left( \frac{m_{\text{C, daf}}}{\text{MW}_{\text{C}}} \text{MW}_{\text{O}_2} \right) + \left( \frac{m_{\text{H, daf}}}{4 \text{MW}_{\text{H}}} \text{MW}_{\text{O}_2} \right) + \left( \frac{m_{\text{N, daf}}}{2 \text{MW}_{\text{N}}} \text{MW}_{\text{O}_2} \right) + \left( \frac{m_{\text{S, daf}}}{\text{MW}_{\text{S}}} \text{MW}_{\text{O}_2} \right) - m_{\text{O, daf}} \right\}}{m_{\text{O}_2, \text{air}}}$$

Another two additional important parameters are the carbon conversion efficiency (CCE %) and the cold gas efficiency (CGE %). CCE% is defined as the ratio of carbon which is converted from the added fuel into gaseous carbon components (gas+ tar) to the carbon in the added fuel (De Jong, 2005) (see **Eq.3- 3**).

$$\text{CCE \%} = \left[ \frac{m_{\text{C, gas+tar}} \Phi_{m, \text{gas+tar}}}{m_{\text{C, fuel (dry)}} \Phi_{m, \text{fuel(dry)}}} \right] \times 100\% \quad \text{Eq.3- 3}$$

CGE% of the gasification is defined as the ratio of the sum of the energy in product gases to the energy of biomass input (biomass energy). The CGE% applied in this work is based on the lower heating value (LHV) of the product gas and is defined as (Siedlecki et al., 2009)(see **Eq.3- 4**):

$$\text{CGE \%} = \left[ \frac{\text{LHV}_{\text{gas}} \Phi_{m, \text{gas}}}{\text{LHV}_{\text{fuel (dry)}} \Phi_{m, \text{fuel (dry)}}} \right] \times 100\% \quad \text{Eq.3- 4}$$

The higher heating value (HHV) of biomass fuels on a d.b. (dry basis) is calculated using a unified formula suggested by Channiwala and Parikh (Channiwala & Parikh, 2002) , and the lower heating value (LHV) of the fuel is estimated by:

$$\text{HHV} = 0.3491\text{C} + 1.1783\text{H} + 0.1005\text{S} - 0.1034\text{O} - 0.0151\text{N} - 0.0211\text{Ash} \text{ [MJ/kg]}$$

$$\text{LHV} = \text{HHV} - 9m_{\text{H}} \times h_{\text{fg}} \quad \text{[MJ/kg]} \quad \text{Eq.3- 5}$$

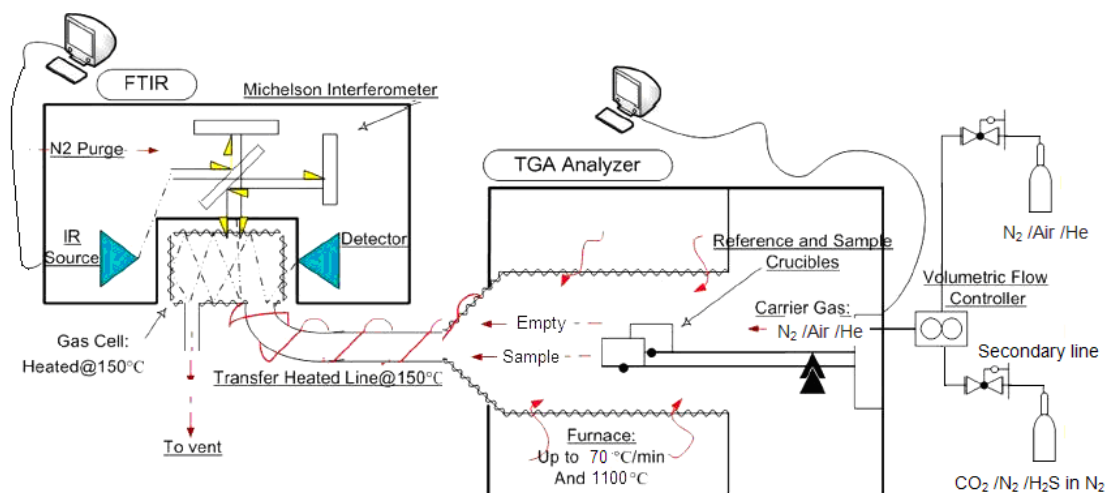
Where: C, H, O, N, and S are percentages of mass fraction carbon, hydrogen, oxygen, nitrogen and sulfur in the dry fuel.  $m_{\text{H}}$  is the mass fraction of hydrogen in the fuel and  $h_{\text{fg}}$  is the enthalpy of vaporization of water ( $\sim 2.26 \text{ MJ/kg}$ ).

## 3.2 TGA-FTIR experiments

### 3.2.1 TGA-FTIR

In order to determine kinetics of char-gas reactions, a TGA-FTIR system has been selected as the analysis tool. A series of experiments has been carried out on a TA Instruments TGA Q600 apparatus coupled with the FTIR (Nicolet 5700). A schematic drawing of the TGA-FTIR system and some pictures of TGA and FTIR are shown in **Figure 3- 8**. The TGA analyzer is capable of providing a simultaneous measurement of heat flow and weight change on the same sample from ambient temperature ( $\sim 20^\circ \text{C}$ ) to  $1500^\circ \text{C}$ . A separate Inconel 600 tube permits introduction of reactive gases into the sample chamber. Some technical details of this TGA instrument are: Platinum/Platinum-Rhodium (Type R) thermocouple, heating rate from ambient to  $1000^\circ \text{C}$  at  $0.1$  to  $105^\circ \text{C/min}$  and sample pans made of platinum ( $40 \mu\text{L}$ ) or alumina ( $110 \mu\text{L}$ ,  $40 \mu\text{L}$ , and  $90 \mu\text{L}$ )(TA-Instrument, 2010). The FTIR spectrometer can be used to identify and quantify gases, such as  $\text{H}_2\text{O}$ ,  $\text{CO}$ ,  $\text{CO}_2$ ,  $\text{CH}_4$ , and  $\text{NH}_3$ , released from pyrolysis. A small, heated stainless-steel line was used as a connection between

these two apparatuses, allowing for purge gas  $N_2$  and released gaseous products to flow from the TGA to the FTIR spectrometer. The sampling line and the gas cell of the FTIR spectrometer were kept at  $150\text{ }^\circ\text{C}$  to avoid the condensation of wax and tar produced during pyrolysis.



FTIR



TGA

Figure 3- 8 A schematic drawing of the TGA-FTIR system (top) modified from the one of (Giuntoli et al., 2009b) and pictures of TGA and FTIR (bottom)

### 3.2.2 Char characterization

After Agrol, willow and DDGS gasification, some their residual char samples (called CFB-Char) which were produced under different operational conditions have been collected from the downcomer of the CFB gasifier. Additionally, since it is fairly inconvenient to study devolatilization process of Agrol, willow and DDGS during gasification in the CFB gasifier, the pyrolysis behavior of these three fuels were investigated using TGA-FTIR. Different heating rates (HR=2, 5, 10, 30, 50, and  $70\text{ }^\circ\text{C/min}$ ) and different pyrolysis temperatures ( $T_{\text{Pyr}}=750, 850\text{ }^\circ\text{C}$ ) were applied for pyrolysis experiments. The gasification behavior of chars (called PYR-Char) obtained after the pyrolysis of three fuels and some selected CFB-Char with  $\text{CO}_2$  was further studied. The physical and chemical properties of chars have been studied by powder X-Ray diffraction (XRD), X-Ray fluorescence (XRF),  $N_2$  adsorption/desorption at  $-196\text{ }^\circ\text{C}$  and scanning electron microscopy (SEM) coupled with energy dispersive scattering (EDS).

1. SEM/EDS analysis was performed using an EVO 50 Series Instrument (LEO ZEISS) equipped with an INCAEnergy 350 EDS micro-analysis system and INCASmartMap for imaging the spatial

variation of elements in a sample (Oxford Instruments Analytical). The accelerating voltage was 25 kV and the spectra collection time was 100 s.

2. XRD powder analysis was carried out using a Philips PW1050/81 diffractometer equipped with a graphite monochromator in the diffracted beam and controlled by a PW1710 unit (CuK $\alpha$ - Ni filtered,  $\lambda = 0.15418$  nm). A  $2\theta$  range from  $5^\circ$  to  $80^\circ$  was examined at a scanning speed of  $70^\circ\text{h}^{-1}$ .
3. XRF analysis was performed using an X-ray fluorescence spectrometer wavelength dispersion (XRF-WD) Panalytical Axios Advanced equipped with an Rh target X-ray tube and a 4 kW generator. 2.5 g of char sample and 2 g of wax were milled for 10 min, and then pressed at 200 kN to obtain a 40 mm diameter pellet. Standardless analyses with a collimation mask of 37 mm were performed. The uncertainty in the measurements was approximately 5 % of the given values.
4. Specific surface area measurements were carried out using a Micromeritics ASAP 2020 instrument. Samples were previously degassed under vacuum, heated up to  $200^\circ\text{C}$  maintained for 200 min at a pressure below  $30\ \mu\text{mHg}$ . Specific surface area was calculated by the Brunauer-Emmett-Teller (BET) method over the  $0.005\text{-}0.1\ p/p^0$  range ( $p/p^0$ : relative pressure;  $p$ : absolute pressure;  $p^0$ : saturation pressure), the micropore area and external surface area were calculated from the  $t$ -plot in the  $3.5\text{-}5.0\ \text{\AA}$   $t$ -value range. The total pore volume was obtained at  $p/p^0 = 0.995$ , the contribution of the micropores was obtained from the  $t$ -plot, whereas the volume of the mesopores was obtained from the BJH method using the adsorption branch (Rouquerol et al., 1999).

### **3.2.3 Char gasification procedure**

The experimental procedures used to perform the gasification of PYR-Char in the TGA are as follows (see **Figure 3- 9**):

1. The temperature is equilibrated at  $35^\circ\text{C}$  for 20 to 30 min in  $\text{N}_2$  atmosphere;
2. The TGA furnace is ramped at the desired heating rate (10, 30, 50,  $70^\circ\text{C}/\text{min}$ ) to the desired pyrolysis temperature ( $T_{\text{Pyr}}=750, 850^\circ\text{C}$ ) in  $\text{N}_2$  atmosphere;
3. The furnace temperature is kept isothermal at the desired pyrolysis temperature  $750$  or  $850^\circ\text{C}$  for 20 min to ensure that the sample is completely pyrolyzed;
4. Introduction of different amounts of  $\text{CO}_2$  ( $\text{CO}_2=10, 20, 30\text{vol.}\%$ ) and rapidly increase the temperature up to the desired gasification temperature ( $T_{\text{Ga}}=900, 1000, 1100^\circ\text{C}$ );
5. Isothermal gasification at the desired temperature ( $T_{\text{Ga}}=900, 1000, 1100^\circ\text{C}$ ) for 20 or 30 min.

In order to achieve different  $\text{CO}_2$  concentrations, a certain amount of pure  $\text{CO}_2$  supplied via a second gas supply line was introduced and further mixed with  $\text{N}_2$  from primary gas supply line. The  $\text{CO}_2$  flow rate was controlled by an external mass flow controller (see **Figure 3- 8**). Before performing the experiments, Agrol, willow and DDGS CFB-Chars were ground to small particles. The particle size distribution of char samples were performed by using a Microtrac S3500 series particle size analyzer. The particle size distribution was determined as well as proper images of very small particles to be seen. Around 90% of chars had a diameter below 0.9 mm. A different temperature program has been applied to CFB-Char. In general, after around 10 mg CFB-Char sample was loaded into an alumina crucible, the temperature was increased from ambient temperature ( $\sim 20^\circ\text{C}$ ) to  $850^\circ\text{C}$  as fast as possible (around 4 minutes) under  $\text{N}_2$  of a flow rate of  $\pm 100\ \text{ml}/\text{min}$  and then keep at an isothermal temperature of  $850^\circ\text{C}$  for 20 min to ensure that volatiles completely released. The following steps were kept the same as those applied for PYR-Char (steps 4-5).

### **3.2.4 Char combustion procedure**

Combustion tests with chars both under isothermal and non-isothermal conditions have been carried out using the TGA. The experimental procedures used to perform char combustion using the TGA analyzer are shown in **Figure 3- 10**. Concerning  $\text{O}_2$  concentration, it assumes that the  $\text{O}_2$  concentration is 21 vol.% when pure air is applied.

For isothermal combustion tests:

- The temperature is equilibrated at  $150^\circ\text{C}$  for 10 min in an  $\text{N}_2$  atmosphere;

- The furnace is ramped at 30 °C/min to the desired combustion temperature (low temperature range (LTR) 400-600 °C, high temperature range (HTR) 750-900 °C) in an N<sub>2</sub> atmosphere;
- The condition is kept isothermal for 20 min to release all volatiles in char samples;
- The N<sub>2</sub> is switched to air or a certain amount of N<sub>2</sub> is introduced to achieve different oxygen concentrations (7.5, 10, 15 and 21vol.%) and subsequent isothermal combustion for 20 to 40 min.

For non-isothermal combustion tests:

- The temperature is equilibrated at 150°C for 10 min in N<sub>2</sub> atmosphere;
- The N<sub>2</sub> is switched to air or a certain amount of N<sub>2</sub> is introduced to achieve different oxygen concentrations (7.5, 10, 15 and 21vol.%) and ramp at desired heating rate to 900 °C;

### ***3.2.5 Sulfidation procedure***

In order to efficiently remove sulfur species from the product gas, desulfurization capacities of different sorbent materials need to be known. In this research, the sulfidation behavior of several metal oxides like ZnO, Fe<sub>2</sub>O<sub>3</sub>, CuO and MnO was investigated using the TGA analyzer. Since H<sub>2</sub>S is the main sulfur species produced from biomass gasification, the main interest is focused on the interaction of the H<sub>2</sub>S gas with different sorbent materials. The experimental procedures used to perform sulfidation using the TGA analyzer are as follows:

1. The furnace temperature is equilibrated at 50 °C for 10 min in N<sub>2</sub> or He atmosphere;
2. The TGA furnace temperature is ramped at 50 °C/min to the desired sulfidation temperature in N<sub>2</sub> or He atmosphere;
3. The TGA furnace temperature is kept isothermal for 20 min to flush away the previous left H<sub>2</sub>S in the secondary supply line;
4. Introduce H<sub>2</sub>S and isothermal sulfidation for 15 to 30 min.

A complete set of experimental parameters used for char gasification and combustion tests and sulfidation is available in **Table A-3** (see Appendix).

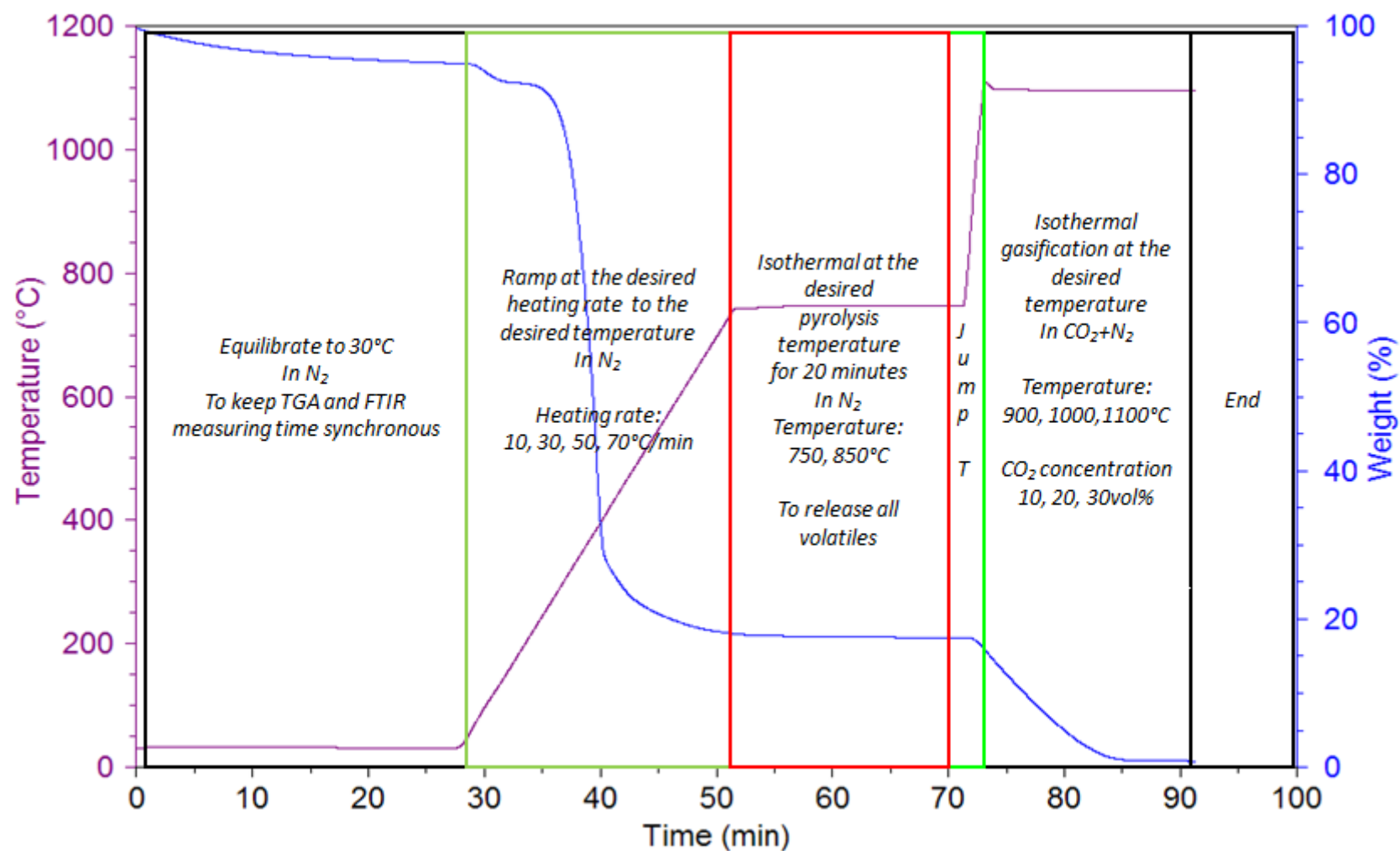


Figure 3- 9 Char gasification experimental procedures

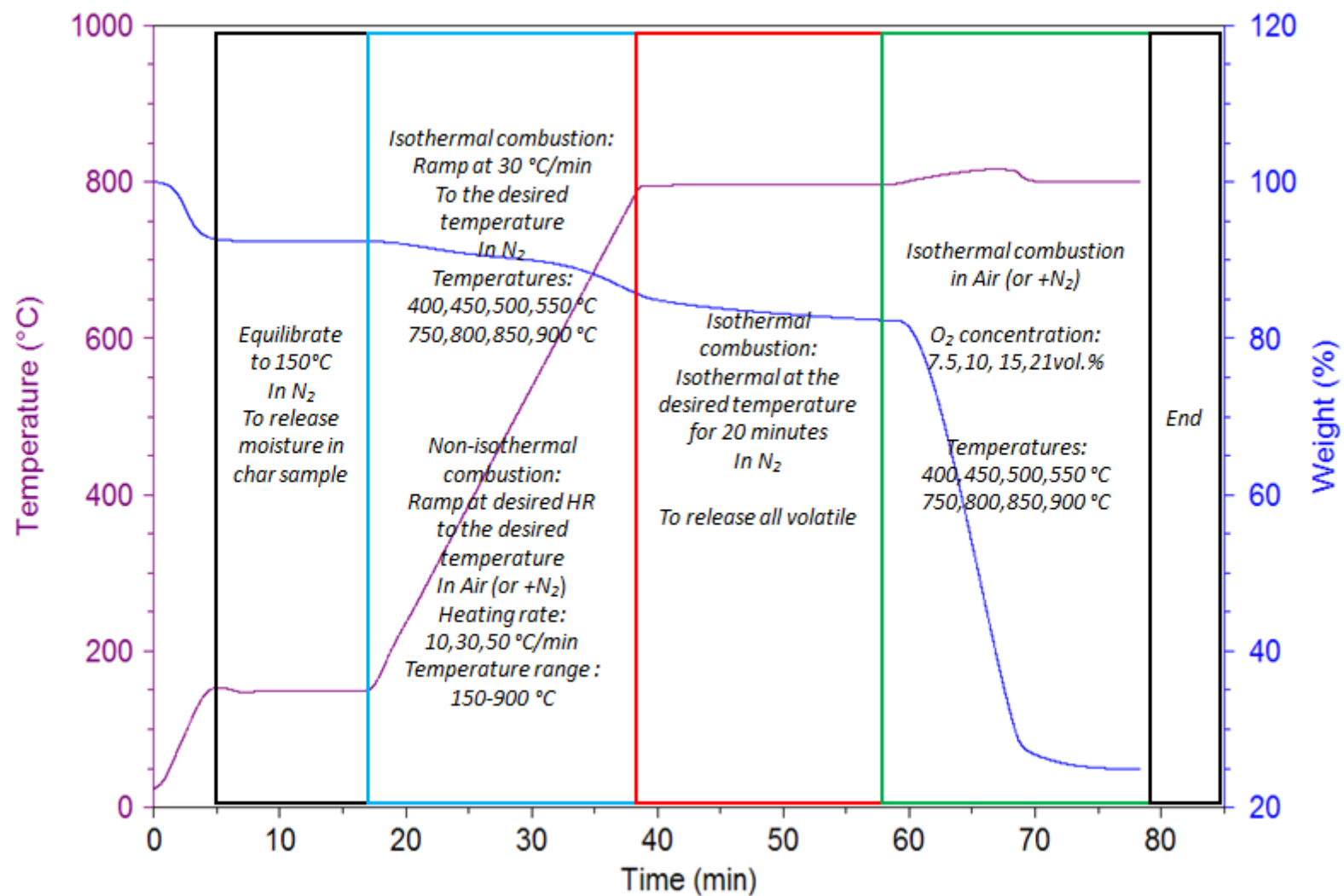


Figure 3- 10 Char combustion experimental procedures

## **4 Thermodynamic modeling of sulfur distribution and capture during biomass gasification**

---

*According to the literature study in chapter 2, the understanding of the formation and distribution of various sulfur compounds during biomass gasification is important. Thus, thermodynamic equilibrium simulation studies concerning sulfur compounds have been performed by using the Factsage<sup>TM</sup> software package version 5.4.1 (GTT Technologies) based on the minimization of the Gibbs energy.*

*Part 1: the distribution of sulfur compounds during the gasification of six different biomass fuels at various temperatures ranging from 700-1200 °C. In this part of the modeling, effects of different gasification conditions, including fuel properties and types, temperature, pressure, ER and minerals content on the behavior of sulfur compounds were systematically investigated. This part of work has been published in the proceeding of the 17<sup>th</sup> European Biomass Conference and Exhibition.*

*Part 2: sulfur capture behavior of various sorbent materials like limestone, lime, CuO, ZnO, FeO and MnO using a simulated gas composition obtained from typical gasifiers. In this part of the modeling, sulfidation and regeneration capacities of different sorbents were examined. This part of the work has been published in the Environmental Progress and Sustainable Energy Journal.*

**Meng, X., de Jong, W., Verkooijen, A.H.M.** 2009. Prediction of sulfur compounds distribution in gasification products of biomass fuels. Proceeding of the 17<sup>th</sup> European Biomass Conference and Exhibition from Research to Industry and Markets, 29 June-3 July, Hamburg, Germany, 940-947.

**Meng, X., de Jong, W., Verkooijen, A.** 2009. Thermodynamic analysis and kinetics model of H<sub>2</sub>S sorption using different sorbents. Environmental Progress & Sustainable Energy, 28(3), 360-371.

As mentioned in previous chapters, sulfur contained in biomass fuels, will be released mainly to  $H_2S$  next to small amounts of other species such as COS and mercaptans during biomass gasification. These sulfur compounds are needed to be removed or reduced to avoid poisoning catalysts. Therefore, to lower their emissions during biomass gasification, the understanding of thermodynamic behavior of sulfur compounds during gasification is needed. Despite the importance of studying the formation of sulfur compounds in gasification of biomass fuels, less information is available in the literature, which is why the first part of the thermodynamic equilibrium simulations with a focus about the partitioning of the various sulfur compounds during the gasification of different biomass fuels over a wide range of potential operational conditions has been performed.

## 4.1 Sulfur distribution modeling procedure

### 4.1.1 Biomass fuels

Six different biomass fuels were selected for the equilibrium calculations: demolition wood (wood B-quality) (WB), miscanthus (MT), straw 97(ST), bio-dried wood (BW), railroad ties (RT), and sewage sludge (SS). WB, MT and ST three fuels used in the Laboratory of Process and Energy at the Delft University of Technology (P&E, TUD) for the CFB gasifier. The compositions of those fuels (reduced to most important elements) are presented in **Table 4- 1** (Siedlecki et al., 2006). Many experiments have been carried out on the CFB gasifier using these fuels in order to identify the influence of a range of process and fuel parameters on the performance of the gasifier with respect to the quality of the product gas in terms of major and minor species produced and the operational behavior of the gasifier.

The feedstock composition data for BW and RT fuels was collected from the paper by van der Drift et al. (Van der Drift et al., 2001). For RT and BW fuels, gasification tests have been done on an atmospheric air-blown CFB gasifier of about 500 kW<sub>th</sub>, which is called BIVKIN and situated at the Netherlands Energy Research Foundation (ECN in Petten, the Netherlands). SS fuel was chosen from the paper by Pinto et al. (Pinto et al., 2008; Pinto et al., 2007), where a detailed introduction about the effect of experimental conditions on the distribution and formation of some sulfur species were presented. For SS fuel, gasification tests were performed on a bench-scale atmospheric fluidized bed gasifier which was circular in cross-section with an inside diameter of 0.08 m and total height of 1.5 m. Detailed information about experimental conditions are available in the relevant references (Pinto et al., 2008; Pinto et al., 2007; Van der Drift et al., 2001).

*Table 4- 1 Fuel characterization from TUD P&E lab (Siedlecki et al., 2006)*

Fuel type	WB	MT	ST
	wt%, a.r.		
moisture	6.2	7.3	6.8
C	47.8	45.2	40.3
H	6.0	5.86	5.45
N	0.75	0.67	0.59
S	0.05	0.11	0.15
Cl	0.04	0.22	0.36
O	44.1	43.5	40.6
SiO <sub>2</sub>	0.214	1.198	7.059
Al <sub>2</sub> O <sub>3</sub>	0.055	0.096	0.089
Fe <sub>2</sub> O <sub>3</sub>	0.084	0.046	0.053
CaO	0.224	0.182	0.476
MgO	0.056	0.128	0.113
Na <sub>2</sub> O	0.022	0.038	0.031
K <sub>2</sub> O	0.046	0.867	2.048
P <sub>2</sub> O <sub>5</sub>	0.014	0.176	0.117
sum	0.714	2.731	9.985
total ash	0.980	3.290	11.59



### 4.1.2 Factsage<sup>TM</sup> modeling

The Equilib module in the Factsage<sup>TM</sup> software package version 5.4.1 (GTT Technologies) employs the Gibbs energy minimization algorithm and thermo-chemical functions of Chemsage and offers considerable flexibility in the way of calculation which may be performed at a user-specified state point. An exhaustive explanation of Factsage<sup>TM</sup> features is available in somewhere else (Bale et al., 2002). In order to simulate the gasification process as close as possible to the actual gasification process, similar experimental conditions have been used in the modeling. The experimental conditions of the gasification tests using six different fuels are shown in **Table 4- 2**.

For the calculation the gas phase was taken as ideal while the liquid and solid phases as pure. Sulfur species in the gaseous phase were represented by the components: H<sub>2</sub>S, COS, CS, CS<sub>2</sub>, S, S<sub>2</sub>, HS, SO, SO<sub>2</sub> and H<sub>2</sub>S<sub>2</sub>, while condensed phase comprised CaS, K<sub>2</sub>SO<sub>4</sub>, Na<sub>2</sub>SO<sub>4</sub>, MgS, SiS, SiS<sub>2</sub> and FeS. Fuels (elemental compositions and mineral species in the ash), gasifying agents (steam, oxygen and air) values were converted to molar bases and entered as reactants in the Factsage<sup>TM</sup> equilibrium program. Water in fuel was specified separately as partly of input data of hydrogen and oxygen. The total elements included in the calculation were C, H, O, N, S, Cl, P, K, Na, Mg, Ca, Si, and Fe, and input data is shown in **Table 4- 3**.

*Table 4- 2 The experimental gasification conditions using different fuels*

Fuel type	SS	BW	ST	MT	RT	WB
Pressure (atm)	1	1	1	1	1	1
Temperature (°C)	850	805	740	747	855	800
Gasifying agent	air/steam	air	O <sub>2</sub> / steam	O <sub>2</sub> / steam	air	O <sub>2</sub> / steam
ER	0.21	0.43	0.33	0.30	0.34	0.34
Steam/ O <sub>2</sub> ratio	-	-	2.3	2.6	-	2.6
SBR	0.9	-	-	-	-	-

*Table 4- 3 Total input data for Factsage<sup>TM</sup> simulation*

mol/ 100g fuel	SS	BW	ST	MT	RT	WB
C	2.64	2.98	3.36	3.76	3.94	3.98
H	5.14	5.58	5.41	5.81	6.17	5.95
O	2.75	5.24	4.62	5.287	5.53	5.56
N	5.16	9.92	0.04	0.05	10.54	0.05
S	0.03365	0.00543	0.00468	0.00343	0.00271	0.00156
Cl	0.00224	0.00053	0.01027	0.00626	0.00039	0.00119
Al	0.05893	0.01775	0.00174	0.00189	0.00072	0.00108
Ca	0.09631	0.03198	0.00848	0.00324	0.00425	0.00399
Fe	0.01539	0.00556	0.00066	0.00057	0.00242	0.00106
K	0.01099	0.01325	0.04348	0.01841	0.00059	0.00097
Mg	0.01687	0.00693	0.00280	0.00317	0.00073	0.00140
Na	0.00609	0.01352	0.00100	0.00122	0.00093	0.00035
P	0.08071	0	0.00105	0.00159	0	0.00012
Si	0	0.05993	0.11749	0.01994	0.00411	0.00356
H <sub>2</sub> O	2.83759	0	5.75366	5.92006	0	5.92006

## 4.2 Sulfur distribution modeling results

### 4.2.1 Comparison of experimental and predicted H<sub>2</sub>S emission

The predicted emission value of H<sub>2</sub>S by using different fuels was compared with the available experimental data and modeling results from literature to test the validity of the Factsage<sup>TM</sup> prediction. The results are shown in **Table 4- 4**.

The results presented in **Table 4- 4** show that all the predicted values are relatively higher than the experimental ones, but being very close to the modeling results from the literature, like RT and BW fuels reported by Kuramochi et al. (Kuramochi et al., 2005). For MT and ST fuels, the predicted values are comparatively satisfactory in view of the fact that no consideration was made of bed materials which were used in the gasification tests. Norman et al. (Norman et al., 1997) mentioned that in the gasification process bed material has a great influence on the predicted outcome of H<sub>2</sub>S and COS. However, the concentration of H<sub>2</sub>S produced from WB fuel was not detected in the experiment probably as a result of limited detection abilities of the equipment. Kuramochi et al. (Kuramochi et al., 2005) reported that the predicted value is 103 ppmv by using a similar fuel in their model. For SS fuel, the result is much higher than the measured value in the quoted paper (Pinto et al., 2008; Pinto et al., 2007). However, a high value of 4000 ppmv by using SS fuel is also predicted by Kuramochi et al (Kuramochi et al., 2005).

*Table 4- 4 The concentration values of H<sub>2</sub>S from modeling and experiments*

Biomass fuels	WB	MT	ST	BW	RT	SS
Temperature(°C)	800	747	739	805	855	850
H <sub>2</sub> S (experimental, ppmv)	-	200	200	230	140	1350
H <sub>2</sub> S (this modeling, ppmv)	144	269	470	462	225	3256
H <sub>2</sub> S(literature modeling, ppmv)	103	-	-	469	225	-

Furthermore, the percentage of sulfur content in the fuel (Fuel-S) converted into H<sub>2</sub>S / COS which is defined by dividing the Fuel-S molar content by the maximum number of moles of H<sub>2</sub>S / COS was also investigated. And the results are shown in **Figure 4- 1**.

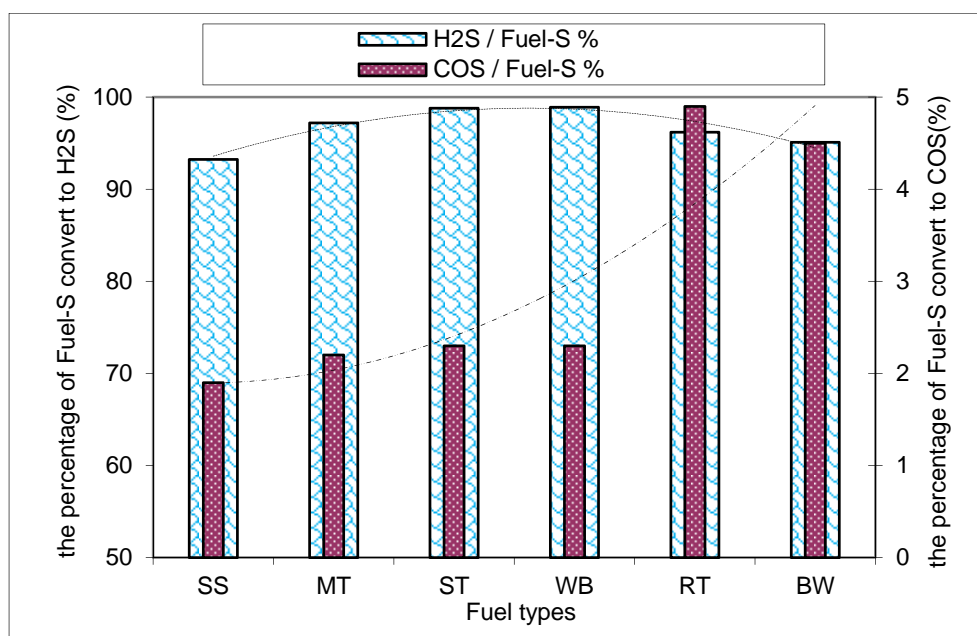


*Figure 4- 1 The relation between Max-H<sub>2</sub>S, Max-COS and Fuel-S content for different fuels*

From **Figure 4- 1** it can be seen that for all the fuels, a special correlation between the maximum concentration of H<sub>2</sub>S and the Fuel-S content is observed. And around 95% Fuel-S is converted into H<sub>2</sub>S during gasification. This observation is also reported by other researchers (Kuramochi et al., 2005; Norheim et al., 2009). For example, Norheim et al. (Norheim et al., 2009) reported that doubling sulfur content leads to a doubling of the H<sub>2</sub>S levels in different temperature intervals. However, the maximum concentration of COS seems to be significantly affected by the gasifying agent used in the gasification process. For MT, ST and WB fuel gasification, which were based on oxygen and steam as the gasifying agent, the observed percentages of the Fuel-S content converted into COS all are round 2.2%. Likewise, for RT and BW fuel gasification, which were based on air as the gasifying agent, the percentage of the Fuel-S content converted into COS both are around 4.6%. According to Attar et al.

(Attar, 1978), the formation of  $\text{H}_2\text{S}$  and the conversion rate depend on large number of factors. Besides the type of fuel used, two groups of variables are reported with a strong impact on the distribution of sulfur during gasification: 1) those that are a function of the initial condition of the fuel, such as volatiles content, ash and its composition and sulfur amount; and 2) those that depend on the operational conditions used, such as reaction time and temperature. Effects of some process conditions were systematically studied in the below sections.

### **4.2.2 Effect of temperature**

Because not all sulfur species concentrations have available experimental data, in this study, the variation of the concentration of  $\text{H}_2\text{S}$  and  $\text{COS}$  as a function of temperature by using different fuels was studied separately and the results are shown in **Figure 4- 2**.

From **Figure 4- 2** it can be seen that an increase in the temperature promotes the formation of the mentioned gaseous sulfur species and leads to an increase in their amounts with varying degrees. For BW and RT fuels it is shown that the predicted results are very similar to the results achieved by Kuramochi et al. (Kuramochi et al., 2005) who studied the effect of temperature on the formation of  $\text{H}_2\text{S}$  by using the same fuels. For WB and ST fuels, the concentration of  $\text{H}_2\text{S}$  slightly increased with an increase of temperature, from 142 to 150 ppmv, and 467 to 492 ppmv, respectively. For MT fuel, a rise of temperature from 900 to 1100 °C led to a significant increase  $\text{H}_2\text{S}$  formation from 281 to 334 ppmv. These predicted results fairly agree with the ones reported by other researchers (Bunt & Waanders, 2008; Gerasimov & Bogacheva, 2001a; Gerasimov & Bogacheva, 2001b; Khan, 1989; Pinto et al., 2008; Stinnett et al., 1974; Van der Drift et al., 2001), who stated that the concentration of  $\text{H}_2\text{S}$  increased with increasing temperature. As a reason for that Khan et al. (Khan, 1989) explained that higher temperatures usually promote the decomposition of sulfur containing tars and hydrocarbons, and thus cause increased  $\text{H}_2\text{S}$  formation and its release into the gas phase. Gerasimov and Bogacheva (Gerasimov & Bogacheva, 2001a) reported that the roles of  $\text{CaS}$  and  $\text{FeS}$  in the condensed phase becomes less pronounced as the temperature increases, which favors the formation of  $\text{H}_2\text{S}$  and  $\text{COS}$  in the gaseous phase. However, Dias and Gulyurtlu (Dias & Gulyurtlu, 2008) reported that increasing temperature from 850 to 900 °C led to a decrease of  $\text{H}_2\text{S}$  from 1081ppmv to 823 ppmv in experimental and predicted results by using RDF fuel. The authors explained that the reduction observed in  $\text{H}_2\text{S}$  with increasing temperature from 850 to 900 °C could be due to the thermal destruction of organic structure in the temperature range 800 to 860 °C, according to Attar et al.(Attar, 1978), thus limiting mass transfer by diffusion at higher temperatures, in particular to the sharp reduction in fuel surface area. The reduction in the surface area limits the accessibility of  $\text{H}_2$  to the sulfur to further form  $\text{H}_2\text{S}$ .

For SS fuel, a different tendency of  $\text{H}_2\text{S}$  formation was observed compared to other fuels. A temperature increase from 725 to 850 °C led to a decrease of  $\text{H}_2\text{S}$ , from 3398 to 3430 ppmv, and with increasing temperature from 850 to 1200 °C, an increase of  $\text{H}_2\text{S}$  from 3430 to 3444 ppmv was observed. The finding is fairly in agreement with those obtained experimentally in reference (Pinto et al., 2008), but contradictory to those in reference (Pinto et al., 2007), in which the author used the same SS fuel but in co-gasification experiments with straw pellets (Pinto et al., 2008) and with coal in reference (Pinto et al., 2007). Furthermore, in both papers, some deviations in relation to the main tendency about the effect of temperature on the  $\text{H}_2\text{S}$  concentration were observed, especially with the temperature range of 800 and 850 °C. For SS fuel, further work is probably required to find out additional information for the explanation of the complex phenomena involved in these processes.

For all the fuels, the concentration of  $\text{COS}$  increased with increasing the temperature, especially for BW fuel, with an increase from 10 to 26 ppmv. Considering that sulfur content in biomass fuels, more  $\text{COS}$  was formed from BW and RT fuels than other fuels. The reason for that can probably be attributed to different gasifying agent used. For other fuels, some amount of steam was used in the gasification process, which could rapidly accelerate  $\text{CO}$  conversion in chain reactions of  $\text{COS}$  flames. For other sulfur species (**Figure A-3**, see Appendix), the temperature had less effect on the formations of  $\text{H}_2\text{S}_2$  and  $\text{CS}_2$ . For SS and RT fuels, to a great extent, the concentration of  $\text{S}_2$  was higher than other

sulfur species and increased rapidly with an increase in temperature. Higher  $\text{SO}_2$  concentrations were obtained for MT and ST fuels, probably due to a higher oxygen concentration used for the reaction conditions in the gasifier.

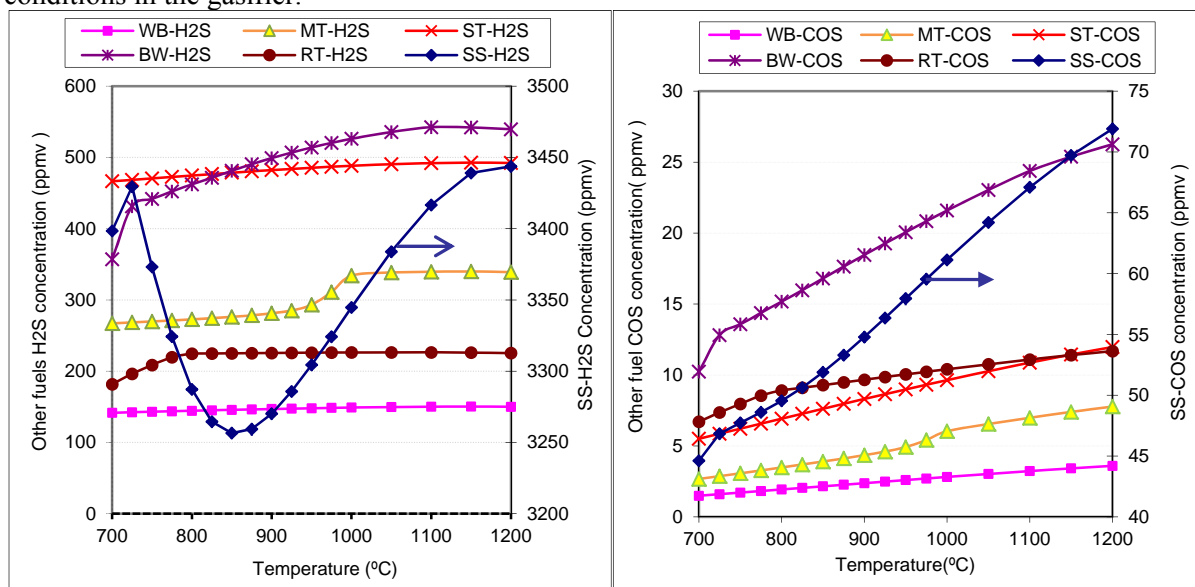


Figure 4- 2 Predicted concentrations of  $\text{H}_2\text{S}$ ,  $\text{COS}$  for the gasification of six biomass fuels at various temperatures

### 4.2.3 Effect of pressure

The variation of the concentration of  $\text{H}_2\text{S}$  and  $\text{COS}$  as a function of pressure by using MT, ST, RT and BW fuels is shown in **Figure 4- 3**.

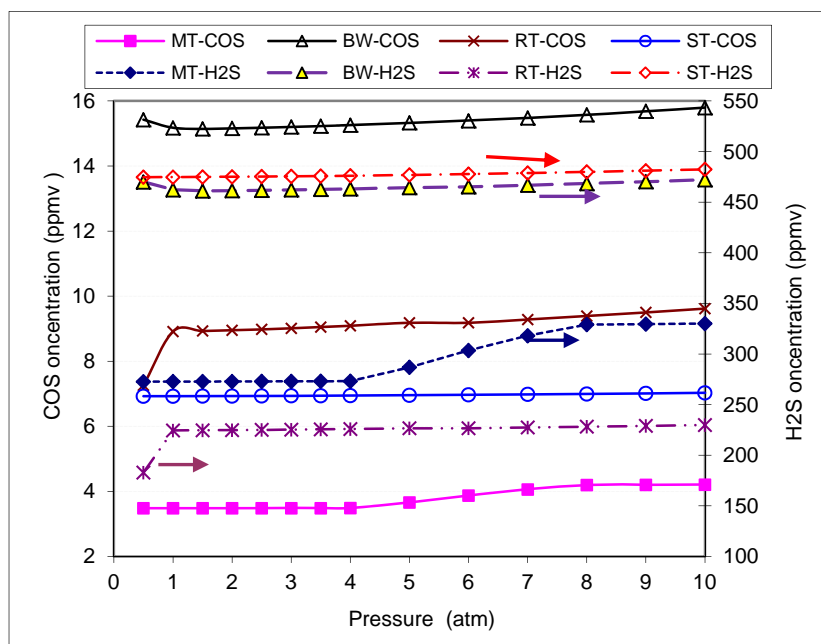


Figure 4- 3 Effect of pressure on  $\text{H}_2\text{S}$  and  $\text{COS}$  formation for gasification of MT, ST, RT and BW fuels at  $800^\circ\text{C}$

From **Figure 4- 3**, it can be seen that an increase of the pressure slightly promotes the formations of  $\text{H}_2\text{S}$  and  $\text{COS}$ , especially for MT fuel. The similar result is reported by Stinnett et al. (Stinnett et al., 1974). The authors mentioned that pressure has very little effect upon the distribution of components in the gas equilibrium at a range of 1 to 50 atm within the temperature range from 1000 to  $3500^\circ\text{F}$ , e.g. the equilibrium mole fraction of  $\text{H}_2\text{S}$  changes by about 3%. For MT fuel, when the pressure

increases from 4 to 8 atm, the concentrations of H<sub>2</sub>S and COS showed a much higher increase and then remained constant. For RT fuel, it seems that reduced pressure gasification can significantly decrease the formations of H<sub>2</sub>S and COS. Their concentrations increased from 183 to 225 ppmv, and 7 to 9 ppmv, respectively, with the pressure changed from 0.5 to 1 atm and then kept almost constant. However, an opposite phenomenon was observed for BW fuel. Unfortunately, there is not so much available experimental data in the literature which can be used to explain these observations.

The other species, except for CS, CS<sub>2</sub>, and H<sub>2</sub>S<sub>2</sub> remained relatively constant in concentrations with varying pressure, and the left sulfur species decreased markedly with increasing pressure (**Figure A-4**, see Appendix). Some similar finding is reported by Nichols et al. (Nichols et al., 1989). They reported that during coal gasification increased pressure shifted the distribution of sulfur among gas phase species; yielding higher H<sub>2</sub>S, COS and lower SO<sub>2</sub> concentration and the levels of H<sub>2</sub>S were about 300 ppm higher at 5atm than H<sub>2</sub>S levels at 1atm. In their study, sulfur species concentrations also were predicted by chemical equilibrium calculations which also show that as pressure increased from 1 to 10 atm the concentration of SO<sub>2</sub> decreased significantly and the concentrations of H<sub>2</sub>S and COS also increased. However, Nichols et al. (Nichols et al., 1989) also reported that the CS<sub>2</sub> levels decrease markedly with increasing pressure, even more so than did the SO<sub>2</sub> levels.

#### **4.2.4 Effect of ER**

The variation of the concentration of H<sub>2</sub>S and COS as a function of ER by using MT, ST, RT and BW fuels are shown in **Figure 4- 4**. From **Figure 4- 4**, it can be seen that an opposite formation trend of H<sub>2</sub>S and COS is observed by using different fuels. For MT and ST fuel, an increase in ER in the range of 0.2 to 0.6 led to higher H<sub>2</sub>S and COS levels, from 255 to 319 ppmv, 443 to 548 ppmv, and 3 to 4 ppmv, 5 to 6 ppmv, respectively. These results agree regarding qualitative trends with experimental and predicted results reported by Dias and Gulyurtlu (Dias & Gulyurtlu, 2008). They reported that H<sub>2</sub>S levels increased from 672 up to 1204 ppmv with increasing ER from 0 to 0.4, and the concentration of sulfur oxidized species such as SO<sub>2</sub> and COS also increased in different proportions. For MT and ST fuels, oxygen-steam was used as gasifying agent in the modeling. The presence of steam maybe acts as a hydrogen donor and then promotes the formation of H<sub>2</sub>S.

For BW and RT fuels, with varying quantities of air and no steam added (see **Table 4- 2**), the main tendency was that ER decrease on the formations of H<sub>2</sub>S and COS. Similar results are also reported by different researchers (Nichols et al., 1989; Pinto et al., 2008; Pinto et al., 2007). Nichols et al. (Nichols et al., 1989) reported that an increase in ER, in the absence of steam produced larger decrease of H<sub>2</sub>S and CS<sub>2</sub> in the obtained product gas and hence resulting in SO<sub>2</sub> formation. An increase in the formation of SO<sub>2</sub> was also observed during our simulation (**Figure A-5**, see Appendix). Pinto et al. (Pinto et al., 2008; Pinto et al., 2007) also reported that the increase of the oxygen flow rate resulted in decreasing the H<sub>2</sub>S content in the product gas within the range of ER value tested from 0 to 0.6. For other sulfur species, except for CS and CS<sub>2</sub>, all increased with an increase of ER by using MT, ST and BW fuels, which partly agrees with the reported results in reference (Jazbec et al., 2004). However, for RT fuel, except for HS and SO<sub>2</sub>, other species decreased with increasing ER (**Figure A-5**, Appendix).

#### **4.2.5 Effect of minerals**

Besides the aforementioned parameters, the minerals in fuel also affect the concentrations of sulfur species. Miura et al. (Miura et al., 1989) claimed that elements such as Fe, Ni, Si, Al, Na, K, Mg, Ca, present in the fuel, might act as catalysts and affected the reaction rates in the gasification process. Khan (Khan, 1989) also investigated the effects of inorganic additives on the yield of gaseous sulfur. The results showed that the addition of CaO to coal significantly reduced the yields of H<sub>2</sub>S and COS. Chen et al. (Chen et al., 1999) also observed that minerals could act as sorbents for the H<sub>2</sub>S, and Ljung and Nordin (Ljung & Nordin, 1997) reported that a high retention of S and Cl due to the presence of high levels of Ca, K and Na in the biomass. Pinto et al. (Pinto et al., 2008; Pinto et al., 2007) reported that sulfur retention in the solids inside the gasifier especially favored by the presence of metals, such as Ca, Zn, Mn, that react with H<sub>2</sub>S to form metal sulfide, Fe also has a strong affinity for H<sub>2</sub>S, forming FeS. Attar and Dupuis (Attar & Dupuis, 1979) reported that part of the sulfur is retained in the solid as

alkaline sulfide due to the reaction of  $H_2S$  with the alkaline minerals and thereby prevent them from entering the gaseous phase. The predicted distribution of solid metallic compounds for gasification of different fuels at different temperatures is shown in **Figure 4- 5**.

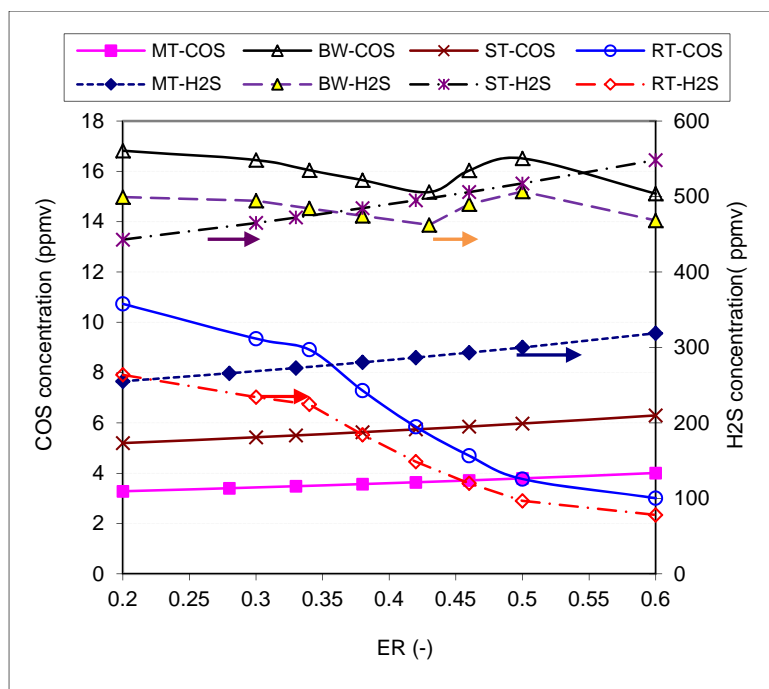


Figure 4- 4 Effect of ER on  $H_2S$  and COS formation for gasification of MT, ST, RT, BW fuels at 800 °C

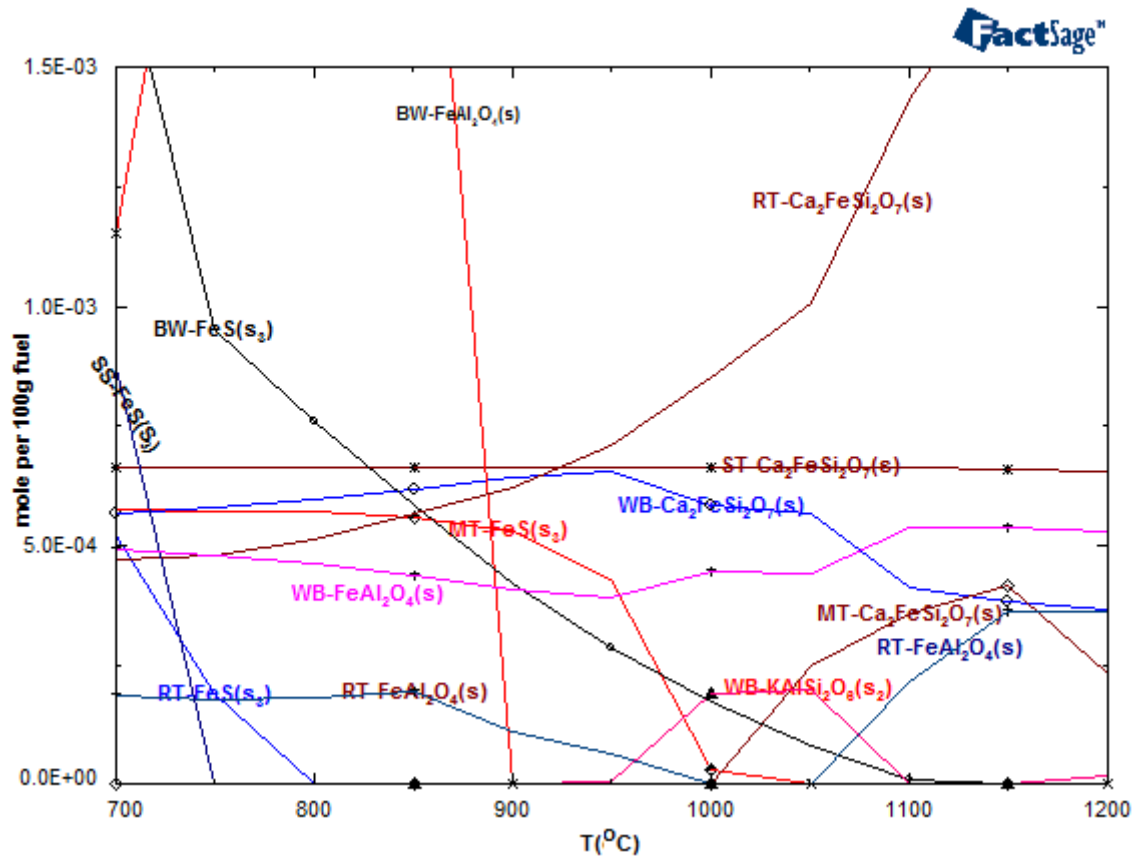


Figure 4- 5 Predicted distributions of solid metallic compounds for the gasification of six biomass fuels at different temperatures

From **Figure 4- 5**, it can be seen that FeS is the only sulfide which can be predicted with a relatively high amount. For WB and ST fuels, there is no FeS predicted in the model, simultaneously similar tendency of H<sub>2</sub>S is observed. For SS, RT, MT, and BW fuels, the disappearance of FeS in the solid phase took place at the temperature of 750, 800, 1000, and 1100 °C, meanwhile, different tendency of H<sub>2</sub>S was also predicted (see **Figure 4- 2**). This finding shows that Fe in fuels has a significant influence on the concentration profile of H<sub>2</sub>S, which agree with the reported results reported by other researchers (Gerasimov & Bogacheva, 2001a; Khan, 1989; Kuramochi et al., 2005; Pinto et al., 2008; Pinto et al., 2007). Other sulfur sulfides favored at low temperature, such as CaS, K<sub>2</sub>SO<sub>4</sub>, Na<sub>2</sub>SO<sub>4</sub>, MgS, SiS and SiS<sub>2</sub>, are almost not predicted at temperatures higher than 700 °C. With increasing temperature, different other kinds of non-sulfur containing solid metallic compounds are formed, which are predominantly Ca<sub>2</sub>FeSiO<sub>7</sub>, KAlSi<sub>2</sub>O<sub>6</sub> and FeAl<sub>2</sub>O<sub>4</sub>.

### 4.3 Conclusion of sulfur distribution modeling

The formation behavior of sulfur compounds during gasification is influenced by fuel characteristics and process conditions such as temperature, pressure and ER. The predicted results show that in the gasification of all the used biomass fuels, H<sub>2</sub>S is the predominant sulfur species and its maximum concentration is closely related to the fuel-S content. For all the fuels, around 95% fuel-S convert into H<sub>2</sub>S during the reaction. However, the percentage of Fuel-S convert into COS is much more affected by the gasifying agent. Minerals in the fuels play an important role in the retention of sulfur in the solid phase, especially the metal Fe. The increase of temperature is in favor of the formation of major gaseous sulfur species with a various increase in their amounts. The H<sub>2</sub>S and COS formation is promoted by an increase in pressure; however, most other kinds of sulfur species show an opposite tendency. ER combined with different gasifying agent seems to have a more complicated influence on all the sulfur species. The fuel characteristics and the process conditions all could affect the formation of sulfur compounds in the gasification process from different points of view. Satisfactory agreement and dissatisfactory variance both are observed considering the comparison with experimental and predicted results in the literature. As a conclusion, although the release of sulfur compounds is a complex issue which could be influenced by various parameters, the Factsage<sup>TM</sup> equilibrium model seems to be useful in predicting their behavior. However, a pure-equilibrium model has its limitations since the reactions and mass transfer in the real gasification process are usually controlled by non-equilibrium factors, which could be the reason why some simulation results cannot be appropriately explained, like the formation of sulfur components by using SS fuel within the temperature range of 800 to 900 °C. Unfortunately, not many experimental data about sulfur species are available to empirically modify the predicted results.

### 4.4 Sulfur capture modeling procedure

After understanding the distribution behavior of sulfur compounds during gasification, the next step is to remove them by using different sorbent materials. Thus, two main objectives have been considered in this part study: (1) to use thermodynamic equilibrium analysis to identify the effective sorbent materials which can chemically bind sulfur to reduce its emissions; and (2) to determine the most effective sorbent among the various materials. Based on the overview of literature (Elseviers & Verelst, 1999; Gasper-Galvin et al., 1998; Westmoreland & Harrison, 1976), the sorbent materials considered in this part study and a summary of their equilibrium products formed during sulfidation reaction are listed in **Table 4- 5**.

Since the product gas composition can vary over a wide range depending on fuel type and gasification operating conditions, three simulated gases based on gas compositions obtained from typical gasifiers (Texaco, Shell and the CFB gasifiers) were used for the thermodynamic analysis of sorption with various sorbents for H<sub>2</sub>S removal. The gas composition of Texaco and Shell are cited from the references (Ben-Slimane & Hepworth, 1994a; Berns et al., 1997). For the third simulated gases, the gas composition was calculated using the Factsage<sup>TM</sup> software where the input data based on DDGS fuel gasified in the CFB gasifier. **Table 4- 6** presents the simulated gas composition used in desulfurization and regeneration (simply called Texaco gas, Shell gas, and CFBG gas).

Because sulfur concentration varies significantly from percent levels in fossil fuels to ppmv levels in biomass fuels, calculations were not conducted for a specific application. For the desulfurization simulation the influence of temperature from 300 to 1500 °C on the equilibrium H<sub>2</sub>S concentration at atmospheric pressure was studied for each case, using the simulated gases as input data. For the regeneration simulation, spent desulfurization sorbent was fed to an equilibrium reactor using various O<sub>2</sub> concentrations. The H<sub>2</sub>S equilibrium concentration, equilibrium products and phase stability diagram for Fe, Mn oxides at various temperatures during regeneration were also calculated using the Factsage<sup>TM</sup> software based on the minimization of the Gibbs energy.

*Table 4- 5 Sorbent considered in the desulfurization simulation and equilibrium products*

Metal type	Considered sorbent	Reaction product at equilibrium phase
Ca	CaCO <sub>3</sub> , CaO, CaCO <sub>3</sub> ·MgCO <sub>3</sub>	CaS
Fe	Fe <sub>3</sub> O <sub>4</sub> , FeO, Fe <sub>2</sub> O <sub>3</sub>	FeS
Mn	MnO <sub>2</sub> , MnO, Mn <sub>3</sub> O <sub>4</sub>	MnS
Cu	CuO	Cu <sub>2</sub> S
Zn	ZnO	ZnS

*Table 4- 6 Simulated gas compositions in desulfurization and regeneration*

Type	CO	CO <sub>2</sub>	H <sub>2</sub>	N <sub>2</sub>	H <sub>2</sub> O	H <sub>2</sub> S	O <sub>2</sub>
Desulfurization (vol.%, wet)							
SHELL	64	0.8	31.6	0.7	1.5	1.4	-
Texaco	39.1	12.3	30.1	0	17.5	1	-
CFBG	14.1	14.9	32.5	1.43	36.8	0.17	-
Regeneration	N <sub>2</sub> as balance					5%, 20%, 40%, 100%	

## 4.5 Sulfur capture modeling results

### 4.5.1 Sulfidation simulation analysis

The sulfidation simulation results of for Texaco, Shell and CFBG gas are shown in **Figure 4- 6** and **Figure 4- 7** and **Figure 4- 8**, respectively. If the H<sub>2</sub>S concentration of 100ppmv is considered allowable (Berns et al., 1997; Elseviers & Verelst, 1999), from these figures it can be seen that iron, manganese, zinc and copper oxides are suitable for desulfurization when the temperature is lower than 500°C for all three simulated gases. The desulfurization capacity of calcium based materials depends more on the simulated gas compositions than other oxides.

#### 4.5.1.1 Zinc Oxide

For Texaco, Shell and CFBG gas, zinc oxide was capable of reducing the H<sub>2</sub>S concentration to a value lower than 50 ppmv up to 700 °C. With increasing temperature from 700 to 800 °C, the H<sub>2</sub>S concentration increased sharply from 53 to 293 ppmv, 42 to 263 ppmv, and 53 to 294 ppmv, respectively. The rapid increase in H<sub>2</sub>S concentration is attributed to the zinc vaporization at temperatures above 700 °C. These results fairly agree with reported values in the literature. Lew et al. (Lew et al., 1989) reported that the kinetics of the ZnO-H<sub>2</sub>S reaction is rapid and ZnO can reduce the H<sub>2</sub>S concentration from 5000 ppmv to less than 10 ppmv. However, zinc sorbents cannot be used at temperatures above 600 °C due to the subsequent vaporization of zinc which results in a rapid decrease in the sulfur capture capacity (Garcia et al., 1997; Ko et al., 2005; Zeng et al., 2000). Westmoreland and Harrison (Westmoreland & Harrison, 1976) reported that zinc is limited to a maximum temperature of approximately 700 °C because of the formation of zinc vapor. Experimental observations in their laboratory have confirmed the formation of zinc vapor in similar atmospheres at temperatures in excess of 700 °C.



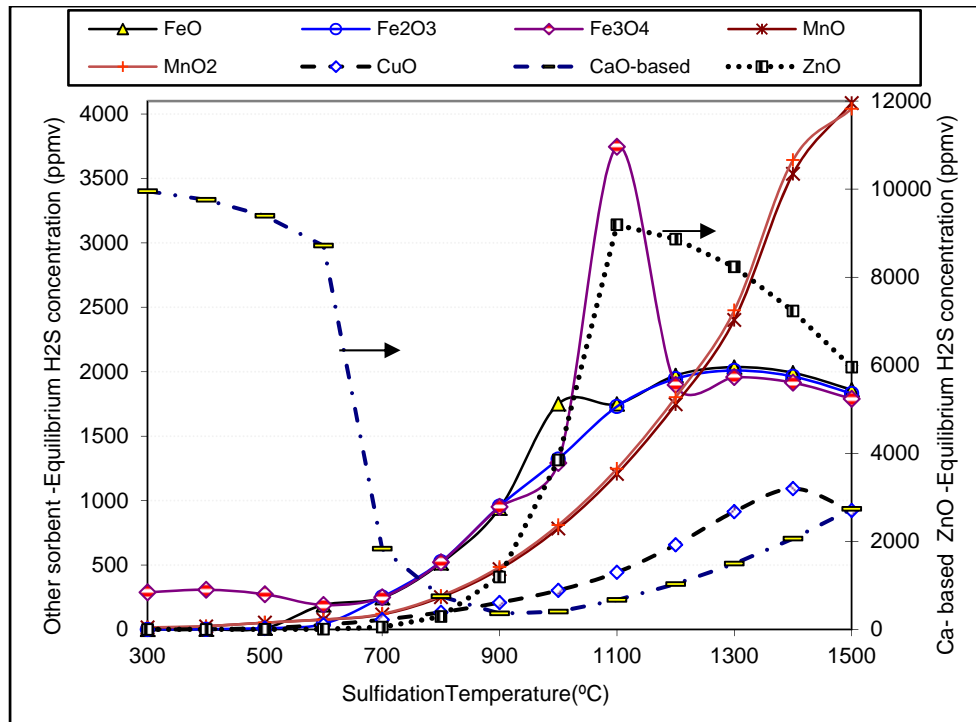


Figure 4- 6  $H_2S$  equilibrium concentration as a function of temperature for Texaco gas with various sorbents

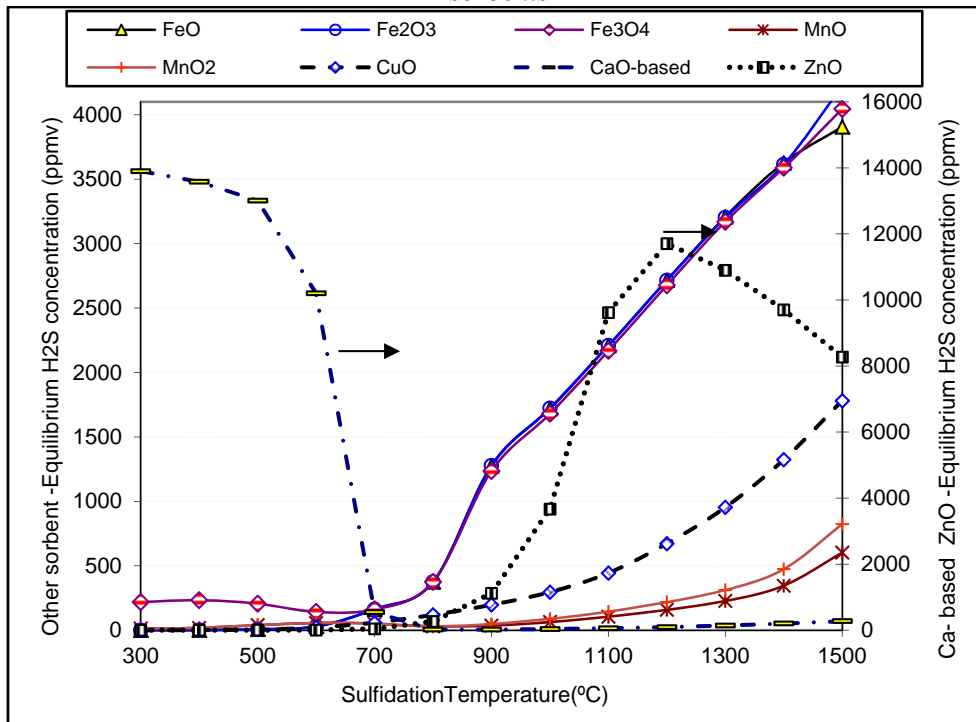


Figure 4- 7  $H_2S$  equilibrium concentration as a function of temperature for Shell gas with various sorbents

#### 4.5.1.2 Manganese Oxides

For Texaco, Shell and CFBG gas, manganese oxides can keep  $H_2S$  concentration lower than 80 ppmv up to 700, 1000 and 500 °C, respectively. These findings fit the reported results by other researchers Berns et al. (Berns et al., 1997) studied sulfidation thermodynamics of different manganese oxide by using Shell gas, and the equilibrium calculations shows that the lower the temperature the lower the equilibrium  $H_2S$  concentration. Shell gas can theoretically be desulfurized with MnO to IGCC specification at temperatures exceeding 900 °C. Ben-Slimane et al. (Ben-Slimane & Hepworth, 1994a;

Ben-Slimane & Hepworth, 1994b; Ben-Slimane & Hepworth, 1995) studied the desulfurization of hot coal-derived fuel gases with Mn-based sorbents. The kinetics studies have shown that manganese oxide is stable for hot gas desulfurization up to around 700 °C with high sulfur capacity between 600 and 700 °C. Westmoreland and Harrison (Westmoreland & Harrison, 1976) also reported that high fractional desulfurization of manganese oxides is predicted for temperatures in excess of 1000 °C and has a great desulfurization potential within the temperature range from 600 to 700 °C.

#### **4.5.1.3 Copper Oxide**

For Texaco, Shell and CFBG gas, at a temperature of 700 °C, a fairly low H<sub>2</sub>S concentration of 76, 59 and 75 ppmv was achieved by using copper oxide, respectively. Higher temperatures led to an increase of H<sub>2</sub>S equilibrium concentration, whereas changed less rapidly compared to zinc oxide. The predicted results are similar to the reported results in the literature. Westmoreland and Harrison (Westmoreland & Harrison, 1976) reported that copper can maintain 95% desulfurization capability to a temperature in excess of 900 °C. Abbasian and Slimane (Abbasian & Slimane, 1998) pointed out that a fortuitous feature of a copper based sorbent is its capability to achieve extremely low levels of H<sub>2</sub>S in the cleaned fuel gas. The optimum desulfurization temperature in terms of sorbent efficiency and utilization for HGD is around 600 °C. The increase of H<sub>2</sub>S concentration at higher temperature is mainly due to high temperatures favoring the complete reduction of copper compounds even in slightly reducing atmosphere. Swisher and Schwerdtfeger (Swisher & Schwerdtfeger, 1992) reported that for Cu-based sorbents, the kinetics of the sulfidation reaction is fast for Cu in the +2 or +1 oxidation states. However, CuO<sub>x</sub> is easily reduced to Cu, which has a slow kinetics for H<sub>2</sub>S removal.

#### **4.5.1.4 Iron Oxides**

Iron oxide desulfurization potential is somewhat lower compared to the other materials. For Texaco, Shell and CFBG gas, FeO and Fe<sub>2</sub>O<sub>3</sub> had the similar sulfur capture capacity as a function of the temperature. A lower H<sub>2</sub>S concentration of 10, 25 and 29 ppmv was achieved using FeO and Fe<sub>2</sub>O<sub>3</sub> up to a temperature of 500 °C for Texaco and CFBG gas, and 600 °C for Shell gas. However, Fe<sub>3</sub>O<sub>4</sub> showed less desulfurization capability at a temperature of lower than 600 °C compared to FeO and Fe<sub>2</sub>O<sub>3</sub>. For all the gases, FeO, Fe<sub>2</sub>O<sub>3</sub> and Fe<sub>3</sub>O<sub>4</sub> had similar low sulfur removal capacity at a temperature higher than 600 °C. Gupta et al. (Gupta et al., 1992) reported that for iron oxide sorbents higher temperatures (>550 °C) lead to severe sorbent decrepitation due to excessive reduction and iron carbide formation. The formation of solid carbon deposition inside sorbent pores and on the surface quickly limits further sulfidation. Focht et al. (Focht et al., 1988) mentioned that at 700 °C Fe<sub>3</sub>O<sub>4</sub> is easily reduced to FeO and the reduction to FeO has been shown to have a detrimental effect on sulfidation. So, although iron oxide has a high sulfur capture capacity and possesses high reactivity for H<sub>2</sub>S, its applicability is limited to measured temperatures of above 600 °C.

#### **4.5.1.5 Calcium Based Materials**

Compared to other materials, dolomite, limestone and lime exhibited fairly similar sulfur removal capabilities and had different sorption tendencies as a function of the temperature. For all the gases, calcium based materials had very low desulfurization capability when the temperature was lower than 900 °C, while for other metal oxides high desulfurization efficiency were observed at same temperature. The H<sub>2</sub>S equilibrium concentration for Texaco and CFBG gas was observed to be much higher than for other metal oxides. Nevertheless, for Shell gas, with very low CO<sub>2</sub> and H<sub>2</sub>O content, the calcium based materials exhibited high desulfurization efficiency at higher temperatures. Similar results have been reported by other researchers (Ben-Slimane & Hepworth, 1994a; Fenouil, 1994; Westmoreland & Harrison, 1976). Westmoreland and Harrison (Westmoreland & Harrison, 1976) reported that the maximum desulfurization of CaCO<sub>3</sub> occurs near 880 °C, the temperature at which CaCO<sub>3</sub> decomposes to CaO. Fenouil et al. (Fenouil, 1994) also pointed out that calcium oxide is an attractive material because it is inexpensive, readily available, and it is an effective sorbent at temperatures within the range from 800 to 1200 °C. Van der Ham et al. (Van der Ham et al., 1996) reported that the sulfidation temperature for Shell gas should be at a level of at least 815 to 845 °C to achieve H<sub>2</sub>S concentration of 20 ppmv.

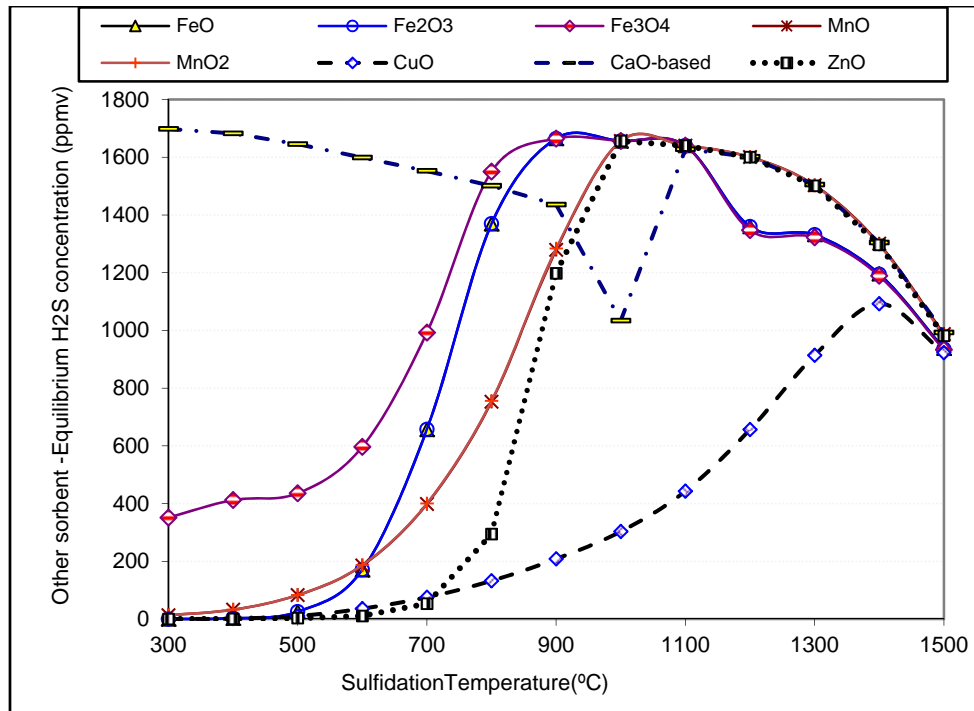


Figure 4- 8  $H_2S$  equilibrium concentration as a function of temperature for CFBG gas with various sorbents

#### 4.5.2 Regeneration simulation analysis

Since regeneration of used sulfur sorbents is of importance for the process economics as well as reducing environmental disposal problems, the regeneration simulation results of zinc oxide, copper oxide and calcium based materials as a function of temperature and  $O_2$  partial pressure are shown in **Figure 4- 9**, **Figure 4- 10** and **Figure 4- 11**, respectively.

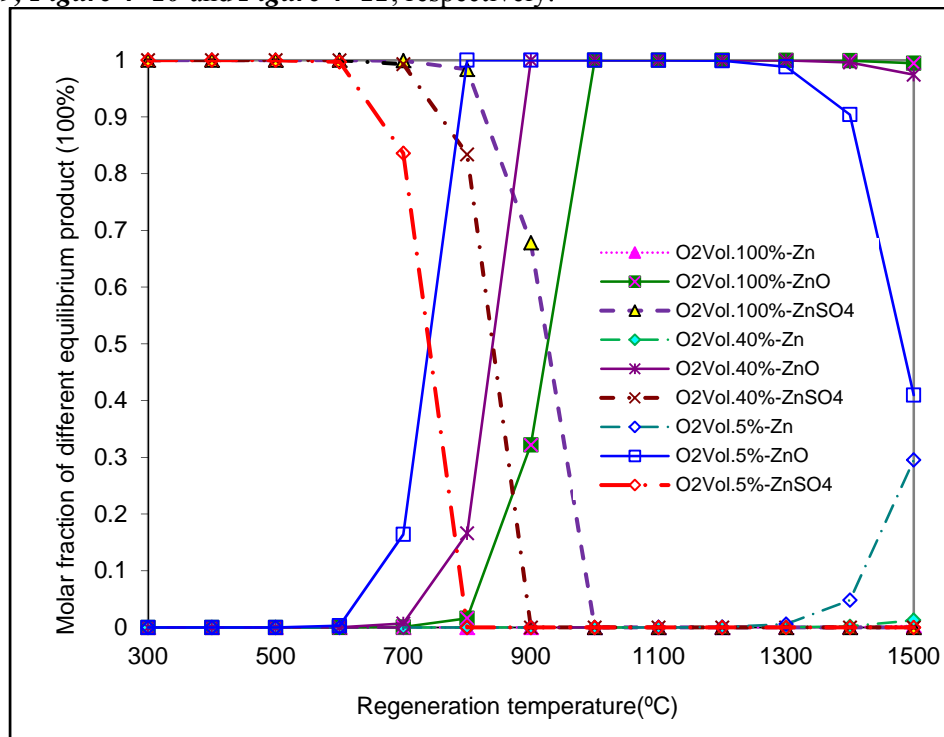


Figure 4- 9  $ZnO$ ,  $Zn$  and  $ZnSO_4$  formation during  $ZnS$  regeneration ( $O_2$  volume fraction in regenerator feed gas: 5%, 40% and 100%)

#### 4.5.2.1 Zinc Oxide

From **Figure 4- 9**, it can be seen that temperatures in excess of 700 °C are required to avoid ZnSO<sub>4</sub> formation and that the minimum regeneration temperature strongly increases with the partial pressure of oxygen. However, regeneration at higher temperatures leads to severe excessive thermal sintering which is reported by Garcia et al. (Garcia et al., 1997). Also from an economic point of view, in order to obtain SO<sub>2</sub> concentration being suitable for H<sub>2</sub>SO<sub>4</sub> production the oxygen molar fraction in the feed gas should be higher than 10%. This implies that regeneration should be carried out at 800°C at least, whereas desulfurization had better to be carried out at much lower temperatures to avoid the volatilization of zinc. In this way, implementation on an industrial scale will yield a more complex unit and different operation temperature could also result a loss the overall thermal efficiency.

#### 4.5.2.2 Copper Oxide

The predicted optimum temperature of operation for hot gas desulfurization by using copper oxide is around 800 °C. From **Figure 4- 10**, it can be seen that the best regeneration temperature is also within the temperature range from 600 to 900°C, which favorably improves the overall thermal efficiency of the process. At a temperature of 900 °C, the main regenerated product was CuO even with different O<sub>2</sub> volume content, while at a temperature higher than 1000 °C, Cu<sub>2</sub>O and CuO were both found in the regenerated sorbents, and Cu<sub>2</sub>O gradually changed to the main product at a temperature higher than 1200 °C. During the regeneration process, Cu in Cu-based sorbents could undergo crystal growth and thermal sintering, decreasing the sulfur capture capacity. Therefore, in order to increase the thermal stability and to maintain copper in the +2 or +1 oxidation states, as well as keep the copper oxide in a highly dispersed state. Alonso et al. (Alonso et al., 2000) suggested that copper-based sorbents are better to be mixed with other metal oxides.

#### 4.5.2.3 Calcium Based Materials

Dolomite, limestone and lime calcium based materials have been widely used in fluidized beds as “in-bed” materials and additives as non-regenerable desulfurization sorbents for decades largely due to their low cost and naturally availability. However, the large quantities of spent sorbents produced with limestone and dolomite contain calcium sulfide which is not environmentally stable and H<sub>2</sub>S could be released in air with high moisture content, and thus requires a further stabilization step to convert calcium sulfide to environmentally acceptable material for landfill disposal. Due to this reason, the regeneration of calcium based materials is also currently considered. From **Figure 4- 11** we can see that the regeneration of CaS need to be performed at temperatures higher than 1100 °C, since CaSO<sub>4</sub> is the main product at lower temperature. A similar result was also reported by Van der Ham et al. (Van der Ham et al., 1996) who reported that for thermo-dynamic reasons the regeneration temperature of calcium based sorbents of at least 1100 to 1200 °C should be applied. Considering the different temperature between sulfidation and regeneration, as well as the overall thermal efficiency and investment cost, the regeneration of calcium based materials still need to be further taken into account. Furthermore, CaSO<sub>4</sub> also has some practical applications such as being used as filler material in constructions.

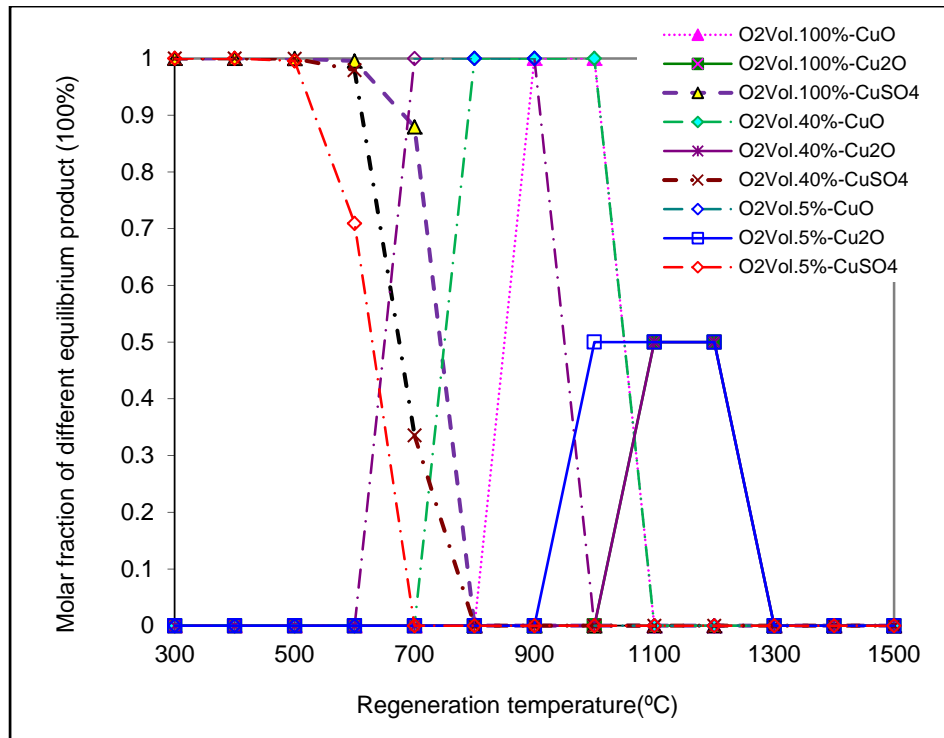


Figure 4- 10  $\text{CuO}$ ,  $\text{Cu}_2\text{O}$  and  $\text{CuSO}_4$  formation during  $\text{Cu}_2\text{S}$  regeneration ( $\text{O}_2$  volume fraction in regenerator feed gas: 5%, 40% and 100%)

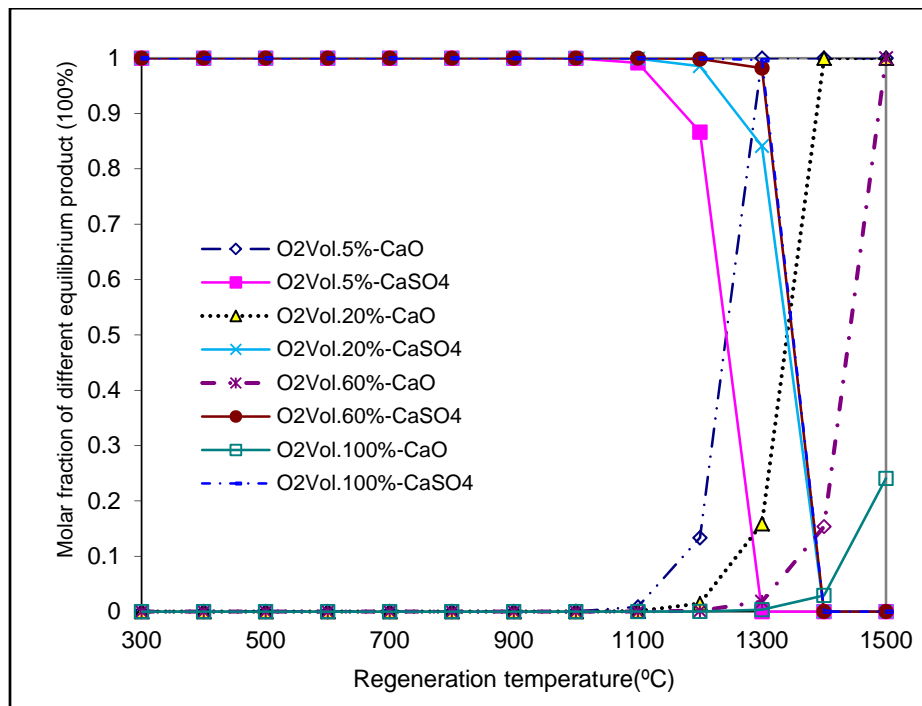


Figure 4- 11  $\text{CaO}$  and  $\text{CaSO}_4$  formation during  $\text{CaS}$  regeneration ( $\text{O}_2$  volume fraction in regenerator feed gas: 5%, 20%, 60% and 100%)

#### 4.5.2.4 Manganese Oxides

Considering that manganese and iron oxide have various states, phase stability diagrams of the Fe-S-O and the Mn-S-O system at different temperatures were calculated. During the regeneration of MnS with  $\text{O}_2$  several reactions can occur (Berns et al., 1997) (see below equations *Eq.4- 1*→*Eq.4- 4*).



Equation **Eq.4- 1** is the most desirable reaction for the regeneration of MnS. Oxidation of Mn oxides could also occur based on equations **Eq.4- 2** and **Eq.4- 3**. The sulfation of MnS as shown in equation **Eq.4- 4** is especially undesirable because the production of manganese sulfate will cause the sorbent pellets to spall and crack. To prevent sulfation, the conditions under which it occurs must be avoided. A phase stability diagram of Mn-S-O at a temperature of 900 and 1500 °C is shown in **Figure 4- 12** ( For results obtained at 600 and 1200 °C, see Appendix **Figure A-6**), where the unit for P(O<sub>2</sub>) and P(SO<sub>2</sub>) is atm.

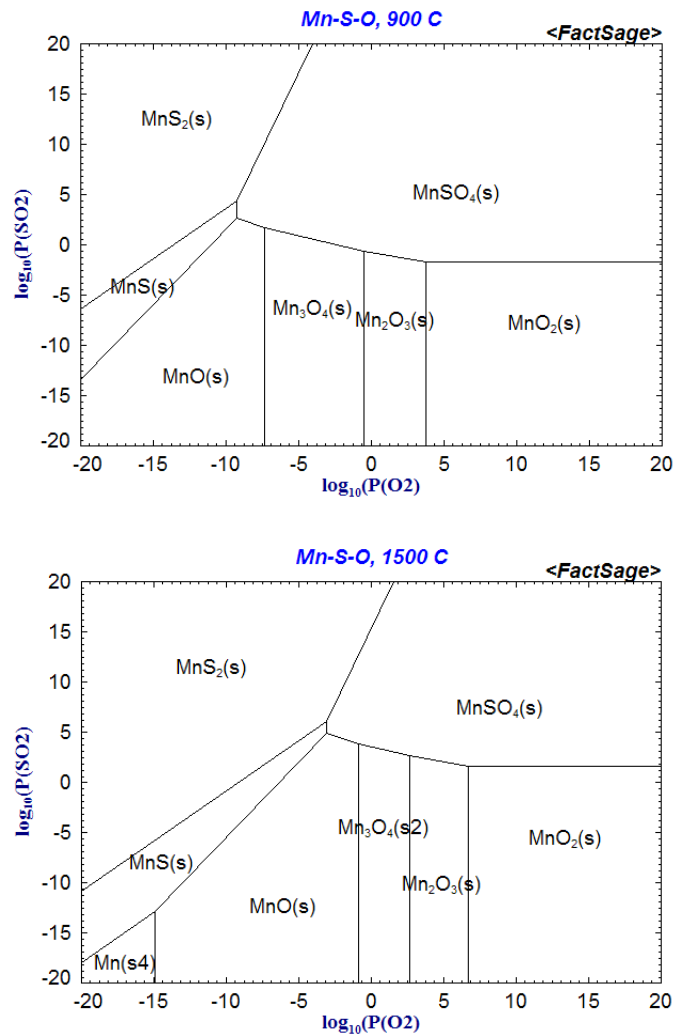


Figure 4- 12 Phase stability diagram for the Mn-S-O system at 900 and 1500 °C

From these figures it can be seen that Mn<sub>2</sub>O<sub>3</sub> and Mn<sub>3</sub>O<sub>4</sub> are the most stable forms, whereas MnO and MnO<sub>2</sub> cannot co-exist. The regeneration should be conducted at a temperature higher than 900 °C when regenerating with oxygen at ambient pressure to prevent the formation of MnSO<sub>4</sub>. Lowering the O<sub>2</sub> and/or the SO<sub>2</sub> partial pressure will result in lower MnSO<sub>4</sub> stability. By using a regeneration gas with O<sub>2</sub> volume content of 5%, 40% and 100% at a temperature of 900 and 1500 °C, the main species in the regenerated products were Mn<sub>2</sub>O<sub>3</sub>, Mn<sub>2</sub>O<sub>3</sub>/Mn<sub>3</sub>O<sub>4</sub>, Mn<sub>3</sub>O<sub>4</sub>, and MnO, Mn<sub>3</sub>O<sub>4</sub>, respectively.

#### 4.5.2.5 Iron Oxides

A phase stability diagram of Fe-S-O system at different temperatures was also plotted to have a better understanding of chemical changes occurring during regeneration reaction. The phase stability diagram of Fe-S-O at a temperature of 900 and 1500 °C is shown in **Figure 4- 13** ( For results obtained at 600 and 1200 °C, see Appendix **Figure A-6**), where the unit for  $P(O_2)$  and  $P(SO_2)$  is atm.

From these figures, it can be seen that FeS, FeSO<sub>4</sub>, Fe<sub>2</sub>(SO<sub>4</sub>)<sub>3</sub>, Fe<sub>2</sub>O<sub>3</sub>, Fe<sub>3</sub>O<sub>4</sub> and FeO different forms may occur as the reaction products. FeSO<sub>4</sub> and Fe<sub>2</sub>(SO<sub>4</sub>)<sub>3</sub> are only stable in some areas with a fairly high SO<sub>2</sub> partial pressure. Thus, during the regeneration process, increasing regeneration temperature or lower O<sub>2</sub> concentration is assumed to be the possible way to overcome sulfate formation. These figures also indicate that the partial pressure of O<sub>2</sub> had less effect than temperature on the regeneration process. At a regeneration temperature of 900 and 1200 °C Fe<sub>2</sub>O<sub>3</sub> was the main species in the regenerated sorbents which is also reported by Fuda et al. (Fuda et al., 1991). By using the regeneration gas with 5vol.% O<sub>2</sub> at a temperature of 1500 °C, Fe<sub>3</sub>O<sub>4</sub> was becoming the main regenerated product, while at 600 °C some Fe<sub>2</sub>(SO<sub>4</sub>)<sub>3</sub> would be produced which should be avoided in the operation.

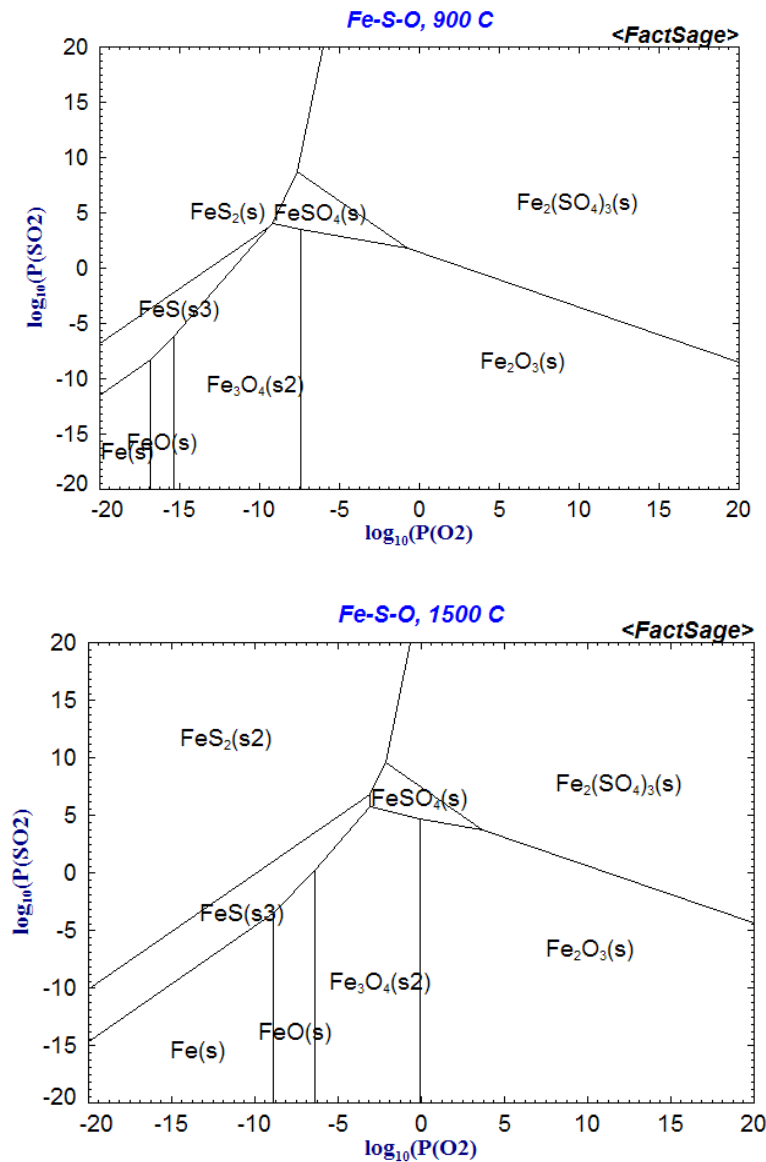


Figure 4- 13 Phase stability diagram for the Fe-S-O system at 900 and 1500 °C

## 4.6 Conclusion of sulfur capture modeling

Sulfidation and regeneration simulations have been performed using the Factsage<sup>TM</sup> equilibrium and phase stability diagram models by applying the free energy minimization method, which appears to be a useful tool for predicting and analyzing performance of sulfur sorbent materials. Even though only single metal oxide systems are examined, the results will favor in the further study of mixed-metal sorbent compounds. Copper, manganese and zinc oxides are the most favorable metals, which are capable of reaching even ppb level at a temperature of about 650 °C. However, evaporation, sintering and excessive temperature rising during regeneration may have a negative impact on their performance, especially at higher temperatures. For desulfurization at temperatures higher than 900 °C, calcium based oxides exhibit a better potential than other metal oxides. However, their desulfurization capabilities are strongly limited by the appropriate temperature range and gas composition especially the H<sub>2</sub>O and CO<sub>2</sub> content. Supporting the oxides on a carrier material or using mixed metal oxides can be one of the most suitable approaches to reduce or solve the volatilization and sintering problems during sulfidation and generation. As a conclusion, the simulation results achieved in this study show a fairly good agreement with predicted and experimental results in the literature. Furthermore, the reaction process involved in the desulfurization process of a real gasifier is much more complicated than is described by just chemical phase equilibrium modeling, thereby this part simulation results can only be used as a reference for improving the efficiency of sorbent utilization and optimize the desulfurization process.



## **5 Biomass gasification in the steam-O<sub>2</sub> blown CFB and the steam blown PBFB gasifiers: Effects of operational conditions on product gas distribution and tar formation**

---

*This chapter presents the experimental results concerning effects of operational conditions (e.g., steam to biomass mass ratio (SBR), oxygen to biomass stoichiometric ratio (ER), gasification temperature, and pressure) and bed materials on the distribution of main product gas, sulfur and tar formation from Agrol, willow and DDGS gasification using the 100 kW<sub>th</sub> steam-O<sub>2</sub> blown CFB and the 30-40kW<sub>th</sub> PBFB gasifiers.*

*The results obtained from three fuels gasification in the CFB gasification has been published in the Biomass and Bioenergy Journal and the 8<sup>th</sup> International Symposium on Gas Cleaning at High Temperature, while results obtained from the PBFB gasifier have been published in the proceedings of the 19<sup>th</sup> European Biomass Conference and Exhibition and the Fuel Journal.*

**Meng, X., de Jong, W., Fu, N., Verkooyen, A.H.M.** 2011. Biomass gasification in a 100 kW<sub>th</sub> steam-oxygen blown circulating fluidized bed gasifier: Effects of operational conditions on product gas distribution and tar formation. *Biomass and Bioenergy*, **35**(7), 2910-2924.

**Meng, X., de Jong, W., Fu, N.J., Verkooyen, A.H.M.** 2010. Primary results of dried distiller's grains with solubles gasification in a 100kW<sub>th</sub> steam-oxygen blown circulating fluidized bed gasifier. *The 8<sup>th</sup> International Symposium on Gas Cleaning at High Temperatures*, Taiyuan, Shanxi, China

Mayerhofer, M., Mitsakis, P., **Meng, X., de Jong, W., Spliethoff, H., Gaderer, M.** 2011. Influence of operational parameters on tar formation and main gas components during allothermal steam gasification. *Proceeding of 19<sup>th</sup> European Biomass Conference and Exhibition from Research to Industry and Markets* 6-10 June, Berlin, Germany.

Mayerhofer, M., Mitsakis, P., **Meng, X., de Jong, W., Spliethoff, H., Gaderer, M.** 2012. Influence of temperature, steam and pressure on tar and gas in allothermal fluidized bed gasification. *Fuel*, **99**, 204-209.

As mentioned in previous chapters, during biomass gasification, several parameters such as gasifier types, reaction temperature, biomass fuels properties, bed materials and gasifying agents have a substantial influence on product gas composition, carbon conversion efficiency and tar formation. The gasifying agents for fluidized bed biomass gasification can be either air, steam, pure oxygen or their combination. Since extensive studies have been published on biomass gasification with air, steam and air steam as gasifying agent, this first part study of this research is mainly focused on understanding how different operational conditions with an emphasis on steam to biomass mass ratio (SBR) affect the main product gas distribution, sulfur and tar formation produced from Agrol, willow and DDGS gasification using the 100 kW<sub>th</sub> steam-oxygen blown circulating fluidized bed (CFB) gasifier.

## 5.1 Biomass gasification using the CFB gasifier

To obtain a clean bio-syngas and to increase the net energy conversion efficiency, the gasification operating conditions need to be optimized. The effects of reaction temperature, ER, SBR and bed materials on the product gas composition and tar formation produced from Agrol, willow and DDGS are presented in the following parts.

As mentioned in chapter 3, an brief summary about experiments and their relevant conditions applied during Agrol, willow and DDGS gasification by using the steam-oxygen blown CFB gasifier at TUD are summarized in **Table A-1**(see Appendix). Among them, a selected summary of process parameters (e.g., SBR, ER, temperature, bed materials, SPA sample) for Agrol, willow and DDGS gasification at TUD is shown in **Table 5- 1**. Concerning four different bed materials used during measurement campaigns at TUD, their compositions have been summarized in **Table 3- 2** in chapter 3. In general, Bed 1 and Bed 2 are Austrian olivines, and the difference between these two Austrian olivines is that Bed 1 was pre-treated by about 1000 redox cycles in a fast internally circulating fluidized bed (FICFB) real gasification process, while bed 2 was untreated natural olivine (Bed 2). Bed 3 was a mixture of quartz sand and pre-treated olivine with a mass ratio around 50:50, while Bed 4 was untreated Scandinavian olivine.

Before detailed discussion, the changing trends of the product gas composition, reactor temperature during experiment as measured versus time during a day's experiment (23rd April, 2010) are presented in **Figure 5- 1**. T\_Aver\_Riser and T\_Aver\_Reactor represent the average temperature of the riser, and of riser and downcomer, respectively.

From this figure, some clear and important points can be concluded:

- 1) A relatively stable temperature profile was established in the whole reactor, which can be seen from the values of T\_Aver\_Riser and T\_Aver\_Reactor. The standard deviation of T\_Aver\_Riser and T\_Aver\_Reactor during stable operation condition was within 7 °C;
- 2) The concentrations of CO and H<sub>2</sub> obtained from Agrol, willow and DDGS were significantly different. However, no significant difference was observed for the concentration of CH<sub>4</sub> for all the fuels and that of CO<sub>2</sub> for Agrol and willow;
- 3) The reactor temperature remained fairly stable and similar during Agrol and willow gasification, while a sharply decreasing trend was observed by using DDGS fuel, which indicates a changed gasification environment inside the reactor. The decrease in the temperature could be due to an increase in steam flow rate and DDGS feeding rate;
- 4) No significant fluctuation was observed in the measured values of all dp-cells during Agrol gasification. A gradually increasing trend of dp-cell 7 and 9 values (downcomer) was found during willow gasification, and almost all dp-cells started to behave differently by changing from willow to DDGS (see **Figure A-7**, Appendix).

Table 5- 1 A selected summary of process parameters setting from Agrol, willow and DDGS gasification at TUD

SPA Sample	0413A	0413B	0413C	0413D	0415A	0415B	0415C	0415D	0415E	0415F
Fuel	Agrol									
Exp. No	A2	A2	A2	A2	A3	A3	A3	A3	A3	A3
SBR (-)	1.52	1.42	1.35	1.35	1.45	1.21	1.13	0.97	1.16	1.25
ER(-)	0.36	0.33	0.42	0.42	0.38	0.38	0.38	0.35	0.35	0.35
Temperature(°C)	730	730	780	820	770	770	775	815	810	810
Bed material	Bed 1	Bed 1	Bed 1	Bed 1	Bed 1	Bed 1	Bed 1	Bed 1	Bed 1	Bed 1
SPA Sample	0419A	0419B	0419C	0419D	0419E	0419F	0419G	0419H	0419I	0325W
Fuel	Willow									
Exp. No	W2	W2	W2	W2	W2	W2	W2	W2	W2	W1
SBR (-)	1.19	0.99	1.27	0.93	1.13	1.22	0.90	1.04	1.14	1.04
ER(-)	0.38	0.38	0.38	0.38	0.38	0.38	0.39	0.39	0.39	0.43
Temperature(°C)	740	740	740	780	780	780	820	820	820	820
Bed material	Bed 1	Bed 1	Bed 1	Bed 1	Bed 1	Bed 1	Bed 1	Bed 1	Bed 1	Bed 3
SPA Sample	0325 A	0423A	0423B	0423C	0423D	0423E	0421A	0421B	0423F	0423G
Fuel	Agrol	Agrol	Agrol	Agrol	Willow	Willow	DDGS	DDGS	DDGS	DDGS
Exp. No	A1	A4	A4	A4	W3	W3	D2	D2	D3	D3
SBR (-)	1.15	1.25	0.98	1.15	0.90	1.14	1.10	0.98	0.95	1.08
ER(-)	0.40	0.33	0.33	0.33	0.34	0.34	0.37	0.37	0.36	0.36
Temperature(°C)	820	770	800	800	800	800	730	740	750	750
Bed material	Bed 3	Bed 2	Bed 2	Bed 2	Bed 2	Bed 2	Bed 1	Bed 1	Bed 2	Bed 2

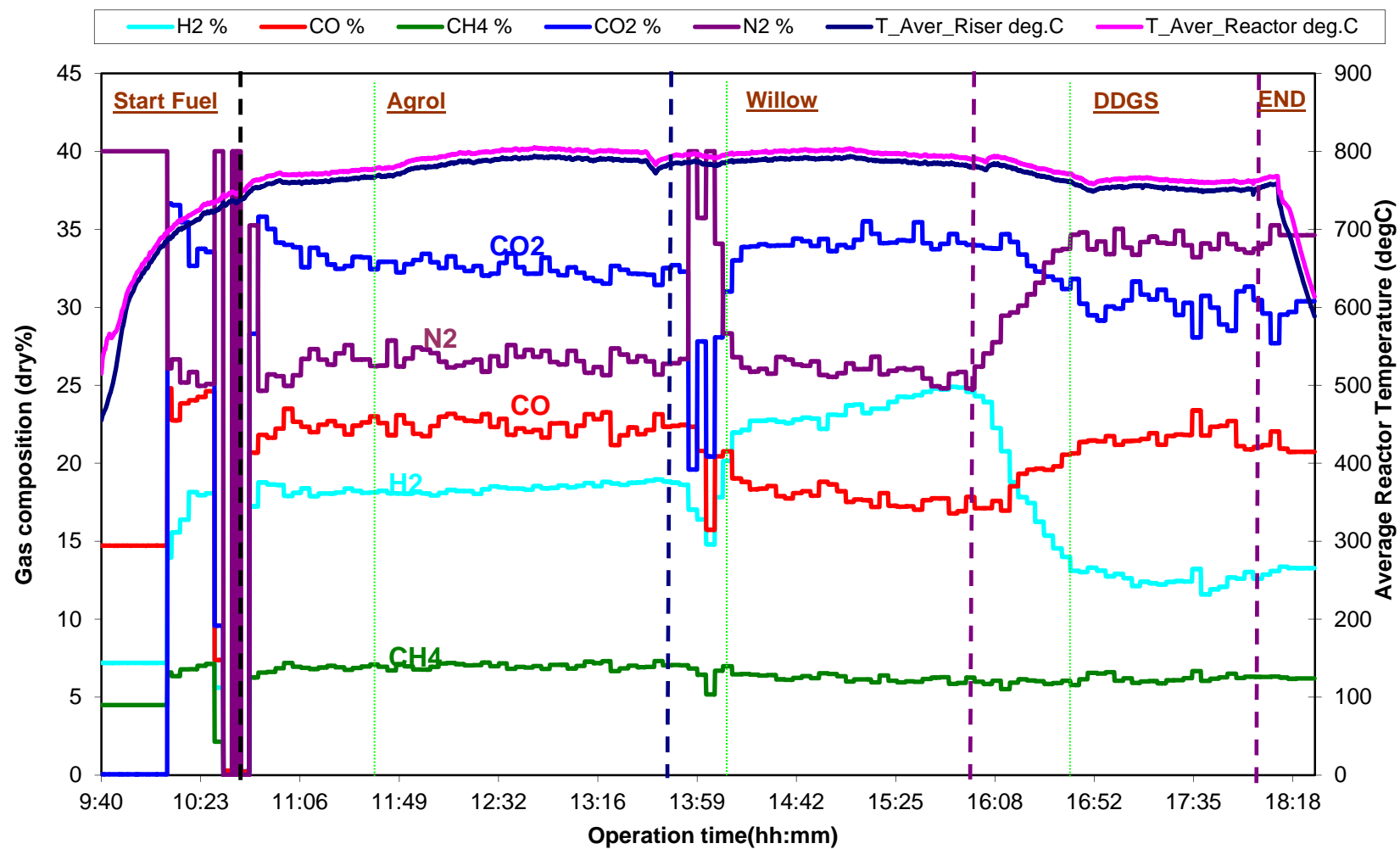


Figure 5- 1 Gas composition and reactor temperature trend lines as measured during the experiment on 23 April 2010

### 5.1.1 Effects of operational conditions on product gas composition

#### 5.1.1.1 Effect on main product gas composition

Effects of temperature, SBR, ER and bed materials on the composition of product gas obtained from Agrol, willow and DDGS gasification in the CFB gasifier is shown in **Figure 5- 2**, **Figure 5- 3** and **Figure 5- 4**, respectively. In these figures, A and W represent Agrol and willow, respectively.

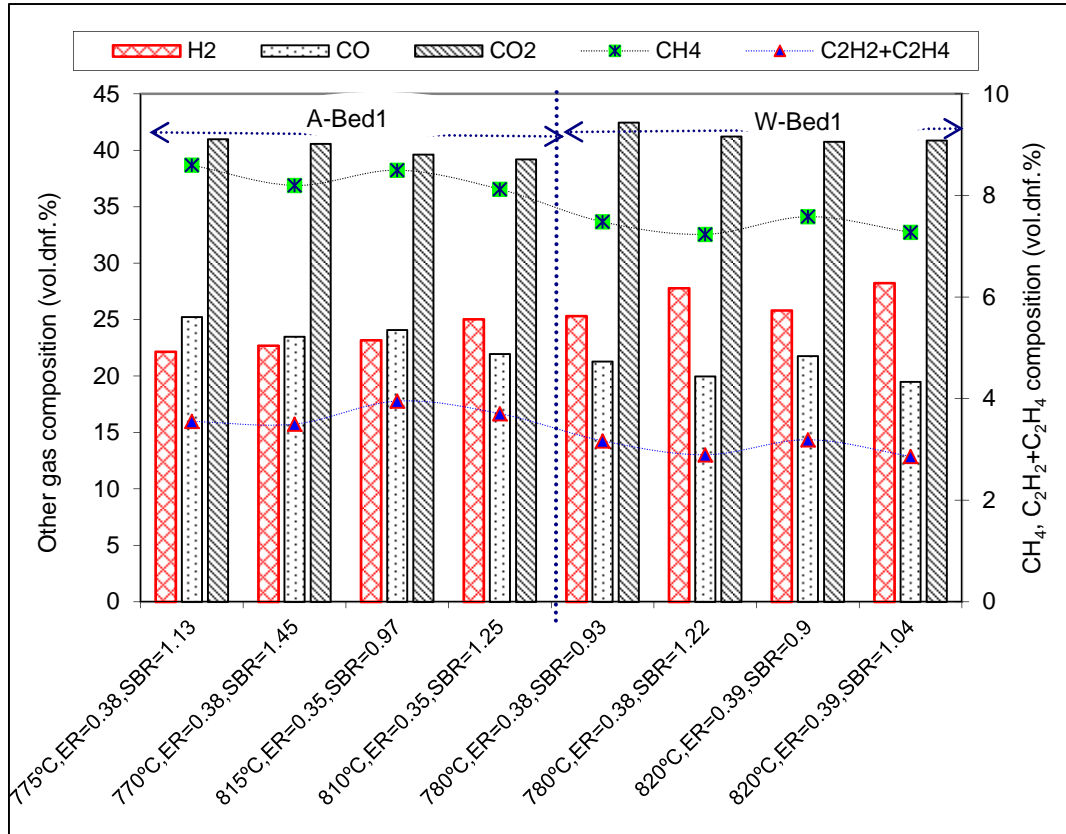


Figure 5- 2 Effects of different operational conditions on the composition of product gas from Agrol (Exp. No A2, A3) and willow (Exp. No W2) using bed 1 at TUD

The concentration of  $N_2$  for Agrol-Bed 1 and willow-Bed 1 at ca. 780 °C was 25vol.% and 21vol.% on a dry basis, respectively. From these three figures, it can be seen that there is a large variation among the product gas composition produced from different fuels as a function of temperature. Generally high temperatures favored the formation of  $H_2$  from all fuels. The concentration of  $H_2$  obtained from willow was higher than that from Agrol, while  $CO$ ,  $CH_4$ ,  $C_2H_2$  and  $C_2H_4$  concentrations followed an opposite trend. The averaged  $H_2$  to  $CO$  mole ratio obtained from Agrol, willow and DDGS over the temperature range from 800 to 820 °C was around 1.0, 1.4 and 0.7, respectively. With increasing SBR, the concentrations of  $CO$ ,  $CH_4$ ,  $C_2H_2$  and  $C_2H_4$  all gradually decreased, while the concentration of  $H_2$  increased with a varying degree depending on fuel types. The concentration of  $CO_2$  obtained from willow was the highest, followed by that from Agrol and DDGS, and no significant change was observed with a variation of the SBR values. However, when the SBR value was increased from 0.98 to 1.16 at a temperature of 800 °C, the concentrations of  $CO$ ,  $CH_4$  and  $C_2H_2$  obtained from Agrol using Bed 2 all slightly increased. Higher ER values increased the concentration of  $CO_2$  in product gas but decreased the concentrations of  $CO$ ,  $CH_4$  and  $H_2$ . The effects of different bed materials on the product gas composition can hardly be determined due to the difference of SBR, ER and the temperature. At similar operational conditions (e.g., 820 °C, SBR~1.15 and ER~0.4), the concentration of  $H_2$  obtained from willow using Bed 1 (~30 vol.%) was higher than using Bed 3 (~26 vol.%) on a dry  $N_2$  free basis (dnf.) which indicated that olivine can improve  $H_2$  production compared to sand. Without feeding any

kaolin into the gasifier, a severe agglomeration was observed during DDGS gasification using Bed 4, which can be seen from **Figure A-8** (see Appendix). When the agglomeration occurred, the fluidization inside the gasifier suddenly stopped, which can be seen from the behavior of the dp-cell 1 and 2 on the riser, and dp-cell 7 and 9 on the downcomer of the CFB gasifier.

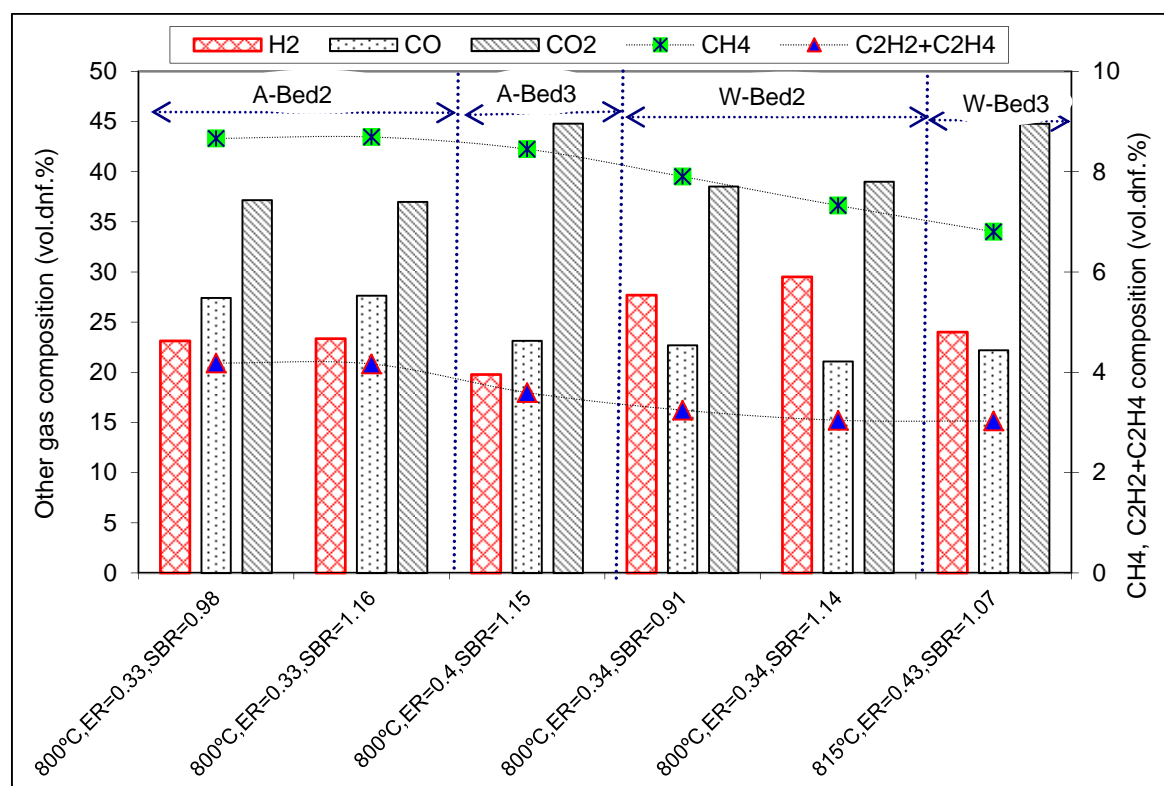


Figure 5- 3 Effects of different operational conditions on the composition of product gas from Agrol and willow using bed 2 (Exp. No A4, W3) and bed 3 (Exp. No A1, W1) at TUD

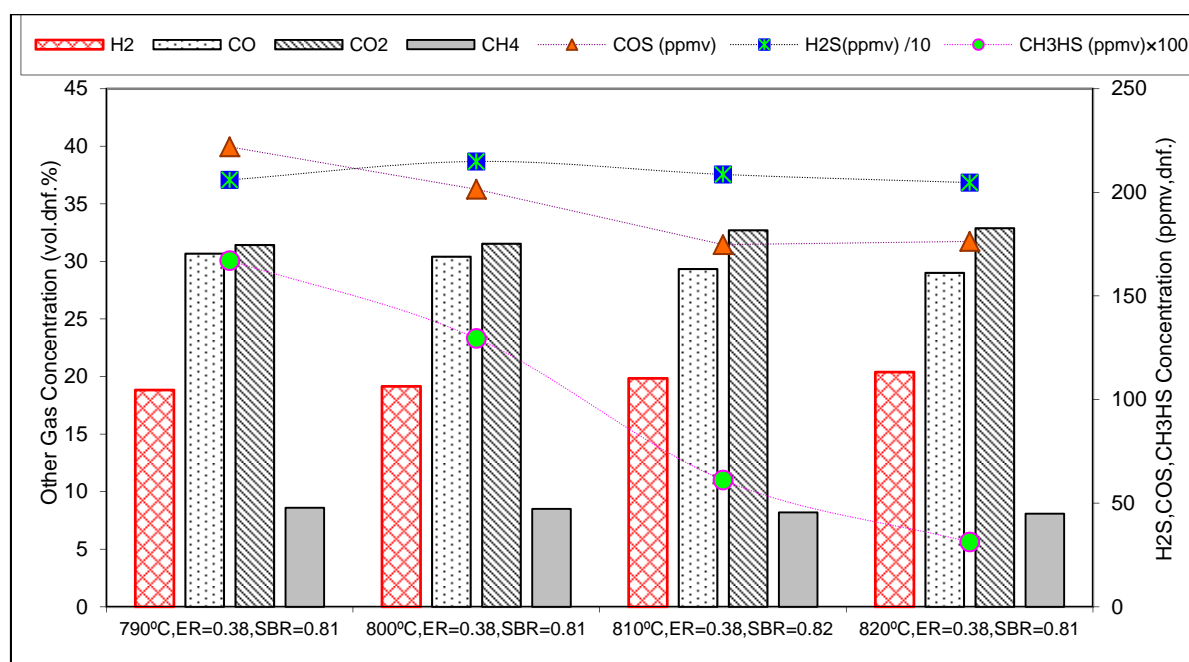


Figure 5- 4 Effects of different operational conditions on the composition of product gas from DDGS using bed 4 (Exp. No D1) at TUD

Most experimental results agreed well with those reported by other researchers. Turn et al. (Turn et al., 1998) reported that light hydrocarbon ( $C_2H_2$ ,  $C_2H_4$ ,  $C_2H_6$ ) concentrations decreased as reactor temperature increased but no noticeable conversion of  $C_2H_2$  and  $C_2H_4$  was observed at lower reactor temperatures from 750 to 800 °C. Gil et al. (Gil et al., 1997), Kumar et al. (Kumar et al., 2009) and Franco et al. (Franco et al., 2003) all reported that the concentration of  $H_2$  increased with increasing the temperature because higher temperature favored endothermic char gasification reaction and steam reforming and cracking of light hydrocarbons and tars. The different behavior of various gaseous species at lower temperatures could be due to the variation in reactivities of chars produced during the pyrolysis step (Orfao et al., 1999) and at higher temperatures could be due to the intensified effect of steam on the decomposition of higher molecular mass components (Qin et al., 2010). Gil et al. (Gil et al., 1999) reported that as ER or SBR was increased the concentrations of CO,  $CH_4$  and  $C_2$ -hydrocarbons decreased due to partial oxidation and steam reforming reactions. Wang and Kinoshita (Wang & Kinoshita, 1992) reported that by varying SBR from 0.4 to 1.0, the concentration of  $H_2$  increased and that of  $CO_2$  remained roughly the same, while the concentration of CO,  $CH_4$  and other light hydrocarbons produced decrease slightly.

### **5.1.1.2 Effect on sulfur species**

Because Agrol and willow both contain less than very low sulfur content (<0.002%), almost no gaseous sulfur species were detected during their experiments. However, a high  $H_2S$  content and well measurable amounts of COS and methyl mercaptan were determined during DDGS gasification. With increasing temperature, the concentration of  $H_2S$  remained fairly stable, whereas the concentrations of COS and methyl mercaptan slightly decreased (see in **Figure 5- 4**). Since for steam- $O_2$  blown CFB gasification of DDGS fuel no reported results are available in the literature, here a simple thermodynamic equilibrium model established by using the Factsage<sup>TM</sup> software package has been used to predict the concentrations of  $H_2S$ , COS and methyl mercaptan. A detailed description about the modeling using Factsage<sup>TM</sup> is available by Meng et al. (Meng et al., 2009), and as well see in chapter 4. The predicted concentration of  $H_2S$  was slightly higher than the measured value, while COS and methyl mercaptan concentrations were lower. The measured average concentrations for  $H_2S$ , COS and methyl mercaptan are around 2300, 200 and 0.8 ppmv, respectively, while the predicted ones are 2600, 40 and 0 ppmv, respectively. Thus during experiments, less  $H_2S$  was produced than predicted by chemical equilibrium calculations, which probably resulted in higher concentrations of COS, methyl mercaptan and other sulfur species. Attar and Dupuis (Attar & Dupuis, 1979) reported that part of the sulfur is retained in the solid as alkali sulfide due to the reaction of  $H_2S$  with the alkali minerals which prevents them from entering the gaseous phase. The mineral elements such as Fe, Ni, Si, Al, Na, K, Mg, Ca present in the fuel may act as catalysts and affect the concentrations of sulfur species during gasification. The presence of high levels of Ca, K and Na in the biomass could lead to a high retention of S and Cl in the ash as presented in previous chapter 4 and one of published papers (Meng et al., 2009). Therefore, the lower measured  $H_2S$  concentration could be attributed to the retention of sulfur in the ash because of the presence of active bed materials and minerals in DDGS fuel. Considering the low sulfur content in biomass fuel and limited measurement capacity and accuracy, equilibrium modeling is already a valuable tool to get an insight into the behavior of sulfur species during biomass gasification.

Besides minerals in the ash, some other operational parameters also affected the concentrations of  $H_2S$  and COS to certain extent. With a variation of SBR, the concentrations of  $H_2S$  and COS obtained from DDGS using Bed 1 and Bed 2 showed a similar change trend. For instance, an increase of SBR from around 1.0 to 1.1 led to a significantly decrease in the concentration of  $H_2S$  obtained from DDGS using Bed 1 from 2700 to 1800 ppmv accompanied with a slightly increase in COS concentration from 116 to 125 ppmv. The predicted results from the Factsage<sup>TM</sup> equilibrium model for DDGS gasification using Bed 1 showed that when SBR was increased from 0.98 to 1.09, a slight decrease in the concentrations of  $H_2S$  and COS from 2640 to 2600 ppmv and 28 to 25 ppmv was observed which partly agree with experimental results. A similar predicted result has been achieved for DDGS gasification using Bed 2. A higher ER led to a decrease in  $H_2S$  concentration but an increase in the concentration of COS. These experimental results only partly agreed with predicted results from

Factsage™ equilibrium model. However, these predicted trends agree with experimental and predicted values reported by Dias and Gulyurtlu (Dias & Gulyurtlu, 2008). They reported that the concentration of H<sub>2</sub>S increased from 672 ppmv up to 1204 ppmv with increasing ER from 0 to 0.4, and the concentration of sulfur oxidizes such as SO<sub>2</sub> and COS also increased in different proportions.

### 5.1.1.3 Effect on CCE%, CGE% and heating values of product gas

The operational conditions also largely influence CCE%, CGE% and heating values of the product gas. In general, a higher temperature and a higher SBR value lead to a higher product gas yield. Effects of operational parameters on CCE%, CGE% and heating values of the product gas obtained from Agrol, willow and DDGS some tests are shown in **Table 5- 2**.

*Table 5- 2 CCE%, CGE% and HHV, LHV of the product gas produced from some Agrol, willow and DDGS gasification tests at TUD*

Fuel	Bed	T	ER	SBR	CCE%	CGE%	HHV_gas	LHV_gas	Product gas/fuel
(-)	(-)	(°C)	(-)	(-)	(%)	(%)	(MJ/kg)	(MJ/kg)	(Nm <sup>3</sup> /kg daf.)
Agrol	Bed 1	770	0.38	1.21	84.2	52.5	3.9	3.6	2.48
Agrol	Bed 1	770	0.38	1.45	74.0	47.0	2.9	2.7	3.08
Willow	Bed 1	780	0.38	1.13	90.5	56.2	4.2	3.8	2.55
Willow	Bed 1	780	0.38	1.22	86.9	55.2	4.0	3.6	2.63
Willow	Bed 2	800	0.34	1.14	91.8	62.1	4.3	4.0	2.81
Willow	Bed 3	820	0.43	1.04	93.5	55.7	4.0	3.7	2.50
DDGS	Bed 2	750	0.36	1.08	96.6	71.5	4.6	4.3	2.82

It can be seen that an increase in SBR led to a higher yield of the product gas, but simultaneously also caused a lower CCE%, CGE% and LHV of the product gas. However, higher temperature largely improved CCE%, CGE% and LHV of the product gas. These results are in agreement with those reported by other researchers. Gil et al. (Gil et al., 1997) reported that by increasing GOR (the ratio of steam and oxygen supplied to biomass fuel supplied on a.r. basis) or decreasing SOR (the mole ratio of steam supplied to oxygen supplied), the LHV of the product gas decreased. The gas yield on a dry basis increased with an increment of GR and bed temperature. A higher temperature in the gasifier bed or lower GR led to higher thermal efficiencies. Wei et al. (Wei et al., 2007) reported that the product gas yield increased with reactor temperature due to enhanced endothermic steam reforming, cracking reactions of the tar and char gasification at elevated temperatures. Turn et al. (Turn et al., 1998) reported that increasing the temperature of the gasifying agents led to an increase in the heating value of the product gas and reduced the tars, soot and char residues. Kinoshita et al. (Kinoshita et al., 1994) reported that the product gas yield and CCE% increase as temperature increases since higher temperatures facilitate tar conversion. Boateng et al. (Boateng et al., 1992) reported that the yield and LHV of the product gas, CCE% and CGE% increased with increasing gasification temperature from 700 to 800 °C.

From **Table 5- 2**, it can also be seen that CCE%, CGE%, the yield and heating values of the product gas obtained from willow were slightly higher than those obtained from Agrol. For instance, under similar operational conditions (e.g., SBR=1.2, ER=0.37, 780 °C, Bed 1), the yield of the product gas produced from willow and Agrol was 2.63 and 2.48 Nm<sup>3</sup>/kg fuel on a daf basis, respectively. Furthermore, it seemed that the product gas yield produced from DDGS was much higher than those from Agrol and willow. For different bed materials, it seemed that Bed 2 was better than Bed 1 on the enhancement of the product gas yield. On another hand, it could be due to some accumulation of ash in the V-cone after several time measurements leading to a slight higher measured pressure drop, since the experiments using Bed 2 was carried out at the last day.



## **5.1.2 Effects of different operational conditions on tar formation/reduction**

### **5.1.2.1 Effect of temperature on tar formation**

The analyzed tar SPA results for Agrol, willow and DDGS are shown in **Figure 5- 5**, **Figure 5- 6** and **Figure 5- 7**, where Total Tar/2, Total Unknown, Sum>C<sub>10</sub>H<sub>8</sub> and Sum>C<sub>10</sub>H<sub>8</sub>UN represent a half of the total tar content, the total unknown tar content, the total tar content heavier than naphthalene and the total unknown tar content heavier than naphthalene, respectively.

From **Figure 5- 5** (Agrol gasification using Bed 1), we can see that with increasing temperature the total tar content produced decreased. The total amounts of class 2 and 4 tars were much higher than those of class 3 and 5 tars. These observations agreed well with the results reported by other researchers. Gil et al. (Gil et al., 1999) and Kinoshita et al. (Kinoshita et al., 1994) all reported that phenol and cresol were predominant only at temperatures below 800 °C, while naphthalene and indene were the major tar components at 900 °C. Narváez et al. (Narvaez et al., 1996) reported that the temperature not only influenced tar formation but also the tar properties by affecting the chemical reactions involved in the whole gasification network. Brage et al. (Brage et al., 2000) reported that with increasing temperature the differences in molecular thermal stability led to a progressive accumulation of non-oxygenated aromatics and favored the formation C<sub>2</sub>H<sub>2</sub> and C<sub>2</sub>H<sub>4</sub> at the expense of phenols. van Paasen and Kiel (van Paasen & Kiel, 2004) reported that tar concentration decreased with temperature varying from 750 to 950 °C, and simultaneously tar composition shifted from alkyl-substituted poly-aromatic hydrocarbons (PAHs) to non-substituted PAHs. Furthermore, from samples 0413C and D, it seemed that a higher temperature favored the decomposition of the heavier tar fraction class 5. When the temperature was increased from 780 to 820 °C, more than 40% of class 5 tar and 60% of Sum>C<sub>10</sub>H<sub>8</sub> UN was reduced, and 26% increase in the fraction of class 3 tar was also observed.

These observations indicate that a higher temperature converts higher molecular weight compounds into smaller molecules. These results seem to partly agree with those reported by Han and Kim (Han & Kim, 2008). They reported that an increase in the temperature had a positive effect on the decomposition of class 1 and 2 tars, while the concentrations of class 3 and 5 tars increased with temperature enhancement. Kiel et al. (Kiel et al., 2004) reported that by varying the temperature no clear change trend of the class 5 tar was found. The concentration of class 4 tar increased with increasing gasification temperature at ER = 0.4, which was largely due to the simultaneous occurrence of many effects such as polymerization reactions. Class 4 tar comprises of a mixture of alkyl-substituted tars and poly-aromatic hydrocarbons which showed a different behavior. Without considering the effects of other operational parameters, a higher temperature led to higher proportions of class 4 and 5 tars. With increasing temperature from 770 to 810 °C (sample 0415A to F), the proportional contributions of class 4 and 5 tars increased from 45 to 65% on the average. For Agrol gasification using Bed 1, the lowest tar content of 5.7 g/Nm<sup>3</sup> and the highest one of 12.4 g/Nm<sup>3</sup> were measured at the temperature of 730 °C with SBR = 1.52 and ER = 0.36, and at 780 °C with SB = 1.35 and ER = 0.42, respectively. These results were surprising because normally at a higher temperature the tar content should be lower. However, as it is well-known, the total tar content produced from biomass gasification does not only depend on the temperature, but also other parameters such as SBR, ER. Somehow lower tar content can be achieved at lower temperature with a suitable combination of other critical operational parameters. For example, Rapagná et al. (Rapagna et al., 2000) also observed a much lower tar concentration of around 2.4 g/Nm<sup>3</sup> at the exit of the gasifier at a temperature of 770 °C using olivine as bed material. Li et al. (Li et al., 2004) reported that the tar yield from biomass gasification decreased when the temperature increased from 700 to 815 °C.

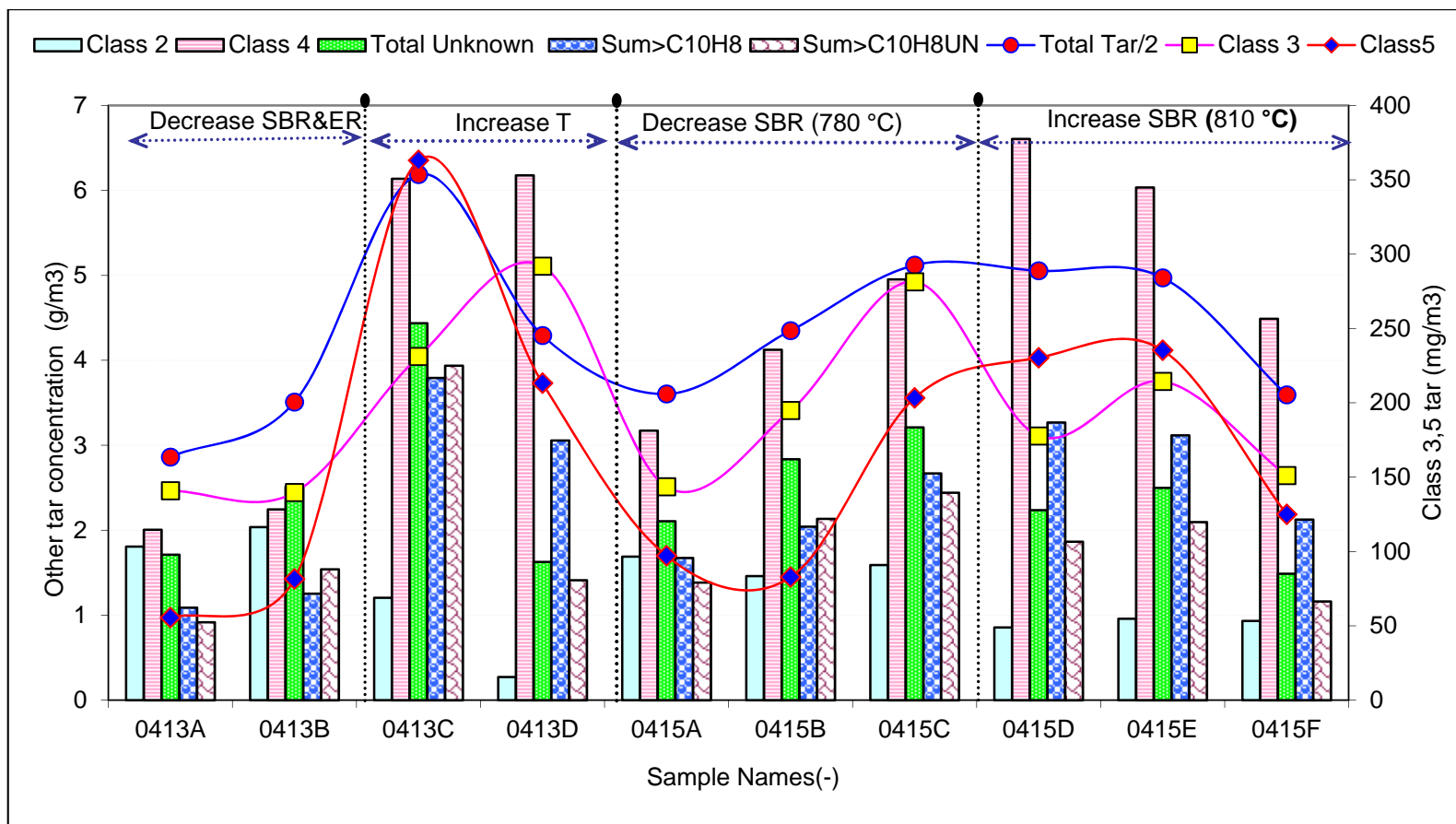


Figure 5- 5 The analyzed SPA results of tar samples from Agrol gasification using bed 1 (Exp. No A2, A3) at TUD

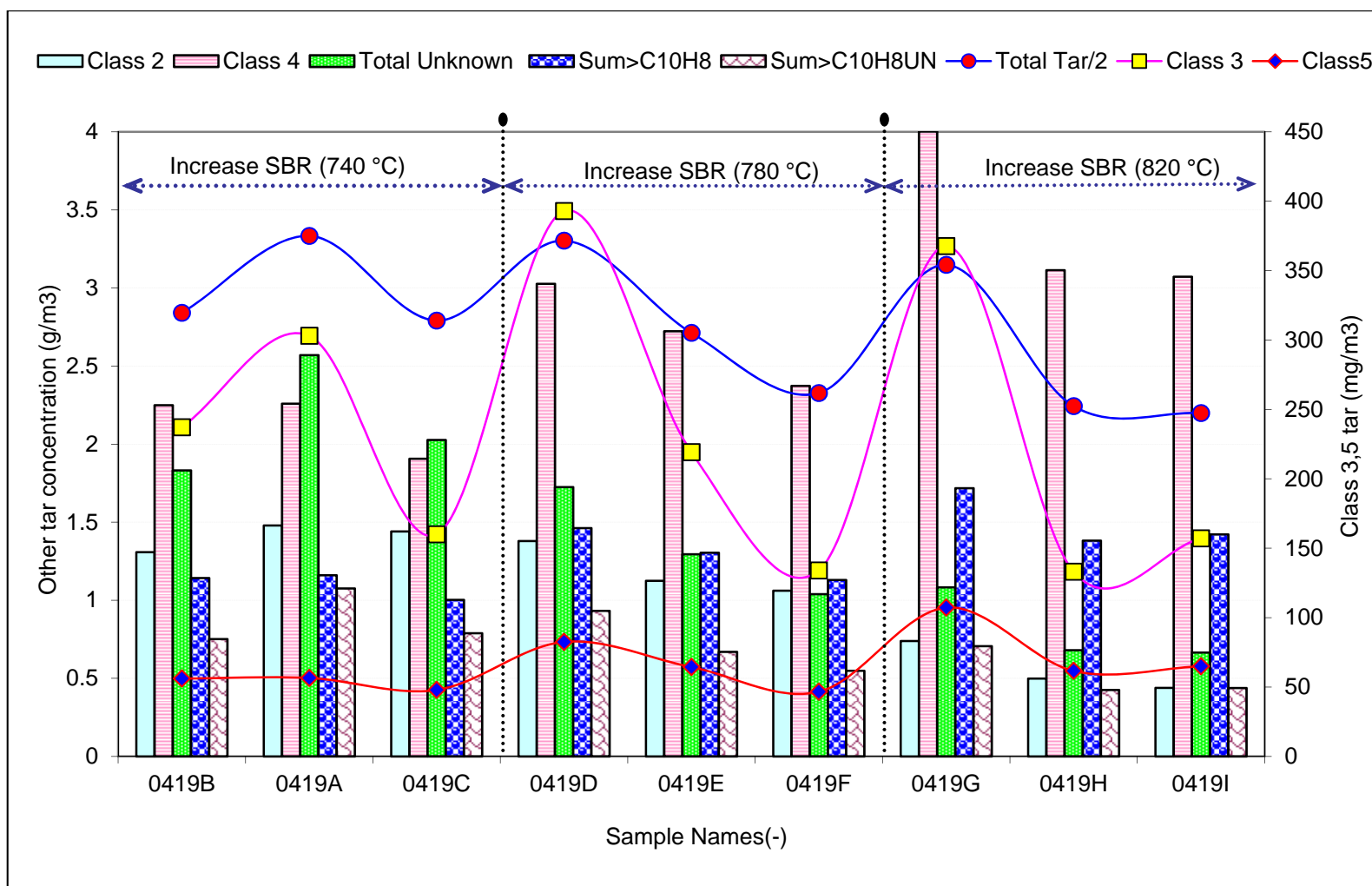


Figure 5- 6 The analyzed SPA results of tar samples from willow gasification using bed 1(Exp. No W2) at TUD

Similar trends were also observed during willow gasification using Bed 1. From **Figure 5- 6** (willow gasification using Bed 1), it can be seen that the total tar content produced from willow gasification decreased with increasing temperature from 740 to 820 °C. Probably due to different fuel properties (e.g., ash content), the total tar content produced from willow was significantly lower than that from Agrol. The lowest and highest tar contents produced from willow were 4.4 and 6.7 g/Nm<sup>3</sup>, which were measured at a temperature of 820 °C with SBR =1.14 and ER = 0.39 (sample 0419I), and at 740 °C with SBR =1.19 and ER = 0.38 (sample 0419A), respectively. During Agrol and willow gasification, a higher temperature led to a higher concentration of class 5 tar components. Regarding this point, van Paasen and Kiel (van Paasen & Kiel, 2004) pointed out that two opposite mechanisms can determine the production of class 5 tar with increasing temperature. Class 5 tar compounds could be produced either from the decomposition of heavy large class 1 tar compounds, or from lighter tar compounds due to PAH growth reactions.

The influence of temperature on tar formation produced from DDGS was difficult to be determined from **Figure 5- 7**. However, the total tar content produced from DDGS gasification using Bed 1 was 7.3 g/Nm<sup>3</sup> (sample 0421A) which was comparatively lower than that from Agrol at similar operational conditions of around 10.2 g/Nm<sup>3</sup> (sample 0415C), and for willow gasification a similar value was obtained of 6.7 g/Nm<sup>3</sup> (sample 0419A). Furthermore, at such a fairly low temperature of 730 °C, the contents of class 2 and 4 tars were only 1 and 1.85 g/Nm<sup>3</sup>, respectively, which is below 2 g/Nm<sup>3</sup> being considered as an important limit for many downstream applications as reported by Aznar et al. (Aznar et al., 1998).

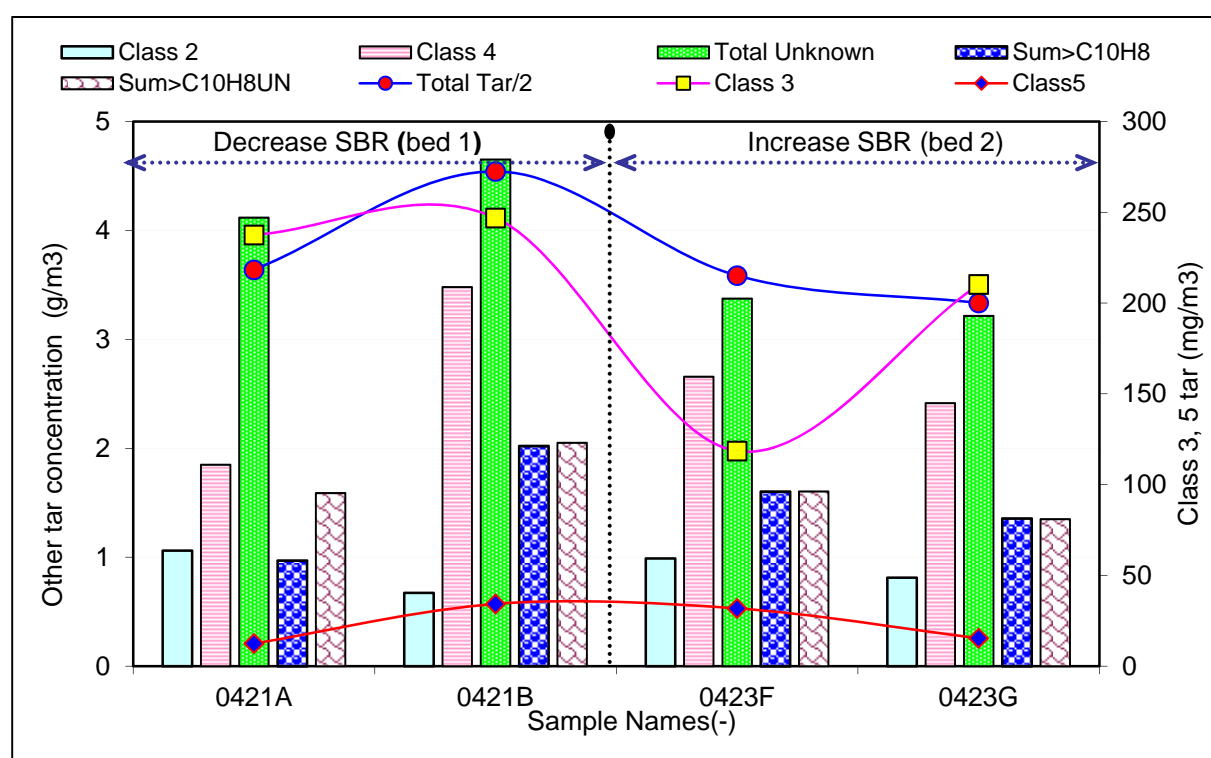


Figure 5- 7 The analyzed SPA results of tar samples from DDGS gasification using bed 1(Exp. No D2) and bed 2 (Exp. No D3) at TUD

### 5.1.2.2 Effects of SBR and ER on tar formation

From **Figure 5- 5**, it can be clearly seen that an increment of SBR significantly promoted tar decomposition during Agrol gasification using Bed 1. With increasing SBR from 1.13 to 1.45 at 770 °C (sample 0415C to A) and SBR from 0.97 to 1.25 at 810 °C (sample 0415D to F), the total tar content both decreased from around 10.2 to 7.2 g/Nm<sup>3</sup>. Generally with increasing SBR the concentrations of class 3, 4 and 5 tars all decreased, while the concentration of class 2 increased.

However, at a temperature of 770 °C, the lowest content of class 5 tar was found at an SBR value of 1.21 instead of 1.45. Furthermore, a slight increase in the concentrations of class 3 and 5 tars was also observed when increasing SBR from 0.97 to 1.16 at a temperature of 810 °C (sample 0415D to E). As aforementioned, the highest tar content obtained from Agrol was around 12.4 g/Nm<sup>3</sup> (sample 0413C) which was measured at a temperature of 780°C and SBR = 1.35 and ER = 0.42. However, under a less favorable tar decomposition circumstance, a much lower tar content of 8.7 g/Nm<sup>3</sup> (sample 0415B) was also observed. These two samples were taken at different days and there might be slight difference inside the gasifier such as the accumulated amount of char content.

Similar trends were observed for willow and DDGS gasification using Bed 1. In **Figure 5- 6**, with increasing SBR from 0.93 to 1.22 at a temperature of 780 °C (sample 0419D to F), the total tar content produced from willow decreased from 6.6 to 4.7 g/Nm<sup>3</sup>. With increasing SBR and a variation in temperature from 780 to 820 °C (samples 0419D to I), the concentrations of class 2 to 5 tars decreased with a varying reduction degree from 20 to 66%, but at a temperature of 740 °C (samples 0419B to C) the concentration of class 2 tar increased with a variation of SBR from 0.99 to 1.27. Furthermore, at a temperature of 820 °C, the lowest concentrations of class 3 and 5 tars were observed at SBR of 1.04 (sample 0419H) instead of at 1.14 (sample 0419I). In **Figure 5- 7**, at a temperature of 730 °C when SBR was increased from 0.98 to 1.1 (sample 0421B to A), the total tar content produced from DDGS decreased from 9.1 to 7.3 g/Nm<sup>3</sup>. More than 45% of class 4 and 60% of class 5 tar were reduced, but the concentration of class 2 largely increased from 0.6 to 1.0 g/Nm<sup>3</sup> and almost no change in the content of class 3 tar.

Similar results were observed for tar compounds produced from Agrol, willow and DDGS gasification using Bed 2 (see in **Figure 5- 7** and **Figure 5- 8**). However, a fairly dramatic change was observed about the class 2 produced from Agrol and willow. With increasing SBR from around 0.9 to 1.15 (sample 0423B to G), the total tar content and the concentrations of class 4 and 5 tars produced from three fuels all decreased. The lowest tar concentrations obtained from Agrol, willow and DDGS were 9.7, 5.3 and 6.7 g/Nm<sup>3</sup>, respectively (sample 0423 A, E and G). Furthermore, it seemed that an increment of SBR from 0.98 to 1.15 at a temperature of 800 °C had a negligible influence on the decomposition of tar produced from Agrol. The total tar content remained around 10 g/Nm<sup>3</sup>, and similar results were also observed when using Bed 1. Unfortunately, the effect of ER on tar formation cannot be clearly concluded from the available SPA results.

From above-stated results, we can see that the compositions and contents of tar produced from three fuels were fairly different. In general, the results reported in this work are similar to those reported by other researchers. Aznar et al. (Aznar et al., 1997) reported that with varying GR from 0.7 to 1.2 more than 85% reduction in total tar was achieved. The different behavior of class 2 to 5 tars produced from Agrol, willow and DDGS could be attributed to their different properties such as the distribution of cellulose, hemicellulose and lignin, and ash contents. According to van Paasen and Kiel (van Paasen & Kiel, 2004), the final tar composition depends on the lignocelluloses composition of biomass fuels. The difference in the concentration of class 2 tar can be largely due to the difference in structure between cellulose and lignin, while the difference in the concentrations of class 4 and 5 tars might be attributed to differences in lignocelluloses composition of the feedstock, since class 4 and 5 tars are mostly PAH compounds which come from aromatic functional group in the molecular structure of lignin.

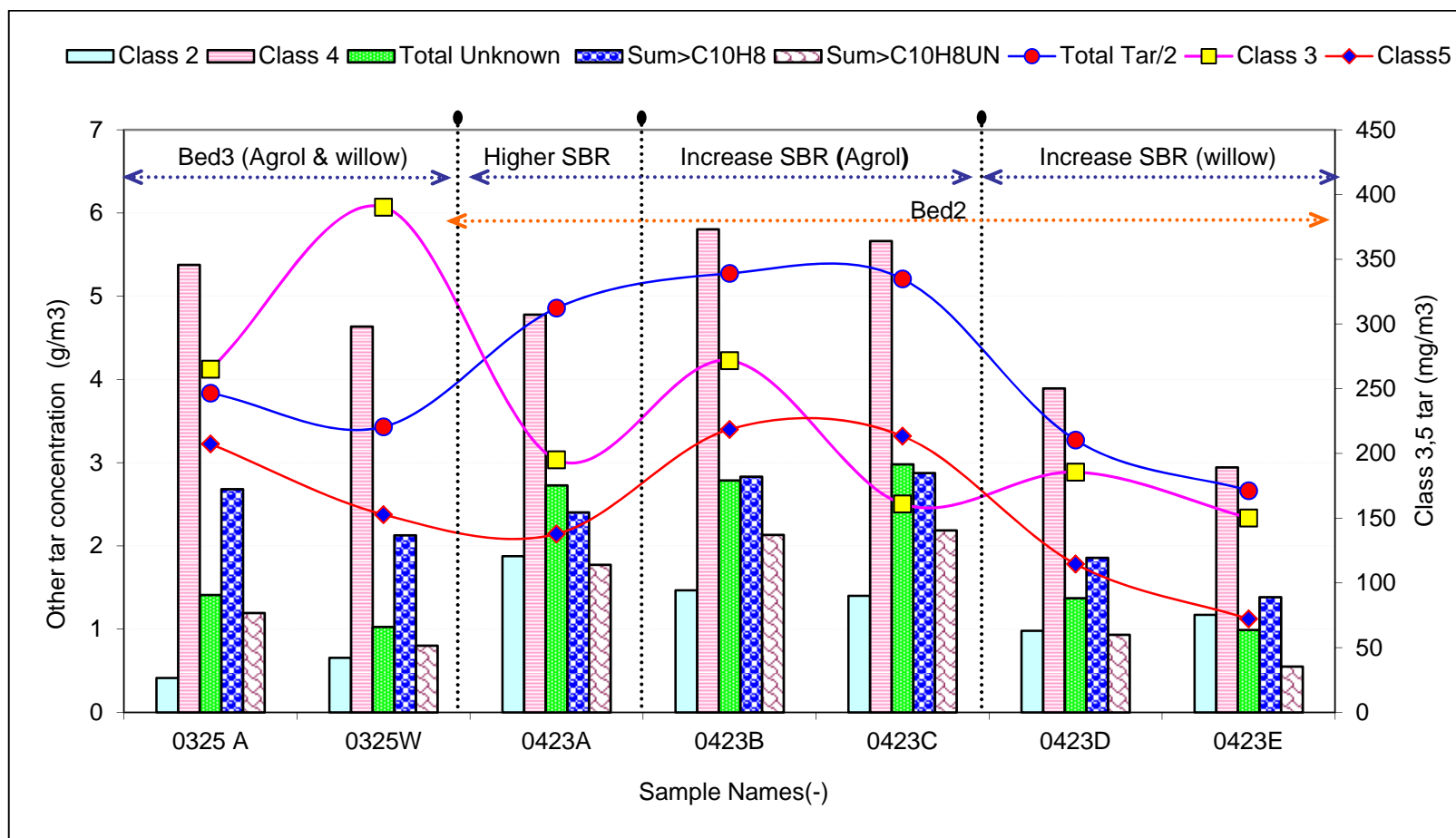


Figure 5- 8 The SPA results of tar samples from Agrol and willow gasification using bed 3 (Exp. No A1, W1) and bed 2 (Exp. No A4, W3) at TUD

### **5.1.2.3 Effect of the types of bed materials**

From **Figure 5- 5** to **Figure 5- 8**, it is difficult to conclude whether Bed 1 or Bed 2 was better regarding tar decomposition. For instance, the total tar content obtained from willow using Bed 2 was  $5.3 \text{ g/Nm}^3$  at  $800^\circ\text{C}$  with  $\text{SBR}=1.14$  and  $\text{ER}=0.34$  (sample 0423E), which was slightly lower than that of  $5.4 \text{ g/Nm}^3$  using Bed 1 at  $780^\circ\text{C}$  with  $\text{SBR}=1.13$  and  $\text{ER}=0.38$  (sample 0419E), while slightly higher than that of  $4.4 \text{ g/Nm}^3$  at  $820^\circ\text{C}$  with  $\text{SBR}=1.14$  and  $\text{ER}=0.39$  (sample 0419I). Furthermore, from these three tar SPA samples, it can also be seen that the concentration of class 5 tar using Bed 2 was much higher than that using Bed 1, while the class 3 tar showed an opposite trend. The concentrations of class 3 and 5 tars in samples 0423E, 0419E and 0419I were 72, 64 and 65  $\text{mg/Nm}^3$ , and 150, 219 and 157  $\text{mg/Nm}^3$ , respectively. Based on these observations, it can be concluded that Bed 1 showed considerable catalytic reactivity towards the decomposition of heavy PAH compounds (class 5 tar). Some fairly interesting observations were also found during Agrol gasification using different bed materials. From SPA samples 0415 D and E and samples 0423B and C, it can be seen that when the temperature was lower than  $820^\circ\text{C}$  and ER lower than 0.35 an increment of SBR from 0.9 to 1.16 had a negligible influence on tar decomposition and compositions. Under these conditions, the averaged total tar content was around  $10 \text{ g/Nm}^3$ . Furthermore, a fairly low tar content of  $7.7 \text{ g/Nm}^3$  was also obtained from Agrol using Bed 3 under a combination of operational conditions of a lower SBR ( $\sim 1.15$ ) with a higher temperature ( $>820^\circ\text{C}$ ) and a higher ER ( $\sim 0.4$ ). These two similar olivine bed materials (Bed 1 and 2) have also been studied by Pecho et al. (Pecho et al., 2008) for the optimization of the biomass gasification under sulfur-free (S-free) and  $\text{H}_2\text{S}$  enriched conditions. They reported that the catalytic activity of Bed 1 increased significantly by redox-type pre-treatment and it also acted as an oxygen carrier from the combustion zone to the gasification zone, whereas fresh olivine Bed 2 had almost no catalytic activity. Their findings can be a good reference for this work. Rauch et al. (Rauch et al., 2004) compared different olivines for biomass steam gasification and found that olivine had high attrition resistance as bed material for fluidized beds and the catalytic activity for tar reforming. Bed 3 showed a less positive influence on tar decomposition than Bed 1. For instance, at the temperature of  $820^\circ\text{C}$  with SBR of 1.04 and ER of 0.4, the total tar content produced from willow gasification using Bed 1 and 3 was  $4.5$  and  $6.9 \text{ g/Nm}^3$ , respectively. The total amount of class 4 and 5 tars was reduced from  $5.4$  to  $3.1 \text{ g/Nm}^3$  and  $153$  to  $62 \text{ mg/Nm}^3$ , respectively.

## **5.2 Conclusion of gasification using the CFB gasifier**

The effects of operational conditions (SBR, ER and temperature) and bed materials on the product gas distribution and tar formation produced from Agrol, willow and DDGS gasification have been investigated using the atmospheric pressure  $100\text{kW}_{\text{th}}$  steam- $\text{O}_2$  blown CFB gasifier. The compositions of the product gas and tar obtained from these fuels are fairly different, but it is difficult to make a clear comparison between them due to some differences in SBR, ER and the temperature used. Under similar operational conditions the concentration of  $\text{H}_2$  obtained from willow was much higher than that obtained from Agrol and DDGS. Among all the experiments, the product gas composition obtained from willow over the temperature range from  $800$  to  $820^\circ\text{C}$  consisted of the highest  $\text{H}_2$  concentration (28 vol.%), followed by Agrol (24 vol.%) and DDGS (20 vol.%) on a  $\text{N}_2$  free basis, respectively. A fairly high amount of  $\text{H}_2\text{S}$  ( $\sim 2300$  ppmv), COS ( $\sim 200$  ppmv) and a trace amount of methyl mercaptan ( $<3$  ppmv) on a  $\text{N}_2$  free basis were also obtained from DDGS gasification. Higher temperatures and SBR were more favorable for  $\text{H}_2$  production but less advantageous for the formation of CO and  $\text{CH}_4$ , whereas a higher SBR also led to a lower CCE%, CGE% and heating values of the product gas due to high steam content in the product gas. Although DDGS fuel has a relatively high K and Cl content, continually adding 3 to 10 % kaolin (based on total feeding rate) into the reactor can successfully avoid agglomeration. Tar produced from the three fuels mainly contains phenol, cresol, naphthalene, indene and pyrene. The total tar content obtained from Agrol was at the maximum of  $12.4 \text{ g/Nm}^3$ , followed by that from DDGS and willow. Higher temperatures and higher SBR were favorable for the tar decomposition. However, it seems that an increment of SBR from 0.9 to 1.16 had a negligible influence on tar obtained from Agrol fuel at a lower temperature ( $<820^\circ\text{C}$ ) and a lower ER ( $<0.35$ ). The content of class 5 tar obtained using Bed 1 was lower than that obtained using Bed 2, which prove

Bed 1 was more reactive on the decomposition of heavy tar compounds. Although at a fairly low temperature of 730 °C, the total tar content produced from DDGS using Bed 1 was 7.3 g/Nm<sup>3</sup> where the contents of class 2 and 4 tars were only 1 and 1.85 g/Nm<sup>3</sup>, respectively, which is near 2 g/Nm<sup>3</sup> being considered as an important limit for many downstream applications. However, DDGS fuel has a high sulfur content which also leads to a high concentration of H<sub>2</sub>S in the product gas. So far, the effects of SBR, ER and temperature on the distribution of H<sub>2</sub>S and COS from DDGS are still not entirely clear. Additional experiments are necessary in order to get a better insight into the reactivity and influences of different bed materials on tar decomposition in combination with reduction of other contaminants e.g., H<sub>2</sub>S.

### 5.3 Biomass gasification using the PBFB gasifier

An overview experimental conditions (e.g., SBR, temperature, pressure) applied during Agrol, willow and DDGS gasification by using the steam blown PBFB gasifier at TUM are summarized in **Table A-2** (see Appendix). Among them, a selected summary of process parameters is shown in **Table 5- 3**. For Agrol and willow, both atmospheric (1 bar) and under pressure (2.5 bar) gasification tests were performed under different SBR ratios (0.83 to 1.2) and different temperatures (750 to 840 °C), while for DDGS only was gasified under atmospheric pressure under similar SBR ratios and slightly lower different temperatures (700 to 800 °C).

*Table 5- 3 Selected process parameters from Agrol, willow and DDGS gasification at TUM*

Experiments	Atmospheric pressure (1 bar)								
SPA Sample	<i>A1</i>	<i>A2</i>	<i>A3</i>	<i>A4</i>	<i>A5</i>	<i>A6</i>	<i>A7</i>	<i>A8</i>	<i>A9</i>
Fuel	Agrol								
SBR	0.83	1	1.2	0.83	1	1.2	0.83	1	1.2
Temperature (°C)	750	750	750	800	800	800	840	840	840
SPA Sample	<i>W1</i>	<i>W2</i>	<i>W3</i>	<i>W4</i>	<i>W5</i>	<i>W6</i>	<i>W7</i>	<i>W8</i>	<i>W9</i>
	Willow								
SBR	0.86	1	1.18	0.86	1	1.18	0.86	1	1.18
Temperature (°C)	750	750	750	800	800	800	840	840	840
SPA Sample	<i>D1</i>	<i>D2</i>	<i>D3</i>	<i>D4</i>	<i>D5</i>	<i>D6</i>			
	DDGS								
SBR	0.9	1.19	0.9	1.19	0.9	1.19			
Temperature (°C)	700	700	750	750	800	800			
Experiments	Under pressure (2.5bar)								
SPA Sample	<i>A10</i>	<i>A11</i>	<i>A12</i>	<i>A13</i>	<i>W10</i>	<i>W11</i>	<i>W12</i>	<i>W13</i>	
Fuel	Agrol				Willow				
SBR	0.84	1.21	0.84	1.21	0.9	1.21	0.9	1.21	
Temperature (°C)	750	750	800	800	750	750	800	800	

#### 5.3.1 Effects of different operational conditions on product gas compositions

Effects of temperature, SBR, and pressure on the composition of product gas obtained from Agrol, willow and DDGS gasification using the PBFB gasifier is shown in **Figure 5- 9**, **Figure 5- 10** and **Figure 5- 11**, respectively. From these figures, it can be seen that temperature and SBR largely influenced the product gas composition produced from three fuels. Generally at atmospheric pressure



an increment of the temperature and/or SBR promoted the formation of  $H_2$  while it simultaneously led to a reduction in the formation of CO and  $CH_4$ . The influence of SBR on the formation of  $H_2$  was much more pronounced at lower temperatures ( $<800^\circ C$ ) than at higher temperatures. These observations agreed fairly well with the results achieved from the CFB gasifier and reported by other researchers (Franco et al., 2003; Gil et al., 1999; Kumar et al., 2009; Qin et al., 2010). Similar to the results obtained concerning the CFB gasifier, the product gas produced from willow gasification contained more  $CO_2$  and  $H_2$  and less CO and  $CH_4$ . The reason could be that the water-gas shift (WGS) reaction is more enhanced during willow gasification thus reducing CO and forming  $CO_2$  and  $H_2$ . The higher content of  $CH_4$  could be due to the higher volatile matter content in Agrol, so that more hydrocarbons were present and thus more  $CH_4$  was formed through cracking reactions in the gasifier. No significant difference was found among the highest concentration of  $H_2$  produced from three fuels gasification using the PBFB gasifier, while the concentration of  $H_2$  produced from DDGS gasification using the CFB gasifier was much lower than that from Agrol and willow.

The effect of pressure on product gas distribution was also investigated during Agrol and willow gasification using the PBFB gasifier. From **Figure 5- 9** and **Figure 5- 10**, it can be seen that under higher pressure (2.5 bar) a different trend of the product gas composition was observed. For Agrol and willow both fuels, when the pressure was increased from 1 to 2.5 bar, the concentrations of  $CO_2$ ,  $CH_4$  and  $H_2$  increased, whereas the concentration of CO decreased. For instance, during Agrol and willow gasification at a higher SBR (around 1.2) and a lower temperature of  $750^\circ C$ , the concentrations of  $H_2$  and  $CH_4$  increased from 44% to 45% and 6.6% to 9.0%, and 47% to 48% and 6.5% to 7.5%, while the concentration of CO contrarily decreased from 18% to 12 %, and 16% to 11%, respectively. Furthermore, at a pressure of 2.5 bar, an increase in the temperature led to an increase in the concentrations of CO and  $H_2$  and a decrease in those of  $CO_2$  and  $CH_4$ . Moreover, during Agrol and willow gasification at a SBR of 1.2, when the temperature was increased from around 750 to  $800^\circ C$ , the concentrations of CO and  $H_2$  increased from 12% to 17%, 11% to 15%, respectively.

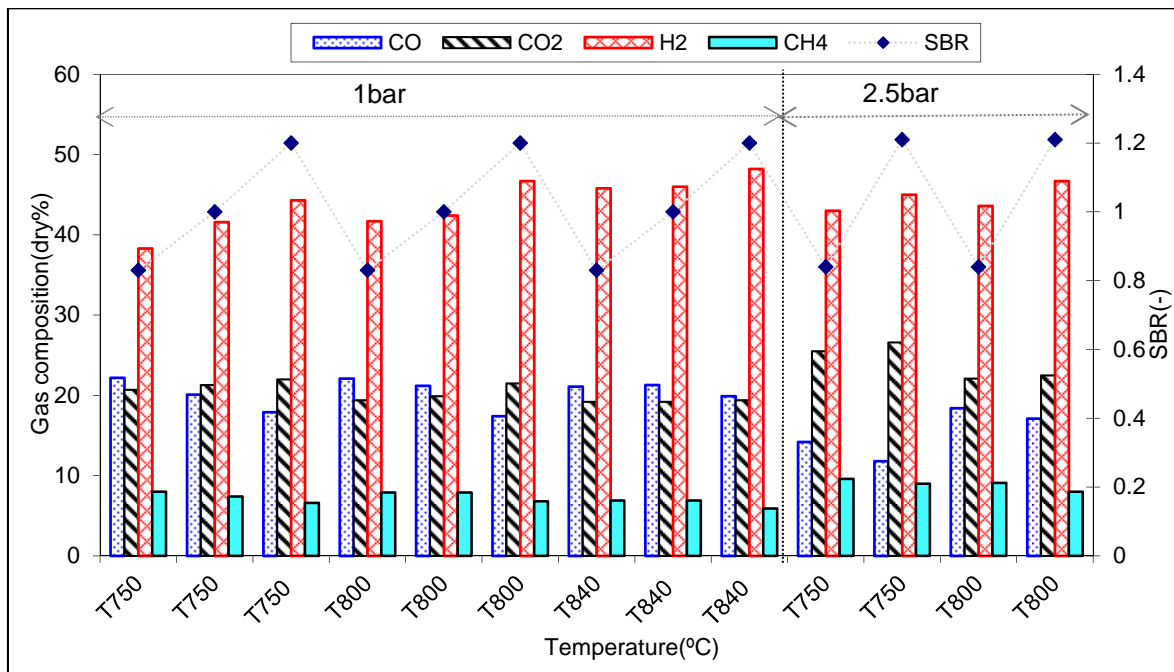


Figure 5- 9 Effects of different operational conditions on the composition of product gas from Agrol (Sample A1-A13) at TUM

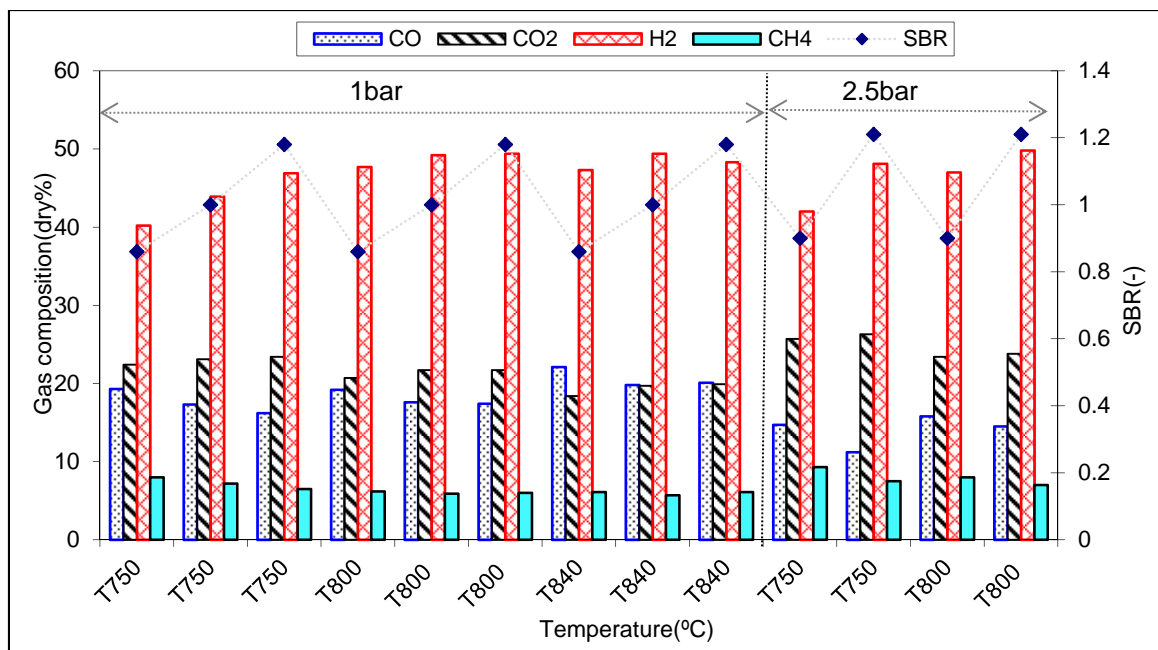


Figure 5- 10 Effects of different operational conditions on the composition of product gas from willow (Sample W1-W13) at TUM

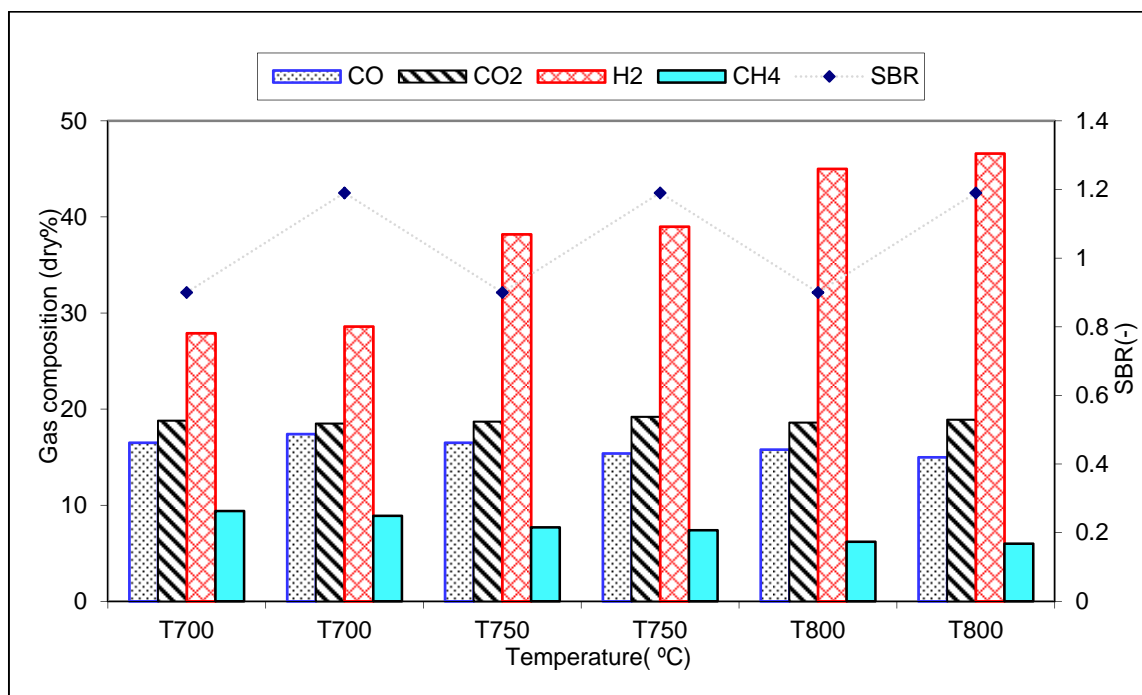


Figure 5- 11 Effects of different operational conditions on the composition of product gas from DDGS (Sample D1-D6) at TUM

These observations are somehow different than those achieved at atmospheric pressure, but there are some explanations available in the literature. Valin et al. (Valin et al., 2010) studied wood sawdust gasification in a steam fluidized bed at 800 °C with varying the pressure from 2 to 10 bar and as total pressure increased from 2 to 10 bar, the yields of CO<sub>2</sub>, CH<sub>4</sub> and H<sub>2</sub> increased by 16%, 53% and 38% respectively, whereas the yield of CO decreased by 33%. They explained that the changes in gaseous yields with pressure can be attributed to the influence of pressure on gas phase reactions (i.e., acceleration of WGS kinetics and reaction rate change in hydrocarbon reactions) and the increase of CH<sub>4</sub> yield with pressure probably due to a change in the secondary pyrolysis reactions scheme under

high pressure. However, Fermoso et al. (Fermoso et al., 2009) studied effects of the main operation variables on the product gas production during the steam-CO<sub>2</sub> co-gasification of bituminous coal and found that at a temperature of 850 °C, an increment in the pressure from 0.5 to 2.0 bar was observed to produce a slight increase in CH<sub>4</sub> and CO<sub>2</sub> to the detriment of H<sub>2</sub> and CO, due to the increase in pressure shifts the equilibrium of methane steam and dry reforming reactions to the side with the fewer moles of gas. Haryanto et al. (Haryanto et al., 2009) performed a thermodynamic analysis regarding the upgrading of syngas derived from biomass gasification and found that there was no considerable influence of increasing pressure at low temperatures (<330 °C). When temperatures were higher than 330 °C, the formation of CO can be suppressed by increasing reaction pressure. However, no significant change in H<sub>2</sub> yield was observed until a temperature of 630 °C. At temperatures higher than 630 °C, increasing pressure from 1 to 3 atmospheres increased the yields of CH<sub>4</sub>, CO<sub>2</sub> and H<sub>2</sub> significantly, while further increment in pressure resulted in a less significant change in their yields.

### ***5.3.2 Effects of different operational conditions on tar formation***

Effects of temperature, SBR, pressure on tar formation obtained from Agrol, willow and DDGS gasification using the PBFB gasifier were also investigated. Generally the total tar concentration decreased with increasing temperature and/or SBR. These observations agreed fairly well with the results achieved from the CFB gasifier and reported by other researchers (Aznar et al., 1998; Gil et al., 1997; Kinoshita et al., 1994; Narvaez et al., 1996; van Paasen & Kiel, 2004). Thus, no more detailed discussion will be presented here, since effects of these two parameters on tar formation have been just discussed in previous 5.1.2 section. Furthermore, a more complete discussion will be presented in next chapter regarding tar formation behavior in the CFB and PBFB gasifiers with a comparison between different online measurement techniques and the SPA method. The influence of pressure on the tar composition was investigated for Agrol and willow fuels. **Figure 5- 12** shows the influence on the tar composition due to a change in the reactor pressure 1 to 2.5 bar at ~750 °C and ~800 °C at an SBR of 0.83 and 1.2.

The formation of different tar compounds during Agrol gasification increased with an increase in the pressure under most operational conditions. For instance, at a temperature of 750 °C with SBR of approximately 0.84, when the pressure was increased from 1.0 to 2.5 bar, the measured concentration of naphthalene and the total tar concentration using the SPA method sharply increased from 0.58 to 1.59, and 5.55 to 7.27g/Nm<sup>3</sup>, respectively. These observations only partly agreed the results reported by other researchers. Knight (Knight, 2000) studied biomass gasification under different pressures and found that the fraction of PAH increased with increasing pressure, while the total tar content decreased with increasing pressure by around 20%, which is mainly due to a decrease of the water soluble tar compounds and phenols, whereas polyaromatic compounds increase. Wolfesberger et al. (Wolfesberger et al., 2009) also found the total tar content to decrease by ~30% when the pressure is increased from 1 to 3 bar at a gasifier temperature of 825 °C.

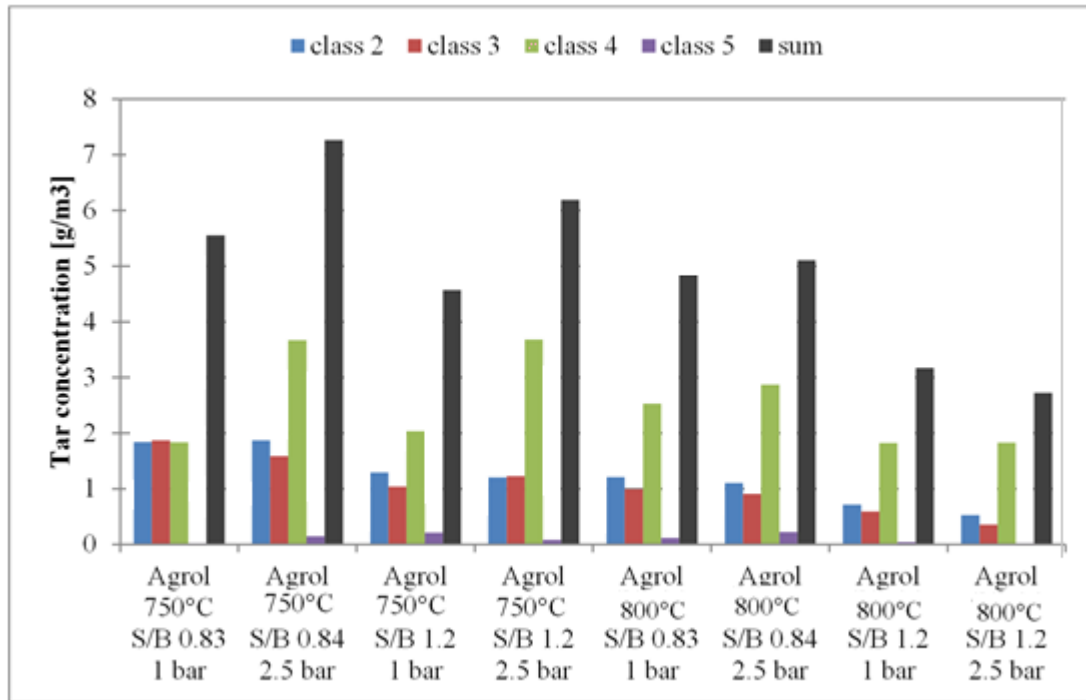


Figure 5- 12 Influence of pressure on tar composition during Agrol gasification (750/800°C S/B 0.83/1.2) adapted from (Mayerhofer et al., 2011)

## 5.4 Conclusion of gasification using the PBFB gasifier

Effects of temperature, SBR and pressure on the product gas and tar composition from three fuels gasification using the PBFB gasifier were investigated. Similar results have been obtained as those from the CFB gasifier. The analyzed results about the influences of the temperature and SBR all confirm that at atmospheric pressure higher temperatures and SBR are more favorable for H<sub>2</sub> production but less advantageous for the formation of CO and CH<sub>4</sub>. Higher pressures appear to promote the formation of CH<sub>4</sub> which will be an advantage for synthetic natural gas (SNG) application. Three different fuels produced different amounts of the tars. Higher temperatures and higher SBR values could promote tar decomposition, a trend which agreed well with the SPA results achieved from the CFB gasifier.

## **6 Tar formation in the steam-O<sub>2</sub> blown CFB and the steam blown PBFB gasifiers: comparison between different on-line measurement techniques and the off-line SPA sampling and analysis method**

---

*Chapter 5 presented the results regarding effects of different operational conditions on the formation of tar produced from Agrol, willow and DDGS gasification on the CFB and PBFB gasifiers. This chapter mainly compares the measured tar results from three different tar measuring techniques in three different ways: on-line analysis behavior of the LIFS and OTA methods, individual tar components quantification of the SPA and LIFS methods and the total tar content analysis using the SPA, LIFS and OTA methods. The possibilities for improving the OTA analyzer have been also recommended based on experimental results. This part of work has been published in the Fuel Processing Technology Journal.*

**Meng, X.,** Mayerhofer, M., Mitsakis, P., de Jong, W., Gaderer, M., Verkooyen, A.H.M., and Spliethoff, H. 2012. Tar formation in a steam-O<sub>2</sub> blown CFB gasifier and a PBFB gasifier (BabyHPR): Comparison between different online measurement techniques and the SPA method. *Fuel Processing Technology*, 100, 16-29.

As mentioned in chapter 1, tar is one of the most problematic compounds which can result in various problems associated with its condensation, aerosol formation and polymerization to form more complex depositing structures. Moreover, tar composition offers quantitative and qualitative information about the gasification conditions, thus quantitative measurement of tar in product gas is important to assess the effectiveness of cleanup and conditioning processes, which is why effectively measure tar during fluidized bed gasification using different techniques was becoming one of the focused areas of this research.

As stated in Chapter 3 and 5, three different tar measurement techniques have been used to quantify tar content produced from Agrol, willow and DDGS gasification during the CFB and PBFB measurement campaign. Since the SPA and LIFS methods can quantify individual tar components, while the LIFS and OTA methods can analyze tar in an on-line way and the OTA method can only measure the total tar concentration, the comparison between these three measurement techniques has been performed in three ways by studying:

- on-line analysis behavior of the LIFS and OTA methods;
- individual tar components quantification of the SPA and LIFS methods; and
- the total tar content analysis using the SPA, LIFS and OTA methods.

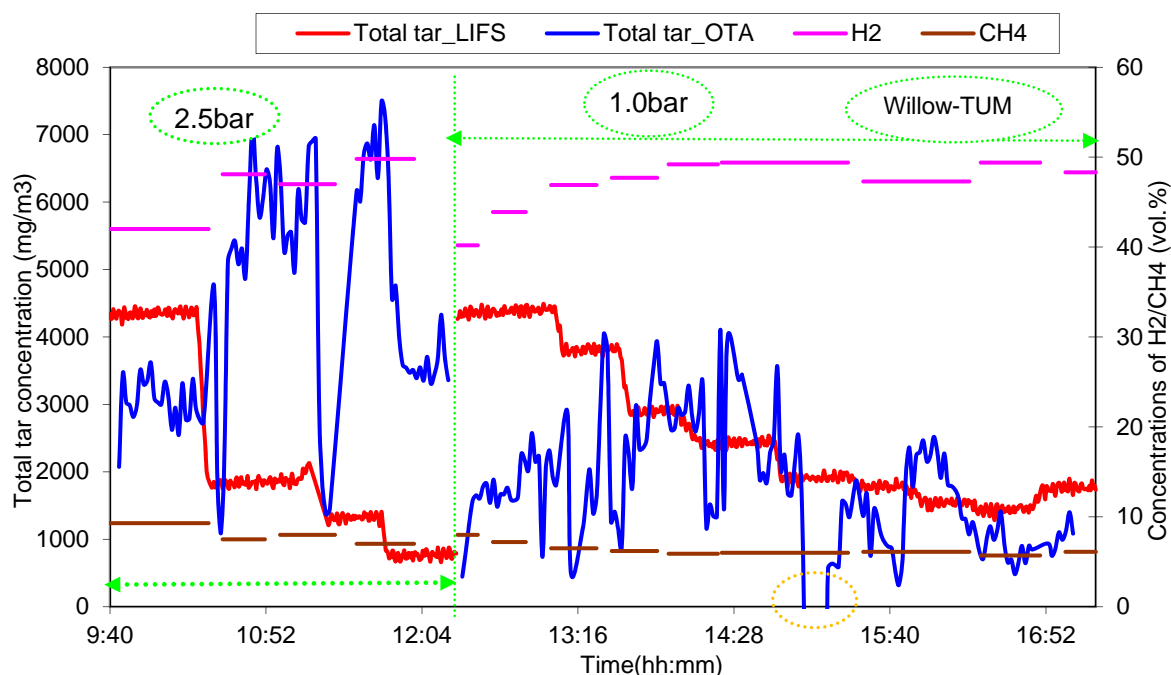
Concerning process parameters (e.g., SBR, ER, temperature, date) for all SPA samples taken from Agrol, willow and DDGS gasification at TUD and TUM, they can be found in **Table 6- 1**.

Table 6- 1 SPA samples for Agrol, willow and DDGS gasification at TUD and TUM

Test name	TUD measurement campaign									
SPA	0415A	0415B	0415C	0415D	0415E	0415F	0421A	0421B	0423F	0423G
Fuel	Agrol						DDGS			
SBR (-)	1.45	1.21	1.13	0.97	1.16	1.25	1.10	0.98	0.95	1.08
ER(-)	0.38	0.38	0.38	0.35	0.35	0.35	0.37	0.37	0.36	0.36
T (°C)	770	770	775	815	810	810	730	740	750	750
SPA	0419A	0419B	0419C	0419D	0419E	0419F	0419G	0419H	0419I	
Fuel	Willow									
SBR (-)	1.19	0.99	1.27	0.93	1.13	1.22	0.90	1.04	1.14	
ER(-)	0.38	0.38	0.38	0.38	0.38	0.38	0.39	0.39	0.39	
T (°C)	740	740	740	780	780	780	820	820	820	
Test name	TUM measurement campaign									
SPA	A1	A3	A7	A9	A10	A11*	A12*	A13*	A0	
Fuel	Agrol									
Date	20100607								20100604	
SBR	0.83	1.2	0.83	1.2	0.84	1.21	0.84	1.21	0.83	
T (°C)	750	750	840	840	750	750	800	800	750	
SPA	W1	W3	W7	W9	W10*	W11*	W12*	W13*		
Fuel	Willow									
Date	20100608				20100609					
SBR	0.86	1.18	0.86	1.18	0.9	1.21	0.9	1.21		
T (°C)	750	750	840	840	750	750	800	800		
SPA	D1	D2	D3	D4	D5	D6				
Fuel	DDGS						Remark * under pressure tests, others all atmospheric tests			
Date	20100609									
SBR	0.9	1.19	0.9	1.19	0.9	1.19				
Temperature (°C)	700	700	750	750	800	800				

## 6.1 On-line analysis comparison

The measured total tar concentration obtained from willow gasification at the PBFB gasifier using the LIFS and OTA methods is shown in **Figure 6- 1**. The term “total tar concentration” used in this study measured by the LIFS method (Total tar\_LIFS) is an underestimation of the total concentration of all tars because it represents the concentration sum of the 14 individual tar compounds and not the overall complete tar content of the gasification process.



*Figure 6- 1 Comparison of on-line tar measurement between the LIFS and OTA methods during willow gasification at TUM (Sample W1-W13)*

As can be seen in **Figure 6- 1**, the total tar concentration changed with varying process parameters (e.g., increasing temperature or SBR), which was measured by using both LIFS and OTA methods. However, when the gasifier ran at constant process parameters (e.g., temperature, SBR remained stable), the measured total tar concentration using the LIFS method remained fairly stable, but using the OTA method it showed much more fluctuations. These observations indicate that both LIFS and OTA methods can measure the change of the gasifier’s performance in real time; however, the LIFS method appeared to quantify tar concentration more accurately than the OTA method. Furthermore, the change trends of H<sub>2</sub> and CH<sub>4</sub> concentration are also presented in **Figure 6- 1**. It can be seen that H<sub>2</sub> concentration increased with decreasing tar concentration, but CH<sub>4</sub> concentration practically showed an opposite trend. For example, CH<sub>4</sub> concentration produced from Agrol gasification at atmospheric pressure at a temperature of 750 °C with SBR =1 was around 6.6 vol.% on a dry basis, but under pressure the concentration increased up to 9.0 vol.% on a dry basis.

Furthermore, it can be observed in **Figure 6- 1** that there is a sharp drop in the measured tar by using the OTA analysis (in light orange circle) at the time around 15:00h PM during willow gasification, which is because at that moment a different carrier gas (N<sub>2</sub>) pressure was set to check how much the pressure of carrier gas affect the measured tar content. From this observation it can be concluded that the carrier gas pressure does largely influence the measured tar content. According to Moersch et al. (Moersch et al., 1997; Moersch et al., 2000), an increase in the carrier gas flow resulted in higher and taller peaks and reduced measurement time, which could affect the measured tar concentration. Therefore, such an operation should be avoided during running measurements. Furthermore, when interpreting the data obtained from the OTA method, it was also observed that the response factor



(RF) determined at different days could cause a noticeable influence on the amount of tar detected, but the measuring range (MR) only affected the detected tar content slightly. For example, the measured results of the total tar content during Agrol gasification on the 1<sup>st</sup> day (4<sup>th</sup> June) measurement from the OTA method are presented in **Figure 6- 2**.

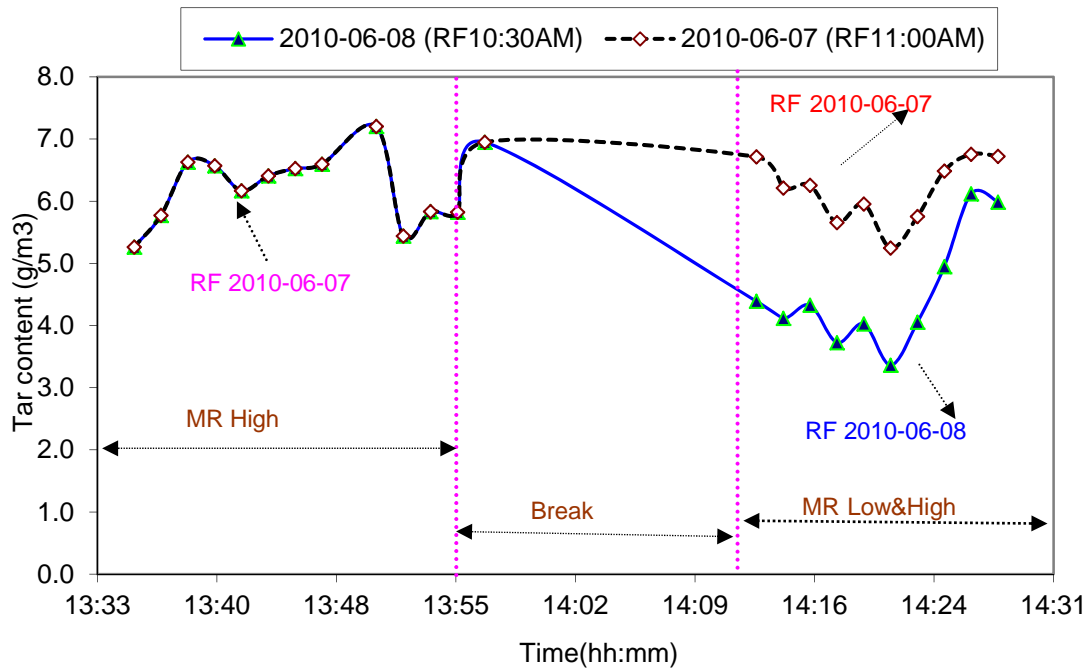


Figure 6- 2 The total tar content measured by the OTA method during Agrol gasification at TUM (Sample A0)

It can be seen from **Figure 6- 2** that the total tar content determined by using the RF value from different days (7<sup>th</sup> and 8<sup>th</sup> June) was fairly different ( $\pm 2.3 \text{ g/m}^3$ ), although it showed a similar fluctuation margin. However, under the same operational conditions, the averaged total tar content measured by using MR High and MR Low & High and the RF determined on 7<sup>th</sup> June was both around  $6.2 \text{ g/m}^3$ . According to the OTA user manual (Ratfish), the sensitiveness limit for the condensable hydrocarbons is about 0.2% of the total HC content in the sample gas, which means that if the total HC content is about  $1000 \text{ mg/Nm}^3$  this could result in a background noise of  $< \pm 20 \text{ mg/Nm}^3$ . Therefore, when the total tar content in the sample gas is around  $6.2 \text{ mg/m}^3$ , the measured value range of  $6.08$  to  $6.3 \text{ mg/m}^3$  is reasonable. From **Figure 6- 2** it can be seen that the highest and lowest tar content measured by using MR Low & High and MR High was  $6.7$  and  $5.3 \text{ mg/m}^3$ , and  $7.2$  and  $5.3 \text{ mg/m}^3$ , respectively. Although the measured total tar content using both MR values had a wider fluctuation margin than it expected, it seems that the MR Low & High was more sensitive than the MR High which is why this range was used during further measurement. However, the large difference between the measured total tar content by using the RF determined on different days was quite remarkable, since except for the RF value determined on different days all other parameters (e.g., carrier gas  $\text{N}_2$  pressure, oven temperature, the MR value) during the calibration remained the same. Therefore, in order to achieve good measurement results by using this OTA analyzer, a regular calibration (i.e., daily) is necessary.

## 6.2 Individual tar component comparison

The measured concentrations of 10 individual tar components from Agrol, willow and DDGS gasification at TUD test rigs using the SPA and LIFS methods are presented in **Figure 6- 3**, **Figure 6- 4** and **Figure 6- 5**, and at TUM in **Figure 6- 6**, **Figure 6- 7** and **Figure 6- 8**, respectively. The considered individual tar components include phenol, o-cresol, m-cresol indene, biphenyl, anthracene,

fluorene, naphthalene, fluoranthene and pyrene. In these figures, o/m-cresol and fluo+pyr represent the concentration sum of o-cresol and m-cresol, and sum of fluoranthene and pyrene, respectively.

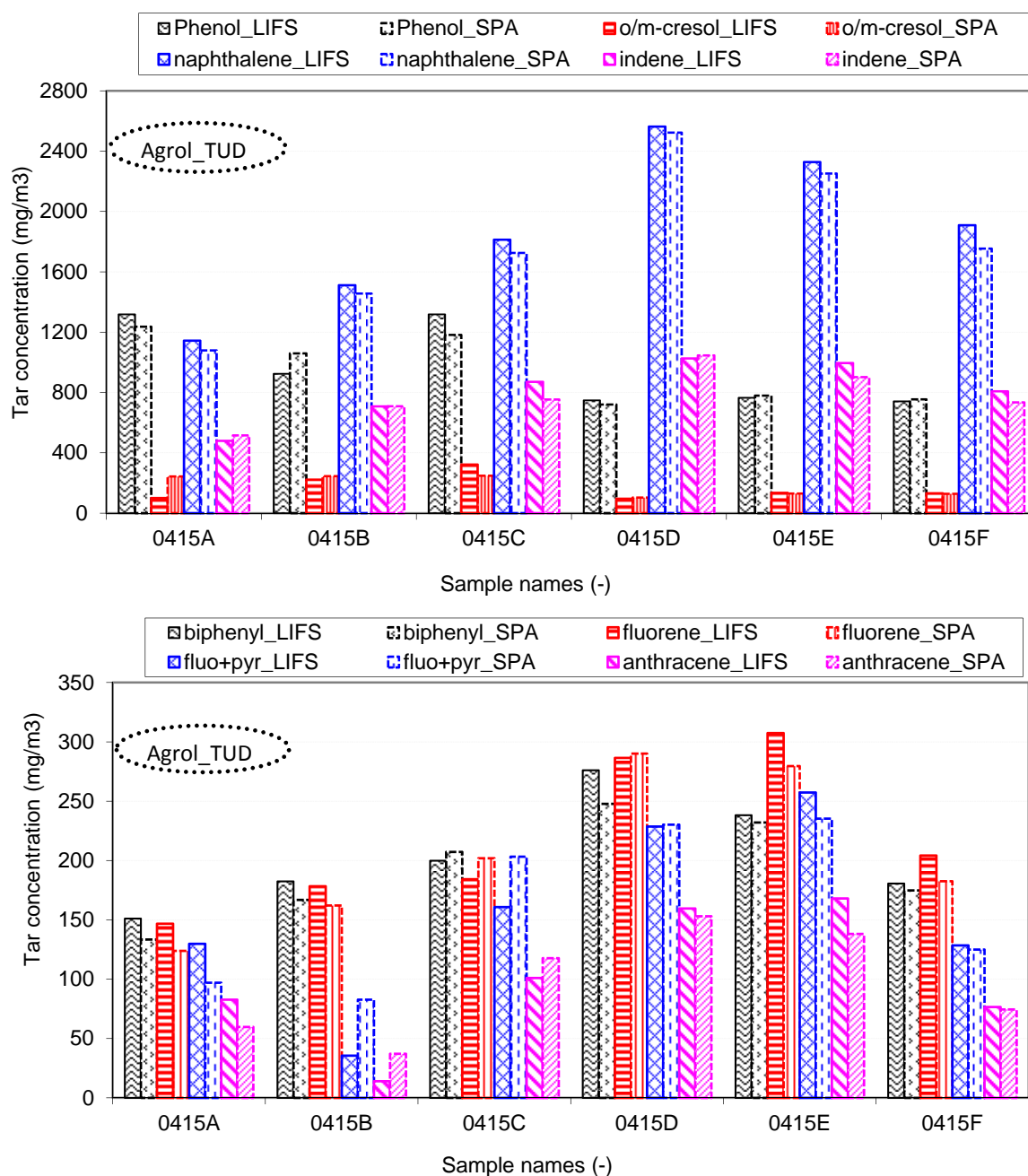


Figure 6- 3 Comparison of individual tar components obtained from Agrol gasification at TUD

### 6.2.1 Individual tar compounds from CFB gasification tests

Several observations can be drawn from the results obtained from the CFB gasification tests at TUD shown in **Figure 6- 3**, **Figure 6- 4** and **Figure 6- 5**. In general, there was a fairly good agreement between the measured results using the SPA and LIFS methods. For most tar components obtained from Agrol and willow gasification, the average difference between the measured values using the SPA and LIFS methods was within  $\pm 10\%$ . A higher difference ( $>30\%$ ) was observed for some heavier tar components such as anthracene, fluoranthene and pyrene quantified during DDGS gasification. For instance, at a temperature of  $730\text{ }^{\circ}\text{C}$  with an SBR value of 1.1 (sample 0421A, see **Figure 6- 5**), the concentrations of anthracene, fluoranthene + pyrene measured using the SPA and LIFS methods were 32 and 23  $\text{mg}/\text{Nm}^3$ , and 16 and 13  $\text{mg}/\text{Nm}^3$ , respectively. The large difference between these two

methods could be due to their low concentration values, since tar concentration lower than 20~30 mg/Nm<sup>3</sup> measured using the SPA method shows much lower accuracy. Under most operational conditions, the concentrations of tar components measured by the LIFS method were higher than those measured by the SPA method, which might be due to some tar loss during the SPA tar sample pretreatment (solvent extraction) before the analysis (Brage et al., 2000).

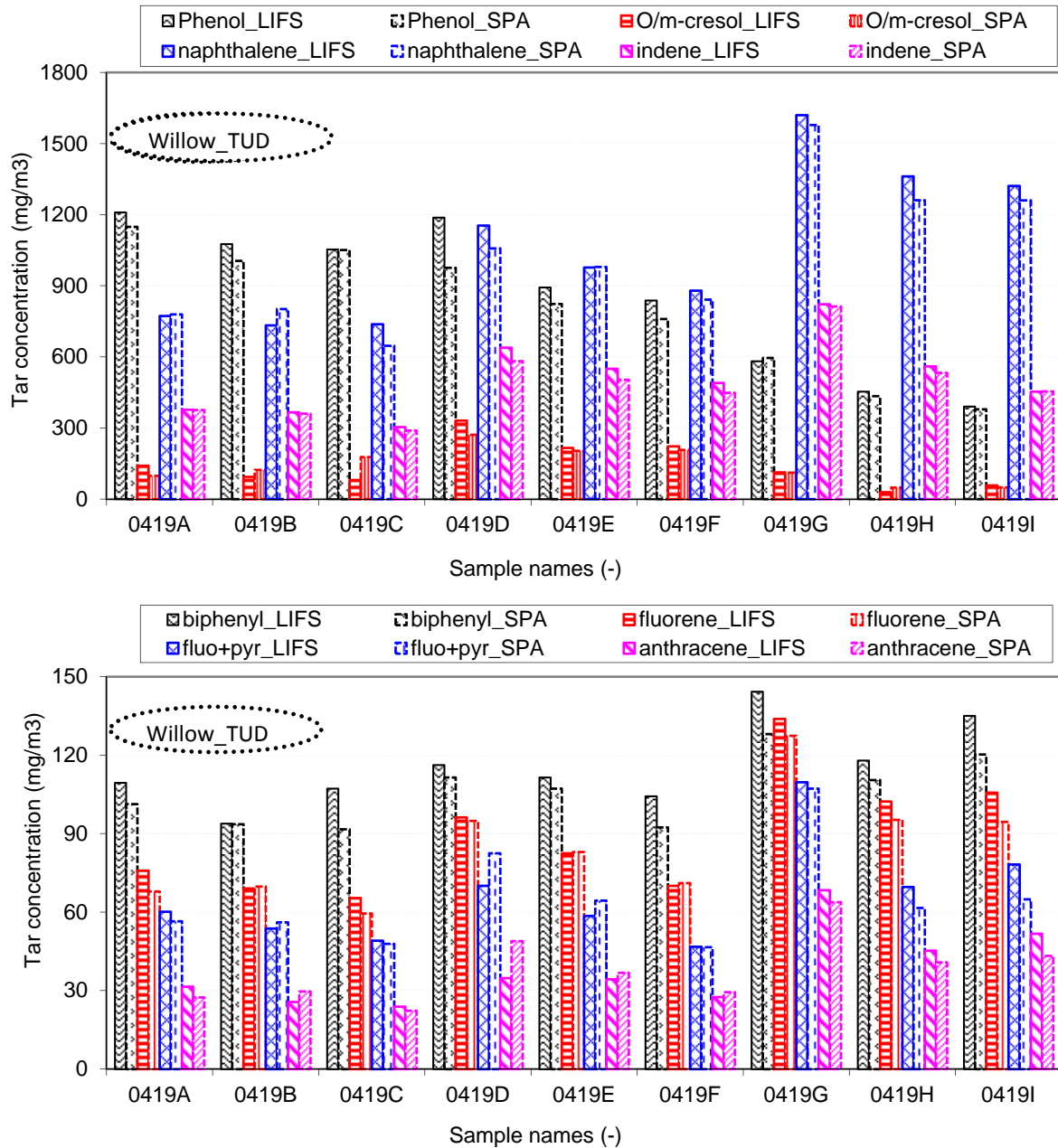


Figure 6- 4 Comparison of individual tar components obtained from willow gasification at TUD

From **Figure 6- 3** and **Figure 6- 4** (also see SBR values in **Table 6- 1**), it can be seen that the concentrations of heavier tar compounds such as indene, naphthalene, biphenyl, anthracene, fluorene, fluoranthene and pyrene, generally decreased with increasing SBR, which is probably due to enhanced steam reforming reactions as reported by most researchers (Li et al., 2004; Meng et al., 2011a; Rapagna et al., 2000). For instance, during Agrol gasification with increasing SBR from 0.97 to 1.25 (sample 0415D to F, see **Figure 6- 3**), the concentration of naphthalene measured using the LIFS and SPA methods decreased from 2.56 to 1.91 g/Nm<sup>3</sup> and 2.52 to 1.75 g/Nm<sup>3</sup>, respectively. During willow

gasification, with increasing SBR from 0.93 to 1.22 (sample 0419 D to F, see **Figure 6- 4**), the measured concentration of naphthalene using the LIFS and SPA methods decreased from 1.15 to 0.88 g/Nm<sup>3</sup> and 1.06 to 0.84 g/Nm<sup>3</sup>, respectively. From these several SPA samples, it can also be seen that the naphthalene concentration obtained from Agrol and willow gasification measured using the LIFS and SPA methods show a good agreement. Higher temperature values generally favored the formation of indene, biphenyl, anthracene, fluorene, naphthalene, fluoranthene and pyrene, but largely reduced the formation of phenol and o/m-cresol. For instance, when the temperature was increased from 780 to 820 °C (sample 0419 E to I, see **Figure 6- 4**) during willow gasification, the measured concentration of naphthalene using the LIFS and SPA methods increased from 0.98 to 1.32 g/Nm<sup>3</sup> and 0.98 to 1.26 g/Nm<sup>3</sup>, respectively. On the other hand, the measured phenol concentration using the LIFS and SPA methods decreased from 0.89 to 0.39 g/Nm<sup>3</sup> and 0.82 to 0.38 g/Nm<sup>3</sup>, respectively.

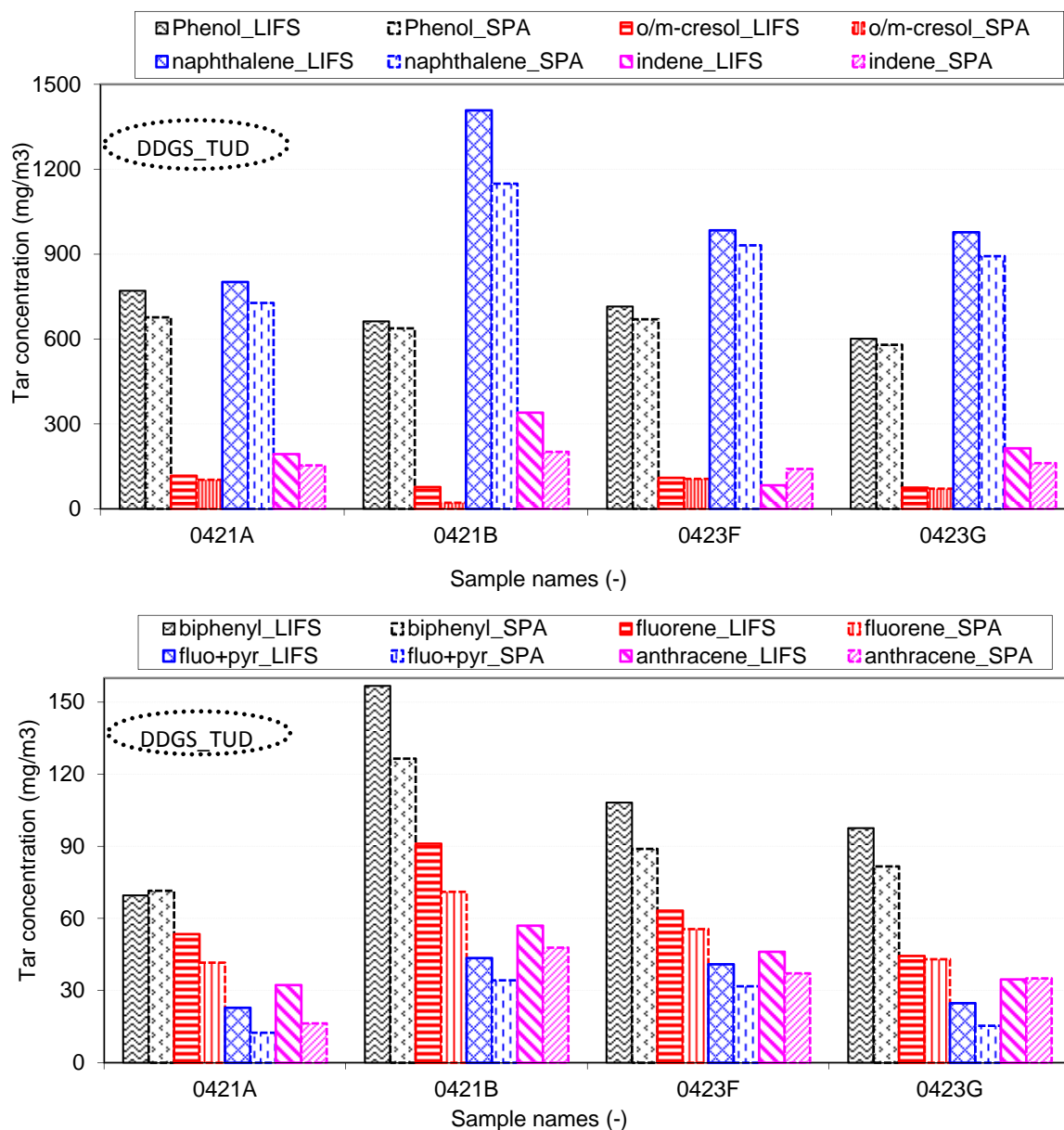


Figure 6- 5 Comparison of individual tar components obtained from DDGS gasification at TUD

## 6.2.2 Individual tar compounds from PBFB gasification tests

Similarly, interesting observations have been made concerning the results from PBFB gasification tests at TUM, which are shown in **Figure 6- 6**, **Figure 6- 7** and **Figure 6- 8**.

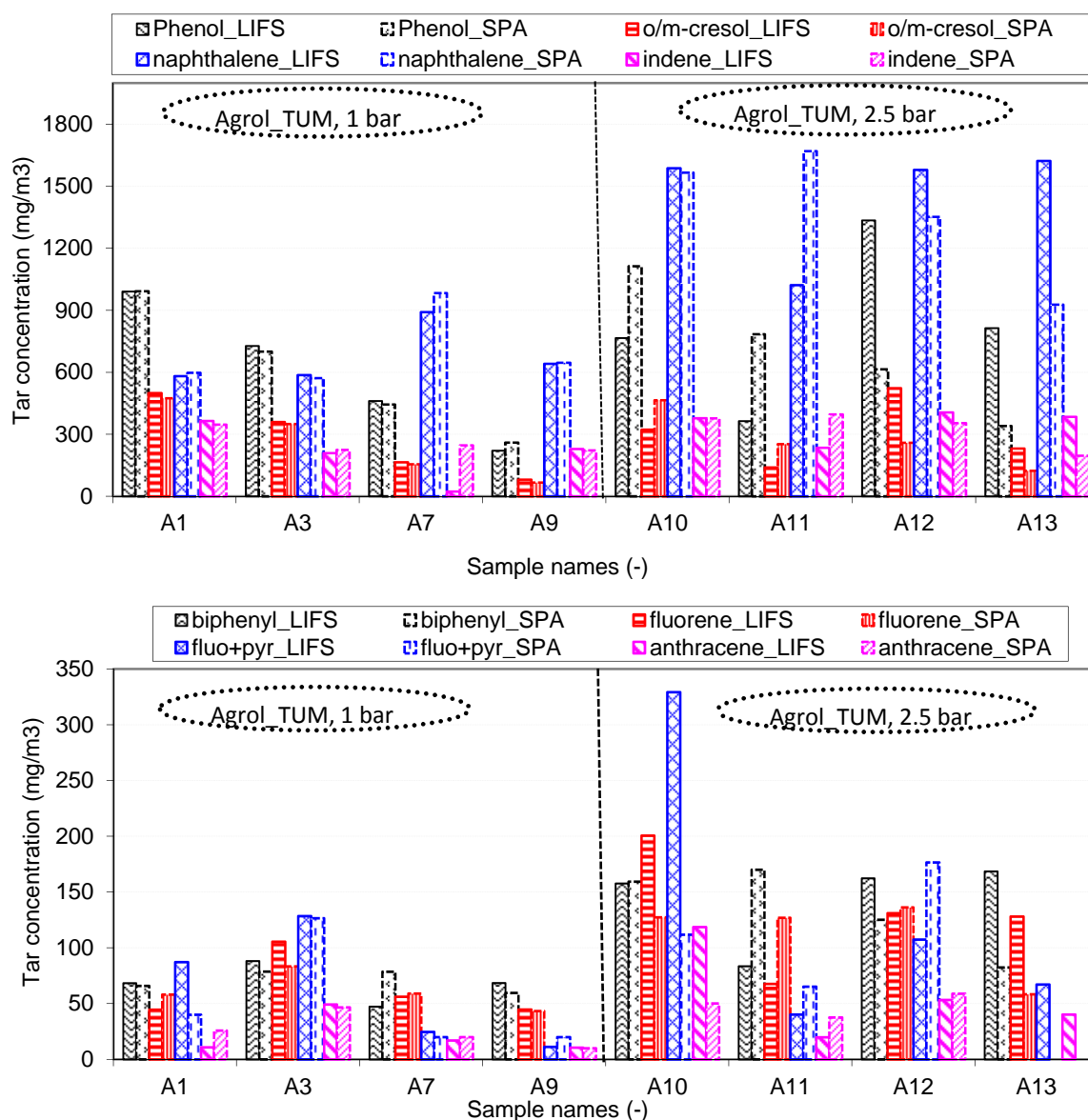


Figure 6- 6 Comparison of individual tar components obtained from Agrol gasification (Sample A1-A13) at TUM

Concerning Agrol and willow gasification at atmospheric pressure, the measured concentrations of tar components such as phenol, o/m-cresol, indene, naphthalene and biphenyl using the SPA and LIFS methods agreed well. For instance, during Agrol gasification at a temperature of 750 °C with an SBR value of 0.83 (sample A1, see **Figure 6- 6**), the measured phenol concentration using the LIFS and SPA methods both were around 0.99 g/Nm<sup>3</sup>. Under similar operation conditions (sample W1), the measured phenol concentration obtained from willow using the LIFS and SPA methods was 1.04 and 0.99 g/Nm<sup>3</sup>, respectively, which shows a good correspondence of both quantification methods for this compound. However, during willow gasification at a temperature of 840 °C (sample W 7 and 9, see **Figure 6- 7**), around 10 mg/Nm<sup>3</sup> of anthracene and the total 50~100 mg/Nm<sup>3</sup> of fluoranthene and pyrene were measured by using the LIFS method, while almost nothing was measured using the SPA method.

Concerning Agrol and willow under pressurized gasification, the measured concentrations of most tar components were fairly different by using the LIFS and SPA methods compared to atmospheric gasification. Regarding all tar compounds obtained from DDGS gasification at temperatures higher



than 750 °C, their concentrations measured by LIFS and SPA agreed fairly well. However, at a temperature of 700 °C with an SBR value of 1.19 (sample D2, see **Figure 6- 8**), the measured o/m-cresol and indene concentrations using LIFS method were both around 0.26 g/Nm<sup>3</sup>, while the values by using SPA method were only 0.13 g/Nm<sup>3</sup>. The aforementioned observations lead to a conclusion that when the tar concentration is low, the measured difference between the LIFS and SPA methods is comparatively high. Moreover, the concentrations of tar compounds such as anthracene, fluoranthene and pyrene produced during most of the operational conditions were generally lower than 100 mg/Nm<sup>3</sup>. Their concentrations obtained from pressurized willow gasification were even lower than 20 mg/Nm<sup>3</sup>. For this case, their measured results using the SPA method may be less accurate.

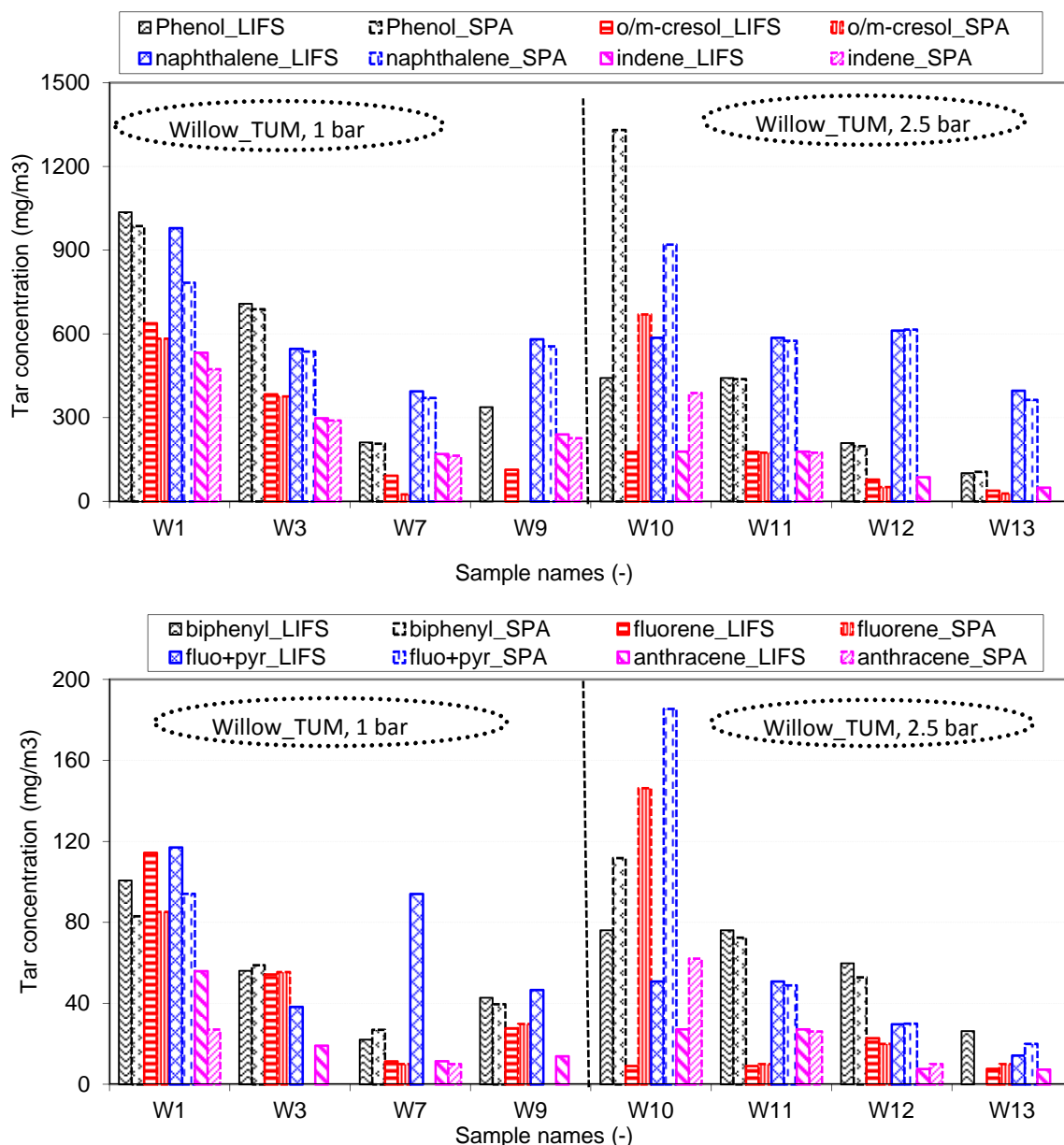


Figure 6- 7 Comparison of individual tar components obtained from willow gasification (Sample W1-W13) at TUM

The concentrations of most tar compounds decreased with increasing SBR. These results agreed well with those obtained from TUD measurements. For instance, with increasing SBR from around 0.9 to 1.2 (sample W1 to W3, D3 to D4) at a temperature of 750 °C, the measured concentration of naphthalene obtained from gasification of willow and DDGS pellets using the LIFS and SPA methods decreased from 0.98 to 0.55 g/Nm<sup>3</sup> and 0.78 to 0.54 g/Nm<sup>3</sup>, and 0.71 to 0.5 g/Nm<sup>3</sup> and 0.71 to

0.46g/Nm<sup>3</sup>, respectively. A higher temperature again significantly reduced the formation of phenol and o/m-cresol, which agree well with the results obtained from the CFB gasification tests at TUD. For instance, with increasing temperature from 750 to 840 °C (Sample A1 to A7, see **Figure 6- 6**; W1 to W7, see **Figure 6- 7**), the measured concentration of phenol obtained from Agrol and willow gasification using LIFS and SPA methods decreased from 0.99 to 0.46 g/Nm<sup>3</sup> and 0.99 to 0.44 g/Nm<sup>3</sup>, and 1.04 to 0.21 g/Nm<sup>3</sup> and 0.99 to 0.21 g/Nm<sup>3</sup>, respectively.

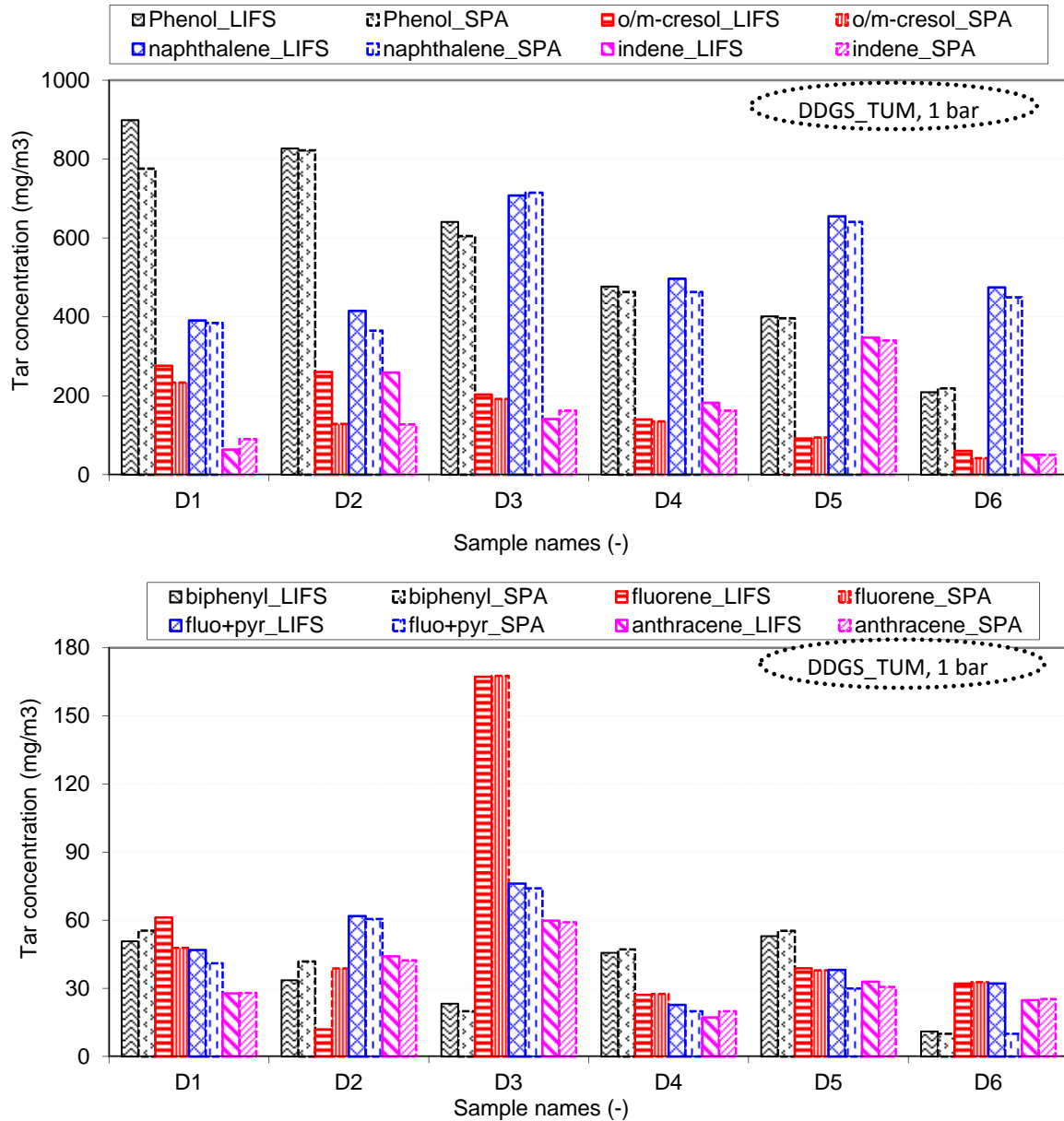


Figure 6- 8 Comparison of individual tar components obtained from DDGS gasification (Sample D1-D6) at TUM

Besides SBR and temperature values, reactor pressure also affected tar formation. Except for o/m-cresol, the formation of other tar compounds during Agrol gasification generally increased with an increase in the pressure under most operational conditions. For instance, at a temperature of 750 °C with SBR of approximately 0.84, when the pressure was increased from 1.0 to 2.5 bar, the measured concentration of naphthalene using the LIFS and SPA methods sharply increased from 0.58 to 1.59g/Nm<sup>3</sup> and 0.6 to 1.57 g/Nm<sup>3</sup>, respectively. However, under the same conditions, the measured concentration of phenol using the LIFS method decreased from 0.99 to 0.77 g/Nm<sup>3</sup>, but increased from 0.99 to 1.11 g/Nm<sup>3</sup> by using the SPA method. Furthermore, when the pressure was increased from 1.0 to 2.5 bar, the measured concentrations of anthracene, fluoranthene and pyrene using LIFS and SPA

method also showed an opposite change trend. According to Knight (Knight, 2000) who studied biomass gasification under different pressures, the fraction of PAH increased with enhancing pressure. The pressure seems to affect the formation of tar obtained from willow gasification in a different way. During willow gasification, the formation of all tar compounds except for naphthalene decreased with increasing pressure under most operational conditions. However, for heavier tar compounds such as biphenyl, anthracene, fluorene, fluoranthene and pyrene, their measured concentrations using the LIFS and SPA methods showed exactly an opposite change trend at lower SBR values. For instance, at a temperature of 750 °C with an SBR of approximate 0.8, when the pressure was increased from 1.0 to 2.5 bar, the measured concentrations of biphenyl, anthracene, fluorene, fluoranthene and pyrene using the LIFS method decreased, while using the SPA method all the aforementioned compound concentrations increased. An explanation for this difference could be that during willow gasification, some blockage in the cyclone occurred which could lead to some tar components being filtered out, cracked or converted in the fixed bed of char/ash that was accumulating in the cyclone. This might be the reason the low tar concentration obtained from willow gasification under pressure.

## 6.3 Total tar concentration comparison

The comparison of the total tar concentration obtained from Agrol, willow and DDGS gasification at TUD and TUM test using different techniques is presented in **Figure 6- 9**. Total tar\_LIFS, Total tar\_SPA and Total tar\_OTA represent the total tar concentration measured by using the LIFS, SPA and OTA method, respectively. Same\_LIFS and Same\_SPA represent the sum of the concentrations of 10 individual tar compounds measured by using the LIFS and SPA methods, respectively.

### 6.3.1 Total tar concentration from CFB gasification tests

Since the OTA analyzer could not be used properly during the TUD measurement campaign, only the total tar concentrations measured by the LIFS and SPA methods were compared. In **Figure 6- 9**, it can be seen that the total concentration of the 10 individual corresponding tar components measured using the LIFS and SPA agreed fairly well. The difference between the measured results from the LIFS and SPA methods under almost all conditions was within  $\pm 6\%$ . The total tar concentration measured by the SPA method was much higher than that by the LIFS method, but showed the same trend with varying process parameters (e.g., SBR, temperature). Higher temperatures and higher SBR values were favorable for the tar decomposition. Since the SPA method is capable of measuring more tar components than the LIFS method, it is not difficult to explain the measured difference between these two methods. From these results, it can be concluded that the LIFS method is a reliable on-line tar measurement technique and can be used to monitor the tar concentration trends as well as the performance of the gasifier in real time under most operational conditions.

### 6.3.2 Total tar concentration from PBFB gasification tests

In **Figure 6- 9**, it can be observed that the total measured concentrations of 10 individual tar compounds obtained from all three fuels gasification at atmospheric pressure using the LIFS and SPA methods agreed reasonably well, but not at that level as in the comparison of the CFB measurements at TUD. This could be due to some handling problems, since the SPA sampling point at TUM is located in a fairly inconvenient place. Furthermore, there was also could be some pressure build up in the SPA tube during sampling. Concerning the total concentration of 10 individual tar compounds obtained from Agrol and DDGS gasification within the temperature range of 750 to 800°C, the averaged difference between the measured results from the LIFS and SPA methods under almost all conditions was within  $\pm 8\%$ . However, as far as the total concentration of 10 individual tar compounds obtained from willow gasification under all operational conditions and from DDGS gasification at the temperature of 700°C is concerned, the averaged difference between the measured results from the LIFS and SPA methods was becoming slightly higher which was within 10-20%. During Agrol and willow pressurized gasification, a high difference was also observed between Same\_SPA and Same\_LIFS. By evaluating these results, it can be concluded that the pressure largely affected the measured tar concentration from the LIFS method.



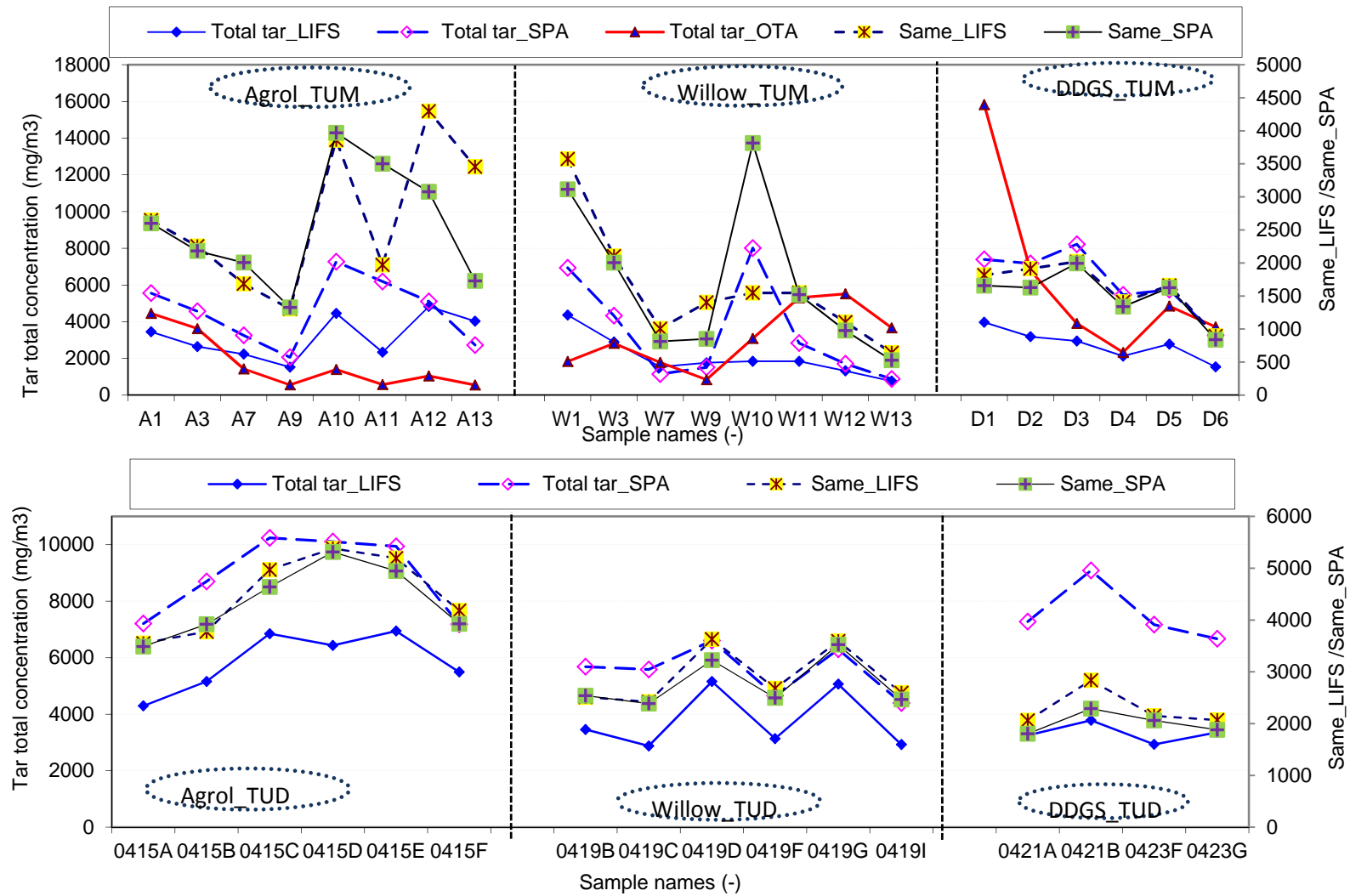


Figure 6- 9 Comparison of the total tar concentration obtained from Agrol, willow and DDGS gasification at TUD and TUM

The total tar concentration measured by the LIFS, SPA and OTA methods showed similar trends with varying process parameters and all decreased with increasing temperature and/or SBR values. However, a large difference was observed among the measured total tar concentration using the LIFS, SPA and OTA methods. Regarding willow gasification within the temperature range of 800 to 850 °C, the total tar concentration measured by using all three methods agreed well, but a large difference was observed at other operational conditions. For DDGS, the total tar concentration measured by the LIFS method was the lowest, followed by that from the OTA and SPA method, except for at a temperature of 700 °C. The measured difference between the SPA and LIFS method was not difficult to explain, since the LIFS method can detect fewer tar compounds. Concerning, the difference between the OTA and SPA method, it could be due to their availability of possibly measure tar components. Furthermore, Moersch et al. (Moersch et al., 2000) also reported that the minimum tar concentration that can be detected by the analyzer is about 50 mg/Nm<sup>3</sup>. In this way, probably some heavy tar components (e.g., fluoranthene, pyrene) with low amounts could not be detected by the OTA analyzer. In **Figure 6- 9**, at the beginning of the measurement during DDGS gasification, the total tar concentration measured by the OTA method was fairly high which was due to the fact that the measured tar content was quantified by using the RF determined later. Thus, this part of data is less accurate.

However, with varying the pressure, the measured total tar concentration by using three different methods showed different trends. Regarding Agrol gasification, when the pressure was increased from 1.0 to 2.5 bar at a temperature of 750 °C with SBR of approximately 0.83 (Sample A1 to 10, see **Figure 6- 6**), the total tar concentration using the LIFS and SPA methods increased from 3.45 to 4.45 g/Nm<sup>3</sup> and 5.55 to 7.27 g/Nm<sup>3</sup>, while it decreased from 4.45 to 1.4 g/Nm<sup>3</sup>, respectively, by using the OTA method. However, when a slightly higher SBR of around 0.9 was applied under similar operational conditions, the total tar concentration obtained from willow gasification measured by using the LIFS method decreased from 4.36 to 1.84 g/Nm<sup>3</sup>, while it increased from 6.94 to 8.0 g/Nm<sup>3</sup> and from 1.83 to 3.09 g/Nm<sup>3</sup>, respectively, when measuring with the SPA and OTA methods. Based on these observations, it can be concluded that the measured results by the OTA method are also largely affected by the pressure just as the LIFS method. Concerning the different tar formation behavior during Agrol and willow gasification under pressurized conditions, some additional experiments may be required in order to understand it better.

## 6.4 Conclusion

The analyzed results from on-line tar measurement campaign showed that the measured concentration of the selected 10 individual corresponding tar compounds obtained from the steam-oxygen blown CFB and the steam blown PBFB atmospheric pressure biomass gasification tests using the off-line SPA and the on-line LIFS methods agreed reasonably well for all three fuels tested under most operational conditions. The total tar concentration measured by the LIFS, SPA and OTA methods showed similar trends with varying process parameters. The LIFS method is a reliable on-line tar measurement technique as its measured results agreed well with that from the SPA method. Both the LIFS and OTA on-line methods can be used as an indicator to monitor the change of the gasifier performance in real time. However, in order to achieve good and reliable tar measurement results, a regular calibration at least daily of the OTA method is very important. The settings of the OTA analyzer used for the measurement should remain the same as those used during the calibration procedure. Since the RF value is very sensitive to all parameters, such as carrier gas flow, MR, and sample gas pressure, a change of any of these parameters could lead to an influence on the actual measurement results to certain extent. For the LIFS method, it will be better if more tar components are calibrated and then quantified during measurement.

## **7 Characterization of different CFB gasification residual chars and comparison of their gasification behavior with TG-derived pyrolysis chars**

---

*Due to the inconvenience of studying the devolatilization process of Agrol, willow and DDGS in the CFB gasifier, the pyrolysis of three fuels and their residual char gasification have been studied by using TGA-FTIR system. This chapter first presents the characterization results of CFB-Chars obtained from different analytical techniques. Then the pyrolysis behavior of three fuels under different heating rates is analyzed. Finally, the gasification behavior of CFB-Char and TG-derived PYR-Char pyrolysis under different operational conditions (e.g., gasification temperature, CO<sub>2</sub> concentration) is compared. The kinetic parameters of char gasification are determined using the volumetric reaction model (VRM) and the shrinking core model (SCM). This part of work has been published in the Energy and Fuels Journal and the Biomass Conversion and Biorefinery Journal.*

**Meng, X., Benito, P., de Jong, W., Basile, F., Verkooijen, A. H. M., Fornasari, G., Vaccari, A.** 2012. Steam-O<sub>2</sub> Blown CFB Biomass Gasification: Characterization of Different Residual Chars and Comparison of Their Gasification Behavior with TG-derived Pyrolysis Chars. *Energy and Fuels*, 26 (1), pp 722–739

**Meng, X., de Jong, W., Fu, N., Verkooijen, A.H.M.** 2011. DDGS chars gasification with CO<sub>2</sub>: a kinetic study using TG analysis. *Biomass Conversion and Biorefinery, Processing of Biogenic Material for Energy and Chemistry*, 1 (4), 217-227.

Chapters 4 to 6 presented the results concerning sulfur distribution and capture, as well as tar formation and measurement techniques during biomass gasification using different fluidized bed gasifiers. As another important issue relating to biomass gasification, char reactivity can be largely influenced by pyrolysis and char reaction conditions. Therefore, this chapter and the following chapter will present the main results concerning char reactions. As mentioned in literature overview study, less research has been focused on studying the morphology and reactivity of char produced from biomass gasification in fluidized beds, in particularly in a steam-O<sub>2</sub> blown CFB gasifier. Subsequently, the combined study of the pyrolysis process and char reactions is also less reported in the literature. Moreover, the gasification behavior of chars produced from some special agriculture residues such as DDGS has seldom been studied. Therefore, the results addressed in this chapter are used to answer abovementioned issues with an emphasis on:

- 1) Chemico-physical characterization of several char samples which were obtained after gasification of three different fuels in the 100 kW<sub>th</sub> steam-O<sub>2</sub> blown CFB gasifier.
- 2) Investigation of the pyrolysis behavior of three different fuels using a TGA-FTIR system
- 3) Study towards the gasification behavior of different char samples under different conditions (e.g., different temperatures, CO<sub>2</sub> concentrations) using the TGA.

## 7.1 Char samples

As mentioned in chapter 3, the gasification behavior of two different types of char samples has been investigated using TGA-FTIR. CFB-Chars were collected from the downcomer of the CFB gasifier after Agrol, willow and DDGS gasification under different operational conditions (See **Table 7- 1**). PYR-Chars were obtained after the pyrolysis of Agrol, willow and DDGS at different heating rates (HR=2, 5, 10, 30, 50, and 70 °C/min) and different pyrolysis temperatures (T<sub>Pyr</sub>=750, 850, 900 °C). Char gasification procedures have been described in chapter 3 (see **Figure 3- 9**). In general, char gasification was performed at different isothermal temperatures (T<sub>Ga</sub> = 900, 1000 and 1100 °C) using different CO<sub>2</sub> concentrations (CO<sub>2</sub> =10, 20 and 30 vol.%).

*Table 7- 1 CFB-Char obtained from Agrol, willow and DDGS gasification*

Char type	Char Agrol A4-15	Char Agrol A11-23	Char willow W4-19	Char willow W12-1	Char DDGS D10-9
Temperature(°C)	700-830	830-850	700-830	830-850	780-830
ER	0.35-0.38	0.35	0.38-0.39	0.38	0.38
SBR	1.0-1.45	1.12	0.9-1.2	1.0	0.81-0.83

## 7.2 Char gasification conversion models

To determine Arrhenius kinetic parameters for char gasification, the volumetric reaction model (VRM) and the shrinking core model (SCM) have been applied. The VRM assumes that the char particle reacts homogeneously with CO<sub>2</sub> and that the particle size remains constant while the density decreases during the reaction (Murillo et al., 2004). The SCM assumes that the reaction initially occurs at the external surface of char and gradually CO<sub>2</sub> diffuses through the gas film, the ash layer and reacts on the un-reacted core surface which keeps on shrinking, but always exists during the reaction progress (Bhat et al., 2001; Lee & Kim, 1996). The overall reaction rates for VRM and SCM are expressed in equation **Eq.7- 1** and **Eq.7- 2**, where X, K<sub>VRM</sub> and K<sub>SCM</sub>, n and C<sub>CO2</sub> represent char conversion (-), the reaction rate constants of the VRM and SCM methods, the reaction order (-) and the concentration of CO<sub>2</sub> (vol.%), respectively. K<sub>VRM</sub> / K<sub>SCM</sub> and X were calculated using equations **Eq.7- 3** and **Eq.7- 4**, where k<sub>0</sub>, Ea, R<sub>g</sub> and T represents the pre-exponential factor (min<sup>-1</sup>), the activation energy (J/mol), the universal gas constant (8.314 J/(mol·K)) and the reaction temperature (K), and m<sub>0</sub>, m<sub>t</sub> and m<sub>f</sub> represents the initial char weight, the char weight at time *t* and the residue char weight, respectively.

$$\frac{dX}{dt} = K_{VRM} (1 - X) C_{CO_2}^n \quad \text{Eq.7- 1}$$

$$\frac{dX}{dt} = 3K_{SCM} (1 - X)^{2/3} C_{CO_2}^n \quad \text{Eq.7- 2}$$

$$K_{VRM} (\text{or } K_{SCM}) = k_0 \exp\left(\frac{-E_a}{R_g T}\right) \quad \text{Eq.7- 3}$$

$$X = \frac{m_0 - m_t}{m_0 - m_f} \quad \text{Eq.7- 4}$$

### 7.3 Characterization of CFB-Char

The properties of CFB-Char samples were studied by XRD, XRF, N<sub>2</sub> adsorption/desorption at -196°C and SEM coupled with EDS. The microstructure and qualitative chemical composition of CFB-Chars were studied by SEM coupled with EDS (see **section 3.2.2** in chapter 3 for detailed descriptions). The SEM images of Agrol, willow and DDGS chars are shown in **Figure 7- 1**, **Figure 7- 2** and **Figure 7- 3**, respectively. It can be observed from these SEM images that Agrol chars were very porous with different superficial cavities and thin walls, which indicates that the fibrous structure of the parent biomass was practically retained. The macropores observed were probably related to the evolution of the volatile matters during the gasification. There were no significant differences between A11-23 and A4-15 samples. Willow chars had also a fibrous morphology, while the structure was more compact and agglomerated which points towards some plastic deformation that might have taken place. Moreover, small particles deposited on the surface of char were observed, which might be attributed to some ashes. DDGS chars had a macroporous structure with rounded pores of different sizes and some particulate matters on the surface. Some slit shaped pores were also observed in the DDGS char. In these samples plastic deformation seemed to take place to a greater extent. The results observed from the EDS analysis revealed that the composition of the CFB-Chars was not completely homogeneous and the inorganic elements were mainly present in the small particles and their amounts varied depending on the zone analyzed. Agrol and willow chars had high contents of K and Ca on the surface with smaller amounts of Mg, Fe, Al, Si and P, while DDGS char had high contents of K and P with some amounts of Na, Ca and Mg observed on the SEM-EDS analysis images (see **Table A- 4** in appendix for element composition in details).

The main composition of the CFB-Char samples obtained by the XRF analysis and their parent fuels is summarized in **Table 7- 2**. The results showed that the inorganic content of the Agrol char was mainly formed by Ca, Fe, K, Mg, and Si. The willow char was mainly composed by Ca and K with minor amounts of Fe, Mg, P and Si, whereas DDGS char was mainly dominated by K and P, with a lesser amount of Ca, Mg and Na. Making a comparison among the inorganic elements in the chars and the original biomass fuels, in general, there is a good agreement between the values, which means that the most abundant elements in their parent fuels were also those present in their residual chars in a higher percentage. However, some deviations from this behavior were observed. For instance, for Agrol a quite larger Fe content was measured in the char together with an increased amount of Mg and Si. This behavior may be due to the deposition of some olivine bed material. The O measured by the XRF analysis is related to the presence of oxygen containing compounds such as oxides or phosphates in the chars; therefore, the largest the O content in DDGS and willow chars would suggest a higher ash content in the chars. In fact from the XRF analysis, it was determined that DDGS char had the highest ash content, followed by willow and Agrol chars, which was in good agreement with the ash contents of the original biomass fuels which are presented in chapter 3. As it can be seen in **Table 7- 2**, although DDGS fuel contained higher S content than willow fuel, there was much lower S contained in DDGS char than willow char, which is probably due to the sulfur retention by Ca in the ash. On the other hand, it should be remarked that although the XRF analysis gives accurate relative concentrations of the elements, the overall mineral content in the chars might be overestimated due to the nature of the samples (Brewer et al., 2009).

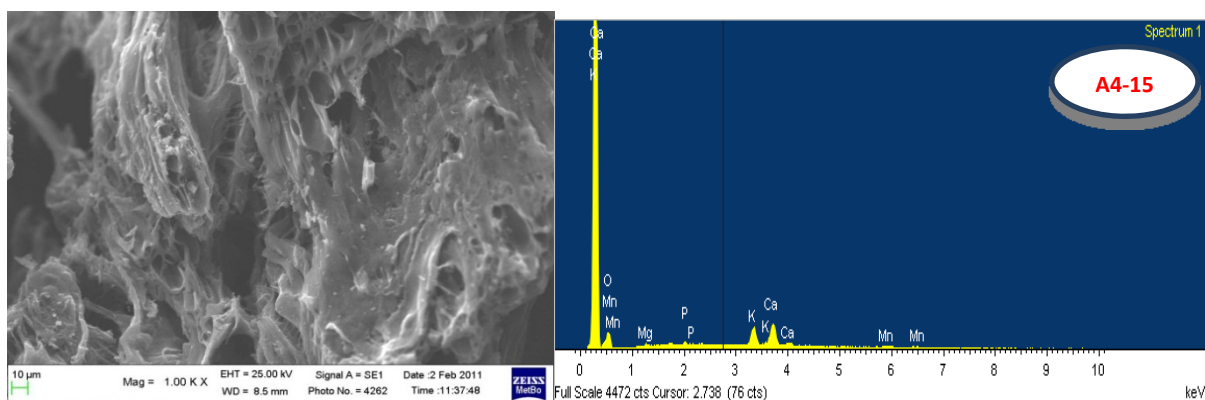
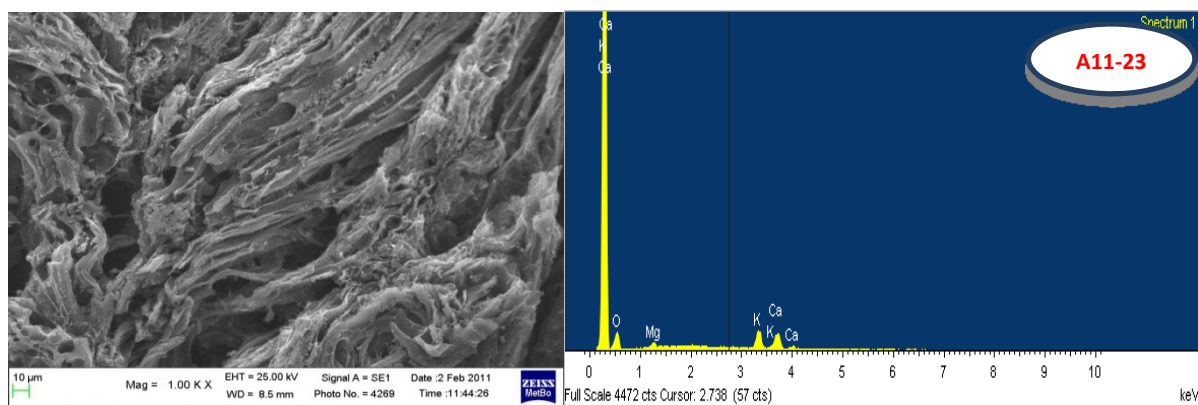


Figure 7- 1 SEM and EDS pictures of Agrol CFB-Chars (Exp. No A3, A6)

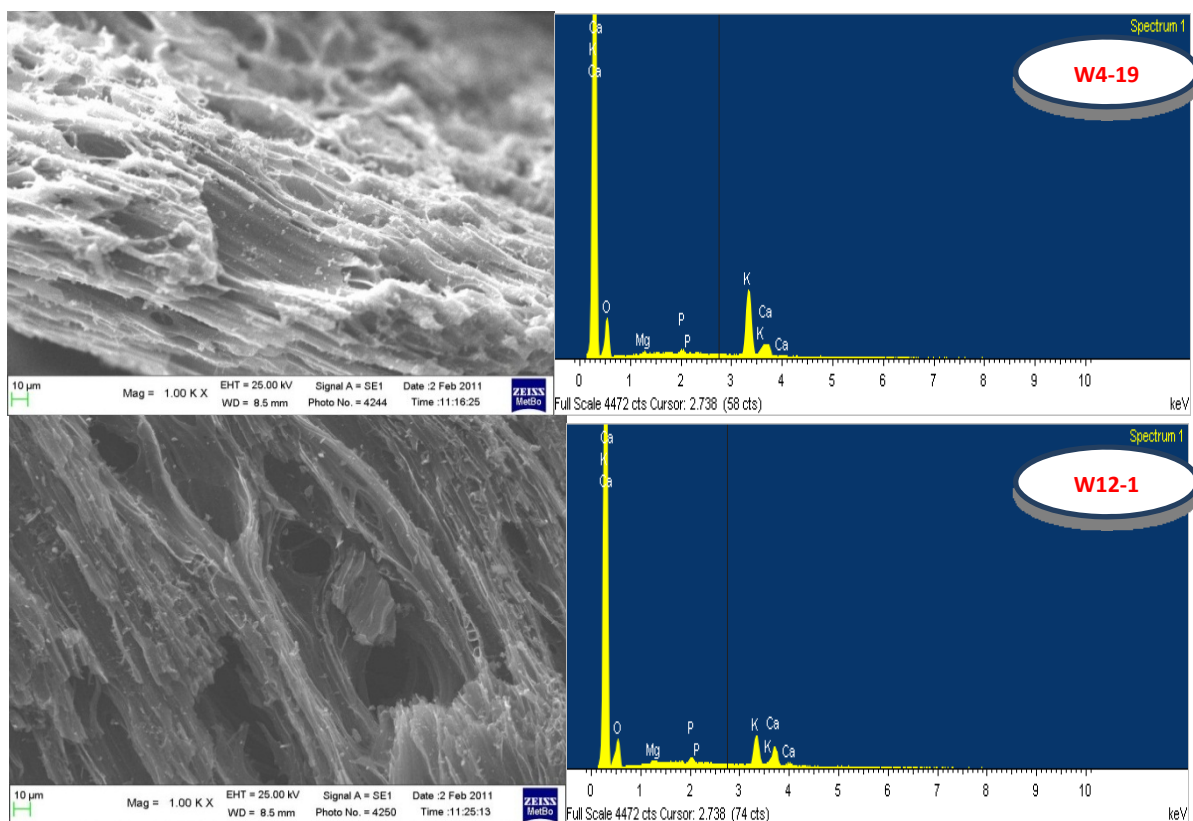


Figure 7- 2 SEM and EDS pictures of willow CFB-Chars (Exp. No W2, W5)

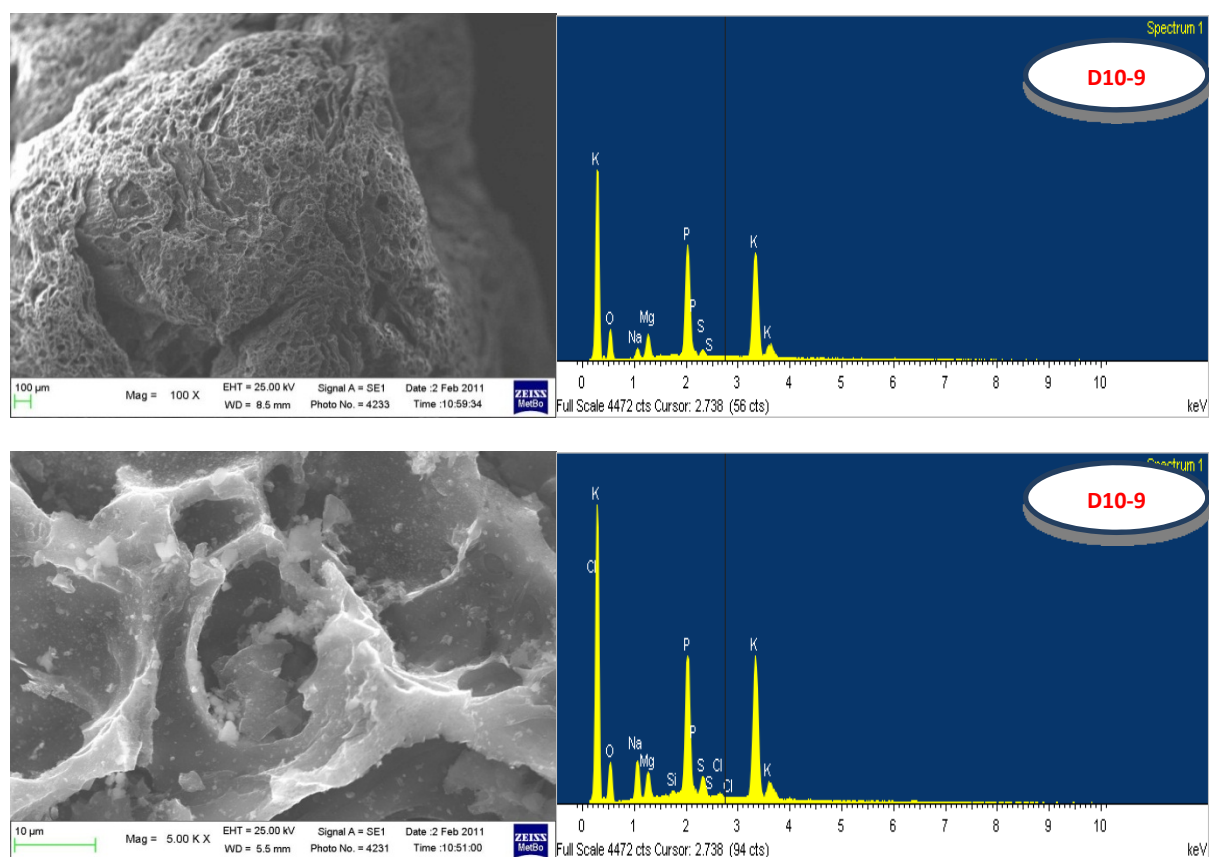


Figure 7- 3 SEM and EDS pictures of DDGS CFB-Char (Exp. No D1)

Table 7- 2 Main composition (mass%, db) of the char samples obtained by XRF analysis

Char /Fuel	Char Agrol A4-15	Char Agrol A11-23	Char willow W4-19	Char willow W12-1	Char DDGS D10-9	Agrol	Willow	DDGS
Al	0.22	0.17	0.44	0.31	0.02	<0.005	0.037	<0.005
Ca	3.74	3.26	10.44	11.60	1.37	0.078	0.470	0.100
Fe	2.03	2.70	1.04	1.12	0.16	0.004	0.034	0.012
K	2.40	2.08	4.60	4.61	11.75	0.044	0.250	1.760
Mg	0.97	1.16	0.89	0.56	1.58	0.017	0.049	0.300
Mn	0.61	0.65	0.22	0.21	0.09	0.012	0.007	0.007
Na	0.02	0.03	0.08	0.06	1.06	0.008	0.021	0.350
O	5.51	5.42	9.89	10.29	15.13	38.2	37.4	31.2
P	0.08	0.10	0.93	0.99	6.02	-*	-	-
S	0.02	0.02	0.11	0.10	0.02	<0.002	<0.002	0.755
Si	1.13	0.88	1.47	1.62	0.28	0.009	0.220	0.053

Remark: \* not available

A comparison of the XRD patterns from different CFB-Char samples is shown in **Figure 7- 4**. It can be seen from these XRD patterns that for all char samples two broad diffraction lines at approximately 23 and 44 ° 2θ were observed over the examined 2θ range (5-80 ° 2θ) which were attributed to the (002) and (101) diffraction lines of a graphite-like structure. Therefore, it may be stated that the gasification temperature might not largely modify the structure of the chars. However, from **Table 7- 1**, it can be also observed that these CFB-Char samples were collected under different SBR and ER values which could slightly influence char structure as well. Unlike for graphite, aromatic rings forming layers of chars are irregularly stacked and randomly arranged. The background observed in the diffraction patterns is related to the presence of amorphous carbon, whereas the low angle (002)



diffraction peak was attributed to the existence of a  $\gamma$ -band on its left side associated with the packing of a saturated structure such as aliphatic side chains (Guerrero et al., 2008; Lu et al., 2002; Lu et al., 2000). Moreover, the shift of the broad(002) peak from  $25^\circ 2\theta$ , as generally observed for graphite carbons (Senneca et al., 2005; Shim et al., 2000), to  $23^\circ 2\theta$  indicated a highly disordered structure of biomass chars (Fu et al., 2009; Guerrero et al., 2008), with a variation from DDGS, willow to Agrol CFB-Chars. The increase of the intensity of the diffraction lines for the Agrol chars appointed that a more regularly ordered carbon lattice structure was achieved, not only in the stacking of the layer but also in a single atomic plane. Since the (101) peak at  $2\theta$  of  $44^\circ 2\theta$  was attributed to graphite-like atomic order within a single plane, a sharper diffraction line for willow and Agrol chars indicated a higher crystallite diameter in these solids (Guerrero et al., 2008). Furthermore, the sharp peaks observed at around  $31$  and  $44^\circ 2\theta$  in the DDGS char were related to the presence of a potassium calcium phosphate, whereas in willow chars the reflection lines of  $\text{SiO}_2$  (quartz) were observed at  $21$ ,  $26$ ,  $42^\circ 2\theta$ .

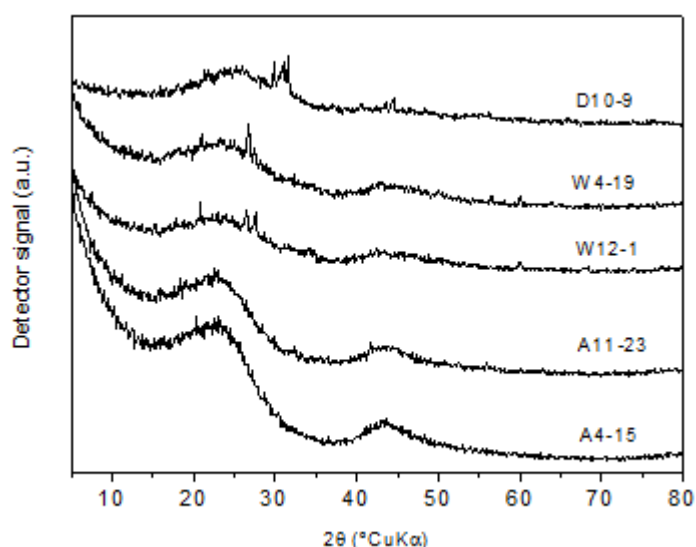


Figure 7- 4 Comparison of the XRD patterns from different CFB-Char samples (Exp. No A3, A6, W2, W5 and D1)

$\text{N}_2$  adsorption/desorption isotherms of three char samples are shown in **Figure 7- 5**. It is remarked that since the diffusion of  $\text{N}_2$  into the micropore network was very slow, in particularly of DDGS CFB-Char, the equilibration of  $\text{N}_2$  took a relatively long time and in some cases the equilibrium could not be reached during the measurement (Cetin et al., 2005). The isotherms were classified according to the International Union of Pure and Applied Chemistry (IUPAC) classification (Sing et al., 1985) (see **Table A- 5**, in Appendix). The shape of the isotherms of the char samples depended on the biomass fuels. Agrol char isotherms were classified as Type I, characteristic for microporous materials ( $< 20 \text{ \AA}$ ), here the  $\text{N}_2$  adsorption takes place at low  $p/p^0$  values and at higher values a plateau is reached, which indicates a very small external surface area. The relatively flat micropore filling pattern indicates the presence of wide micropores and a co-operative filling; this type of isotherms has been classified as Type Ib by Rouquerol et al. (Rouquerol et al., 1999). Ideally type I isotherms are reversible; however, Agrol chars showed a small hysteresis loop due to capillary condensation in mesopores (from  $20$  to  $500 \text{ \AA}$ ). In willow char samples  $\text{N}_2$  adsorption in the low  $p/p^0$  range occurred; however, the  $\text{N}_2$  uptake continues as the relative pressure increased and no plateau is reached, indicating the presence of mesopores with a wide range of sizes and narrow macropores ( $> 500 \text{ \AA}$ ). The hysteresis loops were characteristic for slit-shaped pores. Lastly, the analyzed results showed that the DDGS char was mainly composed by micropores, the differences in the adsorption and desorption branches at low pressure may be related to the condensation of  $\text{N}_2$  in the micropores that could not be evacuated during the desorption part of the analysis; this behavior was previously reported by Lee et al. in biochars produced from cornstover under fast pyrolysis conditions (Lee et al., 2010). BJH pore size distributions obtained from the adsorption branch (see **Figure 7- 5**) indicated that Agrol char



contained mesopores with sizes between 2 to 200 Å and maximum at ca. 30 Å, the average pore diameter was around 40 Å. Willow chars showed slightly larger mesopores, 20 to 400 Å, with an average pore diameter of around 62 Å. On the other hand, no mesopores were observed in the DDGS char. The average pore diameter obtained by the Horvarth-Kavazoe (HK) method for the microporous samples was in the 5-10 Å range with maximum at around 6.8, 6.9 and 5.9 Å for A 4-15, W 12-1 and W 4-19, respectively.

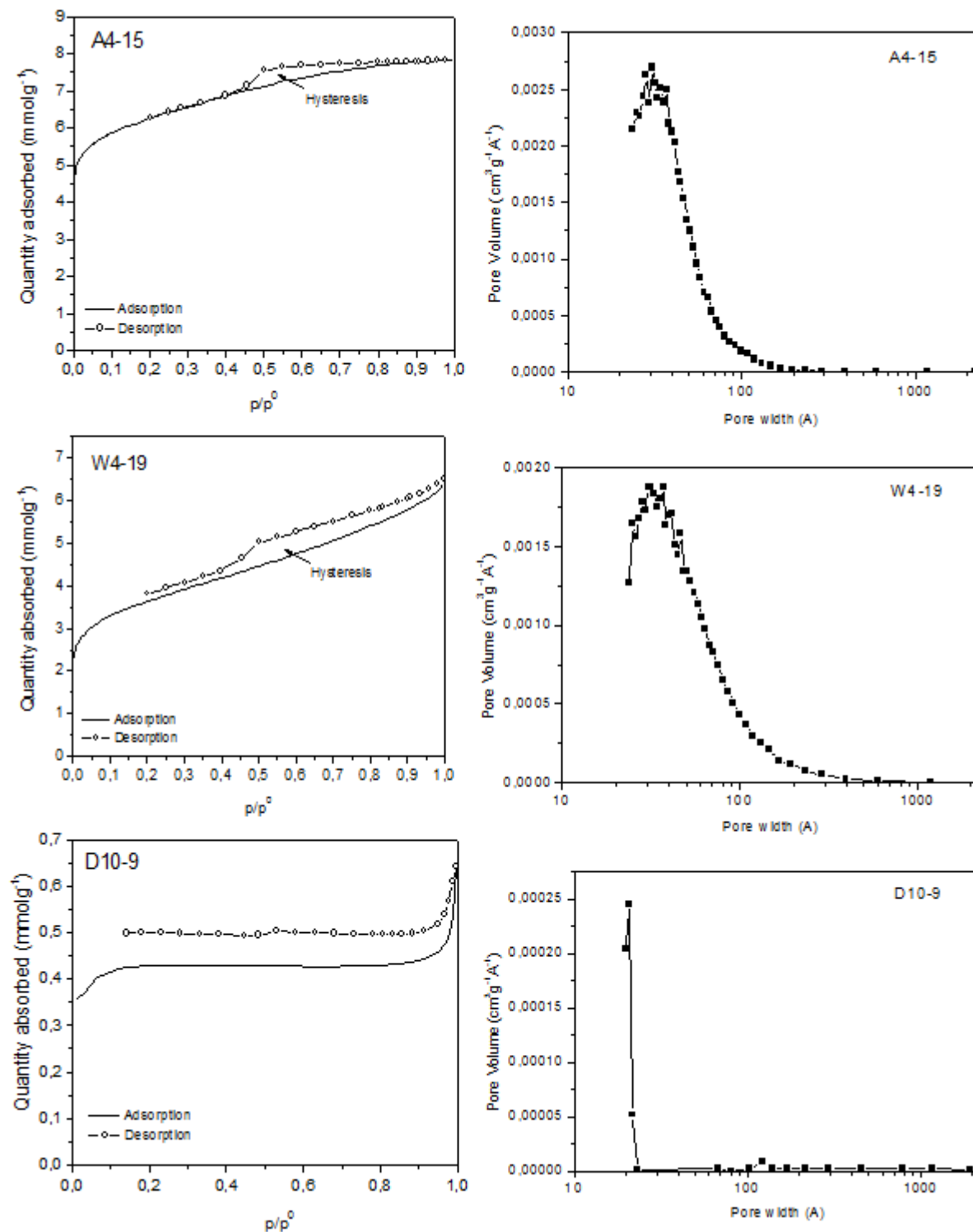


Figure 7- 5 Comparison of the N<sub>2</sub> adsorption/desorption isotherms (left) and BJH pore size distributions (right) from different chars

Specific surface area values obtained by using the BET method are shown in **Table 7- 3**. It can be seen that the Agrol chars had the largest specific surface area ( $S_{\text{BET}}$ ) with a value up to  $521 \text{ m}^2/\text{g}$  (A11-23), followed by willow chars up to  $439 \text{ m}^2/\text{g}$  (W12-1) and DDGS char of  $22.5 \text{ m}^2/\text{g}$ . In all cases a large part of the surface area corresponded to the micropore area ( $S_{\text{m}}$ ). The porosity of the inorganic matter (ashes) in the samples was considered negligible. No significant difference was observed in  $S_{\text{BET}}$  of two Agrol char samples ( $504 \text{ m}^2/\text{g}$  for A4-15) regardless of the gasification temperature applied; while they did differ for two willow char samples ( $296$  and  $439 \text{ m}^2/\text{g}$  for W4-19 and W12-1, respectively): the higher the temperature, the larger the surface area values. The significant difference in  $S_{\text{BET}}$  of different fuel chars could be related to the ash content in parent fuels, since DDGS had a much higher ash content (4.82 wt.%) than willow (2.52 wt.%) and Agrol (0.14 wt.%). The large amount of ash in the DDGS biomass may melt, leading to plastic transformations of the char and blocking of the pores. Moreover, the presence of dead-end pores in the char prevented any access to the adsorbing gas (Sharma et al., 2004). However, the presence of micropores not measured by  $\text{N}_2$  adsorption cannot be ruled out. The total pore volume ( $V_{\text{p}}$ ) values, both due to micropores ( $V_{\text{m}}$ ) and mesopores ( $V_{\text{meso}}$ ) agreed with the specific surface area values, i.e., the large the surface area the large the pore volume.

*Table 7- 3 Specific surface area values of different char samples obtained by  $\text{N}_2$  adsorption/desorption*

Sample	$S_{\text{BET}}$ ( $\text{m}^2/\text{g}$ )	$S_{\text{m}}$ ( $\text{m}^2/\text{g}$ )	$S_{\text{EXT}}$ ( $\text{m}^2/\text{g}$ )	$V_{\text{p}}$ ( $\text{cm}^3/\text{g}$ )	$V_{\text{m}}$ ( $\text{cm}^3/\text{g}$ )	$V_{\text{meso}}$ ( $\text{cm}^3/\text{g}$ )
D10-9	22.5	22	Not available			
W4-19	296	194	102	0.222	0.082	0.121
W12-1	439	348	90	0.259	0.143	0.178
A 4-15	521	404	117	0.272	0.166	0.092
A11-23	504	433	71	0.314	0.218	0.052

## 7.4 Fuel pyrolysis results

### 7.4.1 Fuel pyrolysis behavior

The weight loss (TG, %) and derivative weight loss (DTG, %/min) for Agrol, willow and DDGS at different heating rates (HR=2, 5, 10, 30, 50 and  $70 \text{ }^\circ\text{C}/\text{min}$ ) are shown in **Figure 7- 6**. In **Figure 7- 6**, H2-TG and H2-DTG represents TG and DTG curves for three fuels at HR=2  $^\circ\text{C}/\text{min}$ , respectively, and similar settings as for others.

The results presented in **Figure 7- 6** shows that heating rates largely affect the TG/DTG profiles of Agrol pyrolysis in all stages. In general, the TG/DTG curves shifted towards higher temperature as the heating rates increased. The weight loss started from the starting of the experiment up to approximately  $150\sim 200 \text{ }^\circ\text{C}$  which can be seen from the observable peak in the DTG curves. The first stage weight loss mainly corresponded to the release of the moisture and some light volatile compounds in the biomass sample (Kumar et al., 2008; Mansaray & Ghaly, 1999). Within the temperature range of  $200$  to  $800 \text{ }^\circ\text{C}$ , the volatiles in Agrol were gradually released, which can be seen from another three peaks observed in the DTG curves: a less pronounced shoulder peak, a remarkable main peak and a long tail zone. This pyrolysis behavior is well known and identified for lignocellulosic materials, where the shoulder, the main peak and the long tail are mainly attributed to the decomposition of hemicellulose, cellulose, lignin and extractives (Branca et al., 2005; Giuntoli et al., 2009a; Jensen et al., 1998; Yang et al., 2007). According to Yang et al. (Yang et al., 2007), the decomposition of hemicellulose and cellulose, respectively, occurred within the temperature range of  $220$  to  $315 \text{ }^\circ\text{C}$  and  $315$  to  $400 \text{ }^\circ\text{C}$ , but that of lignin occurred slowly and covered a broad temperature range from  $150$  to  $900 \text{ }^\circ\text{C}$ . The hemicellulose and cellulose related peaks are normally overlapped largely due to the mineral matters present in biomass fuels acting as a catalyst for the decomposition as reported by Lapuerta et al. (Lapuerta et al., 2007) and Varhegyi et al. (Varhegyi et al., 1988).

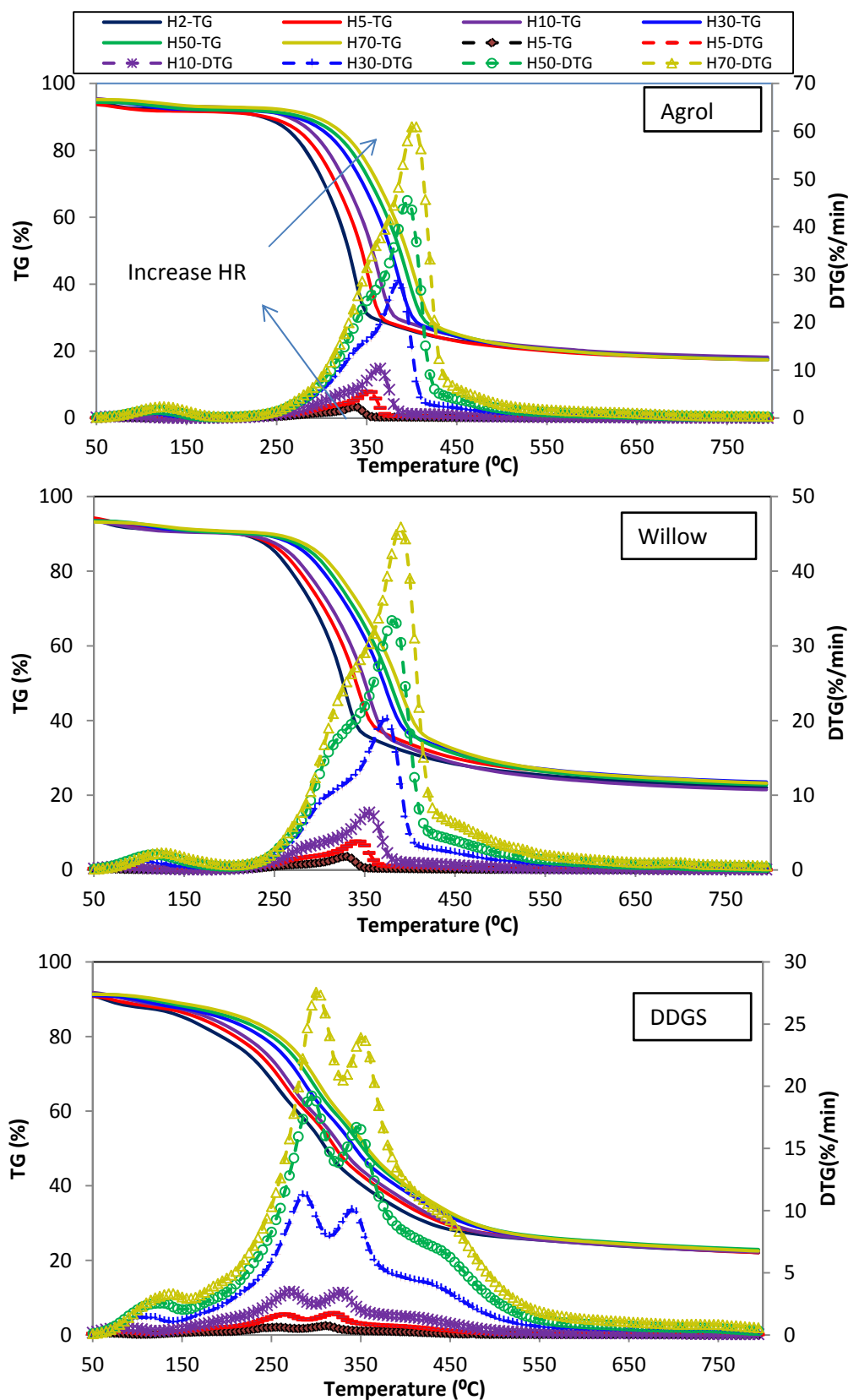


Figure 7- 6 TG and DTG curves for Agrol, willow and DDGS at different heating rates

Similar pyrolysis behavior was observed for willow at different heating rates. However, in general, willow showed a better separation between the hemicellulose and cellulose related peaks. The

shoulder peak occurred at a lower temperature and became more evident. These observations generally agreed with the reported results from other researchers (Biagini et al., 2008; Grønli et al., 2002). Biagini et al. (Biagini et al., 2008) studied the devolatilization of different biomass residues and found that the DTG curves of olive cake and rice husks were fairly similar at various HR values, whereas the shoulder occurred at earlier temperature was more evident for olive cake than rice husks due to their different properties. Grønli et al. (Grønli et al., 2002) reported that hardwoods generally exhibited a more clear-cut separation than softwoods between the first and second reaction zones which were related to the decomposition of hemicellulose and cellulose. Kastanaki et al. (Kastanaki et al., 2002) reported that the less pronounced and well-pronounced shoulder observed respectively in the DTG curve of cotton residue and forest residue indicated a lower amount of hemicellulose in cotton residue than in forest residue. The pyrolysis behavior of DDGS was fairly different from Agrol and willow fuels. The results showed in **Figure 7- 6** indicate that the overall decomposition temperature range of DDGS was definitely broader than those of Agrol and willow. The hemicellulose related peak became into a well-defined peak instead of a shoulder peak. There was also no clear separation between the drying and pyrolysis step. Furthermore, another additional peak was observed in the tail zone of DDGS pyrolysis, which was probably due to some residual compounds remaining from the ethanol fermentation process as reported by Giuntoli et al. (Giuntoli et al., 2009b).

In order to better quantify effects of different heating rates on pyrolysis characteristics of these three fuels, several characteristic devolatilization temperatures and their related rate parameters were introduced here, which were calculated as the method suggested by Grønli et al. (Grønli et al., 2002). **Figure 7- 7** and **Figure 7- 8** show the change trends of characteristic devolatilization temperatures and their related weight loss rates at various heating rates.  $T_{onset}$  and  $T_{offset}$  represent the temperatures when the pyrolysis started and ended, and  $T_{shoulder}$  and  $T_{max}$  represent the temperatures when hemicellulose related shoulder peak and cellulose related main peak occurred, respectively, while  $T_{tail}$  represents the temperature when the peak occurred in the tail zone of DDGS.  $R_{shoulder}$  represents the weight loss rate occurring at the temperature of  $T_{shoulder}$ , and other settings are similar.

From **Figure 7- 7**, it can be clearly seen that characteristic devolatilization temperatures and their related weight loss rates increased with increasing the heating rate, which may be due to heat transfer limitations as reported by Kumar et al. (Kumar et al., 2008) and Aqsha et al. (Aqsha et al., 2011). According to Aqsha et al. (Aqsha et al., 2011), the heat transfer between the crucible and the sample was more efficient at lower heating rates which resulted in a proper drying and pyrolysis process. Contrarily, less efficient heat transfer may occur at higher heating rates which led to a faster increase in the devolatilization rate, thus shifting the peak of the weight loss rate.

As can be seen in **Figure 7- 8**, with increasing the heating rate from 2 to 70 °C/min,  $R_{max}$  observed from Agrol pyrolysis sharply increased from 2.4 to 61 %/min, and meanwhile  $T_{max}$  shifted from approximately 337 to 405 °C. For DDGS, it was difficult to determine  $T_{onset}$  since the variations in DTG curves are hardly detectable. Due to high fluctuation and vibration in DTG curves, all characterized temperatures (except for  $T_{max}$ ) at HR of 2 and 5 °C/min were less accurate and may have  $\pm 0\sim 10$  °C difference. Agrol fuel had the highest  $T_{onset}$ ,  $T_{shoulder}$  and  $T_{max}$  values, followed by willow and DDGS fuels, while DDGS fuel had the highest  $T_{offset}$  value, followed by willow and Agrol fuels, which meant that DDGS fuel had a wider decomposition range ( $T_{offset}-T_{onset}$ ), and Agrol and willow fuels has a similar decomposition range. These observations generally agreed well with the results reported by other researchers (Biagini et al., 2008; Giuntoli et al., 2009b; Grønli et al., 2002). For example, Biagini et al. (Biagini et al., 2008) reported that the higher the heating rate, the higher the values of  $T_{onset}$ ,  $T_{max}$  and  $T_{offset}$ . With increasing the heating rate from 5 to 100 °C/min, the observed  $T_{onset}$  in the DTG curves of rice husks increased from around 257 to 344 °C. Aqsha et al. (Aqsha et al., 2011) found that with increasing the heating rate from 5 to 50 °C/min,  $R_{max}$  observed in the DTG curves of sawdust devolatilization sharply increased from approximately 4 to 26 %/min.

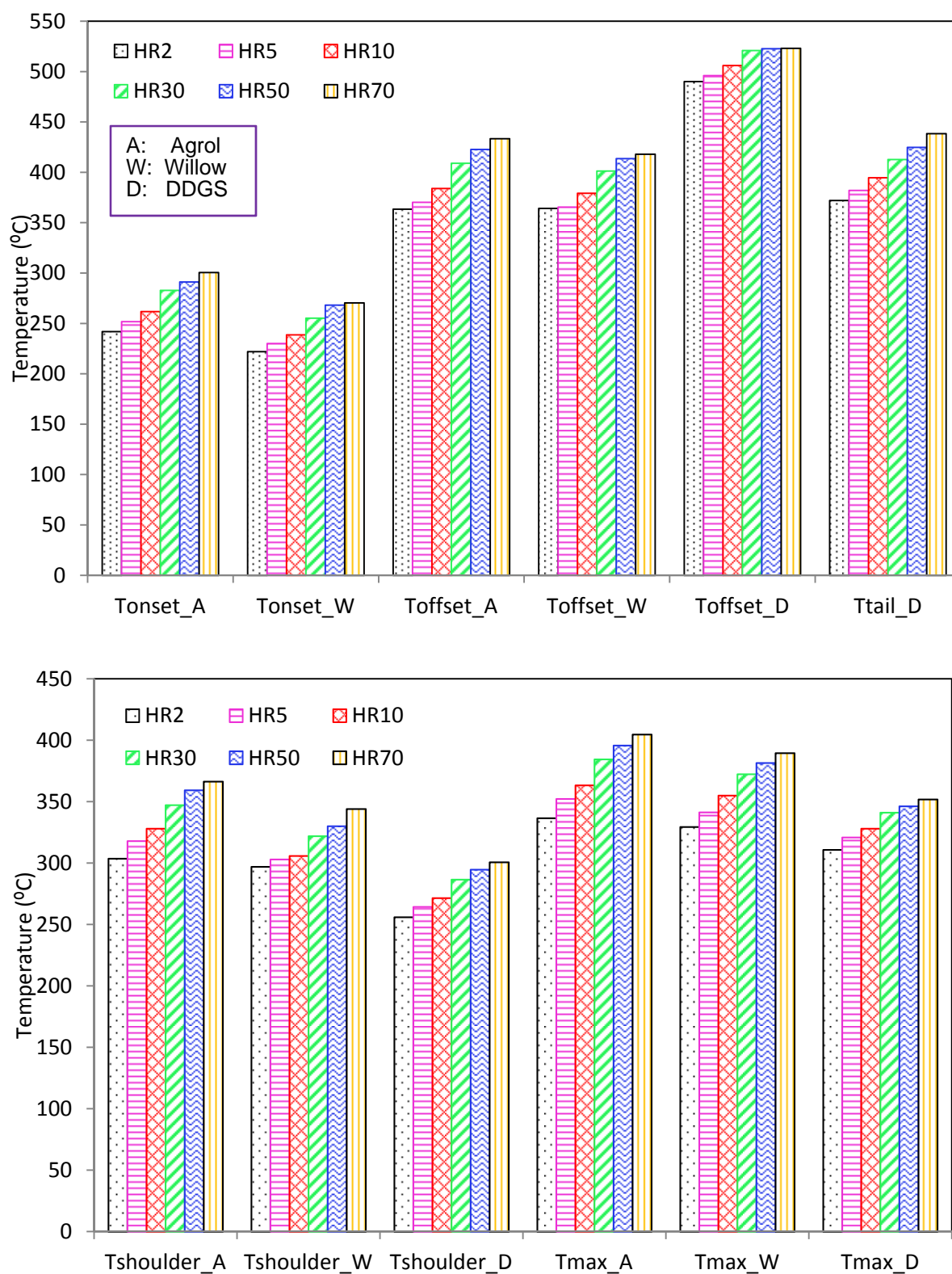


Figure 7- 7 Effects of heating rates on different characteristic devolatilization temperatures for Agrol, willow and DDGS

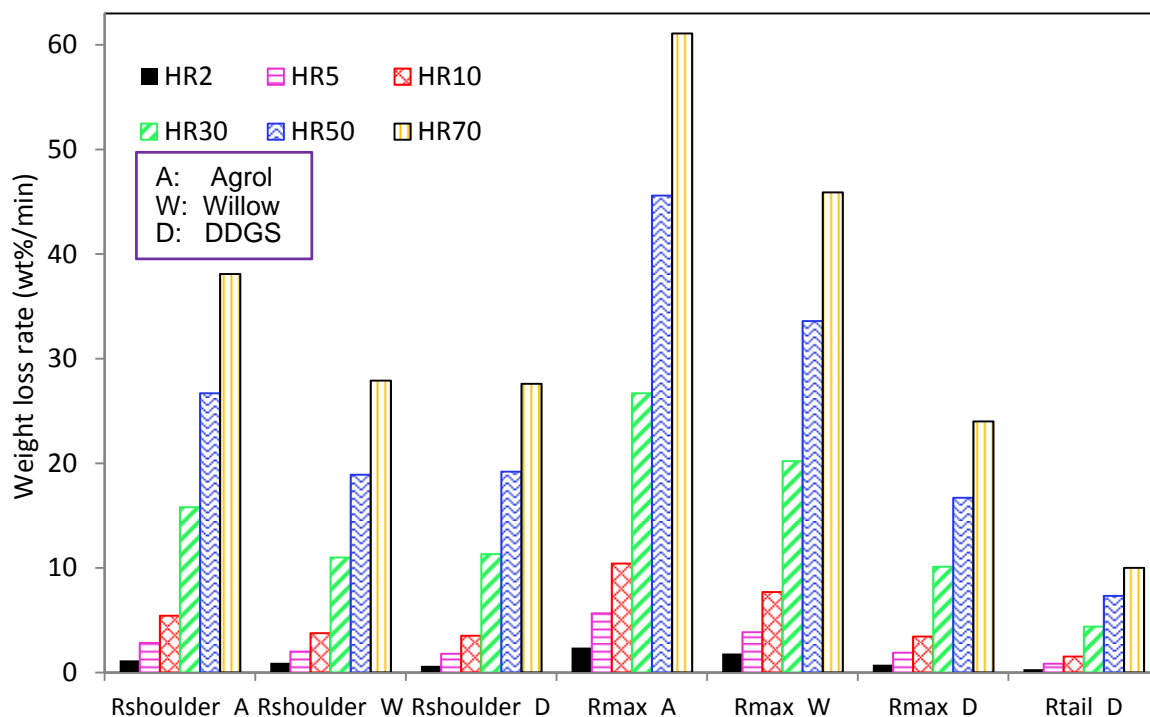


Figure 7- 8 Effects of heating rates on different maximum rates for Agrol, willow and DDGS

#### 7.4.2 Product yields from pyrolysis

Since the yields of the products produced from biomass pyrolysis are largely influenced by pyrolysis conditions, here, the yields of volatile and char produced from Agrol, willow and DDGS gasification under different pyrolysis temperatures ( $T_{PYR}=750, 850, 900$  °C with  $HR=10$  °C/min) are shown in **Figure 7- 9**. In this figure, the yield of volatile is assumed to be equal the total amount of biomass sample minus the sum amount of moisture, ash and char.

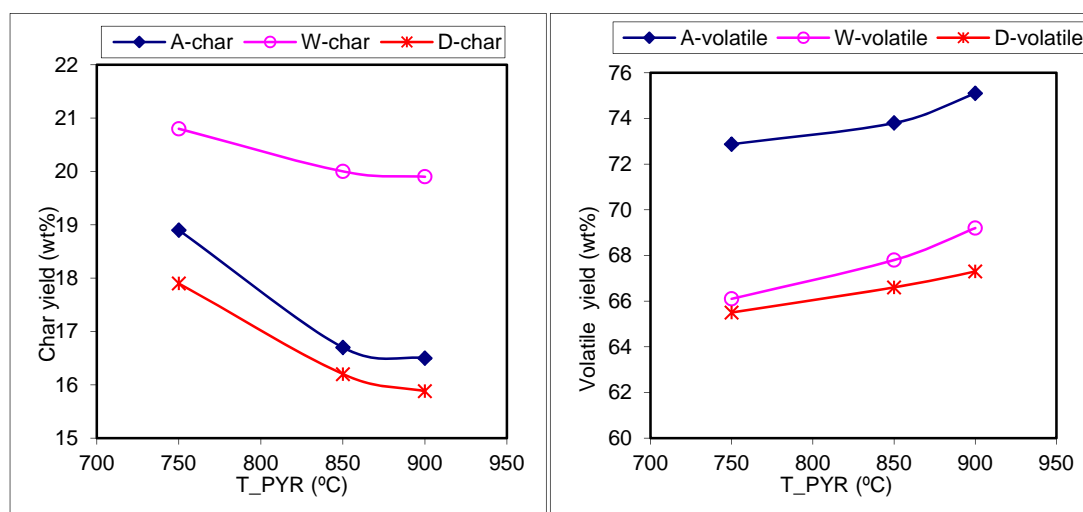


Figure 7- 9 Volatiles and char released from Agrol, willow and DDGS pyrolysis

From **Figure 7- 9**, it can be seen that with increasing pyrolysis temperature from 750 to 900 °C, the yield of char produced from three fuels all decreased, while the yield of the volatile oppositely increased. Among these three fuels, Agrol produced the highest amount of volatile of 72-76 wt. %, while willow produced the highest amount of char 20-21wt.%. These observations generally agree

well with the results reported by Polsongkram and Kuznetsov (Polsongkram & Kuznetsov, 2010), who studied pyrolysis behavior of several woody biomasses and found that the char yield was reduced as the pyrolysis temperature was increased from 61.5-80 wt.% at 250 °C to 24-28 wt.% at 600 °C. Their explanation is that the decrease in char yield could be either due to greater primary decomposition of the wood at the higher temperatures or to secondary decomposition of char residue (Williams & Nugranad, 2000). From **Figure 7- 9**, it can also be seen that the decrease of char yield with increasing temperature from 850 to 900 °C was becoming small. According to Di Blasi et al. (Di Blasi et al., 1999b), the char initially decreased with increasing temperature is due to “ the competition between the primary reactions of char and volatile formation, with the latter becoming more favored. At high temperatures, they tend to become constant, since the variation in the actual degradation temperature of the solid (in relation to the external heating temperature) becomes small, due to the narrow range of temperatures characteristic of biomass pyrolysis, and heat transfer resistances through the packed bed or the particle.”

Besides pyrolysis temperature, the heating rate also influences the yields of char and volatiles to certain extent, which can be seen from **Figure 7- 6**. From **Figure 7- 6**, it can be seen that the heating rate has much less influence on the pyrolysis yield compared to temperature. Almost no change was observed in the yields of volatile and chars when the heating rate was increased from 10 to 70 °C/min. The results agree well with those reported by de Jong (De Jong, 2005), who studied the pyrolysis behavior of several fuels such as miscanthus, Labee wood pellets and Hambach brown coal and found that the yields of char and volatile for all fuels were practically constant with varying heating rate from 10 to 100 °C/min. He explained that the relatively constant char yield within increasing heating rate implied that cross-linking reactions could be unimportant under the process conditions. However, Gheorghe et al. (Gheorghe et al., 2009) found that an increase in the heating rate from 5 to 10 °C/min resulted in a decreasing by 10% for the char yield produced from cherry sawdust. Natarajan and Ganapathy Sundaram (Natarajan & Ganapathy Sundaram, 2009) found that when the heating rate was increased from 20 to 60 °C/min, the yield of solid decreased around 6%, while the yield of volatiles (including gas and liquids) increased around 2-3%. The reason for that could be due to the ash content in the fuel, since the amount and composition of ash catalytically active, may also play an important role on the product distribution of pyrolysis (Di Blasi et al., 2000; Raveendran et al., 1995).

### **7.4.3 Light volatiles from pyrolysis**

The volatiles released from biomass pyrolysis can not all detected and quantified by using FTIR. The measured results of the light volatiles released from Agrol and willow, and DDGS pyrolysis at HR= 10 °C/min are shown in **Figure 7- 10** and **Figure 7- 11**, respectively. From these two figures, it can be seen that the products released from Agrol, willow and DDGS are mainly CO, CO<sub>2</sub> and H<sub>2</sub>O, followed by a small amount of CH<sub>4</sub>. For three fuels, it seemed that their physically absorbed moisture was evolved during the drying process below a temperature of approximately 150 °C and then the pyrolytic water was released continuously up to a temperature range of 500-700 °C. These general observations agreed with the results reported by other researchers (Bassilakis et al., 2001; Giuntoli et al., 2009b).

It can be seen in **Figure 7- 10** that the emissions of CO and CO<sub>2</sub> from Agrol and willow pyrolysis showed remarkable peaks within the temperature range of 340 to 440 °C, and the shapes of their curves were fairly similar to their DTG curves. The release of CO and CO<sub>2</sub> could be largely attributed to the decomposition of the two macro-components (hemicellulose and cellulose) which are normally present in different biomass fuels. However, there are some controversies about which component decomposition chiefly contributes to the release of CO and CO<sub>2</sub>. Jeguirim et al. (Jeguirim et al., 2010) studied the devolatilization kinetics of Miscanthus. They reported that the decomposition of hemicellulose and cellulose components led essentially to CO and CO<sub>2</sub> emissions. Yang et al. (Yang et al., 2007) and Wang et al. (Wang et al., 2011) found that the cellulose decomposition contributed limitedly to the release of CO and CO<sub>2</sub> compared to the release due to hemicellulose decomposition. Their reported results appeared a bit contrarily to the results obtained in this work, since the peak related to the hemicellulose decomposition normally occurred below 315 °C, while the released peaks



of CO and CO<sub>2</sub> observed in this work occurred at around 360 °C which are within the decomposition temperature range of cellulose. This behavior has been well identified and explained by Giuntoli et al. (Giuntoli et al., 2009a). They reported that since the decomposition of cellulose component was highly affected by the presence of inorganic catalysts in the fuel samples (Jensen et al., 1998; Varhegyi et al., 1988), its related peak was usually at lower temperatures than expected from the single cellulose experiments, which is why some researchers found that the contribution of cellulose to the global release of CO and CO<sub>2</sub> was limited compared to those from hemicellulose decomposition (Yang et al., 2007). The release of CH<sub>4</sub> occurred within a widely higher temperature range of 440 to 640 °C, which was because that CH<sub>4</sub> was normally derived by the cracking of methoxyl groups in the lignin part of biomass (Giuntoli et al., 2009a; Yang et al., 2007).

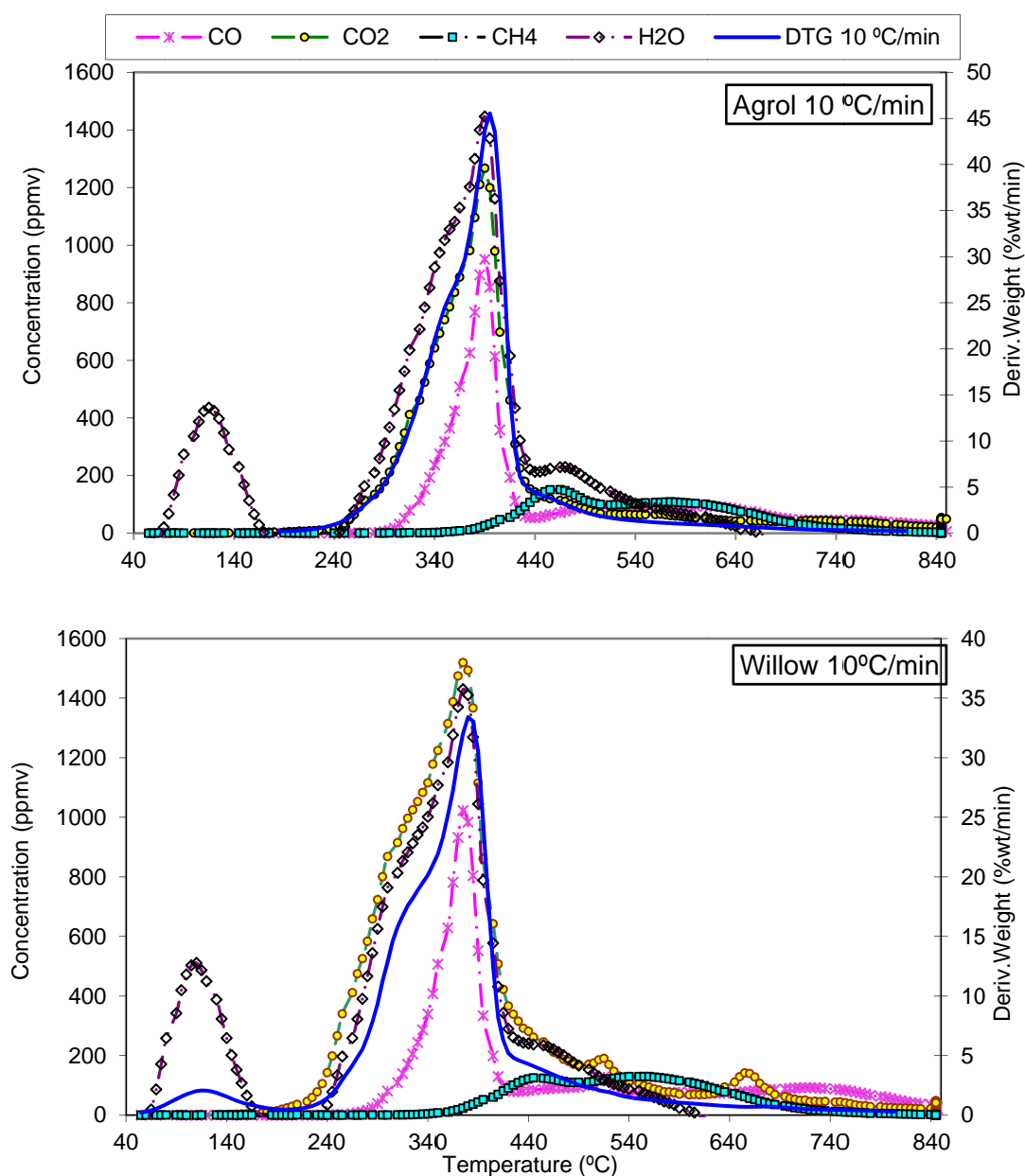


Figure 7- 10 Light volatiles released from for Agrol and willow pyrolysis

It can be seen in **Figure 7- 11** that the emission behavior of CO<sub>2</sub> and CH<sub>4</sub> from DDGS pyrolysis was fairly similar to that from Agrol and willow pyrolysis. However, compared to the release behavior of CO from Agrol and willow pyrolysis, the released CO from DDGS pyrolysis occurred in a wider temperature range, and the decomposition of cellulose and hemicellulose components appeared to



have a less prominent contribution to CO emission. Moreover, a released CO tail peak was observed at a temperature as high as 840 °C. This behavior has also been observed by other researchers. For example, Giuntoli et al. (Giuntoli et al., 2009b) and Jiang et al. (Jiang et al., 2009) observed a release CO tail peak at a temperature of around 890 °C. The release of CO up to high temperatures was largely attributed to secondary reaction of the residues which condensed in the char (Biagini et al., 2008; Giuntoli et al., 2009b; Yang et al., 2007). The aforementioned SEM analysis results also indicated that the surface of DDGS chars contained some condensed particulate matters compared to Agrol and willow chars, which might explain the different CO emission behavior observed between the pyrolysis of three fuels. The condensed particulate matters in DDGS char might lead to the release of CO at high temperatures.

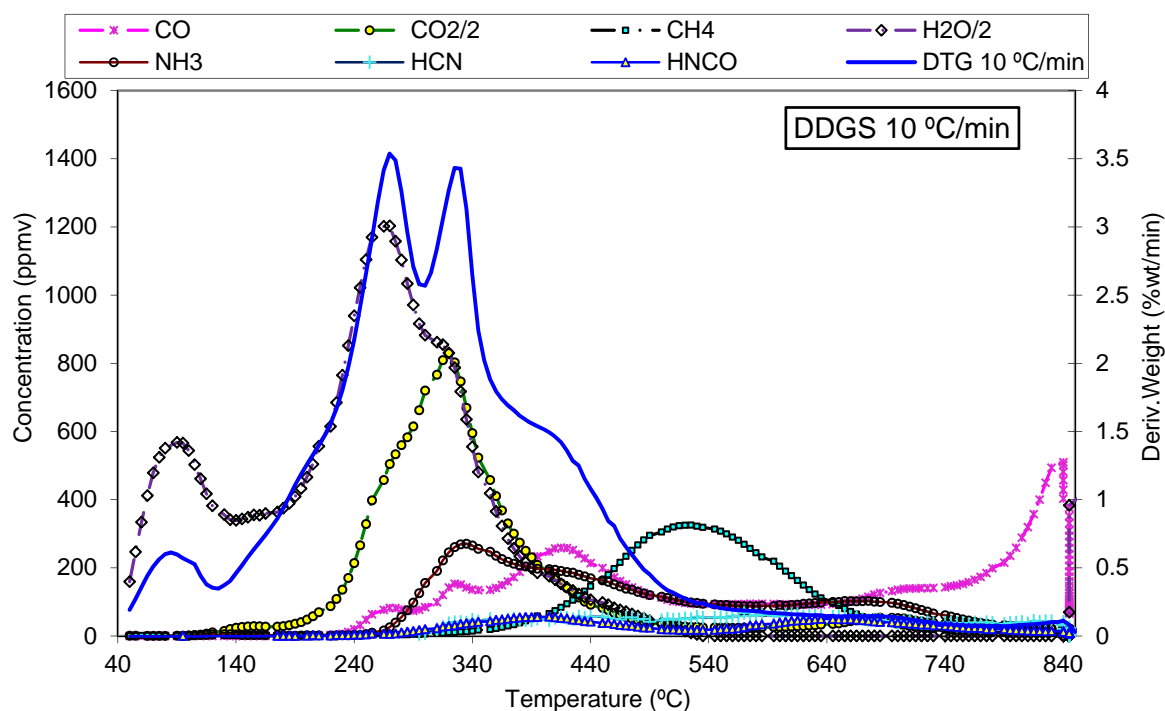
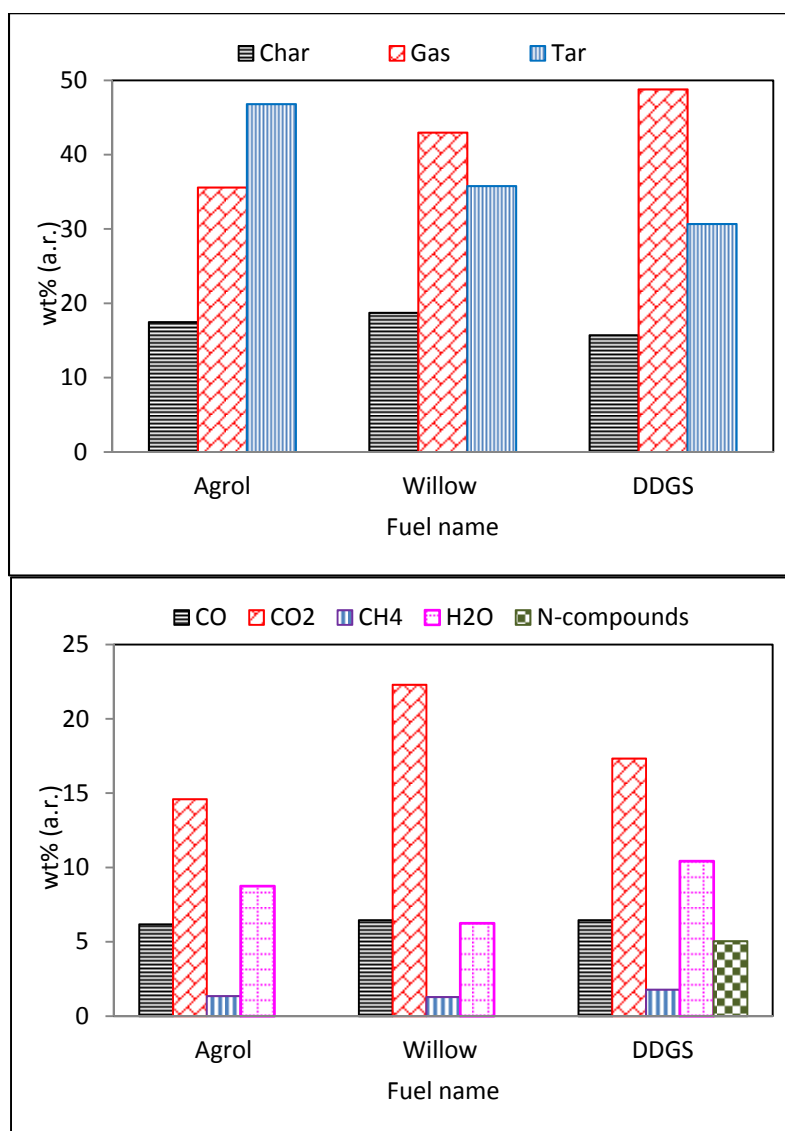


Figure 7- 11 Light volatiles released from for DDGS pyrolysis

Besides  $H_2O$ ,  $CO$ ,  $CO_2$  and  $CH_4$ , some additional amount of N compounds such as  $NH_3$ ,  $HNCO$ , and  $HCN$  were also detected from DDGS pyrolysis. However, the amount of these N compounds released from Agrol and willow pyrolysis were found to be negligible. Among the three N compounds,  $NH_3$  was the main N compound released at low temperatures ( $< 450$  °C) with a released peak of approximately 340 °C, while relatively lower amounts of  $HNCO$  and  $HCN$  were detected and maximum amounts of  $HNCO$  and  $HCN$  released were observed at around 400 and 600 °C, respectively. This behavior agreed well with the observations and explanations reported by other researchers. For example, Giuntoli et al. (Giuntoli et al., 2009b) reported that  $NH_3$  released from their DDGS sample at a temperature of 328 °C is probably due to the decomposition of proteins and eventual free amino acids present in the sample, and a pronounced release peak of  $HNCO$  was observed at 430 °C. Li et al. (Li et al., 2007) reported that  $HNCO$  and  $HCN$  showed a release peak at around 395 and 664 °C, respectively. The different emissions of N compounds observed among Agrol, willow and DDGS pyrolysis could be due to their different structure properties. As well mentioned in a previous study (Meng et al., 2011a) and chapter 3, the N amount (wt.%, dry) present in Agrol, willow and DDGS fuels was around 0.15, 0.69 and 5.52 wt.%, respectively. These values indicate that DDGS fuel contains much higher amount of N than Agrol and willow. A similar conclusion has also been drawn by Giuntoli et al. (Giuntoli et al., 2009b), who reported that almost no N compounds were detected from olive residues and peach stones pyrolysis due to their low N contents (0.8 and 1.4 wt.% N in peach stones and olive residues, respectively).

In order to determine the amount of non-detected product (here it is called tar) released from pyrolysis of three fuels, an overall mass balance was performed between the total amount of gases detected by FTIR (those in **Figure 7- 10** and **Figure 7- 11**) and biomass sample used in TGA, and the results are shown in **Figure 7- 12**, where the amount of tar is equal to the total amount of biomass sample used minus the sum amount of gas, char and ash, while the amount of gas is equal to the amount of gas detected by FTIR plus the amount of water released before 50 °C when the data started to be collected. The item of N-compounds is the sum amount of NH<sub>3</sub>, HNCO and HCN.



*Figure 7- 12 Char, tar and gas released from for Agrol and willow pyrolysis*

From **Figure 7- 12** it can be seen that the yields of CO and CH<sub>4</sub> from Agrol, willow and DDGS were fairly similar, and they are in the range of 6.2-6.5wt.% and 1.3-1.8 wt.%, respectively. Generally these values are consistent with those reported by other researchers (De Jong, 2005; Giuntoli et al., 2009a; Jensen et al., 1998). As above discussed, the difference in CO and CH<sub>4</sub> yields is probably due to different amount hemicellulose and lignin component contained in the fuel samples. Compared to CO and CH<sub>4</sub>, the yields of CO<sub>2</sub> and H<sub>2</sub>O produced from three fuels are much more different. For instance, the yield of CO<sub>2</sub> from Agrol, willow and DDGS is around 15, 22, and 17 wt.%, respectively. These values seem a bit higher compared to those reported by other researchers (De Jong, 2005; Giuntoli et al., 2009a; Jensen et al., 1998). The reason for that could be due to different operational conditions (e.g., pyrolysis temperature, residence time) and fuel properties. Generally the yield of char produced from willow is the highest (19wt.%), followed by that from Agrol (18 wt.%) and DDGS (16wt.%).

The gas yield released from Agrol, willow and DDGS is around 36, 43 and 49 wt.%, respectively. Compared to Agrol and willow, the highest gas yield detected from DDGS is partly attributed the amount of moisture released before 50 °C (ca. 8 wt.%) and N-compounds (ca. 5wt.%), and this fairly agree with the results reported by Giuntoli et al. (Giuntoli et al., 2009b), who reported that the total mass recovery for DDGS was around 35%wt.% on a dry basis.

## **7.5 Char gasification results**

### **7.5.1 Char gasification behavior**

The gasification behavior of PYR-Char and CFB-Char under different operational conditions was examined. **Figure 7- 13**, **Figure 7- 14** and **Figure 7- 15** present the conversion (X) of PYR-Char ( $T_{Pyr}=850$  °C,  $HR=10$  °C/min) and CFB-Char versus time curves at different  $CO_2$  concentrations ( $CO_2=10, 20, 30$  vol.%) and gasification temperatures ( $T_{Ga}=900, 1000, 1100$  °C) for Agrol, willow and DDGS, respectively. In these three figures,  $X_{T900\_0.1}$  means the conversion of PYR-Char (and CFB-Char) when they were gasified at a temperature of 900 °C using 10 vol.%  $CO_2$ , and similar setting as for others.

From **Figure 7- 13**, it can be seen that under relatively unfavorable gasification conditions (e.g.,  $T_{Ga}=900$  °C,  $CO_2=10$  vol.%), Agrol PYR-Chars obtained at  $HR=10$  °C/min all showed a really low conversion of approximately 25%, while Agrol CFB-Chars achieved a conversion higher than 60%. The conversion values of PYR-Chars and CFB-Chars were sharply enhanced with increasing either gasification temperature from 900 to 1100 °C or  $CO_2$  concentration from 10 to 30 vol. %. This observation is fairly reasonable since at a higher temperature, the reaction rate is increased as more energy is supplied to overcome the  $E_a$  barrier as described by the Arrhenius equation (Smith et al., 2001). The incomplete char reaction at lower  $CO_2$  concentration was probably due to the reduction of active sites density by  $N_2$  in high concentration surrounding the surface (Standish & Tanjung, 1988).

Similar results were observed for the gasification of willow and DDGS chars which can be clearly seen in **Figure 7- 14** and **Figure 7- 15**. However, willow and DDGS PYR-Char obtained at  $HR=10$  °C/min and CFB-Char had a much higher conversion when they were under above mentioned unfavorable gasification conditions. According to Di Blasi (Di Blasi, 2009), an enhancement in the char conversion rate is ultimately due to an improvement of several important factors: surface area and accessibility, carbon active sites and catalytic active sites created by indigenous or added inorganic matter and the local gaseous reactant concentration. Consequently, the reactivity is determined by chemical structure, inorganic components and porosity of the samples. Taking into account the results obtained during the characterization of the chars and considering the porosity of the samples (see **Table 7- 3**), it was expected that Agrol char, which showed the largest surface area and highest porosity, should be the most reactive one; however, the opposite behavior was observed. The differences among the reactivities of char samples from different fuels under unfavorable gasification conditions are probably due to catalytic effects of the ashes in the fuels as reported by other researchers (Huang et al., 2009; Zhang et al., 2008).

The aforementioned XRF analysis (see **Table 7- 2**) indicated that DDGS char had the highest alkali content ( $K+Na=12.81$  wt.%), followed by willow char (4.68 wt.%) and Agrol char (2.42 wt.%), while willow char had the highest alkaline earth content ( $Ca+Mg=11.33$  wt.%), followed by Agrol char (4.71wt.%) and DDGS char (2.95 wt.%). According to Huang et al. (Huang et al., 2009), different metals could have different catalytic effects on char  $CO_2$  gasification, and the sequence was  $K-char > Na-char > Ca-char > Fe-char > Mg-char > raw-char$ . Zhang et al. (Zhang et al., 2008) studied the gasification reactivity of biomass chars derived from a wide range of plant origins and concluded that the maximum rate at high conversion range was mainly attributed to the catalytic effect of K. Thus, it is easily understandable that DDGS and willow chars were more reactive than Agrol char due to the enhanced catalytic effects of inorganic elements in their ashes. Moreover, the XRD analysis results also indicated that Agrol char had a higher carbon crystalline order which could also lower its reactivity as reported by Kumar et al. (Kumar & Gupta, 1994), Cetin et al. (Cetin et al., 2004) and Lu

et al. (Lu et al., 2002), probably by lowering the concentration of reaction sites. However, the high ash content present in the char sample could decrease the active surface area of chars (Raveendran & Ganesh, 1998), since the internal structure becomes less accessible to the gaseous reagents for the heterogeneous reactions (Branca et al., 2007). Indeed, SEM and EDS analysis results indicated that DDGS char had more condensed particles on its surface, and it also had much lower  $S_{\text{BET}}$  ( $22.5 \text{ m}^2/\text{g}$ ) compared to willow char ( $296 \text{ m}^2/\text{g}$ ), which may be the reason why DDGS char turned out to be less reactive than willow char. Similarly, DeGroot and Shafizadeh (DeGroot & Shafizadeh, 1984) found that the inorganic content of the lignite char was more than five times greater than that of cottonwood char, but their reactivities were fairly similar. Cetin et al. (Cetin et al., 2004) reported that a higher global char gasification reactivity was observed in the chars obtained from different fuels (e.g., *pinus radiata*, *eucalyptus maculata*) with higher total surface area.

**Figure 7- 16** shows the conversion values of three different PYR-Chars versus time curves at different heating rates (HR=10, 70 °C/min) and different pyrolysis temperatures (T<sub>Pyr</sub>= 750, 850 °C). X\_H10\_T850\_T900 shows the conversion of PYR-Chars obtained at T<sub>Pyr</sub>=850 °C, HR=10 °C/min and gasified at T<sub>Ga</sub>=900 °C using 10 vol.% CO<sub>2</sub>, and similar settings as for others. The results shown in **Figure 7- 16** indicate that just like above-mentioned gasification conditions (e.g., gasification temperature and CO<sub>2</sub> concentration), pyrolysis conditions (e.g., heating rate and pyrolysis temperature) also influenced the conversion of all char samples to some extent.

From **Figure 7- 16**, it can be seen that all PYR-Chars obtained at HR= 70 °C/min achieved much higher conversion values than those obtained at HR= 10 °C/min. Many researchers reported that chars obtained at high heating rates generally had sparse, large internal cavities and macropores structure and/or a higher concentration of active sites which all could lead to a high reactivity (Chen et al., 1997; Guerrero et al., 2005; Kurosaki et al., 2003). Furthermore, an increase in the maximum rate of weight loss and volatile yield observed at high heating rates during pyrolysis also shortened tar vapors residence time in the pores, thus reducing the activities of condensation reactions and preventing char agglomeration and condensation of fragments on the char surface (Fushimi et al., 2003). Previous studies (Meng et al., 2011b; Meng et al., 2011c) also showed that DDGS PYR-Char obtained at HR=10 °C/min was less porous compared to those obtained at HR= 70 °C/min, while willow PYR-Char obtained at HR=10 °C/min has higher condensed particle matter or cross-linking of fragments of the side chain than those obtained at the HR=10 °C/min. Furthermore, PYR-Chars obtained at T<sub>Pyr</sub>= 750 °C showed generally higher conversion than those obtained at T<sub>Pyr</sub>= 850 °C, especially Agrol PYR-Chars when gasified at a temperature of 900 °C. Also reported by some researchers (Fermoso et al., 2009; Kumar & Gupta, 1994; Lu et al., 2002), an increase in pyrolysis temperature appears to substantially decrease the char reactivity, since char structures, as normally reflected by amorphous concentration, aromaticity and crystallite size, became more ordered at higher pyrolysis temperatures thus lowering the concentration of reactive sites.

From **Figure 7- 16**, it can also be seen that there was not too many differences among the conversion of PYR-chars obtained at T<sub>Pyr</sub>= 750 and 850 °C whenever these chars were also obtained at HR=70 °C/min and further gasified at a high temperature of 1100 °C. Furthermore, Agrol and willow chars showed a fairly similar conversion behavior when they were gasified at a temperature of 1100 °C. In this way, it seems that inorganic elements present in the ash of Agrol and willow chars showed less catalytic effects at high temperatures, which might be related to ash sintering as reported by Piotrowska et al. (Piotrowska et al., 2011). Huang et al. (Huang et al., 2009) also reported that Ca was not able to act as catalyst at high temperature since its particles could be inclined to agglomerate, resulting in deactivation.

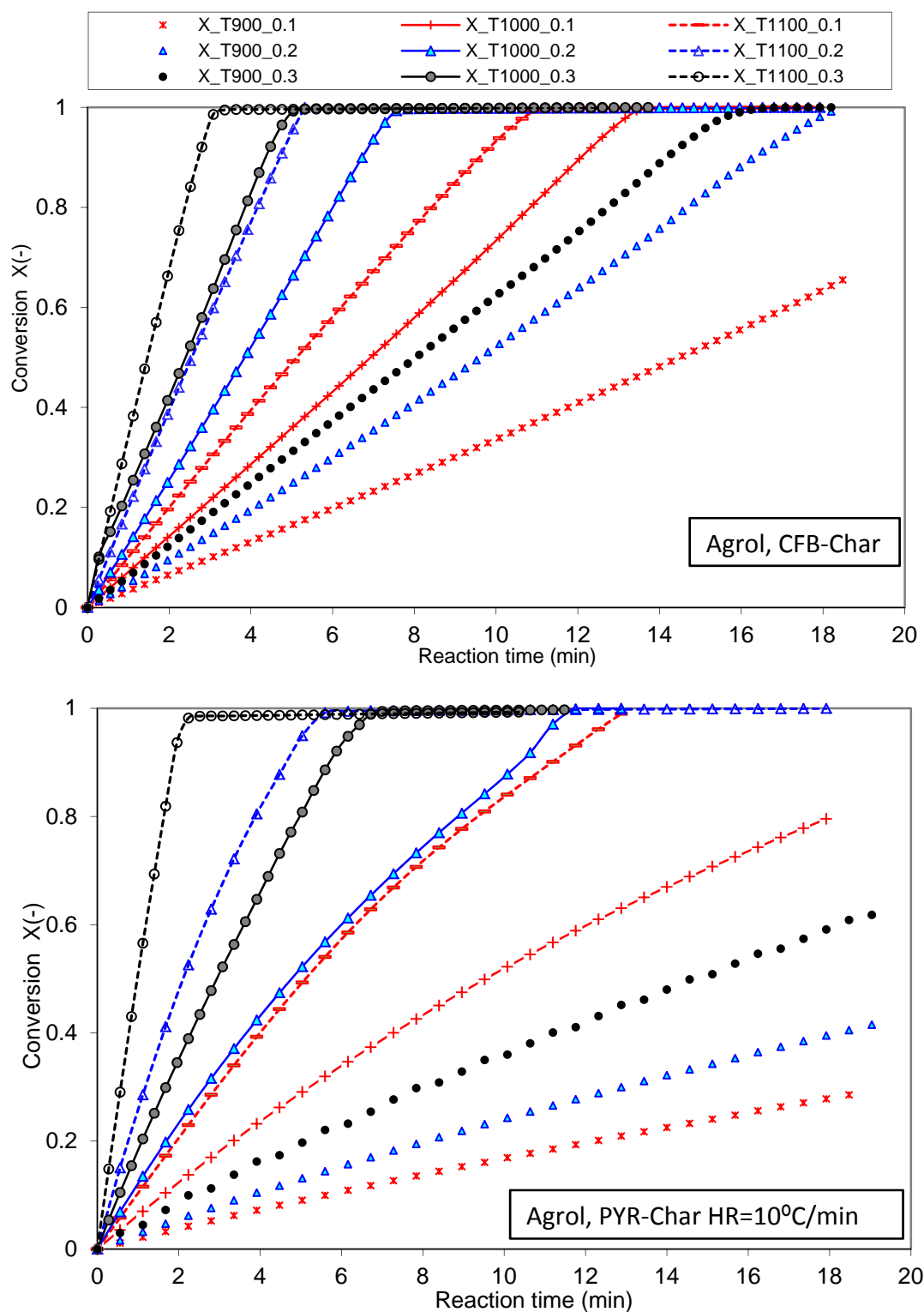


Figure 7- 13 Effects of gasification temperatures and  $CO_2$  concentrations on Agrol char gasification

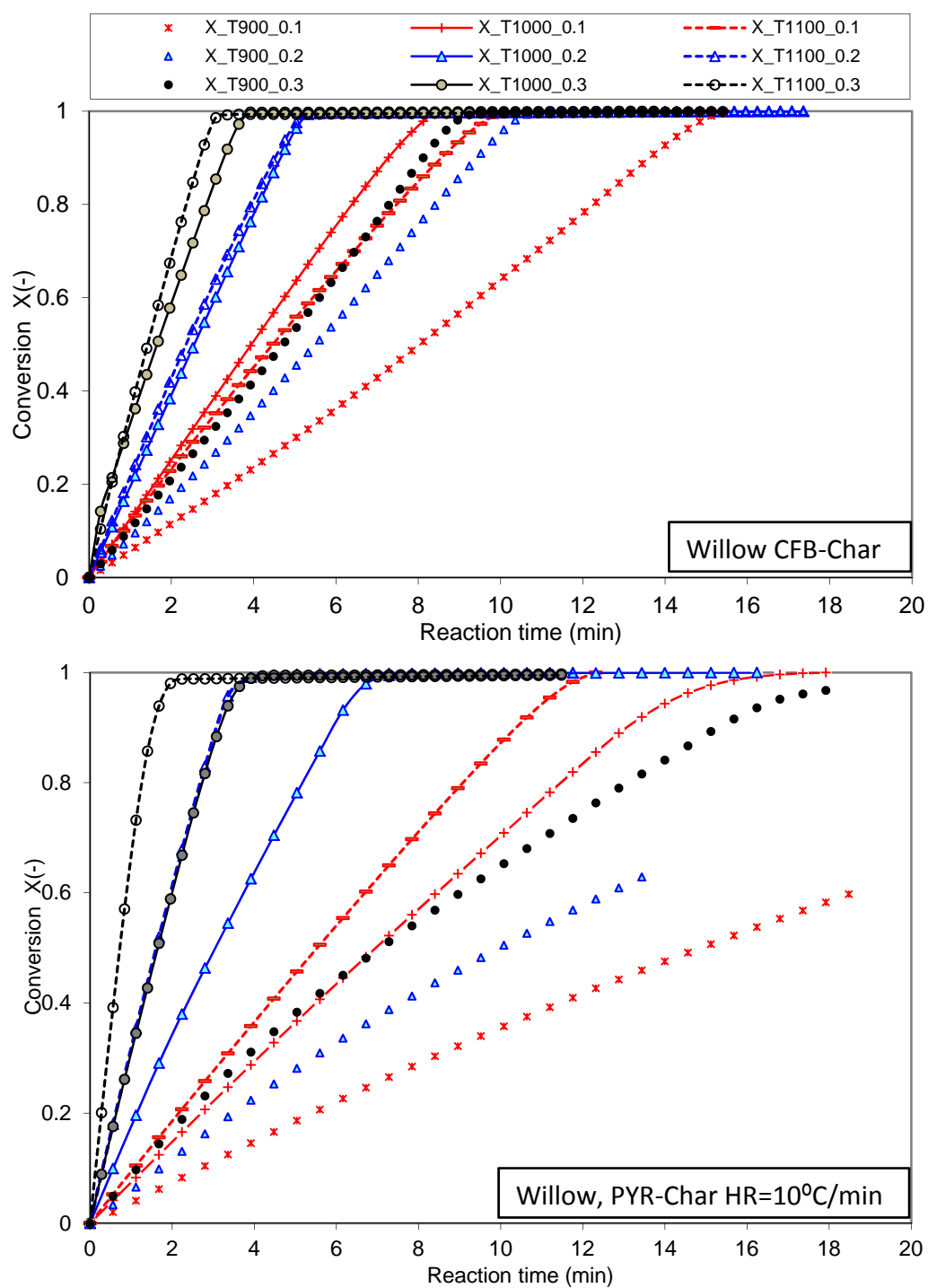


Figure 7- 14 Effects of gasification temperatures and  $CO_2$  concentrations on willow char gasification

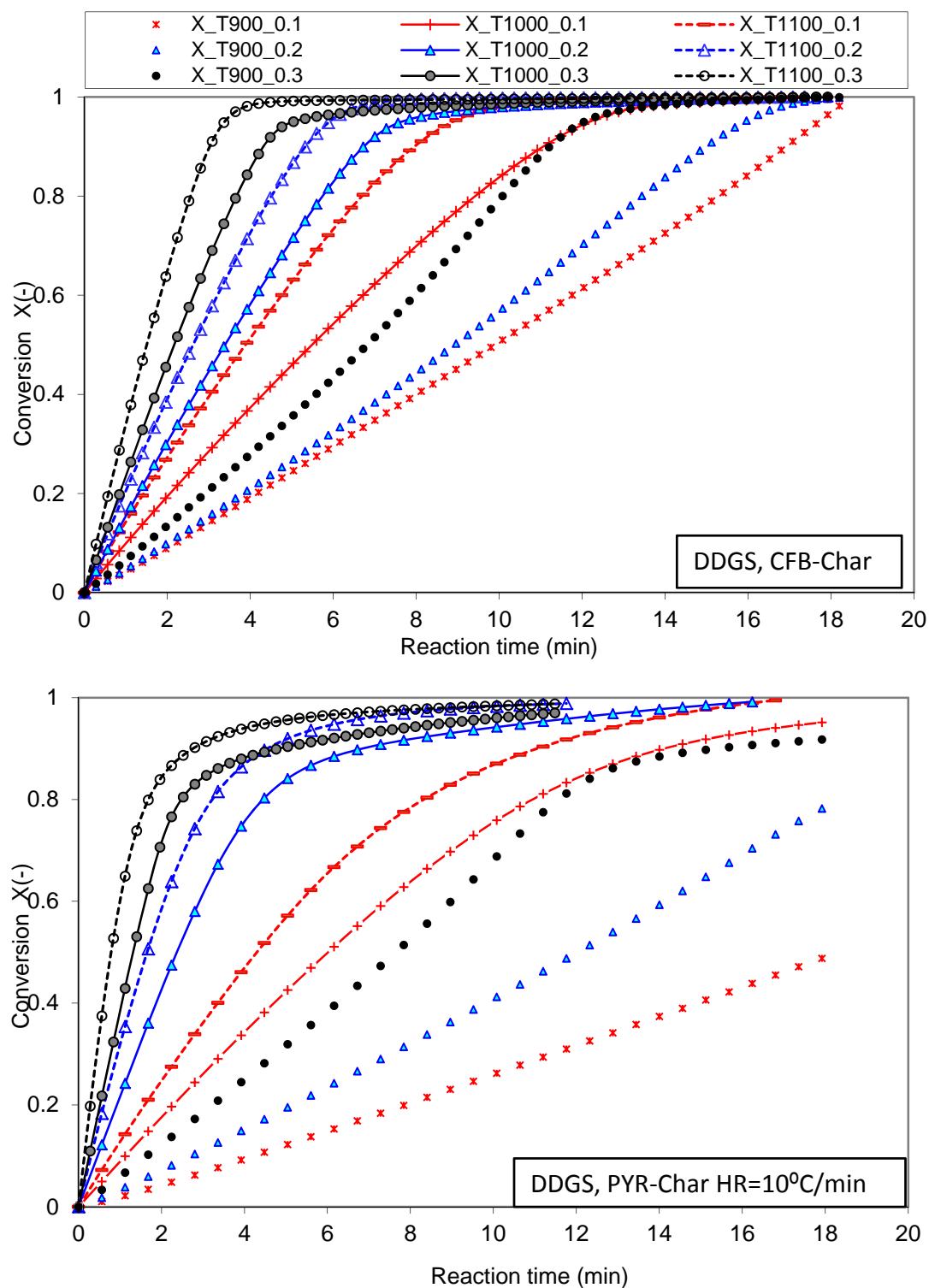


Figure 7- 15 Effects of gasification temperatures and CO<sub>2</sub> concentrations on DDGS char gasification

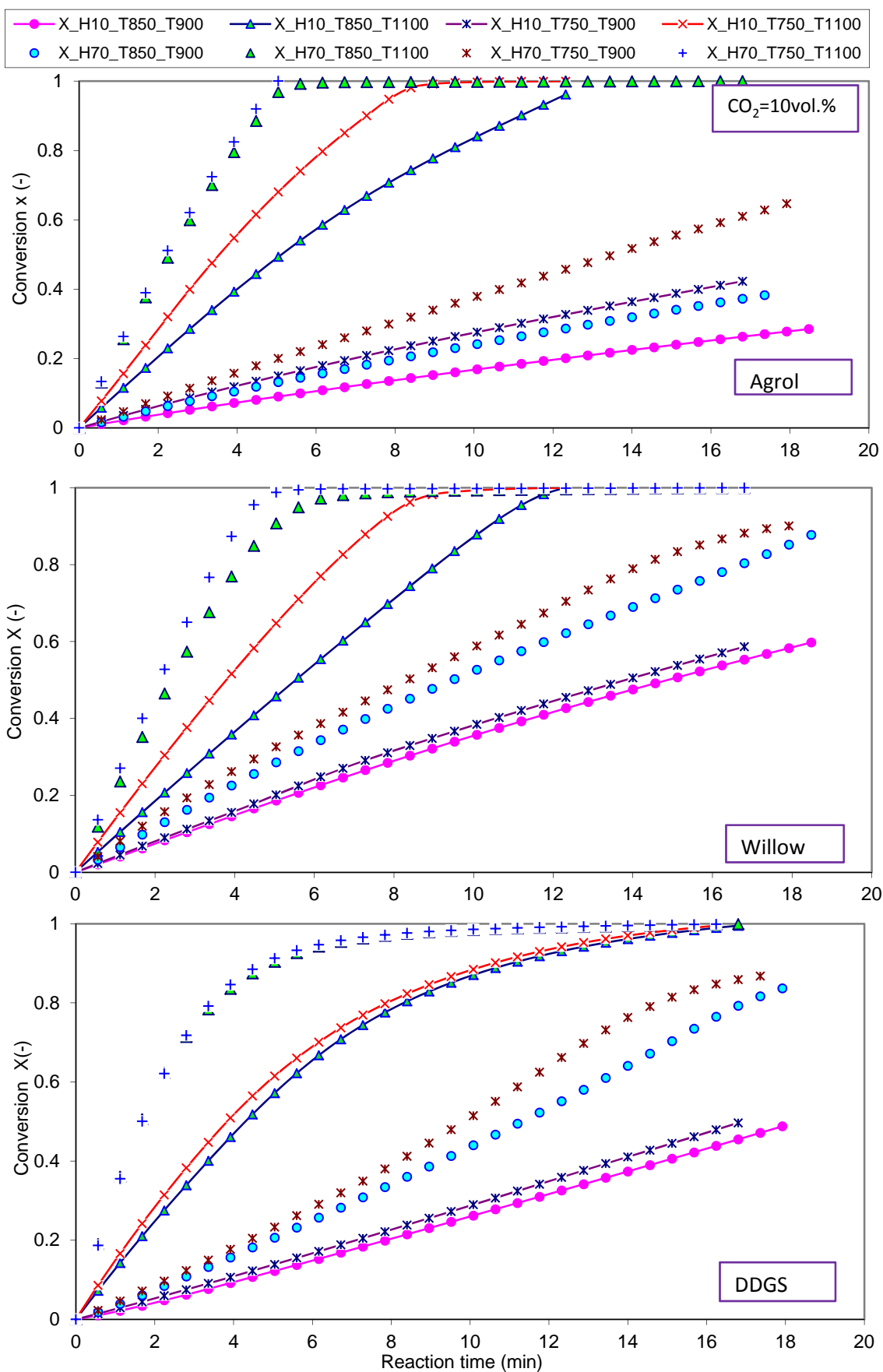


Figure 7- 16 Effects of different heating rates and pyrolysis temperature on PYR-Char conversion  $X$



### 7.5.2 Char gasification kinetics

**Table 7- 4** summarizes the Ea and k0 values calculated for PYR-Chars ( $T_{\text{pyr}}=850$  °C) and CFB-Chars for three fuels using the SCM and VRM models. In **Table 7- 4**, A-H10, A-H70 and A-CFB represent Agrol PYR-Chars obtained at HR=10 °C/min, HR=70 °C/min and Agrol CFB-Char, respectively, and similar settings as for willow and DDGS chars.  $R^2$  is the correlation coefficient, and most of them were above 0.95, which indicates that a fairly good linearity of all correlations was achieved. For all cases, the derived reaction order  $n$  was found to be higher than 2, which might be attributed to a fairly narrow  $\text{CO}_2$  concentration range applied. As such a higher order reaction is considered to be not plausible; the k0 values presented in **Table 7- 4** were therefore calculated based on a first order dependence to  $\text{CO}_2$  concentrations.

Table 7- 4 Kinetic parameters for PYR-Chars ( $T_{\text{pyr}}=850$  °C) and CFB-Chars

Char types	$\text{CO}_2$ (vol.%)	SCM			VRM		
		Ea(kJ/mol)	k0(min <sup>-1</sup> )	R2	Ea(kJ/mol)	k0(min <sup>-1</sup> )	R2
A-H10	0.1	140.2	1.08E+05	0.98	154.5	1.53E+06	0.96
	0.2	170.4	1.83E+06	0.98	181.1	1.84E+07	0.97
	0.3	181.2	6.97E+06	1.00	187.4	4.69E+07	0.99
A-H70	0.1	173.7	5.00E+06	0.98	179.5	3.07E+07	0.96
	0.2	182.2	8.19E+06	0.98	190.1	6.28E+07	0.98
	0.3	190.3	1.67E+07	1.00	202.7	2.12E+08	1.00
A-CFB	0.1	84.2	8.82E+02	0.92	93.8	8.08E+03	0.92
	0.2	91.0	1.67E+03	0.97	95.6	1.02E+04	0.98
	0.3	114.4	1.47E+04	0.96	115.5	6.81E+03	0.96
W-H10	0.1	89.1	1.42E+03	0.96	97.8	1.21E+04	0.95
	0.2	135.8	1.27E+05	0.96	143.2	9.66E+05	0.97
	0.3	160.7	1.63E+06	0.98	162.3	7.40E+06	0.99
W-H70	0.1	96.2	5.31E+03	0.94	96.9	2.23E+04	0.94
	0.2	129.5	1.24E+05	0.96	137.9	1.13E+06	0.97
	0.3	162.9	2.43E+06	0.99	165.0	1.18E+07	0.99
W-CFB	0.1	82.0	1.53E+01	1.00	82.9	6.95E+01	1.00
	0.2	92.3	5.90E+01	1.00	95.1	2.46E+02	1.00
	0.3	113.7	5.52E+02	1.00	115.9	1.64E+02	1.00
D-H10	0.1	102.5	4.68E+03	0.91	115.4	5.97E+04	0.90
	0.2	129.4	6.57E+04	0.89	140.2	7.04E+05	0.89
	0.3	141.9	2.46E+05	0.91	151.7	4.69E+05	0.90
D-H70	0.1	106.4	1.53E+04	0.90	109.2	7.84E+04	0.91
	0.2	124.0	6.19E+04	0.96	125.0	2.75E+05	0.96
	0.3	146.6	4.34E+05	0.95	151.7	1.83E+05	0.95
D-CFB	0.1	55.9	8.52E+01	1.00	57.3	3.79E+02	1.00
	0.2	75.4	3.76E+02	0.92	77.0	1.68E+03	0.92
	0.3	95.2	2.58E+03	0.95	97.5	1.12E+03	0.95

It can be seen from **Table 7- 4** that for all experimental conditions the Ea values calculated using the SCM model were slightly lower than those using the VRM model, and the Ea values increased simultaneously with increasing  $\text{CO}_2$  concentration. Generally, an increase in the heating rate from 10 to 70 °C/min seemed to have no significant influence on the Ea values of PYR-char for all fuels. The calculated Ea values for PYR-Chars using the SCM and VRM models were both within the 90 to 210 kJ/mol range, Ea values for PYR-Chars obtained from Agrol showed the highest Ea range, i.e., 120 to 210 kJ/mol, while those obtained from willow varied within the lowest range of 90-160 kJ/mol. However, compared to PYR-Chars, CFB-Chars showed a much lower Ea value range of 55 to 160 kJ/mol, particularly those obtained from DDGS which had Ea values in the 55 to 100 kJ/mol range. Thus, it can be concluded that higher heating rates could lower the Ea values to some extent.

Furthermore, no significant difference was observed between the Ea values of willow and DDGS PYR-Chars obtained at T<sub>Pyr</sub>=750 and 850 °C, while Agrol PYR-char obtained at T<sub>Pyr</sub>=750 °C had slightly lower Ea values than those obtained at T<sub>Pyr</sub>=850 °C.

In general, the calculated Ea values are comparable to reported values in the literature (Matsumoto et al., 2009; Ollero et al., 2003; Seo et al., 2010). Di Blasi (Di Blasi, 2009) summarized the Ea values for CO<sub>2</sub> gasification of lignocellulosic chars and found that they varied between 88 and 250 kJ/mol. The influences of different factors (e.g., pyrolysis temperature, heating rate) on the Ea values have also been discussed by other researchers. According to Kumar and Gupta (Kumar & Gupta, 1994), the Ea values obtained from wood chars during CO<sub>2</sub> gasification increased with increasing pyrolysis temperature and/or decreasing heating rate. The difference between Ea values obtained from Agrol, willow and DDGS chars might be attributed to the difference in char properties such as the pore structure of char, constituents of ash, char formation condition and carbon structure (Matsumoto et al., 2009). The fairly lower Ea values of CFB-Char obtained from DDGS fuel could be due to high K content in the ash (Di Blasi, 2009; Gómez-Barea et al., 2006; Ollero et al., 2003), since the catalytic effects could increase the reaction rate by lowering the Ea values.

### 7.5.3 Recalculation of TG

The weight loss (TG) curves were recalculated using the calculated Arrhenius parameters and compared with experimental ones to verify the accuracy of the models. The predicted TG curves of two typical cases were selected to show here being representative for the model validation. **Figure 7-17** shows the recalculated weight loss for PYR-Char at different CO<sub>2</sub> concentrations, where PYR-Char was obtained at T<sub>Pyr</sub>=850 °C, HR= 10 °C/min and gasified at T<sub>Ga</sub>=900°C, and **Figure 7-18** shows the recalculated weight loss for CFB-Char at different CO<sub>2</sub> concentrations, where CFB-Char was obtained at T<sub>Pyr</sub>=850 °C and gasified at T<sub>Ga</sub>=1100°C.

Furthermore, TG curves of some other cases are shown in **Figure A-9** and **Figure A-10** (see in Appendix). The legend settings are similar as in **Figure 7-17** and **Figure 7-18**. **Figure A-9** shows the recalculated weight loss for PYR-Char at different gasification temperatures, where PYR-Char was obtained at T<sub>Pyr</sub>=850 °C, HR= 10 °C/min, and gasified at three different temperatures T<sub>Ga</sub>= 900, 1000, 1100 °C using 10 vol.%CO<sub>2</sub>. **Figure A-10** shows the recalculated weight loss for CFB-Char at different gasification temperature, where CFB-Char was obtained at T<sub>Pyr</sub>=850 °C, and gasified at three different temperatures T<sub>Ga</sub>= 900, 1000, 1100 °C using 10 vol.%CO<sub>2</sub>.

It can be seen from **Figure 7-17** that the recalculated TG curves for all PYR-Chars generally showed a fairly good fitting with the experimental results, especially for Agrol PYR-Char wherein almost no differences were observed between the TG curves recalculated from the VRM and SCM models and the experimental results. This could be due to two reasons: first, as well aforementioned, Agrol PYR-Char was the least reactive under unfavorable gasification conditions, thus the effects of external mass transfer contributed in a lesser extent if they existed (see **Table A-6** in Appendix); and second, the catalytic effects of inorganic elements in the ash on char reactivity were less important due to their low amounts, especially K and Na contents. Compared to Agrol PYR-Char, the recalculated TG curves of willow PYR-Char using 10 and 20 vol.% CO<sub>2</sub> also agreed good with the experimental ones, whereas the fitting between the recalculated and experimental TG curves was getting slightly worse using 30 vol.% CO<sub>2</sub> as well as all TG curves of DDGS PYR-Char.

Furthermore, the results presented in **Figure 7-18** also indicate that the recalculated TG curves for all CFB-Chars agree reasonably well with the experimental results, but generally worse as compared to those for PYR-Chars. The above stated gasification results showed that CFB-Chars were getting more reactive than PYR-Chars, especially Agrol CFB-Char at high gasification temperatures. The reason could be that the catalytic effects of inorganic elements on char reactivities were not considered during the modeling calculation, which might be attributed to the difference between the predicted and experimental results of TG curves. Moreover, at high gasification temperature of 1100 °C, the SCM model seemed to be more suitable than the VRM model. According to some researchers (Czakiert &

Nowak, 2009; Hu et al., 2001), the SCM model could be more suitable when the reaction occurred within pore diffusion internal diffusion controlling regime or external diffusion controlling regime.

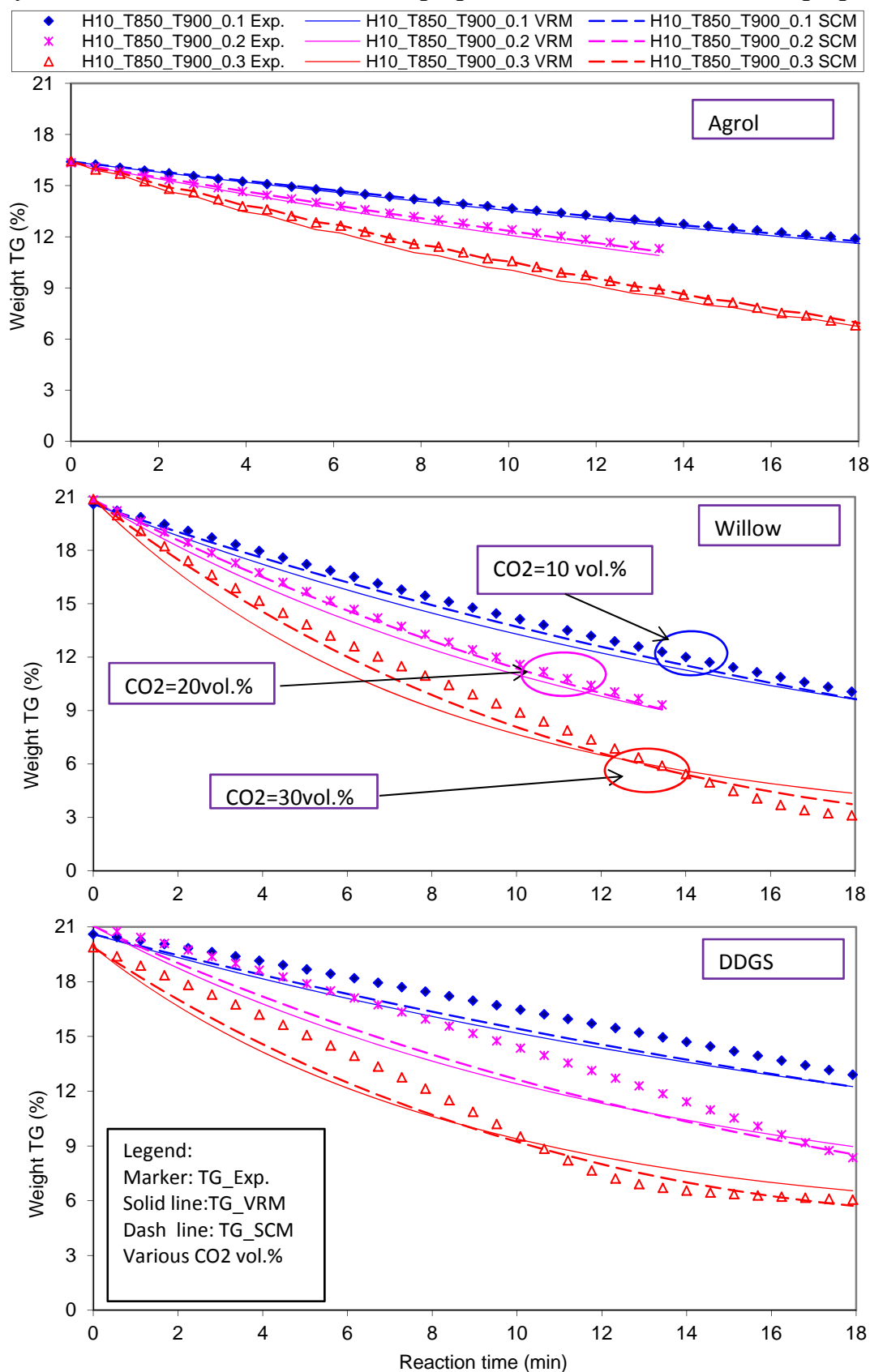


Figure 7- 17 The recalculated weight loss behavior for PYR-Chars at different CO<sub>2</sub> concentrations

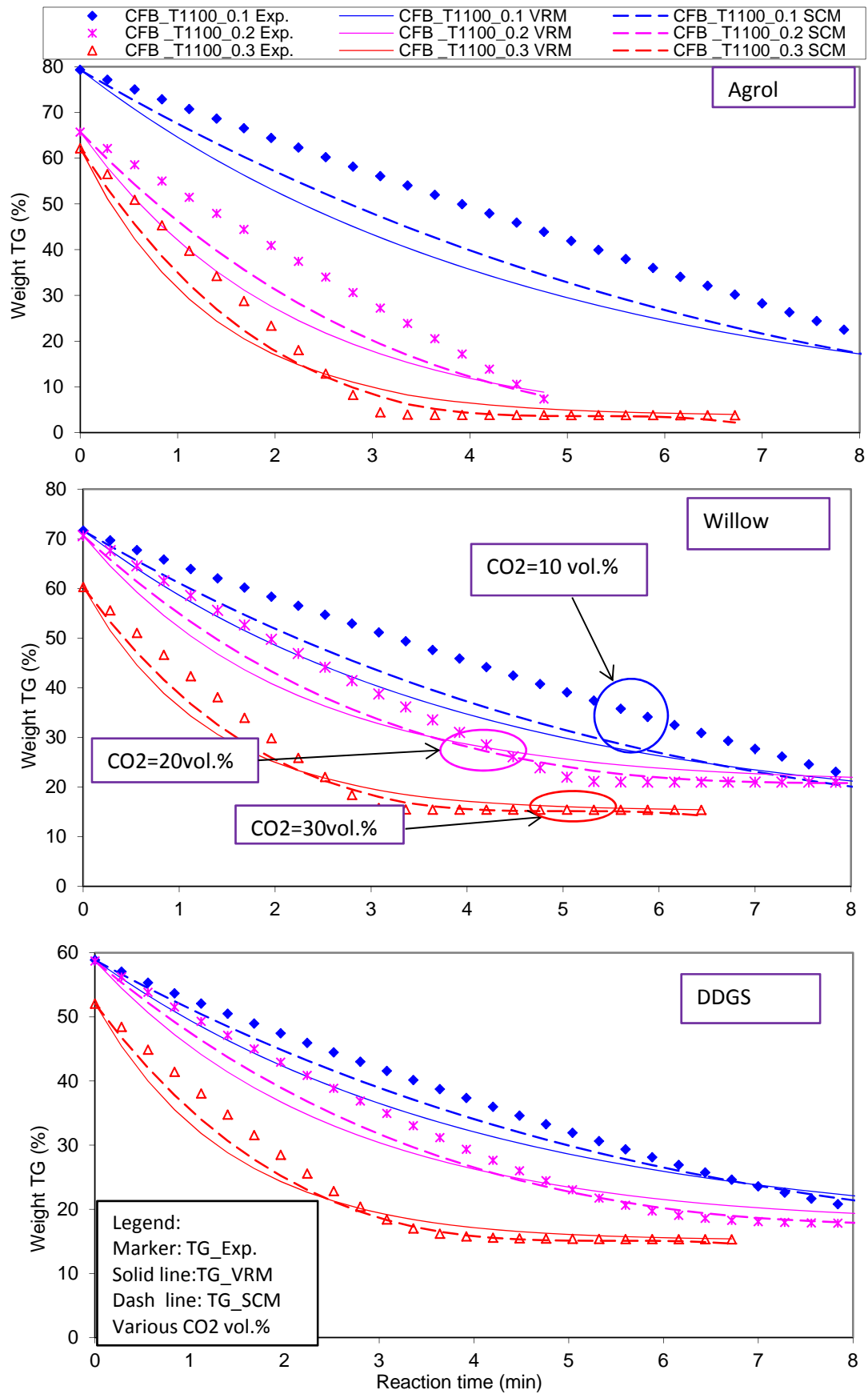


Figure 7- 18 The recalculated weight loss behavior for CFB-Chars at different CO<sub>2</sub> concentrations

From the above observations it can be generally concluded that both the VRM and SCM models are suitable to determine kinetic parameters of char gasification, in particularly for chars which are not so reactive and gasified under low gasification temperature with low CO<sub>2</sub> concentration. However, for reactive chars and with high ash content, enriched in inorganic elements, the catalytic effects of those elements could largely affect the modeling results. In this way, more complicated models, such as the random pore model, which simultaneously consider the effects of pore growth during the initial stages of gasification and the destruction of pores due to the coalescence of adjacent pores (Seo et al., 2010), could be a better choice. Meanwhile, the effects of mass and heat transfer also need to be checked and make sure the reaction occurs within the chemical reaction controlling regime. However, the catalytic influences of inorganic elements on willow and DDGS char gasification are still not well defined and explored in this work. More investigations combining different pre-treatments to lower and/ or increase inorganic elements in the ash content are necessary to get a better insight to their influences.

## **7.6 Conclusion**

The characterization of CFB-Chars obtained from Agrol, willow and DDGS gasification using the 100kW<sub>th</sub> steam-O<sub>2</sub> CFB gasifier by the analysis of XRD, XRF, N<sub>2</sub> adsorption/desorption and SEM coupled EDS allowed to correlate the char reactivity with the chemico-physical properties. Agrol char samples despite showing large specific surface areas had a low reactivity, due to their low ash content and related high crystalline order. On the other hand, the large ash content in willow and DDGS chars, in particularly K component may catalyze its char gasification, balancing the reduced surface area, which would decrease the diffusion of CO<sub>2</sub> within the pores.

SEM images showed that Agrol chars were very porous with different superficial cavities and thin walls, willow chars had a more compact agglomerated structure, while DDGS chars had a macroporous structure with rounded pores of different sizes and some particulate matters on the surface. XRD patterns showed that char samples had a disordered graphite-like structure. The XRF analyzed results showed that the inorganic elements of the Agrol char was formed by Ca, Fe, K, Mg, and Si. The willow char was mainly composed by Ca and K with minor amounts of Fe, Mg, P and Si. However, DDGS char was mainly dominated by K and P, with a lower amount of Ca, Mg and Na.

The pyrolysis behavior of Agrol, willow and DDGS and gasification reactivities of their CFB-Char and PYR-Char were investigated using the TGA-FTIR. The analyzed results showed that Agrol and willow had similar pyrolysis behavior and their characteristic devolatilization temperatures and their related weight loss rates increased with increasing heating rate. Char gasification rate increased with increasing gasification temperature, CO<sub>2</sub> concentration and heating rate, while it decreased with increasing pyrolysis temperature. Generally the calculated activation energy (E<sub>a</sub>) values using the SCM model were slightly lower than those using the VRM model. The calculated E<sub>a</sub> value for PYR-Char using both models were in the range of 90 to 210 kJ/mol, while the calculated E<sub>a</sub> values for CFB-Char were in the range of 55 to 120 kJ/mol. The predicted results using both models showed a reasonably good agreement with experimental results in particularly with those obtained at lower gasification temperature and lower CO<sub>2</sub> concentration. However, for reactive chars and with high ash contents enriched in inorganic elements, the catalytic effects of those elements could largely affect the modeling results using the simplified models.



## **8 Combustion behavior study of willow and DDGS CFB gasification residual chars using TG analysis and COMSOL Multiphysics<sup>TM</sup> modeling**

---

*In the previous chapter 7, the pyrolysis of three fuels and their residual char gasification were studied by using a TGA-FTIR system. This chapter studies the combustion behavior of DDGS and willow chars (as well as pure charcoal, as a comparison) using TG analysis under both isothermal and non-isothermal conditions. A 3D thermogravimetric (TG) furnace model has been built using COMSOL Multiphysics<sup>TM</sup> to better understand temperature and velocity profiles within the TG furnace. This part of work has been published in the Biomass and Bioenergy Journal.*

**Meng, X., de Jong, W., Badri F., Benito, P., Basile, F. Verkooijen, A. H. M. 2012. Combustion study of partially gasified willow and DDGS chars using TG analysis and COMSOL modeling. Biomass and Bioenergy, 39,356-369.**

As mentioned in chapter 7, it is a very important step for most researchers to select suitable kinetic parameters for the reaction of char from the large amount of literature data to perform the modeling of their gasifier processes. So far, few researchers have been focused their work on obtaining reaction kinetic parameters for chars produced from agriculture residues such as DDGS, which leads to some difficulties to simulate DDGS char combustion behavior as well as to perform the modeling of DDGS gasification in a gasifier by applying suitable char kinetics data. Furthermore, it is well known that a certain amount of heat is released during char combustion which can influence the temperature profile inside the reactor to some extent, and this profile is fairly valuable information for choosing suitable temperature control system of the reactor. Therefore, to obtain access to more reliable kinetic data in modeling of biomass gasification in the CFB gasifier, the combustion behavior of partially gasified willow and DDGS residual chars has been investigated using TG analysis. Moreover, to provide a better insight into heat transfer and fluid flow profiles within the TG furnace for the case of char combustion, the used TG furnace has been modeled by using the COMSOL Multiphysics<sup>TM</sup> software version 4.1.

## 8.1 Char combustion conversion models

The applied char combustion procedures have been presented in chapter 3 (see **Figure 3- 10**). The aim of this work is to study the influences of several important factors, such as combustion temperatures (400-600, 750-900 °C), heating rates (HR =10, 30, 50°C/min) and O<sub>2</sub> concentrations (7.5, 10, 15, 21vol. %) on the combustion behavior of willow and DDGS chars. Here, it assumes that O<sub>2</sub> concentrations in the air is 21 vol.%. The particle size distribution of willow and DDGS char samples were performed by using a Microtrac S3500 series particle size analyzer. The particle size distribution was determined as well as proper images of very small particles to be seen. Around 90% of chars had a diameter below 0.9 mm. As a comparison, the combustion behavior of pure charcoal bought from FLUKA Company was also investigated under some experimental conditions. The charcoal is very fine power (<0.1mm) and contains ≤2 % ash and trace amounts of mineral matters. The properties of two selected DDGS and willow CFB-Char samples, and charcoal is shown in **Table 8- 1**.

*Table 8- 1 Willow and DDGS CFB-Char, and charcoal main properties*

Main elements	Ca	Fe	K	Mg	Na	Al	Mn
DDGS char <sup>a</sup>	1.37	0.16	11.75	1.58	1.06	0.02	0.08
willow char <sup>a</sup>	10.44	1.04	4.6	0.89	0.08	0.44	0.22
Charcoal	0.1	0.03	0.02	0.02	0.05	-	0.005

Remark a: All elements from the XRF analysis

Different reaction conversion models have been applied to interpret the experimental data. A general expression (**Eq.8- 1**) was applied to determine Arrhenius kinetic parameters of char combustion, where X, n, C<sub>O2</sub>, k<sub>0</sub>, E<sub>a</sub>, R<sub>g</sub> and T represents char conversion (-), the reaction order (-), O<sub>2</sub> concentration (vol.%), the pre-exponential factor (min<sup>-1</sup>), the activation energy (J/mol), universal gas constant (8.314 J/(mol·K)) and reaction temperature (K), respectively. For char non-isothermal combustion, when the temperature varies with time with a constant heating rate, β =dT/dt, equation **Eq.8- 1** can be reorganized as a function of temperature (**Eq.8- 2**), where β represents the constant heating rate (K/min). The conversion X was calculated the same way by using equation **Eq.8- 4**.

f(X) is a structure factor and this parameter is normally used to describe the effects of available internal surface (e.g., actual surface over initial surface, available active or reactive sites) (Di Blasi, 2009; Risnes et al., 2001). Empirical expressions for f(X) and its integral form g(X) used for common gas solid state reactions models are summarized by Khawam and Flanagan (Khawam & Flanagan, 2006), which are shown in **Table 2- 6**. For isothermal combustion, the VRM model (f(X)=1-X), the SCM model (f(X)=3 (1-X)<sup>1/3</sup>) and zero order model (F0: f(X)=1) were applied, since these models have been widely used by other researchers (Cozzani, 2000; Di Blasi et al., 1999a; Luo & Stanmore,



1992; Zolin et al., 2001). For char non-isothermal combustion, the Flynn-Wall-Ozawa (FWO) method was used to solve **Eq.8- 2**, by applying Doyle's approximation and the integral expression for **Eq.8- 2** is shown as **Eq.8- 3** (Liu, 2009; Sima-Ella et al., 2005).

$$\frac{dX}{dt} = k_0 \exp\left(\frac{-E_a}{R_g T}\right) C_{O_2}^n f(X) \quad \text{Eq.8- 1}$$

$$\frac{dX}{dT} = \frac{k_0}{\beta} \exp\left(\frac{-E_a}{R_g T}\right) C_{O_2}^n f(X) \quad \text{Eq.8- 2}$$

$$\log \beta = \log \frac{k_0 E_a C_{O_2}^n}{g(X)} - 2.315 - \frac{-0.4567 E_a}{R_g T} \quad \text{Eq.8- 3}$$

$$X = \frac{m_0 - m_t}{m_0 - m_f} \quad \text{Eq.8- 4}$$

## 8.2 COMSOL Multiphysics™ modeling procedure

The main TG furnace has been modeled using the COMSOL Multiphysics™ software version 4.1. The geometry of the main TG furnace used in the model is shown in **Figure 8- 1**, and see **Figure A-11** in Appendix for more details.

The main components of the TGA analyzer include the thermobalance, furnace, temperature controller and measurement, purge gas line and other accessories. The thermobalance consist of the individual meter movements, balance beams (including sample platform, platinum liners, and thermocouple wires), tare beams and tare weights, position sensor beams, and sensors. The sample and reference balance assemblies are identical, but mirror images of each other. It is a ceramic alumina beam with the sample platform liner on one end, thermocouple wires running the length of the beam, and a metal bracket mounted on the other end. The metal bracket mounts the beam to the meter movement

To simply the simulation, the geometry for this 3D TG model has been defined as mainly consisting of the furnace tube (walls) with all components inside (two beams with cups at the end and sample in one of the cups). The whole length of the furnace tube is approximately 216 mm of which 94 mm is heated. The external diameter of the inlet and outlet is approximately 25 and 7 mm, respectively, with a thick wall of circa 1 mm. Alumina has been applied as selected material for beams, cups and the inside wall of the furnace, while the sample has been defined as carbon. Air flow is assumed to occur within the furnace tube. The physical and chemical properties of these materials and their relation with temperature have been taken from the COMSOL Multiphysics™ software's own database.

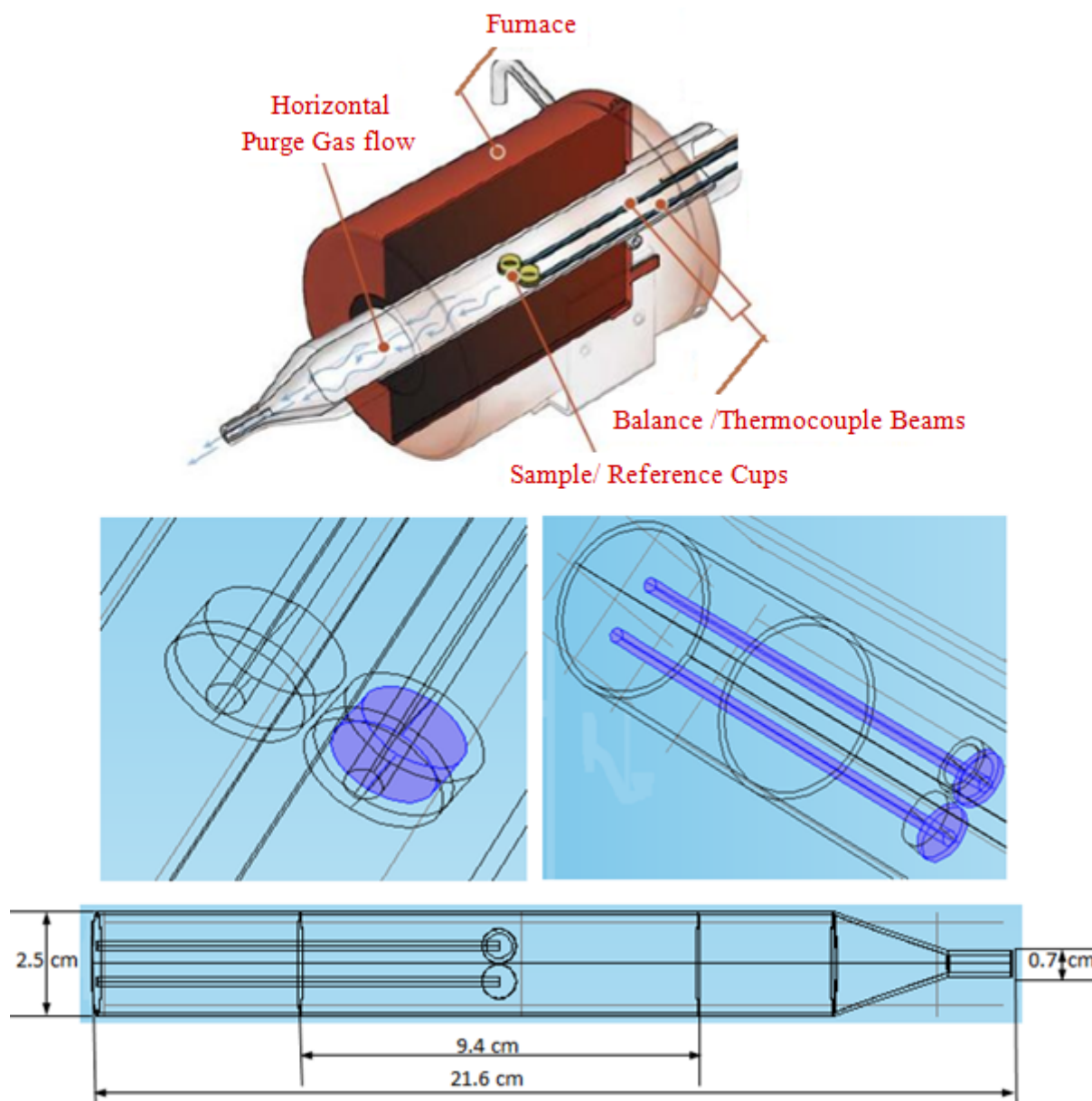


Figure 8- 1 Geometry of the TG furnace used in the COMSOL model

The main equations applied in the TG model and their relevant boundary equations as well as the constants used are summarized in **Table 8- 2**. A general heat transfer equation (**Eq.8- 6**) including conduction, convection and radiation has been used in the model. The conductive item in **Eq.8- 6** equation is described by using Fourier's law of heat conduction which indicates the conductive heat flux is proportional to the temperature gradient and used to model the heat transfer within solid (e.g., alumina beams, plates below the cups). The heat transfer convection within the furnace tube occurs in flow gas domain. Surface to surface radiation is applied to simulate the heat transfer for the heated wall to its adjacent alumina surface due to radiation effect (**Eq.8- 11**). The heat source is to model heat released from char combustion (**Eq.8- 10**). Several boundary conditions are applied to the heat transfer equation: the inlet temperature is assumed to be constant of around room temperature 20 °C (**Eq.8- 7**), the heated wall temperature as assumed to be constant and its value depends on the reaction temperature applied (**Eq.8- 9**), while the outlet temperature and the internal temperature within the furnace tube are derived from an equation of continuity (**Eq.8- 8**).

Table 8- 2 Equations applied in the model and their boundary conditions and constants

Reaction model			
Items		Equations / Values	NO.
General equation		$r = k^f \prod_{i=1}^N c_i^{\nu} = A^f T^f \exp\left(\frac{E_a^f}{R_g T}\right) \prod_{i=1}^N c_i^{\nu}$	Eq.8- 5
Heat transfer			
Items		Equations / Values	NO.
General equation		$\rho_g C_p \frac{\partial T}{\partial t} + \rho_g C_p u \nabla T = \nabla \cdot (\kappa \nabla T) + Q$	Eq.8- 6
Boundary condition / constants	Inlet	$T = T_0,$ <span style="float:right"><math>(T_0 = 293.15K)</math></span>	Eq.8- 7
	Outlet	$-n \cdot (-\kappa \nabla T) = 0$	Eq.8- 8
	External	$T = T_0,$ <span style="float:right"><math>(T_0 = 773.15/1123.15K)</math></span>	Eq.8- 9
	Heat source	$Q = r \bullet \Delta H$	Eq.8- 10
	Surface to surface	$-n \cdot (-K \nabla T) = \varepsilon (G - \sigma T^4)$ $(1 - \varepsilon)G = J_0 - \varepsilon \sigma T^4$	Eq.8- 11
Gas flow			
Items		Equations / Values	NO.
General equation		$\rho_g \frac{\partial u}{\partial t} + \rho_g u \cdot \nabla u = \nabla \cdot \left[ -pI + \mu_g \left( \nabla u + (\nabla u)^T \right) - \frac{2}{3} \mu_g (\nabla \cdot u) I \right] + F \quad (a)$ $\frac{\partial \rho_g}{\partial t} + \nabla \cdot (\rho_g u) = 0 \quad (b)$	Eq.8- 12
Boundary condition / constants	Inlet	$u = -u_0 n,$ <span style="float:right"><math>(u_0 = 7.4 \times 10^{-3} \text{ m/s})</math></span>	Eq.8- 13
	Outlet	$p = p_0,$ <span style="float:right"><math>(p_0 = 0 \text{ pa})</math></span>	Eq.8- 14
	External	$u = 0$	Eq.8- 15

Where:

Variables	Units
$\rho_g$ : The density of fluid gas	kg/m <sup>3</sup>
$C_p$ : The specific heat capacity of the fluid gas	kJ/kg K
$T$ : Temperature	K
$\kappa$ : Thermal conductivity of the materials	W/(m.K)
$u$ : The velocity vector	m/s
$Q$ : Heat source	W/m <sup>3</sup>
$p$ : Static pressure	Pa
$\mu_g$ : The dynamic viscosity of the fluid	Pa·s
$I$ : The identity matrix	-
$F$ : The vector of volume forces	N/m <sup>3</sup>
$\Delta H$ : Heat of combustion reaction	J/mol
$G$ : Total arriving radiative flux- the irradiation	W/m <sup>2</sup>
$J_0$ : The total outgoing radiative flux - the radiosity	W/m <sup>2</sup>
$\sigma$ : the Stefan-Boltzmann constant	W/(m <sup>2</sup> ·K <sup>4</sup> )
$\varepsilon$ : Surface emissivity	-

The Navier–Stokes (NS) equations are applied to model the gas flow within the furnace tube (*Eq.8-12*). The a item in equation *Eq.8-12* is vector equation which represents the conservation of momentum, while b item is the continuity equation and represents the conservation of mass. The volume force is used to incorporate effects of gravity. The boundary conditions applied for the NS equations are the typical no-slip condition on the wall (*Eq.8-15*). The inlet velocity used is calculated from the total inlet flow rate supplied to the furnace (*Eq.8-13*), while the outlet pressure is assumed to be zero (*Eq.8-14*).

## 8.3 Char combustion results

### 8.3.1 Isothermal combustion

*Figure 8-2* shows the weight loss (TG, %) versus time of willow and DDGS CFB-Chars and chacoal in the air with varying the combustion temperature (450, 600, 800 and 900 °C), whereas *Figure 8-3* shows the weight loss (TG, %) versus time of three char samples in the air at two different temperatures (550 and 850 °C) with varying the O<sub>2</sub> concentration (7.5, 15 and 21vol.%). In these two figures, C, D and W represent charcoal, DDGS char and willow char, respectively, and similar as in other figures. T450, T600, T800 and T900 in *Figure 8-2* represent isothermal combustion temperature 450, 600, 800 and 900 °C, respectively, while 7.5%, 15%, 21% in *Figure 8-3* represent the volume fraction of the O<sub>2</sub> concentration 7.5, 15 and 21vol.%, and similar as in other figures.

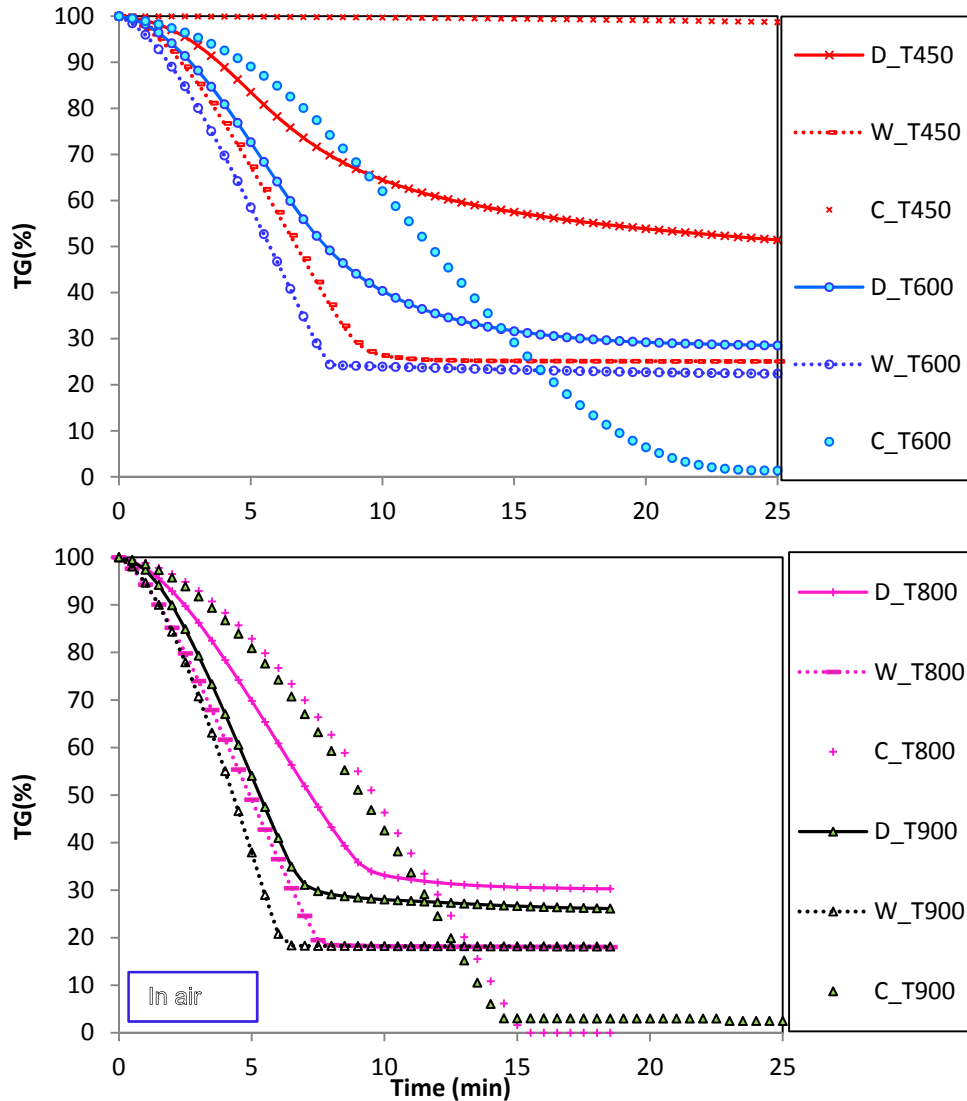


Figure 8- 2 Effects of temperatures (°C) on DDGS and willow chars and charcoal during isothermal combustion in air in the TGA

In **Figure 8- 2** and **Figure 8- 3**, it can be seen that all char conversion values increase with increasing either combustion temperature or O<sub>2</sub> concentration. It is fairly reasonable since an increase in the combustion temperature supplies more energy to the reaction for surmounting activation energy barrier, while an increase in O<sub>2</sub> concentration increase available reactant concentration on the char surface. Under all experimental conditions, willow char was the most reactive, followed by DDGS char and charcoal. Concerning the effect of combustion temperature, at a low temperature of 450 °C, willow char reacted completely within 15 min; however, charcoal only reacted to an extent less than 2%. In general, the conversion values of DDGS char and charcoal combustions observed at a low (450 °C) and high temperature (900 °C) were significantly different, but the conversion value of willow char combustion at a temperature of 450 °C was fairly similar to that observed at 900 °C, as well as those of charcoal obtained at a combustion temperature of 800 and 900 °C. When O<sub>2</sub> concentration was 7.5 vol.% at a temperature of 550 °C, willow char achieved 100% conversion within 25 min, but DDGS char only reacted to an extent less than 70%. From the above observation, it can generally be concluded that the combustion temperature had more influence on DDGS and charcoal than willow char. The different combustion behavior of different char samples at low and high temperatures probably are due to their different properties. Furthermore, different residual weights of ash were obtained after different combustion tests of DDGS and willow chars which indicated that willow and DDGS chars were somewhat inhomogeneous. DDGS char generally contained a higher residual ash amount than willow char. The observations agreed with the results obtained from the EDS and XRF analysis, see chapter 7.

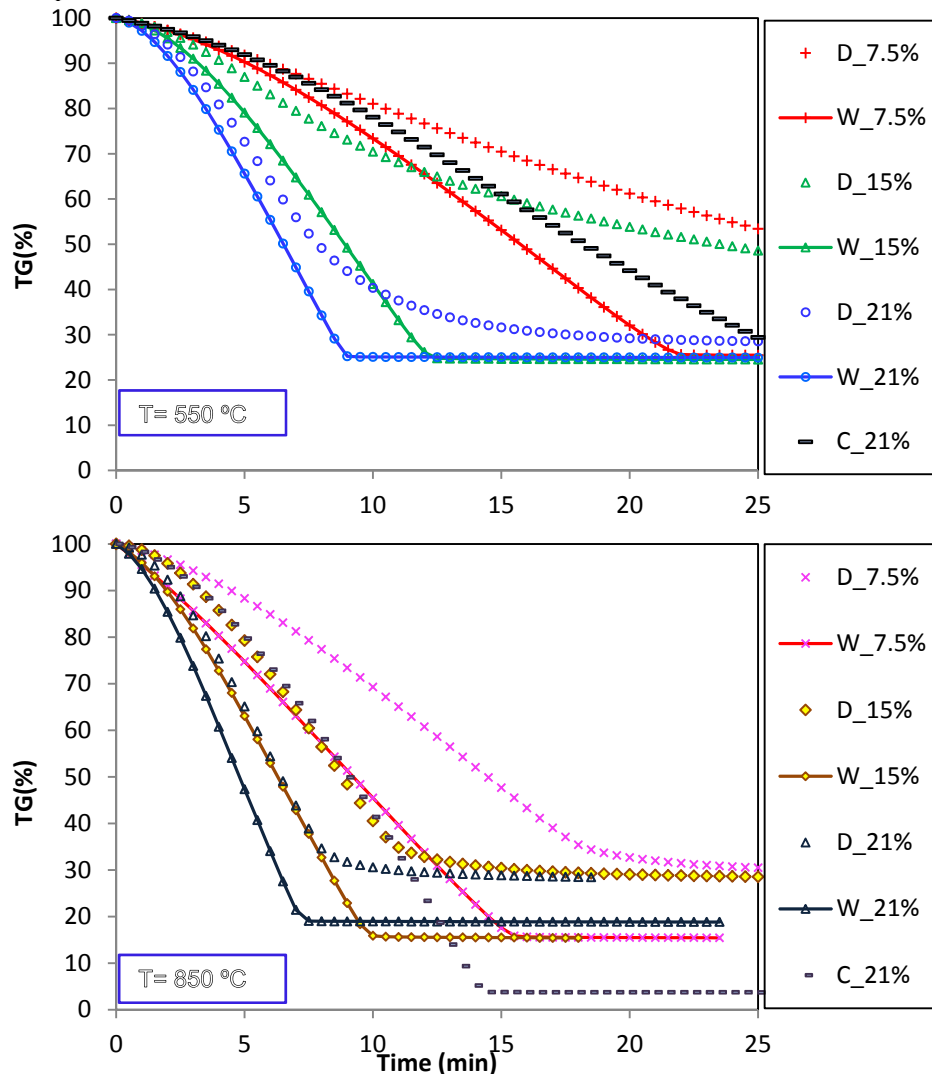
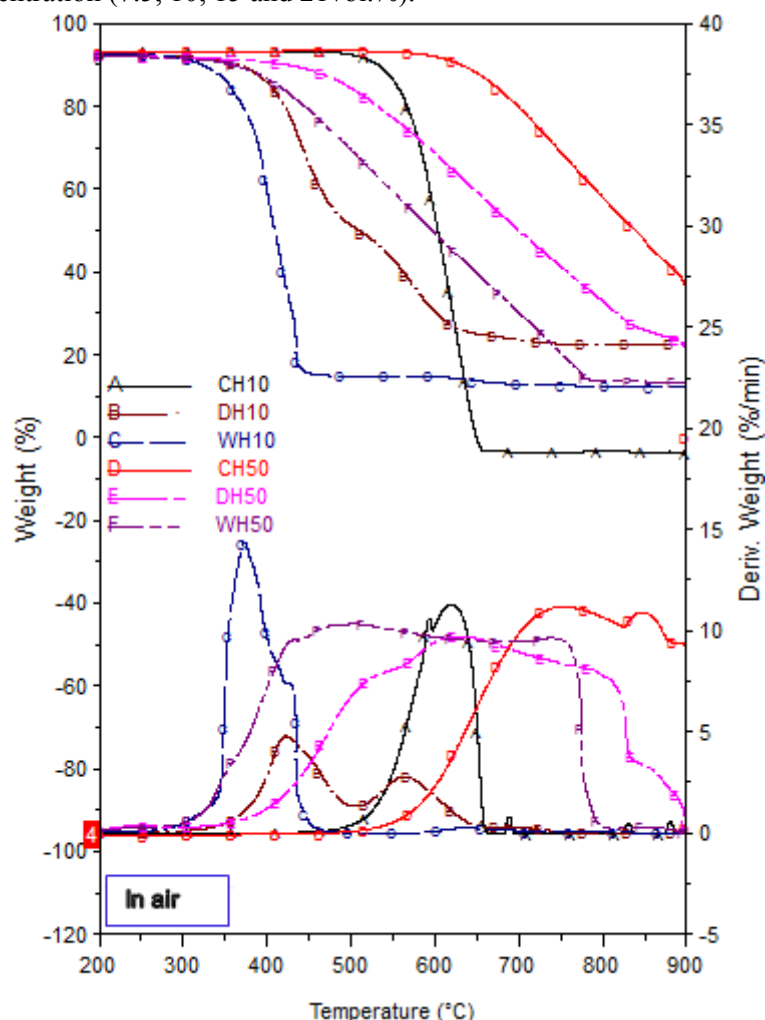


Figure 8- 3 Effects of O<sub>2</sub> concentrations (vol.%) on DDGS and willow char during isothermal combustion in the TGA

### 8.3.2 Non-isothermal combustion

**Figure 8- 4** shows the weight loss (TG, %) and the time derivative of weight loss (DTG, %/min) versus temperature of different chars during non-isothermal combustion in air at HR= 10 and 50 °C/min, while **Figure 8- 5** shows the weight loss (TG, %) and the derivative of weight loss (DTG, %/min) versus temperature of DDGS char during non-isothermal combustion at HR=10 °C/min with varying the O<sub>2</sub> concentration (7.5, 10, 15 and 21vol.%).



*Figure 8- 4 Effects of heating rates on DDGS and willow chars and charcoal non-isothermal combustion in air*

The results shown in **Figure 8- 4** indicate that the combustion of willow char started at the lowest temperature of around 260 °C, while the combustion of charcoal occurred at the highest temperature of around 470 °C. At the low HR of 10 °C/min, the combustion of willow char, DDGS char and charcoal mainly occurred within the temperature range of 300-450, 500-650 and 300-650°C, respectively. Moreover, willow char showed the highest combustion rate and meanwhile this occurred at the lowest temperature of approximately 360 °C, which indicated that willow char is the most reactive among these three chars according to the reported results by other researchers (Entorun & Küçükbayrak, 1996; Kastanaki & Vamvuka, 2006; Rubiera et al., 1999) that, the temperature where the maximum reaction rate occurs can be used as a measure of char reactivity: the lower the maximum peak temperature is, the more reactive the char is.

However, at the relatively higher HR of 50 °C/min, the combustion of these three chars occurred in a much wider temperature range. The DTG curves of three char samples at HR of 50°C/min were also much different compared to those obtained at HR of 10°C/min. For example, the combustion of willow char at HR of 50°C/min mainly occurred within the temperature range of 300-800°C, which is

much wider than the range of 300-450°C obtained at HR of 10 °C/min, and the combustion of DDGS char and charcoal even was up to 900 °C. Generally, a very sharp maximum combustion rate peak (two peaks for DDGS char) was observed during the combustion of three chars at a HR of 10 °C/min, but at a HR of 50 °C/min instead of an evident combustion rate peak, a nearly constant combustion rate was observed in a wide temperature range. These observations generally agreed with the results reported by other researchers. For example, Kastanaki and Vamvuka (Kastanaki & Vamvuka, 2006) studied the combustion reactivity of coal-biomass char blends and reported that combustion of biomass chars started at lower temperatures compared to coal char. Among biomass chars, the combustion of cotton char started at the lowest temperature (282 °C), while the combustion of forest residue char at the highest temperature (354 °C). Tia et al. (Tia et al., 1991) prepared Thai lignite char by pyrolysing the parent lignite at around 900 °C and studied its combustion kinetics using TGA under non-isothermal condition. They reported that the combustion of lignite char started at around 250-300°C and was completed at about 400-500°C for slow HR (<15°C/min), while these temperatures increased to 300 °C and 500- 550°C for high HR (>50°C/min). They also observed that DTG curves obtained at different HR values showed similar behavior as obtained in this work. Their explanation for this behavior is due to the transition of the combustion mechanism from chemical kinetic control to pore diffusion control.

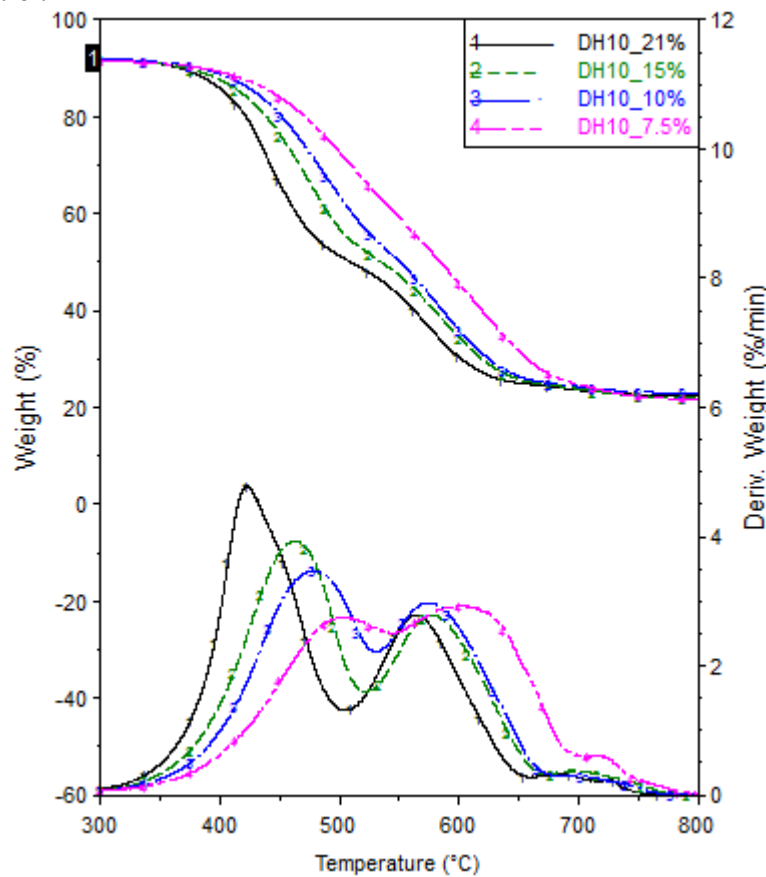


Figure 8- 5 Effects of O<sub>2</sub> concentrations on DDGS char non-isothermal combustion

Interestingly, compared to willow char and charcoal, DDGS char had two obvious combustion peaks at a low HR of 10°C/min. **Figure 8- 5** clearly illustrates that varying the O<sub>2</sub> concentration affected the separation of two peaks, as well as the maximum combustion rate and its associated temperature. The maximum combustion rate of the first and second peak in air occurred at a temperature of around 420 and 565 °C, respectively, while in a 7.5vol.% O<sub>2</sub> environment these shifted to around 500 and 605 °C, respectively. These observations indicate that DDGS char is much different from normal woody biomass, which was also reported by other researchers. For example, Wang et al. (Wang et al., 2009) studied the thermal degradation characteristics and kinetic parameters of distillers grains and solubles (DGS) during pyrolysis and combustion. They observed two obvious zones during DGS combustion and the starting temperature of two zones increased slightly from 180 °C to 220 °C, and from 470 °C

to 490 °C, respectively, with increasing heating rate from 10 to 50 °C/min. Avila and Lester (Avila & Lester, 2008) studied the reactivities of DGS and DDGS char particles at a HR of 10 °C/min in air using TGA (TA Q500). They found that DDG and DDGS chars showed similar behavior due to their same material origin. Two peaks were observed during char combustion which occurred mainly within the temperature range of 300-700 °C. Darvell et al. (Darvell et al., 2010) studied combustion properties of several biomass fuels (e.g., olive residue, shea residue, palm kernel expellers (PKE)) and their derived chars. Different combustion behavior was observed for different chars from their DTG curves. They found that a single peak was observed for the combustion of the PKE and olive residues A and C chars, while two peaks were obtained for the combustion of shea residue and olive residue B char. Similarly, Munir et al. (Munir et al., 2009) reported that the DTG curves for shea meal char showed a two stage combustion process with peaks at a temperature of approximately 390 °C and 420 °C. According to their explanations, this behavior may be due to the nature of the biomass components present in the original material. In the previous chapter, it also pointed out that there were two well-defined peaks occurring during DDGS pyrolysis, whereas only one evident peak observed during Agrol and willow pyrolysis.

### 8.3.3 Kinetic constants for char combustion

**Table 8- 3** summarizes the kinetic constants for three different chars obtained at isothermal combustion and estimated by means of three different conversion models, where  $R^2$  is the correlation coefficient. As can be seen in **Table 8- 3**, most of the correlation coefficients are above 0.95, which indicates that a fairly good linearity of all correlations was achieved. Generally, higher activation energies ( $E_a$ ) were associated with higher pre-exponential constants ( $k_0$ ) which ensured the calculated combustion rate to remain the same; however, the calculated  $E_a$  values for our DDGS and willow chars were much lower, compared to those reported in the literature (Di Blasi et al., 1999a; Janse et al., 1998; Várhegyi et al., 2006; Zolin et al., 2001). For example, almost all  $E_a$  values obtained from the combustions of willow and DDGS chars within the temperature range of 800-900 °C were lower than 30kJ/mol, which indicated that external  $O_2$  diffusion in this temperature range was the rate controlling step instead of chemical reaction kinetic control. Such observations have also been reported by other researchers (Dutta & Wen, 1977; Tseng & Edgar, 1984).

To our surprise, within the temperature range of 400 to 600 °C, willow char obtained an extremely low  $E_a$  value of around 15 kJ/mol, whereas within the similar temperature range, Di Blasi et al. (Di Blasi et al., 1999a) found that  $E_a$  values of several biomass chars (e.g., olive husks, grape residues, and pine wood) combustion in air were within the range of 71 to 100 kJ/mol. Interestingly, the calculated  $E_a$  value using the VRM model for charcoal combustion in air within the temperature range of 450 to 550 °C was around 200 kJ/mol, and in 15 vol.%  $O_2$  within the temperature range of 750 to 900°C was around 125 kJ/mol, which agreed well the values reported in the literature. As aforementioned Di Blasi (Di Blasi, 2009) summarized the  $E_a$  values obtained for lignocellulosic chars combustion and found that they were in the range of 140 to 230kJ/mol with upper boundary values for coal char or graphite combustion in the low temperature zone. This result confirmed that the experimental procedures and conversion models applied in this work were reasonable, and the TG analysis also can be used to estimate char combustion kinetic parameters within some specified condition. However, compared to  $E_a$  values reported in the literature, an  $E_a$  value of approximately 60 kJ/mol obtained from DDGS char combustion seemed to be somewhat on the low side. This probably is due to high ash content in DDGS char sample.



Table 8- 3 Kinetic constants for three different chars isothermal combustion as estimated by different conversion models

Chars			F0			VRM			SCM		
	O <sub>2</sub> (vol.%)	T Range(°C)	Ea(kJ/mol)	k0(min <sup>-1</sup> )	R <sup>2</sup>	Ea(kJ/mol)	k0(min <sup>-1</sup> )	R <sup>2</sup>	Ea(kJ/mol)	k0(min <sup>-1</sup> )	R <sup>2</sup>
Charcoal	21	450-550	166.5	4.56E+09	0.98	199.0	9.35E+11	0.95	187.2	4.50E+10	0.96
	15	750-900	110.1	1.10E+04	0.96	124.8	7.03E+04	0.95	<b>119.7</b>	<b>1.23E+04</b>	<b>0.95</b>
	21	600-900	8.0	7.63E-01	0.99	7.6	1.38E+00	1.00	7.7	3.70E-01	1.00
DDGS	7.5	450-600	45.8	2.75E+02	0.97	52.1	1.39E+03	1.00	49.3	2.40E+02	0.99
	15	450-600	55.4	8.25E+02	0.97	52.9	1.25E+03	0.98	54.7	4.05E+02	0.98
	21	450-600	59.4	1.48E+03	0.93	<b>59.9</b>	<b>3.40E+03</b>	<b>1.00</b>	59.4	8.00E+02	1.00
DDGS	7.5	750-900	22.6	7.93E+00	0.92	22.7	1.57E+01	0.92	22.6	4.05E+00	0.92
	15	750-900	23.1	6.98E+00	0.98	24.3	1.58E+01	1.00	23.6	3.81E+00	1.00
	21	750-900	24.6	8.31E+00	0.96	24.9	1.71E+01	0.91	24.7	4.29E+00	0.94
Willow	7.5	400-500	15.5	7.78E+00	0.97	17.9	2.30E+01	0.95	16.8	4.99E+00	0.96
	15	400-500	14.9	5.52E+00	0.94	16.2	1.39E+01	0.96	15.4	3.14E+00	0.95
	21	400-500	11.0	3.17E+00	0.93	15.8	1.56E+01	0.99	13.3	2.53E+00	1.00
Willow	7.5	800-900	38.9	5.68E+01	1.00	48.7	3.27E+02	1.00	44.6	5.47E+01	1.00
	15	800-900	25.6	1.06E+01	0.98	31.1	3.78E+01	1.00	28.7	7.61E+00	0.99
	21	800-900	18.6	5.17E+00	0.94	20.5	1.28E+01	0.98	19.5	2.93E+00	1.00

As can clearly be seen in **Figure 8- 2** and **Figure 8- 3**, DDGS char contained around 15-30% ash and the catalytic effects of inorganic elements (e.g., K, Na, Ca) could reduce  $E_a$  values (Di Blasi, 2009). Similarly, low  $E_a$  values were also reported by other researchers. For example, Kelebopile et al. (Kelebopile et al., 2011) studied the combustion behavior of three char samples Jing900, Jing1000, and Jing1100 within the temperature range of 500 to 575 °C. These three char samples were prepared from a low volatile bituminous coal in a drop tube furnace (DTF) at a temperature of 900, 1000, and 1100 °C, respectively. They found that the  $E_a$  values for Jing900 and Jing1000 char samples were 50.9 and 83.6 kJ/mol, respectively. They concluded that these fairly low  $E_a$  values were acceptable considering the high ash content (around 56%) in the char samples. Darvell et al. (Darvell et al., 2010) also obtained a much lower  $E_a$  value for olive residue char B combustion (72, 46 kJ/mol depending on model methods), which is lower than those ( $> 140$  kJ/mol) reported by other researchers for olive waste char combustion (Senneca, 2007). Thus, based on the above-stated results from different researchers, the  $E_a$  value obtained in this work for DDGS char combustion seemed to be reasonable. Unfortunately, probably due to the presence of inorganic matter in the willow char (HaykIrI-A ma et al., 2001) and its produced environment (e.g., pyrolysis temperature) during gasification (Patel et al., 1988), willow char seems too reactive to determine its combustion kinetic parameters properly even within the low temperature range of 400 to 500 °C.

The linear iso-conversional model-free FWO method was applied to determine the kinetic constants for the three chars during non-isothermal combustion. **Figure 8- 6** shows FWO plots of DDGS, willow char and charcoal combustion in air at varying conversion ( $X$ ) from 7.5% to 40%, where from the slope of the plots of  $\log \beta$  ( $\beta$ : heating rate °C/min) versus  $1/T$  ( $T$ : reaction temperature, K), the  $E_a$  value at different conversion  $X$  was determined.

From **Figure 8- 6**, it can be seen that generally a fairly good linear correlation was observed at different  $X$  values between  $\log \beta$  and  $1/T$ . For willow, the linear correlation between  $\log \beta$  and  $1/T$  was getting a bit worse when  $X$  was higher than 20%, which indicated that the combustion control mechanism might be slightly different as reported by Liu (Liu, 2009). Furthermore, for the same  $X$  value, the combustion of charcoal occurred at much higher temperature than DDGS and willow char, and this pointed out that charcoal was less reactive.

**Figure 8- 7** presents the calculated  $E_a$  values using the FWO method for DDGS, willow char and charcoal combustion in air at varying  $X$  from 7.5% to 40%, as well as the  $E_a$  values for DDGS and willow chars combustion in 7.5, 10 and 15 vol.%  $O_2$  concentration. The results shown in **Figure 8- 7** indicate that the  $E_a$  values for all three chars largely decrease with increasing  $X$  from 7.5% to 40%. The dependence of the  $E_a$  values on  $X$  is probably due to the change in the combustion control mechanism (Liu, 2009), while the lower  $E_a$  values at higher  $X$  may be attributed to the catalytic effects of the minerals in the ashes of chars and the structural ordering change in the chars (HaykIrI-A ma et al., 2001; Lu et al., 2002). According to HaykIrI-A ma et al. (HaykIrI-A ma et al., 2001), the mineral species showed an important effect on the combustion reactivity of the char samples, and it seemed that the higher the total mineral matter content ( $< 20\%$ ) was, the lower the  $E_a$  value could be. Furthermore, the  $E_a$  values for willow and DDGS chars seemed also to be affected by the  $O_2$  concentration to some extent, since the  $O_2$  concentration could affect the char conversion (Hu et al., 2001).

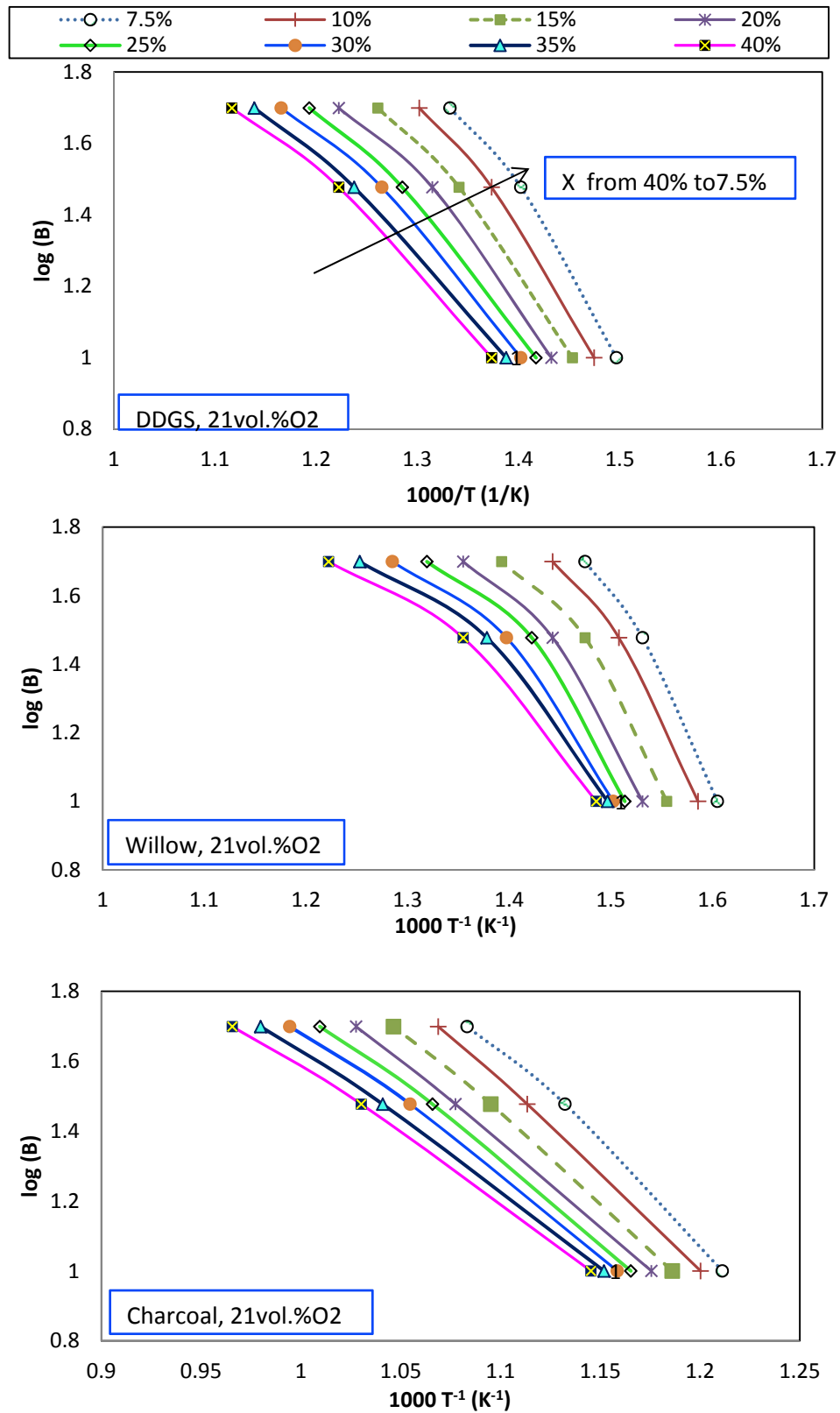


Figure 8- 6 FWO method plots for DDGS, willow char and charcoal at varying conversion

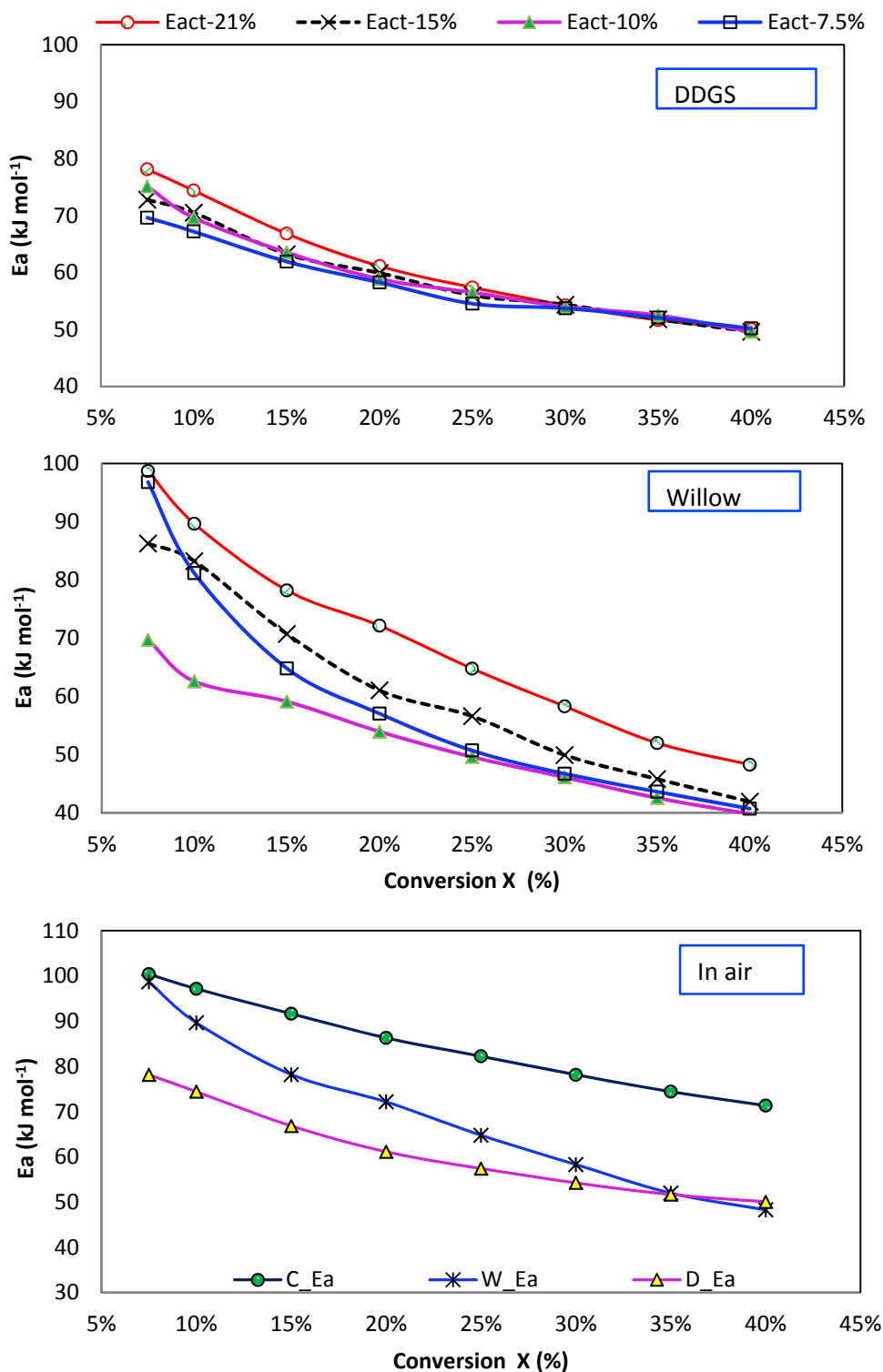


Figure 8- 7  $E_a$  values for DDGS and willow char and carbon at varying conversion and  $O_2$  concentration

### 8.3.4 The recalculated TG curves

Since not all determined kinetic parameters for three chars could represent their true combustion intrinsic kinetics, here only two experimental cases were chosen for the further analysis: DDGS char combustion in air at a temperature of 500 °C and charcoal combustion at a temperature of 850 °C

using 15vol.%O<sub>2</sub>. Although the F0, VRM and SCM three different conversion models were applied to determine for kinetic parameters these two cases, the best TG fittings results for DDGS char and charcoal were predicted by using the VRM and SCM model, respectively. Their predicted and experimental TG curves are presented in **Figure 8- 8**.

The results shown in **Figure 8- 8** indicate that the predicted results for DDGS char using the VRM model and for charcoal using the SCM model agree fairly well their experimental results. These results appeared to be reasonable according to the results reported in the literature (Sorensen et al., 1996a; Sorensen et al., 1996b). In general, the SCM model appeared to more suitable tool when reaction occurred within pore diffusion internal diffusion controlling regime or external diffusion controlling regime (Czakiert & Nowak, 2009; Hu et al., 2001). In the previous chapter, it was also observed during willow and DDGS char gasification that the SCM model was more suitable than the VRM model at higher reaction temperatures (Meng et al., 2011b; Meng et al., 2011c).

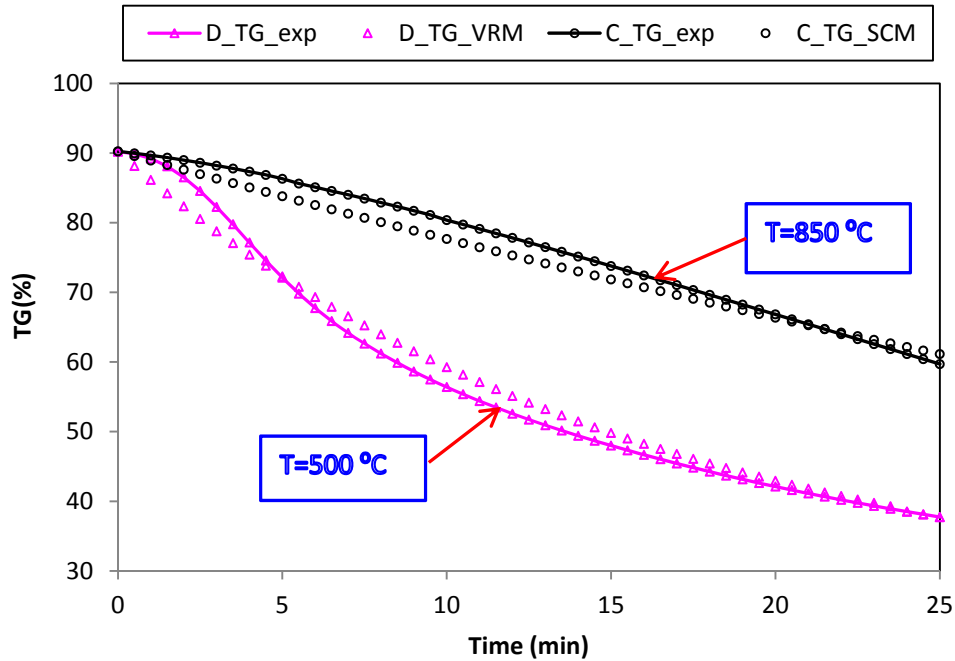


Figure 8- 8 Comparison of experimental and calculated TG curves for DDGS and charcoal

## 8.4 Comsol Multiphysics™ modeling results

In order to better understand the heat transfer and fluid flow within the TG furnace, a 3D TG furnace model was built using the COMSOL Multiphysics™ software version 4.1. Similarly, DDGS char combustion in air at a temperature of 500 °C and charcoal combustion in 15vol.%O<sub>2</sub> at a temperature of 850 °C were simulated, and their derived kinetic parameters (see in **Table 8- 2**) were applied in the sub-model “Reaction model” (**Eq.8- 5** see in **Table 8- 2**) of the 3D TG furnace model.

### 8.4.1 Velocity and temperature distribution without reaction

Temperature and velocity, which are two important parameters related to heat transfer and fluid flow within the TG furnace, both could affect the char combustion conversion reaction. Unfortunately, their profiles within the TG furnace cannot be quantitatively measured due to the limited measuring points assembled in the TG device. **Figure 8- 9** presents an overall temperature and velocity 3D distribution within the TG furnace, where the temperature of the heated wall was set at 500 °C.

The results presented in **Figure 8- 9** indicate that the lowest and highest temperature is observed at the inlet (20 °C) and the heated wall part of the furnace (500 °C), respectively. This observation is fairly reasonable since the gas entered the furnace at atmospheric temperature and was heated up by the heated wall which is the main heat source for the furnace. Downstream the temperature gradually

decreased till round 300 °C which was observed at the outlet of the TG furnace. Obviously, this outlet temperature is higher than the manually measured value from a thermometer which is put at the outlet of the furnace. This could be attributed to the influences of the natural and forced convection at the outlet. The velocity magnitude profile presented in **Figure 8- 9** indicates that the velocity in the middle of the furnace is much higher than near the wall. However, **Figure 8- 9** shows that a clear velocity and temperature profiles near the carbon sample cannot be observed. Thus, another two figures were made in order to investigate effects of between different inlet flow rates and furnace temperatures.

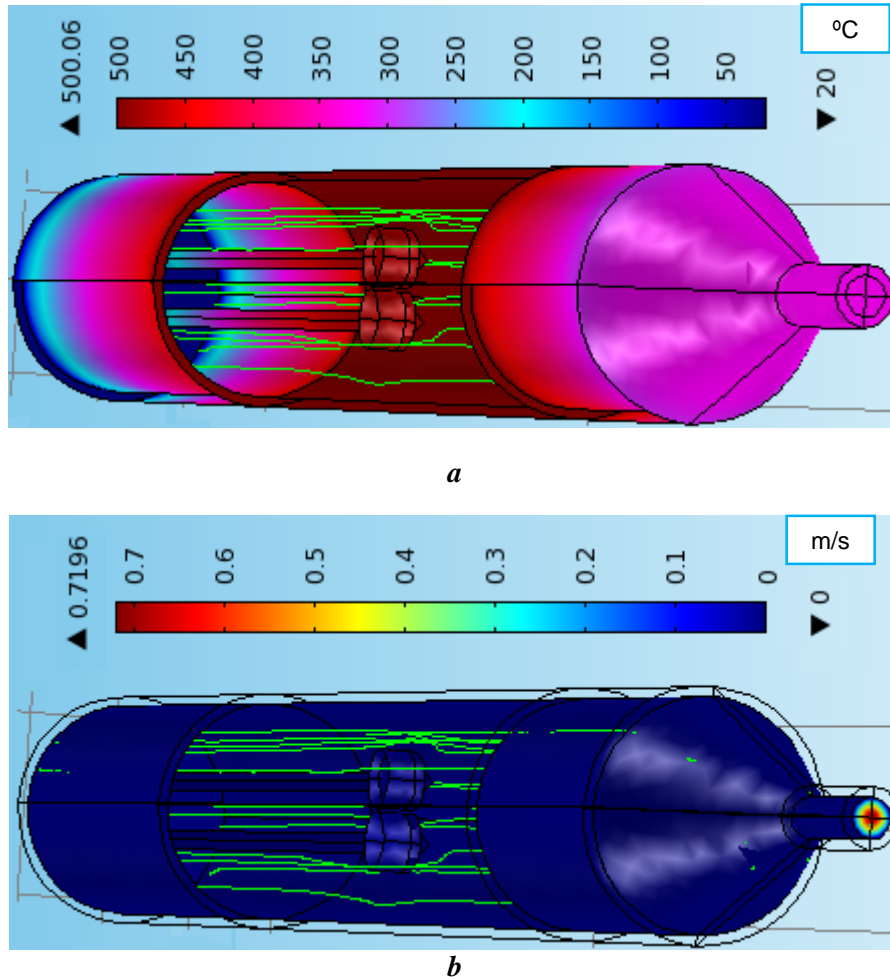


**Figure 8- 9** Temperature (a) and velocity (b) distribution within TG furnace  
(Remark: Green line is velocity streamline)

**Figure 8- 10** presents the temperature distribution nearby the carbon sample at different inlet flow rates (80, 120 and 160mL/min). It can be seen that when the temperature of the furnace was set to 800 °C, the temperature near the carbon sample slightly decreased when the inlet flow rate was increased from 80 to 160mL/min; however, the temperature difference among them was within  $\pm 2$  °C. It seems that the predicted temperature profile change was slightly higher than the obtained experimental value, which was within  $\pm 1$  °C, but do show the similar changing trend. Moreover, the temperature profile presented in **Figure 8- 10** also indicates that the actual temperature nearby the carbon sample is around 15 to 20 °C lower than the set heated wall temperature, depending on the inlet flow rate. This is normal since the middle heated wall is the heat source of the TG furnace and other parts are mainly heated up due to effects of radiation and convection (Comsol, 2010; Goyal et al., 2010).

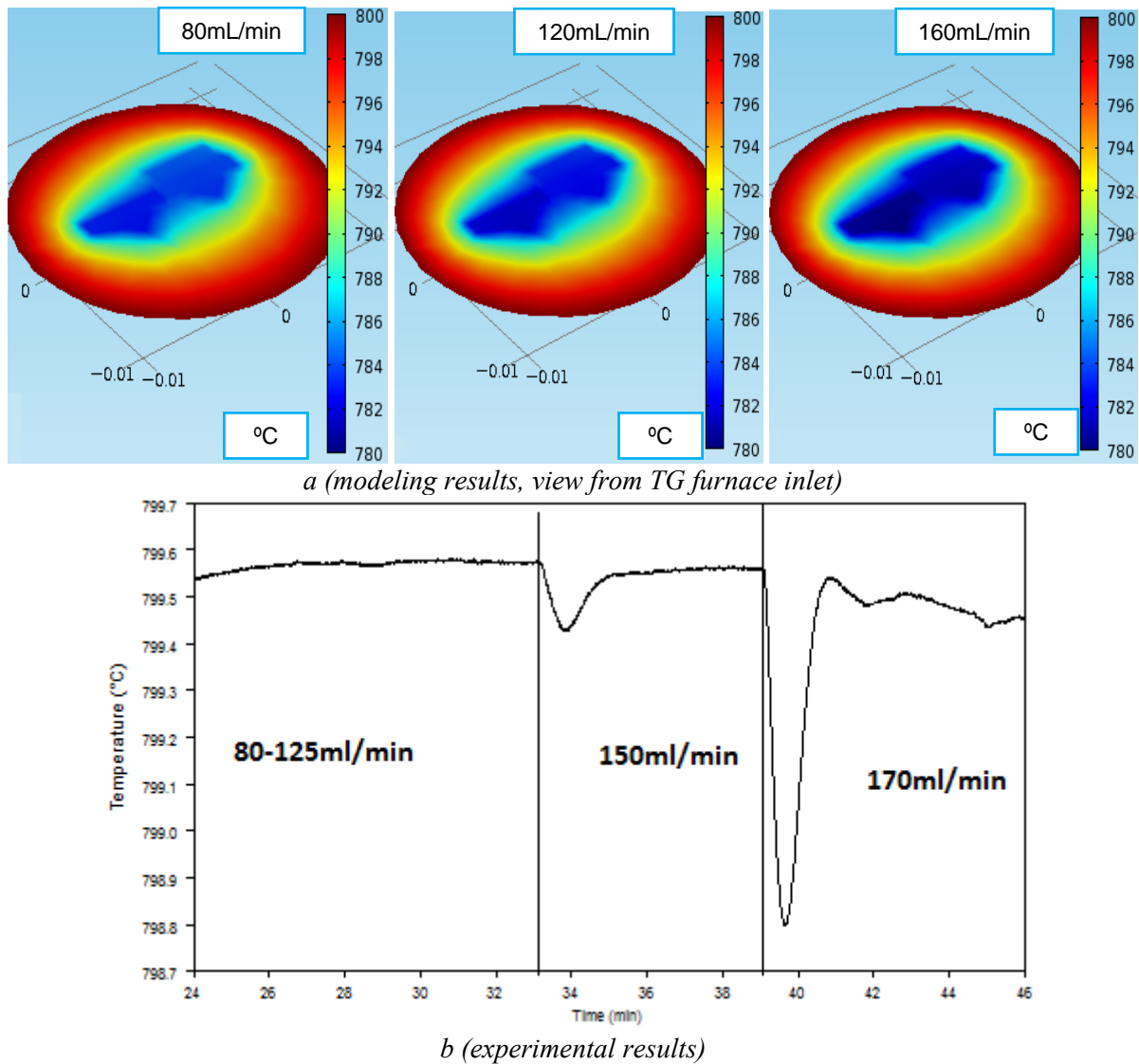


Figure 8- 10 Effects of different flow rates on temperature distribution within TG furnace

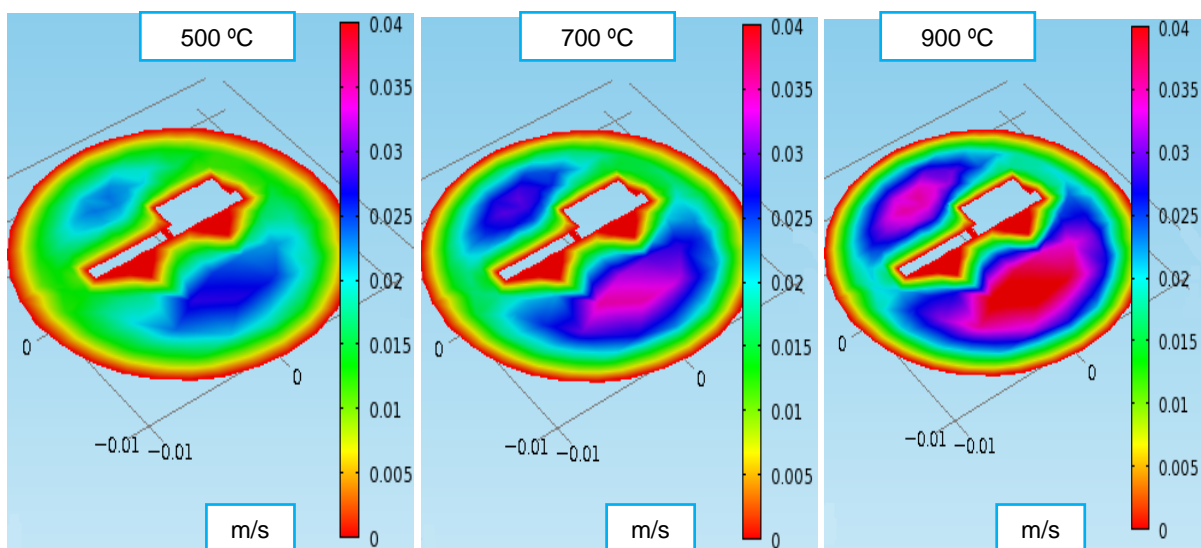


Figure 8- 11 Effects of different temperatures on velocity profile within TG furnace (view from TG furnace inlet)

**Figure 8- 11** presents the velocity magnitude distribution nearby the carbon sample at different temperatures (500, 700 and 900 °C). In general, the velocity magnitude within the TG furnace at different temperatures is fairly similar. When the inlet flow rate was set to 140mL/min, the velocity magnitude increased with increasing the temperature from 500 to 900 °C. The variation in the velocity could be attributed to the change of gas density with temperature (Smith et al., 2001). Furthermore, it can also be seen in **Figure 8- 11** that the velocity along the furnace wall, carbon sample and beams all are around 0, while the maximum value of the velocity is obtained in other “none occupied” zones. These results are reasonable, since the carbon sample and beams were assumed as solid body, thus, the velocity around them was reduced (Petrone et al.; Smirnova & Fend, 2010).

#### **8.4.2 Velocity and temperature distribution with reaction**

Char combustion reaction is highly exothermic (Anthony et al., 1999; Tsai & Scaroni, 1987), and the heat released from the reaction could affect the temperature distribution within the TG furnace, in particular nearby the carbon sample where the reaction occurs. Therefore, the combustion behavior of DDGS char in air at a temperature of 500 °C and pure charcoal in 15vol.% O<sub>2</sub> at a temperature of 850 °C were simulated. **Figure 8- 12** shows the temperature distribution with and without considering char combustion reaction within TGA furnace.

The results shown in **Figure 8- 12** clearly indicate that char combustion does affect the temperature profile within the TG furnace. For example, without considering DDGS char combustion reaction, the predicted temperature near the carbon sample was around 480 °C, associated with a setting temperature of the heated wall of 500 °C. However, when the combustion reaction was taken into consideration, the predicted temperature near the carbon sample was increased to around 494 °C. Meanwhile, the temperature distribution profile within the TG furnace was also simultaneously changed. The maximum temperature of around 505 °C was observed at the “none occupied” zones which are nearby the carbon sample instead of at the heated wall. These observations show a good agreement with the experimental ones. As can be well seen in **Figure 8- 12** (b experimental results), during DDGS char combustion, an increase in the temperature of approximately 12 °C near the sample was also observed, which is really close to the predicted value (14 °C).

Compared to DDGS char combustion, the heat released from pure charcoal combustion obviously has less effect on the temperature distribution within the TG furnace. Similarly, because of the heat produced from the charcoal combustion, a slight increase of approximately 4 °C was observed in the temperature near the carbon sample. This predicted value also agreed well with the experimental value (2 °C see in **Figure 8- 12** (b experimental results)). However, unlike DDGS char combustion, the heat released from the charcoal combustion was not high enough to change the temperature distribution profile within the TG furnace. This is probably due to the difference between their combustion rates. The combustion rate of DDGS char is generally higher than that of pure charcoal. Thus, although the pure charcoal was combusted at a higher temperature, the heat released from its reaction was still much lower than that produced from DDGS char combustion.



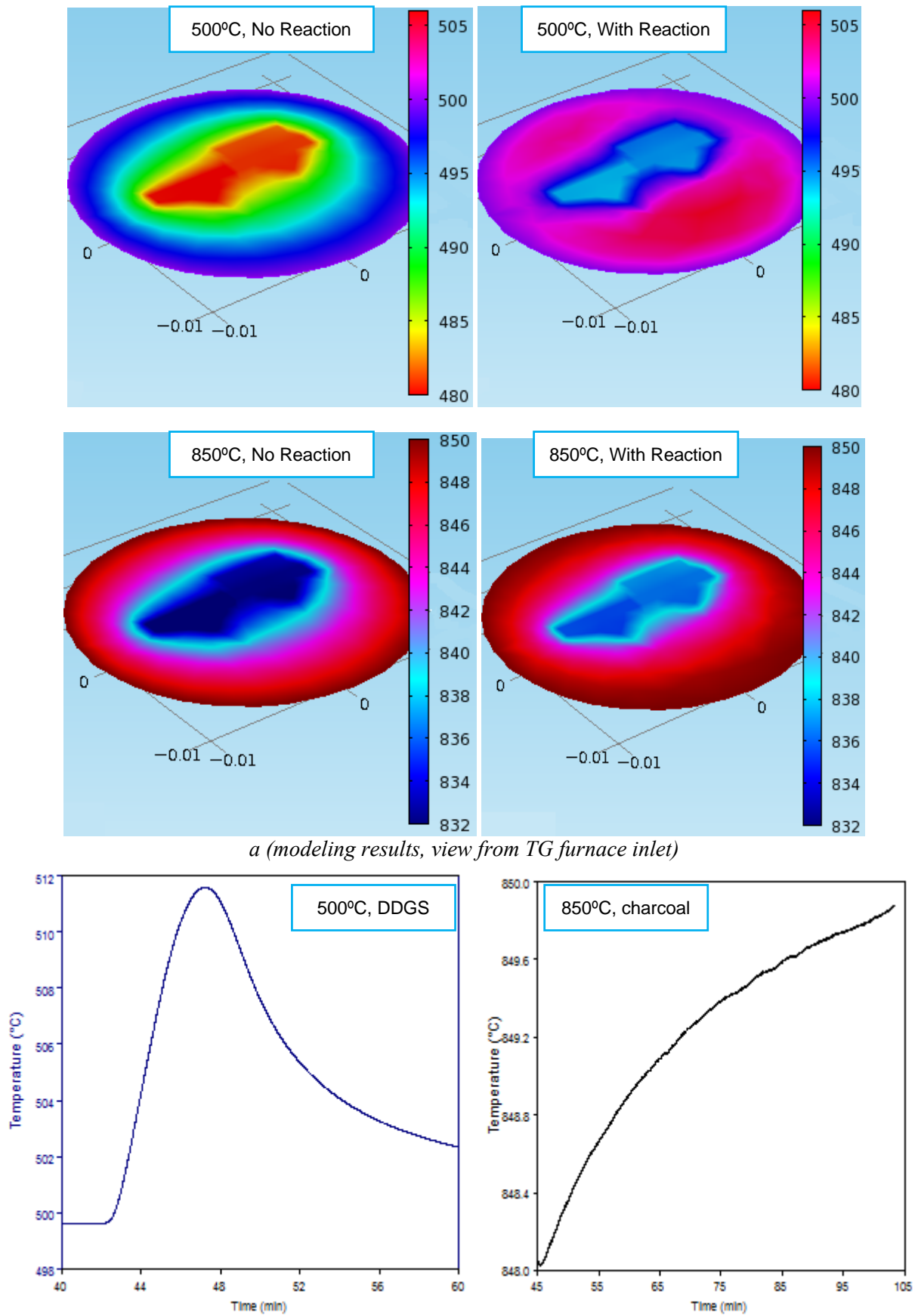


Figure 8- 12 Comparison temperature distribution with and without reaction within TG furnace

Meanwhile, the heat released from the char combustion reaction also slightly increased the velocity within the TG furnace. Similarly, the velocity during DDGS char combustion changed a bit more than that during pure charcoal combustion; however, the overall velocity distribution profile within the TG furnace remained practically the same. Furthermore, the O<sub>2</sub> concentration distribution along the TG furnace tube was also investigated. The predicted results show that there is almost no difference ( $<0.005\text{mol/m}^3$ ) between the bulk O<sub>2</sub> concentration and the O<sub>2</sub> concentration near the surface of carbon sample where the reaction takes place (see in **Figure A-12**, Appendix). The predicted results also confirmed that the external mass transfer had a negligible effect on DDGS char and charcoal combustion under these two experimental conditions (Fogler, 1999).

## 8.5 Conclusion

The combustion behavior of DDGS and willow chars, which were obtained from DDGS and willow gasification using the 100kW<sub>th</sub> steam-O<sub>2</sub> blown CFB gasifier, and pure charcoal was studied using TGA under both isothermal and non-isothermal conditions. Different reaction conversion models were applied to interpret the experimental data in order to obtain kinetic parameters for char combustion. Furthermore, a 3D TG furnace model was built using the COMSOL Multiphysics<sup>TM</sup> software version 4.1 in order to better understand temperature and velocity profiles within the TG furnace with and without considering char combustion reaction.

The results obtained from isothermal combustion experiments showed that the char combustion rate increased with increasing either O<sub>2</sub> concentrations or combustion temperatures. Within the temperature range of 750-900°C, it was impossible to properly determine kinetic parameters for combustion experiments of using DDGS and willow chars, but this was well possible for charcoal under 15% O<sub>2</sub> (Ea was around 120 kJ/mol using the SCM model). Within the temperature range of 400-500 °C, a fairly low Ea value of approximately 15 kJ/mol was obtained for willow char, which indicated that this char is too reactive to determine its combustion kinetic parameters properly. The Ea value obtained from DDGS char within the similar temperature range was around 60 kJ/mol using the VRM model. The results obtained from non-isothermal combustion experiments showed that the combustion temperature ranges of three chars increased with increasing the heating rate. Higher Ea values were obtained at lower conversion values.

The results predicted from the 3D TG furnace COMSOL Multiphysics<sup>TM</sup> model showed that the velocity profile within the TG furnace was affected by the furnace temperature and vice versa. Moreover, the heat produced from char combustion could also affect both temperature and velocity profiles within the furnace to certain extent. In general, a fairly good agreement was observed between the predicted and experimental results. It indicates that this 3D TG furnace COMSOL Multiphysics<sup>TM</sup> model is a useful tool for gaining a better insight into temperature and velocity profiles in the furnace which provide important information for reaction extent control and the furnace design.

## **9 Modeling biomass gasification in the 100kW<sub>th</sub> CFB gasifier using different models**

---

*This chapter describes the modeling of Agrol, willow and DDGS gasification on the 100kW<sub>th</sub> steam-O<sub>2</sub> blown CFB gasifier with an emphasis on the product gas distribution and equilibrium analysis of water-gas shift (WGS) reaction and methane steam reforming (MSR) reaction. Three different types of models: an equilibrium model (EM) and a kinetic model (KM) setup using Aspen plus<sup>TM</sup> software, and a fluidization model (FM) written in C Language and compiled using Bloodshed Dev-C++ software have been developed. The modeling results achieved from different models are compared and validated with the experimental data.*

As mentioned in the literature overview study in chapter 2, a good simulation model can provide plenty of valuable information about the product gas composition. And process optimization can be realized with its help as well as unit scale up. Several reviews of the current knowledge on FB models have been published recently (Basu & Kaushal, 2009; Gómez-Barea & Leckner, 2010; Puig-Arnau et al., 2010). In general, the existing FB models can be divided into three groups: Computational fluid-dynamic models (CFDM), Fluidization models (FM) and Black-box models (BBM) (Gómez-Barea & Leckner, 2010), and among them the FM and BBM models are frequently used. According to (Gómez-Barea & Leckner, 2010), the FM models avoid the details of complex gas-solid dynamic, and assume a multiphase pattern (i.e., two or three phases or regions) in the bed to maintain the fluid-dynamic effects. The flow pattern of the regions is described by semi-empirical correlations. Furthermore, chemical kinetics for gas and solid reactions are usually applied in the FM models as well. The BBM models deal with less or no reaction kinetics involved in the particle conversion process by the means of two approaches: using equilibrium models (EM) or modified equilibrium models (Pseudo-equilibrium models, pseudo-EM).

Although there are many models which have been developed by different researchers, how to define and setup a model probably largely depends on the research objectives and the available experimental information. From the literature review, most published biomass gasification models from the simplest to the most advanced formulation generally agreed reasonably well with the selected experiments. However, the predicted results from different models may be fairly different, and a comparison among them is necessary to see their validity beyond the experimental envelope with which it was derived. In this study, three different models have been set up based on the configuration of the CFB gasifier. The modeling results achieved from different models were compared and validated with the experimental data. Since the distribution of sulfur during biomass gasification under different operational conditions has been predicted in chapter 4, and the main product gas composition is important for its final applications, the main target of these three models is to predict the main product gas composition produced from different fuels at different operational conditions.

## 9.1 Model development

In order to simulate the 100 kW<sub>th</sub> steam-O<sub>2</sub> blown CFB gasifier performance under various operational conditions, three different types of models were developed. The following assumptions are considered in all models:

- The gasifier ran under isothermal conditions and is at steady state.
- The drying and devolatilization takes place instantaneously.
- Fragmentation and attrition of particles does not occur during gasification.
- Char only consists of carbon.
- Particle size distribution is not considered.
- Particle is treated as sphere.

### 9.1.1 Equilibrium model (EM) in Aspen Plus

As mentioned in chapter 2, two approaches are usually applied in equilibrium models: stoichiometric and non-stoichiometric, of which the former requires a defined reaction mechanism and employs equilibrium constants of all constituent reactions, while the latter does not require a specified reaction mechanism and minimizes the Gibbs free energy subject to mass balance and non-negativity constraints of the number of moles of species. Equilibrium models are kinetics free and have been widely used by many researchers for the analysis of the gasification process. Although some thermodynamic equilibrium models have been developed in order to predict the gasifier performance, the calculation to achieve the product gas equilibrium compositions is generally complicated, since mass and energy balances as well as many chemical equations need to be solved simultaneously (Gautam et al., 2010; Jarungthammachote & Dutta, 2007; Li et al., 2001; Zainal et al., 2001). For instance, Jarungthammachote and Dutta (Jarungthammachote & Dutta, 2007) used an equilibrium model to predict the composition of product gas in a down draft waste gasifier. To determine five unknown species (CO, CO<sub>2</sub>, H<sub>2</sub>, CH<sub>4</sub>, and H<sub>2</sub>O) of the product gas, five equations were applied and

generated using mass balance (element balance C, O, H) and equilibrium constant relationships (water-gas shift reaction and methane reaction). To determine equilibrium constants for the reactions, the standard Gibbs free energy of each chemical species at specific temperatures is needed which can be calculated from the values of the standard enthalpy of formation and the standard entropy of formation at the required temperature. Thus, for performing the equilibrium modeling, various thermodynamic properties of different gases are required. Since the Aspen Plus<sup>TM</sup> software contains a large thermal and physical property database and built-in convergence algorithms, in this work, an EM model has been set up by using Aspen Plus<sup>TM</sup> Software in order to simplify the calculation procedure. The CFB gasifier Aspen Plus<sup>TM</sup> EM model flowsheet is presented in **Figure 9- 1** and a brief description of operation block units is summarized in **Table 9- 1**.

In **Table 9- 1**, the Aspen Plus<sup>TM</sup> yield reactor, RYIELD, is applied to simulate biomass decomposition (Block “DEVOLI”), where biomass is converted into its constituting components including C, H, O, S, N, and ash by specifying the yield distribution using a calculator block based on the ultimate analysis. The Aspen Plus<sup>TM</sup> separator, SEP, is applied to simulate carbon conversion (Block “CSEP”), since carbon conversion reported for CFB gasifiers in the literature ranged from 90 to 99% (Doherty et al., 2009). Moreover, there is always a small amount of carbon found together with bed material during cleanup after gasification. Thus, considering carbon conversion obtained from experiments, in the simulation, 10% carbon is separated out as remaining un-reacted and continually circulated through the cyclone. The Aspen Plus<sup>TM</sup> heater, HEATER, is applied to simulate the lab unit steam preheater (Block “PREHEAT”) which is used to preheat steam from 160 to 360 °C. The Aspen Plus<sup>TM</sup> Gibbs reactor, RGIBBS, is used to simulate the CFB gasifier (Block “CFBG”). During gasification, some amounts of N<sub>2</sub> are used to purge dp-cells, feedstock bunkers and ensure the circulation. The preheated steam, O<sub>2</sub> and N<sub>2</sub> are mixed in Block “MIXTURE” and then fed together with the yield volatiles into “CFBG”, where all homogeneous and heterogeneous reactions occur to produce the product gas. CH<sub>4</sub> is the only hydrocarbon taken into consideration in the calculation. After ash is separated from the gas stream (Block “ASHSEP”), the product gas together with un-reacted carbon (Block “CGASMIX”) were fed into the “CYCLONE”, where “SOLID” is separated from the product gas stream. This separated solid is split via “SSPLIT” into two streams which represent the recycled solid and loss carbon, respectively. The ash and loss carbon together represents the total ash out of the system, while the stream “PRODGAS” represents the final product gas obtained from biomass gasification.

As reported by Doherty et al. (Doherty et al., 2009), due to neglect of the enthalpies from chemical bonds of the individual constituents, some enthalpy loss occurs during the transformation from biomass to its constituting components, a heat stream “QHEAT” between Block “DEVOLI” and Block “CFBG” is therefore inserted to simulate the enthalpy difference. With considering “QHEAT” this model is called “heat limited” EM model since the product gas composition is predicted under restricted chemical equilibrium condition by an approach specifying heat duty and temperature. As a comparison, a pure EM model without considering enthalpy difference (No “QHEAT”) is also used to calculate the product gas composition under phase and chemical equilibrium conditions.

### **9.1.2 Kinetic model (KM) in Aspen Plus<sup>TM</sup>**

Although the thermodynamic equilibrium model is relatively simple and can predict the product gas composition produced from different biomass fuels gasification under various operational conditions with reasonable accuracy, equilibrium conditions are difficult to achieve in practical operating conditions. Thus, another type of model, the kinetic model (KM), has been setup by applying kinetics for different reactions which occur during biomass gasification. The 100kW<sub>th</sub> steam-O<sub>2</sub> blown CFB biomass gasifier Aspen Plus<sup>TM</sup> KM model flowsheet is presented in **Figure 9- 2** and the description of the operation block units is available in **Table 9- 1**. Some additional assumptions are considered in this KM model:

- The riser of the gasifier is divided into three regions: bed, upper and exit zone.
- The voidage in the bed zone remains constant and varies with the height of the upper zone.
- Char gasification and combustion reactions occur in the bed zone.

- Homogeneous reactions occur in the upper and the exit zone.

Blocks such as “DEVOLI”, “PREHEAT”, “MIXTURE”, “CYCLONE”, “SSPLIT”, “ASHCM” and “ASHSEP” are similar to those used in the EM model. The Aspen Plus stoichiometric reactor, RSTOIC, is used to simulate the formations of  $\text{H}_2\text{S}$ ,  $\text{HCl}$ ,  $\text{CH}_4$ ,  $\text{C}_2\text{H}_4$  and  $\text{C}_6\text{H}_6$  (Block “RSTOIC”). S and Cl in the fuel are assumed to form only  $\text{H}_2\text{S}$  and  $\text{HCl}$ , respectively. Since tar reaction kinetics is not the main focus during the modeling,  $\text{C}_6\text{H}_6$  is assumed to be the only tar component, and according to Petersen and Werther (Petersen & Werther, 2005a), the amount of  $\text{C}_6\text{H}_6$  formed is assumed to be equal to a 0.6% fractional conversion of carbon. The amount of  $\text{CH}_4$  and  $\text{C}_2\text{H}_4$  formed are calculated partly based on experimental results and modified empirical formula from Hannula and Kurkela (Hannula & Kurkela, 2010), and they are equal to fractional conversion of carbon of 8% and 4.5%, respectively. The Aspen Plus<sup>TM</sup> continuous stirred-tank reactor, RCSTR, is used to simulate char combustion and gasification reactions occurring in bed zone of the CFB gasifier (Block “BENZON”) using reaction kinetics from literature and self-derived TG kinetics, respectively. Homogeneous reactions which followed different reaction kinetics are assumed to occur in the upper zone (Block “UPZONE”) and the exit zone (Block “EXITZONE”) of the CFB gasifier. This KM model is capable of predicting the product gas composition and the carbon conversion under various operational conditions including bed height, ER, SBR and reaction temperature.

All homogeneous and heterogeneous reactions and their reaction rates considered in the KM models and their reaction rates are listed in **Table 9- 2** and **Table 9- 3**, respectively. In the KM model, two types of reaction kinetics are applied, of which one is adapted from Petersen and Werther (Petersen & Werther, 2005a) (called KM-SW) and the other is based on the kinetics obtained from TG tests (called KM-TG) (see **Table 7- 4** in chapter 7 and **Table 8- 3** in chapter 8), respectively.

Among all homogeneous and heterogeneous reactions listed in **Table 9- 2**, the char combustion reaction (R1), the reaction rate for DDGS char combustion applied for KM-TG model was determined from TGA experiments, while for Agrol and willow, a fitting factor of 1.5 and 3.0, respectively, is applied based on their different char reactivities. The splitting factor ( $\alpha$ ) for the reaction (R1) applied for KM-SW model is calculated via the equation in **Table 9- 3**, and it varies from 1.0 to 2.0. Concerning water gas reaction (R4), the splitting factor (1.2) was adopted from Matsui et al. (Matsui et al., 1985) since this value was also used by Petersen and Werther for their simulation (Petersen & Werther, 2005a). **Table 9- 4** summarizes the main input parameters used for Aspen Plus<sup>TM</sup> the EM and KM models.

Table 9- 1 Description of Aspen Plus blocks used in both EM and KM simulation

Reactor block	Block ID	Description
RYIELD	DEVOLI	<ul style="list-style-type: none"> <li>Yield reactor→ models a reactor by specifying the yield of each component. This model is useful when reaction stoichiometry and kinetics are unknown and the yield distribution data or correlations are available.</li> <li>Here, it is used to convert the non-conventional stream 'BIOMASS' into the elements C, H, O, N, S and ash.</li> </ul>
SEP	CSEP	<ul style="list-style-type: none"> <li>Separator – simulates carbon conversion by separating out a specified amount of the carbon.</li> </ul>
SEP	ASHSEP	<ul style="list-style-type: none"> <li>Separator – simulates the ash separation from the product gas.</li> </ul>
SEP	CYCLONE	<ul style="list-style-type: none"> <li>Separator – simulates the CFB cyclone by separating solid from the product gas</li> </ul>
RGIBBS	CFBG	<ul style="list-style-type: none"> <li>Gibbs free energy reactor→ models single-phase chemical equilibrium or simultaneous phase and chemical equilibrium based on Gibbs free energy minimization. This model is useful when temperature and pressure are known while reaction stoichiometry is unknown.</li> <li>Here, it is used to simulate drying, pyrolysis, partial oxidation and gasification in the EM model.</li> </ul>
HEATER	PREHEAT	<ul style="list-style-type: none"> <li>Heater – preheats steam from ca. 160 to ca. 360 °C.</li> </ul>
MIXER	MIXTURE	<ul style="list-style-type: none"> <li>Mixer – mixes the preheated steam, oxygen and purging nitrogen</li> </ul>
MIXER	CGASMIX	<ul style="list-style-type: none"> <li>Mixer – mixes the un-reacted carbon separated in block 'CSEP' with the product gas</li> </ul>
MIXER	ASHCM	<ul style="list-style-type: none"> <li>Mixer – mixes the carbon lost with the ash before leaving the system</li> </ul>
SSPLIT	SSPLIT	<ul style="list-style-type: none"> <li>Splitter – extracts a portion of the carbon to simulate carbon loss in the ash, with the rest recycled</li> </ul>
RSTOIC	RSTOIC	<ul style="list-style-type: none"> <li>Stoichiometric reactor → models a reactor with specified reaction extent or conversion. This model is useful when reaction kinetics is unknown or unimportant but reaction stoichiometry and extent of reaction are known.</li> <li>Here, it is used to model the formations of H<sub>2</sub>S, HCl, CH<sub>4</sub>, C<sub>2</sub>H<sub>4</sub> and C<sub>6</sub>H<sub>6</sub> species.</li> </ul>
RCSTR	BEDZON	<ul style="list-style-type: none"> <li>Continuous stirred-tank reactor → models a reactor with different phase. This model can handle kinetic and equilibrium reactions as well as reactions involving solids. The reaction kinetics can be supplied through the built-in reactions models or a user-defined FORTRAN subroutine.</li> <li>Here, it is used to model char combustion and gasification reactions occurring in bed zone.</li> </ul>
RCSTR	EXITZONE	<ul style="list-style-type: none"> <li>Continuous stirred-tank reactor → here, it is used to model gas reactions at the exit zone.</li> </ul>
RPLUG	UPZONE	<ul style="list-style-type: none"> <li>Plug flow reactor →models a reactor with one-, two-, or three-phases or with coolant streams. This model can handle kinetic reactions including reactions involving solids and reaction kinetics.</li> <li>Here, it is used to model homogenous reactions occurring in the upper zone.</li> </ul>

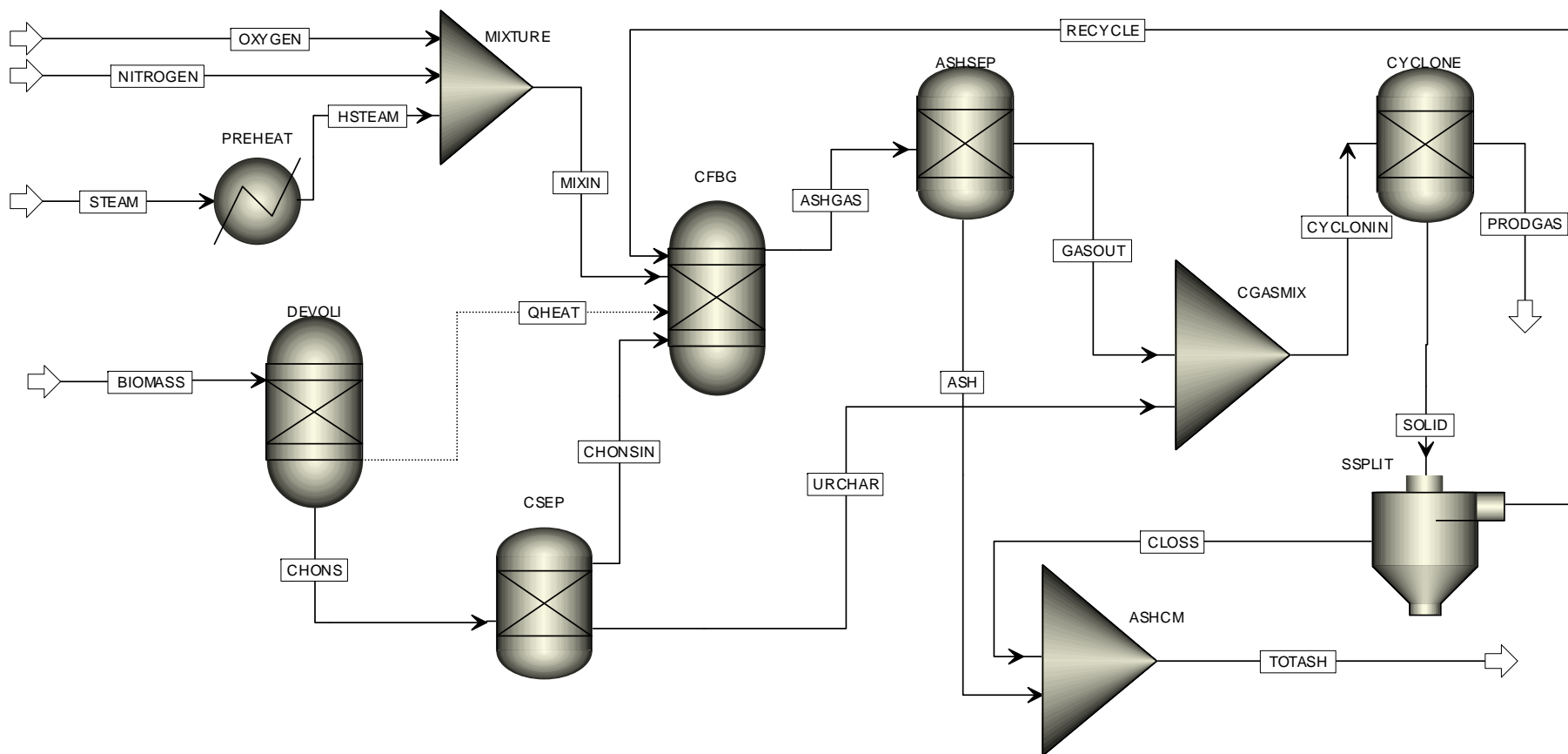


Figure 9- 1 The 100kW<sub>th</sub> steam-O<sub>2</sub> blown CFB biomass gasifier Aspen Plus™ EM model flow sheet



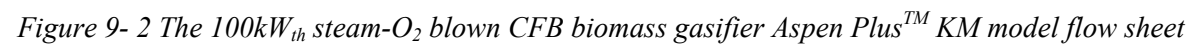


Table 9- 2 Lists of Heterogeneous and homogeneous reactions considered in FM and KM

NO	Reaction name	Reaction expression	Reaction types	FM	KM-SW	KM-TG
R0	Devolatilization	$biomass \rightarrow volatile (VM) + char + \nu_{0,9}C_6H_6 + \nu_{0,5}H_2O_{(g)}$ $VM \rightarrow \nu_{0,1}CO + \nu_{0,2}CO_2 + \nu_{0,3}H_2 + \nu_{0,4}CH_4 + \nu_{0,7}N_2 + \nu_{0,8}C_2H_4$	Instantaneous	√	√	√
R1	Char oxidation	$\alpha C + O_2 \rightarrow 2(\alpha - 1)CO + (2 - \alpha)CO_2$	Kinetic	√	√	√
R2	Boudouard reaction	$C + CO_2 \rightarrow 2CO$	Kinetic	√	√	√
R3	CH <sub>4</sub> production	$C + 2H_2 \rightarrow CH_4$	Kinetic	√	√	√
R4	Water gas reaction	$C + 1.2H_2O \rightarrow 0.8CO + 0.2CO_2 + 1.2H_2$	Kinetic	√	√	√
R5	CO oxidation	$CO + 0.5O_2 \rightarrow CO_2$	Kinetic	√	√	√
R6	H <sub>2</sub> oxidation	$H_2 + 0.5O_2 \rightarrow H_2O$	Kinetic	√	√	√
R7	CH <sub>4</sub> reforming	$CH_4 + H_2O \leftrightarrow CO + 3H_2$	Kinetic	√	√	√
R8	Water gas shift reaction	$CO + H_2O \leftrightarrow CO_2 + H_2$	Kinetic	√	√	√
R9	H <sub>2</sub> S reaction	$CO + H_2S \leftrightarrow COS + H_2$	Equilibrium	×	√	√
R10	CH <sub>4</sub> oxidation	$CH_4 + 0.5O_2 \rightarrow CO + 2H_2$	Kinetic	√	√	√
R11	C <sub>2</sub> H <sub>4</sub> oxidation	$C_2H_4 + O_2 \rightarrow 2CO + 2H_2$	Kinetic	√	√	√
R12	C <sub>6</sub> H <sub>6</sub> oxidation	$C_6H_6 + 3O_2 \rightarrow 6CO + 3H_2$	Kinetic	√	√	√

Remark: √ considered; × not considered

Table 9- 3 Homogenous and heterogeneous reaction rates considered in the FM and KM models

NO	Kinetic rate (kmol/m <sup>3</sup> .s) (Ea: kJ/mol)		Reference:
	KM-SW	FM and KM-TG	
R1	$r1 = 595.7T \exp\left(-149.44/(R_g T)\right) \times (6/d_p) C_{O_2}$ $\alpha = \frac{1+2f_r}{1+f_r} \text{ with } f_r = 4.72 \times 10^{-3} \exp\left(\frac{37.737}{R_g T}\right)$	$r1 = f_0 \times 1.426 \times 10^5 \exp\left(-59.9/(R_g T)\right) C_{O_2}$ <p>For A, D, and W: <math>f_0 = 1.5, 1.0, 3.0</math>, respectively</p>	(Linjewile & Agarwal, 1995; Petersen & Werther, 2005a)
R2	$r2 = \frac{\frac{\rho_{char} F_C (1-X)}{12} \times 4.89 \times 10^{10} \exp\left(-\frac{268.0}{R_g T}\right) C_{CO_2}}{1 + 66 C_{CO_2} + 120 \exp(25.5/R_g T) C_{CO}}$	$r2 = K_0 \exp\left(-Ea_i/(R_g T)\right) C_{CO_2}$ <p>For A, D, and W:  <math>K_0 = 7678.5, 1200, 218.4</math>,  <math>Ea = 96.51, 75.5, 55.06</math>, respectively</p>	(Matsui et al., 1987a; Matsui et al., 1987b)
R4	$r4 = \frac{\frac{\rho_{char} F_C (1-X)}{12} \times 2.39 \times 10^5 \exp\left(-\frac{129}{R_g T}\right) C_{H_2O}}{1 + 31.6 \exp\left(\frac{30.1}{R_g T}\right) C_{H_2O} + 5.36 \exp\left(\frac{59.8}{R_g T}\right) C_{H_2} + 0.83 \exp\left(\frac{96.1}{R_g T}\right) C_{CO}}$		(Matsui et al., 1985; Petersen & Werther, 2005a)
R5	$r5 = 3.16 \times 10^{12} \exp\left(-180.032/R_g T\right) C_{CO}^{1.0} C_{O_2}^{0.25} C_{H_2O}^{0.5}$		(Jensen et al., 1995; Liu & Gibbs, 2003; Petersen & Werther, 2005a)
R6	$r6 = 1.08 \times 10^{13} \exp\left(-125.525/R_g T\right) C_{O_2}^{1.0} C_{H_2}^{1.0}$		(Gómez-Barea & Leckner, 2010; Kilpinen et al., 1991)
R7	$r7 = 3.015 \times 10^6 \exp\left(-124.71/R_g T\right) C_{H_2O}^{1.0} C_{CH_4}^{1.0}$		(Jones & Lindstedt, 1988; Liu & Gibbs, 2003)
R8	$r8 = 2778 \exp\left(-\frac{12.56}{R_g T}\right) \left[ C_{CO} C_{H_2O} - \frac{C_{CO_2} C_{H_2}}{0.0265 \exp(4.177/T)} \right]$		(Gómez-Barea & Leckner, 2010; Macak & Malecha, 1978)
R10	$r10 = 5.0 \times 10^{13} \exp\left(-202.641/R_g T\right) C_{O_2}^{0.8} C_{CH_4}^{0.7}$		(Gómez-Barea & Leckner, 2010; Petersen & Werther, 2005a)
R11	$r11 = 6.45 \times 10^{15} \exp\left(-209.205/R_g T\right) C_{O_2}^{1.18} C_{C_2H_4}^{0.9}$		(Petersen & Werther, 2005a; Srinivasan et al., 1998)
R12	$r12 = 1.58 \times 10^{15} \exp\left(-202.641/R_g T\right) C_{O_2}^{1.0} C_{C_6H_6}^{1.0}$		(Petersen & Werther, 2005a; Srinivasan et al., 1998)

Remark: references are for R1 and R2 used in the KM-SW model

Table 9- 4 The main input parameters for Aspen Plus the EM and KM models

Items	Agrol	Willow	DDGS	Remarks
Moisture ( a.r. %)	8	8	12	Experimental value
Volatile matter	74.7	69.8	67.2	Experimental value
Fixed carbon	16.0	20.1	15.5	Experimental value
Ash content	0.14	2.52	4.82	Experimental value
C (dry %)	51.0	50.3	48.2	Experimental value
H (dry %)	6.26	6.17	6.54	Experimental value
O (dry %)	38.2	37.4	31.2	Experimental value
N (dry %)	0.15	0.69	5.52	Experimental value
S (dry %)	0.002	0.002	0.76	Experimental value
Cl (dry %)	0.01	0.01	0.21	Experimental value
Steam feed rate (kg/h)	11.4, 13.63, 14.7	10.85,13.15, 14.18	14.57, 16.55	Experimental value
Biomass feed rate (kg/h)	11.76	11.67	15.26	Experimental value
Oxygen feed rate (kg/h)	5.15	5.1	5.5	Experimental value
Nitrogen feed rate (kg/h)	4.51	4.51	4.91	Experimental value
Bed height (m)	0.5	0.5	0.5	Assumed
Reaction kinetics	See in <i>Table 9- 3</i>			See in <i>Table 9- 3</i>
Reactor temperature(°C) and pressure (bar)	810, 1.15	780, 1.12	750, 1.15	Experimental value

### 9.1.3 Fluidization model (FM) in C Language

In the third Fluidization model (FM), the CFB gasifier is divided into two regions a bed dense zone and an upper dilute zone. A schematic chart of this FM model is shown in **Figure 9- 3**. Several steps which occur during biomass gasification such as devolatilization, char combustion and gasification and homogeneous reactions are considered in the FM model. In this developed FM model, in the subprocess, the devolatilization process is assumed to be instantaneous, and the released products such as the volatile, char and tar are calculated partly based on literature data the determined data from three fuel pyrolysis experiments using TGA-FTIR (see **Table A- 7** in Appendix). Char produced during devolatilization reacts further with O<sub>2</sub>, steam, CO<sub>2</sub> and H<sub>2</sub>. Furthermore, some additional assumptions are considered in this FM model:

- No lateral mixing of gas in the bed dense zone.
- Heat transfer, particle size and density change are not considered.
- C<sub>6</sub>H<sub>6</sub> is considered as the only tar component.

All homogeneous and heterogeneous reactions and their reaction rates considered in the FM model and their reaction rates are available in **Table 9- 2** and **Table 9- 3**. Hydrodynamic parameters involved in the FM model are summarized in **Table 9- 5**, while **Table 9- 6** summarizes the main input parameters used for the FM model. The gas density and viscosity are calculated based on the ideal gas law and an average value is applied for all the cases.

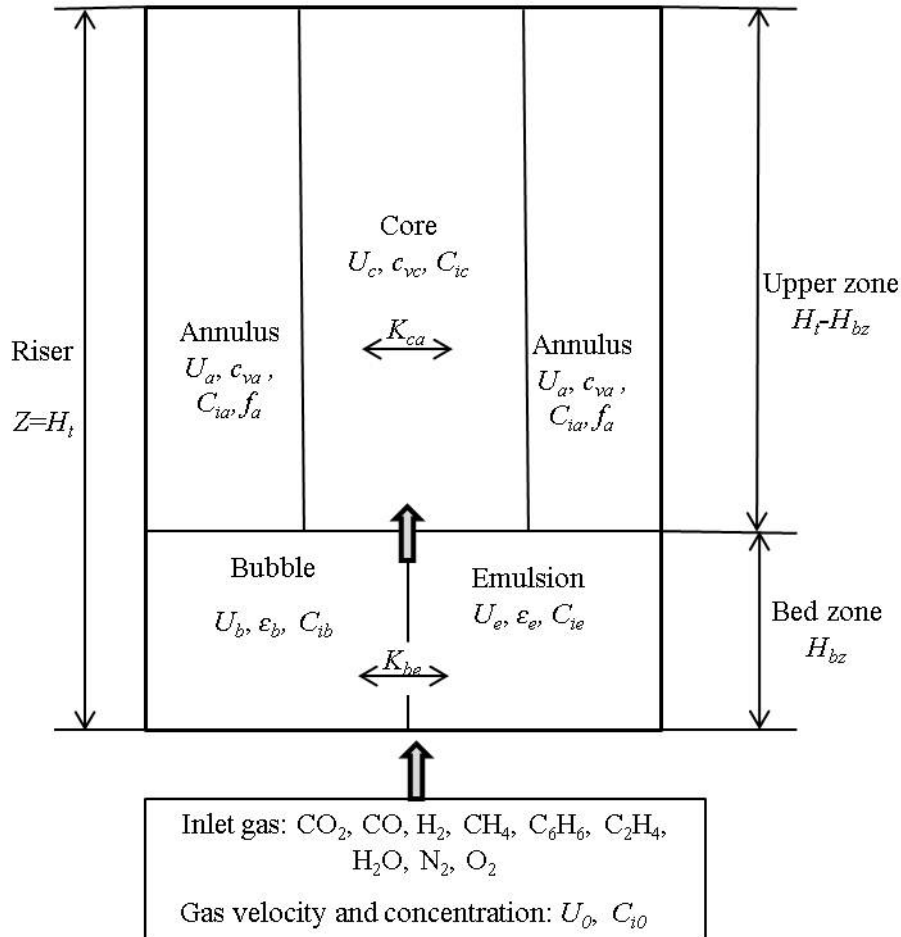


Figure 9- 3 A schematic of the 100kW<sub>th</sub> steam-O<sub>2</sub> blown CFB gasifier riser FM model

Table 9- 5 Hydrodynamic parameters considered in the FM model

Parameters	Correlation	Reference:
Minimum fluidization velocity $U_{mf}$ (m/s)	$150 \frac{(1 - \varepsilon_{mf})}{\phi_s^2 \varepsilon_{mf}^3} \text{Re}_{mf} + 1.75 \frac{1}{\phi_s \varepsilon_{mf}^3} \text{Re}_{mf}^2 = Ar$ $Ar = \frac{\rho_g g d_p^3 (\rho_s - \rho_g)}{\mu_g^2}; \quad \text{Re}_{mf} = \left( \frac{U_{mf} \rho_g d_p}{\mu_g} \right); \quad \frac{(1 - \varepsilon_{mf})}{\phi_s^2 \varepsilon_{mf}^3} \cong 11, \quad \frac{1}{\phi_s \varepsilon_{mf}^3} \cong 14$	(Kunii & Levenspiel, 1991)
Gas velocity in bubble phase ( $U_b$ ), in emulsion phase ( $U_e$ ) and the core ( $U_c$ ), superficial velocity ( $U_0$ ) (m/s)	$U_e = U_{mf} / (1 - \varepsilon_b); \quad U_b = U_0 - U_{mf} + 0.711(gd_b)^{0.5};$ $U_c = (U_b + U_{mf}(1 - \varepsilon_b)) / ((1 - f_a) * (1 - C_{vc}))$	(Kunii & Levenspiel, 1991)
Particle terminal velocity ( $U_t$ )(m/s), dimensionless terminal velocity ( $U_t^*$ )(-), dimensionless particle size ( $d_p^*$ )(-)	$U_t = U_t^* \left[ \frac{\mu_g (\rho_s - \rho_g) g}{\rho_g^2} \right]^{1/3}, \quad U_t^* = \left[ \frac{18}{(d_p^*)^2} + \frac{2.335 - 1.744 \phi_s}{(d_p^*)^{0.5}} \right]^{-1}$ $d_p^* = d_p \left[ \frac{\rho_g (\rho_s - \rho_g) g}{\mu_g^2} \right]^{1/3}$	(Kunii & Levenspiel, 1991)
Solid volume fraction in the core ( $C_{vc}$ ), annulus ( $C_{va}$ ), and exit ( $C_{vez}$ ), Bubble fraction voidage ( $\varepsilon_b$ )(-)	$\overline{C_v} = C_{vez} + (C_{vb} - C_{vez}) \exp(-\alpha(z - H_{bz})) = f_a C_{va} + (1 - f_a) C_{vc}$ $C_{vez} = \frac{K_i^*}{\rho_s (U_0 - U_{t,i})}; \quad \varepsilon_b = (U_0 - U_{mf}) / U_b$	(Kunii & Levenspiel, 1991; Petersen & Werther, 2005a)
Elutriation rate constant ( $K^*$ )(-)	$\frac{K^*}{\rho_g U_0} = 0.0001 + 130 \exp \left[ -10.4 \left( \frac{U_t}{U_0} \right)^{0.5} \left( \frac{U_{mf}}{U_0 - U_{mf}} \right)^{0.25} \right]$	(Gómez-Barea & Leckner, 2010; Kunii & Levenspiel, 1991)
Bubble diameter ( $d_b$ )(m)	$d_b = d_{bm} + (d_{b0} - d_{bm}) \exp(-0.3z/d_t)$ $d_{bm} = 0.65 \left[ \frac{\pi}{4} d_t^2 (U_0 - U_{mf}) \right]^{0.4}; \quad d_{b0} = 0.824 \left[ \frac{\pi}{4} d_t^2 \frac{(U_0 - U_{mf})}{n_{orif}} \right]^{0.4}$	(Horio & Nonaka, 1987; Mori & Wen, 1975; Sadaka et al., 2002)
Mass transfer coefficient between the bubble and emulsion phase ( $K_{be}$ )(-)	Bubble-cloud transfer coefficient: $K_{be} = 4.5 \frac{U_{mf}}{d_b}$	(de Souza-Santos, 2004; Kunii & Levenspiel, 1991; Radmanesh et al., 2006)

Table 9- 6 The main input parameters for the FM model ( A: Agrol, W: willow, D: DDGS)

Items	Symbol	Values			unit	Remarks
CFB riser length	H <sub>t</sub>	5.5			m	Experimental value
CFB riser diameter	d <sub>t</sub>	0.083			m	Experimental value
CFB downcomer diameter	d <sub>d</sub>	0.054			m	Experimental value
Solid particle diameter	d <sub>p</sub>	5.5E-4			m	Experimental value
Gas density	ρ <sub>g</sub>	0.4			kg/m <sup>3</sup>	Calculated
Gas viscosity	μ <sub>g</sub>	5.0E-05			Pa.s	Calculated
Voidage at minimum fluidization stage	ε <sub>mf</sub>	0.45			(-)	(Kunii & Levenspiel, 1991)
Annulus area fraction	f <sub>a</sub>	0.2			(-)	(Löffler et al., 2003)
Gas velocity in the annulus	U <sub>a</sub>	-0.75			m/s	(Petersen & Werther, 2005a)
Voidage in the annulus	C <sub>va</sub>	0.45			(-)	(Löffler et al., 2003)
Bed height	H <sub>bz</sub>	0.5			m	Assumed
Gas initial C <sub>i0</sub> concentrations		A	W	D		See <b>Table A- 7</b> in appendix for details
CO	Ce[i][one]	0.937	0.922	0.800	mol/m <sup>3</sup>	Calculated
CO <sub>2</sub>	Ce[i][two]	1.093	1.076	0.933	mol/m <sup>3</sup>	Calculated
H <sub>2</sub>	Ce[i][three]	2.907	2.879	3.257	mol/m <sup>3</sup>	Calculated
CH <sub>4</sub>	Ce[i][four]	0.444	0.441	0.439	mol/m <sup>3</sup>	Calculated
H <sub>2</sub> O	Ce[i][five]	8.297	8.120	8.730	mol/m <sup>3</sup>	Calculated
O <sub>2</sub>	Ce[i][six]	1.909	1.939	1.672	mol/m <sup>3</sup>	Calculated
N <sub>2</sub>	Ce[i][seven]	1.917	1.991	1.974	mol/m <sup>3</sup>	Calculated
C <sub>2</sub> H <sub>4</sub>	Ce[i][eight]	0.125	0.124	0.123	mol/m <sup>3</sup>	Calculated
Reaction temperature	T	810	780	750	°C	Experimental value
Oxygen feed rate	mO2	5.15	5.10	5.50	kg/h	Experimental value
Steam feed rate	mH2O	11.40	10.85	14.57	kg/h	Experimental value
Nitrogen feed rate	m N2	4.51	4.51	4.91	kg/h	Experimental value
Biomass feed rate	mfuel	11.76	11.67	15.26	kg/h	Experimental value
Density of different fuels	ρ <sub>s</sub>	453	519	521	kg/m <sup>3</sup>	Experimental value
Superficial velocity	U <sub>0</sub>	3.5	3.3	3.2	m/s	Experimental value

The bed dense zone is described using the two-phase model, which consists of a particle-lean bubble phase and a particle-rich emulsion phase (Petersen & Werther, 2005a; Raman et al., 1981; Sadaka et al., 2002). The bubble phase is plug flow without particles while the emulsion phase is completely mixed flow containing gas and particles. Mass transfer occurs between the bubble and emulsion phases. The conservation equations for the gaseous species  $i$  in the bubble and emulsion phases are calculated by using the equations (Eq.9- 1 and Eq.9- 2).

$$U_b \frac{\partial C_{ib}}{\partial Z} = K_{be} (C_{ib} - C_{ie}) + \sum_{g-g} \nu_{ij} R_{ib,g-g} \quad \text{Eq.9- 1}$$

$$U_e \varepsilon_e (1 - \varepsilon_b) \frac{\partial C_{ie}}{\partial Z} = K_{be} \varepsilon_b (C_{ib} - C_{ie}) + (1 - \varepsilon_b) \left[ \varepsilon_e \sum_{g-g} \nu_{ij} R_{ie,g-g} + (1 - \varepsilon_e) \sum_{g-s} \nu_{ij} R_{ie,g-s} \right] \quad \text{Eq.9- 2}$$

Where

- $i$  is the gaseous species  $\text{CO}_2$ ,  $\text{CO}$ ,  $\text{H}_2$ ,  $\text{CH}_4$ ,  $\text{C}_6\text{H}_6$ ,  $\text{C}_2\text{H}_4$ ,  $\text{H}_2\text{O}$ ,  $\text{N}_2$ ,  $\text{O}_2$ .
- $\sum_{g-g} \nu_{ij} R_{ib,g-g}$  and  $\sum_{g-g} \nu_{ij} R_{ie,g-g}$  are the production rate of species  $i$  due to homogeneous reactions occurring in the bubble and emulsion phases, respectively.
- In  $\sum_{g-g} \nu_{ij} R_{ib,g-g}$ ,  $\nu_{ij}$  is the stoichiometric coefficient of gas species  $i$  in reaction  $j$ , while,  $R_{ib,g-g}$  is the reaction rate of gas species  $i$  in reaction  $j$ , similar settings are for  $\sum_{g-g} \nu_{ij} R_{ie,g-g}$  etc.
- $\sum_{g-s} \nu_{ij} R_{ie,g-s}$  is the production rate of species  $i$  due to heterogeneous reactions occurring in the emulsion phase.

The production rates for different gas species are calculated according to their involved reactions and their reaction rates which are presented in **Table 9- 2** and **Table 9- 3**. For example, the production rates of CO in the bubble phase due to gas-gas reactions and in the emulsion phase due to gas-solid reactions are calculated by using the equations **Eq.9- 3** and **Eq.9- 4**, respectively, as follows:

$$R_{\text{CO},g-g} = -r5 + r7 - r8 + r10 + 2r11 + 6r12 \quad \text{Eq.9- 3}$$

$$R_{\text{CO},g-s} = \nu_{0,1} r0 + 2(\alpha - 1)r1 + 2r2 + 0.8r4 \quad \text{Eq.9- 4}$$

Where  $\nu_{0,1}$  is the stoichiometric coefficient of CO during biomass devolatilization (see **Table A- 7** in appendix). The production rate of CO in the emulsion phase due to gas-gas reactions is also calculated by the equation **Eq.9- 3**, since the same reactions are assumed to be occurring in the emulsion phase. For other gas species in emulsion, core and annulus phases, and their production rates are calculated in the same way, and they are available in **Appendix X 1**.

The upper dilute zone is modeled using a core-annulus model (Bi, 2002; Hartge et al., 1999), where the vertical gas convection fluxes of the core phase are directed upward while the annulus phase flow is directed downward. Heterogeneous and homogeneous reactions take place in both zones. Similarly, The conservation equations for the gaseous species  $i$  in the core and annulus phases are calculated by using the equations (Eq.9- 5 and Eq.9- 6).

$$(1 - c_{vc}) U_c \frac{\partial ((1 - f_a) C_{ic})}{\partial Z} = K_{ca} (C_{ia} - C_{ic}) + (1 - f_a) \left[ c_{vc} \sum_{g-s} \nu_{ij} R_{ic,g-s} + (1 - c_{vc}) \sum_{g-g} \nu_{ij} R_{ic,g-g} \right] \quad \text{Eq.9- 5}$$

$$(1 - c_{va}) U_a \frac{\partial (f_a C_{ia})}{\partial Z} = -K_{ca} (C_{ia} - C_{ic}) + f_a \left[ c_{va} \sum_{g-s} \nu_{ij} R_{ia,g-s} + (1 - c_{va}) \sum_{g-g} \nu_{ij} R_{ia,g-g} \right] \quad \text{Eq.9- 6}$$

Where:



- $\sum_{g-g} \nu_{ij} R_{ic,g-g}$  and  $\sum_{g-g} \nu_{ij} R_{ia,g-g}$  are the production rate of species  $i$  due to homogeneous reactions occurring in core and annulus phases, respectively.
- $\sum_{g-s} \nu_{ij} R_{ic,g-s}$  and  $\sum_{g-s} \nu_{ij} R_{ia,g-s}$  are the production rate of species  $i$  due to heterogeneous reactions occurring in core and annulus phases, respectively

The profile of different gas species along the height of the CFB riser is calculated by their balance equations in the bed and upper zone.

**Eq.9- 1** and **Eq.9- 2** equations are integrated for the height  $0 \leq z \leq H_{bz}$  and their boundary conditions are as follows: at  $t=0, z=0, C_{ie} = C_{i0}$

Where:  $C_{i0}$  (mol/m<sup>3</sup>) is the initial concentration of gas species  $i$  which is calculated from biomass devolatilization (see in **Table 9- 6**).

**Eq.9- 5** and **Eq.9- 6** are integrated for the height of  $H_{bz} \leq z \leq H_t$  and their boundary conditions are as follows: at  $z = H_{bz}; (1 - f_a)(1 - c_{vc})U_c C_{ic} = U_b C_{ib} + U_e \epsilon_e (1 - \epsilon_b) C_{ie}$

The FM model has been written in C programming Language and the code is compiled by using Bloodshed Dev-C++ (Petersen & Ringer, 2010), which is a full-featured Integrated Development Environment (IDE) for the C/C++ programming language. The computational flow chart is shown in **Figure 9- 4** and a detailed description of the FM model can be found in **Appendix X 1**.

The equations applied for the gas concentration in different phases are solved with an iterative scheme by employing a finite difference method with a first order of discretization of the integration variable  $z$  (the length of the riser) (Hoffman, 2001). For example, for gaseous species  $i$  in the bubble and emulsion phases, they are calculated as the follows.

$$\begin{aligned}
 tmp1 &= cb[i] \\
 aux1 &= dZ / U_b; aux2 = dZ / (U_{mf} \epsilon_{mf}); aux3 = \epsilon_{mf} (1.0 - \epsilon_b) \\
 cb[i] &= cb[i] - aux1 * K_{be} (cb[i] - ce[i]) + aux1 * \sum_{g-g} \nu_{ij} R_{ib,g-g}; \\
 ce[i] &= ce[i] + aux2 * K_{be} \epsilon_b (tmp1 - ce[i]) + aux3 * aux2 * \sum_{g-g} \nu_{ij} R_{ie,g-g} \\
 &\quad + aux2 * (1.0 - \epsilon_b) (1.0 - \epsilon_{mf}) \sum_{g-s} \nu_{ij} R_{ie,g-s}
 \end{aligned}$$

The convergence criteria applied for these equation iterations are characterized by comparing the variation of gas concentrations when the grid cell ( $\Delta z$ ) of the height is changed. The convergence is assumed to be achieved, if the variation of  $C_{ib}$ ,  $C_{ie}$ ,  $C_{ic}$  and  $C_{ia}$  is less than the given tolerance when the grid of the grid cell ( $\Delta z$ ) of the height is changed.

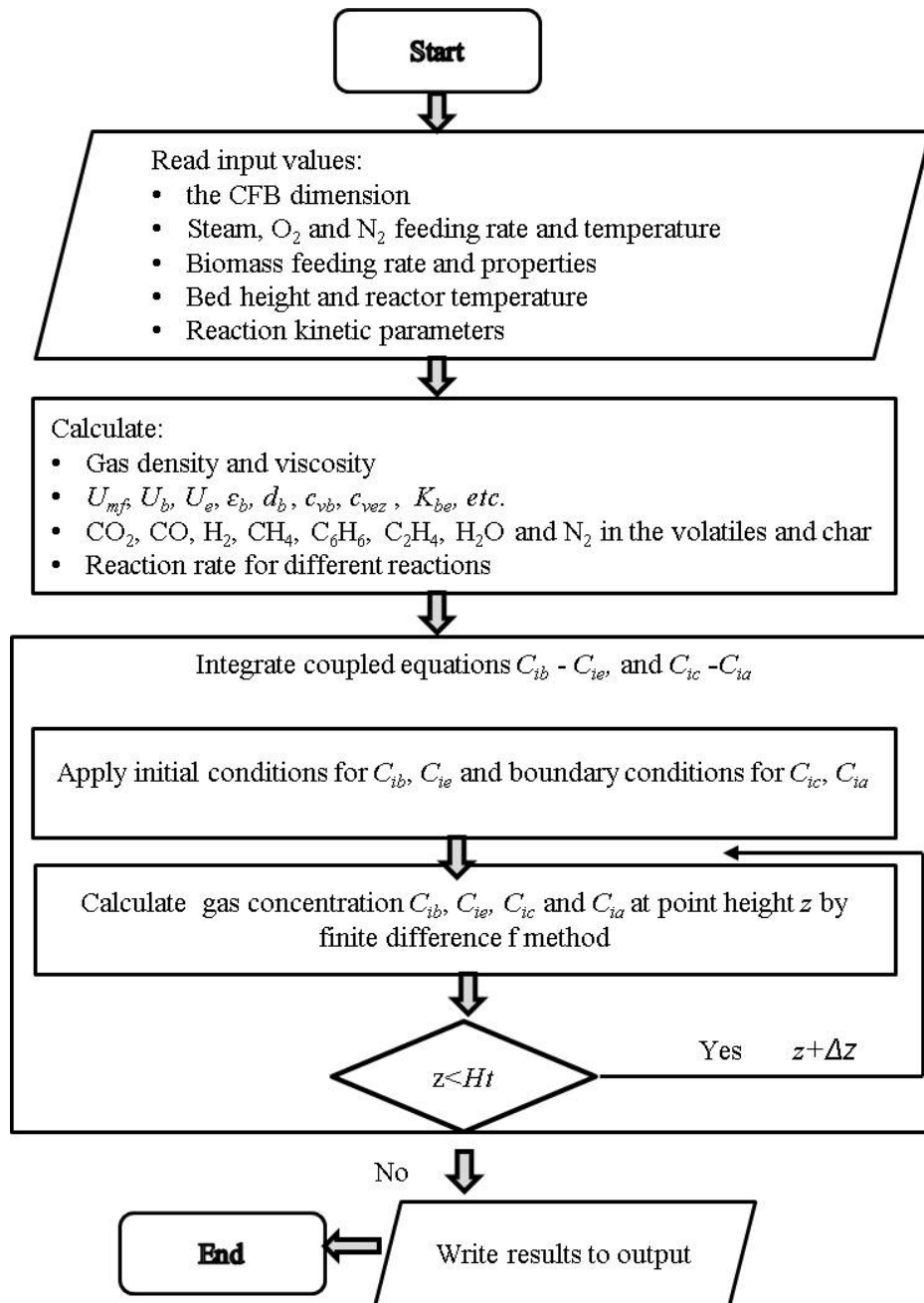


Figure 9- 4 The computational algorithm flow chart of the FM model

## 9.2 Experimental setup and model validation

Agrol, willow and DDGS gasification experiments have been performed using the CFB gasifier. Effects of different operational parameters on the product gas composition and tar formation have been studied in chapters 5 and 6. Thus, here no more additional details will be presented.

## 9.3 Results and discussion

### 9.3.1 Predicted results from the EM models

Figure 9- 5 presents the concentrations of the product gases obtained from Agrol, willow and DDGS which were predicted from the EM models and measured from the experiments. CO-Heq and CO and CO-exp represents the CO concentration predicted from the “heat limited” and the pure EM models, and measured from the experiment, respectively, and similar settings are for other gases.

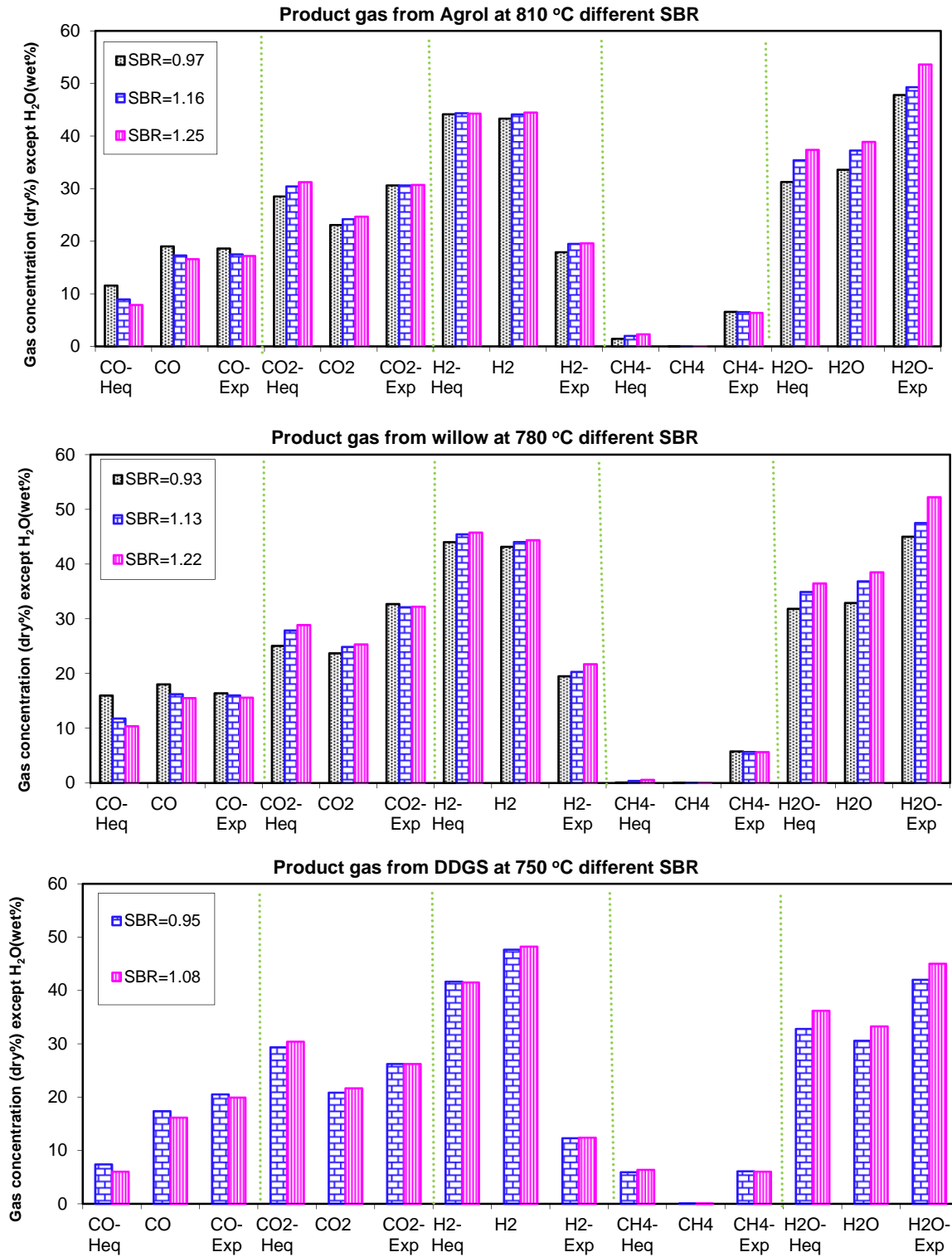


Figure 9- 5 Product gas concentration comparison: predicted values using EM models and measured values

The following observations can be drawn from **Figure 9- 5**:

- 1) In general, the H<sub>2</sub> and H<sub>2</sub>O concentrations predicted from the pure and “heat limited” EM models had no significant difference. However, the predicted H<sub>2</sub> concentrations were around two times as high as the experimental values, and the predicted H<sub>2</sub>O concentrations were lower than the experimental values.

- 2) The CO concentrations predicted from the “heat limited” EM model were lower than the experimental values, while those predicted from the pure EM models were fairly similar to the experimental ones.
- 3) The CO<sub>2</sub> concentrations predicted from the “heat limited” EM model for Agrol and willow were slightly lower than the experimental values, but those for DDGS were higher than the experimental values. The CO<sub>2</sub> concentrations predicted from the pure EM model were lower than the experimental ones.
- 4) Almost no CH<sub>4</sub> or other hydrocarbon compounds were predicted from the pure EM model, but a significant amount predicted by using the “heat limited” EM model. The predicted CH<sub>4</sub> concentrations for Agrol and willow were lower than the experimental values, but those for DDGS agreed fairly well.
- 5) The CO<sub>2</sub>, H<sub>2</sub> and H<sub>2</sub>O concentrations predicted from the pure EM model increased with increasing the SBR value, but the CO concentration decreased. These trends agreed well with experimental ones. However, the CH<sub>4</sub> concentrations predicted from the heat limited EM model for all fuels using heat limited EM increased with increasing SBR, and the H<sub>2</sub> concentration for DDGS decreased.
- 6) The CO<sub>2</sub> and H<sub>2</sub>O concentrations predicted from pure EM model both are lower than the experimental values, while CO concentration is fairly similar to the experimental one. It looks like that O is not in balance. This is because that the total product gas yield predicted from pure EM model is higher than the experimental value. An overall element balance is available in **Table A- 8** (see appendix)

In general, the predicted results from the EM models agree with those reported in the literature (Schuster et al., 2001). According to Puig-Arnavat et al. (Puig-Arnavat et al., 2010), the EM models normally overestimated the yields of H<sub>2</sub> and CO, but underestimated the yields of CO<sub>2</sub>, CH<sub>4</sub> and char. Guekens and Schoeters (Guekens & Schoeters, 1984) and Altafini et al. (Altafini et al., 2003) all reported that thermodynamic equilibrium may not be achieved under low operation temperatures. Kilpinen et al. (Kilpinen et al., 1991) reported that the contents of solid carbon and CH<sub>4</sub> were generally underestimated by the EM models mainly due to the slow kinetics for the char gasification and the CH<sub>4</sub> decomposition. The different results obtained from the heat limited EM model and the pure EM model could be mainly attributed to the equilibrium shifts of the water gas shift reaction (WGS) and the CH<sub>4</sub> steam reforming reaction (MSR).

**Figure 9- 6** shows the equilibrium constant (K<sub>eq</sub>) of the WGS and MSR reactions calculated from the EM models and the experimental results, where K<sub>eq</sub>-WGS-Heq, K<sub>eq</sub>-WGS-Peq and K<sub>eq</sub>-WGS-Exp represent the equilibrium constant of WGS calculated from the “heat limited” EM model, the pure EM model and the experiment, respectively, and similar settings as for the MSR reaction. The values for K<sub>eq</sub> –MRS-Peq are real values divided by 100. For DDGS fuel, the values for K<sub>eq</sub>\_MSR\_Heq and K<sub>eq</sub>-MSR\_Exp are 10 times of the real values. The results presented in **Figure 9- 6** show that:

- 1) Generally there was a significant difference between the K<sub>eq</sub> values for WGS and MSR reactions predicted from the EM models and calculated from the experimental results at the specified reaction temperature.
- 2) For the WGS reaction under most conditions, the value of K<sub>eq</sub>-WGS-Heq was the highest, followed by K<sub>eq</sub>-WGS-Peq and K<sub>eq</sub>-WGS-Exp. This result indicates that under experimental conditions the WGS reaction does not reach equilibrium state, but is closer to the pure equilibrium state than “heat limited” equilibrium state, which could partly explain why the CO concentration predicted from the pure EM models were fairly similar to the experimental ones.
- 3) With increasing the temperature from 740 to 840 °C, the K<sub>eq</sub>-WGS-Peq for all fuels decreased, which indicated a relatively decreasing mole ratio in the total amounts of CO<sub>2</sub> and H<sub>2</sub> to that of CO and H<sub>2</sub>O. Therefore, an increase in the temperature could favor the formations of CO and H<sub>2</sub>O, but inhibit the formations of CO<sub>2</sub> and H<sub>2</sub>. Contrarily, the K<sub>eq</sub>-WGS-Heq for all fuels increased, thus resulted in an opposite formation behavior of these gas species.
- 4) For the MSR reaction under almost all conditions, K<sub>eq</sub>-MRS-Peq was the highest, followed by K<sub>eq</sub>-MRS-Heq and K<sub>eq</sub>-MRS-Exp, particularly for Agrol and willow gasification at higher

temperatures. This observation indicates that the MRS reaction was more influenced by gasification temperature than the WGS reaction. In other words, the CH<sub>4</sub> formation could be enhanced at low temperature, which can explain why the CH<sub>4</sub> concentrations for DDGS predicted from the “heat limited” EM model were closest to the experimental ones.

- 5) With increasing temperature from 740 to 840 °C, the Keq-MRS-Peq for all fuels increased sharply, which indicated a significant increase of the mole ratio in CO and H<sub>2</sub> to that of CH<sub>4</sub> and H<sub>2</sub>O. Therefore, the formation of CH<sub>4</sub> was highly inhibited. Contrarily, the Keq-MRS-Heq for all fuels decreased with increasing temperature, thus the formation of CH<sub>4</sub> was enhanced.

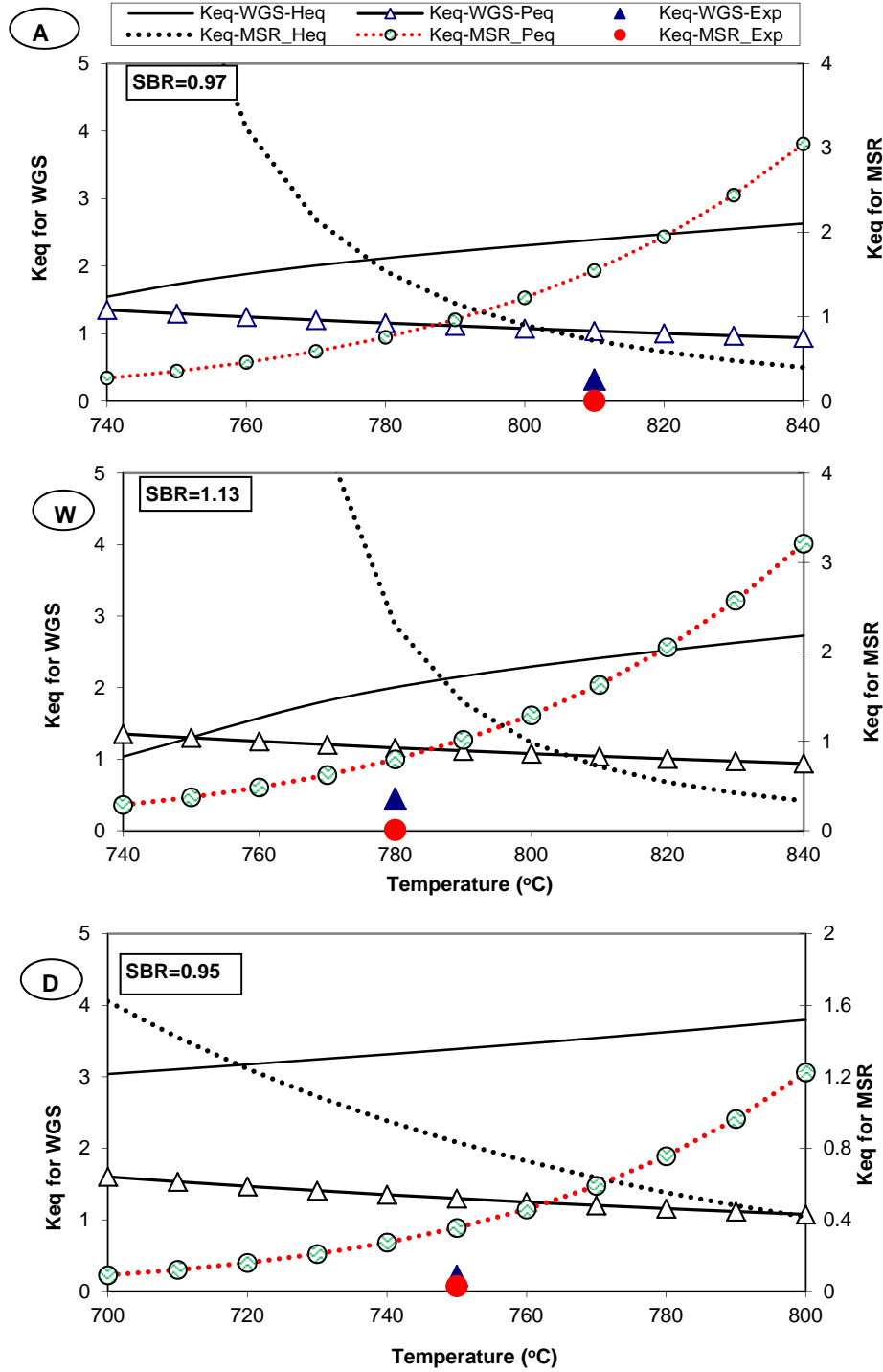


Figure 9- 6 Equilibrium constant (Keq) for reactions WGS and MSR calculated from EM models and experiments

Since the WGS reaction is exothermic (-41kJ/mol) and the MSR reaction is highly endothermic (+242kJ/mol), the different change trends for  $K_{eq}$  versus temperature predicted from the “heat limited” EM and the pure EM model appeared to be fairly reasonable. In the pure EM model, the CFB gasifier was regarded as a perfectly insulated apparatus with fully neglecting heat losses where all reactions reached equilibrium. Therefore, increasing temperature is favorable for the MSR reaction but not for the WGS reaction, which lead to a decrease in the amount of  $CH_4$  and an increase in the amount of CO. However, in the “heat limited” EM model, an additional term “QHEAT” was incorporated to reach and compensate enthalpy balance. Thus, to help the reaction temperature constant, the extents of the equilibria of endothermic reactions (e.g., the MSR reaction) were thereby inhibited, whereas those for exothermic reactions (e.g., the WGS reaction) were oppositely enhanced, which is why a substantial amount  $CH_4$  was predicted from “heat limited” EM model.

### 9.3.2 Predicted results from the KM models

**Figure 9- 7** shows the concentrations of the product gas species obtained from all fuels which were predicted from the KM models and the experiments. CO-SW, CO and CO-Exp represents the CO concentration predicted from the KM-SW model, the KM-TG model and calculated from the experiments, respectively, and similar settings are for other gases. The results shown in **Figure 9- 7** indicate that:

- 1) In general, the concentrations of most product gases predicted from the KM models were much closer to the experimental values than those from the EM models. No large difference was observed between the product gas composition predicted from the KM-SW and KM-TG models.
- 2) Concerning different product gas species, the concentrations of CO and  $C_2H_4$  predicted from the KM models under most conditions were much closer with the experimental values than others. For example, the concentration difference of CO and  $C_2H_4$  for Agrol and willow between the experimental and the predicted was within 0.8%, and the difference between the predicted values from the KM-SW and the KM-TG model was within 0.35%. However, a slightly higher difference of around 3.5-4.0% was observed between the CO concentration for DDGS predicted from the KM models and the experiments.
- 3) The concentrations of  $H_2$ ,  $CH_4$  and  $H_2O$  predicted from the KM models almost all were slightly higher than the experimental ones, especially those obtained from DDGS.  $CH_4$  concentrations for Agrol and DDGS predicted from the KM-TG model were slightly closer to the experimental value than that from the KM-SW model, while for willow that from the KM-SW model was closer. However, an exact opposite trend of the  $H_2$  concentrations was observed for three fuels under almost all conditions.
- 4) The concentrations of  $CO_2$  predicted from the KM models under almost all conditions were lower than the experimental ones. The concentrations predicted from the KM-TG model were generally closer to the experimental value than that from the KM-SW model, and the difference between their predicted values was within 0.8%.
- 5) The predicted concentrations of CO for the three fuels decreased with increasing SBR, while the concentrations for  $H_2O$  and  $CO_2$  increased. These observations agreed well with experimental results as well as those reported by Gil et al. (Gil et al., 1999) and Wang and Kinoshita (Wang & Kinoshita, 1992), who reported that as the SBR value was increased the concentrations of CO decreased due to partial oxidation and steam reforming reactions.
- 6) Under almost all conditions, the concentrations of  $H_2$  predicted from the KM models decreased with increasing SBR, whereas those of  $CH_4$  and  $C_2H_4$  increased. These observations were different from those obtained from the experiments. According to Wang and Kinoshita (Wang & Kinoshita, 1992), the  $H_2$  concentration was influenced by competition between the residence time versus steam injected amounts. In this way if the SBR values were increased at a fixed biomass feed rate, the residence time could be decreased. Consequently, an increase in SBR might result in less  $H_2$  production if the effect of residence time dominated. Umeki et al. (Umeki et al., 2010) reported that an increase in the steam flow rate could simultaneously change SBR (represented by S/C ratio), reaction temperature and residence time, while these parameters all could have an influence on the formation of the gas.

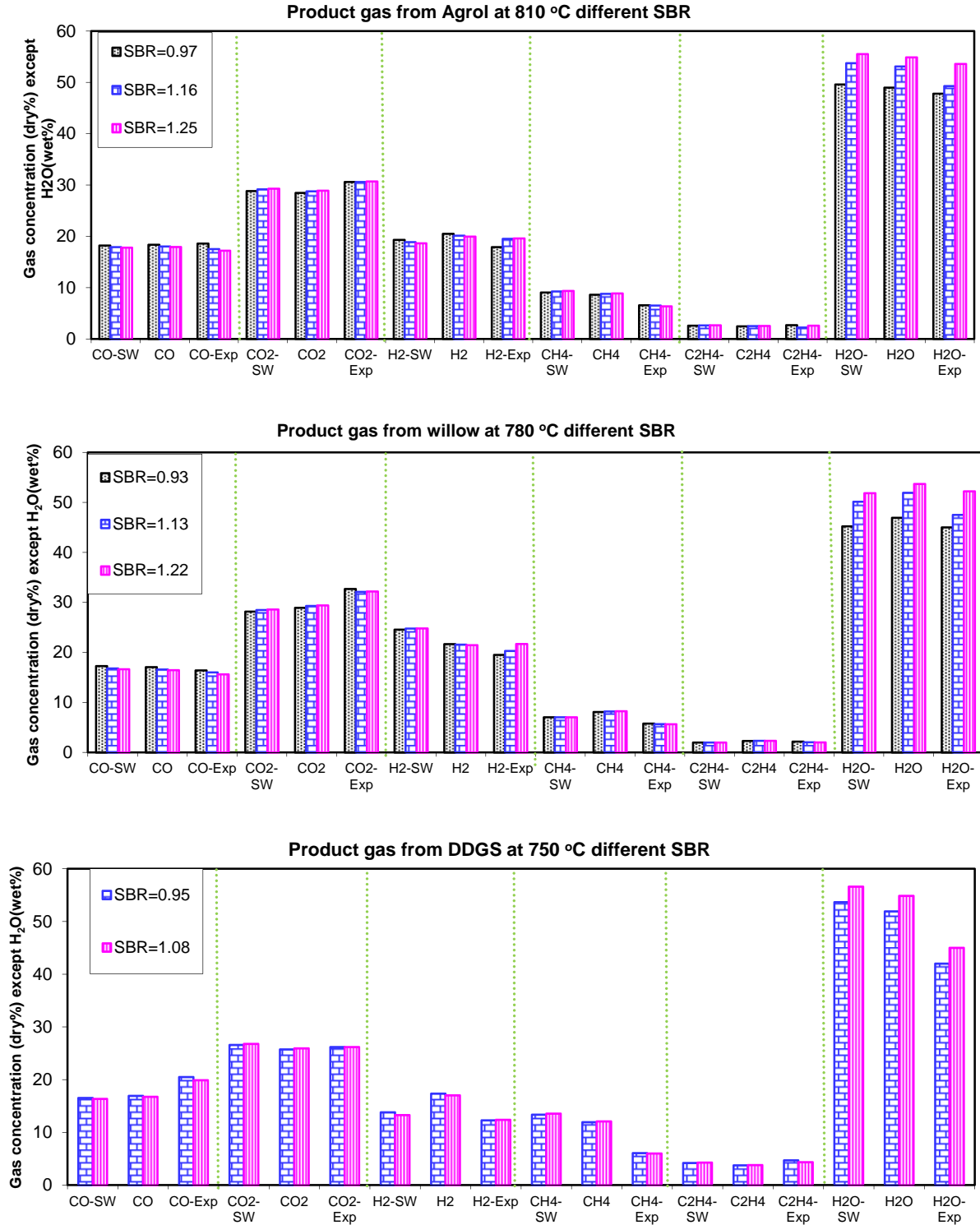


Figure 9- 7 Product gas concentration comparison: predicted values using KM models and measured values

From the above observation, it can be seen that the predicted gas concentrations using the KM-SW and the KM-TG models were fairly similar, and most of them were close to the experimental ones. Concerning all the product gas species, a slightly higher variation was observed between H<sub>2</sub> and CH<sub>4</sub> concentration predicted from the KM-SW and KM-TG models. From **Table 9- 3** it can be seen that there are different char reaction kinetics applied in the KM-SW and the KM-TG models. It appeared that C-O<sub>2</sub> and C-CO<sub>2</sub> reactions influenced the WGS and MSR reactions to some extent which can be seen from their calculated equilibrium constant presented in **Figure 9- 8**. Keq-WGS-SW, Keq-WGS-

TG and Keq-WGS-Exp represent the equilibrium constant of WGS calculated from the KM-SW model, the KM-TG model and the experiments, respectively, and similar setting as for the MSR reaction. The results presented in **Figure 9- 8** show that:

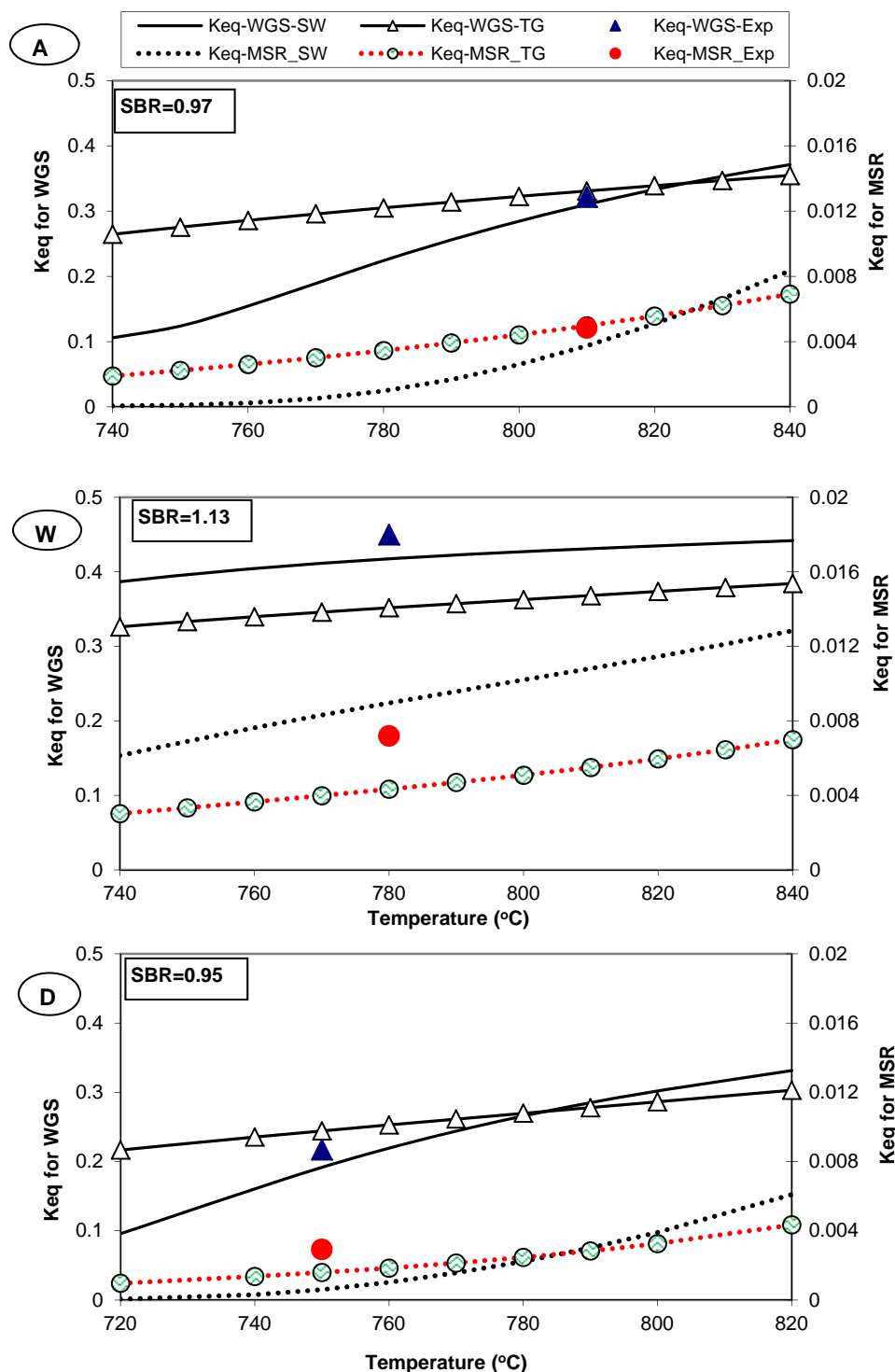


Figure 9- 8 Equilibrium constant (Keq) for reactions WGS and MSR calculated from KM models and experiments

- 1) The Keq-WGS and Keq-MSR values calculated from the KM models for all fuels were much closer to the values from the experimental results than those from the EM models, which indicate that the WGS and MSR reactions occurred actually in kinetic-controlling condition instead of equilibrium controlling condition. It is reasonable since in a gasifier all homogenous



and heterogeneous reactions are impossible to react fast enough in a long enough residence time to reach equilibrium state as normally assumed in EM models.

- 2) With increasing temperature from 740 to 840 °C, the Keq-WGS and Keq-MSR values calculated from the KM models for all fuels increased gradually, but the Keq-WGS and Keq-MSR values calculated from the KM-TG model had a much smoother changing trend compared to those calculated from the KM-SW model. It seems to be unreasonable that an increase in the temperature led to an increase in the Keq-WGS value since this reaction is exothermic. However, due to the shifting of the MSR reaction with an increase in the temperature, a relatively high H<sub>2</sub> amount was simultaneously produced associated with a decrease in the H<sub>2</sub>O amount. This change could possibly increase the calculated Keq value for the WGS reaction.
- 3) For Agrol, willow and DDGS three fuels, the Keq-WGS and Keq-MSR values calculated from the KM-SW and KM-TG models were the closest to the experimental ones. The predicted product gas composition for Agrol also turned out to be the most as similar as the experimental results (see **Figure 9- 7**). From this observation, it can generally be concluded that the WGS and MRS reactions had a related influence on the product gas composition; thus, it is impossible to properly determine CO, CO<sub>2</sub>, H<sub>2</sub> and CH<sub>4</sub> concentration by considering only one reaction equilibrium.
- 4) Considering WGS and MSR reactions, normally the WGS reaction was found to be the most important reaction among all the reactions that controlled the gas composition as reported by Umeki et al. (Umeki et al., 2010), Encinar et al. (Encinar et al., 2002) and Franco et al. (Franco et al., 2003). However, various other reactions such as Boudouard and MSR reactions could also be dominant over a certain temperature range due to the differences in the mineral matter associated catalytic effects and/or the porous structure of different fuels (Franco et al., 2003).

Previous studies showed that operational parameters such as SBR, gasification temperature all influence CCE%, CGE% and LHV of the product gas. Generally a higher temperature and a higher SBR value can lead to a higher product gas yield due to enhanced endothermic steam reforming, cracking reactions of the tar (Wei et al., 2007). Here, the influences of a variation of SBR on CCE%, CGE%, LHV and the yield of the product gas obtained from three fuels predicted using the KM models were compared to the experimental results and the results are summarized in **Figure 9- 9**. In **Figure 9- 9**, the yield of the product gas (kg/kg) is defined as the ratio of the product gas produced (kg/h) to the biomass fuel supplied (kg/h).

From **Figure 9- 9**, it can be seen that an increase in SBR led to a higher yield of the product gas, but simultaneously also caused a lower CCE%, CGE% and LHV of the product gas. For instance, with increasing SBR from 1.13 to 1.22, the yield of the product gas produced from willow increased from 2.4 to 2.5 kg product gas /kg fuel, while CCE%, CGE% and LHV of the product gas values decreased from 90.5 to 86.9%, 56.2 to 55.2% and 3.8 to 3.6 MJ/kg, respectively. Similar trends were also observed for Agrol and DDGS. These trends predicted from the KM models agreed well with those obtained from the experiments as well as those reported by other researchers. For example, Gil et al. (Gil et al., 1997) reported that by increasing GR (the ratio of steam and oxygen supplied to biomass fuel supplied on a.r. basis), the LHV of the product gas and thermal efficiencies decreased. Turn et al. (Turn et al., 1998) reported that the yield of the product gas was improved from 1.1 to 1.6 Nm<sup>3</sup> /kg biomass on a dry ash free basis with increasing SBR from 1.1 to 4.7. Chopra and Jain (Chopra & Jain, 2007) and Kumar et al. (Kumar et al., 2009) reported that CCE% and CGE% might decrease with an increase in SBR since excess steam would lower the gasifier bed temperature. Doherty et al. (Doherty et al., 2009) reported that air preheating increased the product gas heating values and CGE%. Umeki et al. (Umeki et al., 2010) reported that the higher heating value (HHV) of the product gas decreased as SBR (represented by S/C ratio) increased while the gas yield increased, and CGE% decreased with increasing SBR from 2.4 to 2.8. They concluded that the changes in the HHV and the gas yield were attributed to the change in the gas composition and yield affected by the WGS reaction.

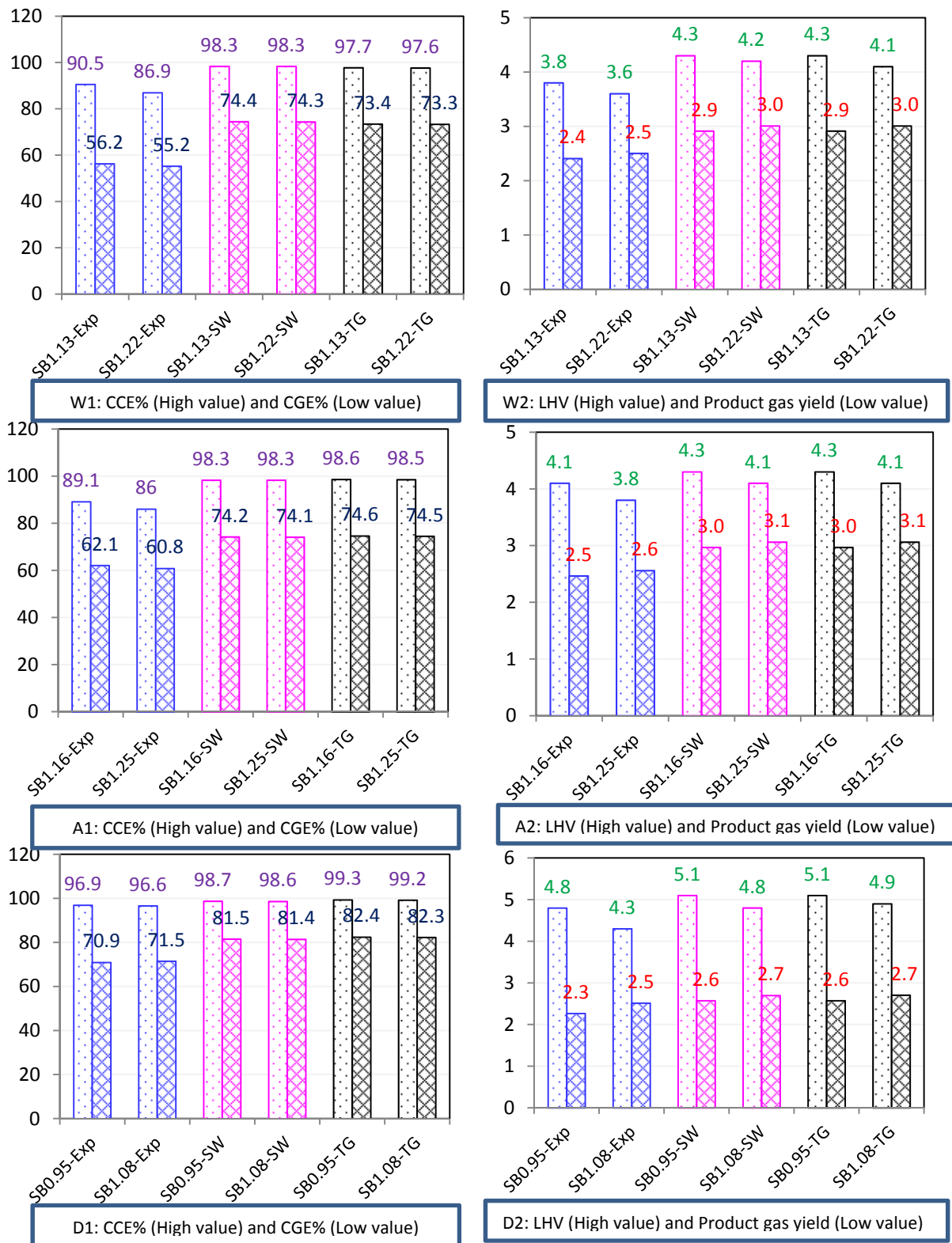


Figure 9- 9 CCE%, CGE% (W1, A1, D1) and LHV(MJ/kg), Product gas yield (kg/kg)(W2, A2, D2) calculated from KM models and experiments

Concerning the LHV of the product gas, it seemed that the product gas LHV produced from DDGS was higher than those from Agrol and willow. This could be due to high  $\text{CH}_4$  concentration contained in the product gas. According to Van der Drift et al. (Van der Drift et al., 2001), the concentration of hydrocarbons could largely influence the heating value of the product gas since these components normally have relatively high heating values. Generally the CCE%, CGE% and LHV and the yield of

the product gas produced from Agrol and willow were fairly similar, particularly considering the values predicted from the KM models. According to obtained experimental results in the previous study (Meng et al., 2011a) and chapter 5, the CCE%, CGE% and the yield of the product gas obtained from willow appeared to be slightly higher than those obtained from Agrol. This could be attributed to higher O/C molar ratio in Agrol fuel as reported by Li et al. (Li et al., 2004), the CGE% decreased with an increasing O/C molar ratio. From **Figure 9- 9**, it can also be seen that the CCE%, CGE%, the yield and LHV of the product gas for three fuels predicted from the KM models generally were slightly higher than those obtained from the experiments, but the predicted values are within the range reported by other researchers (Kumabe et al., 2007; Van der Drift et al., 2001). No significant difference was observed between their values predicted from the KM-SW and KM-TG models.

### **9.3.3 Predicted Results from the FM model**

Besides the Aspen Plus<sup>TM</sup> EM and KM models, the product gas produced from the gasification of three fuels using the CFB gasifier was also predicted by using the FM model, since this type of model has been widely applied for modeling (C) FB gasification process by many other researchers as reported by Gómez-Barea and Leckner (Gómez-Barea & Leckner, 2010). The main input parameters used for the FM model have been summarized in previous sections (see **Table 9- 6**). The concentrations of the product gas components (CO, CO<sub>2</sub>, CH<sub>4</sub>, H<sub>2</sub>, C<sub>2</sub>H<sub>4</sub>, H<sub>2</sub>O) produced from Agrol gasification with SBR=0.97 along the riser is shown in **Figure 9- 10**, where two types of kinetics (SW and TG) have been applied in the FM model. Considering the legend, the mark plus line represents the predicted gas concentration from KM and FM model, while only mark represents the gas concentration obtained from experiments. Since there is not much difference between the predicted results from Aspen Plus<sup>TM</sup> KM-TG and KM-SW models, and the results from the FM model are only compared with those achieved from the Aspen Plus<sup>TM</sup> KM-TG model. From **Figure 9- 10** it can be seen that:

- 1) In general, the change trends of different gas concentrations along the riser predicted from the FM model and KM model are fairly similar. There is no obvious difference observed between the gas concentrations predicted from the FM model by applied SW and TG kinetics, and similar results were also predicted from the KM-SW and the KM-TG models. The outlet CO<sub>2</sub> concentration predicted from FM model by using SW kinetics is slightly higher than that by using TG kinetics, and the same result was also obtained from the KM-SW and KM-TG model, which can be seen in **Figure 9- 7**. Therefore, this observation also validates the correction of the FM model to certain extent.
- 2) Compared to the agreement extent with experimental results, the results predicted from the FM model seemed to be slightly worse than those from the KM model. There were no significant differences between the outlet C<sub>2</sub>H<sub>4</sub> and CH<sub>4</sub> concentrations predicted from the FM model and KM model, and as well as between their variation behavior along the height of the riser. Although the outlet H<sub>2</sub> concentrations predicted from the FM model and KM model both were higher than the experimental values, and the outlet CO concentrations were oppositely lower, the difference between the results from the FM model and experiments are much higher. On the other hand, the outlet H<sub>2</sub>O concentration predicted from the FM model was lower than the experimental value and the CO<sub>2</sub> concentration was higher, while opposite results were predicted from the KM model. From these observations, it can be generally concluded that the WGS reaction was slightly enhanced in the FM model, and the shift equilibrium of the WGS reaction led to higher production CO<sub>2</sub> and H<sub>2</sub>.
- 3) For both FM and KM models, the predicted gas concentrations varied mainly along the height of the riser of approximately 0.5m. This behavior can be attributed to the presence of a dense bed zone which is assumed to be 0.5m high. This observation was also reported by Siedlecki (Siedlecki, 2011), who mentioned that due to the consideration the exit of dense bed zone with a dynamic depth of around 0.49 m in the CSFMB model, a sharp change of all gaseous species at the height of approximately 0.5m was observed.

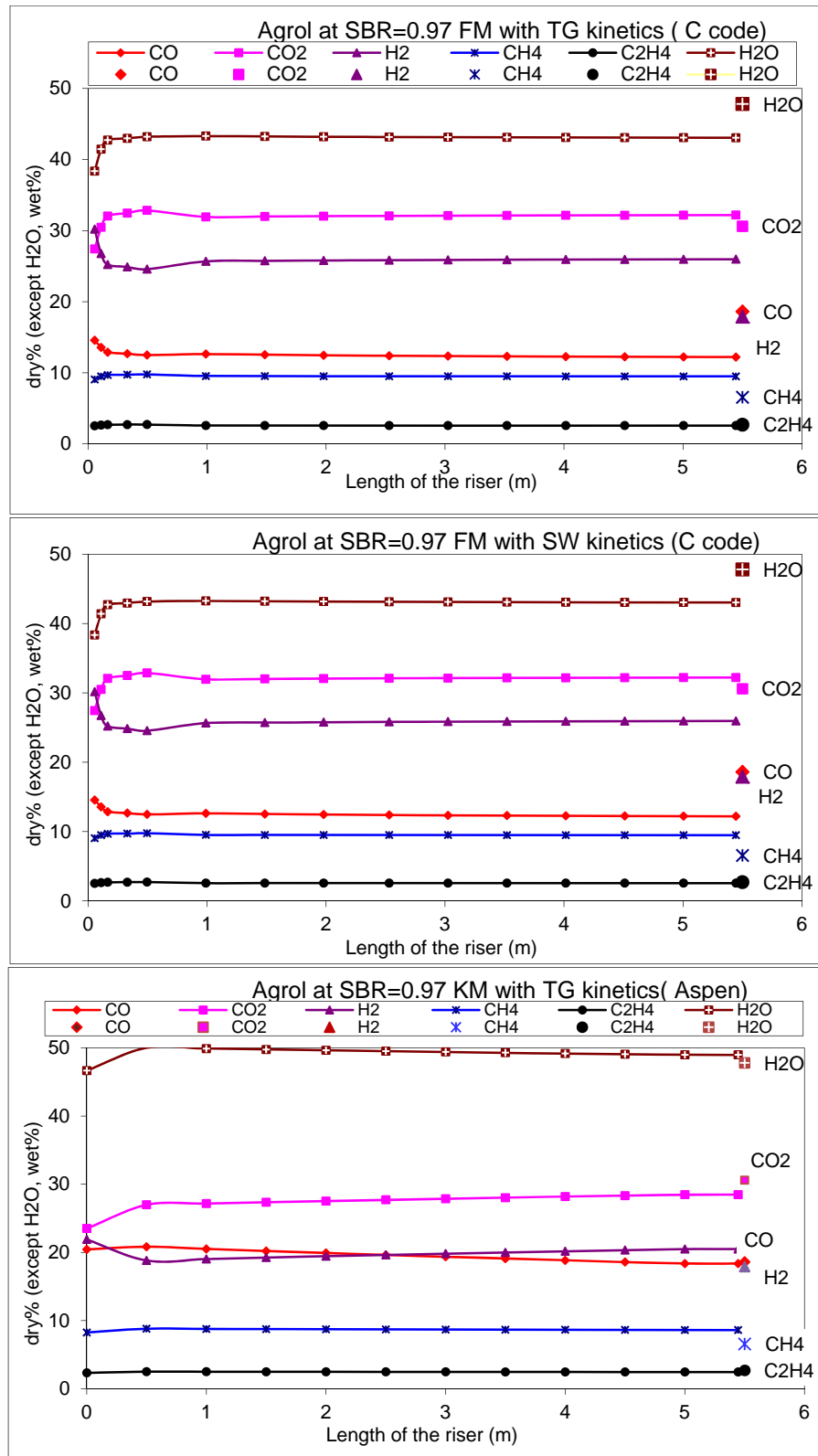


Figure 9- 10 Gas concentration produced from Agrol along the length of the riser predicted from the FM model using SW and TG kinetics and from KM-TG Aspen model

Considering that the concentrations of all gaseous species mainly changed in the bed zone, the zoomed in change profiles of different gases concentration predicted from the FM model in the bed were plotted which are shown in **Figure 9- 11**, where H<sub>2</sub>\_b and H<sub>2</sub>\_e represents the H<sub>2</sub> concentration in the bubble and emulsion phase, respectively, and similar settings are for other gases.

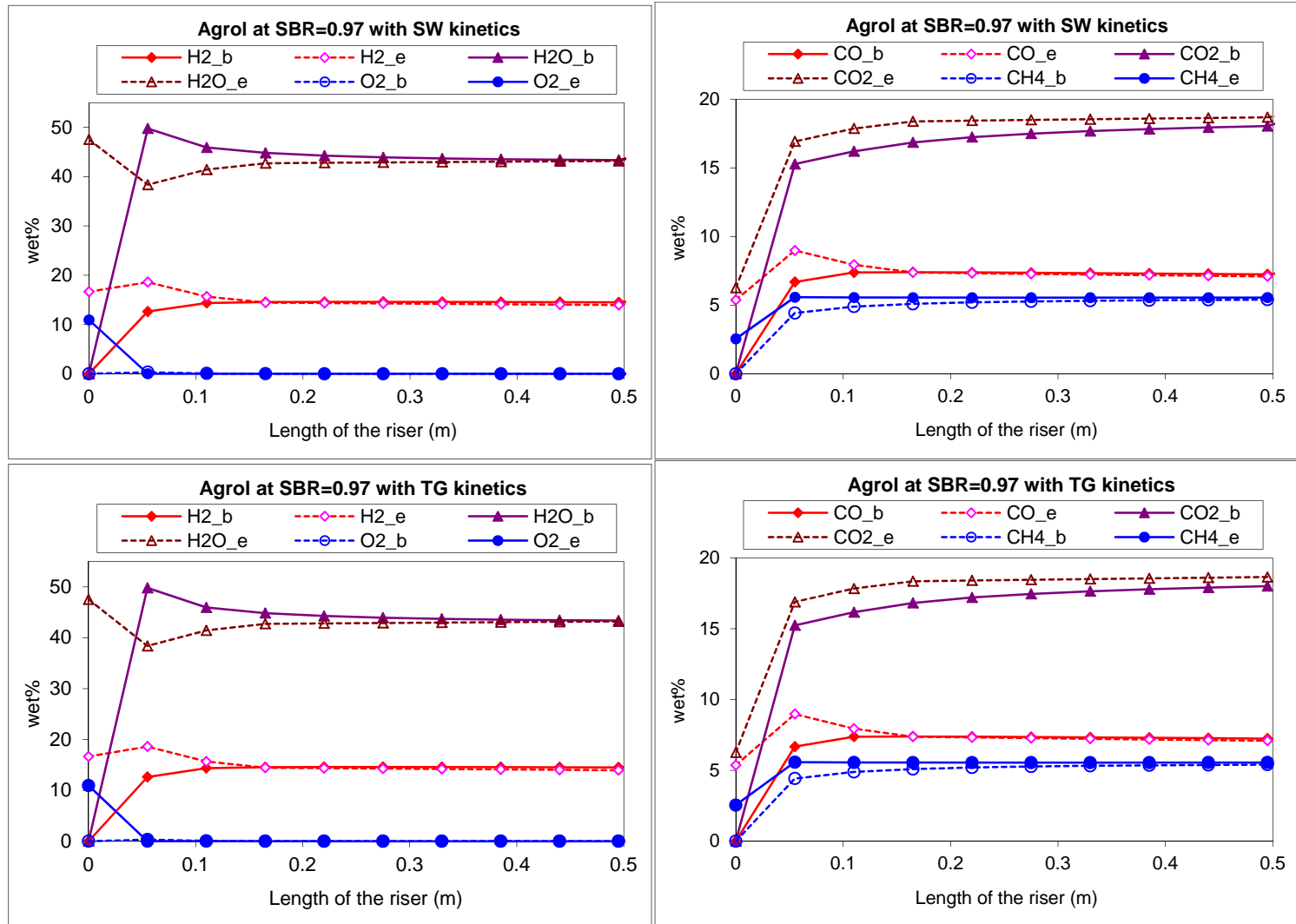


Figure 9- 11 Gas concentration produced from Agrol along the height of the riser predicted from FM model using SW and TG kinetics

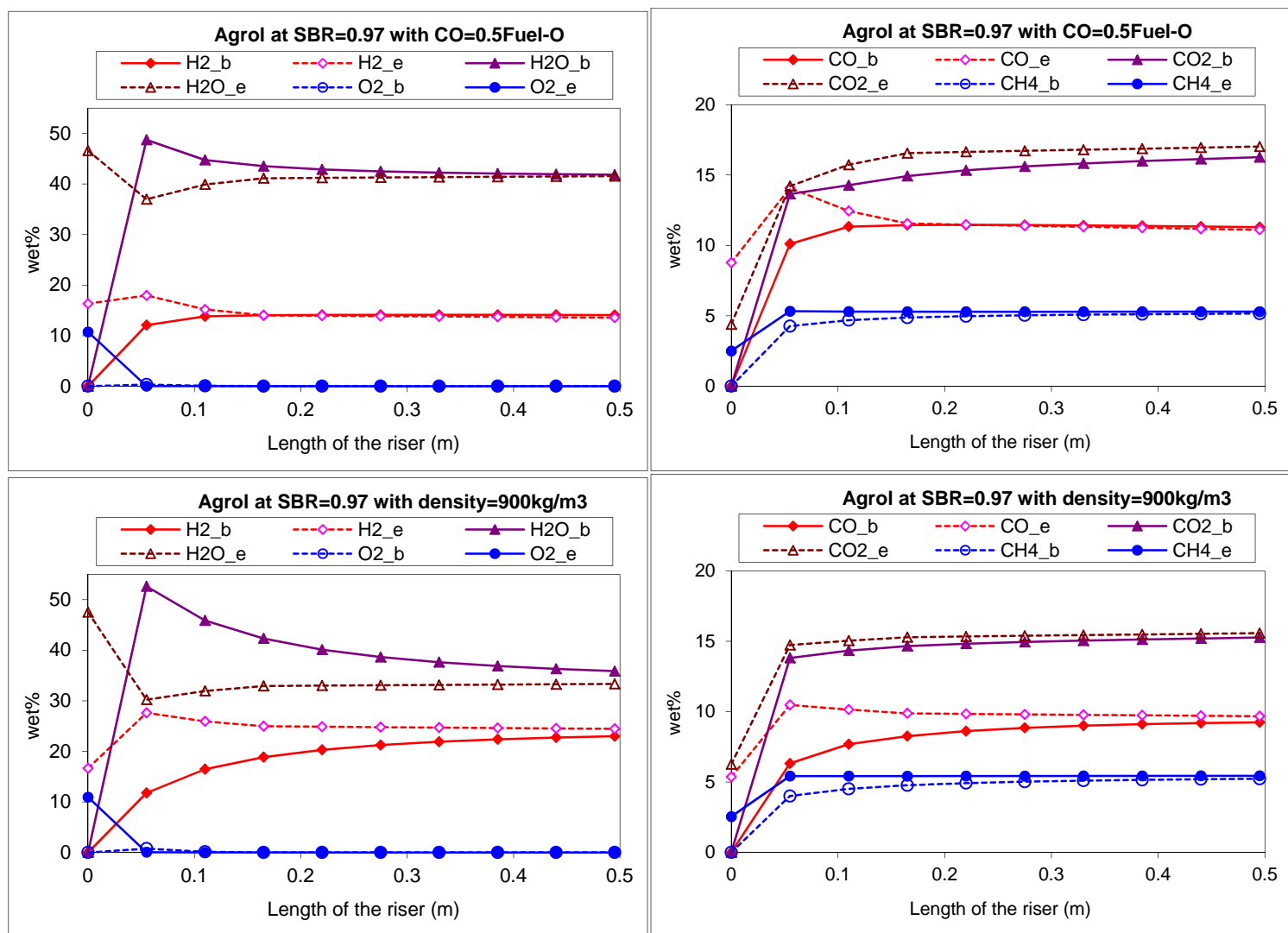


Figure 9- 12 Sensitivity analysis: effects of Agrol devolatilization model (upper) and Agrol density (below) on gas concentrations predicted from FM model

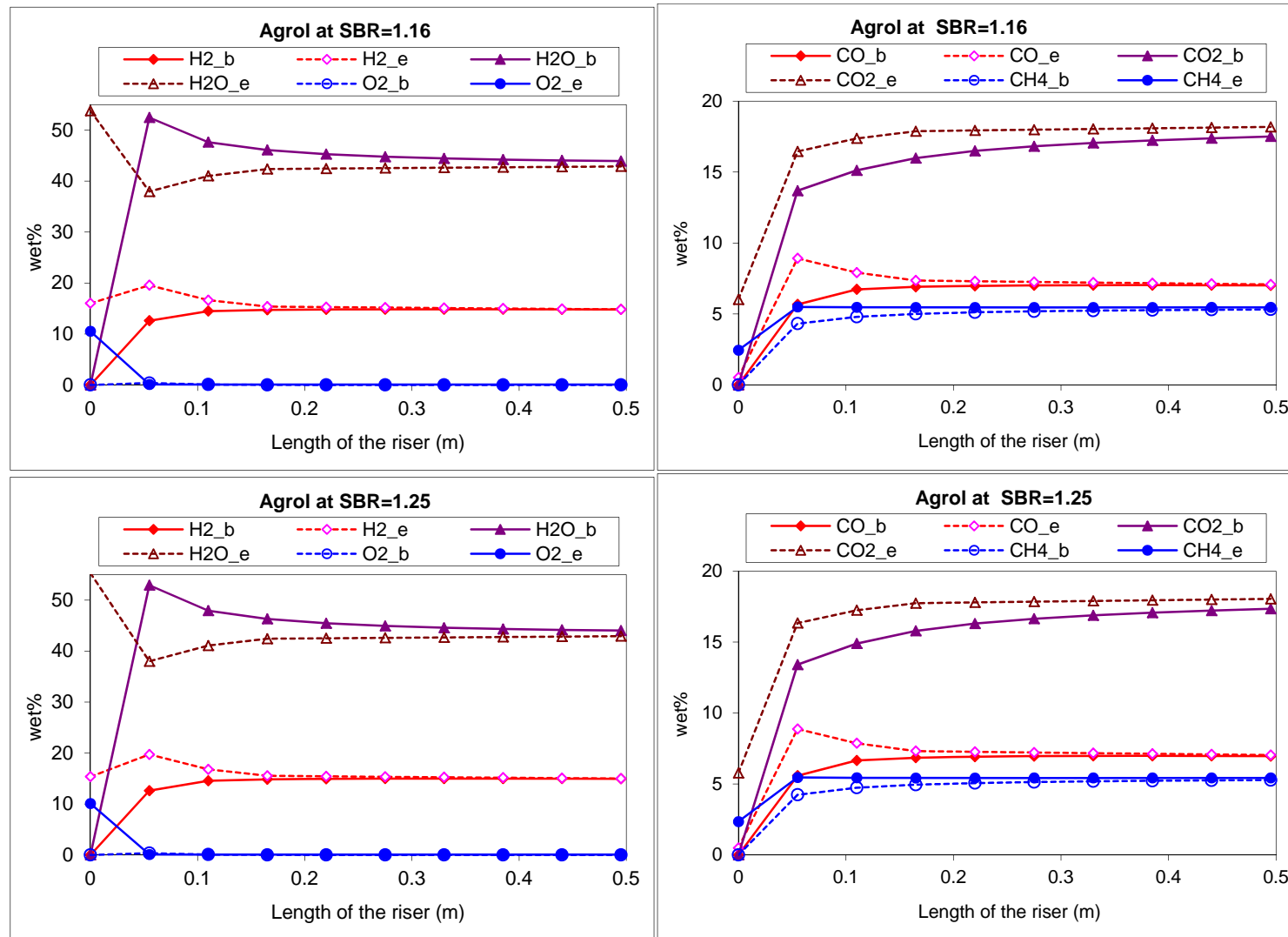


Figure 9- 13 Sensitivity analysis: effects of SBR values on gas concentrations predicted from FM model

The results shown in **Figure 9- 11** indicate that the concentrations of all gases changed differently in bubble and emulsion phases. The difference between gas initial concentrations in the bubble and emulsion phases is attributed to model assumption, since it is assumed that all gases entered only into the emulsion phase in the FM model. However, due to mass transfer occurring between these two phases, the concentrations of all gases gradually reached equilibrium. Once again, there is no obvious difference between the change trends of gas concentrations predicted from the FM model by applying SW and TG kinetics.

- 1) Considering the variation in concentrations of different gas species, the O<sub>2</sub> concentration in emulsion phase sharply decreased to zero largely due to char combustion (R1). This behavior was also observed from the modeling by Siedlecki (Siedlecki, 2011) and De Jong (De Jong, 2005).
- 2) The CH<sub>4</sub> concentration in the emulsion phase is initially increasing possibly due to its formation from Agrol devolatilization (R0) and CH<sub>4</sub> production (R3), and then decreasing largely as a consequence of the MSR reaction (R7). The previous results predicted from the KM model also indicate that the MSR reaction played an important role on CH<sub>4</sub> concentration.
- 3) As reported by De Jong (De Jong, 2005), the decrease in the H<sub>2</sub>O concentration in the bed zone can be attributed to the heterogeneous water-gas reaction (R4). Probably due to H<sub>2</sub> oxidation (R3), the H<sub>2</sub>O concentration slightly increased, and then decreased again because of the WGS reaction.
- 4) The formations of CO, H<sub>2</sub> and CO<sub>2</sub> are much complicated and can be influenced by several reactions (see **Table 9- 2**). For CO<sub>2</sub>, char combustion (R1) and CO oxidation (R5) maybe play a dominant role, thus a continuous increase in the CO<sub>2</sub> concentration is achieved in the bed zone. Although several reactions such as tar oxidation (R12), Boudouard reaction (R2) and char combustion (R1) all could lead to the formation of CO, the predicted CO concentration was still much lower than the experimental value. This is probably due to the shift equilibrium of the WGS reaction and the assumption of the formation behavior of CO during Agrol devolatilization (R0). Similar reasoning might be used to explain the observed difference between the predicted and experimental H<sub>2</sub> concentration.

Unfortunately, the variations of the concentrations of different gases along the riser were not measured during the experiment. However, according to the gas composition measured by Siedlecki (Siedlecki, 2011) at different positions along the riser, above the fuel feed point, the measured H<sub>2</sub>, CH<sub>4</sub> and CO<sub>2</sub> profiles were rather flat, and overall had a slight increasing trend. A maximum of CO concentration was obtained at the fuel feed point, and O<sub>2</sub> concentration decreased sharply from the fuel feed point to zero. The predicted gas concentration profiles from the FM model appear to be fairly consistent with these observations. It concluded that the FM model predicts the main gaseous species profiles along the riser reasonably well, although the major disagreement is found in the outlet concentrations of CO and H<sub>2</sub>, which is often observed as reported by Gómez-Barea & Leckner (Gómez-Barea & Leckner, 2010). Similarly, the concentrations of the product gas components (CO, CO<sub>2</sub>, CH<sub>4</sub>, H<sub>2</sub>, C<sub>2</sub>H<sub>4</sub>, H<sub>2</sub>O) produced from willow and DDGS gasification along the riser were also predicted by using the FM model. And the results are fairly similar (see **Figure A-13** and **Figure A-14** in appendix), thus no additional discussion will be further presented.

### **9.3.4 Sensitivity analysis of the FM model**

In order to test the robustness of this FM model, a sensitivity analysis has been performed. Since there is no significant difference between the predicted results from the FM model by applying SW and TG kinetics, only TG kinetics has been applied in the sensitivity analysis. The following sensitivity analysis included three variables: fuel density, gas composition from Agrol devolatilization and the SBR values. The changes of the predicted results are assessed by comparing with the base case which are the results that presented in **Figure 9- 11**.

According to the summary by Gómez-Barea and Leckner (Gómez-Barea & Leckner, 2010), pyrolysis or devolatilization is demonstrated to be a key step which significantly influences the model results. In



the FM model base case study, it was assumed that 30% O in the fuel (Fuel-O) was converted to CO, while the left O was used to form CO<sub>2</sub>. This assumption is made mainly based on the ratio of the yields of CO and CO<sub>2</sub> produced from Agrol pyrolysis by using TGA-FTIR (see **Figure 7- 12**). However, O in the fuel (Fuel-O) was not only converted to CO and CO<sub>2</sub>, but also some tar which were not detected. Moreover, the yields of CO and CO<sub>2</sub> are affected by the heating rates. More O in the fuel was assumed to convert to CO instead of CO<sub>2</sub> in the CFB model developed by Siedlecki (Siedlecki, 2011). Therefore, the effect of Fuel-O to CO ratio on the predicted product gas composition was investigated, and the results are shown in **Figure 9- 12**, where it is assumed that 50% Fuel-O was converted to CO, while the left Fuel- O to CO<sub>2</sub>.

From **Figure 9- 12**, it can clearly be seen that the concentrations of the product gas components predicted from the FM model were largely influenced by the input Fuel-O to CO ratio. With increasing the ratio of Fuel-O to CO, the CO concentration in the product gas was also increased, meanwhile a decrease in the concentrations of CO<sub>2</sub> and CH<sub>4</sub> was obtained. From this observation, it can be generally concluded that an accurate yield data of the products released from Agrol devolatilization is required in order to develop reliable computational models.

As it is well known, the actual value of fuel density is not easy to determine, but fuel density can largely influence the model results and cause some computational problem as well, since it involves the calculation of most hydrodynamic parameters applied in the FM model. In the FM model base case study, the input value of Agrol density is 453 kg/m<sup>3</sup>, which was calculated by weighting grounded Agrol power in a vessel with a known volume (50mL). The response of the FM model to the variation of the fuel density is shown in **Figure 9- 12**, where the Agrol density is assumed to be 900 kg/m<sup>3</sup>. As expected, the value of fuel density largely influences the formation behavior of CO, CO<sub>2</sub>, H<sub>2</sub> and H<sub>2</sub>O. A higher fuel density value led to a long time for H<sub>2</sub>O to reach equilibrium in the bed.

As one of the most important process variables, the effect of SBR on the formation of the product gas and tar produced from three fuels gasification was mainly studied. Therefore, to further evaluate the functionality and correctness of the FM model, its response to the variation of the SBR values (SBR=1.16, 1.25) was studied as well, and the results are shown in **Figure 9- 13**. According to the experimental results, with increasing the SBR values, the concentrations of CO, CH<sub>4</sub>, H<sub>2</sub>O and C<sub>2</sub>H<sub>4</sub> all gradually decreased, while the concentration of H<sub>2</sub> increased with a varying degree depending on fuel types. No significant change was observed in the CO<sub>2</sub> concentration with a variation of the SBR value. From **Figure 9- 13**, it can clearly be seen that with varying the SBR value, the predicted concentrations of all gaseous species behave in a comparative way. As expected, with increasing SBR values, the predicted concentrations of CO and CH<sub>4</sub> slightly decreased, while the concentrations of H<sub>2</sub>O and H<sub>2</sub> slightly increased. Therefore, considering the behavior of CH<sub>4</sub> and H<sub>2</sub> with varying SBR, it appears that the FM model had a better prediction response than the KM model, since under almost all conditions, the concentrations of H<sub>2</sub> predicted from the KM models decreased with increasing SBR, whereas that of CH<sub>4</sub> on the other hand increased.

### **9.3.5 Comparison of EM, KM and FM models**

The EM, KM and FM three different types of models were applied to simulate the steam-O<sub>2</sub> blown CFB gasifier, and their predicted results were presented in previous sections, respectively. In this section, a brief comparison was made about the product gas composition predicted from EM, KM and FM models. The predicted results for Agrol gasification with SBR=0.97 are shown in **Figure 9- 14**, where EM-Heq, EM-Peq, KM-SW, KM-TG, FM-SW, FM-TG, and Exp. represent gas concentration predicted from “heat limited” EM, pure EM, KM model with SW, TG kinetics, FM model with SW, TG kinetics and calculated from experiments, respectively.

From **Figure 9- 14**, it can be seen that there is a significant variation among the product gas composition predicted from EM, KM, and FM models. As aforementioned, EM model overpredicted H<sub>2</sub> concentration and underpredicted C<sub>2</sub>H<sub>4</sub> and CH<sub>4</sub> concentration to a great extent; however, by applying kinetics for different reactions in the KM and FM models, a substantial improvement was

achieved in their predicted concentrations, although the concentrations of  $H_2$  and  $CH_4$  predicted were still higher than experimental values. Compared to other gas species, the  $C_2H_4$  and  $CO_2$  concentrations predicted from KM and FM model are fairly close to experimental values, especially the  $C_2H_4$  concentration, which indicated that the assumption made in the Agrol devolatilization appears to be reasonable. The CO concentrations predicted from the KM model and pure EM are fairly similar to the experimental values, while the predicted values from other cases are much lower. The predicted  $H_2O$  concentrations from three models all are different to that measured from experiments.

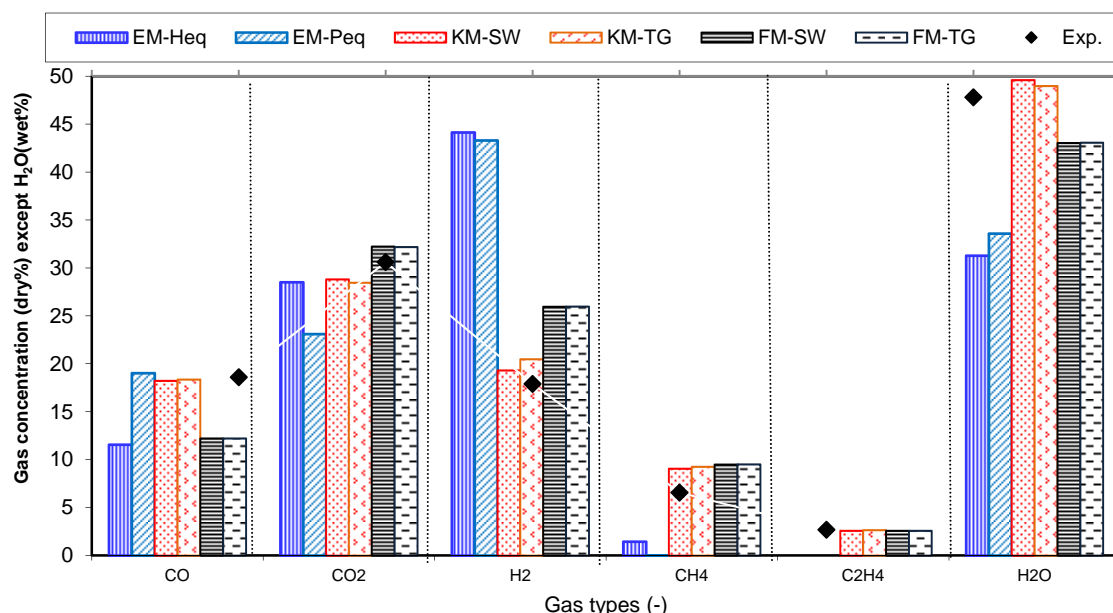


Figure 9- 14 Comparison: the product gas composition predicted from EM, KM and FM models

From these above observations, it can be concluded that the product gas composition predicted from the KM model is the closest to the experimental one, followed by that from the FM and EM model. The MSR and WGS reactions, as well as char reactions play important roles in determining the final CO,  $H_2$ ,  $CH_4$ ,  $CO_2$  and  $H_2O$  concentrations. During gasification in real processes, the WGS and MSR reactions occur in kinetics-controlling region instead of equilibrium controlling condition, and the equilibrium of MSR reaction need much longer time to reach. The product gas composition predicted from the KM-SW, KM-TG, FM-SW and FM-TG are fairly similar, which indicates that char reaction kinetics determined from TG analysis are reasonable, but still cannot fully represent their real kinetics occurring in the real gasifiers. This partly explains that why the results predicted from the FM model are slightly worse than those from the KM model, since more input values are required in the FM model while accurate input data about Agrol devolatilization is still missing. Furthermore, more complicate models generally require more input values and assumptions; therefore, more experiments and analytical instruments are needed in order to obtain reliable and confident input data.

## 9.4 Conclusion

Agrol, willow and DDGS gasification using an atmospheric pressure 100kW<sub>th</sub> steam-O<sub>2</sub> blown CFB gasifier were investigated. Three different types of model: an Equilibrium Model (EM) and a Kinetic Model (KM) setup using Aspen Plus<sup>TM</sup> software, and a Fluidization Model (FM) written in C Language and compiled using Software Bloodshed Dev-C++ were developed to predict the product gas composition under different operational conditions. In general, compared to the product gas composition obtained from experiments,  $H_2$  concentration predicted from the EM models was much higher, while CO,  $CO_2$ ,  $H_2O$  concentrations were slightly lower and almost no  $CH_4$  was predicted from the pure EM model. However, the concentrations of all gas species predicted from the KM models agreed fairly well with those obtained from experiments, except for  $H_2$  and  $CH_4$  produced from DDGS gasification. As expected, an increase in steam/biomass mass ratio (SBR) increased the yield of the product gas, but meanwhile decreased the lower heating value (LHV) of the product gas, CCE % and

CGE%. These trends predicted from the KM models agreed with those obtained from experiments. Both the EM and KM models indicated that the water-gas shift (WGS) reaction and methane steam reforming (MSR) reaction largely influenced the concentration of H<sub>2</sub>, CO, CO<sub>2</sub>, H<sub>2</sub>O and CH<sub>4</sub>. However, it is hardly possible to determine which reaction is more dominant from the predicted results.

In general, the FM model can predict the concentrations of the product gas main components along the height of the riser of the CFB gasifier in a reasonable way in view of varying some process variables, although a relatively high deviation was observed between the simulation and experimental results regarding the outlet H<sub>2</sub> and CO concentrations. The concentrations of the product gas main components appeared to mainly change in the bed zone near the fuel feed point. In this way, a slight decrease in the height of riser may not influence the product gas composition. However, in this FM model, char circulation and tar reaction kinetics are not considered, from previous experimental results, these two parameters play important roles in determine the product gas quality, and then may influence the predicted results to certain extent.

However, due to limited time, this FM model is still in “developing stage”. In order to improve the FM model, several recommendations are suggested: such as check all hydrodynamic parameters which involve in the mass balance equations in the bed and upper zone, especially those applied for the bubble phase; improve biomass devolatilization model by performing some measurements with the heated grid setup to obtain more accurate data regarding the yields of char, tar and volatile gas; refine the model by including the downcomer model, char recycle process and heat transfer; and last but not least extend reaction kinetics by considering tar conversion.



## Chapter 10 Conclusions and recommendations

---

*This chapter summarizes main conclusions drawn from this research work, and proposes some recommendations for further study.*

### 10.1 Conclusions

The main research questions covered in this dissertation concern measurement and reduction of sulfur and tar components during biomass gasification, as well as understand char reaction kinetics, to improve understanding of the gasification process and find ways to enhance the product gas quality and the overall gasification efficiency. The conclusions are given for gasification experiments, the characterization work and the modeling, respectively.

#### 10.1.1 Experimental results from CFB and PBFB tests

- Operational conditions such as gasification temperature, SBR, ER, reactor pressure and bed materials all influenced the main product gas composition produced from Agrol, willow and DDGS gasification. In general, at atmospheric pressure higher temperatures and SBR were more favorable for H<sub>2</sub> production but less advantageous for the formation of CO and CH<sub>4</sub>, whereas a higher SBR also led to a lower carbon conversion efficiency (CCE%), cold gas efficiency (CGE%) and heating values of the product gas. Higher pressures can significantly promote the formation of CH<sub>4</sub> which could be an advantage for SNG application. The product gas compositions obtained from three fuels gasification during the CFB test were different, even for two woody biomasses Agrol and willow. Under similar operational conditions H<sub>2</sub> concentration obtained from willow is the highest, and then that from Agrol and DDGS.
- Due to the low sulfur content contained in Agrol and willow fuels, almost no gaseous sulfur species were detected during gasification experiments. However, a fairly high amount of H<sub>2</sub>S (~2300 ppmv), COS (~200 ppmv) and a trace amount of methyl mercaptan (<3 ppmv) on a N<sub>2</sub> free basis were obtained from DDGS gasification. It appeared that with increasing temperature the concentration of H<sub>2</sub>S remained fairly stable, whereas the concentrations of COS and methyl mercaptan slightly decreased. An increase in the SBR value led to a decrease in the concentration of H<sub>2</sub>S accompanied with slight increase in COS concentration. Due to a relatively high K and Cl content in DDGS fuel, continually adding 3 to 10% kaolin (based on feeding rate) into the reactor was needed to avoid agglomeration.
- Similarly, different amounts of tar were produced from the three fuels, but in all cases it mainly contains phenol, cresol, naphthalene, indene and pyrene. Higher temperatures and higher SBR were favorable for tar decomposition. The content of class 5 tar obtained from three fuels using Bed 1 (treated Austrian olivine) was lower than that using Bed 2 (natural Austrian olivine), which prove Bed 1 was more reactive on the decomposition of heavy tar compounds. At a fairly low temperature of 730 °C, the total tar content produced from DDGS using Bed 1 was 7.3 g/Nm<sup>3</sup> where the contents of class 2 and 4 tars were only 1 and 1.85 g/Nm<sup>3</sup>, respectively. This is near 2 g/Nm<sup>3</sup> being considered as a limit for many downstream applications.
- Three different tar measuring techniques were applied to quantify tar content. The analyzed results showed that the measured concentration of the 10 individual tar species obtained from CFB and PBFB atmospheric pressure tests using the SPA and LIFS methods agreed reasonably well with a difference of less than 10% between the measured tar concentrations. The total tar concentration measured by the LIFS, SPA and OTA methods showed similar trends with varying process parameters. Both the LIFS and OTA methods can be used as an indicator to monitor the change of the gasifier performance in real time; however, it appeared that the LIFS method was a fairly reliable and accurate, and a regular calibration, preferable daily, of the OTA method is required to achieve reliable tar measurement results.

### ***10.1.2 Experimental results from TGA-FTIR tests***

- The analyzed results from TGA-FTIR test showed that Agrol and willow had similar pyrolysis behavior and their characteristic devolatilization temperatures and their related weight loss rates increased with increasing heating rate. The volatiles released from Agrol, willow and DDGS pyrolysis were mainly CO, CO<sub>2</sub> and H<sub>2</sub>O, followed by a small amount of CH<sub>4</sub>. The emissions of CO and CO<sub>2</sub> from Agrol and willow pyrolysis showed remarkable peaks within the temperature range of 340 to 440 °C, while the release of CH<sub>4</sub> occurred within a widely higher temperature range of 440 to 640 °C. Compared to the released behavior of CO from Agrol and willow pyrolysis, the released CO from DDGS pyrolysis occurred in a wider temperature range even up to 840°C. Some additional amounts of N compounds such as NH<sub>3</sub>, HCN, and HNCO were detected from DDGS pyrolysis.
- To determine char reaction kinetics, CFB-Char samples were collected from the downcomer of the CFB gasifier and their properties were studied. SEM images showed that Agrol chars were very porous with different superficial cavities and thin walls. Willow chars had a more compact agglomerated structure, while DDGS chars had a macroporous structure with rounded pores of different sizes and some particulates on the surface. The results observed from the EDS analysis revealed that the composition of the chars was not completely homogeneous. XRD patterns showed that char samples had a disordered graphite-like structure with Agrol showing the highest degree of crystalline order. The XRF analyzed results showed that the inorganic elements in the Agrol char were Ca, Fe, K, Mg, and Si. The willow char was mainly composed by Ca and K with minor amounts of Fe, Mg, P and Si. However, DDGS char was mainly dominated by K and P, with lower amounts of Ca, Mg and Na.
- The gasification behavior of some selected CFB-Char was compared with TG-derived pyrolysis chars (PYR-Char). In general, char gasification rate increased with increasing gasification temperature, CO<sub>2</sub> concentration and heating rate, while it decreased with increasing pyrolysis temperature. At low gasification temperature with low CO<sub>2</sub> concentration, CFB-Chars were much more reactive than PYR-Chars. The calculated activation energy (Ea) values using the SCM model were slightly lower than those using the VRM model. The Ea values for PYR-Char calculated by using both models were in the range of 90 to 210 kJ/mol, while those for CFB-Char were in the range of 55 to 120 kJ/mol. The predicted results using both models showed a reasonably good agreement with experimental results, while at higher gasification temperatures it seemed that the SCM model was becoming more suitable.
- The results obtained from the combustion of willow and DDGS CFB-Chars, and pure charcoal under isothermal conditions showed that the char combustion rate increased with increasing either O<sub>2</sub> concentrations or temperatures. There was a large difference among the determined kinetic parameters for three chars under different conditions. Within the temperature range of 750 to 900 °C, it was impossible to determine kinetic parameters for combustion experiments of DDGS and willow chars, but well possible for very low ash containing charcoal under conditions with 15 vol.% O<sub>2</sub> (Ea was around 120 kJ/mol calculated by using the SCM model). Within the temperature range of 400 to 500°C, an extremely low Ea value of around 15 kJ/mol was obtained for willow char, while the Ea value obtained from DDGS char was around 60 kJ/mol using the VRM model. The non-isothermal combustion experimental results showed that the combustion temperature ranges of three chars increased with increasing heating rate, and higher Ea values were obtained at lower conversion values.

### ***10.1.3 Modeling results***

- Thermodynamic equilibrium modeling results showed that the distribution of sulfur species during gasification was significantly influenced by fuel characteristics and process conditions (e.g., temperature, pressure and ER). The predicted results showed that H<sub>2</sub>S was the predominant sulfur

species during biomass gasification and its maximum concentration was closely related to the Fuel-S content. For all the fuels, around 95% Fuel-S converted into  $\text{H}_2\text{S}$  during the reaction. However, the percentage of Fuel-S converted into COS was largely affected by the gasifying agent applied. Minerals in the fuels played an important role in the retention of sulfur in the solid phase, especially the metal Fe. The increase of temperature was in favor of the formation of major sulfur species with a varying degree.  $\text{H}_2\text{S}$  and COS formation was promoted by an increase of pressure. ER combined with different gasifying agent appeared to have a more complicated influence on all the sulfur species.

- Sulfidation chemical phase equilibrium simulation results showed that copper, manganese and zinc oxides were the most favorable metals, which were capable of reaching even ppb level at a temperature of approximately 650 °C. However, evaporation and/or excessive temperature rising during regeneration had a negative impact on their performance, in particularly at higher temperatures. For desulfurization at a temperature higher than 900 °C, calcium based oxide exhibited a better potential than other metal oxides. However, their desulfurization capabilities were strongly influenced by the temperature range applied and the gas composition especially the  $\text{H}_2\text{O}$  and  $\text{CO}_2$  contents.
- To provide a better insight into heat transfer and fluid flow profiles within the TG furnace for the case of char combustion, the used TG furnace has been modeled using the COMSOL Multiphysics<sup>TM</sup> software. The results predicted from the 3D TG furnace model showed a fairly good agreement with the experimental ones. The predicted temperature increase during DDGS char combustion was around 14 °C which was really close to the value of approximately 12 °C observed from the experiments. The velocity profile within the TG furnace was affected by the furnace temperature and vice versa, and they both affected by the heat produced from char combustion.
- Three different types of models for CFB gasification have been developed to predict the product gas composition and yield, CCE% and CGE% obtained from Agrol, willow and DDGS gasification using the CFB gasifier. Compared to the product gas composition obtained from experiments,  $\text{H}_2$  concentration predicted from the equilibrium models (EM) was much higher, while  $\text{CO}$ ,  $\text{CO}_2$ ,  $\text{H}_2\text{O}$  concentrations were slightly lower and almost no  $\text{CH}_4$  was predicted from the pure EM model. However, the concentrations of all gas species predicted from the kinetic models (KM) agreed fairly well with those obtained from experiments. As expected, an increase in SBR increased the yield of the product gas, but meanwhile decreased the LHV of the product gas, CCE % and CGE%. These trends predicted from the KM models agreed with those obtained from experiments. Both the EM and KM models indicated that the WGS reaction and the MSR reaction largely influenced the concentration of  $\text{H}_2$ ,  $\text{CO}$ ,  $\text{CO}_2$ ,  $\text{H}_2\text{O}$  and  $\text{CH}_4$ .

## **10.2 Recommendations**

- Effects of ER and bed material on tar formation during Agrol, willow and DDGS gasification in the CFB gasifier have still not entirely clearly been elucidated, as well as effects of SBR, ER and temperature on the distribution of  $\text{H}_2\text{S}$  and COS produced from DDGS gasification. Furthermore, an agglomeration phenomenon was observed during DDGS gasification at a temperature higher than 810 °C when no additive kaolin was added. So far, it is still unknown what the initial defluidization temperature for DDGS gasification is without adding additive, as well as how kaolin can avoid the agglomeration problem. Therefore, some additional experiments may be needed to investigate effects of ER and bed materials on tar and sulfur formation, as well as modelling study using Factsage<sup>TM</sup> to get a better insight of the defluidization behavior of DDGS gasification.
- Sulfur capture during DDGS gasification in the CFB gasifier using various developed sorbents was originally planned within this research. However, due to sulfur sorbent materials delivery

problem from the GreenSyngas project partner, in-bed desulfurization unfortunately could not be carried out. Although sulfur capture capabilities of single metal oxides such as ZnO, Fe<sub>2</sub>O<sub>3</sub>, CuO and MnO was tested applying TGA by using an artificial gas H<sub>2</sub>S in N<sub>2</sub> from the gas cylinder, the sulfidation results are far from satisfactory (see **Figure A-15**, Appendix), probably due to the comparatively low flexibility (e.g., low available sorbent surface) of the TGA instrument. Therefore, sulfur capture inside the CFB gasifier and sulfidation of single and mixed metal oxides using a different setup (e.g., a fixed bed) is suggested.

- The physical and chemical characteristics of different CFB-Chars have been studied. However, since char samples from Agrol, willow and DDGS were collected after these fuel gasification tests that were performed under somewhat different operational conditions, it is fairly difficult to determine how operational conditions such as SBR, ER and temperature exactly influence char microstructure. To better understand the morphological structure of Agrol, willow and DDGS chars, some char samples collected under practically identical operational conditions need to be studied. Furthermore, as comparison, the properties of TG-derived pyrolysis char produced under different heating rates are better to be analyzed by different analytical techniques. If possible, the difference in the reactivity between in-situ and ex-situ char needs to be further studied.
- The gasification and combustion behavior of different chars were studied by using the simplified artificial gas CO<sub>2</sub> (or Air) in N<sub>2</sub>. However, during biomass gasification in a real gasifier, char reaction is generally affected by other gas compounds such as H<sub>2</sub> and H<sub>2</sub>O. Therefore, the study of the gasification and combustion behavior of different chars using an artificial product gas is recommended. Furthermore, catalytic influences of inorganic elements on char gasification and combustion rate were observed, but still have not well been defined and systematically explored in this work. More investigations combining different pre-treatments to lower and/or increase inorganic element contents in the ash are necessary in order to get a better insight into their influences.
- The distribution of sulfur species and capture during biomass gasification has been simulated. The Factsage<sup>TM</sup> equilibrium model appeared to be useful in predicting their behaviors. However, a pure-equilibrium model has its limitations since chemical reaction rates and mass transfer in the real gasification process are usually determining conversion. Therefore, the simulation results presented here only can be a reference for understanding sulfur species formation, improving the efficiency of sorbent utilization and optimizing the desulfurization process. This needs to be further validated by experimental data.
- The kinetic parameters for char gasification and combustion were determined by using the simple models, such as volume reaction model (VRM) and shrinking core model (SCM). Char structure change during reaction was not considered. To improve the modeling results, more complicated models such as random pore model, changing grain size model are recommended to interpret the experimental data.
- The modeling of the CFB gasifier in this work mainly focused on the prediction of the product gas composition and the equilibrium analysis of water-gas shift reaction (WGS) and methane steam reforming (MSR) reaction. The FM model is still in “developing stage”, thus need be further improved by checking all hydrodynamic parameters which involve in the mass balance equations in the bed and upper zone, especially those applied for the bubble phase; improving biomass devolatilization model by performing some measurements with the heated grid setup to obtain more accurate data regarding the yields of char, tar and volatile gas; refining the model by including the downcomer model, char recycle process and heat transfer; and extending reaction kinetics by considering tar conversion.



## Bibliography

---

- Abbasian, J., Rehmat, A., Leppin, D., Banerjee, D.D. 1990. Desulfurization of fuels with calcium-based sorbents. *Fuel Processing Technology*, **25**(1), 1-15.
- Abbasian, J., Slimane, R.B. 1998. A regenerable copper-based sorbent for H<sub>2</sub>S removal from coal gases. *Industrial & engineering chemistry research*, **37**(7), 2775-2782.
- Adanez, J., Garcia-Labiano, F., De Diego, L., Fierro, V. 1999. Utilization of calcium acetate and calcium magnesium acetate for H<sub>2</sub>S removal in coal gas cleaning at high temperatures. *Energy & Fuels*, **13**(2), 440-448.
- Adanez, J., Gayán, P., Grasa, G., de Diego, L.F., Armesto, L., Cabanillas, A. 2001. Circulating fluidized bed combustion in the turbulent regime: modelling of carbon combustion efficiency and sulphur retention. *Fuel*, **80**(10), 1405-1414.
- Ahmadi, M., Brage, C., Sjoström, K., Engvall, K., Knoef, H., Van de Beld, B. 2011. Development of an on-line tar measurement method based on photo ionization technique. *Catalysis Today*, **176**(1), 250-252.
- Aho, A., Kumar, N., Eränen, K., Salmi, T., Hupa, M., Murzin, D.Y. 2008. Catalytic pyrolysis of woody biomass in a fluidized bed reactor: Influence of the zeolite structure. *Fuel*, **87**(12), 2493-2501.
- Alonso, L., Palacios, J., Garcia, E., Moliner, R. 2000. Characterization of Mn and Cu oxides as regenerable sorbents for hot coal gas desulfurization. *Fuel Processing Technology*, **62**(1), 31-44.
- Altafini, C.R., Wander, P.R., Barreto, R.M. 2003. Prediction of the working parameters of a wood waste gasifier through an equilibrium model. *Energy conversion and management*, **44**(17), 2763-2777.
- Anthony, E., Jia, L., Caris, M., Preto, F., Burwell, S. 1999. An examination of the exothermic nature of fluidized bed combustion (FBC) residues. *Waste Management*, **19**(4), 293-305.
- Aqsha, A., Mahinpey, N., Mani, T., Salak, F., Murugan, P. 2011. Study of sawdust pyrolysis and its devolatilisation kinetics. *The Canadian Journal of Chemical Engineering*, **9999**, 1-7.
- Atakul, H., Wakker, J.P., Gerritsen, A.W., van den Berg, P.J. 1995. Removal of H<sub>2</sub>S from fuel gases at high temperatures using MnO/[gamma]-Al<sub>2</sub>O<sub>3</sub>. *Fuel*, **74**(2), 187-191.
- Attar, A. 1978. Chemistry, thermodynamics and kinetics of reactions of sulphur in coal-gas reactions: A review. *Fuel*, **57**(4), 201-212.
- Attar, A., Dupuis, F. 1979. The rate and the fundamental mechanisms of the reaction of hydrogen sulfide with the basic minerals in coal. *Industrial & Engineering Chemistry Process Design and Development*, **18**(4), 607-618.
- Avila, C., Lester, E. 2008. The characterization of biomass and their subsequent chars using microscopy and thermogravimetric analysis. University of Nottingham.
- Ayala, R., Gal, E., Gupta, R. 1992. Enhanced durability of high-temperature desulfurization sorbents for moving-bed applications. General Electric Co., Schenectady, NY (United States). Corporate Research and Development Center.
- Aznar, M.P., Caballero, M.A., Gil, J., Martin, J.A., Corella, J. 1998. Commercial steam reforming catalysts to improve biomass gasification with steam-oxygen mixtures. 2. Catalytic tar removal. *Industrial & engineering chemistry research*, **37**(7), 2668-2680.
- Aznar, M.P., Corella, J., Gil, J., Martin, J.A., Caballero, M.A., Olivares, A., Perez, P., Frances, E. 1997. Biomass gasification with steam and oxygen mixtures at pilot scale and with catalytic gas upgrading. Part I: Performance of the gasifier *Developments in Thermochemical Biomass Conversion*, **2**, 1194-1208.
- Babu, B.V. 2008. Biomass pyrolysis: a state of the art review. *Biofuels, Bioproducts and Biorefining*, **2**(5), 393-414.
- Bakker, W.J.W., Kapteijn, F., Moulijn, J.A. 2003. A high capacity manganese-based sorbent for regenerative high temperature desulfurization with direct sulfur production:: Conceptual process application to coal gas cleaning. *Chemical Engineering Journal*, **96**(1-3), 223-235.
- Balat, M., Kirtay, E., Balat, H. 2009. Main routes for the thermo-conversion of biomass into fuels and chemicals. Part I: Pyrolysis systems. *Energy conversion and management*, **50**(12), 3147-3157.
- Bale, C., Chartrand, P., Degterov, S., Eriksson, G., Hack, K., Ben Mahfoud, R., Melançon, J., Pelton, A., Petersen, S. 2002. FactSage thermochemical software and databases. *Calphad*, **26**(2), 189-228.
- Bassilakis, R., Carangelo, R., Wojtowicz, M. 2001. TG-FTIR analysis of biomass pyrolysis. *Fuel*, **80**(12), 1765-1786.
- Basu, P., Kaushal, P. 2009. Modeling of pyrolysis and gasification of biomass in fluidized beds: A review. *Chemical Product and Process Modeling*, **4**(1), 21.
- Basu, P., Sett, A., Gbordzoe, E. 1987. A simplified model for combustion of carbon in a circulating fluidized bed combustor. *Proceedings of the IX International Conference on Fluidized Bed Combustion ASME*, , New York. pp. 738-742.

- Ben-Slimane, R., Hepworth, M. 1994a. Desulfurization of hot coal-derived fuel gases with manganese-based regenerable sorbents. 1. Loading (sulfidation) tests. *Energy & Fuels*, **8**(6), 1175-1183.
- Ben-Slimane, R., Hepworth, M. 1994b. Desulfurization of hot coal-derived fuel gases with manganese-based regenerable sorbents. 2. Regeneration and multicycle tests. *Energy & Fuels*, **8**(6), 1184-1191.
- Ben-Slimane, R., Hepworth, M. 1995. Desulfurization of hot coal-derived fuel gases with manganese-based regenerable sorbents. 3. fixed-bed testing. *Energy & Fuels*, **9**(2), 372-378.
- Berns, J.J., Sadecki, K.A., Hepworth, M.T. 1997. Kinetics of Mn-Based sorbents for hot coal gas desulfurization. Federal Energy Technology Center (FETC), Morgantown, WV, and Pittsburgh, PA.
- Bhat, A., Ram Bheemarasetti, J., Rajeswara Rao, T. 2001. Kinetics of rice husk char gasification. *Energy conversion and management*, **42**(18), 2061-2069.
- Bi, H.T. 2002. Some Issues on Core Annulus and Cluster Models of Circulating Fluidized Bed Reactors. *The Canadian Journal of Chemical Engineering*, **80**(5), 809-817.
- Biagini, E., Fantei, A., Tognotti, L. 2008. Effect of the heating rate on the devolatilization of biomass residues. *Thermochimica acta*, **472**(1-2), 55-63.
- Bioenergy. 2011. Bioenergy: power and heat generation, European commission SETIS strategic energy technology information systems, Vol. 2012, JRC. <http://setis.ec.europa.eu/newsroom-items-folder/bioenergy-power-and-heat-generation>.
- Biomass. 2010. Biomass for Heat and Power, IEA ETSAP - Technology Brief E05 - May 2010 - [www.etsap.org](http://www.etsap.org).
- Boateng, A., Walawender, W., Fan, L., Chee, C. 1992. Fluidized-bed steam gasification of rice hull. *Bioresource technology*, **40**(3), 235-239.
- Boerrigter, H., Calis, H.P., Slort, D.J., Bodestaff, H., Kaandorp, A.J., den Uil, H., Rabou, L.P.L.M. 2004. Gas cleaning for integrated biomass gasification (BG) and Fischer-Tropsch (FT) systems; experimental demonstration of two BG-FT systems. ECN.
- Borgwardt, R.H., Roache, N.F. 1984. Reaction of hydrogen sulfide and sulfur with limestone particles. *Industrial & Engineering Chemistry Process Design and Development*, **23**(4), 742-748.
- Brage, C., Sjöström, K. 1991. Separation of phenols and aromatic hydrocarbons from biomass tar using aminopropylsilane normal-phase liquid chromatography. *Journal of Chromatography A*, **538**(2), 303-310.
- Brage, C., Yu, Q., Chen, G., Sjöström, K. 2000. Tar evolution profiles obtained from gasification of biomass and coal. *Biomass and Bioenergy*, **18**(1), 87-91.
- Brage, C., Yu, Q., Chen, G., Sjöström, K. 1997. Use of amino phase adsorbent for biomass tar sampling and separation. *Fuel*, **76**(2), 137-142.
- Branca, C., Albano, A., Di Blasi, C. 2005. Critical evaluation of global mechanisms of wood devolatilization. *Thermochimica acta*, **429**(2), 133-141.
- Branca, C., Di Blasi, C. 2003. Devolatilization and combustion kinetics of wood chars. *Energy Fuels*, **17**, 1609-1615.
- Branca, C., Iannace, A., Di Blasi, C. 2007. Devolatilization and Combustion Kinetics of Quercus cerris Bark. *Energy & Fuels*, **21**(2), 1078-1084.
- Brewer, C.E., Schmidt Rohr, K., Satrio, J.A., Brown, R.C. 2009. Characterization of biochar from fast pyrolysis and gasification systems. *Environmental Progress & Sustainable Energy*, **28**(3), 386-396.
- Bridgwater, A. 1994. Catalysis in thermal biomass conversion. *Applied Catalysis A: General*, **116**(1-2), 5-47.
- Bridgwater, A. 2003. Renewable fuels and chemicals by thermal processing of biomass. *Chemical Engineering Journal*, **91**(2-3), 87-102.
- Bu, X., Ying, Y., Zhang, C., Peng, W. 2008. Research improvement in Zn-based sorbent for hot gas desulfurization. *Powder Technology*, **180**(1-2), 253-258.
- Bui, T., Loof, R., Bhattacharya, S. 1994. Multi-stage reactor for thermal gasification of wood. *Energy*, **19**(4), 397-404.
- Bunt, J., Waanders, F. 2008. An understanding of the behaviour of a number of element phases impacting on a commercial-scale Sasol-Lurgi FBDB gasifier. *Fuel*, **87**(10-11), 1751-1762.
- Campoy, M., Go mez-Barea, A., Fuentes-Cano, D., Ollero, P. 2010. Tar Reduction by Primary Measures in an Autothermal Air-Blown Fluidized Bed Biomass Gasifier. *Industrial & engineering chemistry research*, **49** (22), 11294-11301.
- Carpenter, D.L., Deutch, S.P., French, R.J. 2007. Quantitative measurement of biomass gasifier tars using a molecular-beam mass spectrometer: Comparison with traditional impinger sampling. *Energy & Fuels*, **21**(5), 3036-3043.
- Cetin, E., Gupta, R., Moghtaderi, B. 2005. Effect of pyrolysis pressure and heating rate on radiata pine char structure and apparent gasification reactivity. *Fuel*, **84**(10), 1328-1334.
- Cetin, E., Moghtaderi, B., Gupta, R., Wall, T. 2004. Influence of pyrolysis conditions on the structure and gasification reactivity of biomass chars. *Fuel*, **83**(16), 2139-2150.

- Chang, J., Leung, D.Y.C., Wu, C., Yuan, Z. 2003. A review on the energy production, consumption, and prospect of renewable energy in China. *Renewable and Sustainable Energy Reviews*, **7**(5), 453-468.
- Channiwala, S., Parikh, P. 2002. A unified correlation for estimating HHV of solid, liquid and gaseous fuels. *Fuel*, **81**(8), 1051-1063.
- Chen, G., Yu, Q., Sjöström, K. 1997. Reactivity of char from pyrolysis of birch wood. *Journal of Analytical and Applied Pyrolysis*, **40**, 491-499.
- Chen, H., Li, B., Zhang, B. 1999. Effects of mineral matter on products and sulfur distributions in hydrolysis. *Fuel*, **78**(6), 713-719.
- Chen, J.S., Gunkel, W.W. 1987. Modeling and simulation of co-current moving bed gasification reactors--Part II. A detailed gasifier model. *Biomass*, **14**(2), 75-98.
- Chopra, S., Jain, A.K. 2007. A review of fixed bed gasification systems for biomass. *Agricultural Engineering International: CIGR Journal*, **Invited Overview No. 5**(IX).
- Comsol, A. 2010. Hydrocarbon Dehalogenation in a Tortuous Microreactor, Model gallery, Model ID: 2182.
- Corella, J., Aznar, M.P., Gil, J., Caballero, M.A. 1999. Biomass gasification in fluidized bed: where to locate the dolomite to improve gasification? *Energy & Fuels*, **13**(6), 1122-1127.
- Corella, J., Sanz, A. 2005. Modeling circulating fluidized bed biomass gasifiers. A pseudo-rigorous model for stationary state. *Fuel Processing Technology*, **86**(9), 1021-1053.
- Cozzani, V. 2000. Reactivity in oxygen and carbon dioxide of char formed in the pyrolysis of refuse-derived fuel. *Industrial & engineering chemistry research*, **39**(4), 864-872.
- Czakiert, T., Nowak, W. 2009. Kinetics of coal char combustion under oxygen-enhanced conditions. *Proceeding of European Combustion meeting 2009, Vienna, Austria, 14-17 April, pp1-6*
- Darvell, L., Jones, J., Gudka, B., Baxter, X., Saddawi, A., Williams, A., Malmgren, A. 2010. Combustion properties of some power station biomass fuels. *Fuel*, **89**(10), 2881-2890.
- Datar, R.P., Shenkman, R.M., Cateni, B.G., Huhnke, R.L., Lewis, R.S. 2004. Fermentation of biomass generated producer gas to ethanol. *Biotechnology and Bioengineering*, **86**(5), 587-594.
- De Jong, W. 2005. Nitrogen compounds in pressurised fluidised bed gasification of biomass and fossil fuels. in: *Process and Energy* Vol. dr, Delft University of Technology. Delft.
- de Souza-Santos, M.L. 2004. *Solid fuels combustion and gasification: modeling, simulation, and equipment operation*. CRC.
- DeGroot, W.F., Shafizadeh, F. 1984. Kinetics of gasification of Douglas Fir and Cottonwood chars by carbon dioxide. *Fuel*, **63**(2), 210-216.
- Demirba, A. 2001. Biomass resource facilities and biomass conversion processing for fuels and chemicals. *Energy conversion and management*, **42**(11), 1357-1378.
- Demirbas, A. 2005a. Bioethanol from cellulosic materials: A renewable motor fuel from biomass. *Energy Sources-Journal of Extraction Conversion and the Environment*, **27**(4), 327-338.
- Demirbas, A. 2002. Hydrogen production from biomass by the gasification process. *Energy sources*, **24**(1), 59-68.
- Demirbas, A. 2005b. Influence of gas and detrimental metal emissions from biomass firing and co-firing on environmental impact. *Energy sources*, **27**(15), 1419-1428.
- Devi, L., Ptasiński, K.J., Janssen, F.J.J.G. 2003. A review of the primary measures for tar elimination in biomass gasification processes. *Biomass and Bioenergy*, **24**(2), 125-140.
- Di Blasi, C. 2009. Combustion and gasification rates of lignocellulosic chars. *Progress in energy and combustion science*, **35**(2), 121-140.
- Di Blasi, C., Branca, C., D'Errico, G. 2000. Degradation characteristics of straw and washed straw. *Thermochimica acta*, **364**(1), 133-142.
- Di Blasi, C., Buonanno, F., Branca, C. 1999a. Reactivities of some biomass chars in air. *Carbon*, **37**(8), 1227-1238.
- Di Blasi, C., Signorelli, G., Di Russo, C., Rea, G. 1999b. Product distribution from pyrolysis of wood and agricultural residues. *Industrial & engineering chemistry research*, **38**(6), 2216-2224.
- Dias, M., Gulyurtlu, I. 2008. H<sub>2</sub>S and HCl formation during RDF and coal co-gasification: a comparison between the predictions and experimental results *Proceedings of the Biomass Gasification Technologies Workshop*, MRC Gebze Campus, Turkey pp. 1-14.
- Doherty, W., Reynolds, A., Kennedy, D. 2009. The effect of air preheating in a biomass CFB gasifier using ASPEN Plus simulation. *Biomass and Bioenergy*, **33**(9), 1158-1167.
- Dutta, S., Wen, C. 1977. Reactivity of Coal and Char. 2. In Oxygen-Nitrogen Atmosphere. *Industrial & Engineering Chemistry Process Design and Development*, **16**(1), 31-37.
- El-Rub, A., Kamel, Z.Y. 2008. Biomass char as an in-situ catalyst for tar removal in gasification systems, Vol. Doctor, University of Twente Enschede, the Netherlands.
- El-Rub, Z.A., Bramer, E., Brem, G. 2004. Review of catalysts for tar elimination in biomass gasification processes. *Industrial & engineering chemistry research*, **43**(22), 6911-6919.

- Elseviers, W., Verelst, H. 1999. Transition metal oxides for hot gas desulphurisation. *Fuel*, **78**(5), 601-612.
- Encinar, J., Gonzalez, J., Gonzalez, J. 2002. Steam gasification of *Cynara cardunculus* L.: influence of variables. *Fuel Processing Technology*, **75**(1), 27-43.
- Entorun, Ç., Küçükbayrak, S. 1996. Effect of mineral matter on the burning profile of lignites. *Thermochimica acta*, **285**(1), 35-46.
- Esplin, G., Fung, D., Hsu, C. 1985. Development of sampling and analytical procedures for biomass gasifiers. *The Canadian Journal of Chemical Engineering*, **63**(6), 946-953.
- Evans, R., Milne, T. 1998. Chemistry of tar formation and maturation in the thermochemical conversion of biomass. Elsevier. pp. 197-198.
- Faaij, A.P.C. 2006. Bio-energy in Europe: changing technology choices. *Energy policy*, **34**(3), 322-342.
- Fan, H.L., Li, C.H. 2005. Testing of iron oxide sorbent for high-temperature coal gas desulfurization. *Energy sources*, **27**(3), 245-250.
- Fang, Y., Huang, J., Wang, Y., Zhang, B. 2001. Experiment and mathematical modeling of a bench-scale circulating fluidized bed gasifier. *Fuel Processing Technology*, **69**(1), 29-44.
- Fenouil, L. 1994. Kinetic and structural studies of the sulfidation of large particles of lime and limestone in coal gas. *Paper presented at AIChE Annual Meeting, San Francisco, CA, Nov. 16.*
- Fenouil, L.A., Lynn, S. 1995. Study of calcium-based sorbents for high-temperature H<sub>2</sub>S removal. 3. Comparison of calcium-based sorbents for coal gas desulfurization. *Industrial & engineering chemistry research*, **34**(7), 2343-2348.
- Fermoso, J., Stevanov, C., Moghtaderi, B., Arias, B., Pevida, C., Plaza, M., Rubiera, F., Pis, J. 2009. High-pressure gasification reactivity of biomass chars produced at different temperatures. *Journal of Analytical and Applied Pyrolysis*, **85**(1-2), 287-293.
- Fischer, G., Schrattenholzer, L. 2001. Global bioenergy potentials through 2050. *Biomass and Bioenergy*, **20**(3), 151-159.
- Focht, G., Ranade, P., Harrison, D. 1988. High-temperature desulfurization using zinc ferrite: reduction and sulfidation kinetics. *Chemical Engineering Science*, **43**(11), 3005-3013.
- Fogler, H.S. 1999. *Elements of chemical reaction engineering*, 3<sup>rd</sup> version. Prentice-Hall, Inc., (now known as Pearson Education, Inc.), New Jersey.
- Franco, C., Pinto, F., Gulyurtlu, I., Cabrita, I. 2003. The study of reactions influencing the biomass steam gasification process. *Fuel*, **82**(7), 835-842.
- Fu, P., Hu, S., Xiang, J., Sun, L., Li, P., Zhang, J., Zheng, C. 2009. Pyrolysis of Maize Stalk on the Characterization of Chars Formed under Different Devolatilization Conditions. *Energy & Fuels*, **23**(9), 4605-4611.
- Fuda, K., Palmer, A.D., Sears, P., Blais, D., Furimsky, E. 1991. Chemical changes occurring during sulphidation and regeneration of iron-containing sorbents. *Fuel*, **70**(1), 100-106.
- Fushimi, C., Araki, K., Yamaguchi, Y., Tsutsumi, A. 2003. Effect of heating rate on steam gasification of biomass. 1. Reactivity of char. *Industrial & engineering chemistry research*, **42**(17), 3922-3928.
- Garcia-Labiano, F., De Diego, L., Adanez, J. 1999. Effectiveness of natural, commercial, and modified calcium-based sorbents as H<sub>2</sub>S removal agents at high temperatures. *Environmental science & technology*, **33**(2), 288-293.
- Garcia, E., Cilleruelo, C., Ibarra, J.V., Pineda, M., Palacios, J.M. 1997. Kinetic study of high-temperature removal of H<sub>2</sub>S by novel metal oxide sorbents. *Industrial & engineering chemistry research*, **36**(3), 846-853.
- Garcia, E., Palacios, J., Alonso, L., Moliner, R. 2000. Performance of Mn and Cu mixed oxides as regenerable sorbents for hot coal gas desulfurization. *Energy & Fuels*, **14**(6), 1296-1303.
- Gasper-Galvin, L.D., Atimtay, A.T., Gupta, R.P. 1998. Zeolite-supported metal oxide sorbents for hot-gas desulfurization. *Industrial & engineering chemistry research*, **37**(10), 4157-4166.
- Gautam, G., Adhikari, S., Bhavnani, S. 2010. Estimation of Biomass Synthesis Gas Composition using Equilibrium Modeling. *Energy & Fuels*, **24**(4), 2692-2698.
- Gebhard, S.C., Wang, D., Overend, R.P., Paisley, M.A. 1994. Catalytic conditioning of synthesis gas produced by biomass gasification. *Biomass and Bioenergy*, **7**(1-6), 307-313.
- Gerasimov, G.Y., Bogacheva, T. 2001a. Modeling of the Transformation of Sulfur Compounds in Oxygen Gasification of Coal Dust. *Combustion, Explosion, and Shock Waves*, **37**(4), 406-412.
- Gerasimov, G.Y., Bogacheva, T. 2001b. Thermodynamic analysis of the process of formation of sulfur compounds in oxygen gasification of coal. *Journal of engineering physics and thermophysics*, **74**(3), 806-812.
- Gheorghe, C., Marculescu, C., Badea, A., Dinca, C., Apostol, T. 2009. Effect of pyrolysis conditions on bio-char production from biomass. *Proceedings of the 3rd WSEAS Int. Conf. on Renewable Energy Sources*, July 1-3 2009, Tenerife Canary Island, Spain. pp. 239-241.

- Gil, J., Aznar, M.P., Caballero, M.A., Francés, E., Corella, J. 1997. Biomass gasification in fluidized bed at pilot scale with steam-oxygen mixtures. Product distribution for very different operating conditions. *Energy & Fuels*, **11**(6), 1109-1118.
- Gil, J., Corella, J., Aznar, M.P., Caballero, M.A. 1999. Biomass gasification in atmospheric and bubbling fluidized bed: Effect of the type of gasifying agent on the product distribution. *Biomass and Bioenergy*, **17**(5), 389-403.
- Giuntoli, J., Arvelakis, S., Spliethoff, H., de Jong, W., Verkoijen, A. 2009a. Quantitative and kinetic thermogravimetric Fourier transform infrared (TG-FTIR) study of pyrolysis of agricultural residues: Influence of different pretreatments. *Energy & Fuels*, **23**(11), 5695-5706.
- Giuntoli, J., De Jong, W., Arvelakis, S., Spliethoff, H., Verkoijen, A. 2009b. Quantitative and kinetic TG-FTIR study of biomass residue pyrolysis: Dry distiller's grains with solubles (DDGS) and chicken manure. *Journal of Analytical and Applied Pyrolysis*, **85**(1-2), 301-312.
- Goldemberg, J., Coelho, S.T., Guardabassi, P. 2008. The sustainability of ethanol production from sugarcane. *Energy policy*, **36**(6), 2086-2097.
- Gómez-Barea, A., Leckner, B. 2010. Modeling of biomass gasification in fluidized bed. *Progress in energy and combustion science*, **36**(4), 444-509.
- Gómez-Barea, A., Ollero, P., Fernández-Baco, C. 2006. Diffusional effects in CO<sub>2</sub> gasification experiments with single biomass char particles. 1. Experimental investigation. *Energy & Fuels*, **20**(5), 2202-2210.
- Goyal, P., Verma, V., Singh, R., Vaze, K. 2010. Thermal Analysis of Joule Heated Ceramic Melter. *Proceedings of the COMSOL Conference 2010*, October 29-30, 2010, Bangalore, India.
- Greensyngas. 2008-2011. Advanced Cleaning Devices for Production of Green Syngas, Vol. 2012. <http://www.eat.lth.se/greensyngas/>.
- Grimm, A., Skoglund, N., Bostrom, D., Ohman, M. 2011. Bed Agglomeration Characteristics in Fluidized Quartz Bed Combustion of Phosphorus-Rich Biomass Fuels. *Energy & Fuels*, **25**(3), 937-947.
- Groeneveld, M.J., Van Swaaij, W. 1980. 39 Gasification of char particles with CO<sub>2</sub> AND H<sub>2</sub>O. *Chemical Engineering Science*, **35**(1-2), 307-313.
- Grønli, M.G., Várhegyi, G., Di Blasi, C. 2002. Thermogravimetric analysis and devolatilization kinetics of wood. *Industrial & engineering chemistry research*, **41**(17), 4201-4208.
- Guekens, A., Schoeters, J. 1984. *Mathematical modelling in gasification*. In: A.V. Bridgewater, Editor, Thermochemical processing of biomass, Butterworths, London.
- Guerrero, M., Ruiz, M., Alzueta, M., Bilbao, R., Millera, A. 2005. Pyrolysis of eucalyptus at different heating rates: studies of char characterization and oxidative reactivity. *Journal of Analytical and Applied Pyrolysis*, **74**(1-2), 307-314.
- Guerrero, M., Ruiz, M.P., Millera, Á., Alzueta, M.U., Bilbao, R. 2008. Characterization of biomass chars formed under different devolatilization conditions: differences between rice husk and eucalyptus. *Energy & Fuels*, **22**(2), 1275-1284.
- Gungor, A., Eskin, N. 2007. Analysis of environmental benefits of CFB combustors via one-dimensional model. *Chemical Engineering Journal*, **131**(1-3), 301-317.
- Gungor, A., Eskin, N. 2008. Two-dimensional coal combustion modeling of CFB. *International Journal of Thermal Sciences*, **47**(2), 157-174.
- Gupta, R., Gangwal, S., Jain, S. 1992. Development of zinc ferrite sorbents for desulfurization of hot coal gas in a fluid-bed reactor. *Energy & Fuels*, **6**(1), 21-27.
- Han, J., Kim, H. 2008. The reduction and control technology of tar during biomass gasification/pyrolysis: an overview. *Renewable and Sustainable Energy Reviews*, **12**(2), 397-416.
- Hannula, I., Kurkela, E. 2010. A semi-empirical model for pressurised air-blown fluidised-bed gasification of biomass. *Bioresource technology*, **101**(12), 4608-4615.
- Hartge, E.U., Luecke, K., Werther, J. 1999. The role of mixing in the performance of CFB reactors. *Chemical Engineering Science*, **54**(22), 5393-5407.
- Haryanto, A., Fernando, S.D., Pordesimo, L.O., Adhikari, S. 2009. Upgrading of syngas derived from biomass gasification: A thermodynamic analysis. *Biomass and Bioenergy*, **33**(5), 882-889.
- Haykiri-Akman, H., Ersoy-Meriboyu, A., Küçükbayrak, S. 2001. Effect of mineral matter on the reactivity of lignite chars. *Energy conversion and management*, **42**(1), 11-20.
- Heinbockel, I., Fett, F. 1995. Simulation of a combined cycle power based on a pressurized circulating fluidized bed combustor. *Heat Recovery System & CHP*, **15**(2), 171-178.
- Herguido, J., Corella, J., Gonzalez-Saiz, J. 1992. Steam gasification of lignocellulosic residues in a fluidized bed at a small pilot scale. Effect of the type of feedstock. *Industrial & engineering chemistry research*, **31**(5), 1274-1282.
- Higman, C., Van der Burgt, M. 2003. *Gasification*. Gulf Professional Publishing.
- Hoffman, J.D. 2001. *Numerical methods for engineers and scientists*. CRC Press.



- Hofmann, P., Panopoulos, K., Aravind, P., Siedlecki, M., Schweiger, A., Karl, J., Ouweltjes, J., Kakaras, E. 2009. Operation of solid oxide fuel cell on biomass product gas with tar levels > 10 g Nm<sup>-3</sup>. *International Journal of Hydrogen Energy*, **34**(22), 9203-9212.
- Horio, M., Nonaka, A. 1987. A generalized bubble diameter correlation for gas-solid fluidized beds. *AIChE Journal*, **33**(11), 1865-1872.
- Horne, P.A., Williams, P.T. 1996. Upgrading of biomass-derived pyrolytic vapours over zeolite ZSM-5 catalyst: effect of catalyst dilution on product yields. *Fuel*, **75**(9), 1043-1050.
- Hu, Y., Nikzat, H., Nawata, M., Kobayashi, N., Hasatani, M. 2001. The characteristics of coal-char oxidation under high partial pressure of oxygen. *Fuel*, **80**(14), 2111-2116.
- Hua, Y., Flamant, G., Lu, J., Gauthier, D. 2004. Modelling of axial and radial solid segregation in a CFB boiler. *Chemical engineering and processing*, **43**(8), 971-978.
- Huang, H.J., Ramaswamy, S. 2009. Modeling biomass gasification using thermodynamic equilibrium approach. *Applied biochemistry and biotechnology*, **154**(1), 14-25.
- Huang, Y., Yin, X., Wu, C., Wang, C., Xie, J., Zhou, Z., Ma, L., Li, H. 2009. Effects of metal catalysts on CO<sub>2</sub> gasification reactivity of biomass char. *Biotechnology advances*, **27**(5), 568-572.
- Huilin, L., Guangbo, Z., Rushan, B., Yongjin, C., Gidaspo, D. 2000. A coal combustion model for circulating fluidized bed boilers. *Fuel*, **79**(2), 165-172.
- Hurt, R.H. 1998. Structure, properties, and reactivity of solid fuels. *Symposium (International) on Combustion*, **27**(2), 2887-2904.
- Hyppanen, T., Lee, Y., Rainio, A. 1991. A three-dimensional model for circulating fluidized bed combustion. *Circulating Fluidized Bed Technology III*, Pergamon Press, Oxford, 563-568.
- Ikenaga, N., Ohgaito, Y., Matsushima, H., Suzuki, T. 2004. Preparation of zinc ferrite in the presence of carbon material and its application to hot-gas cleaning. *Fuel*, **83**(6), 661-669.
- Janse, A.M.C., de Jonge, H.G., Prins, W., van Swaaij, W.P.M. 1998. Combustion kinetics of char obtained by flash pyrolysis of pine wood. *Industrial & engineering chemistry research*, **37**(10), 3909-3918.
- Jappe Frandsen, F. 2005. Utilizing biomass and waste for power production—a decade of contributing to the understanding, interpretation and analysis of deposits and corrosion products. *Fuel*, **84**(10), 1277-1294.
- Jarungthammachote, S., Dutta, A. 2008. Equilibrium modeling of gasification: Gibbs free energy minimization approach and its application to spouted bed and spout-fluid bed gasifiers. *Energy conversion and management*, **49**(6), 1345-1356.
- Jarungthammachote, S., Dutta, A. 2007. Thermodynamic equilibrium model and second law analysis of a downdraft waste gasifier. *Energy*, **32**(9), 1660-1669.
- Jazbec, M., Sendt, K., Haynes, B.S. 2004. Kinetic and thermodynamic analysis of the fate of sulphur compounds in gasification products. *Fuel*, **83**(16), 2133-2138.
- Jeguirim, M., Dorge, S., Loth, A., Trouvé, G. 2010. Devolatilization kinetics of Miscanthus straw from thermogravimetric analysis. *International journal of green energy*, **7**(2), 164-173.
- Jennen, T., Hiller, R., Köneke, D., Weinspach, P.M. 1999. Modeling of gasification of wood in a circulating fluidized bed. *Chemical engineering & technology*, **22**(10), 822-826.
- Jensen, A., Dam-Johansen, K., Wójtcowicz, M.A., Serio, M.A. 1998. TG-FTIR study of the influence of potassium chloride on wheat straw pyrolysis. *Energy & Fuels*, **12**(5), 929-938.
- Jensen, A., Johnsson, J.E., Andries, J., Laughlin, K., Read, G., Mayer, M., Baumann, H., Bonn, B. 1995. Formation and reduction of NO<sub>x</sub> in pressurized fluidized bed combustion of coal. *Fuel*, **74**(11), 1555-1569.
- Jiang, X., Li, C., Wang, T., Liu, B., Chi, Y., Yan, J. 2009. TG-FTIR study of pyrolysis products evolving from dyestuff production waste. *Journal of Analytical and Applied Pyrolysis*, **84**(1), 103-107.
- Jones, W., Lindstedt, R. 1988. Global reaction schemes for hydrocarbon combustion. *Combustion and Flame*, **73**(3), 233-249.
- Jun, H.K., Lee, T.J., Ryu, S.O., Kim, J.C. 2001. A study of Zn-Ti-based H<sub>2</sub>S removal sorbents promoted with cobalt oxides. *Industrial & engineering chemistry research*, **40**(16), 3547-3556.
- Karayilan, D., Dogu, T., Yasyerli, S., Dogu, G. 2005. Mn-Cu and Mn-Cu-V mixed-oxide regenerable sorbents for hot gas desulfurization. *Industrial & engineering chemistry research*, **44**(14), 5221-5226.
- Karellas, S., Karl, J. 2007. Analysis of the product gas from biomass gasification by means of laser spectroscopy. *Optics and Lasers in Engineering*, **45**(9), 935-946.
- Karvan, O., Atakul, H. 2008. Investigation of CuO/mesoporous SBA-15 sorbents for hot gas desulfurization. *Fuel Processing Technology*, **89**(9), 908-915.
- Kastanaki, E., Vamvuka, D. 2006. A comparative reactivity and kinetic study on the combustion of coal-biomass char blends. *Fuel*, **85**(9), 1186-1193.
- Kastanaki, E., Vamvuka, D., Grammelis, P., Kakaras, E. 2002. Thermogravimetric studies of the behavior of lignite-biomass blends during devolatilization. *Fuel Processing Technology*, **77**, 159-166.

- Kelebopile, L., Sun, R., Liao, J. 2011. Fly ash and coal char reactivity from Thermo-gravimetric (TGA) experiments. *Fuel Processing Technology*.
- Kersten, S., Prins, W., Van der Drift, A., Van Swaaij, W. 2003. Experimental fact-finding in CFB biomass gasification for ECN's 500 kW<sub>th</sub> pilot plant. *Industrial & engineering chemistry research*, **42**(26), 6755-6764.
- Khalil, R., Va rhegyi, G., Ja schke, S., Grønli, M.G., Hustad, J. 2008. CO<sub>2</sub> Gasification of Biomass Chars: A Kinetic Study. *Energy & Fuels*, **23**(1), 94-100.
- Khan, M.R. 1989. Prediction of sulphur distribution in products during low temperature coal pyrolysis and gasification. *Fuel*, **68**(11), 1439-1449.
- Khawam, A., Flanagan, D.R. 2006. Solid-state kinetic models: Basics and mathematical fundamentals. *The Journal of Physical Chemistry B*, **110**(35), 17315-17328.
- Kiel, J., Van Paasen, S., Neeft, J., Devi, L., Ptasiński, K., Janssen, F., Meijer, R., Berends, R., Temmink, H., Brem, G. 2004. Primary measures to reduce tar formation in fluidised-bed biomass gasifiers. *ECN, ECN-C-04-014*.
- Kilpinen, P., Hupa, M., Leppaelahti, J. 1991. Nitrogen Chemistry during Gasification A Thermodynamic Analysis AAA-KTF. FKF-91/14 (Abo Akademi).
- Kim, Y., Lee, J., Kim, S.D. 2000. Modeling of coal gasification in an internally circulating fluidized bed reactor with draught tube. *Fuel*, **79**(1), 69-77.
- Kinoshita, C., Wang, Y., Zhou, J. 1994. Tar formation under different biomass gasification conditions. *Journal of Analytical and Applied Pyrolysis*, **29**(2), 169-181.
- Kinoshita, C.M. 1991. Chemical equilibrium computations for gasification of biomass to produce methanol. *Energy sources*, **13**(3), 361-368.
- Klose, W., Wolki, M. 2005. On the intrinsic reaction rate of biomass char gasification with carbon dioxide and steam. *Fuel*, **84**(7-8), 885-892.
- Knight, R.A. 2000. Experience with raw gas analysis from pressurized gasification of biomass. *Biomass and Bioenergy*, **18**(1), 67-77.
- Knoebig, T., Luecke, K., Werther, J. 1999. Mixing and reaction in the circulating fluidized bed-A three-dimensional combustor model. *Chemical Engineering Science*, **54**(13-14), 2151-2160.
- Ko, T.H., Chu, H., Chaung, L.K. 2005. The sorption of hydrogen sulfide from hot syngas by metal oxides over supports. *Chemosphere*, **58**(4), 467-474.
- Koppejan, J., van Loo, S. 2002. Handbook of Biomass Combustion and Cofiring, IEA Bioenergy Task 32: Biomass Combustion and Cofiring, Twente University Press.
- Kumabe, K., Hanaoka, T., Fujimoto, S., Minowa, T., Sakanishi, K. 2007. Co-gasification of woody biomass and coal with air and steam. *Fuel*, **86**(5-6), 684-689.
- Kumar, A., Eskridge, K., Jones, D.D., Hanna, M.A. 2009. Steam-air fluidized bed gasification of distillers grains: effects of steam to biomass ratio, equivalence ratio and gasification temperature. *Bioresource technology*, **100**(6), 2062-2068.
- Kumar, A., Wang, L., Dzenis, Y.A., Jones, D.D., Hanna, M.A. 2008. Thermogravimetric characterization of corn stover as gasification and pyrolysis feedstock. *Biomass and Bioenergy*, **32**(5), 460-467.
- Kumar, M., Gupta, R. 1994. Influence of carbonization conditions and wood species on carbon dioxide reactivity of resultant wood char powder. *Fuel Processing Technology*, **38**(3), 223-233.
- Kunii, D., Levenspiel, O. 1991. *Fluidization engineering*. Butterworth-Heinemann Boston.
- Kuramochi, H., Wu, W., Kawamoto, K. 2005. Prediction of the behaviors of H<sub>2</sub>S and HCl during gasification of selected residual biomass fuels by equilibrium calculation. *Fuel*, **84**(4), 377-387.
- Kurkela, E., Ståhlberg, P., Laatikainen, J., Simell, P. 1993. Development of simplified IGCC-processes for biofuels: supporting gasification research at VTT. *Bioresource technology*, **46**(1-2), 37-47.
- Kurosaki, F., Ishimaru, K., Hata, T., Bronsveld, P., Kobayashi, E., Imamura, Y. 2003. Microstructure of wood charcoal prepared by flash heating. *Carbon*, **41**(15), 3057-3062.
- Kyotani, T., Kawashima, H., Tomita, A., Palmer, A., Furimsky, E. 1989. Removal of H<sub>2</sub>S from hot gas in the presence of Cu-containing sorbents. *Fuel*, **68**(1), 74-79.
- Lappas, A., Samolada, M., Iatridis, D., Voutetakis, S., Vasalos, I. 2002. Biomass pyrolysis in a circulating fluid bed reactor for the production of fuels and chemicals. *Fuel*, **81**(16), 2087-2095.
- Lapuerta, M., Hernandez, J.J., Rodriguez, J. 2007. Comparison between the kinetics of devolatilisation of forestry and agricultural wastes from the middle-south regions of Spain. *Biomass and Bioenergy*, **31**(1), 13-19.
- Laurendeau, N.M. 1978. Heterogeneous kinetics of coal char gasification and combustion. *Prog. Energy Comb. Sci.*, **4**, 221-270.
- Lee, J.S., Kim, S.D. 1996. Gasification kinetics of waste tire-char with CO<sub>2</sub> in a thermobalance reactor. *Energy*, **21**(5), 343-352.

- Lee, J.W., Kidder, M., Evans, B.R., Paik, S., Buchanan III, A., Garten, C.T., Brown, R.C. 2010. Characterization of Biochars Produced from Cornstovers for Soil Amendment. *Environmental science & technology*, **44**(20), 7970-7974
- Leibold, H., Hornung, A., Seifert, H. 2008. HTHP syngas cleaning concept of two stage biomass gasification for FT synthesis. *Powder Technology*, **180**(1-2), 265-270.
- Lettner, F., Timmerer, H., Haselbacher, P. 2007. Deliverable 8: Biomass gasification-State of the art description.
- Lew, S., Jothimurugesan, K., Flytzani-Stephanopoulos, M. 1989. High-temperature hydrogen sulfide removal from fuel gases by regenerable zinc oxide-titanium dioxide sorbents. *Industrial & engineering chemistry research*, **28**(5), 535-541.
- Lew, S., Sarofim, A.F., Flytzani-Stephanopoulos, M. 1992. Sulfidation of zinc titanate and zinc oxide solids. *Industrial & engineering chemistry research*, **31**(8), 1890-1899.
- Li, C., Suzuki, K. 2009. Tar property, analysis, reforming mechanism and model for biomass gasification--An overview. *Renewable and Sustainable Energy Reviews*, **13**(3), 594-604.
- Li, J., Wang, Z., Yang, X., Hu, L., Liu, Y., Wang, C. 2007. Evaluate the pyrolysis pathway of glycine and glycyglycine by TG-FTIR. *Journal of Analytical and Applied Pyrolysis*, **80**(1), 247-253.
- Li, X., Grace, J., Lim, C., Watkinson, A., Chen, H., Kim, J. 2004. Biomass gasification in a circulating fluidized bed. *Biomass and Bioenergy*, **26**(2), 171-193.
- Li, X., Grace, J.R., Watkinson, A., Lim, C.J., Ergudenler, A. 2001. Equilibrium modeling of gasification: a free energy minimization approach and its application to a circulating fluidized bed coal gasifier. *Fuel*, **80**(2), 195-207.
- Li, Z., Flytzani-Stephanopoulos, M. 1997. Cu-Cr-O and Cu-Ce-O regenerable oxide sorbents for hot gas desulfurization. *Industrial & engineering chemistry research*, **36**(1), 187-196.
- Liang, M., Xu, H., Xie, K. 2007. Bench-scale testing of zinc ferrite sorbent for hot gas clean-up. *Journal of Natural Gas Chemistry*, **16**(2), 204-209.
- Liliedahl, T. 2007. Tar analysis, Dept. of Chemical Engineering and Technology Royal Institute of Technology Stockholm, Sweden, Summer School, Julich.
- Linjewile, T.M., Agarwal, P.K. 1995. The influence of product CO/CO<sub>2</sub> ratio on the ignition and temperature history of petroleum coke particles in incipiently gas-fluidized beds. *Fuel*, **74**(1), 12-16.
- Liu, H. 2009. Combustion of Coal Chars in O<sub>2</sub>/CO<sub>2</sub> and O<sub>2</sub>/N<sub>2</sub> Mixtures: A Comparative Study with Non-isothermal Thermogravimetric Analyzer (TGA) Tests. *Energy & Fuels*, **23**(9), 4278-4285.
- Liu, H., Gibbs, B.M. 2003. Modeling NH<sub>3</sub> and HCN emissions from biomass circulating fluidized bed gasifiers. *Fuel*, **82**(13), 1591-1604.
- Ljung, A., Nordin, A. 1997. Theoretical feasibility for ecological biomass ash recirculation: Chemical equilibrium behavior of nutrient elements and heavy metals during combustion. *Environmental science & technology*, **31**(9), 2499-2503.
- Löffler, G., Kaiser, S., Bosch, K., Hofbauer, H. 2003. Hydrodynamics of a dual fluidized-bed gasifier--Part I: simulation of a riser with gas injection and diffuser. *Chemical Engineering Science*, **58**(18), 4197-4213.
- Lorente, E., Millan, M., Brandon, N. 2012. Use of gasification syngas in SOFC: Impact of real tar on anode materials. *International Journal of Hydrogen Energy*, **37**(8), 7271-7278.
- Lu, L., Kong, C., Sahajwalla, V., Harris, D. 2002. Char structural ordering during pyrolysis and combustion and its influence on char reactivity. *Fuel*, **81**(9), 1215-1225.
- Lu, L., Sahajwalla, V., Harris, D. 2000. Characteristics of chars prepared from various pulverized coals at different temperatures using drop-tube furnace. *Energy & Fuels*, **14**(4), 869-876.
- Luo, M., Stanmore, B. 1992. The combustion characteristics of char from pulverized bagasse. *Fuel*, **71**(9), 1074-1076.
- Lv, P., Xiong, Z., Chang, J., Wu, C., Chen, Y., Zhu, J. 2004. An experimental study on biomass air-steam gasification in a fluidized bed. *Bioresource technology*, **95**(1), 95-101.
- Ma, Y., Ge, Q., Li, W., Xu, H. 2008. A sulfur-tolerant Pd/CeO<sub>2</sub> catalyst for methanol synthesis from syngas. *Journal of Natural Gas Chemistry*, **17**(4), 387-390.
- Macak, J., Malecha, J. 1978. Mathematical model for the gasification of coal under pressure. *Industrial & Engineering Chemistry Process Design and Development*, **17**(1), 92-98.
- Maciejewska, A., Veringa, H., Sanders, J., Peteves, S. 2006. Co-firing of biomass with coal: constraints and role of biomass pre-treatment. *Petten, The Netherlands: Institute for Energy*.
- Mansaray, K., Al-Taweel, A., Ghaly, A., Hamdullahpur, F., Ugursal, V. 2000. Mathematical modeling of a fluidized bed rice husk gasifier: Part I-Model development. *Energy sources*, **22**(1), 83-98.
- Mansaray, K., Ghaly, A. 1999. Determination of kinetic parameters of rice husks in oxygen using thermogravimetric analysis. *Biomass and Bioenergy*, **17**(1), 19-31.
- Maschio, G., Lucchesi, A., Koufopoulos, C. 1992. Study of kinetic and transfer phenomena in the pyrolysis of biomass particles. *Advances in Thermochemical Biomass Conversion*, **2**, 11-15.



- Mastellone, M.L., Arena, U. 2008. Olivine as a tar removal catalyst during fluidized bed gasification of plastic waste. *AIChE Journal*, **54**(6), 1656-1667.
- Mathieu, P., Dubuisson, R. 2002. Performance analysis of a biomass gasifier. *Energy conversion and management*, **43**(9-12), 1291-1299.
- Matsui, I., Kojima, T., Kunii, D., Furusawa, T. 1987a. Study of char gasification by carbon dioxide. 2. Continuous gasification in fluidized bed. *Industrial & engineering chemistry research*, **26**(1), 95-100.
- Matsui, I., Kunii, D., Furusawa, T. 1987b. Study of char gasification by carbon dioxide. 1. Kinetic study by thermogravimetric analysis. *Industrial & engineering chemistry research*, **26**(1), 91-95.
- Matsui, I., Kunii, D., Furusawa, T. 1985. Study of fluidized bed steam gasification of char by thermogravimetrically obtained kinetics. *Journal of chemical engineering of Japan*, **18**(2), 105-113.
- Matsumoto, K., Takeno, K., Ichinose, T., Ogi, T., Nakanishi, M. 2009. Gasification reaction kinetics on biomass char obtained as a by-product of gasification in an entrained-flow gasifier with steam and oxygen at 900-1000° C. *Fuel*, **88**(3), 519-527.
- Mayerhofer, M., Mitsakis, P., Meng, X.M., de Jong, W., Spliethoff, H., Gaderer, M. 2011. Influence of operational parameters on tar formation and main gas components during allothermal steam gasification. *Proceeding of 19<sup>th</sup> European Biomass Conference and Exhibition from Research to Industry and Markets* 6-10 June, Berlin, Germany.
- McKendry, P. 2002a. Energy production from biomass (part 1): overview of biomass. *Bioresource technology*, **83**(1), 37-46.
- McKendry, P. 2002b. Energy production from biomass (part 2): conversion technologies. *Bioresource technology*, **83**(1), 47-54.
- McKendry, P. 2002c. Energy production from biomass (part 3): gasification technologies. *Bioresource technology*, **83**(1), 55-63.
- Mears, D.E. 1971. Diagnostic criteria for heat transport limitations in fixed bed reactors. *Journal of Catalysis*, **20**(2), 127-131.
- Meng, X., de Jong, W. 2009. A report on tar analysis and possibility for improvement - the State of the art Literature, Greensyngas Project, Deliverable report 4.4, 22<sup>nd</sup>, October, TU Delft, the Netherlands.
- Meng, X., de Jong, W., Fu, N., Verkooijen, A.H.M. 2011a. Biomass gasification in a 100 kW<sub>th</sub> steam-oxygen blown circulating fluidized bed gasifier: Effects of operational conditions on product gas distribution and tar formation. *Biomass and Bioenergy*, **35**(7), 2910-2924.
- Meng, X., de Jong, W., Fu, N., Verkooijen, A.H.M. 2011b. DDGS chars gasification with CO<sub>2</sub>: a kinetic study using TG analysis. *Biomass Conversion and Biorefinery, Processing of Biogenic Material for Energy and Chemistry*, **4**(1), 217-227.
- Meng, X., de Jong, W., Fu, N., Verkooijen, A.H.M. 2011c. Reaction kinetics study of willow char gasification with CO<sub>2</sub> using TG analysis *The 19<sup>th</sup> European Biomass Conference and Exhibition from Research to Industry and Markets*, 6-10 June 2011, Berlin, Germany. pp. 1551-1557.
- Meng, X., de Jong, W., Fu, N.J., Verkooijen, A.H.M. 2010a. Primary results of dried distillers grains with solubles gasification in a 100kW<sub>th</sub> steam-oxygen blown circulating fluidized bed gasifier. in: *the 8<sup>th</sup> International Symposium on Gas Cleaning at High Temperatures, 2010*. Taiyuan, Shanxi, China.
- Meng, X., De Jong, W., Pal, R., Verkooijen, A.H.M. 2010b. In bed and downstream hot gas desulphurization during solid fuel gasification: A review. *Fuel Processing Technology*, **91**(8), 964-981.
- Meng, X., de Jong, W., Verkooijen, A.H.M. 2009. Prediction of sulphur compounds distribution in gasification products of biomass fuels. *The 17<sup>th</sup> European Biomass Conference and Exhibition from Research to Industry and Markets*, 29 June-3 July, Hamburg, Germany. pp. 940-947.
- Mermoud, F., Salvador, S., Van de Steene, L., Golfier, F. 2006. Influence of the pyrolysis heating rate on the steam gasification rate of large wood char particles. *Fuel*, **85**(10-11), 1473-1482.
- Mettanant, V., Basu, P., Butler, J. 2009. Agglomeration of biomass fired fluidized bed gasifier and combustor. *The Canadian Journal of Chemical Engineering*, **87**(5), 656-684.
- Milne, T., Abatzoglou, N., Evans, R. 1998. Biomass gasifier "tars": their nature, formation, and conversion. *National Renewable Energy Laboratory, NREL/TP-570-25357*.
- Mitsakis, P. 2011. Online analysis of the tar content of biomass gasification producer gas, Vol. Doctor, Technische Universität München. Germany.
- Mitsakis, P., Karellas, S., Spliethoff, H. 2008. Application of laser spectroscopy for the quantitative analysis of biomass gasification tars. *16th European Biomass Conference and Exhibition. From Research to Industry and Markets*, 2-6 June 2008, FERIA Valencia, Spain pp. 652-658.
- Mitsakis, P., Mayerhofer, M., Spliethoff, H. 2009. Qualitative and quantitative analysis of biomass gasification tars by means of laser spectroscopy. *17th European Biomass Conference and Exhibition. From Research to Industry and Markets*, 29 June-3 July 2009, Hamburg, Germany, pp. 639-645.

- Mitta, N.R., Ferrer-Nadal, S., Lazovic, A.M., Parales, J.F., Velo, E., Puigjaner, L. 2006. Modelling and simulation of a tyre gasification plant for synthesis gas production. *Computer Aided Chemical Engineering*, **21**, 1771-1776.
- Miura, K., Hashimoto, K., Silveston, P.L. 1989. Factors affecting the reactivity of coal chars during gasification, and indices representing reactivity. *Fuel*, **68**(11), 1461-1475.
- Moersch, O., Spliethoff, H., Hein, K. 1997. A new system for tar sampling and analysis. *Biomass Gasification and Pyrolysis: State of the Art and Future Prospects*. (Eds: Kaltschmitt, M.; Bridgwater, A.V) CPL Scientific Limited, Newbury, UK, 228-234.
- Moersch, O., Spliethoff, H., Hein, K. 2000. Tar quantification with a new online analyzing method. *Biomass and Bioenergy*, **18**(1), 79-86.
- Mori, S., Wen, C. 1975. Estimation of bubble diameter in gaseous fluidized beds. *AIChE Journal*, **21**(1), 109-115.
- Munir, S., Daood, S., Nimmo, W., Cunliffe, A., Gibbs, B. 2009. Thermal analysis and devolatilization kinetics of cotton stalk, sugar cane bagasse and shea meal under nitrogen and air atmospheres. *Bioresource technology*, **100**(3), 1413-1418.
- Murillo, R., Navarro, M.V., López, J.M., Aylón, E., Callén, M.S., García, T., Mastral, A.M. 2004. Kinetic model comparison for waste tire char reaction with CO<sub>2</sub>. *Industrial & engineering chemistry research*, **43**(24), 7768-7773.
- Narvaez, I., Orio, A., Aznar, M.P., Corella, J. 1996. Biomass gasification with air in an atmospheric bubbling fluidized bed. Effect of six operational variables on the quality of the produced raw gas. *Industrial & engineering chemistry research*, **35**(7), 2110-2120.
- Natarajan, E., Ganapathy Sundaram, E. 2009. Pyrolysis of Rice Husk in a Fixed Bed Reactor. *World Academy of Science, Engineering and Technology*(56), 504-508.
- Neeft, J., Knoef, H., Buffinga, G., Zielke, U., Sjöström, K., Brage, C., Hasler, P., Smell, P., Suomalainen, M., Dorrington, M. 2001. Guideline for sampling and analysis of tars and particles in biomass producer gases. *Proceeding of the conference Progress in thermochemical biomass conversion*. pp. 162-175.
- Neeft, J., Knoef, H., Nederland, S.E.C., Group, B.B.T. 1999. *Behaviour of Tar in Biomass Gasification Systems: Tar Related Problems and Their Solutions*. Novem.
- Nichols, K.M., Hedman, P.O., Smoot, L.D., Blackham, A.U. 1989. Fate of coal-sulphur in a laboratory-scale coal gasifier. *Fuel*, **68**(2), 243-248.
- Nikoo, M.B., Mahinpey, N. 2008. Simulation of biomass gasification in fluidized bed reactor using ASPEN PLUS. *Biomass and Bioenergy*, **32**(12), 1245-1254.
- Nilsson, S., Gómez-Barea, A., Fuentes-Cano, D., Ollero, P. 2012. Gasification of biomass and waste in a staged fluidized bed gasifier: Modeling and comparison with one-stage units. *Fuel*.
- Norheim, A., Lindberg, D., Hustad, J.E., Backman, R. 2009. Equilibrium Calculations of the Composition of Trace Compounds from Biomass Gasification in the Solid Oxide Fuel Cell Operating Temperature Interval. *Energy & Fuels*, **23**(2), 920-925.
- Norman, J., Pourkashanian, M., Williams, A. 1997. Modelling the formation and emission of environmentally unfriendly coal species in some gasification processes. *Fuel*, **76**(13), 1201-1216.
- Nussbaumer, T. 2003. Combustion and co-combustion of biomass: fundamentals, technologies, and primary measures for emission reduction. *Energy & Fuels*, **17**(6), 1510-1521.
- Öhman, M., Nordin, A., Skrifvars, B.J., Backman, R., Hupa, M. 2000. Bed agglomeration characteristics during fluidized bed combustion of biomass fuels. *Energy & Fuels*, **14**(1), 169-178.
- Öhman, M., Pommer, L., Nordin, A. 2005. Bed agglomeration characteristics and mechanisms during gasification and combustion of biomass fuels. *Energy & Fuels*, **19**(4), 1742-1748.
- Okabe, K., Murata, K., Nakanishi, M., Ogi, T., Nurunnabi, M., Liu, Y. 2009. Fischer-Tropsch synthesis over Ru catalysts by using syngas derived from woody biomass. *Catalysis letters*, **128**(1), 171-176.
- Okumura, Y., Hanaoka, T., Sakanishi, K. 2009. Effect of pyrolysis conditions on gasification reactivity of woody biomass-derived char. *Proceedings of the Combustion Institute*, **32**(2), 2013-2020.
- Ollero, P., Serrera, A., Arjona, R., Alcantarilla, S. 2003. The CO<sub>2</sub> gasification kinetics of olive residue. *Biomass and Bioenergy*, **24**(2), 151-161.
- Orfao, J., Antunes, F., Figueiredo, J. 1999. Pyrolysis kinetics of lignocellulosic materials--three independent reactions model. *Fuel*, **78**(3), 349-358.
- Padban, N., Wang, W., Ye, Z., Bjerle, I., Odenbrand, I. 2000. Tar formation in pressurized fluidized bed air gasification of woody biomass. *Energy & Fuels*, **14**(3), 603-611.
- Patel, M.M., Grow, D.T., Young, B.C. 1988. Combustion rates of lignite char by TGA. *Fuel*, **67**(2), 165-169.
- Pecho, J., Schildhauer, T., Sturzenegger, M., Biollaz, S., Wokaun, A. 2008. Reactive bed materials for improved biomass gasification in a circulating fluidised bed reactor. *Chemical Engineering Science*, **63**(9), 2465-2476.

## Bibliography

- Peters, B., Bruch, C. 2001. A flexible and stable numerical method for simulating the thermal decomposition of wood particles. *Chemosphere*, **42**(5-7), 481-490.
- Petersen, I., Werther, J. 2005a. Experimental investigation and modeling of gasification of sewage sludge in the circulating fluidized bed. *Chemical engineering and processing*, **44**(7), 717-736.
- Petersen, I., Werther, J. 2005b. Three-dimensional modeling of a circulating fluidized bed gasifier for sewage sludge. *Chemical Engineering Science*, **60**(16), 4469-4484.
- Petersen, T., Ringer, S. 2010. An electron tomography algorithm for reconstructing 3D morphology using surface tangents of projected scattering interfaces. *Computer Physics Communications*, **181**(3), 676-682.
- Petroleum, B. 2011. BP Energy Outlook 2030, London: BP.
- Petrone, G., Fichera, G., Scionti, M. Thermal and Fluid-dynamical Optimisation of Passengers Comfort in a Touring Bus Cabin. *COMSOL Conference 2008 Hannover*.
- Pinto, F., André, R.N., Lopes, H., Dias, M., Gulyurtlu, I., Cabrita, I. 2008. Effect of Experimental Conditions on Gas Quality and Solids Produced by Sewage Sludge Co-gasification. 2. Sewage Sludge Mixed with Biomass. *Energy Fuels*, **22**(4), 2314-2325.
- Pinto, F., Lopes, H., André, R.N., Dias, M., Gulyurtlu, I., Cabrita, I. 2007. Effect of Experimental Conditions on Gas Quality and Solids Produced by Sewage Sludge Co-gasification. 1. Sewage Sludge Mixed with Coal. *Energy Fuels* **21**(5), 2737-2745.
- Piotrowska, P., Zevenhoven, M., Hupa, M., Giuntoli, J., de Jong, W. 2011. Residues from the production of biofuels for transportation: Characterization and ash sintering tendency. *Fuel Processing Technology*, In Press, Corrected Proof.
- Polsongkram, M., Kuznetsov, G. 2010. Product distribution from woody biomass by fixed-bed pyrolysis process *Modern Technique and Technologies MTT'2010*, 198-200.
- Poston, J.A. 1996. A reduction in the spalling of zinc titanate desulfurization sorbents through the addition of lanthanum oxide. *Industrial & engineering chemistry research*, **35**(3), 875-882.
- Prabir, B. 2010. Biomass gasification and pyrolysis practical design and theory, Elsevier. Oxford.
- Prins, M.J., Ptasiński, K.J., Janssen, F.J.J.G. 2007. From coal to biomass gasification: Comparison of thermodynamic efficiency. *Energy*, **32**(7), 1248-1259.
- Puig-Arnabat, M., Bruno, J.C., Coronas, A. 2010. Review and analysis of biomass gasification models. *Renewable and Sustainable Energy Reviews*.
- Qin, Y.H., Feng, J., Li, W.Y. 2010. Formation of tar and its characterization during air-steam gasification of sawdust in a fluidized bed reactor. *Fuel*, **89**(7), 1344-1347.
- Radmanesh, R., Chaouki, J., Guy, C. 2006. Biomass gasification in a bubbling fluidized bed reactor: experiments and modeling. *AIChE Journal*, **52**(12), 4258-4272.
- Raman, P., Walawender, W.P., Fan, L., Chang, C. 1981. Mathematical model for the fluid-bed gasification of biomass materials. Application to feedlot manure. *Industrial & Engineering Chemistry Process Design and Development*, **20**(4), 686-692.
- Rapagna, S., Jand, N., Kiennemann, A., Foscolo, P. 2000. Steam-gasification of biomass in a fluidised-bed of olivine particles. *Biomass and Bioenergy*, **19**(3), 187-197.
- Ratfisch. Tar analyser TA120-3 user manual.
- Rauch, R., Pfeifer, C., Bosch, K., Hofbauer, H., Swierczynski, D., Courson, C., Kiennemann, A. 2004. Comparison of different olivines for biomass steam gasification. *Proceedings of the conference for Science in Thermal and Chemical Biomass Conversion*, Victoria, Canada. pp. 799-809.
- Raveendran, K., Ganesh, A. 1998. Adsorption characteristics and pore-development of biomass-pyrolysis char. *Fuel*, **77**(7), 769-781.
- Raveendran, K., Ganesh, A., Khilar, K.C. 1995. Influence of mineral matter on biomass pyrolysis characteristics. *Fuel*, **74**(12), 1812-1822.
- Reeve, L. 1958. Desulfurization of coke-oven gas at Appleby--Frodingham. *J. Inst. Fuel*, **31**.
- Risnes, H., Sørensen, L., Hustad, J. 2001. CO<sub>2</sub> reactivity of chars from wheat, spruce and coal. *Proceeding of the conference Progress in thermochemical biomass conversion*. pp. 61-72.
- Rouquerol, F., Rouquerol, J., Sing, K. 1999. Adsorption by Powders and Porous Solids: Principles. *Methodology and Applications (Academic, San Diego, 1999)*.
- Rubiera, F., Arenillas, A., Fuente, E., Miles, N., Pis, J.J. 1999. Effect of the grinding behaviour of coal blends on coal utilisation for combustion. *Powder Technology*, **105**(1-3), 351-356.
- Ruoppolo, G., Ammendola, P., Chirone, R., Miccio, F. 2010. H<sub>2</sub> rich syngas production by fluidized bed gasification of biomass and plastic fuel. *Proceedings Venice 2010, Third International Symposium on Energy from Biomass and Waste*, 8-11 November 2010, Venice, Italy.
- Ruth, L.A., Squires, A.M., Graff, R.A. 1972. Desulfurization of fuels with half-calcined dolomite. First kinetic data. *Environmental science & technology*, **6**(12), 1009-1014.

- Sadaka, S.S., Ghaly, A., Sabbah, M. 2002. Two phase biomass air-steam gasification model for fluidized bed reactors: Part I--model development. *Biomass and Bioenergy*, **22**(6), 439-462.
- Sanz, A., Corella, J. 2006. Modeling circulating fluidized bed biomass gasifiers. Results from a pseudo-rigorous 1-dimensional model for stationary state. *Fuel Processing Technology*, **87**(3), 247-258.
- Sasaoka, E., Sada, N., Manabe, A., Uddin, M.A., Sakata, Y. 1999. Modification of ZnO-TiO<sub>2</sub> high-temperature desulfurization sorbent by ZrO<sub>2</sub> addition. *Industrial & engineering chemistry research*, **38**(3), 958-963.
- Sasaoka, E., Sakamoto, M., Ichio, T., Kasaoka, S., Sakata, Y. 1993. Reactivity and durability of iron oxide high temperature desulfurization sorbents. *Energy & Fuels*, **7**(5), 632-638.
- Scahill, J. 2004. Options for Biomass to Energy Commercial and Emerging Technologies. Biomass - to - Business. in: *National Renewable Energy Laboratory*, [www.emnrd.state.nm.us](http://www.emnrd.state.nm.us).
- Schiffer, H.W. 2008. WEC energy policy scenarios to 2050. *Energy policy*, **36**(7), 2464-2470.
- Schuster, G., Löffler, G., Weigl, K., Hofbauer, H. 2001. Biomass steam gasification-an extensive parametric modeling study. *Bioresource technology*, **77**(1), 71-79.
- Senneca, O. 2007. Kinetics of pyrolysis, combustion and gasification of three biomass fuels. *Fuel Processing Technology*, **88**(1), 87-97.
- Senneca, O., Salatino, P., Masi, S. 2005. The influence of char surface oxidation on thermal annealing and loss of combustion reactivity. *Proceedings of the Combustion Institute*, **30**(2), 2223-2230.
- Seo, D.K., Lee, S.K., Kang, M.W., Hwang, J., Yu, T.U. 2010. Gasification reactivity of biomass chars with CO<sub>2</sub>. *Biomass and Bioenergy*, **34**(12), 1946-1953.
- Sharma, R.K., Wooten, J.B., Baliga, V.L., Lin, X., Geoffrey Chan, W., Hajaligol, M.R. 2004. Characterization of chars from pyrolysis of lignin. *Fuel*, **83**(11-12), 1469-1482.
- Shell International Petroleum Company, I.P., Environment, Environment, E.A.G.B. 2001. *Energy Needs, Choices and Possibilities: Scenarios to 2050*. Shell International Limited.
- Shim, H.S., Hurt, R.H., Yang, N.Y.C. 2000. A methodology for analysis of 002 lattice fringe images and its application to combustion-derived carbons. *Carbon*, **38**(1), 29-45.
- Shirai, H., Kobayashi, M., Nunokawa, M. 1999. Reduction of Fe<sub>2</sub>O<sub>3</sub>-SiO<sub>2</sub> Particle in Air Blown Coal Gasification's Gas. *Kagaku Kogaku Ronbunshu*, **25**(5), 714-720.
- Siedlecki, M. 2011. On the gasification of biomass in a steam-oxygen blown CFB gasifier with the focus on gas quality upgrading: technology background, experiments and mathematical modeling. in: *Process and Energy*, Vol. Doctor, Delft University of Technology. Delft.
- Siedlecki, M., de Jong, W. 2011. Biomass gasification as the first hot step in clean syngas production process-gas quality optimization and primary tar reduction measures in a 100 kW thermal input steam-oxygen blown CFB gasifier. *Biomass and Bioenergy*, **35**(supplement 1), s40-s62.
- Siedlecki, M., Nieuwstraten, R., Simeone, E., de Jong, W., Verkooijen, A. 2009. Effect of Magnesite as Bed Material in a 100 kW<sub>th</sub> Steam-Oxygen Blown Circulating Fluidized-Bed Biomass Gasifier on Gas Composition and Tar Formation. *Energy & Fuels*, **23**(11), 5643-5654.
- Siedlecki, M., van der Nat, K., Simeone, E., de Jong, W. 2006. The first results of gas and solids characterization obtained during steam-oxygen gasification of biomass in a 100kW<sub>th</sub> CFB gasifier. *World Renewable Energy Congress IX*.
- Sima-Ella, E., Yuan, G., Mays, T. 2005. A simple kinetic analysis to determine the intrinsic reactivity of coal chars. *Fuel*, **84**(14-15), 1920-1925.
- Simell, P.A., Leppälähti, J.K. 1992. Catalytic purification of tarry fuel gas with carbonate rocks and ferrous materials. *Fuel*, **71**(2), 211-218.
- Sing, K.S.W., Everett, D.H., Haul, R.A.W., Moscou, L., Pierotti, R.A., Rouquerol, J., Siemieniowska, T. 1985. Reporting physisorption data for gas/solid systems with Special Reference to the Determination of Surface Area and Porosity (Recommendations 1984) *Pure and Applied Chemistry*, **57**(4), 603—619.
- Smirnova, O., Fend, T. 2010. Homogeneous or Inhomogeneous Model for Flow and Heat Transfer in Porous Materials As High Temperature Solar Air Receivers. *The COMSOL Conference 2010, November 17-19, Paris, France*.
- Smith, J., Van Ness, H., Abbott, M. 2001. *Introduction to chemical engineering thermodynamics, Sixth edition*. McGraw-Hill (New York).
- Smolders, K., Baeyens, J. 2001. Hydrodynamic modelling of the axial density profile in the riser of a low density circulating fluidized bed. *The Canadian Journal of Chemical Engineering*, **79**(3), 422-429.
- Sorensen, L.H., Gjernes, E., Jessen, T., Fjellerup, J. 1996a. Determination of reactivity parameters of model carbons, cokes and flame-chars. *Fuel*, **75**(1), 31-38.
- Sorensen, L.H., Saastamoinen, J., Hustad, J.E. 1996b. Evaluation of char reactivity data by different shrinking-core models. *Fuel*, **75**(11), 1294-1300.
- Sotudeh-Gharebaagh, R., Legros, R., Chaouki, J., Paris, J. 1998. Simulation of circulating fluidized bed reactors using ASPEN PLUS. *Fuel*, **77**(4), 327-337.

- Squires, A.M., Graff, R.A., Pell, M. 1971. Desulfurization of Fuel with Calcined Dolomite. I. Introduction and First Kinetic Results. *Chem. Eng. Prog. Symp. Series*, **67**, 23-34.
- Srinivasan, R.A., Sriramulu, S., Kulasekaran, S., Agarwal, P.K. 1998. Mathematical modeling of fluidized bed combustion--2: combustion of gases. *Fuel*, **77**(9-10), 1033-1049.
- Ståhlberg, P., Lappi, M., Kurkela, E., Simell, P., Oesch, P., Nieminen, M. 1998. *Sampling of contaminants from product gases of biomass gasifiers*. Technical Research Centre of Finland.
- Standish, N., Tanjung, A.F.A. 1988. Gasification of single wood charcoal particles in CO<sub>2</sub>. *Fuel*, **67**(5), 666-672.
- Stiegel, G.J., Maxwell, R.C. 2001. Gasification technologies: the path to clean, affordable energy in the 21<sup>st</sup> century. *Fuel Processing Technology*, **71**(1-3), 79-97.
- Stinnett, S.J., Harrison, D.P., Pike, R.W. 1974. Fuel gasification. Prediction of sulfur species distribution by free energy minimization. *Environmental science & technology*, **8**(5), 441-444.
- Sun, R., Zobel, N., Neubauer, Y., Cardenas Chavez, C., Behrendt, F. 2010. Analysis of gas-phase polycyclic aromatic hydrocarbon mixtures by laser-induced fluorescence. *Optics and Lasers in Engineering*, **48**(12), 1231-1237.
- Sutton, D., Kelleher, B., Ross, J.R.H. 2001. Review of literature on catalysts for biomass gasification. *Fuel Processing Technology*, **73**(3), 155-173.
- Swisher, J., Schwerdtfeger, K. 1992. Review of metals and binary oxides as sorbents for removing sulfur from coal-derived gases. *Journal of Materials Engineering and Performance*, **1**(3), 399-407.
- TA-Instrument. 2010. User manual of SDT Q600.
- Tanaka, N. 2010. World Energy Outlook 2010. *International Energy Agency, November*.
- Tancredi, N., Cordero, T., Rodríguez-Mirasol, J., Rodríguez, J.J. 1996. CO<sub>2</sub> gasification of eucalyptus wood chars. *Fuel*, **75**(13), 1505-1508.
- Tar, B.G. 2007. DD CEN/TS 15439:2006 Biomass gasification. Tar and particles in product gases. Sampling and analysis. in: *CEN/TS*, Vol. 15439, CEN.
- Thompson, D., Argent, B. 2002. Prediction of the distribution of trace elements between the product streams of the Prenflo gasifier and comparison with reported data. *Fuel*, **81**(5), 555-570.
- Tia, S., Bhattacharya, S., Wibulswas, P. 1991. Thermogravimetric analysis of Thai lignite--II. Char combustion kinetics. *Energy conversion and management*, **31**(3), 277-284.
- Tsai, C.Y., Scaroni, A.W. 1987. Reactivity of bituminous coal chars during the initial stage of pulverized-coal combustion. *Fuel*, **66**(10), 1400-1406.
- Tseng, H., Edgar, T. 1985. Combustion behaviour of bituminous and anthracite coal char between 425 and 900 °C. *Fuel*, **64**(3), 373-379.
- Tseng, H., Edgar, T. 1984. Identification of the combustion behaviour of lignite char between 350 and 900 °C. *Fuel*, **63**(3), 385-393.
- Turn, S., Kinoshita, C., Zhang, Z., Ishimura, D., Zhou, J. 1998. An experimental investigation of hydrogen production from biomass gasification. *International Journal of Hydrogen Energy*, **23**(8), 641-648.
- Umeki, K., Yamamoto, K., Namioka, T., Yoshikawa, K. 2010. High temperature steam-only gasification of woody biomass. *Applied Energy*, **87**(3), 791-798.
- Valin, S., Ravel, S., Guillaudeau, J., Thiery, S. 2010. Comprehensive study of the influence of total pressure on products yields in fluidized bed gasification of wood sawdust. *Fuel Processing Technology*, **91**(10), 1222-1228.
- van de Kamp, W., de Wild, P., Coda, B., van Paasen, S., Kiel, J. 2005. Sampling and analysis of tar and particles in biomass producer gases. *Energy Research Centre of the Netherlands, report ECN-C--06-046*.
- Van der Drift, A., Van Doorn, J., Vermeulen, J. 2001. Ten residual biomass fuels for circulating fluidized-bed gasification. *Biomass and Bioenergy*, **20**(1), 45-56.
- Van der Ham, A., Heesink, A., Prins, W., Van Swaaij, W. 1996. Proposal for a regenerative high-temperature process for coal gas cleanup with calcined limestone. *Industrial & engineering chemistry research*, **35**(5), 1487-1495.
- van der Meijden, C.M., Veringa, H.J., Rabou, L.P.L.M. 2010. The production of synthetic natural gas (SNG): A comparison of three wood gasification systems for energy balance and overall efficiency. *Biomass and Bioenergy*, **34**(3), 302-311.
- van Paasen, S., Kiel, J., Neeft, J., Knoef, H., Buffinga, G., Zielke, U., Sjoström, K., Brage, C., Hasler, P., Simell, P. 2002. Guideline for sampling and analysis of tar and particles in biomass producer gases, Petten, ECN, ECN-C--02-090.
- van Paasen, S.V.B., Kiel, J.H.A. 2004. Tar formation in fluidized-bed gasification-impact of gasifier operating conditions. *The 2nd world conference and technology exhibition on biomass for energy, industry and climate protection, ECN-RX--04-037*.
- Varhegyi, G., Antal Jr, M.J., Szekeely, T., Till, F., Jakab, E. 1988. Simultaneous thermogravimetric-mass spectrometric studies of the thermal decomposition of biopolymers. 1. Avicel cellulose in the presence and absence of catalysts. *Energy & Fuels*, **2**(3), 267-272.

- Várhegyi, G., Mészáros, E., Antal Jr, M.J., Bourke, J., Jakab, E. 2006. Combustion kinetics of corncob charcoal and partially demineralized corncob charcoal in the kinetic regime. *Industrial & engineering chemistry research*, **45**(14), 4962-4970.
- Varian, B. 2008. Varian GC 450 user manual.
- Villanueva, A., Gómez-Barea, A., Revuelta, E., Campoy, M., Ollero, P. 2008. Guidelines for selection of gasifiers modelling strategies. *16th European biomass conference and exhibition Valencia*, 2-6 June, Spain. pp. 980-986.
- Wang, L., Kumar, A., Hanna, M., Weller, C.L., Jones, D. 2009. Thermal Degradation Kinetics of Distillers Grains and Solubles in Nitrogen and Air. *Energy Sources, Part A*, **31**(10), 797-806.
- Wang, L., Weller, C.L., Jones, D.D., Hanna, M.A. 2008a. Contemporary issues in thermal gasification of biomass and its application to electricity and fuel production. *Biomass and Bioenergy*, **32**(7), 573-581.
- Wang, Q., Luo, Z., Ni, M., Cen, K. 2003. Particle population balance model for a circulating fluidized bed boiler. *Chemical Engineering Journal*, **93**(2), 121-133.
- Wang, S., Guo, X., Wang, K., Luo, Z. 2011. Influence of the interaction of components on the pyrolysis behavior of biomass. *Journal of Analytical and Applied Pyrolysis*, **91**(1), 183-189.
- Wang, X., Jia, J., Zhao, L., Sun, T. 2008b. Mesoporous SBA-15 Supported Iron Oxide: A Potent Catalyst for Hydrogen Sulfide Removal. *Water, Air, & Soil Pollution*, **193**(1), 247-257.
- Wang, Y., Kinoshita, C. 1992. Experimental analysis of biomass gasification with steam and oxygen. *Solar energy*, **49**(3), 153-158.
- Warnecke, R. 2000. Gasification of biomass: comparison of fixed bed and fluidized bed gasifier. *Biomass and Bioenergy*, **18**(6), 489-497.
- Wei, L., Xu, S., Zhang, L., Liu, C., Zhu, H., Liu, S. 2007. Steam gasification of biomass for hydrogen-rich gas in a free-fall reactor. *International Journal of Hydrogen Energy*, **32**(1), 24-31.
- Westmoreland, P.R., Harrison, D.P. 1976. Evaluation of candidate solids for high-temperature desulfurization of low-Btu gases. *Environmental science & technology*, **10**(7), 659-661.
- Williams, P.T., Nugranad, N. 2000. Comparison of products from the pyrolysis and catalytic pyrolysis of rice husks. *Energy*, **25**(6), 493-513.
- Winter, F., Prah, M.E., Hofbauer, H. 1997. Temperatures in a fuel particle burning in a fluidized bed: The effect of drying, devolatilization, and char combustion. *Combustion and Flame*, **108**(3), 302-314.
- Wolfesberger, U., Aigner, I., Hofbauer, H. 2009. Tar content and composition in producer gas of fluidized bed gasification of wood—Influence of temperature and pressure. *Environmental Progress & Sustainable Energy*, **28**(3), 372-379.
- Xie, W., Chang, L., Wang, D., Xie, K., Wall, T., Yu, J. 2010. Removal of sulfur at high temperatures using iron-based sorbents supported on fine coal ash. *Fuel*, **89**(4), 868-873.
- Yang, H., Yan, R., Chen, H., Lee, D.H., Zheng, C. 2007. Characteristics of hemicellulose, cellulose and lignin pyrolysis. *Fuel*, **86**(12-13), 1781-1788.
- Yang, R.T., Shen, M.S. 1979. Calcium silicates: a new class of highly regenerative sorbents for hot gas desulfurization. *AIChE Journal*, **25**(5), 811-819.
- Yrjas, K.P., Zevenhoven, C.A.P., Hupa, M.M. 1996. Hydrogen sulfide capture by limestone and dolomite at elevated pressure. 1. Sorbent performance. *Industrial & engineering chemistry research*, **35**(1), 176-183.
- Yunhau, Z., Huilin, L., Yurong, H., Ding, J., Lijie, Y. 2006. Numerical prediction of combustion of carbon particle clusters in a circulating fluidized bed riser. *Chemical Engineering Journal*, **118**(1-2), 1-10.
- Zainal, Z., Ali, R., Lean, C., Seetharamu, K. 2001. Prediction of performance of a downdraft gasifier using equilibrium modeling for different biomass materials. *Energy conversion and management*, **42**(12), 1499-1515.
- Zeng, Y., Kaytakoglu, S., Harrison, D. 2000. Reduced cerium oxide as an efficient and durable high temperature desulfurization sorbent. *Chemical Engineering Science*, **55**(21), 4893-4900.
- Zevenhoven, R., Kilpinen, P. 2001. *Control of pollutants in flue gases and fuel gases*. Helsinki University of Technology Espoo, Finland.
- Zhang, R., Huang, J., Zhao, J., Sun, Z., Wang, Y. 2007. Sol-gel auto-combustion synthesis of zinc ferrite for moderate temperature desulfurization. *Energy & Fuels*, **21**(5), 2682-2687.
- Zhang, Y., Ashizawa, M., Kajitani, S., Miura, K. 2008. Proposal of a semi-empirical kinetic model to reconcile with gasification reactivity profiles of biomass chars. *Fuel*, **87**(4-5), 475-481.
- Zolin, A., Jensen, A., Jensen, P.A., Frandsen, F., Dam-Johansen, K. 2001. The influence of inorganic materials on the thermal deactivation of fuel chars. *Energy & Fuels*, **15**(5), 1110-1122.

## Appendix

Table A-1 Overview of process conditions setting for Agrol, willow and DDGS gasification at TUD

Exp. NO	D1	D2	D3	A1	A2	A3	A4	A5	A6	W1	W2	W3	W4	W5
Date	15-10-09	21-04-10	23-04-10	25-03-10	13-04-10	15-04-10	23-04-10	17-11-10	23-11-10	25-03-10	19-04-10	23-04-10	29-11-10	01-12-10
Time start	12:00	12:00	16:30	16:20	12:50	11:50	11:00	17:00	11:00	12:20	10:50	13:50	14:30	11:50
Time end	14:00	15:40	18:10	18:20	17:10	17:00	13:30	22:00	18:20	16:20	17:10	16:30	20:30	19:30
Duration	2:00	3:40	1:40	2:00	4:20	5:10	2:30	5:00	7:20	4:00	6:20	2:40	6:00	7:40
Fuel	DDGS	DDGS	DDGS	Agrol	Agrol	Agrol	Agrol	Agrol	Agrol	Willow	Willow	Willow	Willow	Willow
Additive	None	Kaolin	Kaolin	None	None	None	None	None	None	Kaolin	Kaolin	Kaolin	None	None
Bed materials	Bed 4 <sup>A</sup>	Bed 1	Bed 2	Bed 3	Bed 1 <sup>C</sup>	Bed 1	Bed 2 <sup>D</sup>	Bed 2	Bed 2	Bed 3 <sup>B</sup>	Bed 1	Bed 2	Bed 2	Bed 2
Temperature (°C)	780-830	700-760	700-760	800-830	700-830	700-830	700-830	840	840	700-830	700-830	700-830	840	840
Gasifying medium	Steam-O <sub>2</sub>													
Steam flow (kg/h)	10.6-10.9	14.8-16.8	14.5-16.8	11.1-11.6	14.7-15.4	13.6-14.7	11.5-14.6	10-13.6	13.03	11.6-15.9	10.9-14.8	11.5-14.5	12.41	12.41
Biomass flow(kg/h)	13.0-13.6	15.27	15.27	10.1-11.1	10.1-10.8	10.1-11.7	11.72	11.72	11.72	11.1	11.7-12.7	12.71	12.71	12.71
Oxygen flow (kg/h)	4.9-5.0	5.5-2.7	5.49-5.5	5.0-5.5	4.5-5.7	4.7-5.2	4.80-4.90	4.8-5.0	4.8-5.0	5.0-6.0	5-5.6	4.95-5.0	5.55	5.55
L-valve flow (kg/h)	1.4	1.85	1.77	1.4	1.4	1.4	1.4	1.4	1.4	1.4	1.4	1.4	1.4	1.4
Purging N <sub>2</sub> flow(kg/h)	2.47	2.7	2.7	2.7	2.34	2.7	2.7	2.7	2.7	2.7	2.7	2.7	2.7	2.7
Fluidized velocity (m/s)	2.8-3.3	3.3~3.9	3.3-3.9	2.9-3.3	3.5-4.0	2.9-3.8	3-3.6	3-3.6	3-3.6	2.9-3.9	2.9-3.8	3-3.6	3-3.6	3-3.6
SBR (-)	0.81-0.83	0.97-1.10	0.95-1.08	1.00-1.15	1.36-1.52	0.97-1.45	0.98-1.25	0.85-1.16	1.11	1.00-1.15	0.90-1.20	0.9-1.14	0.98	0.98
ER (-)	0.38	0.37	0.36	0.40	0.36-0.42	0.35-0.38	0.33	0.35	0.35	0.40-0.47	0.38-0.39	0.34	0.38	0.38

A: Untreated, used Scandinavian olivine; B: Mixed sand and Used Treated Austrian Olivine; C: Used, treated Austrian olivine; D: Fresh Austrian olivine

*Table A-2 Overview of process conditions setting for Agrol, willow and DDGS gasification at TUM*

SPA Sample	A1	A2	A3	A4	A5	A6	A7	A8	A9	A10	A11	A12	A13
Fuel	Agrol												
Exp. date	20100607												
Steam flow (kg/h)	2.2	2.6	2.4	2.2	2.6	2.4	2.2	2.6	2.4	4.5	5.5	4.5	5.5
Biomass flow(kg/h)	2.6	2.6	2.0	2.6	2.6	2.0	2.6	2.6	2.0	5.3	4.6	5.3	4.6
Pressure (bar)	1	1	1	1	1	1	1	1	1	2.5	2.5	2.5	2.5
SBR	0.83	1	1.2	0.83	1	1.2	0.83	1	1.2	0.84	1.21	0.84	1.21
Temperature (°C)	750	750	750	800	800	800	840	840	840	750	750	800	800
SPA Sample	W1	W2	W3	W4	W5	W6	W7	W8	W9	W10	W11	W12	W13
Fuel	Willow												
Exp. date	20100608									20100609			
Steam flow (kg/h)	1.9	2.2	2.6	1.9	2.2	2.6	1.9	2.2	2.6	4.5	5.5	4.5	5.5
Biomass flow(kg/h)	2.2	2.2	2.2	2.2	2.2	2.2	2.2	2.2	2.2	5.0	4.6	5.0	4.6
Pressure (bar)	1	1	1	1	1	1	1	1	1	2.5	2.5	2.5	2.5
SBR	0.86	1	1.18	0.86	1	1.18	0.86	1	1.18	0.9	1.21	0.9	1.21
Temperature (°C)	750	750	750	800	800	800	840	840	840	750	750	800	800
SPA Sample	D1	D2	D3	D4	D5	D6	A0						
Fuel	DDGS						Agrol						
Exp. date	20100609						20100604						
Steam flow (kg/h)	1.9	2.5	1.9	2.5	1.9	2.5	2.2						
Biomass flow(kg/h)	2.1	2.1	2.1	2.1	2.1	2.1	2.6						
Pressure (bar)	1	1	1	1	1	1	1						
SBR	0.9	1.19	0.9	1.19	0.9	1.19	0.83						
Temperature (°C)	700	700	750	750	800	800	750						



Table A-3 Char combustion and gasification and sulfidation operational parameters

Reaction	Reaction type		Conditions	Parameters
Char gasification	PYR-Char	Isothermal Gasification	Pyrolysis temperature(°C)	750, 850
			Heating rate (°C/min)	10, 30, 50, 70
			CO <sub>2</sub> concentration (vol.%)	10, 20, 30
			Temperature	900, 1000, 1100
	CFB-Char	Isothermal Gasification	CO <sub>2</sub> concentration (vol.%)	10, 20, 30
			Temperature	900, 1000, 1100
Char combustion	CFB-Char	Isothermal Combustion	O <sub>2</sub> concentration (vol.%)	21, 15, 10, 7.5
			Heating rate (°C/min)	30
			Temperature (°C)	LTR: 400, 450, 500, 550, 600 HTR: 750, 800, 850, 900
	CFB-Char	Non-isothermal combustion	O <sub>2</sub> concentration (vol.%)	21, 15, 10, 7.5
			Heating rate (°C/min)	10, 30, 50
			Temperature range (°C)	150-900
	Pure carbon	Isothermal Combustion	O <sub>2</sub> concentration (vol.%)	21
			Heating rate (°C/min)	30
			Temperature (°C)	LTR: 500, 550, 600 HTR: 900
	Pure carbon	Non-isothermal combustion	O <sub>2</sub> concentration (vol.%)	21, 15, 7.5
			Heating rate (°C/min)	10, 30, 50
			Temperature range (°C)	150-900
Sulfidation	ZnO, Fe <sub>2</sub> O <sub>3</sub> CuO, MnO	Isothermal sulfidation	H <sub>2</sub> S concentration (ppmv)	1000, 1500, 2000
			Heating rate (°C/min)	50
			Temperature (°C)	400, 500, 600

*Table A- 4 Elements in SEM-EDS analysis*

Sample	A11-13	A4-15	W4-19	W12-1	D10-9
Element	wt.%	wt.%	wt.%	wt.%	wt.%
C K	89.28	88.65	83.08	88.64	69.05
N K	0.00	0.00	0.00	0.00	0.00
O K	8.82	8.74	14.04	9.47	16.46
Na K	0.00	0.00	0.00	0.06	2.18
Mg K	0.19	0.11	0.07	0.08	1.00
Al K	0.00	0.00	0.00	0.00	0.00
Si K	0.00	0.00	0.00	0.00	0.12
P K	0.05	0.10	0.11	0.15	4.54
S K	0.00	0.00	0.04	0.00	0.68
Cl K	0.00	0.00	0.00	0.00	0.13
K K	0.81	0.90	2.22	0.95	5.51
Ca K	0.77	1.19	0.38	0.64	0.21
Cr K	0.00	0.00	0.00	0.00	0.00
Mn K	0.07	0.20	0.00	0.00	0.00
Fe K	0.00	0.13	0.05	0.00	0.09
Totals	100.00	100.00	100.00	100.00	100.00

Table A- 5 Classification of adsorption isotherms

Types	Descriptions
Type I	The Type I isotherm is concave to the $p/p^\circ$ axis and approaches a limiting value as $p/p^\circ \rightarrow 1$ , which are given by microporous solids ( $<20 \text{ \AA}$ ) having relatively small external surfaces, the limiting uptake being governed by the accessible micropore volume rather than by the internal surface area
Type II	The Type II isotherm is the normal form of isotherm obtained with a non-porous or macroporous adsorbent ( $>500 \text{ \AA}$ ), which represents unrestricted monolayer-multilayer adsorption. Point B (see below figure <i>Types of physisorption isotherms</i> ), the beginning of the almost linear middle section of the isotherm, is often taken to indicate the stage at which monolayer coverage is complete and multilayer adsorption about to begin.
Type III	The Type III isotherm is convex to the $p/p^\circ$ axis over its entire range and therefore does not exhibit a Point B. Isotherms of this type are not common, but there are a number of systems (e.g. nitrogen on polyethylene) which give isotherms with gradual curvature and an indistinct Point B. In such cases, the adsorbate-adsorbate interactions play an important role.
Type IV	Characteristic features of the Type IV isotherm are its hysteresis loop, which is associated with capillary condensation taking place in mesopores (from 20 to 500 $\text{\AA}$ ), and the limiting uptake over a range of high $p/p^\circ$ . The initial part of the Type IV isotherm is attributed to monolayer-multilayer adsorption since it follows the same path as the corresponding part of a Type II isotherm obtained with the given adsorbate on the same surface area of the adsorbent in a non-porous form.
Type V	The Type V isotherm is uncommon; it is related to the Type III isotherm in that the adsorbent-adsorbate interaction is weak, but is obtained with certain porous adsorbents.
Type VI	The Type VI isotherm, in which the sharpness of the steps depends on the system and the temperature, represents stepwise multilayer adsorption on a uniform non-porous surface.

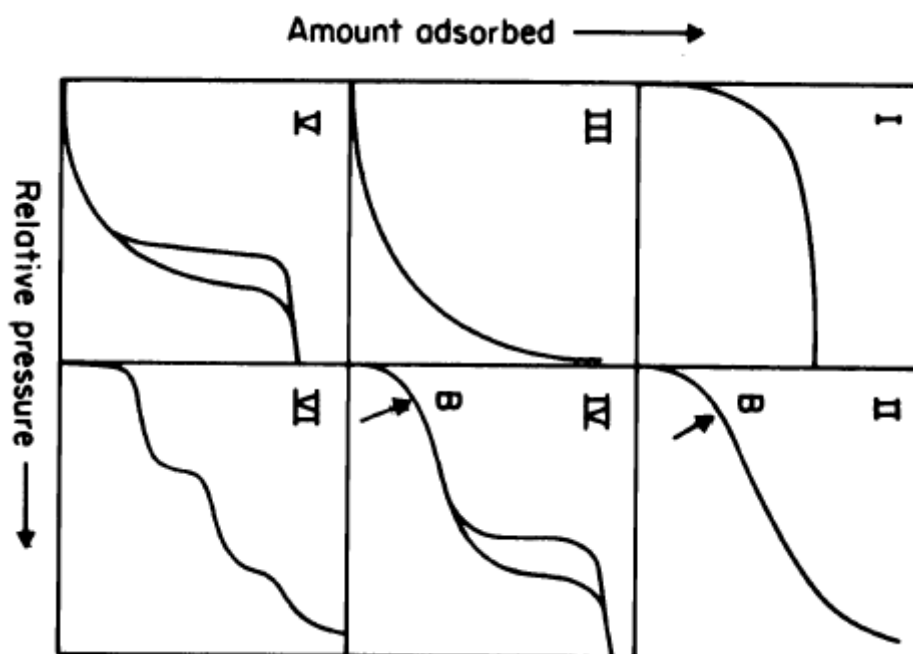
*Types of physisorption isotherms*

Table A- 6 Mass and heat transfer limitation calculation during char gasification

As mentioned in chapter 2, mass and heat transfer limitation during char gasification can be checked according to two criteria: Mears criterion is usually used to estimate effects of external mass transfer (**Eq. A- 1**) and intraphase heat transfer (**Eq. A- 3**), while Weisz-Pater criterion is used to determine the effect of internal mass transfer (**Eq. A- 2**). When these equations are satisfied, it means that effects of external mass transfer, internal mass transfer and intraphase heat transfer effects can be neglected. Since char gasification reaction is the first order of CO<sub>2</sub> concentration, the equations (**Eq.2- 1 to Eq.2- 3**) can be simplified the equations as follows:

$$k_{ex} = \frac{-r'_A \rho_p (1 - \varepsilon_{bed}) R_p}{k_g C_{Ab}} < 0.15 \quad \text{Eq. A- 1}$$

$$C_{wp} = \eta \phi_1^2 = 3(\phi_1 \coth \phi_1 - 1) \ll 1 \quad \text{Eq. A- 2}$$

$$k_{heat} = \left| \frac{-\Delta H (-r'_A) \rho_p (1 - \varepsilon_{bed}) R_p E_a}{h T^2 R_g} \right| < 0.15 \quad \text{Eq. A- 3}$$

Considering parameters involved in the above equations, Thiele modulus ( $\phi_1$ ) is the ratio of the intrinsic chemical reaction rate in the absence of mass transfer limitation to the rate of diffusion through char particle, and it is calculated using equation (**Eq. A- 4**).

$$\phi_1 = R_p \sqrt{\frac{k_1 \rho_p S_a}{D_e}} \quad \text{Eq. A- 4}$$

Mass transfer coefficient ( $k_g$ ) is calculated based on estimation of Reynolds (Re) number and Sherwood (Sh) number using equation (**Eq. A- 5**).

$$k_g = \frac{D_{AB}}{d_p} Sh = \frac{D_{AB}}{d_p} \left( 2 + 0.6 Re^{\frac{1}{2}} Sc^{\frac{1}{3}} \right) = \frac{D_{AB}}{d_p} \left[ 2 + 0.6 \left( \frac{d_p u}{\nu} \right)^{\frac{1}{2}} \left( \frac{\nu}{D_{AB}} \right)^{\frac{1}{3}} \right] \quad \text{Eq. A- 5}$$

Effective diffusivity ( $D_e$ ) is calculated by using gases molecular diffusivity ( $D_{AB}$ ) and Knudsen diffusivity ( $D_{KA}$ ) using equation (**Eq. A- 6**).

$$D_e = \frac{\varepsilon_p}{\tau} \left( \frac{1}{D_{AB}} + \frac{1}{D_{KA}} \right)^{-1} \quad \text{Eq. A- 6}$$

Where:  $\varepsilon_p$  and  $\tau$  are the porosity and the tortuosity, respectively. These two parameters generally depend strongly on the porous char structure and the nature of the biomass and additionally, they change as reaction proceeds. The values of  $\varepsilon_p / \tau$  reported by other researcher [2,3,4] is between 0.14 and 0.30 for many carbonaceous chars. Thus, a middle value of  $\varepsilon_p / \tau = 0.2$  is assumed for the calculation. The binary molecule diffusivity ( $D_{AB}$ ) is calculated by using equation (**Eq. A- 7**) according to Chapman-Enskog formula and also take into account its temperature dependence [2,5],

[2] J.A. Gomez-Barea, P. Ollero and R. Arjona, Reaction–diffusion model of TGA gasification experiments for estimating diffusional effects, *Fuel* 84 (2005), pp. 1695–1704.

[3] M. Groeneveld and W. van Swaaij, Gasification of Char Particles with CO<sub>2</sub> and H<sub>2</sub>O, *Chem Eng Sci* 35 (1980), pp. 307–313

[4] W.M. Rohsenow, J.P. Hartnett and K. Cho YI, *Handbook of heat transfer*: McGraw-Hill New York; 1998

[5] J.A. Gomez-Barea, P. Ollero and A. Villanueva, Diffusional effects in CO<sub>2</sub> gasification experiments with single biomass char particles. 2. Theoretical predictions, *Energy and Fuels* 20 (2006), pp. 2211–2222.

while the Knudsen diffusion ( $D_{KA}$ ) is proportional to  $T^{0.5}$  and independent of both pressure and the presence of other species using equation (**Eq. A- 8**) [6].

$$D_{AB} = 1.67 \times 10^{-5} \left( \frac{T}{298} \right)^{1.75} \quad \text{Eq. A- 7}$$

$$D_{KA} = 0.97 R_{pore} \times \left( \frac{T}{M_w} \right)^{1/2} \quad \text{Eq. A- 8}$$

Most of other parameters were measured and calculated from experimental data, while some of them parameters were obtained from different literatures and see in the below table.

*Table A- 6 Mass and heat transfer limitation calculation during char gasification*

Items	Definition	Units	Values			Reference
			Agrol	Willow	DDGS	
$d_p$	Char diameter, $d_p = 2 R_p$	m	5E-4			Measured
$u$	CO <sub>2</sub> linear velocity	m/s	7.43E-3			Calculated
$\nu$	Kinematic viscosity	m <sup>2</sup> /s	9.78E-5			Calculated[7]
$D_{AB}$	Molecular diffusivity	m <sup>2</sup> /s	1.8E-4			Calculated
$k_g$	Mass transfer coefficient	m/s	0.74			Calculated
$T$	Temperature	K	1173			Experimental
$\varepsilon_{bed}$	Bed porosity	-	0.4			Obtained[8]
$C_{Ab}$	Bulk CO <sub>2</sub> concentration	kmol/m <sup>3</sup>	0.003			Experimental
$D_e$	Effective diffusivity	m <sup>2</sup> /s	7.8E-6			Calculated
$h$	Heat transfer coefficient	kJ/(m <sup>2</sup> ·s·K)	0.33			Calculated [8]
$\Delta H$	Heat of reaction	kJ/kmol	172500			Obtained [2]
$R_g$	Gas constant	kJ/(kmol·K)	8.314			-
$R_{pore}$	Char pore radius	m	5E-8			Measured
$\rho_p$	Char density	kg/m <sup>3</sup>	253	268	421	Measured
$S_a$	Char surface area	m <sup>2</sup> /g	504	296	23	Measured
$E_a$	Activation energy	kJ/kmol	1.87E+5	1.62E+5	1.52E+5	Calculated
$C_{wp}$	Dimensionless number	-	2.6E-2	3.7E-2	3.6E-2	Calculated
$k_{ex}$	Dimensionless number	-	1.5E-4	3.4E-4	9.3E-4	Calculated
$k_{heat}$	Dimensionless number	-	7.2E-7	1.4E-6	3.7E-6	Calculated

[6 ] H.S. Fogler, Elements of chemical reaction engineering, 3rd version, New Jersey: Prentice-Hall, Inc., (now known as Pearson Education, Inc.); 1999

[7] CO<sub>2</sub> viscosity is calculated using: <http://www.lmnoeng.com/Flow/GasViscosity.htm>

[8] J.M. Smith, H.C. Van Ness, M.M. Abbott, Introduction to Chemical Engineering Thermodynamics, Sixth Edition, McGraw-Hill, Singapore, 2001.

Table A- 7 Biomass devolatilization process

Remarks:

1. The amounts of CH<sub>4</sub>, C<sub>2</sub>H<sub>4</sub> and C<sub>6</sub>H<sub>6</sub> formed are equal to fractional conversion of carbon 8%, 4.5% and 0.6%, respectively.
2. The amounts of CO and CO<sub>2</sub> formed are equal to fractional conversion of oxygen 30% and 70%, respectively.
3. Gas volume is calculated based on the ideal gas law.

Items	Unit	Agrol	Willow	DDGS
Biomass feed rate	kg/h	11.76	11.67	15.26
O in fuel	kg/h	4.21	4.04	4.38
H in fuel	kg/h	0.69	0.67	0.92
N in fuel	kg/h	0.02	0.07	0.78
H <sub>2</sub> O in fuel	kg/h	1.20	1.18	1.60
C in fuel	kg/h	5.62	5.44	6.77
Cl in fuel	kg/h	0.00	0.00	0.03
S in fuel	kg/h	0.00	0.00	0.11
Ash in fuel	kg/h	0.02	0.27	0.68
Oxygen feed rate	kg/h	5.15	5.10	5.50
Steam feed rate	kg/h	11.40	10.85	14.57
Nitrogen feed rate	kg/h	4.51	4.51	4.91

*Gas, tar and char mole flow released from biomass devolatilization*

CO	kmol/h	0.079	0.076	0.082
CO <sub>2</sub>	kmol/h	0.092	0.088	0.096
H <sub>2</sub>	kmol/h	0.245	0.237	0.335
CH <sub>4</sub>	kmol/h	0.037	0.036	0.045
H <sub>2</sub> O	kmol/h	0.067	0.065	0.089
O <sub>2</sub>	kmol/h	0.000	0.000	0.000
N <sub>2</sub>	kmol/h	0.001	0.003	0.028
C <sub>2</sub> H <sub>4</sub>	kmol/h	0.011	0.010	0.013
C <sub>6</sub> H <sub>6</sub>	kmol/h	0.000	0.000	0.001
C	kmol/h	0.236	0.229	0.312
Gas mole flow released	kmol/h	0.532	0.516	0.692
Reactor temperature	K	1083.15	1053.15	1023.15
Reactor pressure	bar	1.15	1.12	1.15
Gas volume flow released	L/min	694	672	853
Oxygen volume flow	L/min	58	59	62
Steam volume flow	L/min	483	472	617
Nitrogen volume flow	L/min	58	134	63
Total gas volume flow	L/min	1405	1370	1713
Total gas mole flow	kmol/h	1.487	1.438	1.848

*To be continued*

*To be continued*

Gas and tar initial concentration				
CO	mol/m <sup>3</sup>	0.937	0.922	0.800
CO <sub>2</sub>	mol/m <sup>3</sup>	1.093	1.076	0.933
H <sub>2</sub>	mol/m <sup>3</sup>	2.907	2.879	3.257
CH <sub>4</sub>	mol/m <sup>3</sup>	0.444	0.441	0.439
H <sub>2</sub> O	mol/m <sup>3</sup>	8.297	8.120	8.730
O <sub>2</sub>	mol/m <sup>3</sup>	1.909	1.939	1.672
N <sub>2</sub>	mol/m <sup>3</sup>	1.917	1.991	1.974
C <sub>2</sub> H <sub>4</sub>	mol/m <sup>3</sup>	0.125	0.124	0.123
C <sub>6</sub> H <sub>6</sub>	mol/m <sup>3</sup>	0.006	0.006	0.005
Gas mole fraction				
CO	-	0.149	0.147	0.119
CO <sub>2</sub>	-	0.173	0.172	0.139
H <sub>2</sub>	-	0.461	0.459	0.484
CH <sub>4</sub>	-	0.070	0.070	0.065
H <sub>2</sub> O	-	0.125	0.126	0.128
O <sub>2</sub>	-	0.000	0.000	0.000
N <sub>2</sub>	-	0.001	0.005	0.040
C <sub>2</sub> H <sub>4</sub>	-	0.020	0.020	0.018

Table A- 8 Mass balance for Agrol gasification at SBR=0.97

<i>Pure EM model</i>	Input [kg/h]					Output [kg/h]				deviation	
	Fuel	steam	O <sub>2</sub>	N <sub>2</sub>	Total	Product gas	fly ash	bottom ash	tar	total	%
C	5.62				5.62	5.61		0.01		5.62	0.06
H	0.69				2.09	2.09				2.09	-0.09
O	4.21				20.56	20.56				20.56	-0.01
N	0.02			4.51	4.53	4.53				4.53	0.01
O from oxygen			5.15								
O from steam		10.13									
O from moisture	1.07										
H from steam		1.27									
H from moisture	0.13										
ash	0.02				0.02	0.02				0.02	0.00
Total	11.76	11.40	5.15	4.51	32.82	32.81	0.00	0.01	0.00	32.82	0.00

<i>Experiment</i>	Input [kg/h]					Output [kg/h]				dev	
	Fuel	steam	O <sub>2</sub>	N <sub>2</sub>	Total	Product gas	fly ash	bottom ash	tar	total	%
C	5.62				5.62	4.41			0.18	4.59	18.42
H	0.69				2.09	1.53			0.01	1.55	25.96
O	4.21				20.56	16.26			0.00	16.27	20.89
N	0.02			4.51	4.53	3.79				3.79	16.30
O from oxygen			5.15								
O from steam		10.13									
O from moisture	1.07										
H from steam		1.27									
H from moisture	0.13										
ash	0.02				0.02	0.02				0.02	0.00
Total	11.76	11.40	5.15	4.51	32.82	26.01			0.20	26.21	16.32



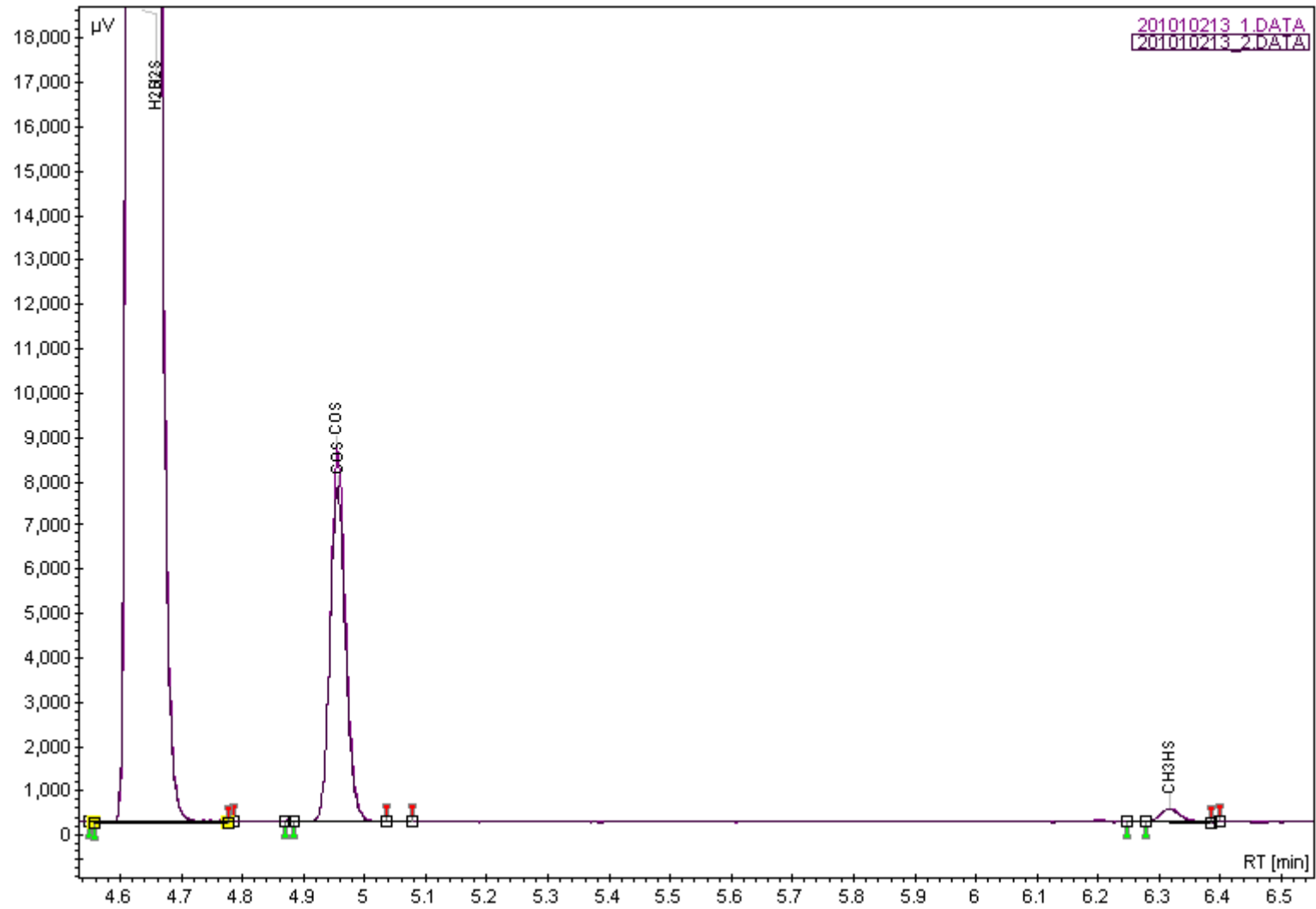


Figure A-1 H<sub>2</sub>S-COS-Methyl Mercaptan GC chromatography curves

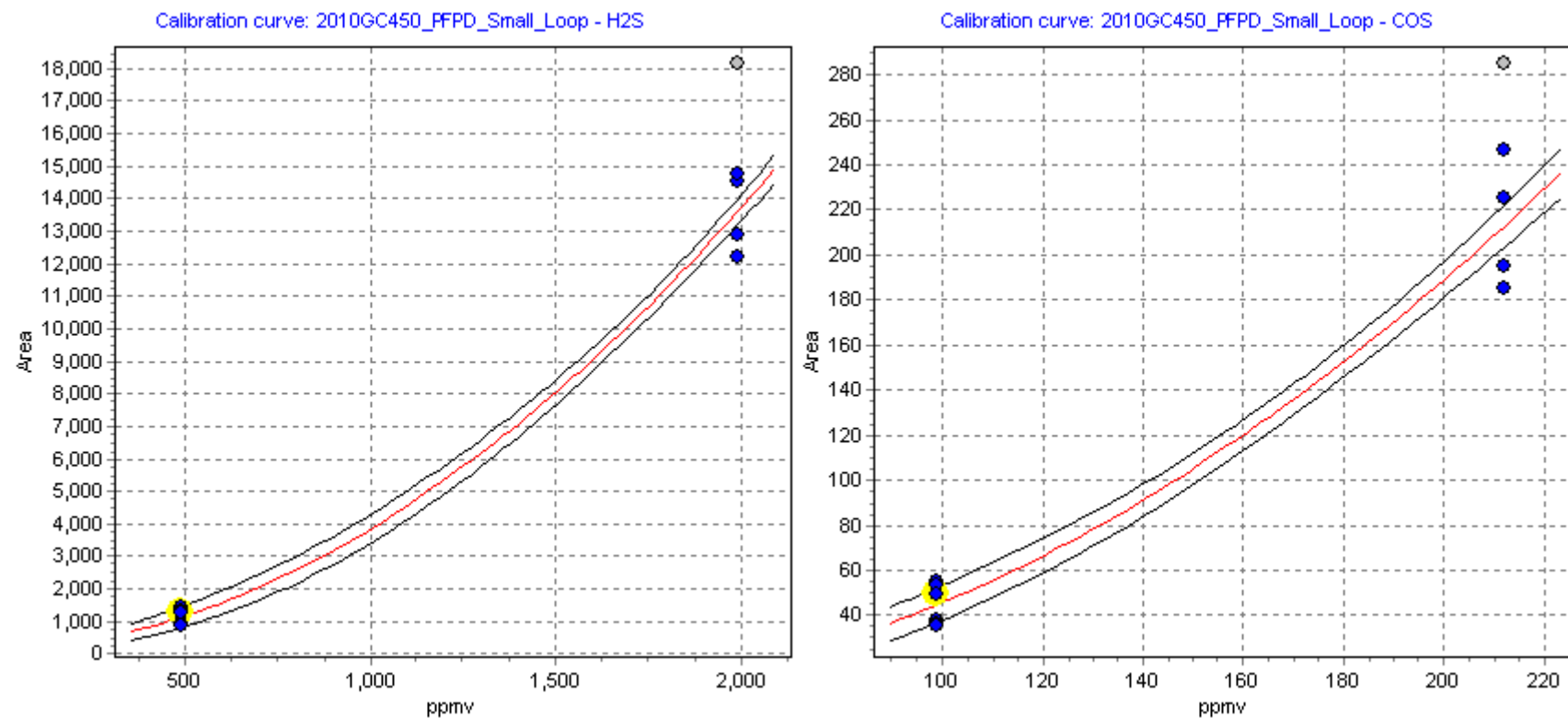


Figure A-2 H<sub>2</sub>S-COS calibration curves

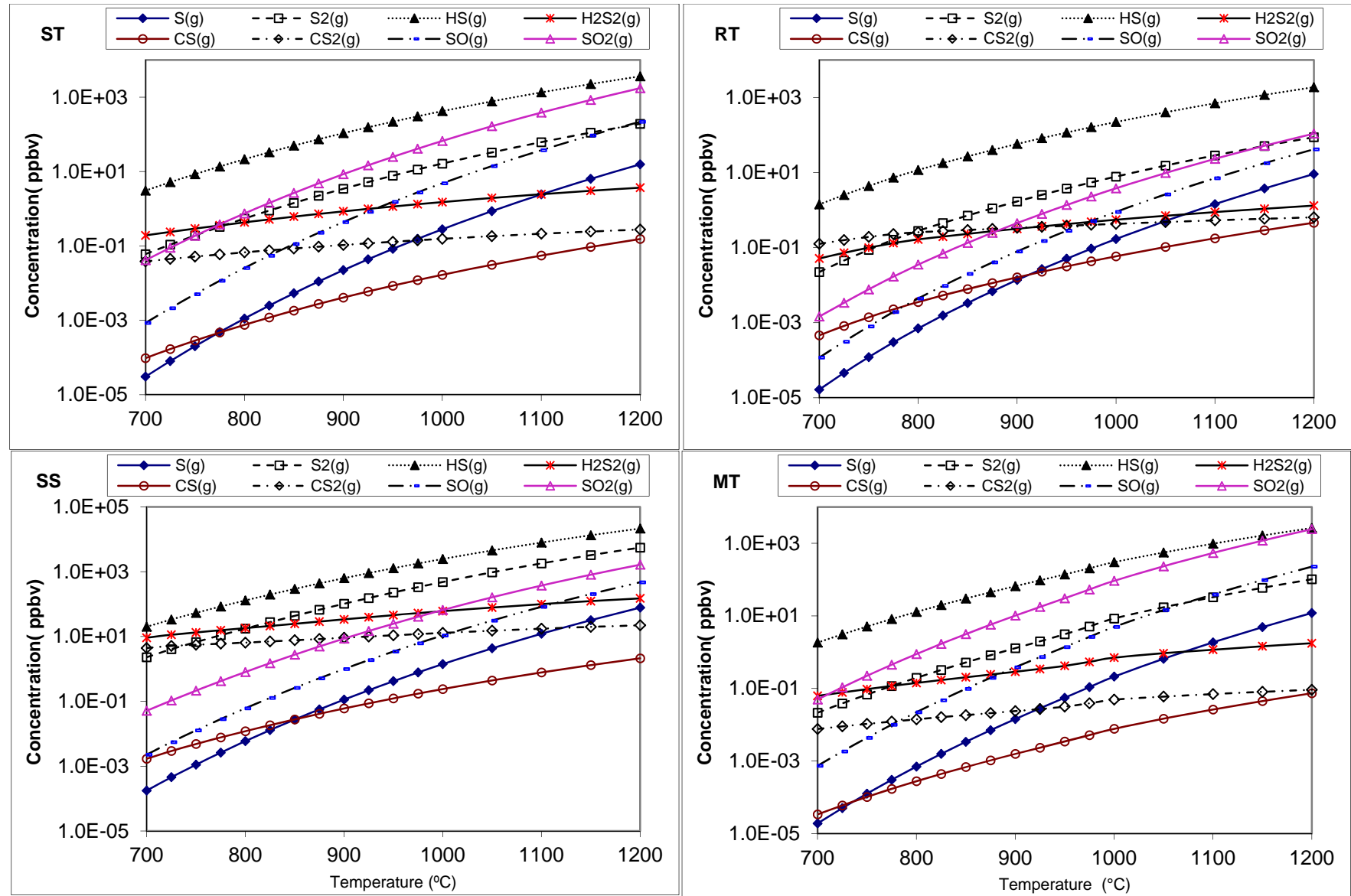


Figure A-3 Predicted concentrations of other sulfur species for the gasification of biomass fuels at various temperatures ( $y = \log(\text{vol. } \%)$ )

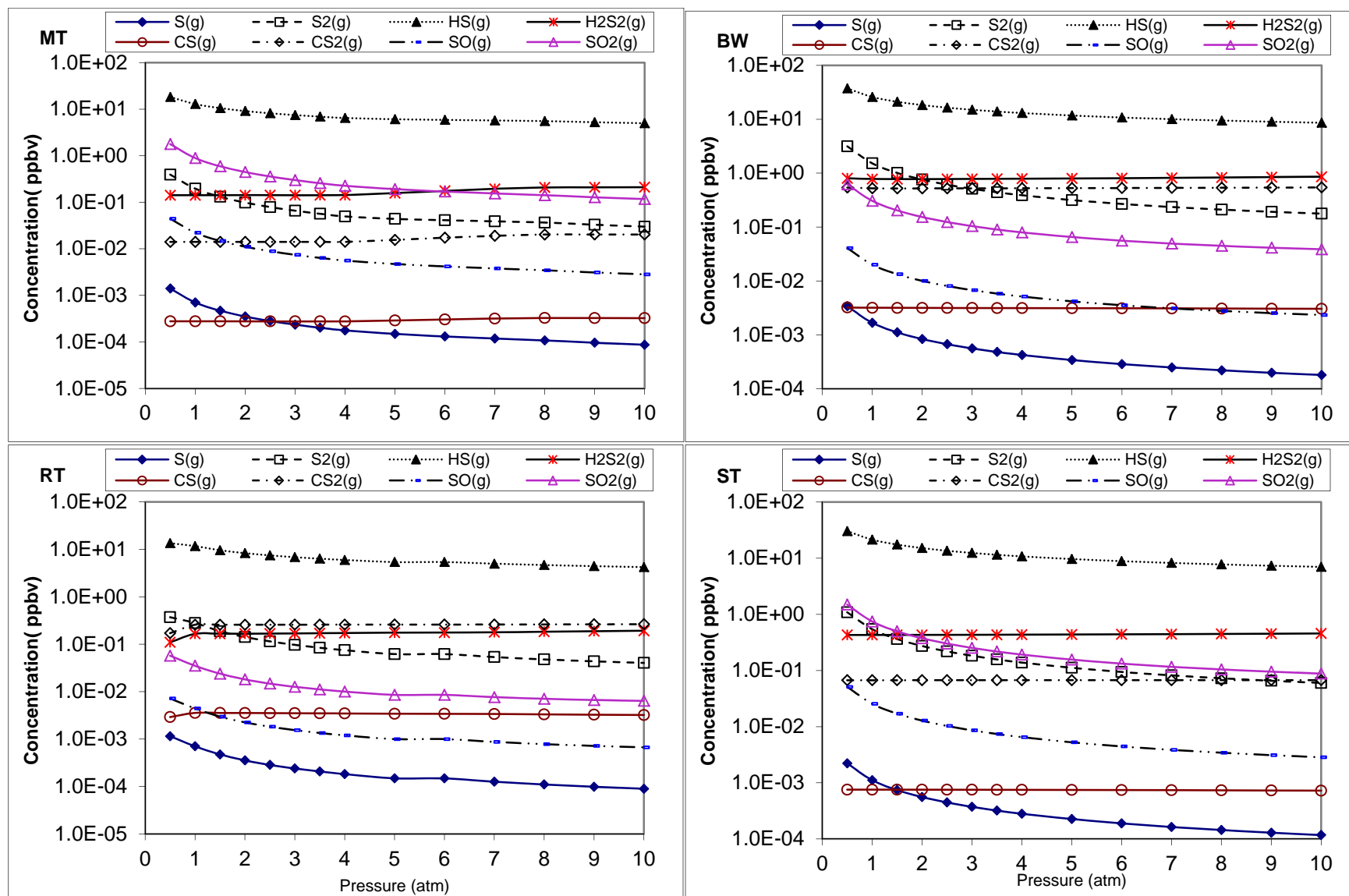


Figure A-4 Effect of pressure on other sulfur species formation for gasification of MT, ST, RT and BW fuels at 800 °C ( $y = \log(\text{vol. \%})$ )

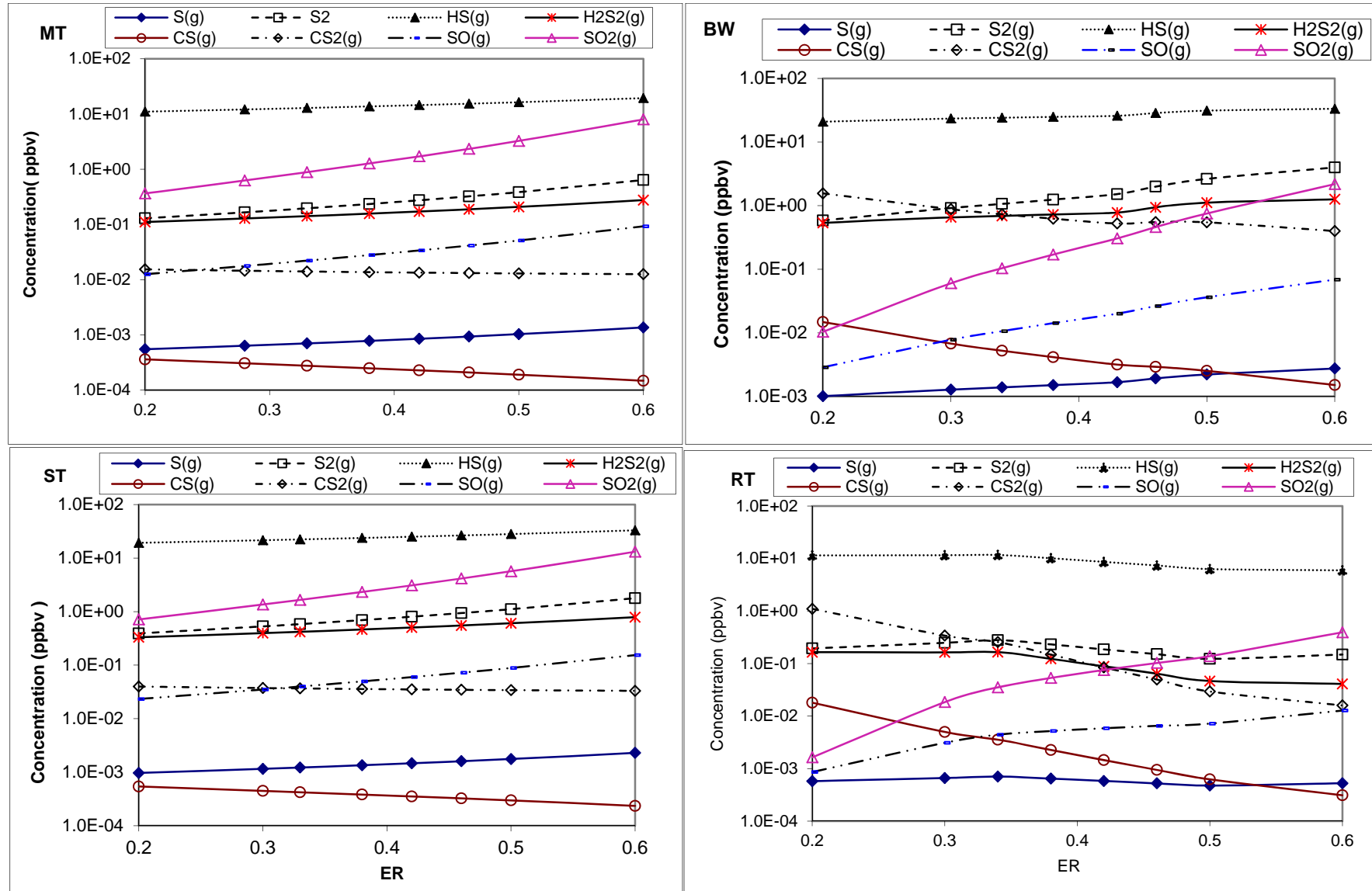


Figure A-5 Effect of ER on other sulfur species formation for gasification of MT, ST, RT and BW fuels at 800 °C ( $y = \log(\text{vol. \%})$ )

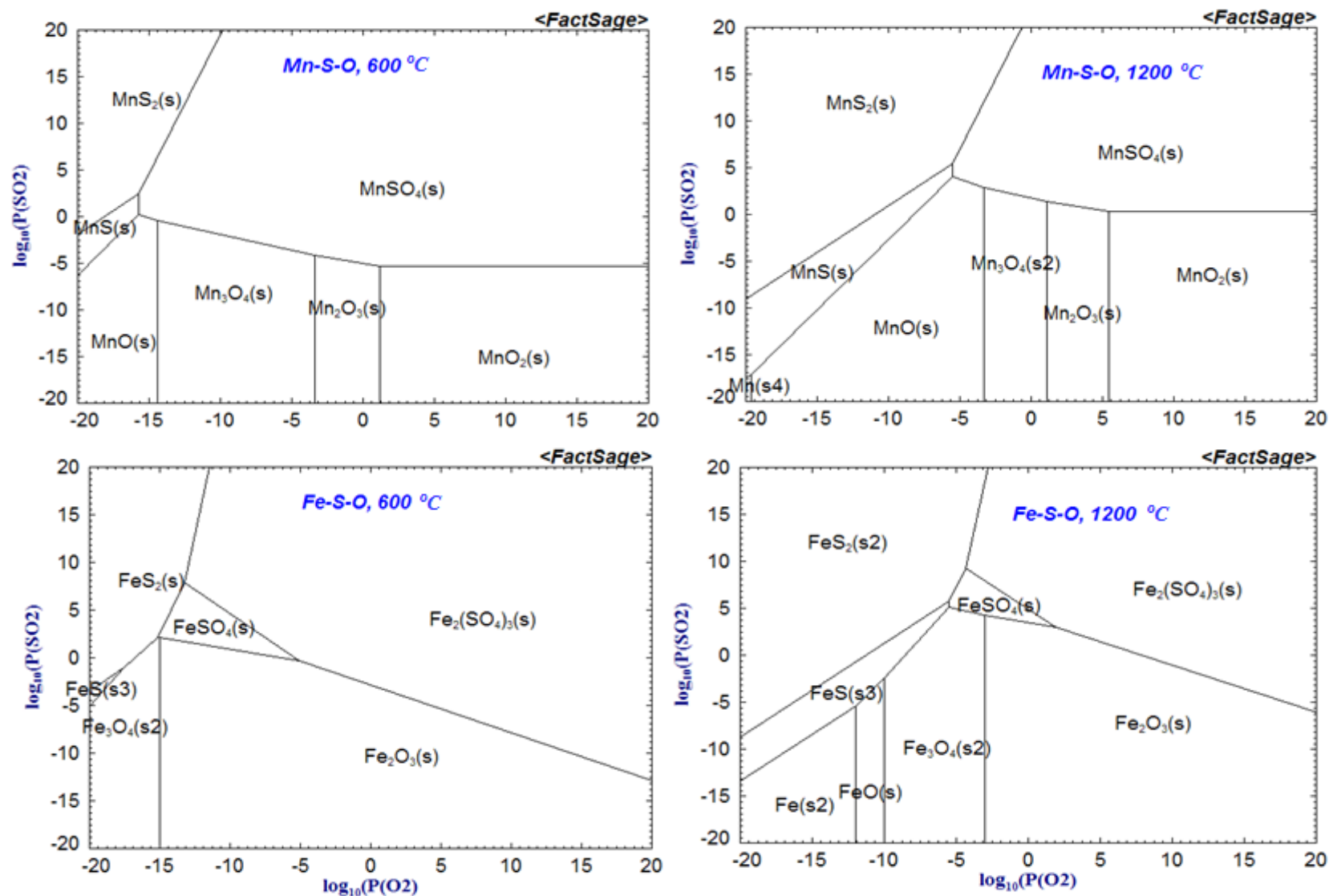
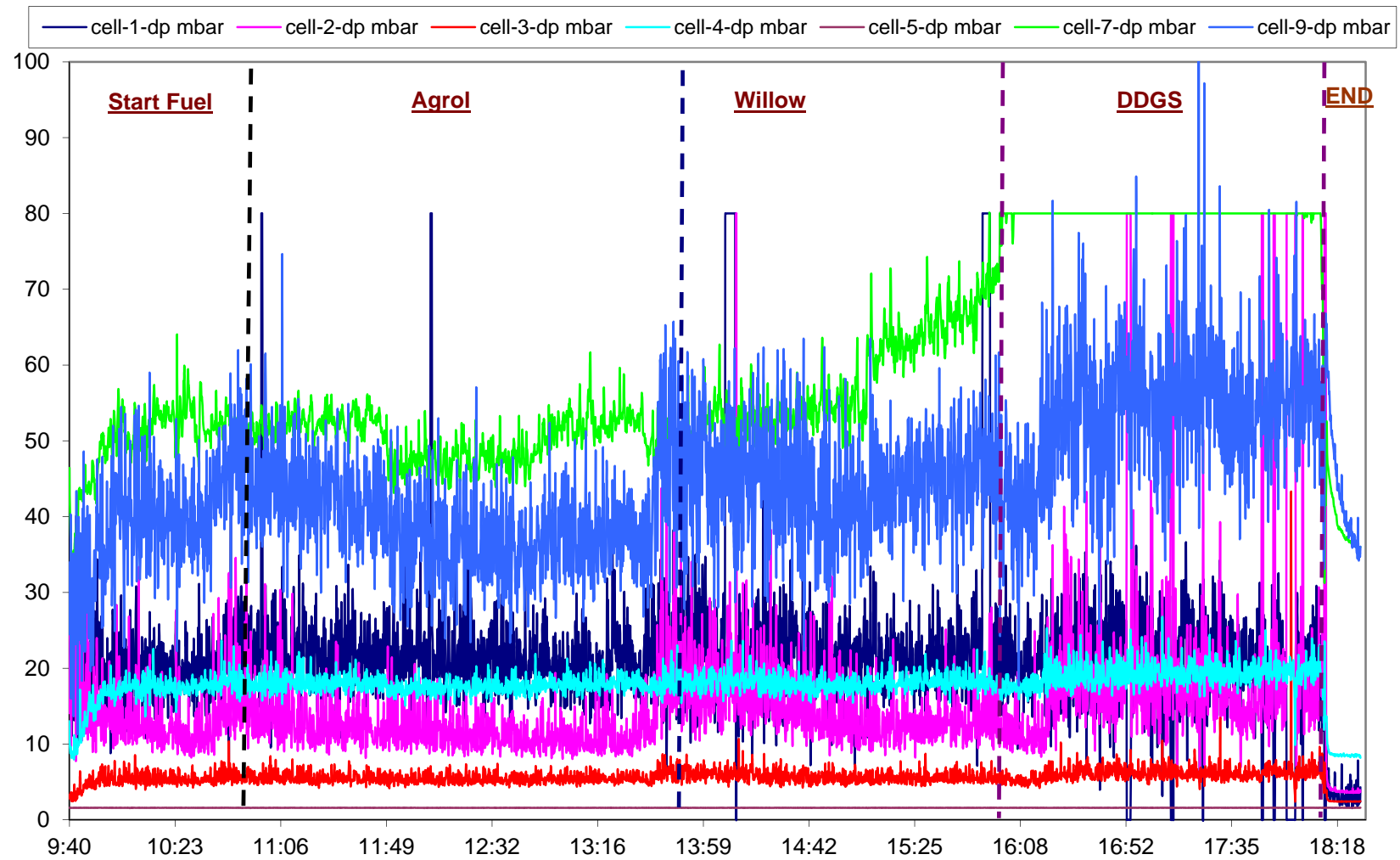


Figure A-6 Phase stability diagrams for the Mn-S-O and Fe-S-O system at 600°C and 1200 °C



*Figure A-7 Several dp-cell trend lines as measured during the experiment on 23 April 2010*

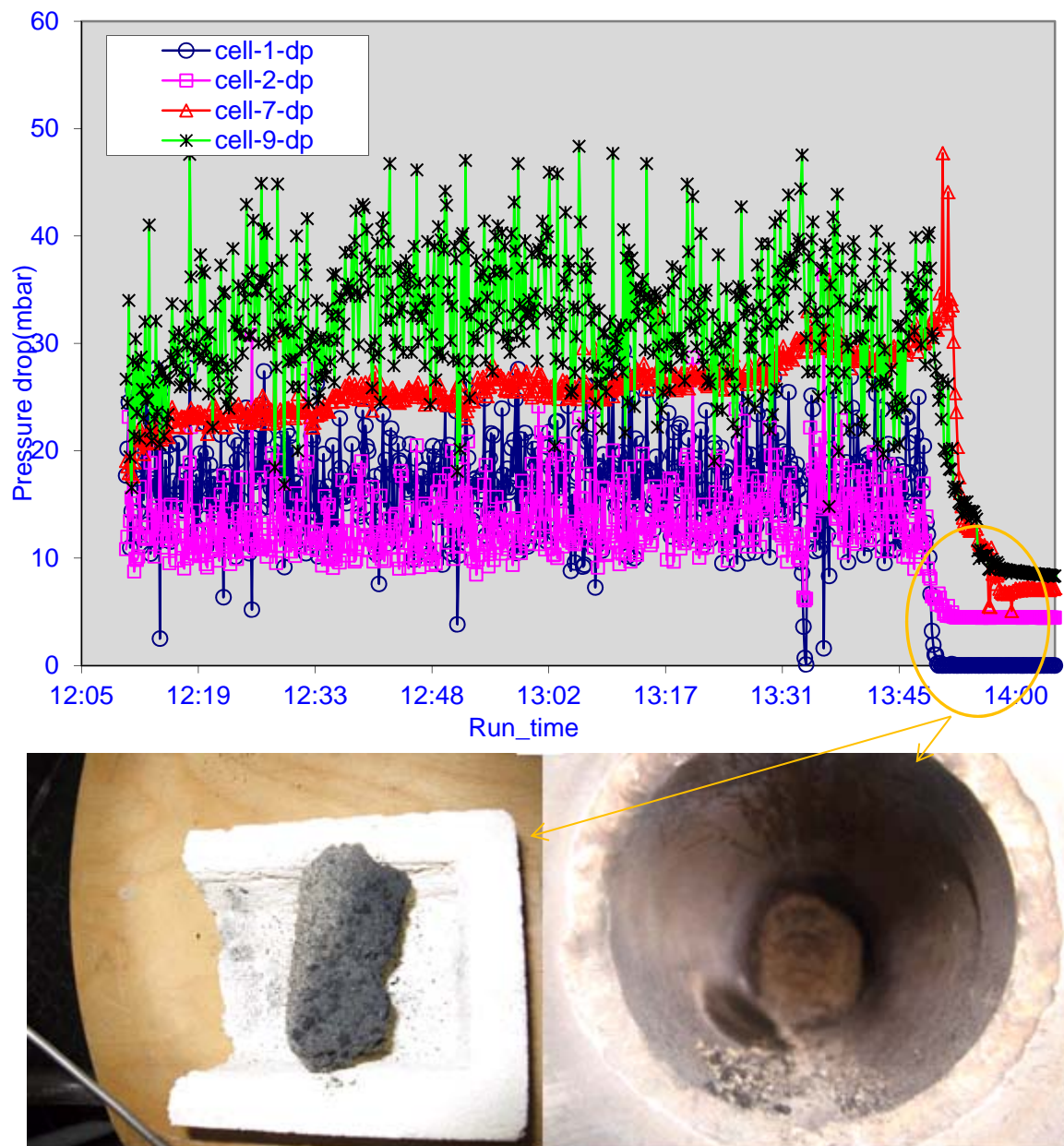


Figure A-8 Several dp-cell behavior (up) and agglomeration pictures (bottom) during DDGS gasification using bed 4 without kaolin (Exp. No D1)



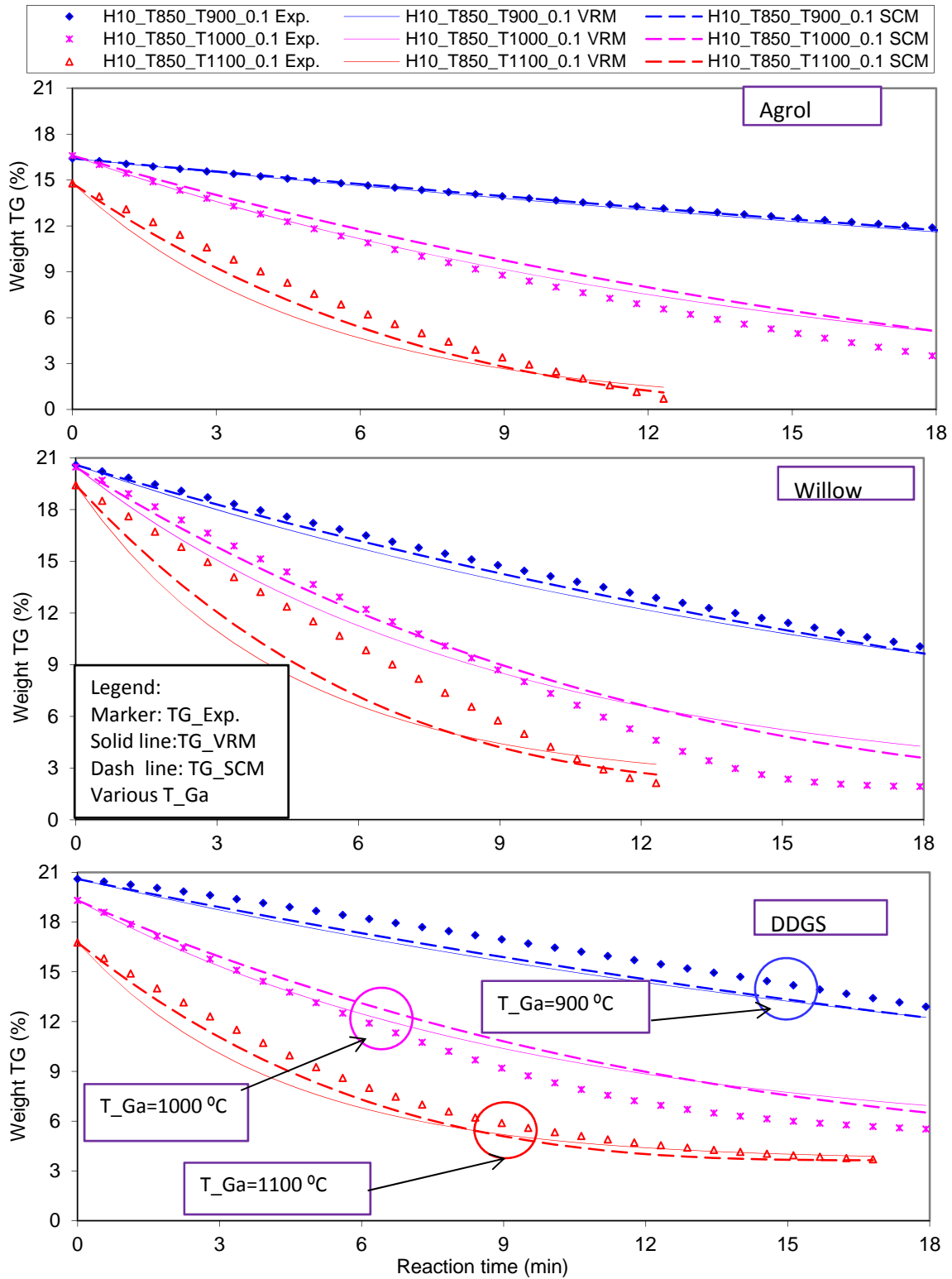


Figure A-9 The recalculated weight loss behavior for PYR-Chars at different gasification temperatures

Remark:

- H10\_T850\_T900\_0.1 represent PYR-Chars at heating rate (10 °C /min) \_pyrolysis temperature ( $T_{Pyr}=850$  °C) \_gasification temperature ( $(T_{Ga}=900$  °C) \_CO<sub>2</sub> concentration (10 vol.%), similar as for others.
- Exp., VRM and SCM represent the TG% values calculated from the experiment, VRM and SCM model, respectively.
- Settings for Agrol, willow and DDGS are the same.

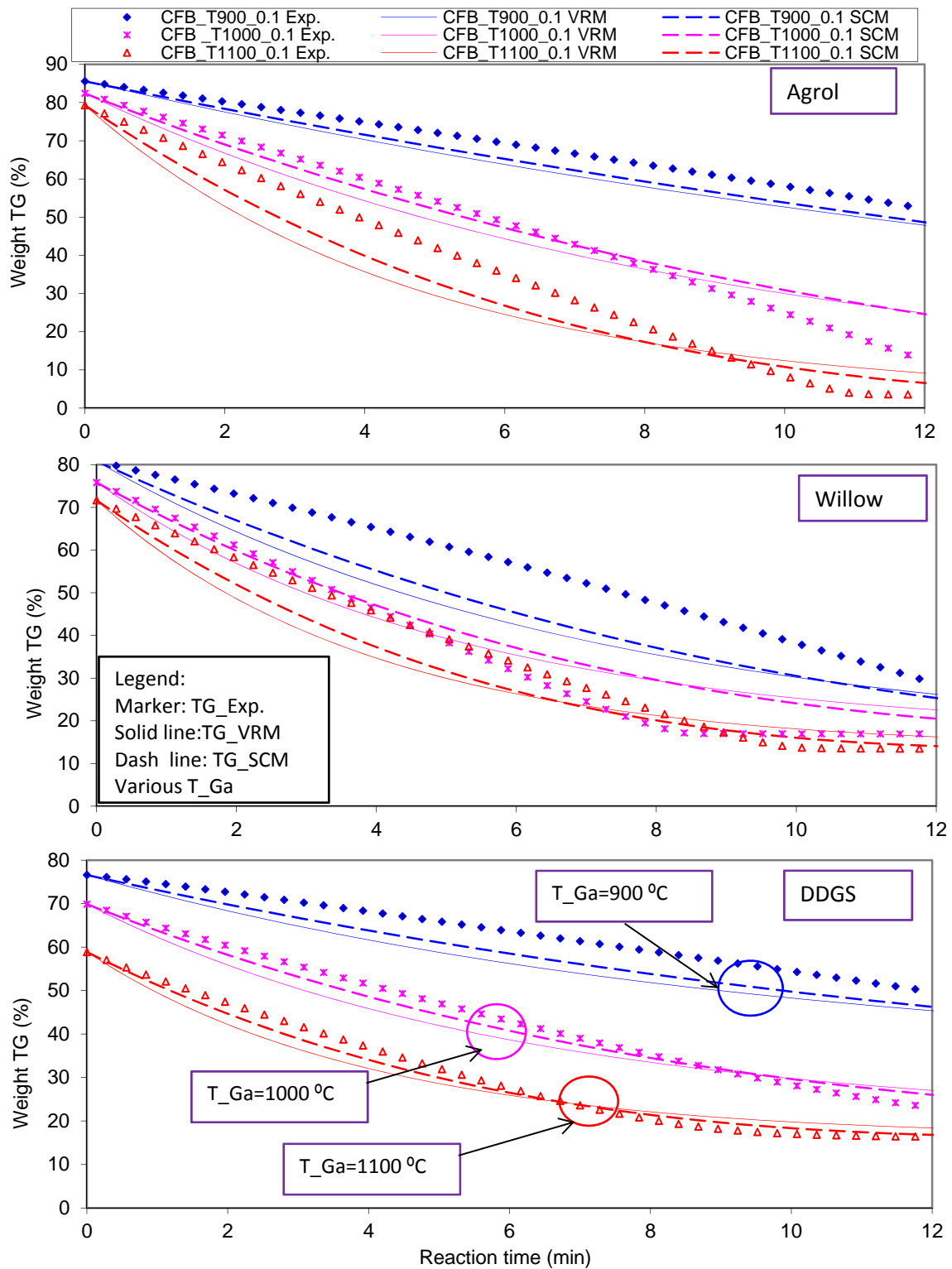
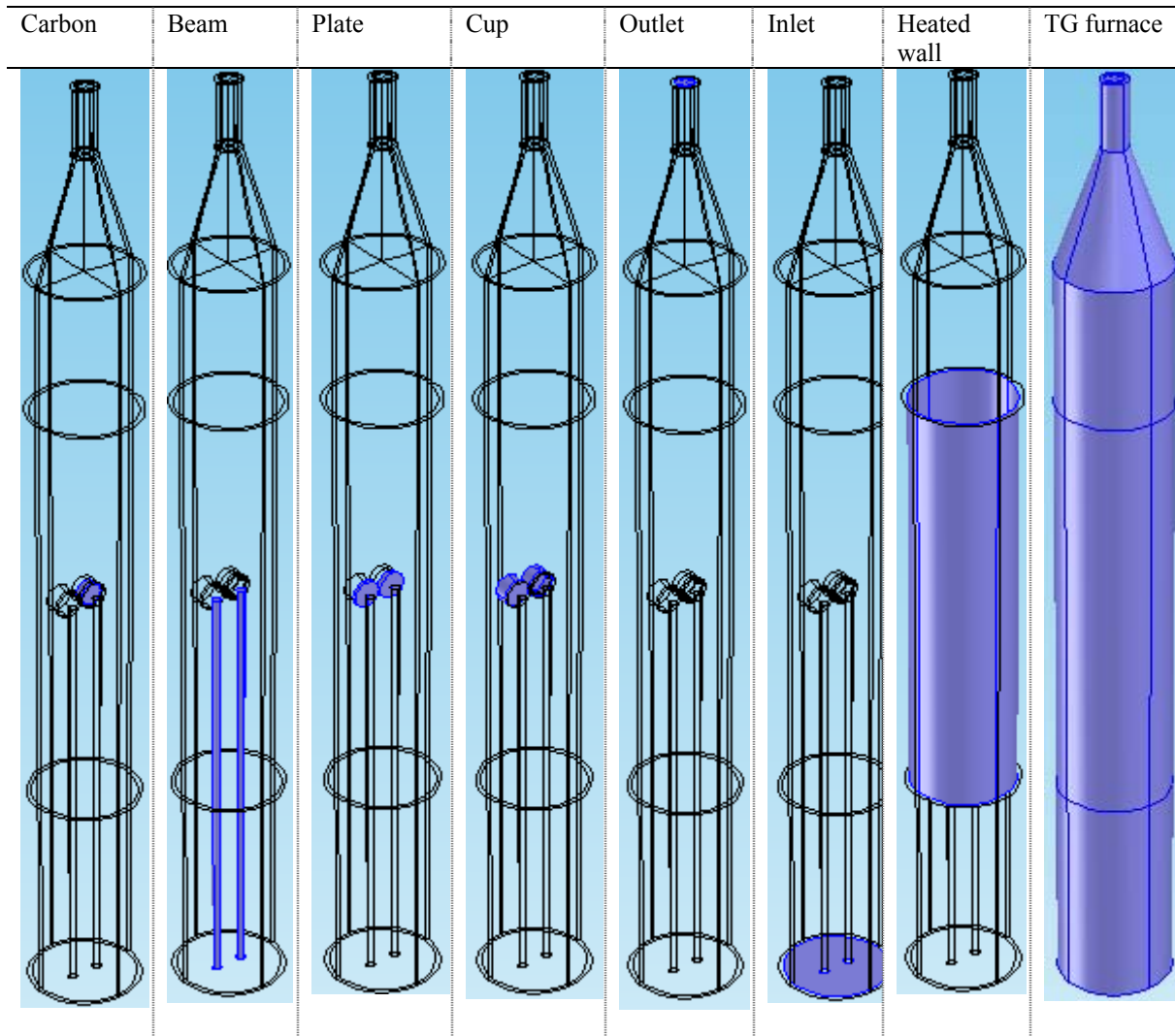


Figure A-10 The recalculated weight loss behavior for CFB-Chars at different gasification temperatures

Remark:

- CFB\_\_T900\_0.1 represent CFB-Chars \_gasification temperature ((T\_Ga=900 °C)\_CO<sub>2</sub> concentration (10 vol.%), similar as for others.
- Exp., VRM and SCM represent the TG% values calculated from the experiment, VRM and SCM model, respectively.
- Settings for Agrol, willow and DDGS are the same.



*Figure A-11 Definitions of different parts in TG furnace COMSOL model*

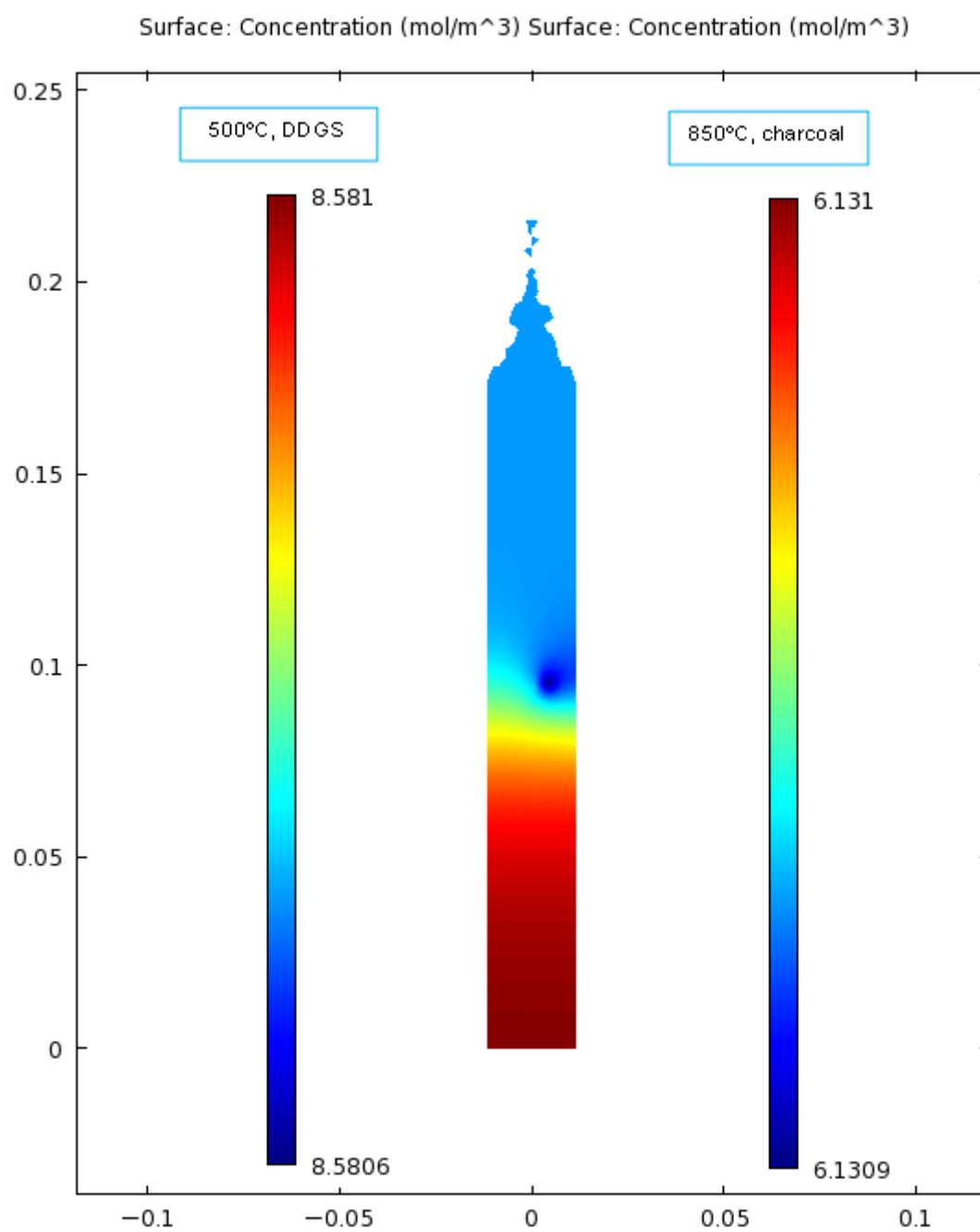


Figure A-12 surface O<sub>2</sub> concentration during DDGS and charcoal combustion

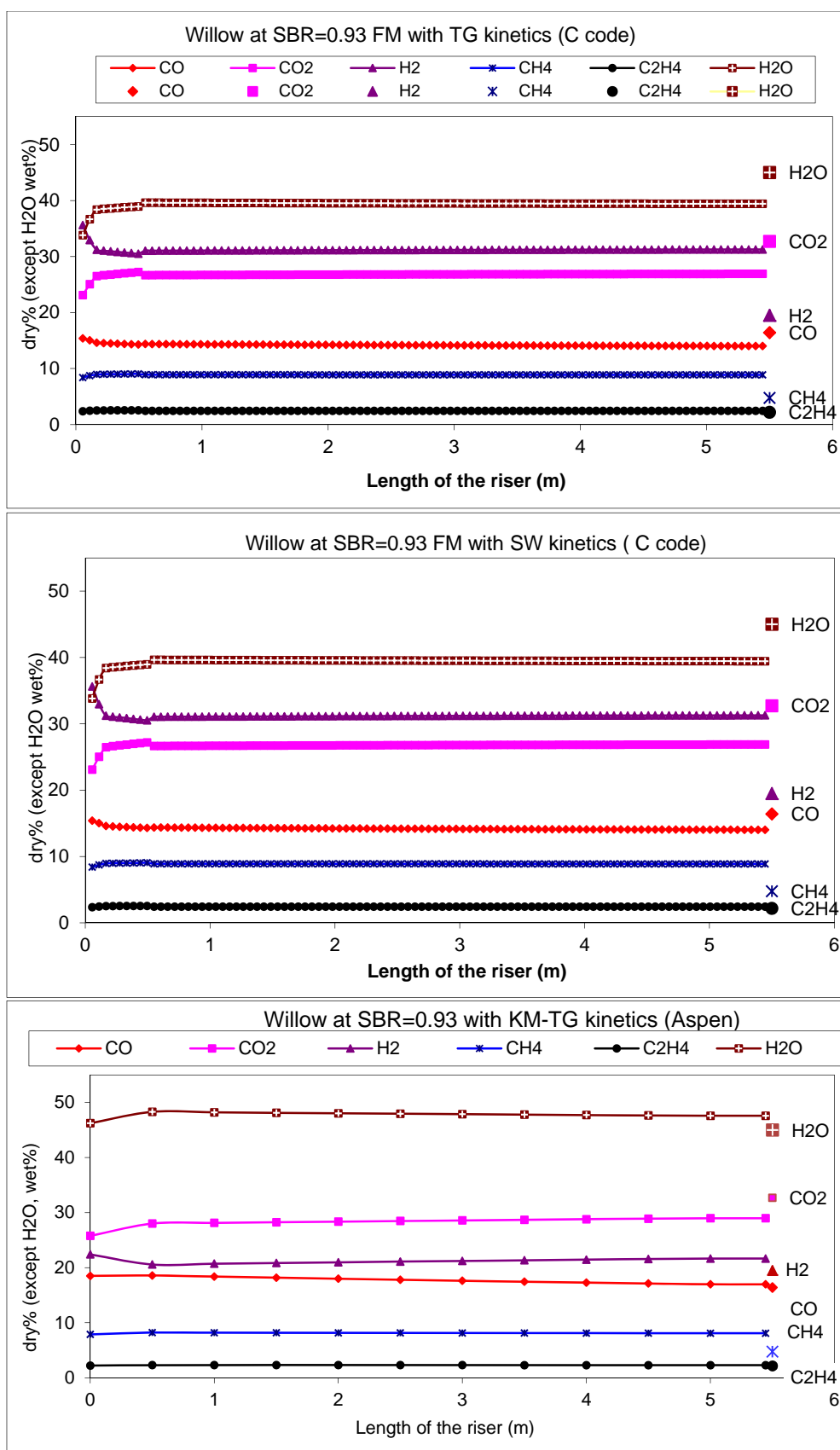


Figure A-13 Gas concentration produced from willow along the length of the riser predicted from the FM model using SW and TG kinetics and from KM-TG Aspen model

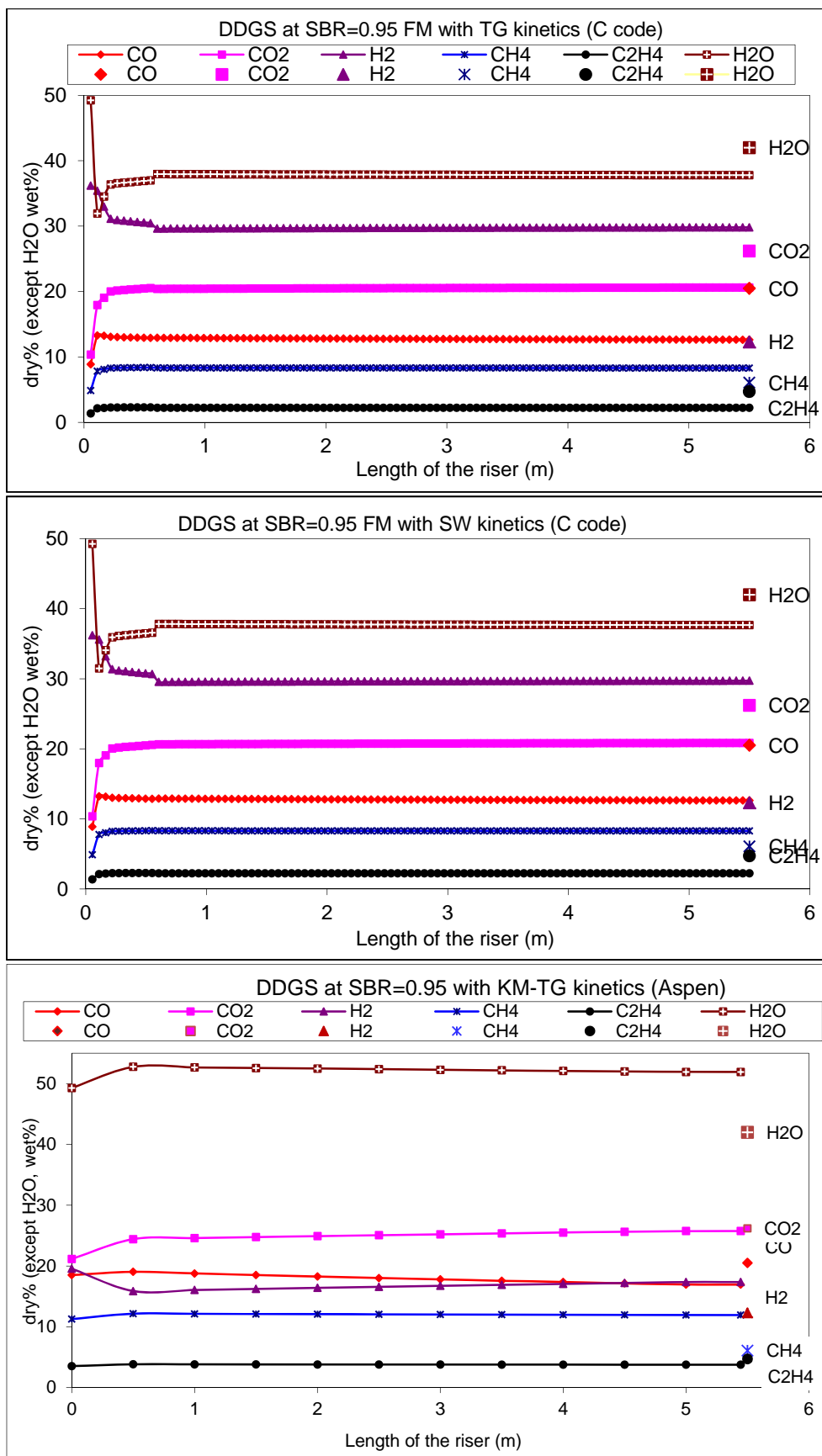


Figure A-14 Gas concentration produced from DDGS along the length of the riser predicted from the FM model using SW and TG kinetics and from KM-TG Aspen model

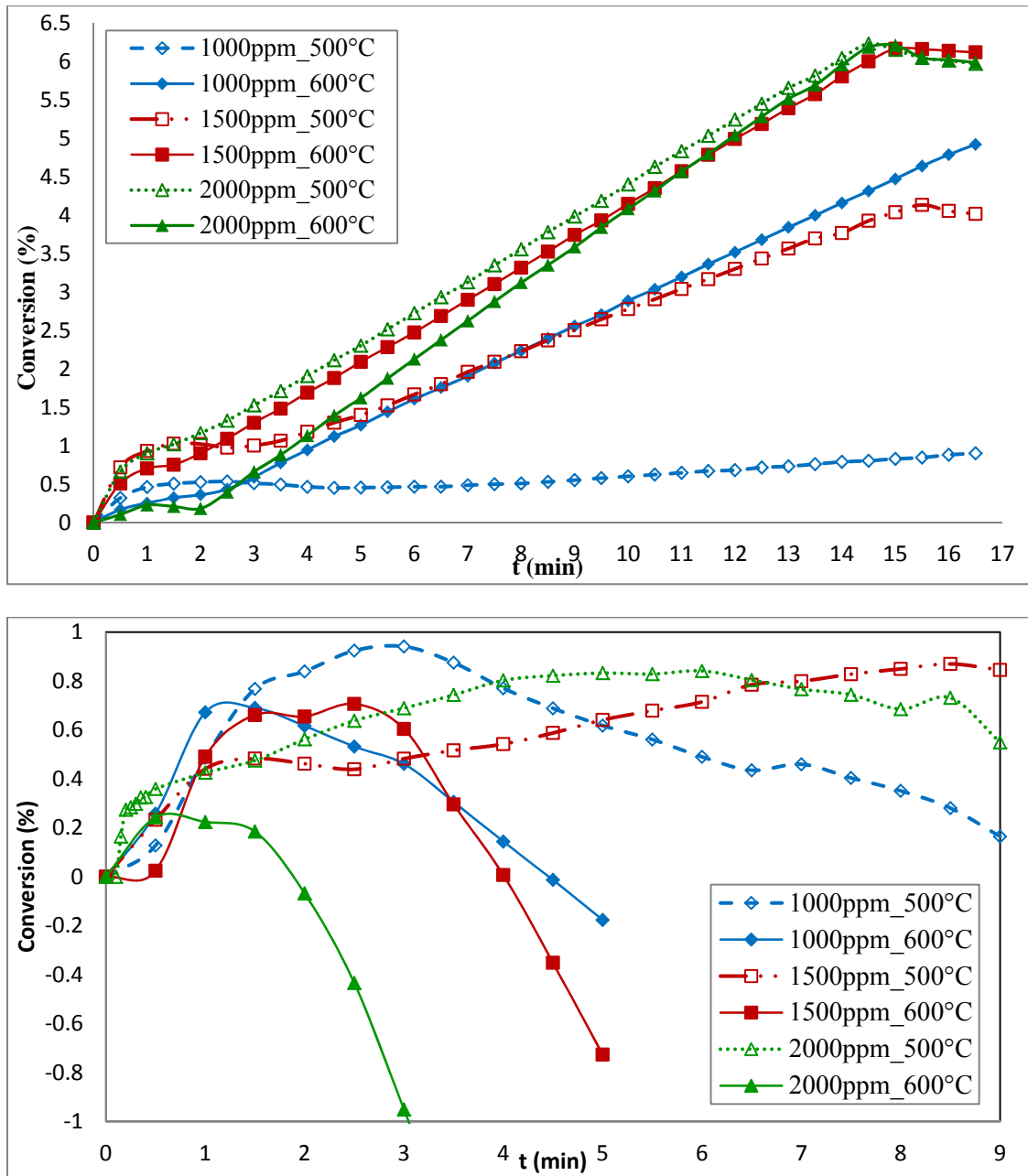


Figure A-15 TGA graph for ZnO (a) and Fe<sub>2</sub>O<sub>3</sub> (b) sulfidation with N<sub>2</sub> as carrier gas

*Appendix X 1 FM code the calculation of the production rate of different gas species*

```
#include "main.h"

void ReactionCoef(INPUT input, double temperature, double cb[], double ce[], double ca[], double
cc[], double z, double dZ, double hd)
{
    const double v15[]={6.0,0.0,3.0,0.0,0.0,0.0,0.0,0.0};
    const double v0[]={0.149,0.173,0.461,0.07,0.125,0.0,0.001,0.02};
    const double beta1=1.2;
    const double mH2O=11.4; //kg/h H2O input to gasifier A11.4, W 13.15, D14.57kg/h
    const double mO2=5.15; //kg/h O2 input to gasifier A 5.15, W 5.1, D 5.5kg/h
    const double mN2=4.51; //kg/h N2 input to gasifier A, W 4.51, D 4.91kg/h
    const double mfuel=0.532; //kmol/h the calculated Agrol input (kmol/h)
    const double rochar=253.0; // kg/m3 Agrol char density
    const double volflow=1405; // L/min inlet gas volume flow rate Agrol
    const double Fvolatile=694; //L/min gas volume flow rate from Agrol pyrolysis
    const double echar=1.0; // carbon ratio in char
    const double X=0.5;
    const double qs=0.81;
    const double time=1.6; // residence time
    const double Ftar=0.006; //mol/m3 the calculated tar

    double
k0,k1,k21,k22,k23,k31,k32,k33,k34,k41,k42,k43,k44,k5,k6,k7,k81,k82,k91,k92,k10,k15,k16,k17;
    double alpha1,tar1;
    double dbm,db0,db,Kbe,Ub,Ue,Eb,Ubr;
    double Uc,Uti,NUti,Ki,Ndp,Cvez,Cvc,alpha;
    double aux1,aux2,aux3,aux4,aux5,tmp1,tmp2;
    double cH2O,cO2,cN2,cfN;
    double Rib,Rieg,Ries;
    double Ricg,Rics,Riag,Rias;
    double T;
    int i;
    T=temperature+273.15;

    //Calculated parameters 0<Z<Hd & Hd<Z<Ht:
    db0=0.824*pow(3.14/4.0*input.dt*input.dt*(input.Uo-input.Umf)/18.0,0.4);
    dbm=0.65*pow(3.14/4.0*input.dt*input.dt*(input.Uo-input.Umf),0.4);
    db=dbm-(dbm-db0)*exp(-0.3*z/input.dt);
    if(db>0.083) db=0.083;
    Ubr=0.711*sqrt(g*db);
    Ub=input.Uo-input.Umf+Ubr;
    Eb=(input.Uo-input.Umf)/Ub;
    Ue=input.Umf/(1.0-Eb);
    Kbe=4.5*input.Umf/db;
    Uc=(Ub+(1-Eb)*input.Umf)/((1.0-input.fa)*(1.0-Cvc));

    Ndp=input.dp*pow((input.rog*g*(input.ros-input.rog)/(input.mug*input.mug)),1.0/3.0);
    NUti=1.0/(18.0/(Ndp*Ndp)+(2.335-1.744*qs)/pow(Ndp,0.5));
    Uti=NUti*pow(input.mug*(input.ros-input.rog)*g/(input.rog*input.rog),1.0/3.0);
    Ki=input.rog*input.Uo*(0.0001+130.0*exp(-10.4*sqrt(Uti/input.Uo)*pow(input.Umf/(input.Uo-
input.Umf),0.25)));
    Cvez=Ki/(input.ros*(input.Uo-Uti));
    if(Cvez<0.0) Cvez=0.0;
```



## Appendix

```
alpha=(0.88-420.0*input.dp)/((input.Uo-Uti)*(input.Uo-Uti)*pow(input.dt,0.6));

//calculate input values fuel (mol/m3/s), oxygen, steam, nitrogen (mol/m3/s)
cfIN=(mfuel*1000.0/60.0)/(Fvolatile/1000.0)/time;
cH2O=(mH2O/18.0*1000.0/60.0)/(volflow/1000.0)/time;
cO2=(mO2/32.0*1000.0/60.0)/(volflow/1000.0)/time;
cN2=(mN2/28.0*1000.0/60.0)/(volflow/1000.0)/time;
tar1=Ftar*1.0;

//calculate reaction coefficients, gas-solid heterogeneous reaction kintetic rate(mol/(m3*s))
alpha1=(1.0+2.0*4.72e-3*exp(37737.0/(Rg*T)))/(1.0+4.72e-3*exp(37737.0/(Rg*T)));
k0=echar*rochar/12.0;
// k1=5.957e+2*T*exp(-149440.0/(Rg*T))*6.0/input.dp; //R1 C+O2=>CO+CO2 KM-SW
k1=1.426e+2*exp(-59900.0/(Rg*T))*1.5; //R1 C+O2=>CO+CO2 KM-TG

//k21=4.89e+7*exp(-268000.0/(Rg*T))*(1.0-X);
//k22=0.066*1.0; // R2 C+CO2=2CO2 kinetic KM-SW
//k23=0.12*exp(25500.0/(Rg*T));
k21=7.679*exp(-96510.0/(Rg*T)); // R2 C+CO2=2CO2 kinetic KM-TG

k31=2.39e+2*exp(-129000.0/(Rg*T))*pow((1.0-X),3.0/3.0); // R3 C+2H2=CH4
k32=3.16e-2*exp(30100.0/(Rg*T));
k33=5.36e-3*exp(59800.0/(Rg*T));
k34=8.25e-5*exp(96100.0/(Rg*T));

k41=2.39e+2*exp(-129000.0/(Rg*T))*pow((1.0-X),3.0/3.0);
k42=3.16e-2*exp(30100.0/(Rg*T)); // R4 C+1.2H2O=0.8CO+0.2CO2+1.2H2
k43=5.36e-3*exp(59800.0/(Rg*T));
k44=8.25e-5*exp(96100.0/(Rg*T));

//gas-gas homogenous reaction kintetic rate(mol/(m3*s))
k5=1.78e+10*exp(-180032.0/(Rg*T)); // R5 CO+0.5O2=CO2
k6=1.08e+10*exp(-125525/(Rg*T)); // R6 H2+0.5O2=H2O CO2H2
k7=1.58e+10*exp(-24343.0/T)*0.0; //CH4+2O2=CO2+2H2O
k81=3015.0*exp(-15000/T); // R7 H4+H2O=CO+3H2
k82=1.0;
k91=2.778*exp(-12560.0/(Rg*T)); //R8 CO+H2O-CO2+H2
k92=0.0265*exp(34730/(Rg*T));
k10=1.585e+10*exp(-24157.0/T)*0.0; // CH4+1.5O2=CO+2H2O this reaction is not considered
in the model, which is why k10=0
k15=1.58e+12*exp(-202641.0/(Rg*T))*tar1; // R12 tar cracking:C6H6+3O2->6CO+3H2
k16=1.58e+10*exp(-202641.0/(Rg*T)); //R10 CH4+0.5O2=CO+2H2
k17=3.71e+12*exp(-209205.0/(Rg*T)); //R11 C2H4+O2=2CO+2H2

//solve homogenous and heterogeneous reaction rates and equation 0<Z<Hd and Hd<Z<Ht:
for (i=0;i<8;i++)
{
    switch (i)
    {
        case 0: //Component1 CO
            //z<Hd
            if(z<hd)
            {
                Rib=v15[one]*k15*cb[six]+k81*(cb[four]*cb[five]-
                cb[one]*pow(cb[three],3.0)/k82)+(k10+k16)*pow(cb[four],0.7)*pow(cb[six],0.8)+2.0*k17*pow(cb[ei
```

```

ght],0.9)*pow(cb[six],1.18)-k5*cb[one]*pow(cb[five],0.5)*pow(cb[six],0.25)-
k91*cb[one]*cb[five]+k91*cb[two]*cb[three]/k92;
    Rieg=v15[one]*k15*ce[six]+k81*(ce[four]*ce[five]-
ce[one]*pow(ce[three],3.0)/k82)+(k10+k16)*pow(ce[four],0.7)*pow(ce[six],0.8)+2.0*k17*pow(ce[ei
ght],0.9)*pow(ce[six],1.18)-k5*ce[one]*pow(ce[five],0.5)*pow(ce[six],0.25)-
k91*ce[one]*ce[five]+k91*ce[two]*ce[three]/k92;
    // Ries=v0[one]*cfIN+2.0*k1*(alpha1-
1.0)*pow(ce[six],1.0)+2.0*k0*k21*ce[two]/(1.0+k22*ce[two]+k23*ce[one])+(2.0-
beta1)*k0*k41*ce[five]/(1.0+k42*ce[five]+k43*ce[three]+k44*ce[one]);
    Ries=v0[one]*cfIN+2.0*k1*(alpha1-1.0)*pow(ce[six],1.0)+2.0*k21*ce[two]+(2.0-
beta1)*k0*k41*ce[five]/(1.0+k42*ce[five]+k43*ce[three]+k44*ce[one]);
    }
    else
    {
        //Hd<z<Ht
        Rieg=v15[one]*k15*cc[six]+k81*(cc[four]*cc[five]-
cc[one]*pow(cc[three],3.0)/k82)+(k10+k16)*pow(cc[four],0.7)*pow(cc[six],0.8)+2.0*k17*pow(cc[ei
ght],0.9)*pow(cc[six],1.18)-k5*cc[one]*pow(cc[five],0.5)*pow(cc[six],0.25)-
k91*cc[one]*cc[five]+k91*cc[two]*cc[three]/k92;
        Riag=v15[one]*k15*ca[six]+k81*(ca[four]*ca[five]-
ca[one]*pow(ca[three],3.0)/k82)+(k10+k16)*pow(ca[four],0.7)*pow(ca[six],0.8)+2.0*k17*pow(ca[ei
ght],0.9)*pow(ca[six],1.18)-k5*ca[one]*pow(ca[five],0.5)*pow(ca[six],0.25)-
k91*ca[one]*ca[five]+k91*ca[two]*ca[three]/k92;
        // Rics=2.0*k1*(alpha1-
1.0)*pow(cc[six],1.0)+2.0*k0*k21*cc[two]/(1.0+k22*cc[two]+k23*cc[one])+(2.0-
beta1)*k0*k41*cc[five]/(1.0+k42*cc[five]+k43*cc[three]+k44*cc[one]);
        // Rias=2.0*k1*(alpha1-
1.0)*pow(ca[six],1.0)+2.0*k0*k21*ca[two]/(1.0+k22*ca[two]+k23*ca[one])+(2.0-
beta1)*k0*k41*ca[five]/(1.0+k42*ca[five]+k43*ca[three]+k44*ca[one]);
        Rics=2.0*k1*(alpha1-1.0)*pow(cc[six],1.0)+2.0*k21*cc[two]+(2.0-
beta1)*k0*k41*cc[five]/(1.0+k42*cc[five]+k43*cc[three]+k44*cc[one]);
        Rias=2.0*k1*(alpha1-1.0)*pow(ca[six],1.0)+2.0*k21*ca[two]+(2.0-
beta1)*k0*k41*ca[five]/(1.0+k42*ca[five]+k43*ca[three]+k44*ca[one]);
    }
    break;
case 1: //Component2 CO2
    //z<Hd
    if(z<hd)
    {

```

```

Rib=v15[two]*k15+k5*cb[one]*pow(cb[five],0.5)*pow(cb[six],0.25)+k7*pow(cb[four],0.7)*pow(cb[
six],0.8)+k91*cb[one]*cb[five]-k91*cb[two]*cb[three]/k92;

```

```

Rieg=v15[two]*k15+k5*ce[one]*pow(ce[five],0.5)*pow(ce[six],0.25)+k7*pow(ce[four],0.7)*pow(ce[
six],0.8)+k91*ce[one]*ce[five]-k91*ce[two]*ce[three]/k92;
    //Ries=v0[two]*cfIN+k1*(2.0-alpha1)*pow(ce[six],0.53)-
k0*k21*ce[two]/(1.0+k22*ce[two]+k23*ce[one])+(beta1-
1.0)*k0*k41*ce[five]/(1.0+k42*ce[five]+k43*ce[three]+k44*ce[one]);
    Ries=v0[two]*cfIN+k1*(2.0-alpha1)*pow(ce[six],0.53)-k21*ce[two]+(beta1-
1.0)*k0*k41*ce[five]/(1.0+k42*ce[five]+k43*ce[three]+k44*ce[one]);
    }
    else
    {
        //Hd<z<Ht

```

```

Ricg=v15[two]*k15+k5*cc[one]*pow(cc[five],0.5)*pow(cc[six],0.25)+k7*pow(cc[four],0.7)*pow(cc[
six],0.8)+k91*cc[one]*cc[five]-k91*cc[two]*cc[three]/k92;

Riag=v15[two]*k15+k5*ca[one]*pow(ca[five],0.5)*pow(ca[six],0.25)+k7*pow(ca[four],0.7)*pow(ca[
six],0.8)+k91*ca[one]*ca[five]-k91*ca[two]*ca[three]/k92;
// Rics=k1*(2.0-alpha1)*pow(cc[six],1.0)-
k0*k21*cc[two]/(1.0+k22*cc[two]+k23*cc[one])+(beta1-
1.0)*k0*k41*cc[five]/(1.0+k42*cc[five]+k43*cc[three]+k44*cc[one]);
// Rias=k1*(2.0-alpha1)*pow(ca[six],1.0)-
k0*k21*ca[two]/(1.0+k22*ca[two]+k23*ca[one])+(beta1-
1.0)*k0*k41*ca[five]/(1.0+k42*ca[five]+k43*ca[three]+k44*ca[one]);
Rics=k1*(2.0-alpha1)*pow(cc[six],1.0)-k21*cc[two]+(beta1-
1.0)*k0*k41*cc[five]/(1.0+k42*cc[five]+k43*cc[three]+k44*cc[one]);
Rias=k1*(2.0-alpha1)*pow(ca[six],1.0)-k21*ca[two]+(beta1-
1.0)*k0*k41*ca[five]/(1.0+k42*ca[five]+k43*ca[three]+k44*ca[one]);
}
break;
case 2: //Component3 H2
//z<Hd
if(z<hd)
{
Rib=v15[three]*k15*cb[six]+3.0*k81*(cb[four]*cb[five]-
cb[one]*pow(cb[three],3.0)/k82)+k91*cb[one]*cb[five]-
k91*cb[two]*cb[three]/k92+2.0*k17*pow(cb[eight],0.9)*pow(cb[six],1.18)-
k6*cb[six]*pow(cb[three],1.0)+2.0*k16*pow(cb[four],0.7)*pow(cb[six],0.8);
Rieg=v15[three]*k15*ce[six]+3.0*k81*(ce[four]*ce[five]-
ce[one]*pow(ce[three],3.0)/k82)+k91*ce[one]*ce[five]-
k91*ce[two]*ce[three]/k92+2.0*k17*pow(ce[eight],0.9)*pow(ce[six],1.18)-
k6*ce[six]*pow(ce[three],1.0)+2.0*k16*pow(ce[four],0.7)*pow(ce[six],0.8);
Ries=v0[three]*cflN+beta1*k0*k41*ce[five]/(1.0+k42*ce[five]+k43*ce[three]+k44*ce[one])-
2.0*k0*k31*ce[three]/(1.0+k32*ce[five]+k33*ce[three]+k34*ce[one]);
}
else
{
//Hd<z<Ht
Ricg=v15[three]*k15*cc[six]+3.0*k81*(cc[four]*cc[five]-
cc[one]*pow(cc[three],3.0)/k82)+k91*cc[one]*cc[five]-
k91*cc[two]*cc[three]/k92+2.0*k17*pow(cc[eight],0.9)*pow(cc[six],1.18)-
k6*cc[six]*pow(cc[three],1.0)+2.0*k16*pow(cc[four],0.7)*pow(cc[six],0.8);
Riag=v15[three]*k15*ca[six]+3.0*k81*(ca[four]*ca[five]-
ca[one]*pow(ca[three],3.0)/k82)+k91*ca[one]*ca[five]-
k91*ca[two]*ca[three]/k92+2.0*k17*pow(ca[eight],0.9)*pow(ca[six],1.18)-
k6*ca[six]*pow(ca[three],1.0)+2.0*k16*pow(ca[four],0.7)*pow(ca[six],0.8);
Rics=beta1*k0*k41*cc[five]/(1.0+k42*cc[five]+k43*cc[three]+k44*cc[one])-
2.0*k0*k31*cc[three]/(1.0+k32*cc[five]+k33*cc[three]+k34*cc[one]);
Rias=beta1*k0*k41*ca[five]/(1.0+k42*ca[five]+k43*ca[three]+k44*ca[one])-
2.0*k0*k31*ca[three]/(1.0+k32*ca[five]+k33*ca[three]+k34*ca[one]);
}
break;
case 3: //Component4 CH4
//z<Hd
if(z<hd)
{

```

```

        Rib=v15[four]*k15-k7*pow(cb[four],0.7)*pow(cb[six],0.8)-k81*(cb[four]*cb[five]-
cb[one]*pow(cb[three],3.0)/k82)-(k10+k16)*pow(cb[four],0.7)*pow(cb[six],0.8);
        Rieg=v15[four]*k15-k7*pow(ce[four],0.7)*pow(ce[six],0.8)-k81*(ce[four]*ce[five]-
ce[one]*pow(ce[three],3.0)/k82)-(k10+k16)*pow(ce[four],0.7)*pow(ce[six],0.8);
        Ries=v0[four]*cfIN+k0*k31*ce[three]/(1.0+k32*ce[five]+k33*ce[three]+k34*ce[one]);
    }
    //Hd<z<Ht
    else
    {
        Ricg=v15[four]*k15-k7*pow(cc[four],0.7)*pow(cc[six],0.8)-k81*(cc[four]*cc[five]-
cc[one]*pow(cc[three],3.0)/k82)-(k10+k16)*pow(cc[four],0.7)*pow(cc[six],0.8);
        Riag=v15[four]*k15-k7*pow(ca[four],0.7)*pow(ca[six],0.8)-k81*(ca[four]*ca[five]-
ca[one]*pow(ca[three],3.0)/k82)-(k10+k16)*pow(ca[four],0.7)*pow(ca[six],0.8);
        Rics=k0*k31*cc[three]/(1.0+k32*cc[five]+k33*cc[three]+k34*cc[one]);
        Rias=k0*k31*ca[three]/(1.0+k32*ca[five]+k33*ca[three]+k34*ca[one]);
    }
    break;
case 4: //Component5 H2O
    //z<Hd
    if(z<hd)
    {

```

```

        Rib=k6*cb[six]*pow(cb[three],1.0)+2.0*k7*pow(cb[four],0.7)*pow(cb[six],0.8)+2.0*k10*pow(cb[fo
ur],0.7)*pow(cb[six],0.8)-k81*(cb[four]*cb[five]-cb[one]*pow(cb[three],3.0)/k82)-
k91*cb[one]*cb[five]+k91*cb[two]*cb[three]/k92;

```

```

        Rieg=k6*ce[six]*pow(ce[three],1.0)+2.0*k7*pow(ce[four],0.7)*pow(ce[six],0.8)+2.0*k10*pow(ce[fo
ur],0.7)*pow(ce[six],0.8)-k81*(ce[four]*ce[five]-ce[one]*pow(ce[three],3.0)/k82)-
k91*ce[one]*ce[five]+k91*ce[two]*ce[three]/k92+cH2O;
        Ries=v0[five]*cfIN-beta1*k0*k41*ce[five]/(1.0+k42*ce[five]+k43*ce[three]+k44*ce[one]);
    }
    //Hd<z<Ht
    else
    {

```

```

        Ricg=k6*cc[six]*pow(cc[three],1.0)+2.0*k7*pow(cc[four],0.7)*pow(cc[six],0.8)+2.0*k10*pow(cc[fo
ur],0.7)*pow(cc[six],0.8)-k81*(cc[four]*cc[five]-cc[one]*pow(cc[three],3.0)/k82)-
k91*cc[one]*cc[five]+k91*cc[two]*cc[three]/k92;

```

```

        Riag=k6*ca[six]*pow(ca[three],1.0)+2.0*k7*pow(ca[four],0.7)*pow(ca[six],0.8)+2.0*k10*pow(ca[fo
ur],0.7)*pow(ca[six],0.8)-k81*(ca[four]*ca[five]-ca[one]*pow(ca[three],3.0)/k82)-
k91*ca[one]*ca[five]+k91*ca[two]*ca[three]/k92;
        Rics=-beta1*k0*k41*cc[five]/(1.0+k42*cc[five]+k43*cc[three]+k44*cc[one]);
        Rias=-beta1*k0*k41*ca[five]/(1.0+k42*ca[five]+k43*ca[three]+k44*ca[one]);
    }
    break;

```

```

case 5: //Component6 O2

```

```

    //z<Hd
    if(z<hd)
    {
        Rib=-3*k15*cb[six]-0.5*k5*cb[one]*pow(cb[five],0.5)*pow(cb[six],0.25)-
0.5*k6*cb[six]*pow(cb[three],1.0)-2.0*k7*pow(cb[four],0.7)*pow(cb[six],0.8)-
(1.5*k10+0.5*k16)*pow(cb[four],0.7)*pow(cb[six],0.8)-k17*pow(cb[eight],0.9)*pow(cb[six],1.18);
        Rieg=-3*k15*ce[six]-0.5*k5*ce[one]*pow(ce[five],0.5)*pow(ce[six],0.25)-
0.5*k6*ce[six]*pow(ce[three],1.0)-2.0*k7*pow(ce[four],0.7)*pow(ce[six],0.8)-

```

```

(1.5*k10+0.5*k16)*pow(cc[four],0.7)*pow(cc[six],0.8)-
k17*pow(cc[eight],0.9)*pow(cc[six],1.18)+cO2;
    Ries=v0[six]*cfIN-k1*pow(cc[six],1.0);
}
//Hd<z<Ht
else
{
    Ricg=-3*k15*cc[six]-0.5*k5*cc[one]*pow(cc[five],0.5)*pow(cc[six],0.5)-
0.5*k6*cc[six]*pow(cc[three],1.0)-2.0*k7*pow(cc[four],0.7)*pow(cc[six],0.8)-
(1.5*k10+0.5*k16)*pow(cc[four],0.7)*pow(cc[six],0.8)-k17*pow(cc[eight],0.9)*pow(cc[six],1.18);
    Riag=-3*k15*ca[six]-0.5*k5*ca[one]*pow(ca[five],0.5)*pow(ca[six],0.5)-
0.5*k6*ca[six]*pow(ca[three],1.0)-2.0*k7*pow(ca[four],0.7)*pow(ca[six],0.8)-
(1.5*k10+0.5*k16)*pow(ca[four],0.7)*pow(ca[six],0.8)-k17*pow(ca[eight],0.9)*pow(ca[six],1.18);
    Rics=-k1*pow(cc[six],1.0);
    Rias=-k1*pow(ca[six],1.0);
}
break;
case 6: //Component7 N2
//z<Hd
if(z<hd)
{
    Rib=0.0;
    Rieg=cN2;
    Ries=v0[seven]*cfIN;
}
//Hd<z<Ht
else
{
    Ricg=0.0;
    Riag=0.0;
    Rics=0.0;
    Rias=0.0;
}
break;
case 7: //Component8 C2H4
//z<Hd
if(z<hd)
{
    Rib=v15[eight]*k15-k17*pow(cb[eight],0.9)*pow(cb[six],1.18);
    Rieg=v15[eight]*k15-k17*pow(cc[eight],0.9)*pow(cc[six],1.18);
    Ries=v0[eight]*cfIN;
}
//Hd<z<Ht
else
{
    Ricg=-k17*pow(cc[eight],0.9)*pow(cc[six],1.18);
    Riag=-k17*pow(ca[eight],0.9)*pow(ca[six],1.18);
    Rics=0.0;
    Rias=0.0;
}
break;
}
if(z<hd)
{
    aux1=dZ/Ub;

```

```

aux2=dZ/(input.Umf*input.Emf);
aux3=(1.0-Eb)*input.Emf;
tmp1=cb[i];
cb[i]=cb[i]-aux1*Kbe*(cb[i]-ce[i])+aux1*Rib;
ce[i]=ce[i]+aux2*Kbe*Eb*(tmp1-ce[i])+aux3*aux2*Rieg+aux2*(1.0-Eb)*(1.0-input.Emf)*Ries;
if(cb[i]<0) cb[i]=0.0;
if(ce[i]<0) ce[i]=0.0;
}
else
{
Cvc=Cvez+(input.Cvb-Cvez)*exp(-alpha*(z-hd));
aux4=dZ/((1.0-Cvc)*Uc*(1.0-input.fa));
aux5=dZ/((1.0-input.Cva)*input.fa*input.Ua);
tmp2=cc[i];
cc[i]=cc[i]-input.Kca*(cc[i]-ca[i])*aux4+aux4*(1.0-input.fa)*(Cvc*Rics+(1.0-Cvc)*Ricg);
ca[i]=ca[i]+input.Kca*(tmp2-ca[i])*aux5+aux5*input.fa*(input.Cva*Rias+(1.0-input.Cva)*Riag);
if(cc[i]<0) cc[i]=0.0;
if(ca[i]<0) ca[i]=0.0;
}
}
}

```

## List of publications

---

### *Journal papers:*

1. **Meng, X.**, De Jong, W., Verkooijen, A. 2009. Thermodynamic analysis and kinetics model of H<sub>2</sub>S sorption using different sorbents. *Environmental Progress & Sustainable Energy*, **28**(3), pp. 360-371.
2. **Meng, X.**, de Jong, W., Fu, N., Verkooijen, A.H.M. 2011. Biomass gasification in a 100 kW<sub>th</sub> steam-oxygen blown circulating fluidized bed gasifier: Effects of operational conditions on product gas distribution and tar formation. *Biomass and Bioenergy*, **35**(7), 2910-2924.
3. **Meng, X.**, De Jong, W., Pal, R., Verkooijen, A.H.M. 2010. In bed and downstream hot gas desulfurization during solid fuel gasification: A review. *Fuel Processing Technology*, **91**(8), 964-981.
4. **Meng, X.**, de Jong, W., Fu, N., Verkooijen, A.H.M. 2011. DDGS chars gasification with CO<sub>2</sub>: a kinetic study using TG analysis. *Biomass Conversion and Biorefinery, Processing of Biogenic Material for Energy and Chemistry*, 1 (4), 217-227.
5. **Meng, X.**, Benito, P., de Jong, W., Basile, F., Verkooijen, A.H.M., Fornasari, G. and Angelo Vaccari, A. 2012. Characterization of different residual chars obtained from biomass gasification in a 100kW<sub>th</sub> steam-O<sub>2</sub> blown CFB gasifier, *Energy and Fuels*, **26**(1), 722-739.
6. **Meng, X.**, de Jong, W., Badri F., Benito, P., Basile, F., Verkooijen, A. H. M. 2012. Combustion study of partially gasified willow and DDGS chars using TG analysis and Comsol modeling, *Biomass and Bioenergy*, **39**, 356-369.
7. **Meng, X.**, Mitsakis, P., Mayerhofer, M., de Jong, W., Gaderer, M., Verkooijen, A.H.M., and Spliethoff, H. 2012. Tar formation in a steam-O<sub>2</sub> blown CFB gasifier and a PBFB gasifier (BabyHPR): Comparison between different online measurement techniques and the SPA method, *Fuel Processing Technology*, **100**, 16-29.
8. Mayerhofer, M., Mitsakis, P., **Meng, X.**, de Jong, W., Spliethoff, H., Gaderer, M. 2012. Influence of temperature, steam and pressure on tar and gas in allothermal fluidized bed gasification, *Fuel*, **99**, 204-209.
9. Nilsson P. T., Malik A., **Meng X.**, Pagels J., de Jong W., Gudmundsson A., Verkooijen A. H. M., Sanatil M. 2012. Methodology for sampling and characterization of sub-micron high temperature particles present in the product gas from a CFB biomass gasifier, submitted to *Applied Energy*.

### ***Conference papers:***

1. **Meng, X.**, de Jong, W., Verkooijen, A.H.M. 2009. Prediction of sulfur compounds distribution in gasification products of biomass fuels, Proceeding of 17<sup>th</sup> European Biomass Conference and Exhibition from Research to Industry and Markets, 29 June-3 July, Hamburg, Germany. pp. 940-947.
2. **Meng, X.**, de Jong, W., Fu, N.J., Verkooijen, A.H.M. 2010. Primary results of dried distiller's grains with solubles gasification in a 100kW<sub>th</sub> steam-oxygen blown circulating fluidized bed gasifier, the 8<sup>th</sup> International Symposium on Gas Cleaning at High Temperatures, 2010. Taiyuan, Shanxi, China
3. **Meng, X.**, de Jong, W., Fu, N., Verkooijen, A.H.M. 2011c. Reaction kinetics study of willow char gasification with CO<sub>2</sub> using TG analysis, Proceeding of 19<sup>th</sup> European Biomass Conference and Exhibition from Research to Industry and Markets, 6-10 June, Berlin, Germany.
4. Mayerhofer, M., Mitsakis, P., **Meng, X.**, de Jong, W., Spliethoff, H., Gaderer, M. 2011. Influence of operational parameters on tar formation and main gas components during allothermal steam gasification, Proceeding of 19<sup>th</sup> European Biomass Conference and Exhibition from Research to Industry and Markets, 6-10 June, Berlin, Germany.

### ***Project deliverables:***

1. **Meng, X.**, and de Jong, W. 2009. A report on tar analysis and possibility for improvement - the State of the art Literature, Greensyngas Project, Deliverable 4.4, 22<sup>nd</sup>, October, TU Delft, the Netherlands.
2. **Meng, X.**, and de Jong, W. 2011. Comparison of on-line measurement techniques and standard tar measurements, Deliverable D4.5, January, 2011, TU Delft, the Netherlands.
3. **Meng, X.**, and de Jong, W. 2011. Summary of reviews on contaminants identification and cleaning system results, Deliverable D8.3, March, 2011. TU Delft, the Netherlands.
4. **Meng, X.**, and de Jong, W. 2011. Demonstration of in-bed S capture in interaction with in-bed tar reduction, Milestone M4.1, March, 2011.



## Acknowledgments

---

In Chinese, we have one popular saying “guāng yīn sì jiàn, rì yuè rú suō” (光阴似箭，日月如梭) which means “Time flies”, it does so! It feels that I just started this PhD journal yesterday, now four years is going to reach the end. This book contains not only the fruits of my four years of hard work, but also a bucket of wonderful and amazing memory which have been brought by my dear colleagues, friends and family. With this opportunity, I would like express my deepest and truest gratitude to all of you for your contribution to my PhD work.

First of all, immense gratitude to my promotor professor Adrian Verkooijen and my daily superior Dr. Wiebren de Jong, who allowed all this come into being. Thank you sincerely for giving me this great opportunity to carry out this research and continue my research dream in the Netherlands. Thank you for encouraging, guarding, fully supporting and trusting my work. No words can really express how much this opportunity means to me and brightens up my dark moments when I was struggling to find a job in this strange and unfamiliar country. Adrian and Wiebren, *hartelijk dank voor alles uit het diepst van mijn hart*.

Secondly, grateful thanks to the European Commission in the framework of the FP7 Integrated Project “GreenSyngas” for founding this work. Thank project coordinator professor Mehri Sanati from Lund University (ULUND) for organizing this project. Thank all project partners, in particular Lantmännen for supplying biomass fuels, Michael Müller from Jülich GmbH for performing fuel characterization analysis, XRF lab of the C.S.B. of University of Bologna (UNIBO) for X-ray fluorescence analysis, and Markus Koch from BKG GmbH & CoKG for delivering olivine materials. Thank Mattias, Panagiotis from Technical University Munich, Patrik from ULUND, Patricia from UNIBO for co-performing measurement campaigns.

Experiments require lots of practical operational skills and labour work. I express my deep thanks to: Marcin and Eleonora, and Jacopo for patiently helping me to get familiar with the CFB gasifier and TGA-FTIR setups and solve experimental problems; Yair, Alex, John, and Weipeng for helping me to prepare and clean up “experimental messy”; Michel for helping me to purchase chemical products and understand GC 450 system; and Andre, Daniel, Jesper, Jan, Eugene, Martijn, Eveline, Judith, Helma, Ilona, Leslie and Rob for your mechanical, electrical and managerial support. Also, my highly appreciation is for my students Yuan, Ningjie, Kevin and Fatemeh who have contributed to this book.

Many thanks also surely go to my dear Chinese friends: Yongju, Zuopeng, Yuan, Ming, Xiaoqian, Liyan, Jie, Xiaohua, Huaiyu, Bowen, Ningjie, Zhaochuang, Xin, Nana... Thanks for the chatting, discussion and gathering; and to my all the rest of P&E colleagues: Teunis for helping me with software issues, Theo and Richard for helping my Inburgeringsexamen, and JuanMa, Aravind, Gianluca, Carsten, Bart, Hrishikesh, Yash, Nafiseh, Wijitra and others who are not listed; and to my old colleagues in SDERI. Thanks for your close presence that brought a colourful memory to me.

*Natuurlijk*, I express deepest thanks to my family: my parents for all support and understanding to my each decision; my sister (Xiangjie) and brother (Xiangsuo) to take care of my parents in China; my dear husband Rinko for always encouraging and enduring me; my parents-in-law (Henny and Theo), sister-in-law (Rianka) and all Rijnhout family for your kindness, care and consideration which make me feel at home; and also my little lovely son Johannes MengLong, thank you “baobao” for being here, enjoying and sharing this special moment together with mum and dad.

Last but not least, I would like also to thank to Jonathan de Vries, Anders Ekerot and Ruud Börger from COMSOL BV for technical support of the modelling; Titus de Leeuw, Ilco Houben and Els Verdonck from TA instruments for helping TGA maintenance and training; Gernot Hellier from Ratfish GmbH for modifying the on-line tar analyzer; Willem Jan Buys from Varian company for assisting me GC installation and calibration; and Paul Keijzer for helping GCU unit modification. And finally with my full heart I wish you all the best with your future carrier, study and life.



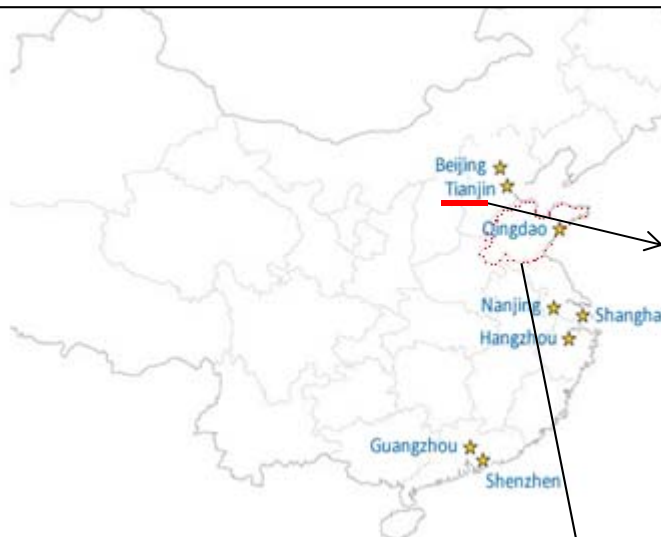
## Curriculum Vitae

**Come to the Netherland:** 18 December, 2007 (for Rinko)

**PhD study:** 08/2008—11/2012 Energy Technology section, 3mE Faculty, Delft University of Technology

**Postdoc:** 12/2012- Energy Technology section, 3mE Faculty, Delft University of Technology

**Dutch level:** Past “Inburgeringsexamen (A2)” and “Staatsexamen NT2 Programma I (B1)”



**Master study:** 2003-2006, Tianjin University

- **Major:** Built Environment and Equipment Engineering
- **Final assignment:** Research on optimization of alkali-catalyzed transesterification of waste cooking oil (WCO) for biodiesel fuel production
- **Co-research:** Study on combined desulfurization and denitrification using active carbon in circulating fluidized bed

**Part-time job:**

- **Editor** of “Gas & Heat Journal”
- **Manager assistant** of China and Netherlands Government Cooperate FTEI project (development and demonstration of feasible technologies for environmental infrastructure in China’s western small cities) in Tianjin office.

**Birth Place:** 6 October, 1980, Shan County, Heze district, Shandong Province, China

**High school:** 1995-1999, Shanxian NO.1 high school, Shan County, China



**Bachelor study:** 1999-2003, Shandong Institute of Architecture and Engineering, Jinan, China

- **Major:** Built Environment and Equipment Engineering
- **Final assignment:** Designing of Air-conditioning system and refrigeration house of Shandong Institute of Architecture and Engineering Scholarship Report Hall (honored)

**Full-time job:** 3/2006-12/2007, research assistant, in Energy Research Institute of Shandong Academy of Science (SDERI)

- **Main research:** Optimization of biodiesel production from chicken fats and oleaginous microbe oils which are produced from lignocelluloses by pretreatment, hydrolysis, fermentation and transesterification
- **Co-research:** Mechanism study of catalytic cracking and steam reforming of multi-lump biomass tar for hydrogen production